



Friedrich-Schiller-Universität Jena

---

Chemisch-Geowissenschaftliche Fakultät

# Design of Functional Polymer Architectures by RAFT Polymerization

## Dissertation

zur Erlangung des akademischen Grades  
doctor rerum naturalium (Dr. rer. nat.)

vorgelegt dem Rat der Chemisch-Geowissenschaftliche Fakultät der  
Friedrich-Schiller-Universität Jena

von Diplom-Chemiker Christian Pietsch  
geboren am 03.01.1984 in Naumburg/Saale

Gutachter:

1. Professor Dr. Ulrich S. Schubert (Universität Jena)
2. Jun.-Professor Dr. Felix H. Schacher (Universität Jena)
3. Professor Dr. Philipp Vana (Universität Göttingen)

Tag der öffentlichen Verteidigung: 18.09.2013

*“If you want to understand function, study structure”*

Francis Crick



---

## Table of contents

---

<i>Table of contents</i>	V
<i>Documentation of authorship</i>	1
<i>1 Introduction</i>	7
<i>2 Modern polymerization techniques towards stimuli-responsive properties</i>	11
<i>2.1 Controlled radical polymerization techniques</i>	11
<i>2.2 Stimuli-responsive properties for polymeric sensor application</i>	15
<i>3 Controlled radical polymerization of functional monomers</i>	19
<i>4 Responsive block copolymers: Well-defined synthesis and self-assembly</i>	29
<i>5 Poly(methyl methacrylate) based nanoparticles for cellular uptake</i>	37
<i>Summary</i>	43
<i>Zusammenfassung</i>	47
<i>References</i>	51
<i>List of abbreviations</i>	59
<i>Curriculum vitae</i>	61
<i>Publication list</i>	63
<i>Acknowledgements / Danksagung</i>	69
<i>Declaration of authorship / Selbstständigkeitserklärung</i>	73
<i>Publications P1-P12</i>	75



---

## Documentation of authorship

---

This section contains a list of the individual author contributions to the publications reprinted in this thesis.

### Publication P1

U. Mansfeld, C. Pietsch, R. Hoogenboom, C. R. Becer, U. S. Schubert "Clickable initiators, monomers and polymers in controlled radical polymerizations – a prospective combination in polymer science", *Polym. Chem.* **2010**, *1*, 1560–1598.

- |                 |  |
|-----------------|--|
| U. Mansfeld:    | conceptual development, preparation of manuscript: chapters 2, 3, 4.3 and parts of chapters 4.1, 5 and 6   |
| C. Pietsch:     | conceptual development, preparation of manuscript: chapters 4.2, 7 and parts of chapters 3.3, 4.1, 5 and 6 |
| R. Hoogenboom:  | correction of the manuscript, supervision  |
| C. R. Becer:    | preparation of the manuscript: introduction, conclusion  |
| U. S. Schubert: | correction of the manuscript, supervision  |

### Publication P2

C. Pietsch, U. S. Schubert, R. Hoogenboom "Aqueous polymeric sensors based on temperature-induced polymer phase transitions and solvatochromic dyes", *Chem. Commun.* **2011**, *47*, 8750–8765 (including cover page).

- |                 |  |
|-----------------|--|
| C. Pietsch:     | conceptual development, manuscript preparation: all chapters and cover preparation |
| U. S. Schubert: | correction of the manuscript, supervision  |
| R. Hoogenboom:  | correction of the manuscript, supervision  |

Publication P3

R. Menzel, A. Breul, C. Pietsch, J. Schäfer, C. Friebe, E. Tauscher, D. Weiß, B. Dietzek, J. Popp, R. Beckert, U. S. Schubert "Blue-emitting polymers based on 4-hydroxythiazoles incorporated in a methacrylate backbone", *Macromol. Chem. Phys.* **2011**, *212*, 840–848 (including cover page).

- R. Menzel: conceptual contribution, syntheses of thiazole monomers, manuscript preparation and cover preparation
- A. Breul: polymerizations, manuscript preparation
- C. Pietsch: conceptual contribution, polymerizations, manuscript and cover preparation
- J. Schäfer: characterization optical properties
- C. Friebe: characterization
- E. Tauscher: conceptual contribution
- D. Weiß: supervision R. Menzel
- B. Dietzek: correction of the manuscript, supervision J. Schäfer
- J. Popp: correction of the manuscript
- R. Beckert: correction of the manuscript, supervision R. Menzel
- U. S. Schubert: correction of the manuscript, supervision

Publication P4

A. M. Breul<sup>+</sup>, C. Pietsch<sup>+</sup>, R. Menzel, J. Schäfer, A. Teichler, M. D. Hager, J. Popp, B. Dietzek, R. Beckert, U. S. Schubert "Blue emission of side-chain pendant 4-hydroxy-1,3-thiazoles in polystyrenes synthesized by RAFT polymerization", *Eur. Polym. J.* **2012**, *48*, 1339–1347.

<sup>+</sup> Both authors contributed equally to this paper.

- A. M. Breul: polymerizations, manuscript preparation
- C. Pietsch: polymerizations, kinetic study, manuscript preparation
- R. Menzel: syntheses of thiazole monomers
- J. Schäfer: characterization optical properties
- A. Teichler: film characterization
- M. D. Hager: correction of the manuscript, supervision A. Breul
- J. Popp: correction of the manuscript
- B. Dietzek: correction of the manuscript, supervision J. Schäfer
- R. Beckert: correction of the manuscript, supervision R. Menzel
- U. S. Schubert: correction of the manuscript, supervision



## Publication P5

C. Pietsch<sup>+</sup>, J. Schäfer<sup>+</sup>, R. Menzel, R. Beckert, J. Popp, B. Dietzek, U. S. Schubert "Förster resonance energy transfer in poly(methyl methacrylates) copolymers bearing donor–acceptor 1,3-thiazole dyes", *J. Polym. Sci., Part A: Polym. Chem.* **2013**, *51*, 4765–4773.

<sup>+</sup> Both authors contributed equally to this paper.

C. Pietsch:	conceptual development, synthesis of all copolymers, polymer characterization, manuscript preparation
J. Schäfer:	FRET investigation, fluorescence characterization, manuscript preparation
R. Menzel:	syntheses of thiazole monomers, correction of the manuscript
R. Beckert:	correction of the manuscript, supervision R. Menzel
J. Popp:	correction of the manuscript
B. Dietzek:	correction of the manuscript, supervision J. Schäfer
U. S. Schubert:	correction of the manuscript, supervision

## Publication P6

C. Pietsch, A. Vollrath, R. Hoogenboom, U. S. Schubert "A fluorescent thermometer based on a pyrene-labeled thermoresponsive polymer", *Sensors* **2010**, *10*, 7979–7990.

C. Pietsch:	fluorescence investigation, characterization, manuscript preparation
A. Vollrath:	DLS studies
R. Hoogenboom:	conceptual development, correction of the manuscript, supervision
U. S. Schubert:	correction of the manuscript, supervision

## Publication P7

D. Heine, C. Pietsch, U. S. Schubert, W. Weigand "Controlled radical polymerization of styrene-based models of the active site of the [FeFe]-hydrogenase", *J. Polym. Sci., Part A: Polym. Chem.* **2013**, *51*, 2171–2180 (including cover page).

D. Heine:	conceptual contribution, syntheses of [FeFe]-Hydrogenase monomers, characterization, manuscript and cover preparation
C. Pietsch:	conceptual contribution, performing of copolymerization's, IR and SEC characterization, manuscript and cover preparation
U. S. Schubert:	conceptual contribution, correction of the manuscript, supervision
W. Weigand:	correction of the manuscript, supervision

Publication P8

C. Pietsch, U. Mansfeld, C. Guerrero-Sanchez, S. Hoepfner, A. Vollrath, M. Wagner, R. Hoogenboom, S. Saubern, S. H. Thang, C. R. Becer, J. Chiefari, U. S. Schubert "Thermo-induced self-assembly of responsive poly(DMAEMA-*b*-DEGMA) block copolymers into multi- and uni-lamellar vesicles", *Macromolecules*, **2012**, *45*, 9292–9302 (including cover page).

- C. Pietsch: block copolymer synthesis, polymer characterization, LCST investigations, manuscript and cover preparation
- U. Mansfeld: cryo-TEM investigations, correction of the manuscript
- C. Guerrero-Sanchez: supervision synthesis, correction of the manuscript
- S. Hoepfner: cryo-TEM investigation, supervision and manuscript correction
- A. Vollrath: DLS studies
- M. Wagner: Zeta potential measurements
- R. Hoogenboom: correction of the manuscript
- S. Saubern: correction of the manuscript
- S. H. Thang: CTA synthesis, correction of the manuscript
- C. R. Becer: conceptual contribution, correction of the manuscript
- J. Chiefari: correction of the manuscript
- U. S. Schubert: conceptual contribution, correction of the manuscript, supervision

Publication P9

A. Krieg, C. Pietsch, A. Baumgaertel, M. D. Hager, C. R. Becer, U. S. Schubert „Dual hydrophilic polymers based on (meth)acrylic acid and poly(ethylene glycol) – synthesis and water uptake behavior”, *Polym. Chem.* **2010**, *1*, 1669–1676.

- A. Krieg: syntheses of copolymers and macroinitiators, manuscript preparation
- C. Pietsch: syntheses of copolymers, kinetic study and manuscript preparation
- A. Baumgaertel: MS characterization
- M. D. Hager: correction of the manuscript
- C. R. Becer: correction of the manuscript
- U. S. Schubert: correction of the manuscript, supervision

## Publication P10

I. Y. Perevyazko, A. Vollrath, C. Pietsch, S. Schubert, G. M. Pavlov, U. S. Schubert "Nanoprecipitation of poly(methyl methacrylate)-based nanoparticles: Effect of the molar mass and polymer behavior", *J. Polym. Sci., Part A: Polym. Chem.* **2012**, *50*, 2906–2913.

- I. Y. Perevyazko: characterization via AUC and viscosity, manuscript preparation  
A. Vollrath: nanoparticle preparation, characterization by SEM and DLS, manuscript preparation  
C. Pietsch: syntheses of all polymers, SEC characterization and manuscript preparation  
S. Schubert: correction of the manuscript, supervision A. Vollrath  
G. M. Pavlov: correction of the manuscript, supervision I. Perevyazko  
U. S. Schubert: correction of the manuscript, supervision

## Publication P11

A. Vollrath, D. Pretzel, C. Pietsch, I. Y. Perevyazko, R. Menzel, S. Schubert, G. M. Pavlov, D. Weiß, R. Beckert, U. S. Schubert "Preparation, cellular internalization and biocompatibility of highly fluorescent PMMA nanoparticles", *Macromol. Rapid Commun.* **2012**, *33*, 1791–1797.

- A. Vollrath: nanoparticle preparation, characterization, manuscript preparation  
D. Pretzel: cell studies, biocompatibility tests and manuscript preparation  
C. Pietsch: syntheses of all copolymers, characterization and manuscript preparation  
I. Y. Perevyazko: characterization via AUC and pUC  
R. Menzel: syntheses of thiazole monomers, correction of the manuscript  
S. Schubert: correction of the manuscript, supervision A. Vollrath  
G. M. Pavlov: correction of the manuscript, supervision I. Perevyazko  
D. Weiß: correction of the manuscript, supervision  
R. Beckert: correction of the manuscript, supervision R. Menzel  
U. S. Schubert: correction of the manuscript, supervision

Publication P12

A. Vollrath, A. Schallon, C. Pietsch, S. Schubert, T. Nomoto, Y. Matsumoto, K. Kataoka, U. S. Schubert "A toolbox of different sized and labeled PMMA nanoparticles for cellular uptake investigations", *Soft Matter*, **2013**, *9*, 99–108.

- |                 |  |
|-----------------|--|
| A. Vollrath:    | labeling, nanoparticle preparation, characterization, manuscript preparation |
| A. Schallon:    | cell studies, CLMS investigation and manuscript preparation                  |
| C. Pietsch:     | syntheses of copolymers, characterization, manuscript preparation            |
| S. Schubert:    | correction of the manuscript, supervision A. Vollrath                        |
| T. Nomoto:      | CLMS studies   |
| Y. Matsumoto:   | CLMS studies, supervision T. Nomoto  |
| K. Kataoka:     | conceptual contribution, correction of the manuscript, supervision           |
| U. S. Schubert: | conceptual contribution, correction of the manuscript, supervision           |

Declaration of the supervisor:

---

(Prof. Dr. Ulrich. S. Schubert)

---

# 1 Introduction

---

After the developments of the first synthetic polymer by Baakeland at the beginning of the 20<sup>th</sup> century (phenol formaldehyde resins, “Bakelite”) the research field of synthetic polymers started.<sup>[1, 2]</sup> At this time the macromolecular structure of polymers was not known but several polymers based on modified natural products were established for industrial applications. In 1920s Staudinger proved the existence of large covalent chain macromolecules and established the concept of macromolecular chemistry (primary-valence chain systems).<sup>[3-5]</sup>

Today a large number of industrial used synthetic polymers are produced by chain growth polymerizations that were developed in the 1930s to 1960s. The chemistry of vinylic/acrylic monomers was at this time still a new field, where *e.g.* *poly(methyl methacrylate)* (PMMA, Plexiglas) was developed in 1933 by the pioneering work of Otto Röhm.<sup>[6]</sup> Two further representative examples are the Ziegler-Natta polymerization and the anionic polymerization by Szwarc.<sup>[7, 8]</sup> After these developments an exponential grow of new polymeric materials occurred, although very few new industrial polymers were introduced in recent decades.

Nowadays the interests of (academic) polymer scientist are more focused on controlling the molecular architecture and structure of macromolecules. The aim is the understanding of structure-properties relationships regarding polymer chain length, composition and architecture (Figure 1). In this context modern *controlled radical polymerization* (CRP) techniques<sup>[9, 10]</sup> provide the possibility to control the macromolecular chain structure, the polymer architecture, the molar mass and the functionalization (side and endgroup). The most applied techniques up today for this controlled design are the *reversible addition-fragmentation chain transfer* (RAFT)<sup>[11, 12]</sup> polymerization, the *atom transfer radical polymerization* (ATRP)<sup>[13, 14]</sup> and the *nitroxide-mediated polymerization* (NMP)<sup>[15, 16]</sup> method. The unique features of the RAFT polymerization are the good tolerance to several functional groups and the possibility to polymerize a wide range of different monomers.

The scope of this thesis is the development and design of new copolymer systems with advanced macromolecular structure with a focus on the controlled construction of polymer chains including functionalities and block segments. The conception is based on the RAFT polymerization method for the synthesis of polymeric material, which allows this “microstructural” constitution. More specifically, this thesis aims to investigate structure-property relationships thereby focusing on the incorporation of functional groups and its applications. The functionalities include dyes with sensing/“antenna” structures for

diagnostics as well as responsive block copolymers for controlled stimuli-induced self-assembly. These advanced polymeric structures strongly influence the properties, like the phase separation morphologies, self-assembly or stimuli-responsive behavior of the corresponding copolymer (Figure 1).

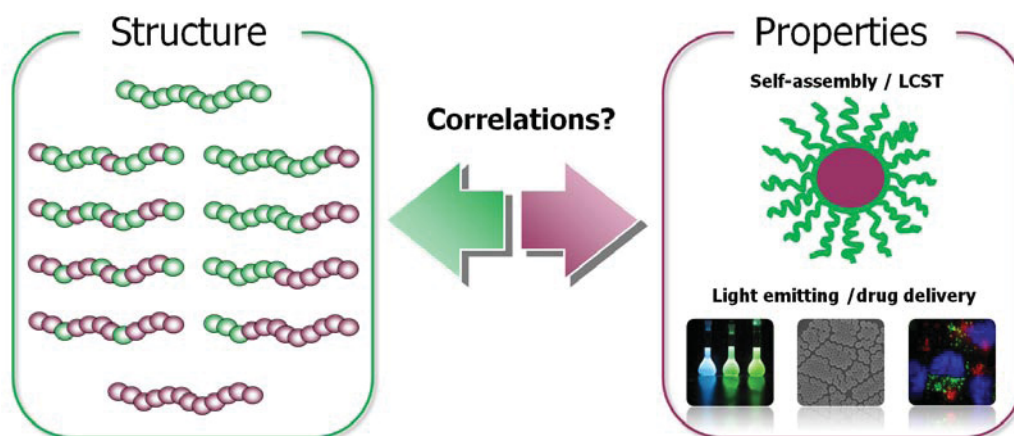


Figure 1 Correlation between molecular structures and macroscopic properties.

A comprehensive overview about the design of polymer architectures by RAFT polymerization including the incorporation of different functionalized monomers can be found in **Chapter 2.1** of this thesis. Therein the RAFT polymerization method and its mechanism is further discussed in detail. The implementation of functionalities (e.g. dyes) in combination with the thermo-responsive phase separation of copolymers opens a window for applications in sensor systems or in diagnostics. **Chapter 2.2** provides an overview of the research that guided the way from fundamental studies of the thermo-responsive phase separation of aqueous polymer solutions to polymeric sensor systems.

The incorporation of functional groups into polymer chains, in particular the use of light-emitting or light absorbing dyes is an appealing design criterion and represents an important challenge. Light-emitting or absorbing copolymers reveal high potential for applications in various fields, like in *förster resonance energy transfer* (FRET) pairs for diagnostics.<sup>[17-19]</sup> An essential requirement for these constructs is the incorporation of chromophores into the polymer without changes in their optical properties, e.g. the quantum yield. Polymerization strategies which open avenues to fulfill this requirement are provided by the RAFT method, which was applied for several dye-functionalized methacrylates and styrene derivatives (**Chapter 3**). The preparation of multifunctional and well-defined macromolecules *via* the RAFT process is also demonstrated. Additionally the proof for the controlled/living polymerization is provided based on a kinetic analysis.

Besides the investigations of controlled polymerization of functional monomers the interest of many researchers was attracted towards the constructions of more complex structures, like block or comb copolymers. In this research field the morphologies, self-organization towards polymersomes and advanced stimuli-responsive behavior, e.g. phase separation in response to an external stimulus, are of great interest.<sup>[20-28]</sup> Such “responsive” materials can act in response to changes in environmental parameters like temperature, pH value or light. In this context the preparation of amphiphilic block copolymers, which undergo a thermo-sensitive self-organization, in particular the formation of micelles or vesicular structures is of great interest. The polymer architecture plays a key role for this self-organization and has to be carefully designed. For this purpose a library of double thermo-responsive block copolymers with different ratio between both segments were synthesized by RAFT polymerization. The characteristics regarding the thermo induced self-assembly depending on the block length is part of **Chapter 4**. Moreover, this chapter provides the synthesis and characterization of dual hydrophilic statistical and block copolymers of acrylic monomers. Next to the exploration of self-assembled structures of block copolymers an additional procedure was investigated to generate tailor-made nano-objects. The design of labeled polymeric nanostructures with tailored properties has attracted great attention not only in chemistry, but also in other disciplines like biology. The combination of chromophores and advanced polymer structure opened up opportunities for preparation of labeled polymeric *nanoparticles* (NP). **Chapter 5** contains analysis of the polymeric NP systems with respect to their corresponding NP size, used chromophores and stability. Furthermore, such fluorescent polymeric NPs have been studied in cellular uptake in terms of potential diagnostic devices. In this final chapter well-defined and differently sized NPs, prepared by nanoprecipitation of dye-functionalized PMMA derivatives, are presented.





---

## 2 Modern polymerization techniques towards stimuli-responsive properties

---

Parts of this chapter have been published: P1) U. Mansfeld, C. Pietsch, R. Hoogenboom, C. R. Becer, U. S. Schubert, *Polym. Chem.* **2010**, *1*, 1560–1598; P2) C. Pietsch, U. S. Schubert, R. Hoogenboom, *Chem. Commun.* **2011**, *47*, 8750–8765.

The investigation of structure-property relationship of macromolecules represents an intensive research field in polymer chemistry. In fact, the molecular structure of the polymer determines the macroscopic properties, e.g. the morphologies, the self-assembling or the stimuli-responsive behavior in aqueous solutions.<sup>[20-23, 29]</sup> Therefore an important aspect is the construction of advanced polymer architectures to study the corresponding polymer properties. In this context modern *controlled radical polymerization* (CRP) techniques represent suitable methods to construct well-defined copolymer structures with stimuli-responsive behaviors. Also the combination of thermo-responsiveness with a second response towards other environmental parameters, like changes in the pH value, within one polymer chain, is achievable. These modern controlled polymerization platforms represent suitable synthetic tools for their construction, whereby the functionalization of the polymer and the control over the polymer chain length as well as composition is provided. In detail the controlled incorporation of dyes or other functional groups can be generated by using functional monomers or initiators. Within this polymerization method the study of thermo-responsive phase separation and dye based polymeric sensor systems could be realized and investigated in detail regarding the development of structure-property relationships.

### 2.1 Controlled radical polymerization techniques

The synthesis of well-defined polymers has been the ultimate challenge of polymer chemists in the last decades. The development of anionic polymerization by Szwarc *et al.* in 1956 opened new avenues and a new field of materials research.<sup>[8, 30]</sup> Besides, polymeric materials have improved the quality of our lives in all areas from engineering to electronics and even medical applications.<sup>[29, 31, 32]</sup> Following the invention of anionic polymerization, other possible types of living and/or controlled radical polymerizations have been intensively studied.<sup>[16, 33-35]</sup> One of the most significant CRP techniques to date is the *reversible*

*addition-fragmentation chain transfer* (RAFT) polymerization.<sup>[11, 12, 36, 37]</sup> This polymerization method requires the usage of a dedicated compound or *chain transfer agent* (CTA) to gain control over the polymerization of various monomeric structures.

The unique features of the RAFT polymerization are the good tolerance to several functionalities (e.g., incorporation of dyes or functional groups for click chemistry)<sup>[38, 39]</sup> and the possibility to construct a wide range of different architectures, e.g., comb, block, gradient and star copolymers, respectively.<sup>[40]</sup> A good control over the molar mass and *polydispersity index* (PDI) can be obtained by this type of controlled radical polymerization technique. The RAFT polymerization was developed in 1998 by the *Commonwealth Scientific and Industrial Research Organization* (CSIRO) in Australia, using sulfur based compounds as chain transfer agent.<sup>[11]</sup> These CTA's are based on thiocarbonylthio (S=CS) compounds, providing effective and versatile control of the radical polymerization process. The CTA's can be divided in four classes of RAFT agents: dithioesters, trithiocarbonates, xanthates and dithiocarbamates.<sup>[41, 42]</sup> Schematic representation of different CTA agents used in this work are shown in Figure 2.

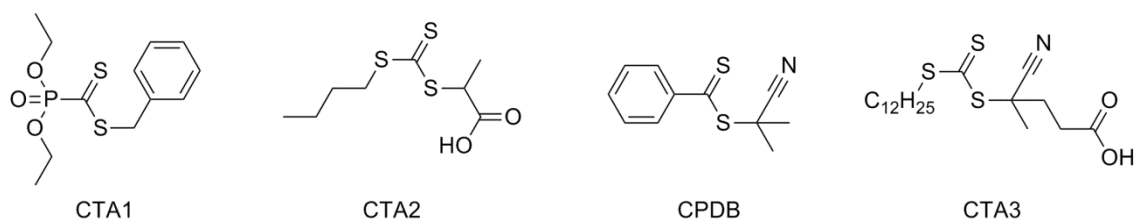


Figure 2 Schematic representation of the CTA agents used in the controlled radical polymerization (CTA1: Benzyl (diethoxyphosphoryl)dithioformate, CTA2: 2-(Butylthiocarbonothioylthio) propanoic acid, CPDB: 2-Cyano-2-propyl dithiobenzoate CTA3: 4-Cyano-4-[(dodecylsulfanylthiocarbonyl) sulfanyl]pentanoic acid).

The concept of the RAFT method is based on a degenerative chain control, which induces an equilibrium between propagating macroradical-chains and dormant polymeric RAFT agents bearing the thiocarbonylthio moieties at the end of the polymer chain.<sup>[12, 40]</sup> A rapid exchange *via* a reversible deactivation process between the dormant and the active radical is required to obtain control over the polymerization process. The main equilibrium of the mechanism of the RAFT process is illustrated in Figure 3. In the ideal case the radicals start growing at the same time and have equal opportunities for growth, resulting in a linear increase of chain length with monomer conversion and a narrow molar mass distribution.

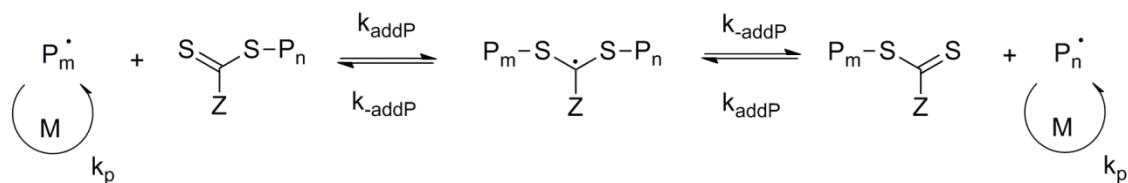


Figure 3 Schematic representation of the main equilibrium of the RAFT mechanism ( $k_p$  represents the polymerization rate,  $M$  the monomer and  $P_{n,m}$  polymer chains).

It is possible to polymerize a wide range of monomers, e.g. methacrylates, acrylates, styrenes, acrylamides and vinyl esters with the RAFT technique. Also a large variety of functional groups can be polymerized utilizing the RAFT process; important functionalities are carboxylic acids, alcohols, amines, triple bonds, epoxides, sulfates and azides.

The selective functionalization of macromolecules is one of the ultimate challenges for polymer chemists, while the synthesis of tailor-made polymer architectures represents another important goal. The preparation of such multifunctional and well-defined macromolecules requires a smart selection of the controlled polymerization procedure in combination with appropriate functionalization reactions. The synthesis of end- or side-functional macromolecules could be achieved by using functional initiators, monomers or end capping techniques. However, these specific functional groups might have enormous effects on the polymerization rate, control over the polydispersity index and the composition of the copolymers.

Fortunately, a decade ago, the “click” chemistry concept was introduced by Sharpless *et al.* that stimulated the development of a wide range of efficient coupling reactions that enable nowadays the preparation of not only telechelic polymers but also of side-group functionalized polymers using clickable initiators, monomers and polymers.<sup>[43-46]</sup> Sharpless and coworkers drew attention to several highly efficient organic reactions and called them “click” reaction.<sup>[47, 48]</sup> Several other efficient organic reactions have since then been claimed to be “click” reactions since they fulfilled all or most of the click chemistry criteria, which can be listed as modular and wide in scope, high efficiency and high yields, no or inoffensive byproducts, readily available starting materials and reagents, no solvent or a benign solvent, and simple purification techniques (no chromatographic procedures).<sup>[46]</sup>

The concept of “click” chemistry combined with the concept of controlled radical polymerizations represents an ideal pair for the preparation of tailor-made macromolecular architectures. The striking advantage of this combination can be clearly seen by the variety of “clicked” architectures that become within reach by using clickable polymers as building blocks. These clickable polymers act as basic modules for further functionalization reactions to engineer more complex architectures or to tune the properties of the polymeric material. (Figure 4).

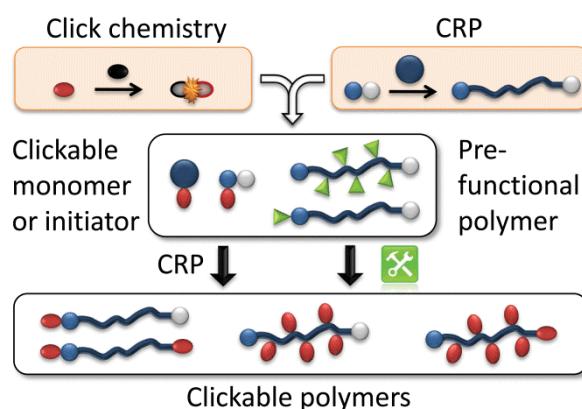


Figure 4 Schematic representation for the construction of different functional polymer architectures.

An example for the post modification of polymers represents the cleavage of the chain transfer agent leading to thiol-terminated polymers, which can easily be prepared by RAFT polymerization. These thiol-terminated polymers can subsequently be clicked not only to unsaturated double bonds but also to alkyne and para-fluoro groups making the combination of RAFT polymerizations with thio-click chemistry a powerful method.<sup>[49, 50]</sup>

Another advantage of this “click” approach is the possible functionalization of polymers with fluorescence dyes (e.g. pyrene), where the degree of functionalization (in the side groups) can be varied, or the simultaneous incorporation of several dyes to explore energy transfer applications.

The combination of controlled radical polymerization techniques and click reactions has become a unique synthetic route for preparing highly functional tailor-made macromolecules. The preparation of new well-defined functional polymers has, thus, become accessible to develop novel polymer structures or properties.

## 2.2 Stimuli-responsive properties for polymeric sensor application

The determination of the temperature is one of the most important analytical methods in chemical laboratories. Among chemical,<sup>[51-56]</sup> pH,<sup>[57, 58]</sup> chemomechanical<sup>[59]</sup> and calorimetric sensors, optical temperature<sup>[60]</sup> sensors play an important role in polymer science. A new class of optical temperature sensors has been therefore developed and received significant attention for the development of sensory materials in the last years. The here discussed sensors are based on stimuli-responsive polymers<sup>[25, 26, 61-63]</sup> that sharply respond with a phase transition to environmental parameter changes such as the temperature, pH value, UV/Vis light or chemical changes. Stimuli-responsive polymer systems can be polymers in solutions, hydrogels, self-assembled aggregates and nanoparticles.<sup>[25-27, 57, 60-65]</sup> The access and the possibility to control the polymer properties<sup>[29]</sup> (e.g. architecture) and the flexibility of processing in combination with a tunable solubility (e.g. ratio of hydrophobic/hydrophilic monomers) make them very promising and advantageous for sensor materials. For sensing purposes, the polymer phase transition can be translated into a sensory signal by incorporation of solvatochromic dyes<sup>[56, 66]</sup> that specifically change their optical or emissive properties upon changing the environmental parameters (Figure 5).

The sensing approach based on the combination of a responsive polymer phase transition and a solvatochromic dye allows simple and fast detection of, e.g., the temperature by measuring the absorbance or fluorescence of the solution. The high sensitivities arise from the incorporated solvatochromic dye molecules, which respond to minor local environmental changes that occur upon the temperature induced polymer phase transition. For temperature-sensing in aqueous solution, the most important polymer phase transition is the so-called *lower critical solution temperature* (LCST), i.e. the polymer is dissolved at lower temperatures and precipitates upon increasing the temperature.

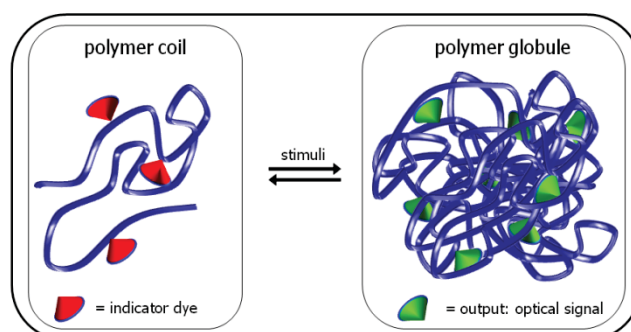


Figure 5 Schematic representation of the polymeric sensors based on polymer phase transitions (coil-to-globule) and solvatochromic dyes.

The driving force for the study of polymeric temperature sensors in the last 20 years is twofold: (i) the development of new functional (temperature) sensor systems utilizing stimuli-responsive polymers and (ii) to gain an in-depth understanding of polymer chain conformations and/or phase transitions in solution. Widely used experimental techniques<sup>[25]</sup> for the determination of these coil-to-globule/LCST transitions are (i) calorimetry<sup>[67-69]</sup> (thermodynamics of phase separation), (ii) viscosity determination<sup>[67]</sup> (hydrodynamic consequences), (iii) light scattering measurements<sup>[70-73]</sup> (size of the coil or globule), (iv) UV/Vis or fluorescence spectroscopy<sup>[74-77]</sup> (molecular resolution of the thermo-reversible phase separation) and additionally, (v) IR<sup>[78]</sup> and NMR spectroscopy.

These techniques are used for fundamental research on stimuli-responsive polymers providing novel insights into the elementary mechanism like the equilibrium transition states or the kinetic/thermodynamic processes of the phase separation and the structure of individual polymer coils as well as the effects of various specific/non-specific interactions (hydrogen bonding, electrostatic, hydrophobic/hydrophilic interactions) between the polymer chains, side/end-groups and/or the solvent.

Additional information can be obtained with polymeric fluorescent sensors, because numerous parameters like fluorescence decay times, fluorescence intensity, quenching efficiency, energy transfer and fluorescence polarization can be determined. The most challenging problems of optical sensors are the reversibility over a long time, the signal stability and photobleaching of the chromophore. Nonetheless, covalently embedding the chromophore into a polymer backbone or in a nanoparticle/hydrogel protects the chromophore making the combination very promising.

The temperature-induced polymer phase separation (demixing) in solution is called LCST transition and can be described by the Flory–Huggins theory.<sup>[79]</sup> During these coil-to globule transitions the polymer chains change from a fully dissolved, hydrated state (hydrophilic) into a collapsed non-hydrated state (hydrophobic). This sharp entropy-driven collapse has a strong influence on the microenvironment of the repeating units of the polymer. The (majority of) water molecules are released into the bulk water during this transition and, therefore, a hydrophilic–hydrophobic (polarity) change occurs in the microenvironment of the polymer. By attaching a solvatochromic chromophore to the polymer chain, this microenvironmental polarity change during the temperature induced polymer phase transition can be translated into a colorimetric or fluorescent sensing signal.

The majority of such sensor designs are based on dye functionalized stimuli-responsive poly(*N*-iso-propylacrylamide), PNIPAM,<sup>[25, 67]</sup> while more recently polymers based on poly(ethyleneglycol) (PEG) functionalized methacrylates,<sup>[80-82]</sup> *i.e.* POEGMA, became popular alternatives too. The poly(di(ethylene glycol) methyl ether methacrylate), PDEGMA (two units of EG), has a LCST around 27 °C. The popularity of PNIPAM is largely based on its LCST of 32 °C,<sup>[25]</sup> which is close to the human body temperature.

Besides these polymers other alternatives are known, showing a LCST behavior in aqueous solution, namely poly(2-dimethylaminoethyl methacrylate), PDMAEMA, poly(vinyl methyl ether), PVME, poly(ethyleneglycol), PEG and poly(2-ethyl-2-oxazoline), POx, as depicted in Figure 6.

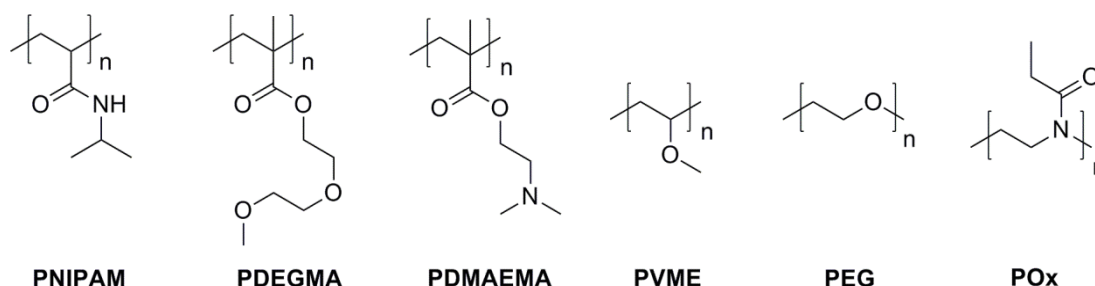


Figure 6 Schematic representation of the chemical structures of polymers with a LCST behavior in water.

The LCST of these thermo-responsive polymers strongly depends on the hydrophilic-hydrophobic character of the repeating unit. In addition, the LCST temperature range of these copolymers can be tuned over the full temperature range of ambient water by controlling the hydrophilic/hydrophobic balance of the polymer by copolymerization. Some thermo-responsive polymers, e.g. PNIPAM or POEGMA, show a sharp phase transition and a good reversibility in water, which is crucial for accurate and reliable sensors applications. The syntheses of responsive copolymers are usually performed by radical polymerization techniques. The most commonly used technique is *free radical polymerization* (FRP) in bulk or solution. However, controlled radical polymerization methods are preferred due to the possibility to control the polymer architecture, composition and chain length. The RAFT polymerization has been mostly used for the construction of these polymeric sensors due to the good tolerance to functional groups.

The synthesis of the desired dye functional macromolecules as well as the preparation of different architectures and their wide range of applications, such as temperature or pH sensors, drug delivery systems and light harvesting antennas are discussed in the next chapter. Also detailed insights into the temperature-induced polymer phase transitions of a polymeric sensor will be provided.





---

### 3 Controlled radical polymerization of functional monomers

---

Parts of this chapter have been / will be published: P3) R. Menzel, A. Breul, C. Pietsch, J. Schäfer, C. Friebe, E. Tauscher, D. Weiß, B. Dietzek, J. Popp, R. Beckert, U. S. Schubert, *Macromol. Chem. Phys.* **2011**, *212*, 840–848; P4) A. M. Breul, C. Pietsch, R. Menzel, J. Schäfer, A. Teichler, M. D. Hager, J. Popp, B. Dietzek, R. Beckert, U. S. Schubert, *Eur. Polym. J.* **2012**, *48*, 1339–1347; P5) C. Pietsch, J. Schäfer, R. Menzel, R. Beckert, J. Popp, B. Dietzek, U. S. Schubert, *J. Polym. Sci., Part A: Polym. Chem.* **2013**, *51*, 4765–4773; P6) C. Pietsch, A. Vollrath, R. Hoogenboom, U. S. Schubert, *Sensors* **2010**, *10*, 7979–7990; P7) D. Heine, C. Pietsch, U. S. Schubert, W. Weigand, *J. Polym. Sci., Part A: Polym. Chem.* **2013**, *51*, 2171–2180.

The incorporation of functional groups into copolymer chains, in particular the incorporation of light-emitting chromophores or light absorbing dye's, is an important design criterion for the construction of advanced polymeric materials. These light-emitting copolymers are the subject of intense research due to their potential applications in various fields. In general, they have been successfully applied in *organic light-emitting diodes* (OLEDs),<sup>[83, 84]</sup> as sensor systems in biochemical and environmental applications,<sup>[60, 85]</sup> in *dye-sensitized solar cells* (DSSCs)<sup>[86, 87]</sup> and for the construction of antenna systems mimicking light-harvesting photosynthetic proteins in plants by incorporating donor and acceptor dye-units to allow *förster resonance energy transfer* (FRET).<sup>[88, 89]</sup>

There are three major synthetic pathways to prepare dye-functionalized polymers: (i) the use of a dye functionalized monomer, (ii) using a functionalized initiator or chain transfer agent and (iii) application of efficient post-polymerization reactions. The post functionalization method has to fulfill some important criterion for a successful incorporation, e.g., using an activated ester monomer or an efficient “click” reaction. On the other hand functional monomers can be used to synthesize pendant functionalized polymers, whereby the functionalized monomer can be homopolymerized or copolymerized to obtain versatile random-, block- or comb copolymers. The chosen controlled radical polymerization processes in this work is the RAFT polymerization method. The RAFT technique was applied for polymerization of dye-functionalized methacrylates and styrene derivatives. The functionalities of these monomers are based on light-emitting chromophores, i.e. the 4-hydroxy-1,3-thiazole dye (**1** to **4**), pyrene dye (**7**) or even more complex structure like the [2Fe2S] clusters (**5** and **6** based on a [FeFe]-hydrogenase model) as depicted in Figure 7. The synthesis of the dye-functionalized methacrylates is straightforward, whereby

the used synthetic route involved the esterification of methacryloyl chloride with the corresponding alcohol functionalized dye. The styrene based monomers were synthesized via a substitution reaction using vinylbenzyl chloride and the corresponding alcohol functionalized dye.

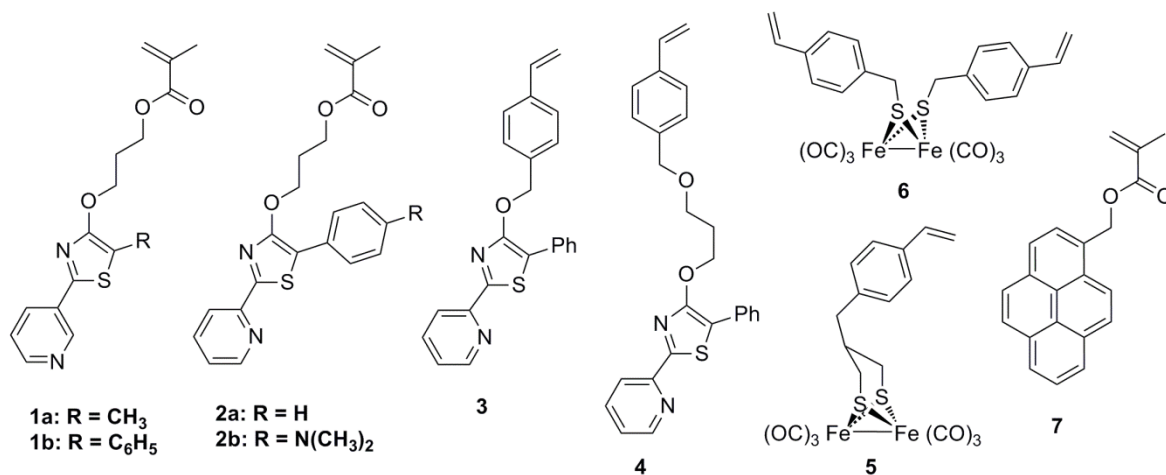


Figure 7 Schematic representation of the used dye-functionalized methacrylates and styrene monomers as well as the [FeFe] functionalized styrenes.

The polymerization of the dye functionalized monomers can be limited in case if reactive groups are present, which interfere with the radical polymerization process. This limitation is in particular given for the polymerization of metal containing monomers, e.g. for the styrene derivatives **5** and **6**, where the metal and the CO groups are known for interactions with the propagating radical.<sup>[90-92]</sup>

The selection of the chromophore should be carefully made not only from a synthetic point of view, but also for their fluorescence and absorption properties. Usually, classic chromophores like coumarines, naphthalenes and quinolines have low quantum yields, strong solvent dependency of their electronic properties, excimer formation,<sup>[93]</sup> and a low photostability. To overcome these restrictions a novel non-classical fluorescence emitter has been developed: the 4-hydroxy-1,3-thiazole dye. The thiazole chromophores generally show very-high room-temperature fluorescence and quantum yields ranging from 0.7 up to unity, in combination with a large Stokes shift, making them very promising for light harvesting polymers.<sup>[94, 95]</sup> These mentioned points are essential for an efficient FRET in a donor/acceptor based copolymer.

The RAFT polymerization was chosen as an efficient method for the polymerization of the thiazole-functionalized methacrylates (**1a**, **1b**). The reaction temperature was set to 70 °C with a reaction time of 16 h in order to ensure an optimal value of conversion combined with low PDI values. The two obtained copolymers revealed a narrow molar-mass

distribution with PDI values below 1.2 (see TABLE 1) as well as a statistical distribution of the dye units along the copolymer chain, as indicated by similar conversion of both monomers. This observation indicates also similar reactivity of both the dye functionalized monomer and MMA. The targeted dye content of 3% was nearly reached for both copolymers **P1** and **P2** (calculated from the integration of the  $^1\text{H}$  NMR spectra).

TABLE 1 Selected characterization data for the obtained copolymers **P1** and **P2**.

Entry	[MMA]/ [dye]	[M]/[CPDB]/ [Initiator]	MMA/dye conv [%] <sup>[a]</sup>	<i>t</i> (h)	<i>M<sub>n</sub></i> [g/mol] <sup>[b]</sup>	PDI <sup>[b]</sup>	DP	Dye [mol%] <sup>[c]</sup>
<b>P1</b>	MMA/ <b>1a</b>	97/3:1:0.25	60 / 65	16	7 400	1.17	71	2
<b>P2</b>	MMA/ <b>1b</b>	97/3:1:0.25	67 / 67	16	8 400	1.19	77	2

[a] Calculated from GC peak integrals, and the UV UV-detector peak areas:  $A_{\text{polymer}}/(A_{\text{polymer}} + A_{\text{monomer}})$ .

[b] Calculated from SEC ( $\text{CHCl}_3/\text{triethylamine}/\text{iso-propanol} = 94/4/2$ ) using PMMA calibration. [c] Calculated from  $^1\text{H}$  NMR spectra using the integrated areas of aromatic dye signals and the  $-\text{OCH}_3$  MMA signals.

The proof of the controlled radical polymerization of these thiazole monomers was provided by kinetic investigations, using semi-logarithmic plot of  $\ln([M]_0/[M]_t)$  versus time and plotting molar masses against monomer conversion. In detail, the polymerization kinetics were determined for the copolymerization of styrene and **3** in toluene with 2-(butylthiocarbonothioylthio)propanoic acid, CTA2, and a  $[M]/[\text{CTA2}]$  ratio of 250. The polymerization kinetics for the RAFT polymerizations have been investigated by determination of the styrene conversion using  $^1\text{H}$  NMR spectroscopy (the styrene signals were overlapping with the thiazole styrene vinyl signals, therefore, estimation of the total conversion), and the molar masses as well as polydispersity indices by *size exclusion chromatography* (SEC). A linear slope of  $\ln([M]_0/[M]_t)$  could be observed for styrene of nearly 7 h, followed by a decrease in the slope (Figure 8). Such a decrease in  $\ln([M]_0/[M]_t)$  is commonly observed due to either the occurrence of termination reactions (for styrene mostly recombination reactions) or a decrease in initiator concentration, which results from a steadily decreasing concentration of the radical source (AIBN).<sup>[96]</sup> The decrease in radical concentration for the RAFT polymerization of styrene is described in literature by a recombination of the growing radical chains or by recombination of AIBN-derived cyanoisopropyl radicals.<sup>[97]</sup>

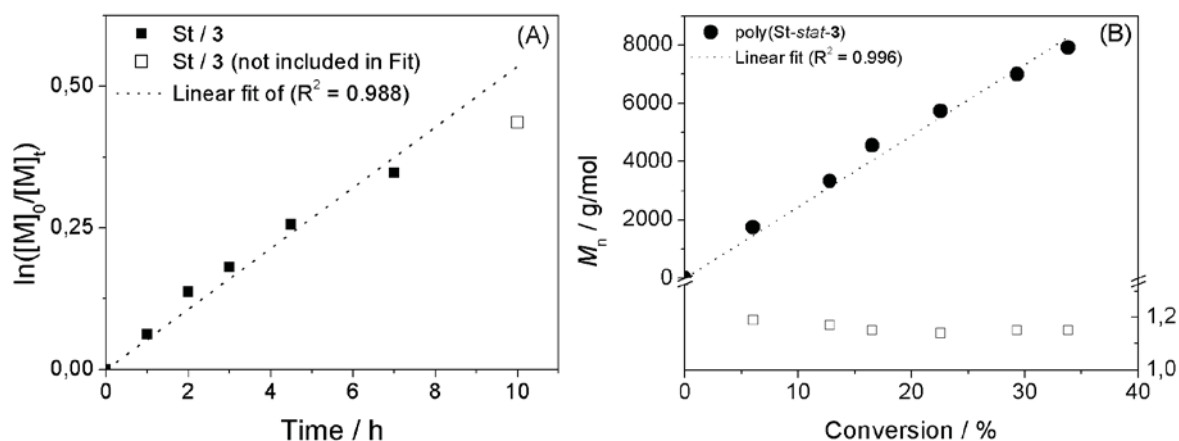


Figure 8 A) Kinetic analysis of the monomer conversion of styrene and 1,3-thiazole functionalized styrene 3 during the RAFT polymerization at 80 °C in toluene. B)  $M_n$  values and polydispersity indices versus monomer conversion for the copolymerization.

The linear increase of  $M_n$  values with monomer conversion in combination with low polydispersity indices (under 1.20) evidences that the RAFT polymerization of styrene and thiazole styrene proceeded in a controlled manner (Figure 8b). The linear fit demonstrates clearly that the molar mass of the copolymers can be tuned in a well-defined manner.

In a next step artificial light-harvesting systems based on polymeric structures to mimic natural light-harvesting systems have been designed and characterized using 2-(pyridine-2-yl) 4-hydroxy-1,3-thiazole dyes **2a** and **2b**. The design strategy was to incorporate the monomeric dye units into a linear copolymer for optimal energy transfer between them. The thiazole dyes **2a** and **2b** were constructed for the usage as energy donor and acceptor dye for this FRET investigation.

In detail a series of statistical donor-acceptor copolymers (in total five copolymers) based on a PMMA backbone was synthesized using the RAFT polymerization technique. Within this series, the ratios of donor to acceptor were varied (Figure 9) starting from the donor copolymer (**PD**) following by an increasing amount of acceptor (**PDA1-3**) ending by the acceptor copolymer (**PA**). The thiazole donor (**2a**) and acceptor monomers (**2b**) were explicitly synthesized to construct donor-acceptor systems along a polymer chain (Figure 9). In doing so the thiazole structure of **2a** was expanded with an electron donating dimethylamino group at the phenyl ring in order to increase the charge transfer character (the pyridine acts as the electron acceptor) of the longest-wavelength  $\pi$ - $\pi^*$  transition. This induces a red shift of the absorption and emission. The monomer **2a** exhibits a bathochromically shifted absorption (416 nm,  $\Delta = 40$  nm) and emission spectra (526 nm,  $\Delta = 77$  nm) together with a reduced quantum yield ( $\Phi_F = 61\%$ ) compared to **2a** in chloroform.

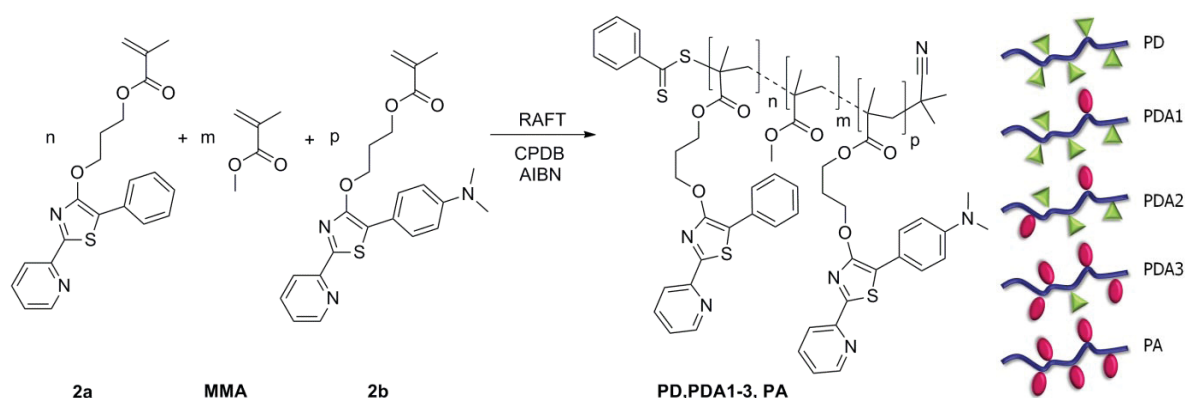


Figure 9 Schematic representation of the RAFT polymerization of MMA with **2a** and **2b** using the CTA CPDB and the radical initiator AIBN. Right: Illustration of the functionalized donor-acceptor copolymers **PD**, **PDA1-3** and **PA**.

The polymerizations were carried out using 2-cyano-2-propyl dithiobenzoate, CPDB, as CTA and 2,2'-azobis(*iso*-butyronitrile), AIBN, as radical initiator. The polymerizations of the monomers were performed in toluene with a monomer concentration of 2.0 mol L<sup>-1</sup>. The polydispersity index values measured by SEC are below 1.3, demonstrating a good control over the copolymer characteristics (TABLE 2). The monomer conversions of the MMA units were estimated by <sup>1</sup>H NMR spectroscopy *via* the signals of the protons of the corresponding double bonds. The conversion of all methyl methacrylate units was around 65 to 80% after 13 h of polymerization time.

The emission spectrum of **2a** shows a distinct overlap with the absorption of **2b** resulting in a large overlap integral. From the steady state spectra the Förster distance was calculated to be  $R_0 = 39 \text{ \AA}$ . The polymers **PDA1-3** have statistically distributed donor and acceptor molecules with calculated donor/acceptor ratios (mol%) of 10.5/1.5, 4.7/3.5 and 1.6/4.8, respectively.

TABLE 2 Overview of the synthesized donor-acceptor copolymers by RAFT polymerization.

Entry	[MMA]/[2a]/[2b]	$M_n$ [g/mol] <sup>[a]</sup>	PDI <sup>[a]</sup>	DP <sub>SEC</sub>	$M_n$ [g/mol] <sup>[b]</sup>	PDI <sup>[b]</sup>	ratio <sup>1</sup> NMR % <sup>[c]</sup> [MMA]/[2a]/[2b]
<b>PD</b>	95/ 5/ 0	7 000	1.21	57	n/a	n/a	92.1/ 7.9/ 0
<b>PDA1</b>	94/ 5/ 1	10 600	1.20	76	8 900	1.18	87.7/ 10.8/ 1.5
<b>PDA2</b>	94/ 3/ 3	11 100	1.26	87	9 100	1.25	91.8/ 4.7/ 3.5
<b>PDA3</b>	94/ 1/ 5	12 400	1.26	102	9 800	1.30	83.6/ 1.6/ 4.8
<b>PA</b>	95/ 0/ 5	7 000	1.22	58	n/a	n/a	93.2/ 0/ 6.8

[a] Calculated from SEC (DMAc) using PMMA calibration. [b] Calculated from SEC (CHCl<sub>3</sub>) using PMMA calibration. [c] Calculated from integrated areas of (CH<sub>3</sub>)<sub>2</sub>N- signals the ester CH<sub>2</sub>-O-, and the CH<sub>3</sub>- side-group signals.

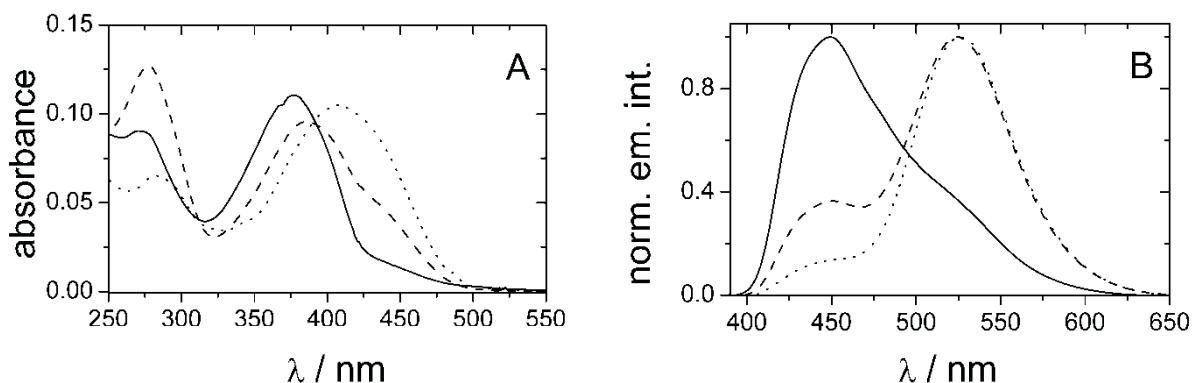


Figure 10 A) Absorption spectra and B) normalized emission spectra of **PDA1** (solid line), **PDA2** (dashed line) and **PDA3** (dotted lines) measured in chloroform at room temperature. The excitation wavelength was  $\lambda_{Ex} = 376$  nm.

The distances between the chromophores within the copolymers **PDA1-3** are heterogeneous distributed. This leads to three cases of donor-acceptor copolymers: (i) donor dominated copolymer, (ii) acceptor dominated copolymer and (iii) a copolymer with a balanced donor-acceptor ratio. This general classification is experimentally derivable from steady-state absorption and emission spectra (Figure 10). The spectra resemble the donor or acceptor spectra depending on the donor-acceptor ratio.

In a next step the energy transfer efficiencies for **PDA1-3** were calculated with reference to the fluorescence intensity of **PD**. The transfer efficiency increases from 0.35 to 0.74 and 0.87 for **PDA1**, **PDA2** and **PDA3**, respectively. The transfer rates for the D/A copolymers increased as a function of acceptor dye units. The present study shows the strong interplay of the ratio between the donor and acceptor chromophore along the polymer chain for the energy transfer. The shown copolymers can act as antenna structures for light harvesting systems.

After having studied the light-emitting properties of several thiazole based copolymers it was desirable to broaden the range of polymerizable functions to open a new window for more applications. Such potential application is e.g. the production of hydrogen. Nature provides a highly efficient tool for hydrogen evolution and uptake, the enzyme *hydrogenase*.<sup>[98, 99]</sup> Hydrogenases are proteins that are able to convert protons catalytically into hydrogen in a reversible two electron redox process.<sup>[100-102]</sup> The embedding of such active “core structures” into an appropriate copolymer might be very useful to develop synthetic analogues. For this purpose, copolymers with defined superstructures could be the ultimate goal. The first controlled radical polymerization of styrene-based models of the active site of the [FeFe]-hydrogenase could be performed using the RAFT polymerization technique.

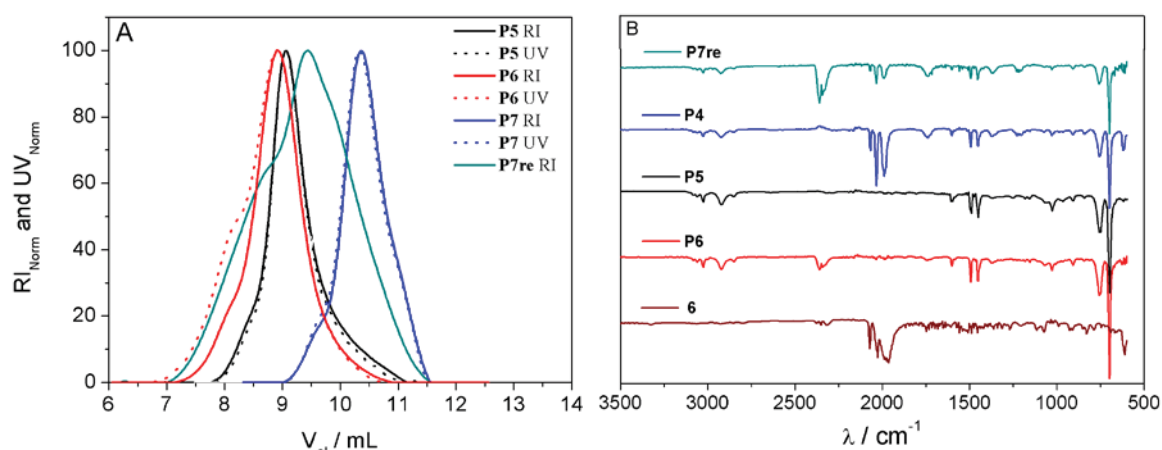


Figure 11 A) SEC trace of the synthesized copolymers (UV/VIS detector at 490 nm) and B) IR spectra of different [FeFe] cluster copolymers and styrene monomer **6**.

Different model complexes based on styrene were prepared including a propanedithiolato-bridged (**5**) and a bifunctional styrene iron complex (**6**), see Figure 7. These model complexes were copolymerized with styrene using free radical (**P3**) and the RAFT polymerization process (**P4** to **P7**, TABLE 3). The polymerization behavior of the hydrogenase models was analyzed in detail. It could be shown that the model complex can be incorporated into copolymers; the obtained copolymers exhibited narrow molar mass distributions (PDI values below 1.3, TABLE 3). The UV absorption of the copolymer on the SEC profile (Figure 11A) indicates the presence of the [FeFe]-core<sup>[103]</sup> in the obtained copolymers. Another confirmation for the successful incorporation of the cluster into the copolymer could be provided by IR spectroscopy (Figure 11B). The copolymers exhibited strong signals for the CO vibration in the IR-region at 2 067, 2 033 and 1 987 cm<sup>-1</sup>, respectively. The signals correspond to these of the monomeric models (**6**).

TABLE 3 Overview of reaction conditions and characterization data of the obtained copolymers via RAFT copolymerization.

Entry	M/M <sub>dye</sub> /CTA	[M/M <sub>dye</sub> ]: [CTA]:[Init.]	T (°C)	Conc. (mol/L)	t (h)	M <sub>n</sub> [g/mol] <sup>[a]</sup>	PDI <sup>[a]</sup>	Conv.
<b>P4</b>	St/ <b>6</b> / --	245/5:--:1	70	2.0	13	28 400 <sup>[b]</sup>	5.4 <sup>[b]</sup>	n/a
<b>P5</b>	St/ <b>5</b> / CTA1	199/1:1:0.25	70	4.0	18	7 400	1.23	n/a
<b>P6</b>	St/ <b>6</b> / CTA2	248/2:1:0.25	80	4.0	14	9 700	1.24	32
<b>P7</b>	St/ <b>6</b> / CPDB	98/2:1:0.25	70	2.0	24	2 800	1.18	n/a
<b>P7re</b>	St/ <b>6</b> / CPDB	98/2:1:0.25	70	2.0	26	6 000	1.6	n/a
<b>P8</b>	DEGMA/ <b>7</b> / CPDB	95/5:1:0.25	70	2.0	12	29 000	1.20	n/a

[a] Calculated from SEC (CHCl<sub>3</sub>/triethylamine/iso-propanol = 94/4/2) using PS calibration. [b] Calculated from SEC (DMAc, LiCl) using PS calibration.

The presence of the [FeFe]-hydrogenase models were also proven by AAS and NMR spectroscopy as well as with cyclic voltammetric measurements. It could be shown that the [FeFe]-hydrogenase mimic copolymers, as well as the monomeric originating complexes exhibit electrocatalytic proton reduction at a low potential of  $-2.2$  V.

The manifold possibilities to incorporate chromophores into the polymer backbone may provide a platform for applications as polymeric sensor systems. Thermoresponsive polymers that undergo such a solubility transition by variation of temperature represent important materials for the development of “smart” systems as already described in Chapter 2.2.

In this content it would be advantageous to construct a fluorescent thermometer based on a dye-labeled thermoresponsive polymer. To translate the LCST transition of a copolymer into a fluorescent response, the polymer was functionalized with pyrene resulting in a variation of the emission based on the pyrene microenvironment change from hydrophilic to hydrophobic during the LCST transition.

For this purpose, a well-defined fluorescent copolymer based on PDEGMA functionalized with pyrene units (**P8**) was synthesized by RAFT polymerization. It was demonstrated by temperature controlled fluorescence investigations that this polymer acts as a soluble fluorescent temperature sensor in water (Figure 12A). At temperatures below the polymer phase transition, the polymer chains are hydrated as demonstrated by DLS (Figure 12B) and, thus, the pyrene molecules are exposed to the polar aqueous environment driving excimer formation. Above the LCST phase transition of the polymer, the polymer chains are dehydrated and demix from the aqueous solution providing a less polar environment for the pyrene inside the polymer aggregates.

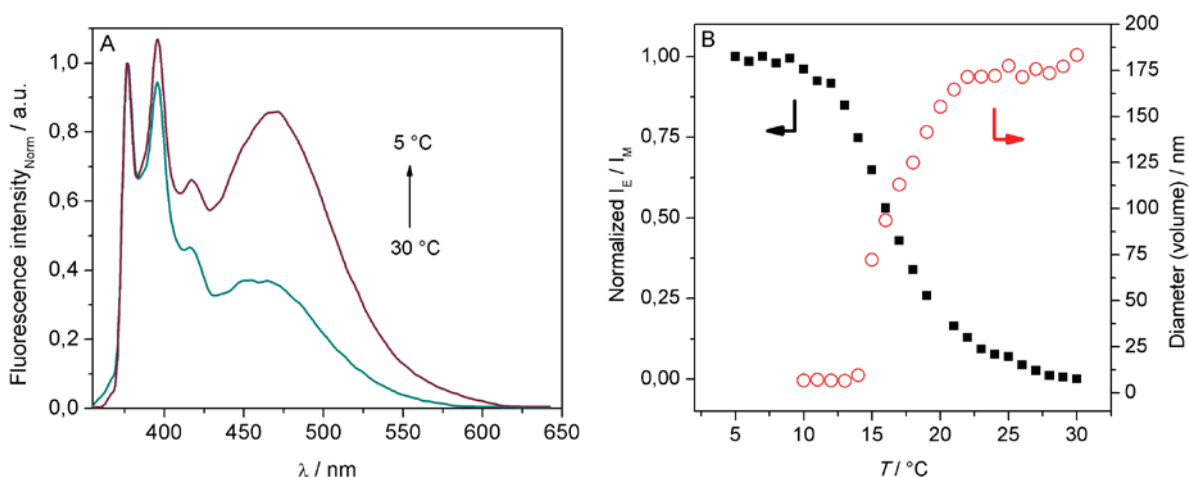


Figure 12 A) Normalized fluorescence intensity (377 nm) at 5 °C (purple) and 30 °C (green) of a solution of pyrene-labeled copolymer **P8** in water. B) The ratio of excimer (467 nm) to monomer (395 nm) emission intensities ( $I_E/I_M$ , black squares) and the hydrodynamic radius of the polymer globules (DLS, open red circles) as function of temperature.



During the phase transition, a gradual decrease in the normalized ratio of excimer emission to monomer emission intensities ( $I_E/I_M$ ) ratio could be observed (Figure 12), which can be used to detect the temperature of the solution in between 11 and 21 °C, *i.e.*, the temperature sensing regime. Interpretation of the  $I_E/I_M$  ratio as sensing signal is believed to make the sensor more robust compared to looking at individual emission intensities since it will be less dependent on the polymer concentration. Turbidimetry and DLS demonstrated that the polymer phase transition also occurred in the observed temperature sensing regime confirming that indeed the polymer phase transition induces the change in  $I_E/I_M$  ratio of the attached pyrene molecules.

The temperature responsive behavior of PDEGMA copolymers is widely tunable by incorporation of hydrophobic or hydrophilic monomers, which opens new avenues towards biomedical, sensor or drug delivery applications. The incorporation of a second temperature responsive monomer in a block copolymer structure can lead to a thermo-induced self-assembly behavior and will be in the focus of the next chapter.



---

## 4 Responsive block copolymers: Well-defined synthesis, characterization and self-assembly

---

Parts of this chapter have been published: P8) C. Pietsch, U. Mansfeld, C. Guerrero-Sanchez, S. Hoepfener, A. Vollrath, M. Wagner, R. Hoogenboom, S. Saubern, S. H. Thang, C. R. Becer, J. Chiefari, U. S. Schubert, *Macromolecules*, **2012**, *45*, 9292–9302. P9) A. Krieg, C. Pietsch, A. Baumgaertel, M.D. Hager, C. R. Becer, U. S. Schubert, *Polym. Chem.* **2010**, *1*, 1669–1676.

Stimuli-responsive polymers, which undergo phase transitions in response to an external stimulus, have gained the interest of many researchers in the past decade.<sup>[25-28]</sup> Such “smart” materials can act with a property change in response to changes in temperature, pH value, light, or magnetic field.<sup>[60, 104]</sup> The area of stimuli-responsive polymers represents nowadays a strongly growing area in polymer research and, in particular, the investigation regarding lower critical solution temperature behavior has attracted significant interest. Particular attention in this context has been paid to the thermo-sensitive self-organization of amphiphilic block copolymers, especially on the formation of micelles or vesicular structures in aqueous solution. Numerous reports described the micellization of diblock copolymers containing thermosensitive block segments.<sup>[104-108]</sup> The formed vesicles or polymersomes are usually spherical shell structures with a hydrophobic core-layer and a hydrophilic internal and external corona, which are made from amphiphilic block copolymers.<sup>[22, 23, 109]</sup> Polymer vesicles, which respond to external stimuli such as a change in temperature or the pH value, represent attractive candidates for applications in encapsulation or drug delivery systems.<sup>[27, 110, 111]</sup>

LCST polymers are soluble below a certain temperature because of the formation of hydrogen bonds between water molecules of the hydration shell and the polymer chains. By passing the *cloud point temperature* ( $T_{CP}$ ), the polymer starts to precipitate due to weakening of these hydrogen bonds and due to hydrophobic polymer–polymer interactions because the entropy term becomes dominant in the Gibbs equation. Another factor is the release of water molecules during this transition.

A number of PEG functionalized poly(meth)acrylates have been reported to exhibit a LCST behavior.<sup>[80, 112, 113]</sup> In particular, different oligo(ethylene glycol) methyl ether methacrylate (OEGMA)-based polymers received significant attention as temperature sensitive materials. By variation of the side chain length, the  $T_{CP}$  of these copolymers can be tuned, which makes them very attractive systems.<sup>[80, 82, 114]</sup> The homopolymer of DEGMA has a  $T_{CP}$

around 27 °C, which can be increased by copolymerizing with a more hydrophilic monomer.<sup>[80, 112, 114, 115]</sup> Acidic monomers like acrylic acid (AA) and methacrylic acid (MAA) were chosen as such hydrophilic comonomers, resulting in pH- and temperature-responsive polymeric material.

In a first step the synthesis and characterization of dual hydrophilic analogues of statistical and block copolymers of acrylic acid or methacrylic acid with oligo(ethylene glycol) acrylates (OEGA) *via* controlled radical polymerization techniques were designed in order to extend the scope of these interesting properties. These kind of polymers with various architectures are of great interest in the field of polymer science due to their wide range of possible applications, e.g. in drug-delivery systems, dispersing agents and absorbent materials.<sup>[23, 116-118]</sup> To obtain block, comb and statistical copolymers, two synthetic routes were used, namely using macromonomers and/or *macro chain transfer agents* (macroCTA) to prepare the targeted polymeric structures. An overview of the applied polymerization route and the resulting copolymer structures is given in Figure 13.

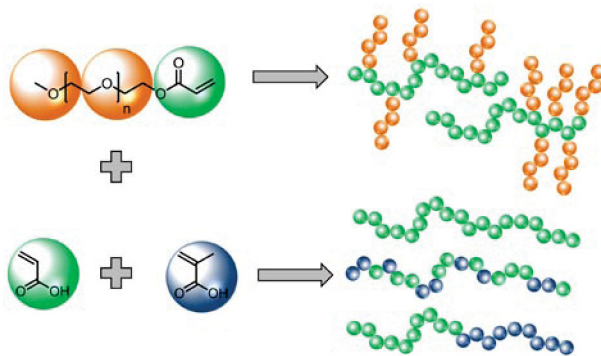


Figure 13 Schematic representation of the used monomers and the resulting macromolecular architectures obtained by the applied RAFT polymerization procedure.

In the present study, the macromonomer approach was applied to obtain statistical and block comb copolymers based on AA and OEGA. The synthesis of polymers based on AA or MAA via CRP techniques can be challenging due to the acidic nature of the free carboxylic acid. The RAFT polymerization method allows the use of acidic monomers and also the application of polar solvents like ethanol or water. As a consequence this technique is the most widely employed CRP method to prepare water soluble polymers.<sup>[119]</sup>

The block copolymers of AA and OEGA were prepared in a sequential monomer addition process using the RAFT method, whereby AA was polymerized first resulting in a macroCTA. Afterwards OEGA was added and the polymerization solution was further heated (**P9 – P11**). The statistical copolymers based on AA and OEGA were synthesized under similar conditions (**P12 – P14**). An overview of the molecular characteristics of these copolymers is given in TABLE 4. Well-defined dual hydrophilic linear and comb based

copolymers of acrylic acid and poly(ethylene glycol) acrylate could be prepared as indicated by the mono-modal SEC elugramms and the low PDI values. The polymers were characterized in detail by  $^1\text{H}$  NMR spectroscopy and *matrix assisted laser desorption ionization time of flight* (MALDI-TOF) mass spectrometry. Further investigation of the water uptake behavior of some selected copolymers showed an interesting water absorbing behavior of the block copolymer.

TABLE 4 Overview of selected characteristics of the prepared statistical (s) and block (b) copolymers of OEGA and AA.

Entry	Feed AA/OEGA	$M_n$ (theo) [g/mol] <sup>[a]</sup>	$M_n$ (SEC) [g/mol] <sup>[b]</sup>	PDI <sup>[b]</sup>	Ratio $^1\text{H}$ NMR [%] AA:OEGA <sup>[c]</sup>
POEGA	0/8	3 800	3 000	1.15	0:100
P9 (b)	35/5	4 800	6 000	1.20	87:13
P10 (b)	45/5	5 700	6 600	1.25	---
P11 (b)	70/5	7 700	11 000	1.20	93: 7
P12 (s)	35/5	4 800	6 400	1.28	81:19
P13 (s)	45/5	5 700	7 100	1.21	---
P14 (s)	70/5	7 700	8 100	1.38	91: 9

[a] Calculated according to formula ( $M_n(\text{theo.}) = ([M]/[\text{CTA}] \times \text{conv.} \times M_{\text{Monomer}}) + M_{\text{CTA}}$ ). [b] Calculated from SEC (DMAc, LiCl) using PS calibration. [c] Calculated from integrated areas of OEGA signals and AA signals.

Block copolymers can be responsive to two different stimuli at the same time, such as temperature and the pH value, as demonstrated for block copolymers of poly(*N*-isopropylacrylamide-*block*-acrylic acid), (PNIPAM-*b*-PAA)<sup>[120]</sup> and poly(dimethylaminoethyl methacrylate-*block*-methyl methacrylate), (PDMAEMA-*b*-PMMA).<sup>[121]</sup> The thermo-responsive self-organization of amphiphilic block copolymers in aqueous solution has been described in the literature for several systems.<sup>[104, 106-108, 122-124]</sup> Besides OEG based monomers, DMAEMA can be used as a comonomer, which results in a pH- and temperature-responsive copolymer, too.<sup>[125]</sup> Various  $T_{\text{CP}}$ 's of PDMAEMA have been reported in literature ranging from 20 to 80 °C, which is an indication that the LCST strongly depends on the molar masses and the used pH value due to partial (de)protonation of the basic nitrogen atoms of DMAEMA.<sup>[125-129]</sup> However, the thermo-induced self-assembly of poly(DMAEMA-*b*-DEGMA) was, to the best of our knowledge, not yet reported.

A library of double thermo-responsive poly(DMAEMA-*b*-DEGMA) copolymers was synthesized using the RAFT polymerization technique in a sequential monomer addition approach. Within this series, the ratios of DMAEMA and DEGMA were varied ranging from 100% DMAEMA to 100% DEGMA with composition changes in 20% steps. The polymerizations were carried out using a trithiocarbonate (CTA3) as CTA and VAZO-88 as radical initiator (see Figure 14).

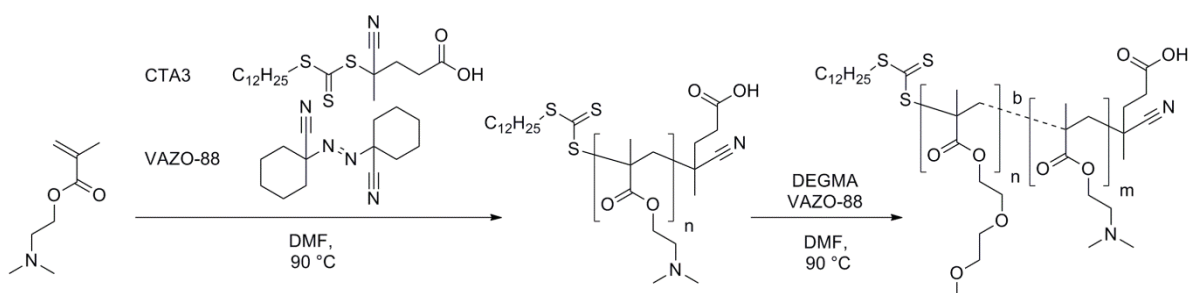


Figure 14 Schematic representation of the poly(DMAEMA-*b*-DEGMA) synthesis using the RAFT polymerization with CTA3 and radical initiator VAZO-88.

The first block segment was polymerized in DMF followed by the polymerization of DEGMA. In TABLE 5 the molar masses and polydispersity indices measured by SEC are summarized demonstrating good control over the first blocks (PDI < 1.23) and relatively good control for most block copolymers (PDI < 1.35, except **B4**).

The conversion of DMAEMA (by  $^1\text{H}$  NMR spectroscopy) was around 70 to 80% after 10 hours of polymerization. Then the polymerization was stopped to retain a high RAFT end-group functionality. A clear molar mass shift could be observed for the block copolymers in the SEC analysis. For the final copolymers, the ratio between both block segments were determined by  $^1\text{H}$  NMR spectroscopy using the integrated areas of DMAEMA signals ( $(\text{CH}_3)_2\text{N-}$  at 2.26 ppm) and the DEGMA ( $\text{CH}_2\text{-O-}$  at 3.54 to 3.66 ppm) ethylene glycol side-group signals

TABLE 5 Overview of the composition of the obtained block copolymers of poly(DMAEMA-*b*-DEGMA) with increasing ratio of DEGMA.

Entry	$M_n$ (SEC <sub>1</sub> ) [g/mol] <sup>[a]</sup>	PDI <sup>[a]</sup>	$M_n$ (SEC <sub>2</sub> ) [g/mol] <sup>[b]</sup>	PDI <sup>[b]</sup>	$M_n$ (SEC <sub>3</sub> ) [g/mol] <sup>[c]</sup>	PDI <sup>[c]</sup>	Ratio $^1\text{H}$ NMR [%] DMAEMA:DEGMA <sup>[d]</sup>
H4 (h)	15 200	1.21	13 500	1.43	28 700	1.22	100: 0
B1 (q)	20 800	1.29	24 700	1.44	29 700	1.36	94: 6
B2 (q)	21 800	1.25	24 100	1.41	30 200	1.34	87: 13
B3 (b)	26 900	1.27	27 400	1.52	---	---	66: 34
B4 (b)	35 100	1.54	36 600	1.48	---	---	64: 36
B5 (q)	39 700	1.35	24 000	1.70	---	---	51: 49
B6 (b)	26 600	1.32	27 100	1.33	33 500	1.24	20: 80
H6 (h)	23 600	1.23	23 700	1.29	27 800	1.20	0:100

Copolymer structure: h = homopolymer, q = quasi diblock copolymer, b = diblock copolymer. [a] Calculated from SEC (DMF, LiBr) using PS calibration. [b] Calculated from SEC (DMAc, LiCl) using PS calibration. [c] Calculated from SEC ( $\text{CHCl}_3$ /triethylamine/*iso*-propanol = 94/4/2) using PS calibration. [d] Calculated from integrated areas of DMAEMA signals ( $(\text{CH}_3)_2\text{N-}$ ) and the DEGMA ( $\text{CH}_2\text{-O-}$ ) side-group signals. [e] Block copolymer reached the exclusion limit of the SEC.

The thermoresponsive properties of this library of poly(DMAEMA-*b*-DEGMA) were firstly studied by heating the polymer solutions in deionized water. This induces a LCST transition, *i.e.* the solutions become turbid above the characteristic  $T_{CP}$  indicating the collapse of the polymer chains (two phase system). The  $T_{CP}$ 's of the homo- and block copolymers were determined by turbidimetry measurements in deionized water at different concentrations. All  $T_{CP}$  transitions from the turbidimetry measurement of the block copolymers are plotted in Figure 15 against the molar ratio of PDMAEMA to provide a better overview. A roughly linear behavior of the  $T_{CP}$  transitions with increasing amount of mol% DMAEMA in the block copolymers could be observed. Two  $T_{CP}$  values were observed for **B5** (ratio 50/50 mol%) indicating the double thermo-responsive behavior in aqueous solution. The turbidimetry curve of this copolymer shows a weak transition at 33 °C followed by a rearrangement and, therefore, a second transition at 49 °C.

In order to evaluate the aggregation behavior of the chosen copolymer, **B5** was investigated in further detail by DLS. The distribution of the block copolymer assemblies at temperatures below and above the phase transition is illustrated in Figure 15. Below the cloud point at 25 °C the polymer chains are fully soluble and, therefore, a hydrodynamic diameter smaller than 10 nm was obtained, corresponding most probably to individual hydrated polymer chains, taking into account also the molecular dimensions of the block copolymers. An increase in temperature results in an increase in the diameter of the polymer aggregates to ~100 nm (Figure 15 state 2), indicating the temperature-induced aggregation of the polymer chains. The first transition of the polymer solution is observed at a temperature of 31 °C, *i.e.*, when the collapse of the PDEGMA takes place.

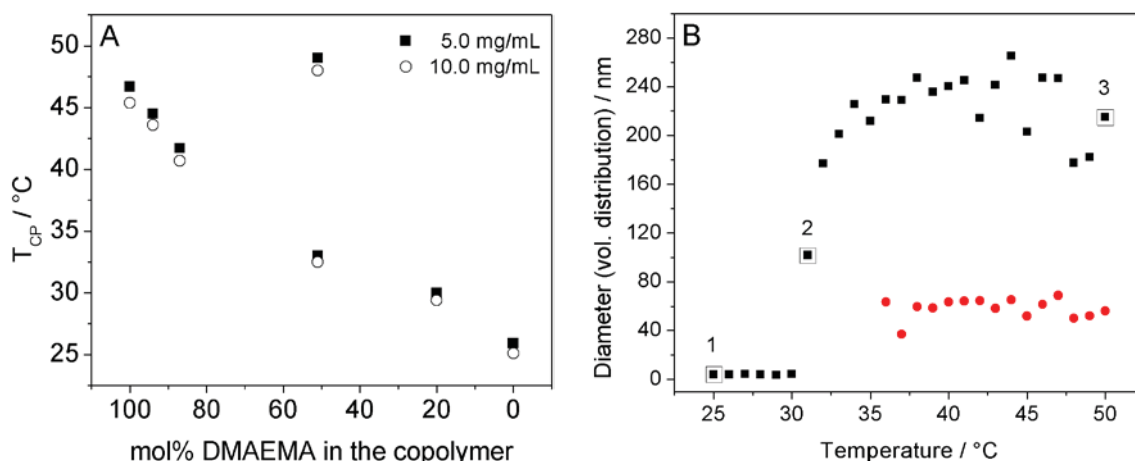


Figure 15 A) Cloud points of the studied block copolymers of poly(DMAEMA-*b*-DEGMA) at 5.0 and 10.0 mg mL<sup>-1</sup>; B) The hydrodynamic diameter (volume distribution) of the **B5** block copolymer chains (1) and globules (2,3), showing two distributions (black and red points) at 1.0 mg mL<sup>-1</sup> as a function of temperature.

By further increasing the temperature, a rearrangement is observed, which is reflected in the appearance of a second distribution. Above 36 °C two distributions are formed with a hydrodynamic diameter of 65 and 240 nm, respectively (Figure 15 state 3). The formed structures appear to be stable in solution, as the aggregate size remains constant even at further elevated temperatures.

The temperature induced phase transition of the selected block copolymer **B5** was further investigated by temperature dependent  $^1\text{H}$  NMR spectroscopy to obtain a deeper insight into the aggregation behavior. The  $^1\text{H}$  NMR spectrum of the block copolymer at 25 °C shows the characteristic signals of poly(DMAEMA-*b*-DEGMA); the corresponding temperature series is plotted in Figure 16a. In the  $^1\text{H}$  NMR spectra, the signals at 3.3 to 3.9 ppm represent the groups of poly(DEGMA) and the signals at 2.3 ppm ( $\text{CH}_3\text{-N-}$ ) represent the poly(DMAEMA) block. It is observable that the DEGMA signals at 3.5 to 3.9 ppm decrease significantly, denoting the collapse of the DEGMA block by increasing the temperature from 25 to 40 °C. Also all other signals (backbone and DMAEMA) decrease by increasing temperature leading to broad signals due to the reduced flexibility of the polymer chains. The PDMAEMA block is still visible at 45 °C ( $\text{CH}_3\text{-N-}$  at 2.2 ppm) as it is supposed that it forms a kind of corona around the hydrophobic PDEGMA aggregates. Unexpectedly, further increasing the temperature from 50 to 65 °C is accompanied by an increase for some signals corresponding to DMAEMA and to DEGMA, respectively (Figure 16a). The shifted signals indicate a different microenvironment of (at least parts of) the DMAEMA and DEGMA groups and are supposed to correlate to the corresponding rearrangement of the block copolymer. This second assembly might be induced by the collapse of the DMAEMA block (at 49 °C). The transformation of the PDMAEMA block is indicated by the high-field shift of the DMAEMA signal.

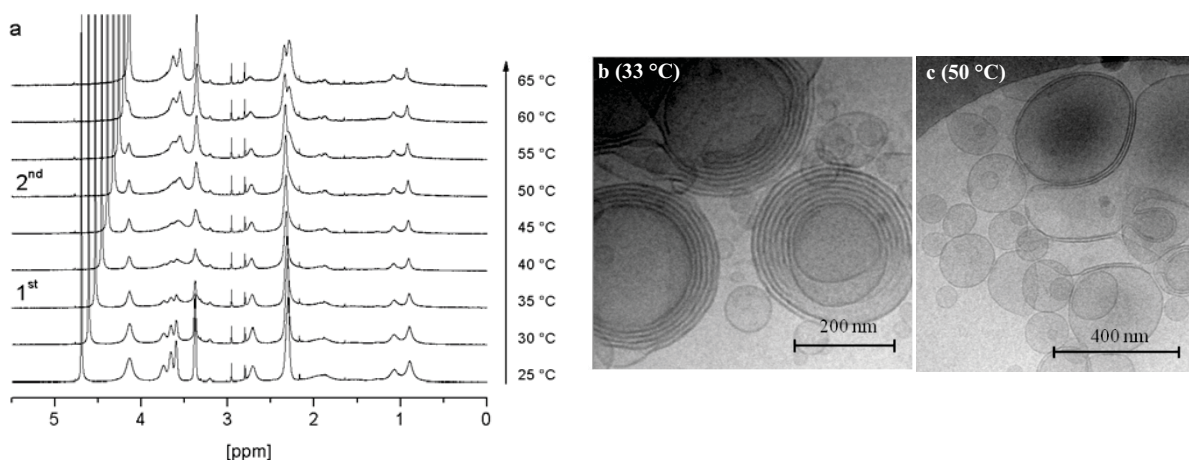


Figure 16 a) Temperature dependent  $^1\text{H}$  NMR spectra in  $\text{D}_2\text{O}$ : b,c) Cryo-TEM images of **B5** block copolymer solution at  $\sim 33$  and  $50$  °C in  $\text{H}_2\text{O}$  (preheated,  $5.0 \text{ mg mL}^{-1}$ ) showing the formation of multilamellar and unilamellar vesicles.



The double responsive behavior of poly(DMAEMA-*b*-DEGMA) motivated the utilization of cryo-TEM to visualize the associated structures. The cryo-TEM images of solutions which were vitrified at a blotting temperature of approximately 33 °C are depicted in Figure 16b. At this temperature, which is above the  $T_{CP}$  of PDEGMA and below the  $T_{CP}$  of PDMAEMA, the presence of large *multilamellar vesicles* (MLV) with a diameter of approximately 200 nm and *unilamellar vesicles* (ULV), which are significantly smaller (40 to 90 nm), can be observed. The cryo-TEM micrograph shows that the MLVs have a layered structure with comparable distance between the individual lamellae and represent an onion-like form. In this case a molecular arrangement of the copolymer can be assumed that resembles the structure depicted in Figure 16b (PDEGMA dark; PDMAEMA light). The formation of MLV is based on the one hand on the hydrophilic-hydrophobic character of the block copolymers and on the other hand on the volume fractions of the individual blocks, respectively. For thermo-sensitive block copolymers the individual blocks show a selective, thermally driven solubility and, therefore, the overall hydrophilic-hydrophobic character can be changed by temperature variations.

The block copolymer was subsequently heated to a temperature above the  $T_{CP}$  of DMEAEMA (above 47 °C, Figure 16c) and the resulting structures were investigated by cryo-TEM. In contrast to the sample which was investigated at 33 °C the formation of preferentially unilamellar, large vesicles could be observed.

The thermo-responsive behavior of the selected block copolymer **B5** was further investigated by temperature variable zeta potential (also known as electrokinetic potential) measurements to gain a deeper insight in the polyelectrolyte nature of the block copolymer during the polymer phase transitions (Figure 17A). The zeta-potential measurements reveal that two reversible thermo-induced transitions are present without showing any hysteresis behavior in the graph (Figure 17A, black squares).

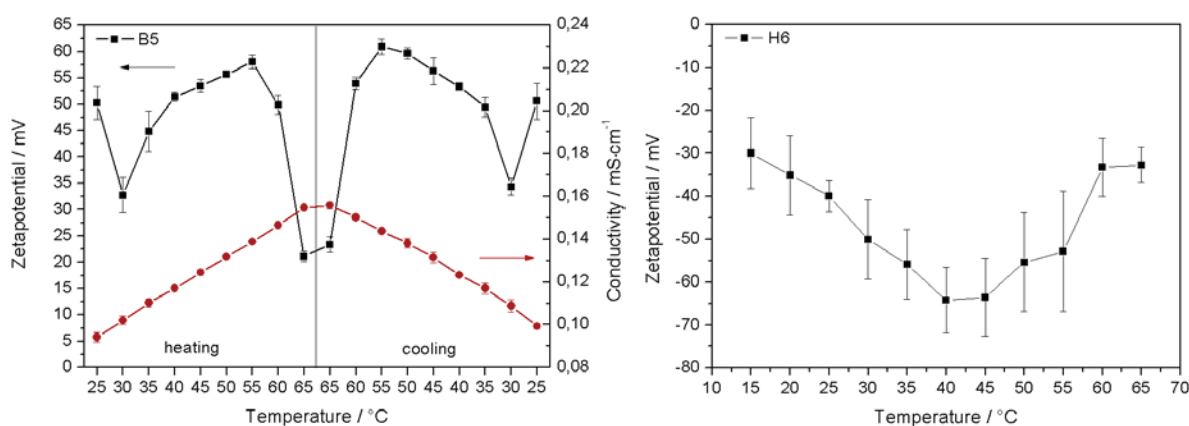


Figure 17 A) Temperature variable zeta potential measurements (black squares) of block copolymer **B5** solution (2.5 mg mL<sup>-1</sup>) and B) of homopolymer **H6** (2.5 mg mL<sup>-1</sup>).

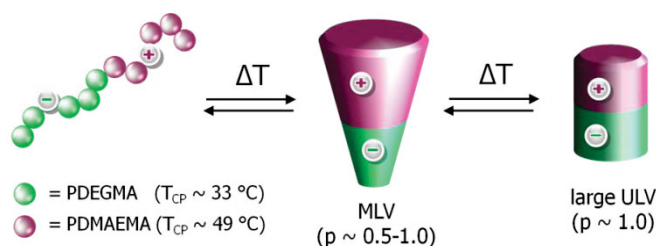


Figure 18 Proposed model for the aggregation of the double responsive transition of the block copolymer (green cycles DEGMA and purple cycles DMAEMA units).

The first transition takes place at around 30 °C and the second transition around 55 to 60 °C, whereby a strong decrease in the zeta potential is observed.

Based on these experimental observations a model for the aggregation of the double responsive transition of the block copolymer structures at different temperatures was developed which is schematically illustrated in Figure 18. In this configuration the PDEGMA block (negatively charged based on the zeta-potential measurements as shown in Figure 17) became insoluble at the first LCST transition temperature and is collapsed in the lamellar structure. The still soluble PDMAEMA block (positively charged) stabilizes the individual shells by a layer-by-layer assembly and promotes the preferential formation of multilamellar onion-like vesicles. With further increasing temperature also the solubility of the PDMAEMA decreases. As a result, the volume of the hydrophobic part of the copolymer increases and the inter-bilayer energy changes. Simultaneously, the decreasing size of the hydrophilic corona block is seen as an additional driving force for the modified aggregation behavior due to altered volume-fraction and space requirements. This effect was, e.g., already observed for PS-*b*-PAA aggregates,<sup>[24]</sup> where shorter corona fractions generally resulted in the formation of larger structures.<sup>[130]</sup> Additionally, the altered charge balance within the structures favors the formation of larger and unilamellar vesicles.

It can be concluded that variable temperature <sup>1</sup>H NMR spectroscopy, zeta potential and cryo-TEM investigations revealed the temperature induced formation of MLV structures at elevated temperatures which convert into ULV at higher temperatures. This transition could be assigned to the changes of the volume ratios as well as to the ionic interplay between the block copolymers at different temperatures. In particular the ionic contributions of the negatively charged PDEGMA block and the positively charged PDMAEMA block are supposed to support the layer-by-layer assembly at 33 °C, which favors the formation of MLV vesicles. Further increase of the temperature changes again the volume ratio between the blocks as the solubility of the second block occurs, furthermore the second LCST transition is associated with a changed electrostatic balance between the blocks. This results in the preferential transition of MLVs to ULVs. The present study assumes a facile interplay of the volume ratio and the changes of the ionic interactions.

---

## 5 Poly(methyl methacrylate) based nanoparticles for cellular uptake

---

Parts of this chapter have been published: P10) I. Y. Perevyazko, A. Vollrath, C. Pietsch, S. Schubert, G. M. Pavlov, U. S. Schubert, *J. Polym. Sci., Part A: Polym. Chem.* **2012**, *50*, 2906–2913; P11) A. Vollrath, D. Pretzel, C. Pietsch, I. Y. Perevyazko, R. Menzel, S. Schubert, G. M. Pavlov, D. Weiß, R. Beckert, U. S. Schubert *Macromol. Rapid Commun.* **2012**, *33*, 1791–1797; P12) A. Vollrath, A. Schallon, C. Pietsch, S. Schubert, T. Nomoto, Y. Matsumoto, K. Kataoka, U. S. Schubert, *Soft Matter*, **2013**, *9*, 99–108.

Polymeric *nanoparticles* (NP) have been extensively studied in the last decades as potential drug or gene delivery vehicles.<sup>[131, 132]</sup> NP formation using the nanoprecipitation method<sup>[133]</sup> is nowadays a commonly used technique.<sup>[134]</sup> Among numerous other manufacturing methods (e.g. emulsion polymerization), it is a very simple and convenient way for the production of NPs with desired sizes and defined surfaces.<sup>[135, 136]</sup> A variety of different polymers can be used for nanoprecipitation, such as poly(lactide-co-glycolide),<sup>[137]</sup> poly( $\epsilon$ -caprolactone),<sup>[138]</sup> acetalated dextran,<sup>[139]</sup> poly(styrene), poly(methyl methacrylates)<sup>[140, 141]</sup> and its different copolymers. The nanoprecipitation or solvent evaporation process represents a process based on the diffusion of the organic solution (*i.e.*, polymer solvent) into an aqueous phase leading to the precipitation of the polymer into small colloidal particles.

The first aim of this investigation focused on the influence of the polymer molar mass and the polymer-solvent interactions (e.g. polymer concentration) on the formation of NP using the nanoprecipitation method. For this purpose, a homologous series of poly(methyl methacrylate)s (PMMA) with varying *degrees of polymerization* (DP) of 50 up to 2 000 was developed.

Subsequently, nanoprecipitation was performed in an automated and systematic manner to vary different initial concentrations of polymer and solvent/non-solvent ratios. The NP formulations were examined in terms of particle size and size distribution as well as zeta-potential values. The conditions for the preparation of stable and uniform NP regarding the molar mass and polymer concentration were determined.

For this purpose, a range of PMMA samples were synthesized using the RAFT polymerization technique using AIBN as radical initiator, ethanol as solvent, and CPDB as CTA. The monomer concentration, the polymerization time and the [M]:[CTA] ratio were varied in order to obtain the desired molar mass of PMMA. In TABLE 6 the chosen

conditions for the MMA polymerization are shown. To reach molar masses ( $M_n$ ) over 100 000 g mol<sup>-1</sup> long polymerization times are not preferred due to possible termination reactions (e.g. coupling of the polymer chains). Instead the monomer concentration was increased up to 7.03 mol L<sup>-1</sup> as well as the [M]:[CTA] ratio.

TABLE 6 Selected polymerization and characterization data of polymers **PMMA 1** to **5**.

Entry	[M]/[CTA]/ [AIBN]	Conc [mol L <sup>-1</sup> ]	Time, h	$M_n$ (SEC) [g/mol] <sup>[a]</sup>	$M_w$ (SEC) [g/mol] <sup>[a]</sup>	PDI <sup>[a]</sup>	DP <sub>SEC</sub>
<b>PMMA 1</b>	40/1/0.25	2.0	13	6 800	7 700	1.13	66
<b>PMMA 2</b>	200/1/0.25	2.0	13	17 200	20 200	1.17	170
<b>PMMA 3</b>	400/1/0.25	2.0	20.5	31 500	39 700	1.26	312
<b>PMMA 4</b>	1 200/1/0.25	7.03	16	85 000	106 000	1.25	846
<b>PMMA 5</b>	4 000/1/0.25	7.03	16	204 000	274 000	1.34	2 035

[a] Calculated from SEC (DMAc, LiCl) using PMMA calibration.

A homologous series of PMMAs with molar masses ranging from  $M_n = 6\,800$  g mol<sup>-1</sup> up to high molar masses of  $M_n = 204\,000$  g mol<sup>-1</sup> could be realized *via* the RAFT process. All PMMA samples are well-defined, indicated by a mono-modal molar mass distribution as well as by low PDI values ranging from 1.13 to 1.34. The SEC chromatographs of the different PMMA samples are depicted in Figure 19A. To study the influence of the polymer molar mass on the NP formation *via* nanoprecipitation, it is crucial to maintain the same initial conditions for each nanoprecipitation process. It could be shown that the particle size is strongly affected by the initial polymer concentration: Higher concentrations lead to an increasing number of molecules per volume of the solvent which, in turn, leads to the formation of larger particles. However, equality of the initial polymer concentration will not reflect the same conditions for the nanoprecipitation process in case of polymers with various molar mass, since macromolecular coils will occupy different volumes owing to the different length of a polymer chain. Therefore the same “degree of dilution” was used, which is represented by the Debye parameter ( $c$  [ $\mu$ ]). A SEM image and the corresponding size-distribution of nanoparticles prepared from **PMMA 3** are shown in Figure 19B.

In conclusion, the investigation has shown that it is crucial to work with highly diluted polymer solutions to obtain well-defined particles on the basis of a certain polymer. It is an interplay of polymer molar mass, hydrodynamic volume and solvent quality for the formation of stable NP suspensions. Primarily the key factor for the particle preparation is the volume fraction occupied by the macromolecular polymer coil in the solution instead of the polymer concentration.

Recent progress in the area of nanosciences enabled the development of various NP devices as powerful tools in the pharmaceutical area for drug delivery systems, but also in other scientific fields, like diagnostics and nanotechnology.<sup>[132, 142, 143]</sup>

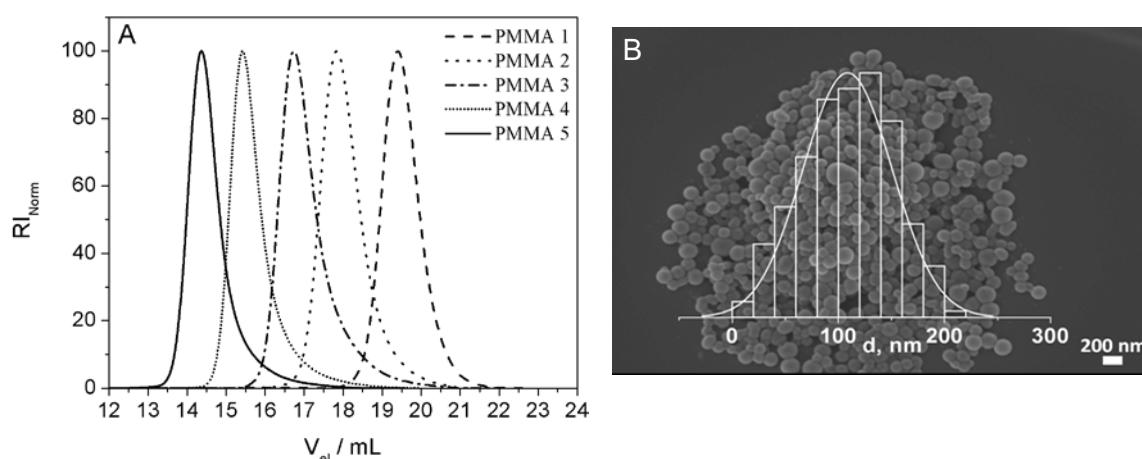


Figure 19 A) SEC chromatograms of the obtained PMMA polymers; B) SEM image and corresponding size-distribution of NPs prepared from **PMMA 3** solutions in THF.

In particular for diagnostic applications, like live cell imaging, the investigation of labeled NP (1 to 1 000 nm) is rapidly expanding.<sup>[144-147]</sup> The use of fluorescent polymeric NP represents a suitable alternative to avoid potential toxicity of metal-based NP (e.g. quantum dots).<sup>[143, 148]</sup> The covalent incorporation of dyes into the polymer backbone and the subsequent NP preparation provides a protection against external influences; a defined dye-particle ratio and, therefore, more defined fluorescent NPs. Moreover, the fluorescence properties of the dye are maintained, which is essential for the subsequent analysis of particle-cell interactions, e.g. via *confocal laser scanning microscopy* (CLSM). For the preparation of dye labeled NP systems two approaches can be explored, namely using a dye-functionalized monomer or a post functionalization of the copolymer with an activated dye. Both synthetic routes are schematically presented in Figure 20.

For the design of the labeled NP's, a yellow light-emitting thiazole-dye was attached to the methacrylate monomer by an esterification reaction (**2b**). The non-classical thiazole dye is similar in structure to the luciferin dye of fireflies and shows excellent fluorescent properties.<sup>[94, 95]</sup> The resulting dye-functionalized methacrylate (**2b**) was statistically copolymerized with MMA using the RAFT polymerization methodology (Figure 20). The reaction was carried out using AIBN as a radical initiator and CPDB as a chain transfer agent. The ratio of non-functionalized MMA to the dye-functionalized monomer was 138:2, leading to a final conversion rate of 70% of the copolymers with a DP of 100. The dye-functionalized methacrylates were statistically distributed in the polymer backbone due to the same reactivity of both monomers. The low degree of labeling (1 to 3%) ensured the preservation of the properties of the PMMA homopolymer. As determined by SEC, the final copolymer (**P15**) revealed a molar mass of  $M_n = 8\,500\text{ g mol}^{-1}$  with a polydispersity index value of 1.19.

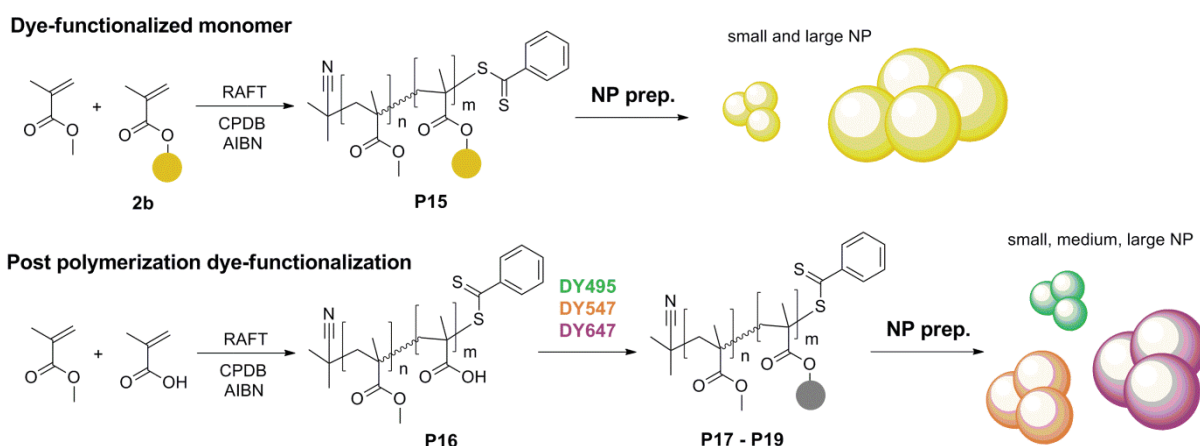


Figure 20 Schematic representation of the two synthetic routes to dye labeled polymeric NPs.

Similar molar mass distributions recorded by both RI and UV detector clearly demonstrate that the thiazole dye was incorporated into the copolymer (Figure 21). The ratio of the MMA units and the thiazole dye in the copolymer (**P15**) was determined to be 2.9 mol% by  $^1\text{H}$  NMR spectroscopy.

Nanoprecipitation was used as suitable tool for preparation of differently sized NPs.<sup>[133, 141]</sup> The final particle size was tuned by variation of the initial polymer concentration in the organic phase and/or by changing the dropping method (polymer solution into water or water into polymer solution).<sup>[149]</sup> The particle sizes and distribution were examined by DLS. The diameter of the NP suspensions were determined to be  $d = 120$  nm for small NPs and  $d = 600$  nm for the large ones, respectively. The resulting size distributions were monomodal with  $\text{PDI}_{\text{particle}}$  values between 0.03 and 0.26.

In a further study the dye labeled PMMA copolymers were chosen as a model system to investigate the diagnostic applications of the corresponding NPs such as imaging of cells taking up particles. An important criterion for this investigation represents the biocompatibility of these PMMA nanospheres. Therefore, the biocompatibility of the particle suspensions was proven by cytotoxicity assay and microscopic evaluation of viability using a live/dead staining. In order to prove the efficient internalization of the particles into cells, mouse fibroblasts L929 were incubated with 120 and 600 nm sized nanosuspensions. The internalization of NPs into cells were monitored by CLSM and representative micrographs are shown in Figure 21B. On the basis of the relative size distribution of their corresponding fluorescence signal, a differentiation of small and large particles was possible. It is known that PMMA particles are taken up by cells and it can be assumed that this cellular uptake of PMMA particles in the studied size range is mediated in a similar fashion *via* an endocytotic or phagocytotic pathway.<sup>[150]</sup>

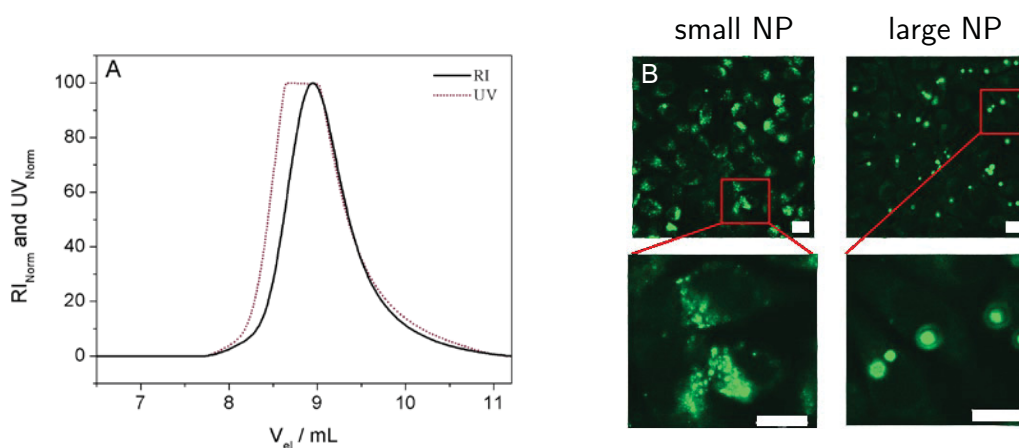


Figure 21 A) SEC elugram of poly(MMA-stat-2b) **P15**; B) confocal fluorescence images of L929 (scale bar indicates 10  $\mu\text{m}$ ).

After studying the influence of molar mass on the NP sizes and the potential to produce non-toxic particle suspensions with tailor-made size and good biocompatibility, it was desirable to investigate the pathway of the particles into the cells. For such a study well-defined NPs in size, shape, surface functionalities and dye label are beneficial.

Within the last decade, the cellular uptake of NPs with respect to various physical, chemical, and biological parameters have been studied by several groups.<sup>[151-153]</sup> For this purpose, different NPs based on organic as well as inorganic substances were used, what implicate a variation in surface charge, structure, aggregation behavior in cell media, and density next to size. This hampers general statements concerning an “optimal” particle size. Nevertheless, the size of the NPs was found to play a key role in the final particle–cell interaction and uptake.<sup>[154, 155]</sup> In addition, the internalization of particles into cells is further influenced by their surface charge: An increased positive charge leads to a higher cellular uptake due to electrostatic interactions with the negatively charged cell membrane.<sup>[156]</sup>

The present study focused on the investigations of cell interaction of polymeric NPs with well-defined characteristics based on PMMA derivatives. To provide the possibility of functionalization, carboxylic acid groups were introduced into the PMMA chain (Figure 20). For this purpose, MMA was copolymerized with MAA using the RAFT polymerization method (**P16**), reaching a final conversion of 87% (both monomers). MMA and MAA are statistically distributed in the polymer backbone due to the same reactivity of both.<sup>[157]</sup> The calculated ratio of 91 to 9% of MMA to MAA by  $^1\text{H}$  NMR spectroscopy fits well to the calculated theoretical value of 90 to 10% in the copolymer. A molar mass of  $M_n = 16\,000\text{ g mol}^{-1}$  with a polydispersity index of 1.15 was determined by SEC. Afterwards, the methacrylic acid units of **P16** were labeled with various dyes (**Dy495** (green excitation, **P17**), **Dy547** (orange excitation, **P18**) and **Dy647** (red excitation, **P19**) for tracking the NPs (see Figure 20, **P17** to **P19**).<sup>[158]</sup>

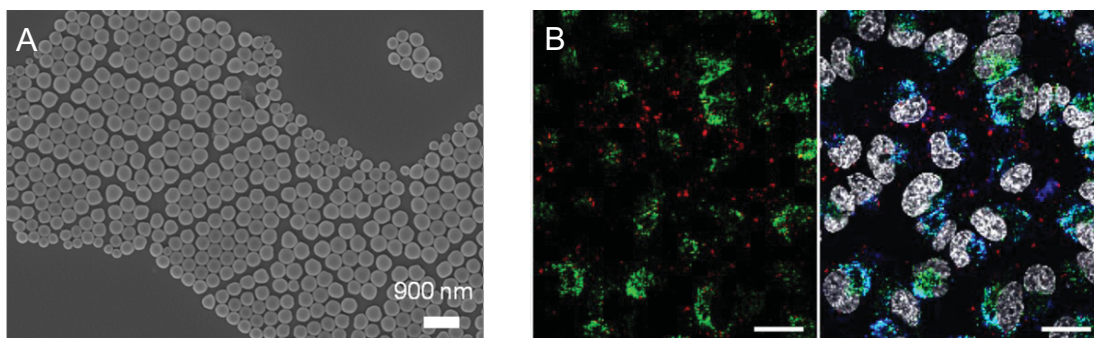


Figure 22 A) Representative SEM image of large particles of poly(MMA-stat-MA<sup>dye</sup>) copolymer; B) confocal microscope images of HeLa cells incubated with two different particle suspensions. Overlay of stained lysosomes (LysoTracker, green) and large NP<sup>red</sup> (left) and overlay (right) of large NP<sup>red</sup> (red), medium NP<sup>orange</sup> (blue), lysosomes (green) and cell nuclei (white, Hoechst 33342). The scale bars indicate 20 μm.

Differently labeled copolymers were formulated into differently sized NPs with narrow size distribution (small NP,  $d = 80$  nm; medium NP,  $d = 170$  nm and large NP  $d = 360$  nm) under appropriate conditions of nanoprecipitation and were subsequently characterized by DLS and SEM (Figure 22A). Additionally, the zeta potential of the NP was measured in water (pH 6), resulting in values of  $\sim 30$  mV (positive due to cationic amine groups of the dyes) for all nanoparticle suspensions. Zeta potential values larger than 20 mV indicate high repulsion forces and colloidal stability of the NPs in suspension.<sup>[159]</sup> Mixtures of the differently sized and labeled NPs were applied for internalization studies using monolayer cultured HeLa cells. For this purpose, the intracellular distribution of the NPs after incubation was studied in living cells by CLSM (Figure 22B). A strong co-localization was observed between small and medium sized NPs, whereas for large NPs only a marginal co-localization was detected. Further investigation regarding the cellular fate of the differently sized NPs showed that medium sized nanoparticles were detected in the late endosomes/lysosomes, whereas the large nanoparticles exhibit little co-localization with LysoTracker (Figure 22B). To identify different uptake mechanism depending on particle size, different inhibitors were used. It was shown that nanoparticles with  $d < 200$  nm (small NP) were internalized via clathrin-dependent endocytosis, whereas those with  $d > 300$  nm (large NP) were uptaken via macropinocytosis.

In conclusion a detailed size dependent uptake of well-defined nanoparticles prepared by nanoprecipitation of dye-functionalized PMMA derivatives was presented. With this approach a detailed study of possible pathways into cells and the cellular uptake mechanism was possible.



---

## Summary

---

Modern polymerization techniques based on *controlled radical polymerization* (CRP) procedures have drawn significant scientific interest in the last decades based on the possibility to prepare complex polymer architectures. In this context the *reversible addition-fragmentation chain transfer* (RAFT) polymerization represents one of the most versatile and robust technique in the toolbox of CRP polymerizations, since it is applicable for a wide range of monomers and functionalities. RAFT polymerization as the key methodology in this work facilitates the preparation of (multi)functional polymeric material under conventional conditions.

The presented thesis provides an overview of the defined synthesis procedures of polymers with tailored structures and functionalities with the ability to form nanostructures *via* self-assembly or nanoprecipitation. A variety of strategies for the preparation of functional polymers are explored, namely incorporation of functionalized monomers and the construction of block copolymer segments. In detail the research in this thesis focused on the defined synthesis of polymers with tailored photophysical properties and stimuli-responsive assembly behavior (Figure 23).

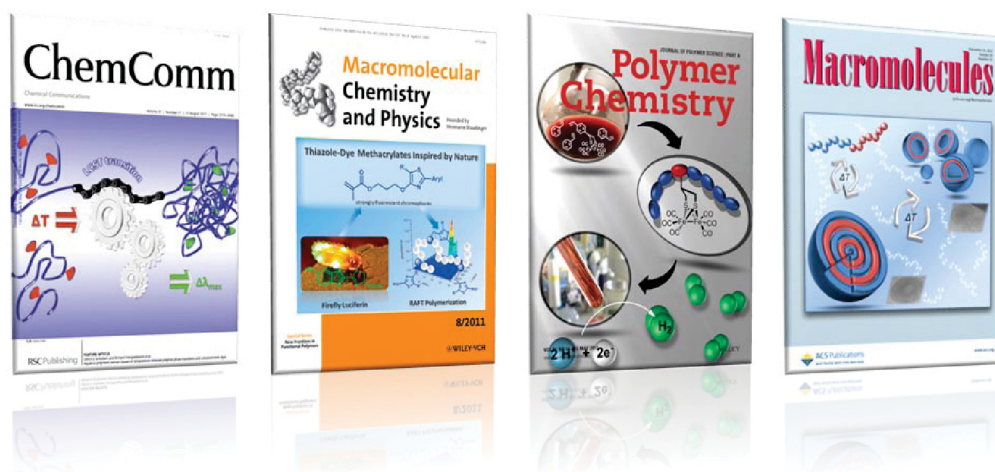


Figure 23 Overview about polymers with tailored structures and functionalities illustrated by cover images of publications included in this thesis: Chem. Commun. (Chapter 2), Macromol. Chem. Phys. (Chapters 3 and 5), J. Polym. Sci., Part A: Polym. Chem. (Chapter 3) and Macromolecules (Chapter 4).

It could be demonstrated that various 4-hydroxythiazole, pyrene and [2Fe2S] cluster units functionalized to monomers can be (co)polymerized using the RAFT technique. Furthermore it could be shown that these monomers can be copolymerized in a controlled manner. The polymers containing derivatives of 4-hydroxythiazoles were studied as new light-harvesting systems and blue-fluorescing chromophores were compiled. In a further step the combination of energy donor and acceptor thiazole dyes were explored regarding the investigation of an energy transfer (FRET) between them along the polymer chain. In the D/A copolymer high energy transfer efficiencies were observed by optimization of the D/A ratio and these copolymer can act as antenna structures for light harvesting systems.

After the examination of the light-emitting properties of several thiazole based copolymers it was desirable to broaden the range of functional monomers to open new windows for other applications including the production of hydrogen. For this purpose, [FeFe]-hydrogenase styrene models were developed and the first controlled radical polymerization of these models is described. It could be shown that the biomimetic metal centers keep their activity and redox behavior after polymerization and inclusion into the copolymer chain.

The manifold possibilities to incorporate chromophores into copolymer backbones enables the possibility for applications as polymeric sensor systems. In this context, thermo-responsive polymers that undergo a lower critical solution temperature transition by variation of the temperature are important systems for the development of smart materials. A well-defined fluorescent copolymer based on PDEGMA functionalized with pyrene side-chain units was synthesized by RAFT polymerization. Temperature dependent fluorescence measurements demonstrated that this polymer acts as a soluble fluorescent temperature sensor.

Investigations of the LCST behavior have attracted significant interest in polymer research. Particular attention in this regard has been paid to the thermo-sensitive self-organization of amphiphilic block copolymers, especially on the formation of micelles or vesicular structures. The RAFT polymerization method was used for the preparation of a library of double thermo-responsive diblock copolymers, namely poly(DMAEMA-*b*-DEGMA) block copolymers. The phase transitions of these block copolymers in aqueous solutions were studied in detail. Within this library of block copolymers, a block ratio of 50:50 resulted in a double responsive LCST behavior. This block copolymer was further investigated to elucidate the self-assembly behavior. Variable temperature <sup>1</sup>H NMR spectroscopy, zeta potential, and cryo-TEM investigations revealed the temperature induced formation of multilamellar vesicular (MLV) structures and subsequent transition in large unilamellar (ULV) structures.

Besides the investigation of self-assembled block copolymer structures, another approach for the generation of nanostructures was explored. The nanoprecipitation process was utilized

to generate nano-sized colloidal particles. Fine-tuning of the NPs was investigated and it could be shown that the corresponding NP size, incorporation of chromophores and stability can be controlled. The influence of the molar mass and polymer concentration on the NPs size was demonstrated. Furthermore, possible applications of fluorescent polymeric nanoparticles in cellular uptake as diagnostic tools were illustrated and the cellular uptake mechanism was revealed.

In conclusion, this thesis presented the preparation of new functional smart polymeric materials. The embedding of several dyes in polymer backbones, thermo-responsive block copolymer system and tailored nanoparticles are highlighted and represent an important contribution to actual research fields. The gained knowledge will be the fundament for new developments and investigations. Future research will be directed towards the design and self-assembly of block copolymers and nanoparticles as new tools for delivery vehicles or nanocontainers (*e.g.* for therapies), whereby specific attention will be focused on the encapsulation and transport of guest molecules. In combination with chromophores the advanced nanostructure can be used not only in diagnostic application (*e.g.* as sensor) but also to better understand the formed morphologies and self-assembled architectures.



---

## Zusammenfassung

---

Moderne Polymerisationstechniken, basierend auf *kontrollierten radikalischen Polymerisationsprozessen* (CRP), führten in den letzten Jahrzehnten zu einem beeindruckenden wissenschaftlichen Interesse. Ein Grund für die zunehmende Bedeutung dieser Technik ist die Möglichkeit der Synthese vielfältiger und komplexer Polymerarchitekturen. Die reversible Additions-Fragmentierungs-Kettentransfer (RAFT) Polymerisation ist in diesem Zusammenhang eine der leistungstärksten und robustesten Varianten im „Werkzeugkasten“ der CRP-Polymerisationen. Diese Methode ermöglicht es, auf eine große Auswahl maßgeschneiderter Monomere und Funktionalitäten für zielgerichtete Anwendungen zurückzugreifen. Die RAFT-Technik, auf die sich die vorliegende Arbeit fokussiert, stellt folglich ein Schlüsselement für die Synthese von (multi)funktionalen Polymermaterialien unter konventionellen Polymerisationsbedingungen dar.

Die vorliegende Dissertation behandelt die definierte Makromolekülsynthese maßgeschneiderter Strukturen und Funktionalitäten, sowie die Möglichkeit der Präparation von Nanostrukturen durch Selbstorganisation oder Nanofällung. In diesem Zusammenhang wurden verschiedene Strategien zum Aufbau solcher Makromoleküle intensiv untersucht. Neben dem Einbau funktionaler Monomere in das Polymerrückgrat, erfolgte die Synthese von Blockcopolymersegmenten unterschiedlicher Blocklänge.

Die vorliegende Forschungsarbeit behandelt im speziellen die RAFT-(Co)Polymerisation von Methacrylaten und Styrol-Bausteinen für den Aufbau hochfunktionalisierter Polymere mit definierten photophysikalischen Eigenschaften bzw. „stimuli-responsivem“ Verhalten (Figure 24).

In diesem Zusammenhang wurden verschiedene 4-Hydroxythiazole, Pyrene und [2Fe2S]-Cluster funktionalisierte Monomere (co)polymerisiert. Es konnte ebenfalls gezeigt werden, dass die Polymerisation dieser Monomere kontrolliert („quasi-lebend“) verläuft. Insbesondere Makromoleküle, basierend auf 4-Hydroxythiazolen, stellten sich als moderne Lichtsammleinheiten mit einer zusätzlichen Fluoreszenz im blauen Bereich des elektromagnetischen Spektrums heraus. Des Weiteren wurde, durch Kombination aus einem Donor- (D) und einem Akzeptorfarbstoff (A), der Energietransfer zwischen beiden Chromophoren entlang des Polymerrückgrats untersucht. Die Optimierung der D/A Verhältnisse führte zu hohen Energietransferraten, welches die Anwendung dieser Systeme als sogenannte „Antennenstrukturen“ für Lichtsammleinheiten, ermöglicht.

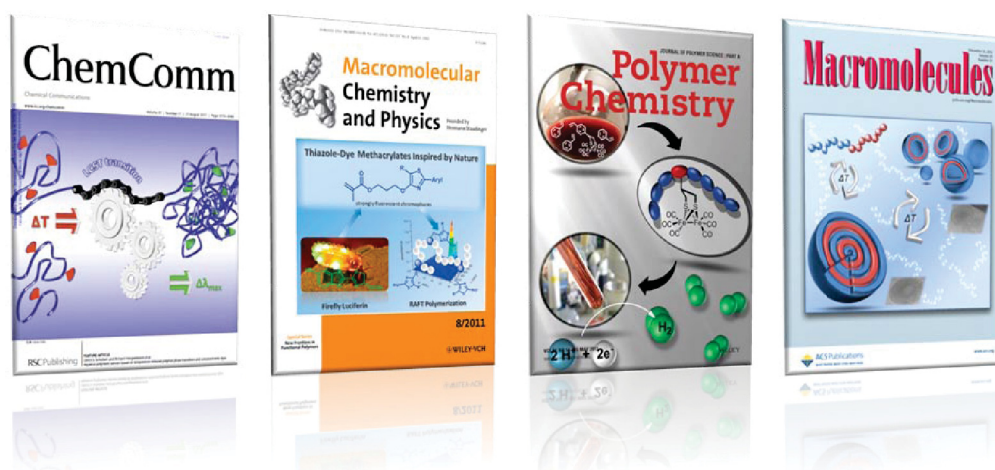


Figure 24 Übersicht maßgeschneiderter Polymerarchitekturen, welche durch Titelblätter ausgewählter Publikationen der Dissertation illustriert sind: Chem. Commun. (Kapitel 2), Macromol. Chem. Phys. (Kapitel 3 und 5), J. Polym. Sci., Part A: Polym. Chem. (Kapitel 3) und Macromolecules (Kapitel 4).

Nach Untersuchung der Licht-emittierenden Eigenschaften verschiedener Thiazol-basierter Copolymere, stand die Erweiterung der Auswahl von Monomerfunktionalitäten im Mittelpunkt. Dabei lag der Fokus auf der Untersuchung neuartiger Anwendungen, wie z.B. moderne Systeme der Wasserstoffentwicklung. Darauf aufbauend wurden Styrol-Modelle der [FeFe]-Hydrogenase entwickelt und ihre kontrollierte radikalische (Co)Polymerisation erstmalig beschrieben. Es konnte gezeigt werden, dass die Aktivität und das Redoxverhalten des biomimetischen Metallzentrums der [FeFe]-Hydrogenase nach dem Einbau in die Polymerkette erhalten bleibt.

Daneben ermöglichen die vielfältigen Variationen des Einbaus von Chromophoren in polymere Strukturen eine Anwendung als Polymer-basierte Sensoren. In diesem Kontext spielt das Phasenverhalten von Polymeren mit unterer kritischer Lösungstemperatur (LCST) eine entscheidende Rolle. Mittels RAFT-Polymerisation konnte ein solches Polymer, bestehend aus PDEGMA mit zusätzlich fluoreszierenden Pyrene-basierten Seitengruppen, gezielt synthetisiert werden. Fluoreszenzuntersuchungen zeigten, dass dieses Copolymer als Temperatursensor in Lösung agieren kann.

Des Weiteren ist das Auftreten von Mischungslücken bei Temperaturerhöhung (hydrophil zu hydrophob) von Polymerlösungen in den letzten Jahrzehnten Gegenstand intensiver Forschung, u. a. bezüglich der thermosensitiven Selbstorganisation von amphiphilen Blockcopolymeren zu Mizellen bzw. vesikulären Strukturen. Für die Synthese einer entsprechenden Polymerbibliothek wurde die RAFT-Methode genutzt, um Poly(DMAEMA-*b*-DEGMA) Blockcopolymere herzustellen. Die detaillierte Charakterisierung der erhaltenen Verbindungen in Lösung zeigte ein doppelt ansprechbares LCST Verhalten für Blockcopolymere mit gleichen Blocklängen.

Durch temperaturabhängige Untersuchungen mittels  $^1\text{H}$  NMR Spektroskopie, elektrophoretischer Lichtstreuung und cryo-Transmissions-Elektronenmikroskopie (cryoTEM) konnte hierbei die Bildung multilamellarer, vesikulärer Strukturen, welche bei Temperaturerhöhung in größere unilamellare Strukturen übergehen, gezeigt werden.

Neben der Charakterisierung selbstorganisierender Blockcopolymerer wurde der Prozess der Nanofällung, als eine weitere Variante zur Generierung von Nanopartikeln, untersucht. In diesem Zusammenhang konnte der Einfluss der Molmasse und der Polymerkonzentration auf die Partikelgröße und die Stabilität, sowie der Einbau von Farbstoffen, untersucht werden. Des Weiteren wurden Studien zur Zellaufnahme von fluoreszierenden Nanopartikeln durchgeführt, welche sich anschließend als mögliches Werkzeug im diagnostischen Bereich etablieren ließen.

Zusammenfassend präsentiert die vorliegende Dissertation die Synthese neuartiger, funktionaler Polymermaterialien. Der Einbau verschiedener Farbstoffe in Makromoleküle, das thermosensitive Verhalten von Blockcopolymeren und die Präparation definierter Nanopartikelsysteme wurden aufgezeigt und liefern einen wertvollen Beitrag zu aktuellen Forschungsthemen. Die gewonnenen Erkenntnisse werden in das zukünftige Design und den Aufbau selbstorganisierender Blockcopolymerstrukturen und nanopartikulärer Systeme einfließen, um neuartige Transportvehikel oder Nanocontainer (z.B. für Therapie Zwecke) zu entwickeln. Besonderes Augenmerk liegt auf dem Einschluss und dem Transport von niedermolekularen Substanzen (Gastmolekülen). In der Kombination mit Farbstoffen können diese Nanostrukturen im diagnostischen Bereich Anwendungen finden (z.B. als Sensor) oder dazu genutzt werden, ein besseres Verständnis der gebildeten Morphologien und selbstorganisierenden Architekturen zu erhalten.





---

## References

---

- [1] W. Hesse, in *Ullmann's Encyclopedia of Industrial Chemistry*, Wiley-VCH Verlag GmbH & Co. KGaA, **2000**.
- [2] R. Stepto, K. Horie, T. Kitayama, A. Abe, *Pure Appl. Chem.* **2003**, *75*, 1359-1369.
- [3] H. Staudinger, *Ber. Dtsch. Chem. Ges.* **1920**, *53*, 1073-1085.
- [4] H. Staudinger, J. Fritsch, *Helv. Chim. Acta* **1922**, *5*, 785-806.
- [5] H. Ringsdorf, *Angew. Chem. Int. Ed.* **2004**, *43*, 1064-1076.
- [6] [http://www.rohmhaas.com/history/ourstory/innovation\\_plexiglastriumphs.htm](http://www.rohmhaas.com/history/ourstory/innovation_plexiglastriumphs.htm) (last accessed 22<sup>nd</sup> april 2013).
- [7] K. Ziegler, E. Holzkamp, H. Breil, H. Martin, *Angew. Chem.* **1955**, *67*, 541-547.
- [8] M. Szwarc, *Nature* **1956**, *178*, 1168-1169.
- [9] G. Odian, *Principles of Polymerization*, 4th ed., New York: Wiley-Interscience, **2004**.
- [10] A. H. E. Müller, K. Matyjaszewski, *Controlled and Living Polymerizations*, WILEY-VCH, Weinheim, Germany, **2009**.
- [11] J. Chiefari, Y. K. Chong, F. Ercole, J. Krstina, J. Jeffery, T. P. T. Le, R. T. A. Mayadunne, G. F. Meijs, C. L. Moad, G. Moad, E. Rizzardo, S. H. Thang, *Macromolecules* **1998**, *31*, 5559-5562.
- [12] G. Moad, E. Rizzardo, S. H. Thang, *Aust. J. Chem.* **2012**, *65*, 985-1076.
- [13] J. S. Wang, K. Matyjaszewski, *J. Am. Chem. Soc.* **1995**, *117*, 5614-5615.
- [14] K. Matyjaszewski, J. H. Xia, *Chem. Rev.* **2001**, *101*, 2921-2990.
- [15] C. J. Hawker, *J. Am. Chem. Soc.* **1994**, *116*, 11185-11186.
- [16] C. J. Hawker, A. W. Bosman, E. Harth, *Chem. Rev.* **2001**, *101*, 3661-3688.
- [17] B. N. G. Giepmans, S. R. Adams, M. H. Ellisman, R. Y. Tsien, *Science* **2006**, *312*, 217-224.
- [18] E. A. Jares-Erijman, T. M. Jovin, *Nat. Biotechnol.* **2003**, *21*, 1387-1395.
- [19] K. E. Sapsford, L. Berti, I. L. Medintz, *Angew. Chem. Int. Ed.* **2006**, *45*, 4562-4589.
- [20] F. S. Bates, *Science* **1991**, *251*, 898-905.
- [21] F. S. Bates, G. H. Fredrickson, *Physics Today* **1999**, *52*, 32-38.

- [22] B. M. Discher, Y.-Y. Won, D. S. Ege, J. C.-M. Lee, F. S. Bates, D. E. Discher, D. A. Hammer, *Science* **1999**, *284*, 1143-1146.
- [23] D. E. Discher, A. Eisenberg, *Science* **2002**, *297*, 967-973.
- [24] L. Zhang, A. Eisenberg, *J. Am. Chem. Soc.* **1996**, *118*, 3168-3181.
- [25] H. G. Schild, *Prog. Polym. Sci.* **1992**, *17*, 163-249.
- [26] E. S. Gil, S. M. Hudson, *Prog. Polym. Sci.* **2004**, *29*, 1173-1222.
- [27] D. Schmaljohann, *Adv. Drug Delivery Rev.* **2006**, *58*, 1655-1670.
- [28] C. Weber, R. Hoogenboom, U. S. Schubert, *Prog. Polym. Sci.* **2012**, *37*, 686-714.
- [29] K. Matyjaszewski, *Prog. Polym. Sci.* **2005**, *30*, 858-875.
- [30] M. Szwarc, M. Levy, R. Milkovich, *J. Am. Chem. Soc.* **1956**, *78*, 2656-2657.
- [31] V. Ladmiral, G. Mantovani, G. J. Clarkson, S. Cauet, J. L. Irwin, D. M. Haddleton, *J. Am. Chem. Soc.* **2006**, *128*, 4823-4830.
- [32] E. R. Gillies, J. M. J. Fréchet, *Drug Discovery Today* **2005**, *10*, 35-43.
- [33] M. Ouchi, T. Terashima, M. Sawamoto, *Chem. Rev.* **2009**, *109*, 4963-5050.
- [34] K. Matyjaszewski, J. Xia, *Chem. Rev.* **2001**, *101*, 2921-2990.
- [35] M. Kamigaito, T. Ando, M. Sawamoto, *Chem. Rev.* **2001**, *101*, 3689-3746.
- [36] G. Moad, E. Rizzardo, S. H. Thang, *Aust. J. Chem.* **2006**, *59*, 669-692.
- [37] G. Moad, E. Rizzardo, S. H. Thang, *Aust. J. Chem.* **2009**, *62*, 1402-1472.
- [38] C. Pietsch, R. Hoogenboom, U. S. Schubert, *Angew. Chem. Int. Ed.* **2009**, *48*, 5653-5656.
- [39] C. Pietsch, R. Hoogenboom, U. S. Schubert, *Polym. Chem.* **2010**, *1*, 1005-1008.
- [40] G. Moad, E. Rizzardo, S. H. Thang, *Aust. J. Chem.* **2005**, *58*, 379-410.
- [41] R. T. A. Mayadunne, E. Rizzardo, J. Chiefari, J. Krstina, G. Moad, A. Postma, S. H. Thang, *Macromolecules* **2000**, *33*, 243-245.
- [42] J. Chiefari, R. T. A. Mayadunne, C. L. Moad, G. Moad, E. Rizzardo, A. Postma, S. H. Thang, *Macromolecules* **2003**, *36*, 2273-2283.
- [43] H. C. Kolb, M. G. Finn, K. B. Sharpless, *Angew. Chem. Int. Ed.* **2001**, *40*, 2004-2021.
- [44] D. Fournier, R. Hoogenboom, U. S. Schubert, *Chem. Soc. Rev.* **2007**, *36*, 1369-1380.
- [45] W. H. Binder, R. Sachsenhofer, *Macromol. Rapid Commun.* **2007**, *28*, 15-54.
- [46] C. R. Becer, R. Hoogenboom, U. S. Schubert, *Angew. Chem. Int. Ed.* **2009**, *48*, 4900-4908.

- [47] D. D. Diaz, S. Punna, P. Holzer, A. K. McPherson, K. B. Sharpless, V. V. Fokin, M. G. Finn, *J. Polym. Sci., Part A: Polym. Chem.* **2004**, *42*, 4392-4403.
- [48] P. Wu, A. K. Feldman, A. K. Nugent, C. J. Hawker, A. Scheel, B. Voit, J. Pyun, J. M. J. Frechet, K. B. Sharpless, V. V. Fokin, *Angew. Chem. Int. Ed.* **2004**, *43*, 3928-3932.
- [49] A. B. Lowe, *Polym. Chem.* **2010**, *1*, 17-36.
- [50] Charles E. Hoyle, Christopher N. Bowman, *Angew. Chem. Int. Ed.* **2010**, *49*, 1540-1573.
- [51] B. Adhikari, S. Majumdar, *Prog. Polym. Sci.* **2004**, *29*, 699-766.
- [52] O. S. Wolfbeis, *J. Mater. Chem.* **2005**, *15*, 2657-2669.
- [53] F. Baldini, et al. (eds.), in *Optical Chemical Sensors, Vol. 224*, 1 ed., Springer, Dordrecht, The Netherlands, **2006**, 297-322.
- [54] C. McDonagh, C. S. Burke, B. D. MacCraith, *Chem. Rev.* **2008**, *108*, 400-422.
- [55] O. S. Wolfbeis, *Adv. Mater.* **2008**, *20*, 3759-3763.
- [56] M. I. J. Stich, L. H. Fischer, O. S. Wolfbeis, *Chem. Soc. Rev.* **2010**, *39*, 3102-3114.
- [57] A. Richter, G. Paschew, S. Klatt, J. Lienig, K.-F. Arndt, H.-J. Adler, *Sensors* **2008**, *8*, 561-581.
- [58] J. Han, K. Burgess, *Chem. Rev.* **2009**, *110*, 2709-2728.
- [59] H.-J. Schneider, K. Kato, R. Strongin, *Sensors* **2007**, *7*, 1578-1611.
- [60] J. Hu, S. Liu, *Macromolecules* **2010**, *43*, 8315-8330.
- [61] R. Liu, M. Fraylich, B. Saunders, *Colloid Polym Sci* **2009**, *287*, 627-643.
- [62] D. Roy, J. N. Cambre, B. S. Sumerlin, *Prog. Polym. Sci.* **2010**, *35*, 278-301.
- [63] S. Dai, P. Ravi, K. C. Tam, *Soft Matter* **2009**, *5*, 2513-2533.
- [64] M. Annaka, T. Tanaka, *Nature* **1992**, *355*, 430-432.
- [65] Y. Qiu, K. Park, *Adv. Drug Delivery Rev.* **2001**, *53*, 321-339.
- [66] C. Reichardt, *Chem. Rev.* **1994**, *94*, 2319-2358.
- [67] M. Heskins, J. E. Guillet, *J. Macromol. Sci.-Chem.* **1968**, *2*, 1441-1455.
- [68] H. G. Schild, D. A. Tirrell, *J. Phys. Chem.* **1990**, *94*, 4352-4356.
- [69] J. Zhao, R. Hoogenboom, G. Van Assche, B. Van Mele, *Macromolecules* **2010**, *43*, 6853-6860.
- [70] S. Fujishige, K. Kubota, I. Ando, *J. Phys. Chem.* **1989**, *93*, 3311-3313.
- [71] K. Kubota, S. Fujishige, I. Ando, *J. Phys. Chem.* **1990**, *94*, 5154-5158.

- [72] V. Aseyev, S. Hietala, A. Laukkanen, M. Nuopponen, O. Confortini, F. E. Du Prez, H. Tenhu, *Polymer* **2005**, *46*, 7118-7131.
- [73] P. Kujawa, F. Tanaka, F. M. Winnik, *Macromolecules* **2006**, *39*, 3048-3055.
- [74] P. Vyskocil, J. Ricka, T. Binkert, *Helv. Phys. Acta* **1989**, *62*, 243-245.
- [75] F. M. Winnik, *Polymer* **1990**, *31*, 2125-2134.
- [76] J. Duhamel, *Acc. Chem. Res.* **2006**, *39*, 953-960.
- [77] H. Ringsdorf, J. Simon, F. M. Winnik, *Macromolecules* **1992**, *25*, 7306-7312.
- [78] Y. Maeda, T. Higuchi, I. Ikeda, *Langmuir* **2000**, *16*, 7503-7509.
- [79] U. W. Gedde, in *Polymer Physics*, 1st ed., Kluwer Academic Publishers, Dordrecht, The Netherlands, **1995**, 55-69.
- [80] S. Han, M. Hagiwara, T. Ishizone, *Macromolecules* **2003**, *36*, 8312-8319.
- [81] S. Saeki, N. Kuwahara, M. Nakata, M. Kaneko, *Polymer* **1976**, *17*, 685-689.
- [82] J.-F. Lutz, Ö. Akdemir, A. Hoth, *J. Am. Chem. Soc.* **2006**, *128*, 13046-13047.
- [83] A. C. Grimsdale, K. Leok Chan, R. E. Martin, P. G. Jokisz, A. B. Holmes, *Chem. Rev.* **2009**, *109*, 897-1091.
- [84] O. Nuyken, S. Jungermann, V. Wiederhirn, E. Bacher, K. Meerholz, *Monatsh. Chem.* **2006**, *137*, 811-824.
- [85] D. T. McQuade, A. E. Pullen, T. M. Swager, *Chem. Rev.* **2000**, *100*, 2537-2574.
- [86] X. Liu, R. Zhu, Y. Zhang, B. Liu, S. Ramakrishna, *Chem. Commun.* **2008**, *0*, 3789-3791.
- [87] G. D. Sharma, P. Suresh, J. A. Mikroyannidis, *Synth. Met.* **2010**, *160*, 1427-1432.
- [88] D. A. Friesen, T. Kajita, E. Danielson, T. J. Meyer, *Inorg. Chem.* **1998**, *37*, 2756-2762.
- [89] M. Sykora, K. A. Maxwell, J. M. DeSimone, T. J. Meyer, *Proc. Natl. Acad. Sci. U. S. A.* **2000**, *97*, 7687-7691.
- [90] C. U. Pittman, M. D. Rausch, *Pure Appl. Chem.* **1986**, *58*, 617-622.
- [91] D. Seyferth, H. P. Withers, *Inorg. Chem.* **1983**, *22*, 2931-2936.
- [92] S. I. Pomogailo, G. I. Dzhardimalieva, V. A. Ershova, S. M. Aldoshin, A. D. Pomogailo, *Macromol. Symp.* **2002**, *186*, 155-160.
- [93] M. Aguiar, F. E. Karasz, L. Akcelrud, *Macromolecules* **1995**, *28*, 4598-4602.
- [94] E. Täuscher, D. Weiß, R. Beckert, H. Görls, *Synthesis* **2010**, *2010*, 1603-1608.
- [95] R. Menzel, E. Täuscher, D. Weiß, R. Beckert, H. Görls, *Z. Anorg. Allg. Chem.* **2010**, *636*, 1380-1385.

- [96] E. V. Chernikova, A. V. Tarasenko, E. S. Garina, V. B. Golubev, *Polymer Science Series A* **2006**, *48*, 1046-1057.
- [97] G. Moad, Y. K. Chong, R. Mulder, E. Rizzardo, H. Thang San, in *Controlled/Living Radical Polymerization: Progress in RAFT, DT, NMP & OMRP, Vol. 1024*, American Chemical Society, **2009**, 3-18.
- [98] A. I. Krasna, D. Rittenberg, *J. Am. Chem. Soc.* **1954**, *76*, 3015-3020.
- [99] M. Frey, *ChemBioChem* **2002**, *3*, 153-160.
- [100] M. W. W. Adams, *FEMS Microbiol. Lett.* **1990**, *75*, 219-237.
- [101] D. J. Evans, C. J. Pickett, *Chem. Soc. Rev.* **2003**, *32*, 268-275.
- [102] C. Tard, C. J. Pickett, *Chem. Rev.* **2009**, *109*, 2245-2274.
- [103] A. T. Fiedler, T. C. Brunold, *Inorg. Chem.* **2005**, *44*, 1794-1809.
- [104] J. Du, R. K. O'Reilly, *Soft Matter* **2009**, *5*, 3544-3561.
- [105] I. Dimitrov, B. Trzebicka, A. H. E. Müller, A. Dworak, C. B. Tsvetanov, *Prog. Polym. Sci.* **2007**, *32*, 1275-1343.
- [106] M.-H. Li, P. Keller, *Soft Matter* **2009**, *5*, 927-937.
- [107] S. Qin, Y. Geng, D. E. Discher, S. Yang, *Adv. Mater.* **2006**, *18*, 2905-2909.
- [108] Y. Li, B. S. Lokitz, C. L. McCormick, *Angew. Chem. Int. Ed.* **2006**, *45*, 5792-5795.
- [109] M. Antonietti, S. Förster, *Adv. Mater.* **2003**, *15*, 1323-1333.
- [110] J. Coelho, P. Ferreira, P. Alves, R. Cordeiro, A. Fonseca, J. Góis, M. Gil, *The EPMA Journal* **2010**, *1*, 164-209.
- [111] O. Onaca, R. Enea, D. W. Hughes, W. Meier, *Macromol. Biosci.* **2009**, *9*, 129-139.
- [112] J.-F. Lutz, A. Hoth, *Macromolecules* **2005**, *39*, 893-896.
- [113] J.-F. Lutz, *J. Polym. Sci., Part A: Polym. Chem.* **2008**, *46*, 3459-3470.
- [114] C. R. Becer, S. Hahn, M. W. M. Fijten, H. M. L. Thijs, R. Hoogenboom, U. S. Schubert, *J. Polym. Sci., Part A: Polym. Chem.* **2008**, *46*, 7138-7147.
- [115] T. Ishizone, A. Seki, M. Hagiwara, S. Han, H. Yokoyama, A. Oyane, A. Deffieux, S. Carlotti, *Macromolecules* **2008**, *41*, 2963-2967.
- [116] M. P. Patel, M. B. Johnstone, F. J. Hughes, M. Braden, *Biomaterials* **2000**, *22*, 81-86.
- [117] Y. Oda, S. Kanaoka, S. Aoshima, *J. Polym. Sci., Part A: Polym. Chem.* **2010**, *48*, 1207-1213.
- [118] H. M. L. Thijs, C. R. Becer, C. Guerrero-Sanchez, D. Fournier, R. Hoogenboom, U. S. Schubert, *J. Mater. Chem.* **2007**, *17*, 4864-4871.
- [119] A. B. Lowe, C. L. McCormick, *Prog. Polym. Sci.* **2007**, *32*, 283-351.

- [120] C. M. Schilli, M. Zhang, E. Rizzardo, S. H. Thang, Y. K. Chong, K. Edwards, G. Karlsson, A. H. E. Müller, *Macromolecules* **2004**, *37*, 7861-7866.
- [121] F. L. Baines, N. C. Billingham, S. P. Armes, *Macromolecules* **1996**, *29*, 3416-3420.
- [122] M. Arotçaréna, B. Heise, S. Ishaya, A. Laschewsky, *J. Am. Chem. Soc.* **2002**, *124*, 3787-3793.
- [123] A. Blanazs, S. P. Armes, A. J. Ryan, *Macromol. Rapid Commun.* **2009**, *30*, 267-277.
- [124] J. Weiss, C. Bottcher, A. Laschewsky, *Soft Matter* **2011**, *7*, 483-492.
- [125] D. Fournier, R. Hoogenboom, H. M. L. Thijs, R. M. Paulus, U. S. Schubert, *Macromolecules* **2007**, *40*, 915-920.
- [126] V. Bütün, S. P. Armes, N. C. Billingham, *Polymer* **2001**, *42*, 5993-6008.
- [127] F. A. Plamper, M. Ruppel, A. Schmalz, O. Borisov, M. Ballauff, A. H. E. Müller, *Macromolecules* **2007**, *40*, 8361-8366.
- [128] F. A. Plamper, A. Schmalz, A. H. E. Müller, *J. Am. Chem. Soc.* **2007**, *129*, 14538-14539.
- [129] S.-i. Yamamoto, J. Pietrasik, K. Matyjaszewski, *Macromolecules* **2008**, *41*, 7013-7020.
- [130] S. J. Holder, N. A. J. M. Sommerdijk, S. J. Williams, R. J. M. Nolte, R. C. Hiorns, R. G. Jones, *Chem. Commun.* **1998**, 1445-1446.
- [131] K. Riehemann, S. W. Schneider, T. A. Luger, B. Godin, M. Ferrari, H. Fuchs, *Angew. Chem. Int. Ed.* **2009**, *48*, 872-897.
- [132] N. Sanvicens, M. P. Marco, *Trends Biotechnol.* **2008**, *26*, 425-433.
- [133] H. Fessi, F. Puisieux, J. P. Devissaguet, N. Ammoury, S. Benita, *Int. J. Pharm.* **1989**, *55*, R1-R4.
- [134] S. Schubert, J. J. T. Delaney, U. S. Schubert, *Soft Matter* **2011**, *7*, 1581-1588.
- [135] C. E. Mora-Huertas, H. Fessi, A. Elaissari, *Int. J. Pharm.* **2010**, *385*, 113-142.
- [136] C. Vauthier, K. Bouchemal, *Pharm. Res.* **2009**, *26*, 1025-1058.
- [137] T. Govender, S. Stolnik, M. C. Garnett, L. Illum, S. S. Davis, *J. Controlled Release* **1999**, *57*, 171-185.
- [138] H. Zhang, W. Cui, J. Bei, S. Wang, *Polym. Degrad. Stab.* **2006**, *91*, 1929-1936.
- [139] S. Hornig, T. Heinze, *Biomacromolecules* **2008**, *9*, 1487-1492.
- [140] A. Vollrath, S. Schubert, N. Windhab, C. Biskup, U. S. Schubert, *Macromol. Rapid Commun.* **2010**, *31*, 2053-2058.

- [141] S. Hornig, T. Heinze, C. R. Becer, U. S. Schubert, *J. Mater. Chem.* **2009**, *19*, 3838-3840.
- [142] D. F. Emerich, C. G. Thanos, *J. Drug Targeting* **2007**, *15*, 163-183.
- [143] W. J. Stark, *Angew. Chem. Int. Ed.* **2011**, *50*, 1242-1258.
- [144] A. Merkoci, *Biosens. Bioelectron.* **2010**, *26*, 1164-1177.
- [145] C. J. Xu, L. Y. Mu, I. Roes, D. Miranda-Nieves, M. Nahrendorf, J. A. Ankrum, W. A. Zhao, J. M. Karp, *Nanotechnology* **2011**, *22*, 1-17.
- [146] K. H. Chung, M. Y. Cho, M. H. Sung, H. Poo, Y. T. Lim, *Chem. Commun.* **2011**, *47*, 8889-8891.
- [147] G. Tosi, L. Bondioli, B. Ruozi, L. Badiali, G. M. Severini, S. Biffi, A. De Vita, B. Bortot, D. Dolcetta, F. Forni, M. A. Vandelli, *J. Neural Transm.* **2011**, *118*, 145-153.
- [148] K. H. Lee, *J Nucl Med* **2007**, *48*, 1408-1410.
- [149] I. Y. Perevyazko, J. T. Delaney, Jr., A. Vollrath, G. M. Pavlov, S. Schubert, U. S. Schubert, *Soft Matter* **2011**, *7*, 5030-5035.
- [150] A. Bettencourt, A. J. Almeida, in *J. Microencapsulation*, **2012**.
- [151] J. A. Kim, C. Aberg, A. Salvati, K. A. Dawson, *Nat. Nanotechnol.* **2012**, *7*, 62-68.
- [152] V. Mailander, K. Landfester, *Biomacromolecules* **2009**, *10*, 2379-2400.
- [153] L. E. Euliss, J. A. DuPont, S. Gratton, J. M. DeSimone, *Chem. Soc. Rev.* **2006**, *35*, 1095-1104.
- [154] G. M. Whitesides, *Nat. Biotechnol.* **2003**, *21*, 1161-1165.
- [155] M. Gaumet, R. Gurny, F. Delie, *Eur. J. Pharm. Sci.* **2009**, *36*, 465-473.
- [156] J. Dausend, A. Musyanovych, M. Dass, P. Walther, H. Schrezenmeier, K. Landfester, V. Mailander, *Macromol. Biosci.* **2008**, *8*, 1135-1143.
- [157] J. Brandrup, E. H. Immergut, E. A. Grulke, in *Polymer Handbook*, 4 ed., Wiley-Interscience, **1999**.
- [158] J. Pauli, T. Vag, R. Haag, M. Spieles, M. Wenzel, W. A. Kaiser, U. Resch-Genger, I. Hilger, *Eur. J. Med. Chem.* **2009**, *44*, 3496-3503.
- [159] R. H. Müller, *Zetapotential und Partikelladung in der Laborpraxis*, Wissenschaftliche Verlagsgesellschaft, Stuttgart, Germany, **1996**.





---

## List of abbreviations

---

$[M]_0$	Monomer concentration at zero time
$[M]_t$	Monomer concentration at time t
A	Acceptor
AA	Acrylic acid
AAS	Atomic absorption spectroscopy
AIBN	2,2'-Azobis( <i>iso</i> -butyronitrile)
ATRP	Atom transfer radical polymerization
AUC	Analytical ultracentrifugation
CLMS	Confocal laser scanning microscopy
CPDB	2-Cyano-2-propyl dithiobenzoate
Cryo-TEM	Cryogenic transmission electron microscopy
CRP	Controlled radical polymerization
CSIRO	Commonwealth Scientific and Industrial Research Organization
CTA	Chain transfer agent
CTA1	Benzyl (diethoxyphosphoryl)dithioformate
CTA2	2-(Butylthiocarbonothioylthio)propanoic acid
CTA3	4-Cyano-4-[(dodecylsulfanylthiocarbonyl)sulfanyl]pentanoic acid
d	Diameter
$\delta$	Chemical shift
D	Donor
DEGMA	Di(ethylene glycol) methyl ether methacrylate
DLS	Dynamic light scattering
DMAEMA	2-Dimethylaminoethyl methacrylate
DMF	Dimethylformamid
DMAc	Dimethylacetamid
DP	Degree of polymerization
DSSC	Dye-sensitized solar cell
$\varepsilon$	Extinction coefficient
FRP	Free radical polymerization
FRET	Förster resonance energy transfer
$I_E/I_M$	Excimer emission to monomer emission intensities
IR spectroscopy	Infrared spectroscopy
$k_p$	Polymerization rate

$\lambda$	Wavelength
LCST	Lower critical solution temperature
MAA	Methacrylic acid
macroCTA	Macro chain transfer agents
MALDI-TOF	Matrix assisted laser desorption ionization time of flight
MLV	Multilamellar vesicles
MMA	Methyl methacrylate
$M_n$	Number average molar mass
NIPAM	<i>N</i> - <i>iso</i> -propylacrylamide
NMP	Nitroxide mediated polymerization
NP	Nanoparticle
NMR spectroscopy	Nuclear magnetic resonance spectroscopy
OEGA	Oligo(ethylene glycol) methyl ether acrylate
OEGMA	Oligo(ethylene glycol) methyl ether methacrylate
OLED	Organic light-emitting diode
$\Phi_F$	Quantum yield
PEG	Poly(ethyleneglycol)
PDEGMA	Poly[di(ethylene glycol) methyl ether methacrylate]
PDMAEMA	Poly[2-dimethylaminoethyl methacrylate]
PDI	Polydispersity index
$PDI_{particle}$	Polydispersity of particle size distribution
PMMA	Poly(methyl methacrylate)
PO <sub>x</sub>	Poly(2-ethyl-2-oxazoline)
PS	Polystyrene
PVME	Poly(vinyl methyl ether)
$R_0$	Förster distance
RAFT	Reversible addition fragmentation chain transfer polymerization
RI	Refractive index
SEC	Size-exclusion chromatography
SEM	Scanning electron microscopy
$t$	Time
$T$	Temperature
$T_{CP}$	Cloud point temperature
UV/vis	Electron absorption spectroscopy
ULV	Unilamellar vesicles
$\bar{\nu}$	Wavenumber
$V_{el}$	Elution volume

---

## Curriculum vitae

---



Christian Pietsch

---

### Personal Information

Gender **Male**  
Date of Birth **03<sup>th</sup> January 1984**  
Place of Birth **Naumburg / Saale, Germany**

### Education

10/08 - present **PhD-student, Chemistry, Friedrich-Schiller-University Jena,**  
Laboratory of Organic and Macromolecular Chemistry  
PhD-thesis: "*Design of functional polymer architectures by RAFT Polymerization*", Supervisor: Prof. Dr. Ulrich S. Schubert.

05/10 – 07/10 **Guest researcher at CSIRO, Melbourne, Australia**  
Topic: "*Blockcopolymers via RAFT polymerization*"

11/07 - 08/08 **Execution of diploma thesis, Eindhoven University of Technology,**  
Eindhoven, The Netherlands  
Diploma-thesis: "*Responsive copolymers as soluble polymeric sensors*"

10/03 - 09/08 **Academic degree diploma (equivalence to MSc), Chemistry,**  
*Friedrich-Schiller-University Jena, Germany*  
Specialization: polymer and organic chemistry

08/94 - 07/03 **Aquirement of University-Entrance diploma, Lepsius Gymnasium**  
*Naumburg, Germany*

Jena, 30. April 2013

---

Christian Pietsch



---

## Publication list

---

*Peer-reviewed publications:*

- [01] **C. Pietsch**, R. Hoogenboom, U. S. Schubert "Soluble polymeric dual sensor for temperature and pH value", *Angew. Chem. Int. Ed.* **2009**, *48*, 5653–5656.
- [02] **C. Pietsch**, M. W. M. Fijten, H. M. L. Thjis, R. Hoogenboom, U. S. Schubert "Unexpected reactivity for the RAFT copolymerization of oligo(ethylene glycol) methacrylates", *J. Polym. Sci.; Part A.; Polym. Chem.* **2009**, *47*, 2811–2820.
- [03] **C. Pietsch**, R. Hoogenboom, U. S. Schubert "PMMA based soluble polymeric temperature sensors based on UCST transition and solvatochromic dyes", *Polym. Chem.* **2010**, *1*, 1005–1008.
- [04] U. Mansfeld, **C. Pietsch**, R. Hoogenboom, C. R. Becer, U. S. Schubert "Clickable initiators, monomers and polymers in controlled radical polymerizations – a prospective combination in polymer science", *Polym. Chem.* **2010**, *1*, 1560–1598.
- [05] A. Krieg, **C. Pietsch**, A. Baumgaertel, M. D. Hager, C. R. Becer, U. S. Schubert "Dual hydrophilic polymers based on (meth)acrylic acid and poly(ethylene glycol) – synthesis and water uptake behavior", *Polym. Chem.* **2010**, *1*, 1669–1676.
- [06] **C. Pietsch**, A. Vollrath, R. Hoogenboom, U. S. Schubert "A fluorescent thermometer based on a pyrene-labeled thermoresponsive polymer", *Sensors* **2010**, *10*, 7979–7990.
- [07] R. Menzel, A. Breul, **C. Pietsch**, J. Schäfer, C. Friebe, E. Tauscher, D. Weiß, B. Dietzek, J. Popp, R. Beckert, U. S. Schubert "Blue-emitting polymers based on 4-hydroxythiazoles incorporated in a methacrylate backbone", *Macromol. Chem. Phys.* **2011**, *212*, 840–848.

- [08] M. A. Kostianinen, **C. Pietsch**, R. Hoogenboom, R. J. M. Nolte, J. J. L. M. Cornelissen "Temperature-switchable assembly of supramolecular virus-polymer complexes", *Adv. Funct. Mater.* **2011**, *21*, 2012–2019.
- [09] **C. Pietsch**, U. S. Schubert, R. Hoogenboom "Aqueous polymeric sensors based on temperature-induced polymer phase transitions and solvatochromic dyes", *Chem. Commun.* **2011**, *47*, 8750–8765.
- [10] A. M. Breul, **C. Pietsch**, R. Menzel, J. Schäfer, A. Teichler, M. D. Hager, J. Popp, B. Dietzek, R. Beckert, U. S. Schubert "Blue emission of side-chain pendant 4-hydroxy-1,3-thiazoles in polystyrenes synthesized by RAFT polymerization", *Eur. Polym. J.* **2012**, *48*, 1339–1347.
- [11] I. Y. Perevyazko, A. Vollrath, **C. Pietsch**, S. Schubert, G. M. Pavlov, U. S. Schubert "Nanoprecipitation of poly(methyl methacrylate)-based nanoparticles: effect of the molar mass and polymer behavior", *J. Polym. Sci., Part A: Polym. Chem.* **2012**, *50*, 2906–2913.
- [12] A. Vollrath, D. Pretzel, **C. Pietsch**, I. Y. Perevyazko, R. Menzel, S. Schubert, G. M. Pavlov, D. Weiß, R. Beckert, U. S. Schubert "Preparation, cellular internalization and biocompatibility of highly fluorescent PMMA nanoparticles", *Macromol. Rapid Commun.* **2012**, *33*, 1791–1797.
- [13] A. Vollrath, A. Schallon, **C. Pietsch**, S. Schubert, T. Nomoto, Y. Matsumoto, K. Kataoka, U. S. Schubert "A toolbox of different sized and labeled PMMA nanoparticles for cellular uptake investigations", *Soft Matter*, **2013**, *9*, 99–108.
- [14] **C. Pietsch**, U. Mansfeld, C. Guerrero-Sanchez, S. Hoepfener, A. Vollrath, M. Wagner, R. Hoogenboom, S. Saubern, S. H. Thang, C. R. Becer, J. Chiefari, U. S. Schubert "Thermo-induced self-assembly of responsive poly(DMAEMA-*b*-DEGMA) block copolymers into multi- and uni-lamellar vesicles", *Macromolecules*, **2012**, *45*, 9292–9302.
- [15] D. Heine, **C. Pietsch**, U. S. Schubert, W. Weigand "Controlled radical polymerization of styrene-based models of the active site of the [FeFe]-hydrogenase", *J. Polym. Sci., Part A: Polym. Chem.* **2013**, *51*, 2171–2180.

- [16] **C. Pietsch**, J. Schäfer, R. Menzel, R. Beckert, J. Popp, B. Dietzek, U. S. Schubert "Förster resonance energy transfer in donor-acceptor 1,3-thiazole dyes in poly(methyl methacrylates)", *J. Polym. Sci., Part A: Polym. Chem.* **2013**, *51*, 4765–4773.

*Submitted publication:*

- [17] M. Wagner, **C. Pietsch**, L. Tauhardt, A. Schallon, U. S. Schubert "Characterization of cationic polymers for gene delivery by asymmetric flow field-flow fractionation and analytical ultracentrifugation", *J. Chromatogr. A*, manuscript submitted.

*Publication under preparation:*

- [18] **C. Pietsch**, M. Wagner, U. Mansfeld, C. Guerrero-Sanchez, S. Hoepfener, J. Chiefari, U. S. Schubert "Thermo- and pH-induced self-assembly of responsive poly(DMAEMA-*b*-DEGMA) block copolymers into vesicular structures", manuscript under preparation.

*Non-refereed publications:*

- [19] R. Hoogenboom, **C. Pietsch**, U. S. Schubert "Temperature responsive poly(oligoethylene glycol methacrylate)s: From unexpected reactivities to dual sensors" *PMSE Prepr.* **2009**, *101*, 1035–1036.
- [20] **C. Pietsch**, R. Menzel, A. M. Breul, M. D. Hager, R. Beckert, U. S. Schubert "Blue emitting thiazole based copolymers by RAFT polymerization" *Polym. Prepr.* **2012**, *242*, 210–211.
- [21] S. Schubert, A. Vollrath, I. Perevyazko, **C. Pietsch**, J. T. Delaney, G. M. Pavlov, U.S. Schubert "High-throughput nanoprecipitation of functional polymers" *Polym. Prepr.* **2012**, *242*, 282–283.
- [22] A. Krieg, **C. Pietsch**, M. D. Hager, C. R. Becer, U. S. Schubert "Dual hydrophilic polymers based on (meth)acrylic acid and poly(ethyleneglycol) – synthesis and water uptake behavior" *Polym. Prepr.* **2012**, *242*, 357–358.

*Oral contributions:*

- [01] C. Pietsch, M. W. M. Fijten, R. Hoogenboom, U. S. Schubert "Responsive copolymers as dual sensors", **HTE DPI meeting**, *Darmstadt*, Germany, June **2009**.
- [02] C. Pietsch, H. M. L. Thjis, M. W. M. Fijten, R. Hoogenboom, U. S. Schubert "Responsive copolymers as soluble polymeric sensors", **EPF conference**, *Graz*, Austria, July **2009**.
- [03] C. Pietsch, H. M. L. Thjis, M. W. M. Fijten, R. Hoogenboom, U. S. Schubert "Temperature responsive poly(oligoethylene glycol methacrylate)s: From unexpected reactivities to dual sensors", **Evonik Röhm GmbH**, *Darmstadt*, Germany, August **2009**.
- [04] C. Pietsch, R. Menzel, R. Hoogenboom, R. Beckert, U. S. Schubert "Polymeric sensors based on polymer phase transition and thiazole dyes", **EPF conference**, *Granada*, Spain, June **2011**.
- [05] C. Pietsch, J. Schäfer, R. Menzel, A. Schallon, R. Hoogenboom, R. Beckert, U. S. Schubert, "RAFTing macromolecular architectures", **HTE DPI meeting**, *Darmstadt*, Germany, June **2012**.

*Poster presentations:*

- [01] C. Pietsch, M. W. M. Fijten, R. Hoogenboom, U. S. Schubert "Responsive copolymers as soluble polymeric sensors", **DPI annual meeting**, *Antwerpen*, Belgium, November **2008**.
- [02] C. Pietsch, M. W. M. Fijten, R. Hoogenboom, U. S. Schubert "Responsive copolymers as soluble polymeric sensors", **ABC**, *Basel*, Switzerland, January **2009**.
- [03] C. Pietsch, M. W. M. Fijten, R. Hoogenboom, U. S. Schubert "Responsive copolymers as soluble polymeric sensors for temperature and pH value", **CRP meeting**, *Ol Fosse d'Outh, Houffalize*, *Belgium*, September **2009**.



- [04] C. Pietsch, M. W. M. Fijten, R. Hoogenboom, U. S. Schubert “Responsive copolymers as soluble polymeric sensors for temperature and pH value”, **DPI annual meeting**, *Eindhoven*, The Netherlands, November **2009**.
- [05] C. Pietsch, R. Menzel, A. M. Breul, R. Beckert, U. S. Schubert “New blue emitting polymers based on 4-hydroxythiazoles incorporated in methacrylate backbones”, **DPI annual meeting**, *Bergen op Zoom*, The Netherlands, November **2010**.
- [06] C. Pietsch, C. Guerrero-Sanchez, A. Vollrath, U. Mansfeld, S. Hoepfner, R. Hoogenboom, J. Chiefari, U. S. Schubert, “Thermo-induced self-assembly of stimuli-responsive block copolymers of poly(DEGMA-*b*-DMAEMA)”, **DPI annual meeting**, *Zeist*, The Netherlands, November **2011**.
- [07] C. Pietsch, D. Heine, W. Weigand, U. S. Schubert, “Controlled Radical Polymerization of Styrene-Based Models of the Active Site of the [FeFe]-Hydrogenase”, **DPI annual meeting**, *Zeist*, The Netherlands, November **2012**.



---

## Acknowledgement / Danksagung

---

An dieser Stelle möchte ich ein paar Worte des Danks an die Menschen richten, die zum Gelingen dieser Arbeit beigetragen haben.

Zuerst möchte ich mich bei meinem wissenschaftlichen Betreuer Prof. Dr. Ulrich S. Schubert für die Möglichkeit bedanken, meine Doktorarbeit in seiner Arbeitsgruppe anfertigen zu dürfen. Er hat mir die Möglichkeit gegeben ein spannendes und hochinteressantes Thema zu bearbeiten, wobei ich viel Freiraum für eigene Ideen und Vertrauen bei der Ausgestaltung bekam und dafür vielen Dank Uli.

Weiterhin möchte ich mich für die Einbindung in gemeinsame Projekte und Kooperationen, die damit verbundenen zahlreichen Diskussionen und Anregungen, welche zum Gelingen dieser Arbeit beigetragen haben, bedanken. Namentlich gilt mein Dank dem Proexzellenz Projekt „PhotoMic“, dem *Dutch Polymer Institut (DPI)*, sowie Evonik und der BASF SE. Insbesondere danke ich dem DPI für die finanzielle Unterstützung.

I would like to thank my direct supervisor Prof. Richard Hoogenboom during my PhD time for his important contribution, his huge knowledge and for all the discussions. We had fruitful video conference, mostly Friday morning with the first cup of coffee. I would like to say thank you for replying to my questions with prompt emails and the continuous support over the last years.

Dear Dr. Remzi Becer and dear Dr. Carlos Guerrero-Sanchez I would like to say at this point thank you very much for initiating the idea to do my research stay in Melbourne, Australia at the *Commonwealth Scientific and Industrial Research Organization (CSIRO)*. I'm really grateful for the possibility to spend some month in the group of Dr. San H. Thang and Dr. John Chiefari and to work together with you, Carlos. I really enjoyed working in "Down Under", learned the RAFT agent synthesis with  $\text{CS}_2$  and for new achievement in RAFT polymerization. I especially thank Carlos, Simon, San, Christina, Matthias, Erika and Christian for the nice atmosphere, the good and successfully time in Australia.

Ferner gilt ein großes Dankeschön den Kooperationspartnern des „PhotoMic“ Projektes. Ich möchte mich bei Prof. Rainer Beckert, Prof. Benjamin Dietzek und Prof. Jürgen Popp ganz herzlich für Gespräche, Anregungen und die intensive Zusammenarbeit bedanken. Ganz besonders möchte ich mich an dieser Stelle bei Roberto Menzel für die exzellente Zusammenarbeit und die Einblicke in die Welt der Thiazolfarbstoffe bedanken. Für den

Ausflug in die zeitaufgelöste Spektroskopie, in Energietransferraten und noch viel mehr Physik, möchte ich Johann Schäfer sehr danken. Es war immer sehr angenehm mit dir zusammen zuarbeiten. Hier sei besonders Alexander Breul erwähnt, mit dem ich zusammen dieses faszinierende Projekt bearbeiten durfte.

Prof. Wolfgang Weigand, Ihnen und ihrer Arbeitsgruppe möchte ich herzlich danken, vor allem Daniel Heine für zahlreiche Synthesen der [FeFe]-Hydrogenase Modelle, die vielen Diskussionen, die Erforschung der Polymerisationsmöglichkeiten dieser Systeme und die zahlreichen gemeinsamen Studien.

Ferner gilt ein großes Dankeschön den Mitarbeitern der Arbeitsgruppe, die wesentlich zum Gelingen dieser Arbeit beigetragen haben. Uli Mansfeld und Dr. Stephanie Höppener für sehr viele Stunden des Messens meiner Proben am cryo-TEM. Es sind so tolle Bilder entstanden! An dieser Stelle möchte ich nochmal die sehr gute Zusammenarbeit mit euch erwähnen, ohne diese hätten wir nicht so erfolgreich das Manuskript anfertigen können. Antje Vollrath und Igor Perevyazko möchte ich für den Ausflug in die Welt der Nanopartikel danken. Sie sind ein Teil meiner Dissertation geworden und ich konnte viele neue Einblicke gewinnen, wobei ich das Potential dieser Nanotransporter erleben konnte. Dr. Anja Schallon und Dr. David Pretzel danke ich für die vielen Einblicke in die Biologie, die Ihr für mich als „Vollblutchemiker“ doch etwas näher und auch verständlicher gemacht habt. Anja, ich möchte mich an dieser Stelle für dein Vertrauen in meine Fähigkeiten, deine große Unterstützung und die zahlreichen Kooperationen, welche zu sehr tollen Ergebnissen führten und führen werden, bedanken.

Bei Conny Bader möchte ich mich für das Gefühl als „Oberarzt“ bedanken, da sie nach meiner Synthesepanung die Reaktionsapparatur aufbaute und ich nur für die Zugabe des Schwefelkohlenstoffs durch eine Spritze gerufen wurde. Anschließend erhielt ich 2 Tage später das isolierte Zwischenprodukt. Das war ein tolles Gefühl.

Ich möchte mich bei Dr. Grit Festtag und Nicole Fritz für tadellos arbeitende SEC Systeme und für das Messen der NMR Spektren (auch bei verschiedenen Temperaturen) und die Benutzung des 300 NMR Spektrometers bei Dr. Wolfgang Günther Gabriele Sentis und Birgit Friedrich bedanken. Michael Wagner und Antje Vollrath möchte ich für viele DLS und Zeta-Potential Messungen danken.

Ferner gilt mein Dank Dr. Anja Baumgaertel und Katrin Knop für MALDI Analysen, Renzo Paulus für DSC Untersuchungen, Christian Friebe für Cyclovoltammetrie Messungen und für angefertigten AAS-Analysen möchte ich Sandra Köhn danken. Ich schulde auch dank meiner Hiwi-Studentin Leonore Steuer für die Hilfe im Labor. Den Hausmeistern gilt ebenfalls ein besonderer Dank für den fast täglichen Transport der Chemikalien vom Institut zum TO.

Ganz vielen lieben Dank an meinen Labor-Kollegen Katrin und Andreas. Wir haben zusammen das Labor 3.21 eingeräumt und fast die ganze Promotionszeit zusammen gearbeitet. Dabei haben wir SEC Kurven, die mehr nach den Alpen aussahen, autopolymerisierte Monomer, einen größeren Wasserschaden im Labor und ganz viel Musik erlebt (bei so mancher Auswahl musste ich allerdings flüchten). Auch wenn öfters die Pipetten, Stifte und Rührfische von Katrin „gemopst“ wurden (ab dem Zeitpunkt musst ich die Polymerisation immer ohne durchführen ☺), hatten wir eine sehr schöne Zeit. An die merkwürdige Sache mit der Acetonflasche („Katrin du weißt wovon ich rede“) kann ich mich noch gut erinnern. Unser „Wikipedia-Lexikon Andreas“ werde ich sehr vermissen. Wir hatten viele gemeinsamen RAFT Sessions und auch immer Streit um die Heißluftpistole. Mit dir war es eine super Zeit, die ich nie vergessen werde. Auch die zwei „neuen“ Sarah und Tobi, welche jetzt in meinem Abzug arbeiten „dürfen“ möchte ich mich für die gute Arbeitsatmosphäre bedanken. Sarah, ich fand es toll, dass ich dir die RAFT beibringen konnte. Bitte behalte dein Lachen, damit begeisterst du alle im Gebäude. Tobi, wenn es mit deinen Lebensmittelfarbstoffen nicht klappt, dann iss sie einfach alle auf, es merkt keiner. Für euch zwei schreibe ich hier noch folgendes: „Bassline-junkie“ und das werde ich nicht vergessen.

Auch meinen Büro-Kollegen: Andreas, Anke, Hendrik, Markus und Tobi möchte ich für die schöne Zeit danken. Wir haben öfters viel gelacht, just in diesem Moment denke ich wie ich z. B. die Mirkowelle und den Wasserkocher gleichzeitig an gemacht habe und wir einen „Feuerball“ sehen durften... Markus, du bekommst zuerst viel Respekt, wie du die anionische Polymerisation aufgebaut hast, ist echt klasse und vor allem das bisher noch nix explodiert ist ☺. Unsere Leidenschaft für die Gitarre und das „rumklimpern“ im Büro hat uns zusammengeschweißt und eine tolle Freundschaft entstehen lassen. Anke, entschuldige dass wir dich so oft geärgert haben, aber insgesamt hatten wir doch einigen Spaß. Chris, du bist ja immer öfters bei uns im Büro, bei dir möchte ich mich für die tollen Motto-Partys bedanken.

Insgesamt möchte ich mich bei der „Schubert-group“ für die tolle Atmosphäre und die zahlreich zusammen verbrachten Stunden bedanken. Sei es beim Grillen vorm TO, auf so manch einer Cocktail-Party, beim Kubb oder Volleyball spielen oder in der Havanna-Bar. Vielen, vielen Dank. Die gemeinsame Zeit hinterlässt aber auch sein Spuren, ihr seid mir alle ans Herz gewachsen. Ohne euch wäre alles nur halb so schön gewesen: Antje, Berny, Torsten, Kristian, Matthias, Renzo, Bobby, Sofia, BANja, Christine, Lutz, Caro, Uli, Sebastian, Igor, Mirko, Stefan, Franzi, David, Tobias, Benedikt, Esra, Stephanie, Jürgen und Anna.

So Antje nun kommen wir nochmal zu dir, unserem "Flummy", danke für die viele gute Laune, deine Begeisterung und Lebensenergie und die vielen lustigen Momente die wir zusammen verbracht haben. Die legändere Schneeballschlacht werde ich nicht vergessen. Die Radtouren mit dir Matthias waren immer toll und eine super Ablenkung vom Chemiealltag. Liebe Anja, an dieser Stelle möchte ich mich nochmals bei dir bedanken für die großartige Unterstützung und dein Vertrauen in mein Chemiewissen. Du hast tolle Ideen und ich „durfte“ sofort loslegen größere Mengen an Polymeren zu synthetisieren. Ich wünsche dir viel Erfolg und Kraft bei deinen ehrgeizigen Vorhaben. Uwe, Martin und Micha euch gebührt Dank für zahlreiche Hilfestellung bei synthetischen Problemen und ein immer offenes Ohr zum diskutieren. Einen Dank möchte ich auch (T)Anja, Sylvia und Tanja aussprechen für das erfolgreiche managen der gesamten Gruppe.

Auch meinen vielen Freunden in Jena möchte ich danken, vor allem Andy, Carsten, Ulle, Harry, Daniel, Roberto, Dirk und Kristina. Wir haben eine tolle Zeit zusammen erlebt. Andy, Carsten und Ulle euch gebührt besonderer Dank für die vielen Mountainbike-Touren die wir unternommen haben um ein wenig abzuschalten.

Ein ganz besonderes Dankeschön möchte ich an dieser Stelle an meine Familie richten für den großen Rückhalt und dass ihr mir in jeder Hinsicht beigestanden habt. Ihr habt mich unterstützt wo ihr konntet, auch wenn ihr wenig von Chemie oder Polymeren verstanden habt, ihr wusstet dass es mein Lebensweg werden wird.

Die letzten Zeilen gehören allein meiner wunderbaren Freundin Alex. Du hast es geschafft mir in allen erdenklichen Situationen viel Rückhalt zugeben. Ohne deine großartige Unterstützung, deine Ermutigungen und deine Kraft hätte ich es nicht so erfolgreich geschafft. Vielen Dank für deine Sichtweise auf verschiedenste Dinge, deine „Antennen“ und die vielen Diskussion über Chemie und Biologie. Du bist mein Licht am Horizont.

---

## **Declaration of authorship / Selbstständigkeitserklärung**

---

Ich erkläre, dass ich die vorliegende Arbeit selbständig und unter Verwendung der angegebenen Hilfsmittel, persönlichen Mitteilungen und Quellen angefertigt habe.

I certify that the here presented work is, to the best of my knowledge, original and the results of my own investigations, except as acknowledged, and has not been submitted, either in part or whole, for a degree at this or any other university.

Jena, 30. April 2013

---

Christian Pietsch





---

## Publications P1-P12

---

- P1:** *Polym. Chem.* **2010**, *1*, 1560–1598. Reproduced by permission of The Royal Society of Chemistry.
- P2:** *Chem. Commun.* **2011**, *47*, 8750–8765. Reproduced by permission of The Royal Society of Chemistry.
- Cover:** *Chem. Commun.*, **2011**, 8706. Reproduced by permission of The Royal Society of Chemistry.
- P3:** *Macromol. Chem. Phys.* **2011**, *212*, 840–848. Reprinted with permission. Copyright © 2011 WILEY-VCH Verlag GmbH & Co. KGaA, Weinheim.
- Cover:** *Macromol. Chem. Phys.* **2011**, *Vol. 212, Issue 8*. Reprinted with permission. Copyright © 2011 WILEY-VCH Verlag GmbH & Co. KGaA, Weinheim.
- P4:** *Eur. Polym. J.* **2012**, *48*, 1339–1347. Reprinted with permission. Copyright © 2012 Elsevier.
- P5:** *J. Polym. Sci., Part A: Polym. Chem.* **2013**, *51*, 4765–4773. Reprinted with permission. Copyright © 2013 Wiley Periodicals, Inc.
- P6:** Open access journal.
- P7:** *J. Polym. Sci., Part A: Polym. Chem.* **2013**, *51*, 2171–2180. Reprinted with permission. Copyright © 2013 Wiley Periodicals, Inc.
- Cover:** *J. Polym. Sci., Part A: Polym. Chem.* **2013**, *Vol. 51, Issue 10*. Reprinted with permission. Copyright © 2013 Wiley Periodicals, Inc.
- P8:** Reprinted with permission from *Macromolecules*, **2012**, *45*, 9292–9302, Copyright © 2012 American Chemical Society.
- Cover:** Reprinted with permission from *Macromolecules*, December 11, **2012** Vol. 45, No. 23. Copyright © 2012 American Chemical Society.
- P9:** *Polym. Chem.* **2010**, *1*, 1669–1676. Reproduced by permission of The Royal Society of Chemistry.
- P10:** *J. Polym. Sci., Part A: Polym. Chem.* **2012**, *50*, 2906–2913. Reprinted with permission. Copyright © 2012 Wiley Periodicals, Inc.
- P11:** *Macromol. Rapid Commun.* **2012**, *33*, 1791–1797 and *Macromol. Rapid Commun.* **2013**, *34*, 280. Reprinted with permission. Copyright © 2012 WILEY-VCH Verlag GmbH & Co. KGaA, Weinheim.
- P12:** *Soft Matter*, **2013**, *9*, 99–108. Reproduced by permission of The Royal Society of Chemistry.



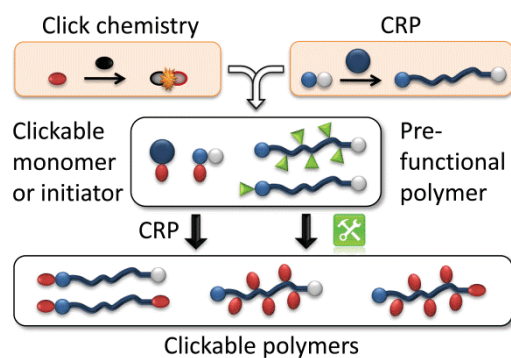
## Publication P1:

*Clickable initiators, monomers and polymers in controlled radical polymerizations – a prospective combination in polymer science*

---

U. Mansfeld, C. Pietsch, R. Hoogenboom, C. R. Becer, U. S. Schubert

*Polym. Chem.* **2010**, *1*, 1560–1598





# Clickable initiators, monomers and polymers in controlled radical polymerizations – a prospective combination in polymer science

Ulrich Mansfeld,<sup>abc</sup> Christian Pietsch,<sup>abc</sup> Richard Hoogenboom,<sup>b</sup> C. Remzi Becer<sup>\*ab</sup> and Ulrich S. Schubert<sup>\*abc</sup>

Received 30th May 2010, Accepted 2nd July 2010

DOI: 10.1039/c0py00168f

Preparation of multifunctional and well-defined macromolecules requires a smart selection of the most suitable controlled polymerization technique in combination with appropriate click reactions. In this review, we provide an overview on the use of various “clickable” initiators and monomers as well as on the postpolymerization modifications that have been widely used to construct clickable macromolecules. As such, this contribution will aid polymer chemists to select a suitable combination of CRP and click methodologies to design the target structures.

## 1. Introduction

The synthesis of well-defined polymers has been the ultimate challenge of polymer chemists in the last decades. The development of anionic polymerization by Szwarc *et al.* opened new avenues and a new field of materials research.<sup>1,2</sup> Besides, polymeric materials have improved the quality of our lives in all areas from engineering to electronics and medical applications.<sup>3–5</sup> Following the invention of anionic polymerization, other possible types of living and/or controlled polymerizations, cationic and radical, have been widely studied.<sup>6–9</sup> The most significant controlled radical polymerization (CRP) techniques to date could be listed as atom transfer radical polymerization (ATRP),<sup>6–8</sup> nitroxide-mediated radical polymerization (NMP)<sup>9,10</sup>

and reversible addition-fragmentation chain transfer polymerization (RAFT).<sup>11,12</sup> Each of these techniques requires the use of a dedicated metal/ligand complex, chain transfer agent (CTA) or nitroxide mediator to gain control over the polymerization of various monomeric structures. All these parameters have been extensively investigated in detail and reported by numerous research groups. Consequently, nowadays well-defined polymers can be successfully synthesized and characterized by performing these techniques under specific conditions.

After significant advances in the controlled/“living” radical polymerization techniques over the last years, functionalization of the macromolecules has been the following challenge for polymer chemists. Synthesis of end- or side-functional macromolecules has been achieved by using functional initiators, monomers or end capping techniques. However, these specific functional groups might have enormous effects on the polymerization rate, control over the polydispersity index and the composition of the polymers. Fortunately, a decade ago, the click chemistry concept was introduced by Sharpless *et al.* that enables nowadays the preparation of not only telechelic polymers but also side-group functionalized polymers using clickable initiators, monomers or polymers.<sup>13–21</sup> Sharpless and coworkers

<sup>a</sup>Laboratory of Organic and Macromolecular Chemistry, Friedrich-Schiller-University Jena, Humboldtstr. 10, 07743 Jena, Germany. E-mail: ulrich.schubert@uni-jena.de; c.r.becer@warwick.ac.uk

<sup>b</sup>Laboratory of Macromolecular Chemistry and Nanoscience, Eindhoven University of Technology, P. O. Box 513, 5600 MB Eindhoven, The Netherlands

<sup>c</sup>Dutch Polymer Institute (DPI), P. O. Box 902, 5600 AX Eindhoven, The Netherlands



Ulrich Mansfeld

Ulrich Mansfeld studied chemistry at the Friedrich-Schiller-University Jena (Germany; 2003–2008) and accomplished the master thesis at the Eindhoven University of Technology (Netherlands) under the supervision of Prof. Ulrich S. Schubert. In 2009, he began his PhD studies working in the fields of controlled radical polymerizations and supramolecular chemistry.



Christian Pietsch

Christian Pietsch studied chemistry at the Friedrich-Schiller-University Jena (Germany). He completed his MSc in 2008 at the University of Technology in Eindhoven (Netherlands), where he worked on the synthesis of stimuli-responsive copolymers under the supervision of Prof. Ulrich S. Schubert. He continued as a PhD student in Jena working on responsive copolymers as well as living radical polymerization and dye-labeled polymers. Recently, he spent two months at CSIRO (Melbourne, Australia), where he carried out research on RAFT polymerizations.

drew attention to several highly efficient organic reactions, such as the copper-catalyzed [3 + 2] Huisgen cycloaddition reaction (CuAAC), which has developed into the most widely employed click reaction.<sup>22,23</sup> This reaction requires a copper salt and a ligand as catalysts but proceeds very rapidly and selectively at room temperature.<sup>24</sup> Several other efficient organic reactions have been claimed to be “click” reactions since they fulfilled all or some of the click chemistry criteria, which can be listed as modular and wide in scope, high efficiency and high yields, no or inoffensive byproducts, stereospecific, readily available starting materials and reagents, no solvent or a benign solvent, and simple purification techniques.<sup>17</sup>

Metal-free click reactions have attracted the greatest attention in recent years since they eliminate the main disadvantage of CuAAC click reactions: the use of a copper catalyst.<sup>17,25</sup> This opens new avenues to rapid and efficient reactions that can be

employed in, *e.g.*, living organisms.<sup>26</sup> Several types of metal-free click-like reactions have been developed and the most prominent ones are thiol-ene,<sup>19,27,28</sup> thiol-yne,<sup>29,30</sup> thiol-*para*-fluoro,<sup>31,32</sup> nitrile oxide-alkyne cycloaddition,<sup>33</sup> pyridyl disulfide exchange,<sup>34–36</sup> and Diels–Alder reactions.<sup>37–39</sup> These reactions have pros and cons in comparison to each other. Each of them can be used for certain monomers, initiators or polymerization techniques. Therefore, one should carefully design the synthetic route to prepare the desired functional polymer.

The aim of this review is to provide an insight on the selection of the most suitable CRP technique and click reaction for the synthesis of the desired tailor-made macromolecule. The range of functional initiators and monomers are listed in tables for each CRP technique. Hereby, click reactions performed before (“preclick”) and after (“postclick”) the polymerization initiated by a functional initiator or propagated with a functional monomer are discussed. The special focus will be on the combinations of CRP and click chemistry techniques rather than discussing each of them in details.

## 2. Overview on click reactions used in combination with controlled radical polymerization techniques

In the following section the click reactions that have been used in combination with CRP are briefly summarized while referring to the original literature (Scheme 1).

The most widely applied click reaction has been the copper-catalyzed azide-alkyne 1,3-dipolar cycloaddition (CuAAC) as shown in Scheme 1.<sup>40</sup> Sharpless *et al.* defined this type of cycloaddition as the ideal click reaction and the reaction principle has been employed in various fields of synthetic chemistry, *i.e.* medicinal chemistry, polymer chemistry, material chemistry, inorganic chemistry and, in particular, organic chemistry.<sup>13</sup> This reaction proceeds very rapidly in aqueous medium and even under ambient conditions. The major drawback of this reaction



**Richard Hoogenboom**

*Richard Hoogenboom was born in 1978 in Rotterdam (Netherlands) and studied chemical engineering at the Eindhoven University of Technology (TU/e; Netherlands). In 2005, he obtained his PhD under the supervision of Ulrich S. Schubert (TU/e) and continued working as project leader for the Dutch Polymer Institute. After postdoctoral training with Martin Möller at the RWTH Aachen (Humboldt fellowship) and Roeland J. M. Nolte at the Radboud University Nijmegen*

*(NWO veni-grant), he was appointed as associate professor at Ghent University from July 2010. His research interests include stimuli-responsive polymers, supramolecular polymers, and poly(2-oxazoline)s.*



**C. Remzi Becer**

*C. Remzi Becer was born in 1980 in Izmir, Turkey. He received his BSc degree in 2003 at the Chemistry Department of the Istanbul Technical University (ITU). In 2005, he received his MSc degree in Polymer Science and Technology at the ITU. He completed his PhD study titled as “Controlling Polymer Architectures” in 2009 under the supervision of Ulrich S. Schubert at the Eindhoven University of Technology (Netherlands) and the Friedrich-Schiller-University Jena*

*(Germany). Since late 2009, he has been a Marie Curie Research Fellow in the University of Warwick (United Kingdom). His research interests include controlled living polymerization techniques, click reactions and glycopolymers.*



**Ulrich S. Schubert**

*Ulrich S. Schubert was born in Tübingen in 1969. He studied chemistry at the Universities of Frankfurt and Bayreuth (both Germany) and the Virginia Commonwealth University, Richmond (USA). His PhD thesis was executed at the University of Bayreuth and the University of South Florida Tampa. After postdoctoral training with Professor Lehn at the Université Strasbourg (France) he moved to the Technische Universität München (Germany) to obtain*

*his Habilitation in 1999. From 1999 to 2000 he held a temporal position as professor at the Center for NanoScience, Universität München (Germany). From 2000 to 2007 he was Full-Professor at the Eindhoven University of Technology. Currently he holds a chair at the Friedrich-Schiller-University Jena.*

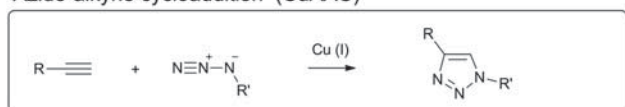
is the necessity of using a copper salt, which requires a purification step following the click reaction.<sup>41</sup>

Nevertheless, this drawback can be overcome by choosing alkynes with higher reactivity. For instance, cyclooctyne derivatives can undergo strain-promoted azide-alkyne click reactions in biological environments.<sup>42</sup> Similarly, electron-deficient alkynes and activated alkynes also provide highly efficient reactions.<sup>43</sup> Apparently, alkyne compounds play a crucial role in many different click-like reactions. As an example, Tunca and Hizal *et al.* demonstrated the synthesis of A<sub>2</sub>-B<sub>2</sub> 4-miktoarm star copolymers using the Glaser coupling as an alkyne-alkyne homocoupling reaction (AAC),<sup>44</sup> which is a copper-catalyzed reaction that reaches completion at room temperature in three

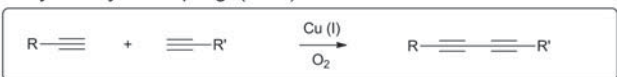
days.<sup>45</sup> Recently, Lutz and Heaney *et al.* reported the cycloaddition of alkynes with nitrile oxides (NOAC)<sup>46</sup> in combination with CRP as a potential click reaction.<sup>33</sup> This reaction proceeds at room temperature, in polar medium, in the absence of transition metal catalyst, in high yields and is highly regioselective. Besides alkynes, also nitriles can react with azides in a zinc-catalyzed cycloaddition<sup>47</sup> and can be used in combination with CRP.<sup>48</sup>

Alkynes do not only react with azides<sup>49</sup> or its own kind but also react with thiols, known as thiol-yne click reaction.<sup>29,30</sup> This represents a very efficient reaction and results in addition of two thiol compounds per alkyne molecule, which can be either added by a base-catalyzed Michael addition or by a photo-initiated

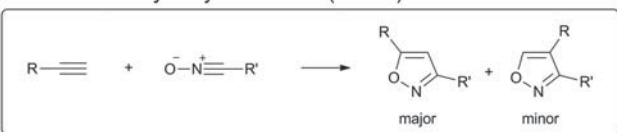
#### Azide-alkyne cycloaddition (CuAAC)



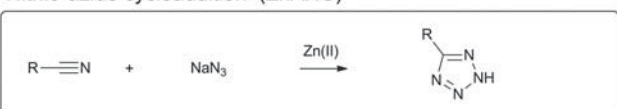
#### Alkyne-alkyne coupling (AAC)



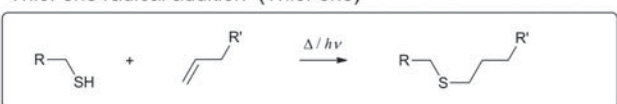
#### Nitrile oxide-alkyne cycloaddition (NOAC)



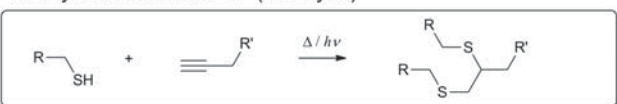
#### Nitrile-azide cycloaddition (ZnANC)



#### Thiol-ene radical addition (Thiol-ene)



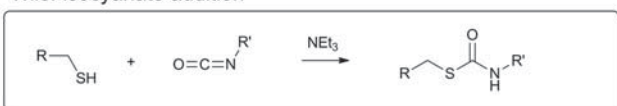
#### Thiol-yne radical addition (Thiol-yne)



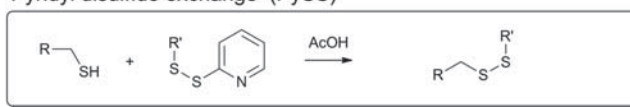
#### Michael addition (MAdd)



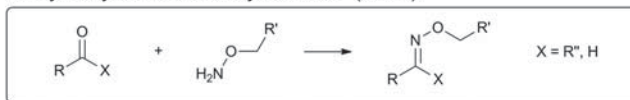
#### Thiol-isocyanate addition



#### Pyridyl disulfide exchange (PySS)



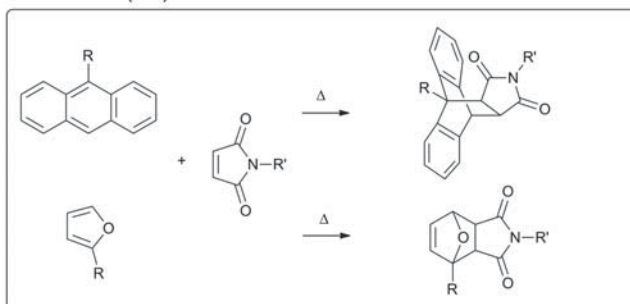
#### O-Hydroxylamine-carbonyl addition (Oxim)



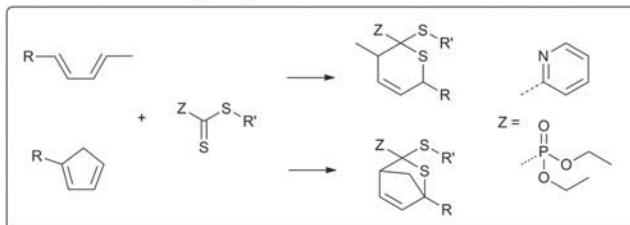
#### Ring-opening reaction of epoxides (RO)



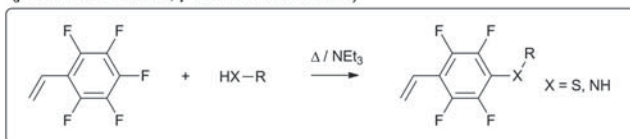
#### Diels Alder (DA)



#### Hetero Diels Alder (HDA)



#### para-Fluoro-nucleophile substitution (para-fluoro-thiol, para-fluoro-amine)



**Scheme 1** Schematic representation of the click reactions that have been used in combination with controlled radical polymerization techniques.

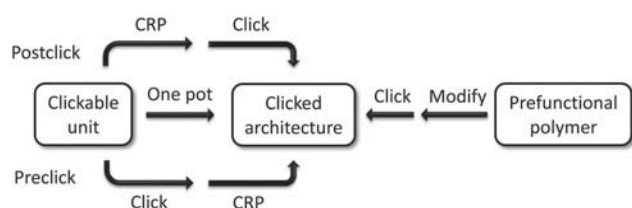
Anti-Markovnikov-addition.<sup>29,50</sup> Thiol compounds have been in the focus of click reactions in the last couple of years due to their high reactivity towards common functional groups, *i.e.* alkene, alkyne, isocyanate and pentafluorophenyl.<sup>51</sup> The thiol-ene click reaction has been utilized by several groups for the synthesis of dendrimers, the side-chain functionalization of well-defined backbones and for the synthesis of block copolymers.<sup>19,28,52</sup> Advantages and disadvantages of this type of click reaction have been discussed in several review articles.<sup>10,53</sup> Other thiol-based click reactions can be counted as thiol-maleimide addition (MAdd),<sup>28</sup> thiol-isocyanate addition<sup>54</sup> and pyridyl disulfide exchange (PySS).<sup>36</sup> Thiol-terminated polymers can be easily obtained by RAFT polymerization of a wide range of monomers and a subsequent cleavage of the chain transfer agent. However, hetero Diels–Alder (HDA) reaction using a dedicated chain transfer agent can be employed without a transformation of the RAFT agent to prepare AB block copolymers.<sup>55</sup> Commonly, the Diels–Alder reaction (DA) has been employed to construct miktoarm star polymers<sup>56</sup> or to engineer self-healing polymers by reversible crosslinking.<sup>57</sup>

A frequently used reaction for bioconjugation is the oxime formation (Oxim) that has been applied in the conjunction of carbonyl-functionalized proteins and aminoxy-functionalized polymers.<sup>58</sup> Furthermore, the ring-opening reaction of epoxides as a well-known spring-loaded reaction<sup>13</sup> is used in combination with the CRP of glycidyl methacrylate mostly to introduce other clickable functionalities<sup>59</sup> or for attachment on surfaces.<sup>60</sup>

In practice, some combinations of click reactions and CRP techniques are most commonly applied which will be discussed in detail in the following sections.

### 3. Strategies towards clicked polymer architectures

There are at least four common ways to combine controlled radical polymerization techniques and click chemistry to construct various clicked polymeric architectures. Thereby, each approach has its inherent drawbacks and amenities. The strategies are summarized in Scheme 2 and will be discussed in a general way in the following.



**Scheme 2** Schematic representation of the strategies towards clicked architectures.

#### 3.1 Postclick strategy

By using functional initiators or monomers with clickable moieties for controlled radical polymerizations, clickable polymers can be achieved to construct various architectures by clicking post to the polymerization.

As a limitation, the clickable functionality must not interfere with the polymerization process or has to be protected to gain

control over the polymerization and, thus, yielding well-defined polymers with high functional group fidelity up to sufficient monomer conversions. Moreover, most functional monomers or initiators are not commercially available and have to be synthesized prior to the polymerization.

The clickable polymer represents a platform for versatile click functionalization, while retaining the polymer characteristics *i.e.* chain length, monomer composition and molar mass dispersity. Herein, the approach has a wide scope by means of construction flexibility, in contrast to the preclick approach (see below), since different functional polymers can be prepared from a single batch of a clickable macromolecule. Furthermore, the same molar mass and its distribution allow for a better comparison of changes related to the functionality.

The postclick approach offers high functional group fidelity compared to the postmodification approach. In particular, for the polymerization of clickable monomers each repeating unit of the resultant polymer bears the clickable unit in contrast to a prefunctional homopolymer that have to be modified with the clickable moiety after polymerization. Accordingly, using  $\alpha$ -functionalized initiators each chain is monoterminally functionalized, while end-group functionalization *via* the postmodification are limited by the yield of the final modification step.

#### 3.2 Preclick strategy

Clicked polymeric architectures can be also obtained by using functional initiators or monomers with clickable moieties that are clicked prior to the polymerization in a so-called “preclick” route. This method is predominantly used if the clickable units interfere with the radical process or the temperature of the polymerization and can not be sufficiently protected.

As a limitation, the clicked moiety must be stable under the applied polymerization conditions. It should be mentioned that Diels–Alder adducts tend to undergo retro Diels–Alder reactions at elevated temperatures and, hence, are not in principle amenable for this strategy. However, the stability range of the Diels–Alder adducts is strongly system dependent.<sup>61,62</sup> Recently, some literature examples discussed the polymerizability and stability of related clicked initiators and monomers. Maleimide functionalities are often protected by the reversible Diels–Alder reaction with furan to make it more compatible with radical polymerization processes, which was demonstrated by Sanyal and coworkers using a furan-maleimide methacrylate. This monomer was polymerized by a free radical polymerization procedure at 65 °C and deprotected *via* retro-DA at 125 °C.<sup>63</sup> Syrett *et al.* reported an ATRP reaction with a clicked initiator linked *via* the maleimide-furan adduct, where the polymerization was successfully performed at 50–60 °C and the retro Diels–Alder reaction occurred at 120 °C.<sup>64</sup> By using a clicked initiator with the maleimide-anthracene adduct significantly higher thermal stability was observed upon the retro Diels–Alder reaction. In addition, Barner-Kowollik *et al.* investigated a hetero Diels–Alder cycloadduct of a dithioester and cyclopentadiene that was rapidly formed at room temperature and cleaved above 80 °C.<sup>65</sup> By contrast, the Huisgen 1,3-dipolar cycloaddition of alkynes with azides represents a prominent reaction for this strategy, since the triazole ring is stable under the typically applied polymerization conditions. Furthermore, the bulkiness of the clicked unit should



not disturb the polymerization process by causing slow propagation or deactivating of the catalytic system.

In case the clicked monomers can be successfully polymerized *via* CRP, this procedure provides the highest control over the incorporation of the clicked functionality into polymeric architectures, while having the lowest scope by means of construction flexibility:

On the one hand, the click reaction has been performed with small molecules (monomers or initiators) that can be easily purified and analyzed. Hereon, subsequent polymerization is carried out with less reactive material leading to high functional-group fidelity, whereby no further functionalization is required. However, in order to obtain clicked architectures with different clicked functionalities, the click reaction as well as the polymerization has to be carried out for each clicked architecture. This method has been successfully employed for the preparation of comb-shaped polymers with almost quantitative functionalization of each repeating unit.<sup>66,67</sup>

### 3.3 Simultaneous/one pot strategy

In many cases the catalyst used in the ATRP polymerization, *i.e.* CuBr/PMDETA (*N,N,N',N'',N'''* pentamethyldiethylene triamine), is the same as for the click reaction that allows a simultaneous/one-pot process of polymerization and click reaction. The combination of the Cu(I)-catalyzed Huisgen cycloaddition and a CRP process allows the one-pot synthesis of a wide range of products, *i.e.*  $\alpha$ -functional- (clickable initiator), grafted- (clickable monomer), star-shaped polymers and polymeric networks, respectively. The simultaneous process means that CRP and click reaction occur at the same time during the polymer synthesis. In contrast to a one-pot process, whereas at first the polymerization and then the click reaction are performed or *vice versa* (subsequent addition of the second compound). The advantage of this strategy in contrast to the “preclick” or “postclick” way is that for clicked polymeric architectures only one synthesis step and one purification step is required. However, it should be noted that the click reaction generally proceeds much faster than the ATRP and, thus, most click coupling reactions will occur during the initial stages of the polymerization.

The first example of this combined route was demonstrated by Haddleton *et al.* in 2005 using an azide-functionalized ATRP initiator for the polymerization of methyl methacrylate as indicated by a linear relationship of the first order kinetic plot. The efficiency of the click reaction was investigated in the presence of alkyne-functional dyes.<sup>68</sup> Another example of simultaneous click and CRP with an unprotected propargyl methacrylate was also reported by Haddleton *et al.* It was shown that the copper-catalyzed azide-alkyne click reaction proceeds much faster compared to the ATRP.<sup>69</sup> The authors could also show that the ratio of rate constants for the polymerization and the click process can be controlled by varying the solvent, the temperature or the concentration of the catalyst. Thus, it was demonstrated that the rate of CuAAC in DMSO is slower than the polymerization, whereas in DMF or toluene the click reaction is faster than the polymerization. The measured PDI values of the synthesized copolymers were found to be below 1.3.<sup>69</sup> As a limitation, the clickable functionality must be used without a protection group to allow the Huisgen cycloaddition and, hence, side reactions can occur.

Also the one-pot/tandem process is often used for the preparation of clicked polymeric architectures by using ATRP polymerization and CuAAC. This approach uses the same catalytic system for both the click reaction as well as ATRP, but sequentially. Thereby, both ways are possible: At first the click reaction followed by the polymerization or *vice versa* (in the manner that the second compound was added later). In contrast, if all components are added at once, the click reaction can be performed at room temperature, while after full conversion, the temperature was raised to initiate the polymerization.<sup>70</sup> In all cases well-defined copolymers were obtained. Dubois *et al.* discussed these different routes and showed that both the preclick as well as the one-pot route give similar results in molar mass and PDI values, whereby the postclick route leads to an increase of the polydispersity index from 1.3 to 1.5.<sup>70</sup>

### 3.4 Postmodification strategy

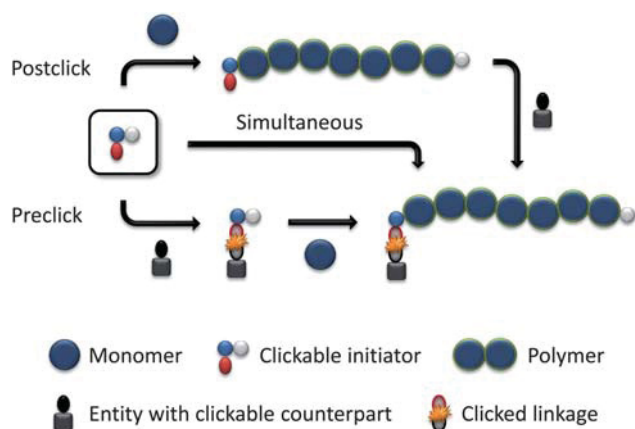
Prefunctional polymers with latent groups prepared by CRP can be modified with clickable moieties to obtain clickable polymers. The modification reaction must be efficient, since it correlates to the fidelity of functional groups in the modified polymer. Mostly, purification steps are necessary, since even efficient modification reactions are not quantitative. In this case, modification as well as clicking are carried out at the polymer, which might complicate in principle the purification and analysis. In particular, incomplete modification is critical for pendant functional polymers, since the unreacted functionalities are attached to the same polymer backbone as the converted ones and, thus, can not be separated as it can be done for endgroup-modified polymers.

As an advantage, the starting materials by means of initiators and monomers are in most cases commercially available or can be easily synthesized allowing for large scale experiments. This approach can be used for terminal and pendant functionalized polymers, except for comb-shaped polymers, since electronic and steric effects may hinder full transformation. This method is in particular suitable for clicked architectures where the clickable as well as the clicked moiety interfere with the polymerization process.

It should be noted that in a narrower sense the described reactions are defined as click reactions for the conjunction of small molecules, since they feature among other characteristics a high efficiency and selectivity allowing for the equimolar usage of the click counterparts. However, the conjunction of polymers using these reactions leads not always to full conversion probably due to sterical hindrance or affected diffusion of the polymer chains.<sup>53</sup> To drive the reaction to completion, an excess of one clickable polymer can be used. If the click reaction is completed, the typical problems of purification due to the equal solubility behavior of both product and educt polymer can be overcome by adding a click-functionalized resin containing the click counterpart related to the excess one.<sup>71,72</sup> The subsequent purification of the desired clicked architecture can be then easily performed by filtration of the clicked resin.

## 4. Clickable initiators

The use of functional initiators in controlled radical polymerization processes lead to terminal-functionalized polymers in one



**Scheme 3** Schematic representation of the strategies using clickable initiators.

step. Thereby, two possible routes can be employed using clickable initiators. As illustrated in Scheme 3, click reactions can be performed either after the polymerization (postclick) or prior to the polymerization (preclick). For ATRP initiators only  $\alpha$ -clickable polymers are inherently possible in one step. With the ability of the synthesis of initiators/transfer agents for NMP and RAFT with functional groups on both the initiating as well as on the mediating fragment the toolbox expands and  $\omega$ -clickable polymers as well as  $\alpha,\omega$ -clickable polymers are accessible in a one step procedure. The advantage of the clickable initiator approach compared to the clickable monomer route is the lower concentration of the clickable unit. Hence, side reactions are reduced and protection is not strictly necessary while leading to a controlled polymerization with a high degree of functionalization of the clickable moiety. In the following, an overview of potential clickable initiators is given and is summarized in Tables 1 to 7. Possible combinations and the restrictions of CRP and click reactions are discussed. Unless otherwise noted, all selected initiators belong to the postclick approach.

#### 4.1 Atom transfer radical polymerization (ATRP)

ATRP is the most widely employed CRP technique using the clickable initiator approach because of the easy preparation of functional initiators. Different types of initiators are discussed in the following subsections (Tables 1–3).

**Alkyne-functionalized initiators.** The first report on the combination of click chemistry and a controlled radical polymerization technique was published by van Hest *et al.* in 2005 showing the facile approach towards block copolymers *via* the azide-alkyne cycloaddition.<sup>73</sup> By using propargyl 2-bromoisobutyrate (Entry 1) as clickable initiator terminal alkyne-functionalized polystyrenes and polyacrylates were synthesized. The initiator is based on a common ATRP initiator group, which is an  $\alpha$ -halo ester. The terminal alkyne was protected with a trimethylsilyl group (TMS) to prevent possible side reactions under the polymerization conditions: (i) Complexation with the copper catalyst,<sup>73–75</sup> (ii) subsequent homocoupling of alkynes,<sup>44</sup> (iii) chain transfer by hydrogen abstraction from the alkyne<sup>76</sup> and interference with propagating radicals leading to crosslinking.<sup>77</sup>

Nevertheless, the TMS group was found to be instable under the polymerization conditions using CuBr/PMDETA as catalyst that leads to a loss of protecting group up to 70%.<sup>78</sup> The loss was ascribed to a nucleophilic attack to the TMS group by one of the nitrogen atoms of PMDETA. As a consequence, the less nucleophilic ligand bipyridine (bpy) was chosen to reduce the deprotection although it is not the optimum catalyst for ATRP reactions and does not avoid the decomposition completely.<sup>78</sup> Another strategy uses the more stable triisopropylsilyl group (TIPS) instead of TMS revealing no loss during the polymerization.<sup>78</sup> This might be due to the bulky character of the protecting group that hinders the nucleophilic attack of the metal/ligand complex. The alkyne-functionalized initiators bearing either a chlorine or a bromine atom as an initiating moiety were frequently reported for the polymerization of styrene, acrylates, methacrylates and *N*-isopropylacrylamide, whereby in some cases the terminal alkyne was protected with TMS<sup>33,44,76,79,80</sup> or not protected.<sup>81–86</sup> Haddleton and coworkers used the unprotected alkyne initiator depicted in Entry 1 for the random copolymerization of methyl methacrylate (MMA) and hostasol methacrylate (HMA) ( $M_n = 15\,000\text{ g mol}^{-1}$ , PDI = 1.2–1.3).<sup>82</sup> The  $\alpha$ -functionalized fluorescent copolymer was clicked onto cotton and both Wang and Merrifield resins using the Huisgen [2 + 3] cycloaddition. Recently, Tunca and coworkers used the protected initiator (Entry 1) for the preparation of block copolymers of styrene and divinylbenzene to form multiarm star polymers with terminal alkyne groups.<sup>87–89</sup> At first, styrene was polymerized to obtain linear alkyne-functional PS (up to  $M_n = 6\,000\text{ g mol}^{-1}$ , PDI = 1.1). Subsequently, the prepared PS was used as macroinitiator in the polymerization of divinylbenzene leading to a crosslinked second block that form the core of the multiarm star polymer (up to  $M_w = 250\,000\text{ g mol}^{-1}$ , PDI = 1.2). Besides the initiator depicted in Entry 1, its analogue propargyl 2-halopropionate (Entry 2) was also used as clickable initiator for the polymerization of acrylates and NIPAM without any protection.<sup>90,91</sup>

In most cases of the unprotected initiators, good control over the polymerization was achieved yielding alkyne-functional polymers with low PDI values. In these cases, the undesired chain transfer and termination reactions are suppressed to a negligible amount by decreasing the reaction time<sup>84</sup> and keeping the polymerization at low conversions to reduce the termination reactions at the  $\omega$ -end of the chain. The bromine atom is often substituted in a postmodification reaction with sodium azide to yield heterotelechelic polymers bearing an alkyne and an azide end group, respectively. Furthermore, side reactions involving the alkyne functionality were suppressed by using low alkyne concentrations according to a high monomer-to-initiator ratio<sup>92</sup> or by using relatively low temperatures,<sup>85,91</sup> *i.e.* 40 °C for the polymerization of *t*BMA<sup>85</sup> or NIPAM.<sup>91</sup> In contrast, the polymerization of styrene was conducted for 6 h at 90 °C with the initiator depicted in Entry 1 as nonprotected alkyne initiator revealing significant termination reactions as indicated by SEC measurements.<sup>86</sup> It should be noted that direct polymerization throughout the triple bond is hindered, because radical transfer reactions from the styrene or methacrylate radical are suppressed by their low reactivity (Q-values, r-values).

Most of the alkyne-functionalized ATRP initiators are based on the  $\alpha$ -halo isobutyrate group. This class of alkyl halides possesses high activation rates due to the suitable radical-stabilization

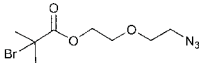
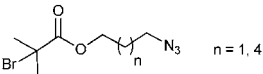
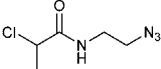
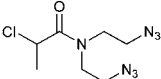
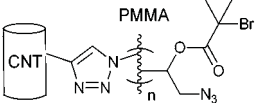
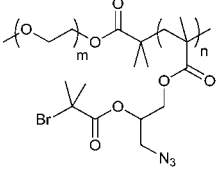
**Table 1** Alkyne-containing initiators for ATRP (poC = postclick, prC = preclick, simult = simultaneous)

Entry	Structure	Click	CRP	Monomer (Abbr./Entry)	Strategy	Ref
1		CuAAC	ATRP	St, MA, OEGA <i>t</i> BA, NIPAM, <i>t</i> BMA, DEAEMA, HMA	poC	73,76,78–81, 83–89,103,104
		AAC NOAC	ATRP ATRP	St St	poC poC	44 33
2		CuAAC	ATRP	NIPAM, EEA	poC	90,91
3		CuAAC	ATRP	NIPAM, <b>46</b> , <b>53</b>	prC	95
4		CuAAC	ATRP	St, <i>t</i> BA, MMA	simult	96
5		CuAAC	ATREP	St, VBA, <b>50</b>	simult	83
6		CuAAC	ATRP	St	poC	97
7		CuAAC	ATRP	St	poC	98
8		CuAAC	ATRP	MMA	prC	99
9		CuAAC	ATRP ROP	St, MMA, <i>t</i> BA DMAEMA, NIPAM	poC	71,94,100
			ATRP ROP	St	prC	101
10		CuAAC	ATRP	<i>t</i> BA	poC	102

effects of the tertiary carbon and the vicinal ester group resulting in a high initiation efficiency, which is required to control molar masses and molar mass distributions.<sup>93</sup> In most of the present cases, this type of initiator is used for ATRP regardless of the

polymerized monomer class, *e.g.* styrenes, acrylates or methacrylates. However, normally the initiator structure is carefully chosen for each given monomer and its reactivity.<sup>6,93</sup> Therefore, special focus appear not to be on the optimal initiator structure for

**Table 2** Azide-containing initiators for ATRP (poC = postclick, prC = preclick, simult = simultaneous)

Entry	Structure	Click	CRP	Monomer	Strategy	Ref
11		CuAAC	ATRP	DMAEMA, St	poC	92,106,107
12		CuAAC	ATRP	MMA, DEAEMA, HEMA, KSPMA, HMA, NIPAM, DMAEMA, DEAM, St	poC, simult	68,82,94,109–112
13		CuAAC	ATRP	NIPAM	poC	113
14		CuAAC	ATRP	NIPAM	poC	110
15		CuAAC	ATRP	St, <i>n</i> BMA	poC, prC	114
16		CuAAC	ATRP	DEGMA	poC	104

control, but on the accessibility of an alkyne-functionalized one. Practically,  $\alpha$ -bromoisobutyryl bromide is commercial available and is mostly functionalized *via* esterification reaction with propargyl alcohol.

The most widely employed catalytic system is CuBr and PMDETA again regardless of the initiator or monomer type. Besides, other catalytic systems, *e.g.* CuCl/tris(2-(dimethylamino)-ethyl)amine (Me<sub>6</sub>TREN) for the polymerization of NIPAM<sup>91,94</sup> or 1,1,4,7,10,10-hexamethyltriethylenetetramine (HMTETA),<sup>44</sup> could provide better control over the polymerizations. The catalytic activity of the metal complex and, hence, the ability to control the polymerization can be correlated to the ability to stabilize the Cu(II) oxidation state, thus forming a reducing Cu(I) complex.<sup>93</sup> The polymerization can proceed relatively fast even at low temperatures when a catalyst with a high activity is used.<sup>6</sup> PMDETA is a good ligand for Cu(I) with moderate activity between the less active bpy (two magnitudes lower in activation rate) and the more active Me<sub>6</sub>TREN (two magnitudes higher in activation rate) and, therefore, can be used for a wide range of monomers.<sup>93</sup>

Besides the attachment of propargyl alcohol, the alkyne moiety can also be incorporated onto an ATRP initiator by the

reaction of propargyl amine with  $\alpha$ -haloisobutyryl halides. An example is shown in Entry 3.<sup>95</sup> Hereby, a combination of the pre- and the postclick approach was utilized. The initiator was clicked prior to the polymerization with azide-functionalized dansyl as a fluorescent label. By using this compound as initiator in ATRP different random copolymers of alkyne- or azide-functionalized acrylamides were obtained: Poly(NIPAM-*r*-propargylacrylamide) ( $M_n = 20\,000\text{ g mol}^{-1}$ , PDI = 1.3) and poly[NIPAM-*r*-(3-azidopropylacrylamide)] ( $M_n = 10\,000\text{ g mol}^{-1}$ , PDI = 1.2). The pendant clickable polymers were attached onto an azide-functionalized silica particle in an elegant layer-by-layer click approach to yield thermoresponsive microcapsules after removal of the silica template.<sup>95</sup>

In Entry 4 an initiator is shown where the alkyne is linked to the mediating bromide *via* an *o*-nitrobenzyl ester as a photo-cleavable group.<sup>96</sup> The initiator was used in a one-pot click-CRP reaction for the polymerization of either St, *t*BA or MMA in the presence of azide-functionalized PEO or PS to prepare photo-cleavable block copolymers as clicked structures with the labile group between the polymer blocks: PEO-*b*-PS ( $M_n = 38\,000\text{ g mol}^{-1}$ , PDI = 1.2), PEO-*b*-*t*BA ( $M_n = 63\,000\text{ g mol}^{-1}$ , PDI = 1.2), PS-*b*-PMMA ( $M_n = 38\,000\text{ g mol}^{-1}$ , PDI = 1.2–1.3).

The initiator can bear more than one alkyne functionality. Multifunctional initiators can be used to create two or three dimensional architectures such as star polymers or networks. The initiator depicted in Entry 5 contains two bromoisobutyrate groups as well as two propargyl groups (unprotected alkynes) and is used in atom transfer radical emulsion polymerization in water to synthesize crosslinked nanoparticles of styrene and vinylbenzyl azide.<sup>83</sup> An example that can be better analyzed by means of molar mass and its polydispersity index is described for the initiator depicted in Entry 6 bearing both two alkyne and two bromoisobutyrate groups. The polymerization of styrene was carried out for 2 h at 110 °C without the protection of the terminal alkyne groups ( $M_n = 4\,000\text{ g mol}^{-1}$ , PDI = 1.1–1.2), while the subsequent alkyne-azide cycloaddition leads to figure-of-eight-shaped polymers.<sup>97</sup>

Another alkyne-functionalized initiator (Entry 7) is functionalized with one bromoisobutyrate as well as two propargyl groups.<sup>98</sup> Thereby, one alkyne moiety was clicked with an azide-functionalized poly(ethyleneglycol) (PEG) and was subsequently utilized in the polymerization of styrene without protecting the second alkyne moiety that resulted in a “tadpole-shaped” architecture after the second click reaction.<sup>98</sup>

In addition, a trialkyne-functionalized initiator (Entry 8) was synthesized by the substitution reaction of propargyl

bromide with pentaerythritol followed by the attachment of  $\alpha$ -bromoisobutyryl bromide on the remaining alcohol groups.<sup>99</sup> The initiator was used in a preclick approach: First, azido-PS prepared by RAFT ( $M_n = 2\,500\text{ g mol}^{-1}$ , PDI = 1.1) was clicked onto the initiator. Thereby, the molar mass distribution increased to 1.2 due to the presence of small amounts of macroinitiator, where only two PS-chains were attached. Subsequently, the PS-macroinitiator was used in the polymerization of MMA to yield 4-arm stars ( $M_n = 34\,000\text{ g mol}^{-1}$ , PDI = 1.3–1.4). The high polydispersity was assigned to a lack of control in the initial stages of the polymerization.

Furthermore, alkyne-functionalized initiators were combined with other polymerization techniques or methods by incorporating, *e.g.*, alcohol groups for ring-opening polymerization (ROP) (Entry 9), whereby the polymerization techniques do not interfere with each other and can be applied simultaneously<sup>100</sup> or subsequently.<sup>101</sup> Besides the incorporation of  $\alpha$ -haloisobutanoyl halides (halide = Cl, Br) into small molecules they can also be incorporated into alcohol-functionalized polymers to form ATRP macroinitiators as shown in Entry 10.<sup>102</sup> In this example, polystyrene was synthesized *via* anionic polymerization and functionalized with propargyl bromide and  $\alpha$ -bromoisobutanoyl bromide to provide an alkyne-functionalized ATRP macroinitiator. Polymerization of *t*BA yielded mid-chain alkyne-

**Table 3** Other click-functionalized initiators for ATRP (poC = postclick, prC = preclick)

Entry	Structure	Click	CRP	Monomer (Abbr./Entry)	Strategy	Ref
17		DA MAdd	ATRP ATRP	<i>t</i> BA, MMA OEGMA, 45, SMA	poC prC poC	115,117,120,121,125 64 66,122,123
18		MAdd	ATRP	NIPAM	prC	35,58
19		DA	ATRP	St, MMA	poC	87,89,121,124,125
20		DA	ATRP	St	–	126
21		Thiol-ene	ATRP	St, MMA	poC	127
22		PySS	ATRP	St, <i>t</i> BMA, MMA	poC prC	34,128,129 35,58
23		Oxim	ATRP	NIPAM, HEMA, OEGMA	poC	131,132

functionalized PS-*b*-PtBA block copolymers ( $M_n = 15\,000\text{ g mol}^{-1}$ , PDI = 1.2–1.3).

**Azide-functionalized initiators.** The cycloaddition counterparts to the alkyne-functionalized initiators are azide-functionalized ones. The common procedure for their syntheses is the functionalization of a basic framework with (i) an azide *via* substitution reaction of an alkyl halide with sodium azide and (ii) with  $\alpha$ -haloisobutyrate as the ATRP initiating fragment *via* esterification of an amine or alcohol function.

One can mistrust the requirement of azide-functionalized initiators, since the azide functionality can be easily and efficiently introduced by substitution of the mediating halide with sodium azide. However, the degree of azide functionalization that can be reached with the initiator approach is higher compared to the postmodification route. The reason lies in the nature of controlled radical polymerizations: Termination reactions always occur and, hence, not all polymer chains retain the halide at the  $\omega$ -terminus which is the bottleneck for the degree of functionalization that can be reached *via* postmodification. In contrast, using functional initiators, every chain that is initiated by the initiator bears the azide moiety at the  $\alpha$ -terminus independently from termination reactions.

The azide moiety is used without protection during polymerization, although some side reactions were described: (i) Cyclization reactions between the azide and the propagating radical that causes low initiator efficiency,<sup>68,92</sup> (ii) 1,3-cycloaddition of azides with the double bond of the monomer occurs in the absence of a catalyst at high temperatures and long reaction times, at which the amount decreases in the order of acrylates > acrylamides >> methacrylates > styrenes.<sup>105</sup>

To reduce the side reactions to a negligible amount, short reaction times<sup>92,106</sup> and low temperatures<sup>92,107</sup> are preferably used. It was shown that the polymerization at room temperature completely suppressed side reactions involving the azide.<sup>108</sup> Hence, monomer classes are favored that can be polymerized at moderate temperatures.

In contrast, it was shown that the azide group does not act as an initiating species itself as indicated by controlled polymerizations with an azide-containing initiator.<sup>92</sup>

The initiator structure depicted in Entry 11 (top) was used for the polymerization of *N,N*-dimethylamino-2-ethyl methacrylate (DMAEMA)<sup>92,106</sup> in THF with CuBr/HMTETA at 60 °C in a controlled way (PDI = 1.1–1.3). However, the initiator efficiency was low ( $f = 0.4$ ) due to intramolecular cyclization at the early stages of the polymerization involving the azide and the propagating radical.<sup>92</sup> Therefore, the “preclick” method was utilized to circumvent these side reactions as the azide-functionalized initiator was “clicked” onto an alkyne-functionalized poly( $\epsilon$ -caprolactone) (PCL). As expected, an increase in the initiation efficiency to  $f = 0.85$  could be observed when using the “clicked” PCL macroinitiator.<sup>92</sup> This is a good example where the preclick method is used since the postclick route failed in parts due to side reactions involving the clickable unit.

The initiator structure depicted in Entry 11 (bottom) containing a cleavable *p*-alkoxybenzyl ester was used in bulk polymerization of styrene at 90 °C, whereby no termination reactions were observed ( $M_n = 4\,000\text{ g mol}^{-1}$ , PDI = 1.1–1.2).<sup>107</sup>

The spacer between the initiating fragment and the azide function seems to have a significant influence on the initiation efficiency in terms of intramolecular cyclization: The initiator depicted in Entry 12 shows, despite a controlled polymerization of MMA ( $M_n = 6\,000\text{ g mol}^{-1}$ , PDI = 1.2–1.3), a reduced initiation efficiency for the hexyl spacer (70 to 80%) compared to the propyl spacer (100%).<sup>68</sup> Hence, the initiator efficiency can be optimized by choosing an initiator structure by means of a spacer that prevents cyclization in the early stages of the polymerization.

In Table 2, 3-azidopropyl 2-bromoisobutyrate (APBIB) has been the most widely used azide-functionalized initiator (Entry 12,  $n = 1$ ). Controlled polymerization of St ( $M_n = 4\,500\text{ g mol}^{-1}$ , PDI = 1.3),<sup>109</sup> NIPAM ( $M_n = 10\,000\text{ g mol}^{-1}$ , PDI = 1.1–1.2),<sup>110</sup> and DMAEMA ( $M_n = 10\,000\text{ g mol}^{-1}$ , PDI = 1.1–1.2) have been reported.<sup>111</sup>

Moreover, Haddleton and coworkers used the azide-functionalized initiator depicted in Entry 12 for the random copolymerization of MMA and hostasol methacrylate (HMA) ( $M_n = 8\,000\text{ g mol}^{-1}$ , PDI = 1.2).<sup>82</sup> The  $\alpha$ -functionalized fluorescent copolymer was clicked onto cotton and both Wang and Merrifield resins using Huisgen [2 + 3] cycloaddition.

In addition, Topham and coworkers have polymerized a number of acrylates and methacrylates (MA) in a controlled way using APBIB as initiator:<sup>112</sup> 2-Aminoethyl methacrylate hydrochloride ( $M_n = 7\,000\text{ g mol}^{-1}$ , PDI = 1.1–1.2), 2-(diethylamino)ethyl methacrylate (DEAEMA) ( $M_n = 21\,000\text{ g mol}^{-1}$ , PDI = 1.3), DMAEMA ( $M_n = 7\,000\text{ g mol}^{-1}$ , PDI = 1.3), 2-hydroxyethyl methacrylate (HEMA) ( $M_n = 7\,000\text{ g mol}^{-1}$ , PDI = 1.3), 2-hydroxypropyl methacrylate (HPMA) ( $M_n = 5\,000\text{ g mol}^{-1}$ , PDI = 1.2), 2-(methacryloyloxy)ethyl phosphorylcholine ( $M_n = 15\,000\text{ g mol}^{-1}$ , PDI = 1.2), glycerol monomethacrylate ( $M_n = 11\,000\text{ g mol}^{-1}$ , PDI = 1.2), potassium 3-sulfopropyl methacrylate (KSPMA) ( $M_n = 20\,000\text{ g mol}^{-1}$ , PDI = 1.2), and methyl chloride-quaternized 2-(dimethylamino)-ethyl methacrylate ( $M_n = 5\,000\text{ g mol}^{-1}$ , PDI = 1.2).

Furthermore, 2-chloropropionamide linked with an ethyl spacer to the azide moiety (Entry 13) was utilized in the controlled polymerization of NIPAM ( $M_n = 12\,000\text{ g mol}^{-1}$ , PDI = 1.3).<sup>113</sup> The *N,N*-diazido-2-chloropropionamide (Entry 14) was used in the polymerization of NIPAM to incorporate two azide functionalities on the same chain end ( $M_n = 10\,000\text{ g mol}^{-1}$ , PDI = 1.1)<sup>110</sup> In this way, 3-arm star polymers can be prepared.

Besides the initiators discussed above, there are also azide-functionalized macroinitiators available. An elegant example of a multi-clickable initiator that is attached to a carbon nanotube (CNT) is shown in Entry 15.<sup>114</sup> Poly(glycidyl methacrylate) (PGMA) is functionalized in a ring-opening reaction with sodium azide and subsequently reacted with 2-bromoisobutyryl bromide to yield a multi-clickable polymeric macroinitiator. This multi-azide-functionalized polymer was clicked onto a multialkyne-functionalized CNT, whereby the excess of azide functions over the alkyne ones preserve free azides on the surface of the carbon nanotube. This coated CNT was used to click PEG in a grafting-onto approach as well as to polymerize St or *n*BMA in a grafting-from approach to yield amphiphilic polymer brushes on carbon nanotubes.

A similar macroinitiator was prepared from a copolymer (PEG-*b*-PGMA), whereby the poly(glycidyl methacrylate) was functionalized in a ring-opening reaction with sodium azide and subsequently reacted with 2-bromoisobutryl bromide to yield a multi-clickable polymeric macroinitiator (Entry 16).<sup>104</sup> Polymerization of DEGMA yielded azide-functionalized PEO-*b*-[PGMA-*g*-(N<sub>3</sub>)(PDEGMA)] ( $M_n = 52\,000\text{ g mol}^{-1}$ , PDI = 1.2). In a grafting-onto approach alkyne-functionalized PDEAEMA was attached *via* click reaction to obtain coil-rod double hydrophilic diblock copolymers.

**Maleimide-functionalized initiators.** Another frequently used click reaction is the Diels–Alder reaction that becomes more and more prominent in combination with controlled radical polymerizations in the field of material science.<sup>57,115–121</sup>

A widely used example is the [4 + 2] cycloaddition of maleimide and anthracene, whereby both moieties can be used as clickable functions attached to common ATRP initiators. The maleimide function must be protected, since it can act as a polymerizable monomer leading to crosslinking and a significant decrease of clickable fidelity after polymerization.<sup>122</sup> Therefore, the maleimide is protected prior to the polymerization *via* Diels–Alder reaction with furan that can be easily cleaved after the polymerization in a retro Diels–Alder reaction by heating the protected polymer. Besides, the maleimide can also undergo Michael addition with thiols as a Michael acceptor (Entry 17, 18).<sup>35,58,66,122,123</sup>

An often used maleimido initiator is depicted in Entry 17. In general, the maleimide was attached to 2-bromoisobutyrate in a stepwise fashion. At first, maleic anhydride reacts with furan to protect the double bond. Subsequently, the imide was formed with ethanolamine under reflux and as the last step commercially available 2-bromoisobutryl bromide was reacted.<sup>122</sup> This protected initiator was utilized *via* the postclick approach in the homopolymerization of MMA<sup>115,117,120,121</sup> (up to  $M_n = 3\,000\text{ g mol}^{-1}$ , PDI = 1.1–1.2), OEGMA (up to  $M_n = 32\,000\text{ g mol}^{-1}$ , PDI = 1.2),<sup>122</sup> (2,2-dimethyl-1,3-dioxolan-4-yl)methyl methacrylate (up to  $M_n = 35\,000\text{ g mol}^{-1}$ , PDI = 1.2),<sup>122</sup> *t*-butyl acrylate (*t*BA)<sup>115</sup> (up to  $M_n = 3\,000\text{ g mol}^{-1}$ , PDI = 1.2) and the random copolymerization of different methacrylates<sup>66,123</sup> containing protected alkyne, ketosol and hostasol or rhodamine B as fluorescent dyes ( $M_n = 10\,000\text{ g mol}^{-1}$ , PDI = 1.2). In none of these cases, side reactions were observed or discussed. Furthermore, this initiator was used in preclick approaches by Haddleton and coworkers for the polymerization of MMA at 50 °C (up to 55 000 g mol<sup>-1</sup>, PDI < 1.2).<sup>64</sup> Thereby, the alcohol-functionalized maleimide was clicked *via* DA reaction with an alcohol-functionalized furan or anthracene moiety and was subsequently reacted with 2-bromoisobutryl bromide to obtain clicked dual-initiators with ATRP-mediating moieties on both click counterparts.

The anthracene-functionalized initiator depicted in Entry 19 was synthesized from commercially available 9-anthracenemethanol and 2-bromoisobutryl bromide<sup>124</sup> and was utilized in the homopolymerization of MMA<sup>87,124</sup> (up to  $M_n = 30\,000\text{ g mol}^{-1}$ , PDI = 1.1) and styrene<sup>121</sup> ( $M_n = 5\,000\text{ g mol}^{-1}$ , PDI = 1.1).

Tunca and coworkers used the initiator shown in Entry 19 for the preparation of block copolymers of styrene and divinylbenzene to form multiarm star polymers with terminal anthracene

groups.<sup>125</sup> At first, styrene was polymerized to obtain linear anthracene-functional PS (up to  $M_n = 6\,000\text{ g mol}^{-1}$ , PDI = 1.1). Subsequently, the prepared PS was used as macroinitiator in the polymerization of divinylbenzene leading to a crosslinked second block that form the core of the multiarm star polymer (up to  $M_w = 75\,000\text{ g mol}^{-1}$ , PDI = 1.5). Furthermore, anthracene functional PS (prepared with the initiator shown in Entry 19) as well as alkyne functional PS (prepared with the initiator shown in Entry 1) were used as macroinitiators for the ATRP of divinylbenzene yielding multiarm star polymers with terminal alkyne and anthracene groups ( $M_w = 250\,000\text{ g mol}^{-1}$ ).<sup>89</sup> The orthogonality of the two clickable groups were utilized in a sequential double click reaction to selectively attach azide-functionalized P*t*BA and maleimide-functionalized PMMA.

In addition, commercially available 9-chloromethylanthracene was applied as initiator in the polymerization of styrene ( $M_n = 4\,500\text{ g mol}^{-1}$ , PDI = 1.2) using CuCl/bpy as catalytic system in THF (Entry 20).<sup>126</sup> Although the prepared polymers were not yet applied in a Diels–Alder reaction, the terminal anthracene moiety represents a potential group for this click reaction.

**Ene-functionalized initiators.** Since the thiol-ene reaction is a rather new type of click reaction, only one example of an ATRP initiator was published so far to the best of our knowledge (Entry 21).<sup>127</sup> Hawker and coworkers reported an alkene-containing  $\alpha$ -bromoisobutyrate type of initiator. The polymerization of St and MMA was carried out yielding terminal alkene-functionalized polymers. In a postmodification reaction with sodium azide, the  $\omega$ -bromide could be easily exchanged with an azide moiety to form a heterotelechelic clickable polymer. The orthogonality of the subsequent thiol-ene and CuAAC click reaction was proven by stepwise “clicking”, whereby the thermal thiol-ene reaction was preferred due to possible side reactions of the alkyne during UV-light exposure.

**Pyridyl-disulfide-functionalized initiators.** Another click-like reaction that is used in combination with ATRP is the pyridyl disulfide exchange which is important in particular in bioconjugation.<sup>128,129</sup> It is a metal-free reaction and can be considered as a click reaction in a broader sense. The reaction is not an oxidative radical coupling reaction of thiols but a nucleophilic exchange reaction, whereby the formed thiolate must be a good leaving group. It is reported that pyridyl disulfides are known to undergo direct coupling with free thiols under ambient conditions in bioconjugation, whereby 2-pyridinethione is released as a good leaving group.<sup>34</sup> The pyridyl disulfide moiety can be considered as a protected thiol and can be used in radical polymerizations. However, side reactions in terms of chain coupling and transfer involving the disulfide were observed at high conversions and at high amounts of catalyst (catalyst to initiator ratio of 1 : 1). Side reactions could be reduced by using less catalyst<sup>130</sup> (catalyst to initiator ratio of 1 : 0.2) or by changing the catalytic system from CuBr/bpy to CuCl/bpy<sup>34</sup> which decreases the amount of free radicals.

An ATRP initiator with a pyridyl disulfide moiety is depicted in Entry 22 and was introduced by Maynard and coworkers.<sup>34</sup> It was used for the homopolymerization of MMA ( $M_n =$

10 000 g mol<sup>-1</sup>, PDI = 1.2), *N*-acetyl-*D*-glucosamine-functionalized methacrylate<sup>128</sup> ( $M_n = 13\,000$  g mol<sup>-1</sup>, PDI = 1.1), *N*-hydroxysuccinimidyl methacrylate<sup>129</sup> ( $M_n = 10\,000$  g mol<sup>-1</sup>, PDI = 1.3), 2-THP-protected HEMA<sup>129</sup> ( $M_n = 10\,000$  g mol<sup>-1</sup>, PDI = 1.3), *t*-butyl methacrylate (*t*BMA)<sup>129</sup> ( $M_n = 5\,000$  g mol<sup>-1</sup>, PDI = 1.5), HEMA<sup>34</sup> ( $M_n = 16\,000$  g mol<sup>-1</sup>, PDI = 1.2–1.3), and St<sup>129</sup> ( $M_n = 13\,000$  g mol<sup>-1</sup>, PDI = 1.2).

In contrast to these postclick approaches for bioconjugation also the preclick approaches are conducted with retention of the bioactivity.<sup>35</sup> As advantages of the grafting-from approach the following issues can be pointed out: (i) The purification of the bioconjugate from catalyst and monomer is simplified compared to the purification from the polymer in the grafting-onto approach and (ii) the placement of the polymer is predetermined facilitating the synthesis and characterization.<sup>58</sup> Herein, 2-bromoisobutyrate as an ATRP initiator functionalized with either pyridyl disulfide (Entry **22**) or maleimide (Entry **18**) was clicked prior to the polymerization onto the free cysteine of a protein (Bovine Serum Albumin or T4 lysozyme). Using these protein macroinitiators NIPAM could be polymerized *in situ* (PDI = 1.3).<sup>35,58</sup>

**Initiators for oxime formation.** A well-known reaction in bioconjugation is the oxime formation of aminoxy-functionalized compounds with carbonyl-containing proteins. Due to the tolerance of functional groups in controlled radical polymerizations,  $\alpha$ -functionalized polymers could be synthesized using *t*-butoxycarbonyl-protected (Boc) aminoxy-initiators for ATRP as shown by Maynard and coworkers.<sup>131,132</sup> Thereby, no termination reactions occurred during the polymerization induced by the protected aminoxy functionalization. After polymerization the aminoxy group can be easily deprotected with trifluoroacetic acid. As depicted in Entry **23**, the aminoxy moiety was linked *via* a tetra(ethylene glycol) spacer to either 2-bromoisobutyrate for the polymerization of methacrylates or 2-chloropropionate for the polymerization of acrylamides. In this way,  $\alpha$ -functionalized polymers were obtained with NIPAM ( $M_n = 16\,000$  g mol<sup>-1</sup>, PDI = 1.1), HEMA ( $M_n = 40\,000$  g mol<sup>-1</sup>, PDI = 1.2), and oligo(ethylene

glycol) methacrylate (OEGMA) ( $M_n = 23\,000$  g mol<sup>-1</sup>, PDI = 1.2–1.3).<sup>131,132</sup>

#### 4.2 Reversible addition fragmentation chain transfer (RAFT)

In principle, all types of monomers which can be polymerized by free radical polymerization can also be polymerized by RAFT using the appropriate type of RAFT agents, *i.e.* dithiobenzoates, trithiocarbonates and xanthates.<sup>11,12</sup> AIBN has been the most widely used initiator for RAFT polymerization. In general, clickable moieties are attached to the initiating fragment (R group) of the chain transfer agents. The advantage of the R group compared to the mediating group (Z group) is the high end-group fidelity of the resulting polymer. The related clickable CTAs are depicted in Tables 4 to 6.

**Alkyne-functionalized CTAs.** Alkyne-containing CTAs are mostly prepared by an esterification of propargyl alcohol with an activated acid on the RAFT agent. The alternative route is using a halogen alkyne compound and the potassium salt of the dithioester or trithiocarbonate *via* a nucleophilic substitution.

The first report on click chemistry and the RAFT process for the preparation of diblock copolymers of styrene and vinyl acetate *via* polymer-polymer conjugation was provided by Barner-Kowollik and coworkers ( $M_n = 12\,100$  g mol<sup>-1</sup>, PDI = 1.1–1.2).<sup>133</sup>

Another combination of click chemistry and the RAFT process was published by Hawker *et al.* in 2006 showing the facile formation of clickable micelles from block copolymers of protected acrylic acid and styrene polymerized with an alkyne-functionalized RAFT agent (Entry **24**). Azide-alkyne cycloaddition is possible with the terminal alkyne-functionalized block copolymers. Protection of the terminal alkyne with the trimethylsilyl group was not necessary in this case.<sup>134</sup>

Furthermore, a similar approach to well-defined block copolymers was reported using a TMS-protected alkyne dithiobenzoate as shown in Entry **24**. Terminal alkyne-functionalized

**Table 4** Alkyne-containing chain transfer agents for RAFT (poC = postclick, prC = preclick)

Entry	Structure	Click	CRP	Monomer	Strategy	Ref
24		CuAAC	RAFT	MA, THPA, St, NIPAM	poC	133–136,143,144
25		CuAAC	RAFT	AM, St, MA, 4VP, NIPAM, MMA	poC prC	137–140,145,146 147
26		CuAAC	RAFT	St, <i>n</i> BA	prC	142
27		Thiol-yne	RAFT	NIPAM	poC	141
27		CuAAC	RAFT	VAc, NVP, St, <i>n</i> BA	prC	142



**Table 5** Azide-containing chain transfer agents for RAFT (poC = postclick, prC = preclick)

Entry	Structure	Click	CRP	Monomer	Strategy	Ref
28		CuAAC	RAFT	St, VAc, DMA	poC	99,133,148
29		CuAAC	RAFT	St, DMA, NIPAM, nBA, OEGA	poC	148–152,156
30		CuAAC	RAFT	NIPAM, DMA	poC	105,157,158
31		CuAAC	RAFT	VAc	poC, prC	135,144,153–155

poly(styrene) was synthesized at 60 °C in a controlled way ( $M_n = 8\,200\text{ g mol}^{-1}$ , PDI = 1.1) and it was shown that the molar mass linearly increased with monomer conversion.<sup>133</sup> The same RAFT agent was used for the polymerization of an *O*-methacryloyl

mannose monomer resulting in an alkyne-functionalized glyco-polymer ( $M_n = 4\,300\text{ g mol}^{-1}$  and PDI = 1.1–1.2).<sup>135</sup> Similarly, an alkyne-functionalized RAFT agent bearing an unprotected alkyne group was used for the polymerization of styrene and

**Table 6** Other click-functionalized chain transfer agents for RAFT (poC = postclick, prC = preclick)

Entry	Structure	Click	CRP	Monomer	Strategy	Ref
32		CuAAC	RAFT	HPMAM, MMA, St, OEGA, NIPAM	poC	159
33		PySS	RAFT	nBA, OEGA, NIPAM	poC, prC	162,36,163, 160,161
34		PySS	RAFT	OEGA, St	poC	164
35		HDA	RAFT	St, <i>i</i> BoA	poC	38,39,55,165–170
36		MAdd	RAFT	NIPAM	prC	171

NIPAM at 70 to 80 °C. Different homopolymers were synthesized in a molar mass range between 2 700 to 3 700 g mol<sup>-1</sup> for poly(styrene) and 4 900 to 11 000 g mol<sup>-1</sup> for poly(NIPAM).<sup>136</sup>

Also a terminal alkyne-functionalized trithiocarbonate (Entry 25) has been used for the RAFT polymerization of different monomers by Brittain.<sup>137,138</sup> For example, surface-mediated RAFT polymerization of styrene and methyl acrylate resulted in poly(St-*b*-MA) with a molar mass of  $M_n = 34\,000$  g mol<sup>-1</sup>.<sup>137</sup> Furthermore, the same group reported on the modification of silica nanoparticles using the tandem approach of RAFT polymerization of styrene and click chemistry.<sup>138</sup>

The chain transfer agent as shown in Entry 25 was clicked to azido end-functionalized poly(isobutylene) and was subsequently used as a clicked macro-RAFT agent for the polymerization of NIPAM ( $M_n = 24\,800$ – $53\,200$  g mol<sup>-1</sup>, PDI < 1.1). First order kinetic plots for the polymerization of NIPAM were obtained and revealed that this monomer polymerizes in a controlled way.<sup>139</sup>

The alkyne-functionalized chain transfer agent depicted in Entry 25 was reported by another research group for the polymerization of 4-vinylpyridine (NVP) initiated with AIBN at 80 °C resulting in a polymer with a molar mass of 13 600 g mol<sup>-1</sup> with a PDI value of 1.4.<sup>140</sup>

Hyperbranched polymers were prepared by thiol-yne click chemistry by Perrier *et al.* using the alkyne-terminated transfer agent shown in Entry 26. After a postmodification step to cleave the RAFT agent into a thiol it was clicked (by UV light at room temperature with yields over 95%) to form a styrene hyperbranched polymer.<sup>141</sup> Furthermore, a xanthate type of RAFT agent (Entry 27) containing an alkyne group has been used for the polymerization of VAc and NVP by Klumperman.<sup>142</sup> In all cases, xanthates were first clicked and then used as functionalized RAFT agents in the polymerization of VAc ( $M_n = 3\,900$  g mol<sup>-1</sup>, PDI = 1.2–1.3), NVP ( $M_n = 5\,400$  g mol<sup>-1</sup>, PDI = 1.1–1.2), St ( $M_n = 7\,500$  g mol<sup>-1</sup>, PDI = 1.1–1.2) and *n*BA ( $M_n = 10\,000$  g mol<sup>-1</sup>, PDI = 1.1).<sup>142</sup> Semi-logarithmic kinetic plots indicated controlled polymerizations using these RAFT agents.

It seems that the protection of the alkyne group is not strictly necessary. As shown above, there are examples for both protected and unprotected CTAs demonstrating that polymers with high end-group fidelity (> 90%) can be prepared. The temperature and the ratio between the alkyne terminated RAFT agent and the monomer play an important role to achieve a sufficient control over the polymerization.

**Azide-functionalized CTAs.** The common procedure for the synthesis of azide-containing CTAs is the esterification of 2-azidoethanol and an activated acid of the RAFT agent. The two largest classes of RAFT agents (dithiobenzoates and trithiocarbonates) have been mostly used as azido-functionalized chain transfer agents.

The azide moiety is used without protection during the polymerization, although some side reactions were described. To decrease the amount of side reactions, low temperatures and/or low conversions are favored that will be discussed in the following.

The dithiobenzoate RAFT agents depicted in Entry 28 were used for the bulk polymerization of styrene at 60 °C and provide a good control over the polymerization ( $M_n = 1\,900$  to  $5\,300$  g mol<sup>-1</sup>, PDI = 1.1<sup>143</sup> and  $M_n = 3\,200$  to  $11\,000$  g mol<sup>-1</sup>,

PDI = 1.1<sup>133</sup>). Moreover, Sumerlin *et al.* using the initiator listed in Entry 28 for the polymerization of St and DMA resulting in azido functional PS ( $M_n = 5\,500$  to  $12\,000$  g mol<sup>-1</sup>, PDI = 1.1–1.3) and poly(DMA) ( $M_n = 10\,800$  to  $21\,800$  g mol<sup>-1</sup>, PDI = 1.30).<sup>148</sup> A thionaphthoyl RAFT agent containing the azide functionality (Entry 28) was also used for the polymerization of styrene in bulk at 80 °C ( $M_n = 2\,400$  g mol<sup>-1</sup>, PDI = 1.1). A linear relationship in the semi-logarithmic kinetic plot was reported indicating that the concentration of propagating chains are almost constant throughout the reaction.<sup>99</sup>

Among the azide-functionalized RAFT agents belonging to the class of the trithiocarbonates, the CTA with a C<sub>12</sub>-side chain is frequently used for the RAFT polymerization of acrylamides (Entry 29): First order kinetic plots for this CTA indicate a constant concentration of propagating chains.<sup>148,149</sup> In addition, Gondi *et al.* used the initiator depicted in Entry 29 with AIBN for the controlled polymerization of styrene ( $M_n = 5\,100$ – $8\,600$  g mol<sup>-1</sup>, PDI = 1.1–1.2) and DMA ( $M_n = 5\,000$ – $10\,000$  g mol<sup>-1</sup>, PDI = 1.1–1.2).<sup>148</sup> Furthermore, the same group reported on the synthesis of poly(DMA-*b*-NIPAM) using this azido-RAFT agent. In this way, telechelic polymers were synthesized: PNIPAM ( $M_n = 2\,700$  g mol<sup>-1</sup>, PDI = 1.1–1.2), PDMA ( $M_n = 4\,200$  g mol<sup>-1</sup>, PDI = 1.1) and poly(DMA-*b*-NIPAM) ( $M_n = 6\,000$  g mol<sup>-1</sup>, PDI = 1.15).<sup>149</sup> In addition, NIPAM was polymerized with the initiator shown in Entry 29 at 60 °C in a controlled way resulting in azido end-functionalized polymers ( $M_n = 16\,300$  g mol<sup>-1</sup>, PDI = 1.1), which were further used for protein coupling by the copper-catalyzed azide-alkyne cycloaddition.<sup>150</sup> The RAFT agent depicted in Entry 29 was also applied for the preparation of 3-miktoarm star polymers by using a combination of RAFT, ring-opening polymerization and click chemistry. After the polymerization at 70 °C of *n*BA ( $M_n = 3\,500$  g mol<sup>-1</sup>, PDI = 1.1), OEGA ( $M_n = 4\,800$  g mol<sup>-1</sup>, PDI = 1.1) or NIPAM ( $M_n = 4\,600$  g mol<sup>-1</sup>, PDI = 1.1) propargyl diol was clicked to the azide.<sup>151</sup> Furthermore, an azide-functionalized CTA (Entry 29) was used for the preparation of hyperbranched polymers. For this purpose, a propargyl acrylate was clicked onto the CTA and subsequently copolymerized with St or NIPAM.<sup>152</sup> Perrier *et al.* used a trithiocarbonate (Entry 30) for the RAFT polymerization of NIPAM ( $M_n = 2\,600$ – $10\,600$  g mol<sup>-1</sup>, PDI = 1.1), but side reactions involving the azido moiety occurred such as 1,3-dipolar cycloaddition with electron-deficient olefins, *i.e.* NIPAM.<sup>105</sup> The cycloadditions to the triazoline or to the pyrazoline (by a second addition of NIPAM) were confirmed by high resolution mass spectrometry.<sup>105</sup>

As depicted in Entry 31, an azide-functionalized xanthate has been used for the polymerization of VAc ( $M_n = 6\,800$  g mol<sup>-1</sup>, PDI = 1.15)<sup>155</sup> as well as for grafting to an alkyne side-chain functional copolymer.<sup>153</sup> A xanthate-terminated dextran was prepared by using click chemistry of an azido RAFT agent shown in Entry 31. The resulting macro-CTA was used for the bulk polymerization of VAc resulting in a block copolymer. The molar mass linearly increased by conversion, although the polydispersity index was increasing.<sup>154</sup> A similar xanthate was used for the bulk polymerization of VAc at 80 °C resulting in a broader molar mass distribution at higher monomer conversion (PDI > 1.4).<sup>155</sup>

**Heterodifunctional CTAs for orthogonal click chemistry.** A difunctional CTA with clickable moieties on both the initiating

as well as on the mediating side was described by Stenzel and Barner-Kowollik *et al.* using a RAFT agent that combines clickable units for dipolar cycloaddition and pyridyl disulfide exchange as two orthogonal click reactions (Entry 32). The reported RAFT agent bears an azide and a dithiopyridine group at the R and Z fragments, respectively. St, NIPAM, and OEGA were polymerized in a controlled way as indicated by kinetic investigations. In contrast, the polymerizations of HPMAM and MMA could not be performed in a controlled manner, since the trithiocarbonate CTA is less suitable for methacrylates. Well-defined heterotelechelic polymers were observed for St ( $M_n = 5\,000\text{--}14\,000\text{ g mol}^{-1}$ , PDI = 1.1), NIPAM ( $M_n = 3\,200\text{--}16\,200\text{ g mol}^{-1}$ , PDI = 1.12 to 1.14) and OEGA ( $M_n = 7\,500\text{--}12\,500\text{ g mol}^{-1}$ , PDI = 1.1).<sup>159</sup>

**Pyridyl-disulfide-containing CTAs.** The chain transfer agent depicted in Entry 33 (top) was used by Davis and coworkers for the homopolymerization of OEGA.<sup>36</sup> The PDI values of the OEGA homopolymers ( $M_n = 12\,000\text{--}34\,000\text{ g mol}^{-1}$ ) were smaller than 1.20 for all samples and for one sample of the block copolymerization with *n*BA (by increasing the conversion the molar mass distribution broadened). The high end-group fidelity of the pyridyl disulfide groups was indicated by <sup>1</sup>H NMR spectroscopy. Furthermore, the same RAFT agent (Entry 33) was used by Davis *et al.* for the polymerization of NIPAM and OEGA resulting in different molar masses and polydispersity indices:<sup>160–163</sup> POEGA ( $M_n = 15\,500\text{--}23\,000\text{ g mol}^{-1}$ , PDI = 1.2–1.3) and PNIPAM ( $M_n = 5\,100\text{--}18\,000\text{ g mol}^{-1}$ , PDI = 1.2–1.5).<sup>163</sup> The PySS end group is often used for the preparation of polymer bioconjugates, *e.g.* with BSA *via* the free thiol group. Semilogarithmic kinetic plots are reported for the RAFT polymerization of OEGA and NIPAM with the CTA pictured in Entry 33 (top) by Bulmus and Davis showing a linear relationship between  $\ln[[M]_0/[M]]$  and reaction time, which indicates a constant level of radical concentration during the polymerization.<sup>163</sup> The symmetric trithiocarbonate RAFT agents depicted in Entry 34 were used for the polymerization of OEGA at 70 °C and provide a good control over the polymerization ( $M_n = 4\,600\text{--}23\,400\text{ g mol}^{-1}$ , PDI = 1.2–1.3). With these homopolymers a chain extension using styrene was performed resulting in block copolymers of type ABA ( $M_n = 19\,100\text{--}37\,900\text{ g mol}^{-1}$ , PDI = 1.2–1.3).<sup>164</sup>

**Functional CTAs for hetero Diels–Alder reactions.** Besides an alkyne or an azide moiety on the RAFT agent, the C=S double bond (dienophile) was directly used as a clickable group for hetero Diels–Alder reactions with dienes (Scheme 1, HDA). This approach represents a straightforward pathway to block copolymers without an additional synthesis step for a postmodification or any other preparation step. The first study on this approach was reported by Barner-Kowollik, Stenzel and coworkers in 2008. The authors prepared polymer conjugates of PS polymerized by RAFT and a diene-terminated poly( $\epsilon$ -caprolactone). The use of these electron-deficient dithioesters (Entry 35) allow the polymerization of styrene in a controlled manner ( $M_n = 2\,200\text{--}2\,800\text{ g mol}^{-1}$ , PDI = 1.1).<sup>38</sup> This class of RAFT agents was also used for the polymerizations of St and isobornyl acrylate (*i*BoA) with different molar masses (stopped at low monomer conversion to ensure high end-group fidelity). All obtained polymers were well-defined and have low polydispersity indices. The prepared polymers were clicked *via* the HDA with cyclopentadienyl- or 2,4-hexadiene-endcapped polymers.<sup>38,39,55,165–170</sup>

**Functional CTAs for Michael addition.** A functional CTA for Michael addition was described by Sumerlin *et al.* using a RAFT agent with a maleimide end group (Entry 36). After the modification with BSA the RAFT polymerization of NIPAM was performed resulting in polymer-protein conjugation with a molar mass of  $240\,000\text{ g mol}^{-1}$ .<sup>171</sup>

### 4.3 Nitroxide-mediated radical polymerization (NMP)

For nitroxide-mediated polymerizations very few examples of clickable initiators were described up to now. In comparison to ATRP and RAFT polymerizations, usually higher reaction temperatures are necessary for NMP. This decreases the number of suitable click functionalities that can be used during the polymerization without exceeding acceptable amounts of side reactions.

It was shown that unimolecular initiators such as phenylethyl-alkylated 2,2,6,6-tetramethylpiperidinylnitroxide (TEMPO) and 2,2,5-trimethyl-4-phenyl-3-azahexane-3-nitroxide (TIPNO) can be functionalized without influencing the control over the polymerization.<sup>172–174</sup> Thereby, the functionalization can be performed in principle at the initiating as well as at the mediating fragment of the alkoxyamine. Until now, clickable moieties are only attached to the initiating fragment. The advantage of this side compared to the mediating side is the high end-group fidelity of the resulting polymer. This is caused by the nature of the NMP process: The incorporation of a functional group at the initiating chain end is done in one step, whereas the incorporation of a certain functionality at the mediating chain end contains many reaction steps until the final polymer is formed, which increases the probability of side reactions.

The general synthetic strategy towards a functional unimolecular initiator is the radical coupling reaction of TIPNO or of the commercially available TEMPO with a functionalized vinyl compound activated by a manganese(III) salen complex (Jacobsen's reagent).<sup>175</sup> The related clickable initiators for NMP are shown in Table 7.

**Alkyne-functionalized initiators.** In Entry 37 an alkyne-functionalized alkoxyamine based on PhEt-TIPNO is shown that was synthesized according to the general radical coupling of TIPNO and 4-(trimethylsilylethynyl)styrene that was obtained by Sonogashira reaction of 2-bromostyrene and trimethylsilyl acetylene.<sup>176</sup>

The alkyne was protected with the TMS group to reduce the possible side reactions under polymerization conditions: (*i*) chain transfer by hydrogen abstraction from the alkyne as well as polymerization along the triple bond leading to cross-linking<sup>76,77,176,177</sup> and (*ii*) addition of nitroxide radicals to the triple bond.<sup>178</sup> It can be noted that even a small loss of nitroxide during polymerization has a large impact on the controlled character of the polymerization, since it shifts the equilibrium towards the free propagating radical resulting in a significant increase in termination and transfer reactions in particular at higher conversions.

The protected initiator (Entry 37) was used in the homopolymerization of styrene resulting in  $\alpha$ -functionalized clickable PS ( $M_n = 24\,000\text{ g mol}^{-1}$ , PDI = 1.1) after deprotection with tetrabutylammonium fluoride (TBAF). In contrast to ATRP, no uncontrolled deprotection of the TMS-alkyne was noticed

**Table 7** Clickable initiators for NMP (poC = postclick, prC = preclick)

Entry	Structure	Click	CRP	Monomer (Abbr./Entry)	Strategy	Ref
37		CuAAC	NMP	St	poC	176
38		CuAAC	NMP	St	poC	179–181
		AAC	ATRP	MMA	poC	45
39		CuAAC	NMP	St	poC	182–184
		AAC	ROP	ε-CL	poC	45
40		CuAAC	NMP	–	–	185
41		CuAAC	NMP	–	–	175
42		CuAAC	NMP	St, <i>t</i> BA St, NIPAM, <i>n</i> BA	poC prC	174 176,188
43		DA	NMP	St	poC	118
			ATRP	<i>t</i> BA	prC	119,190
			NMP	St		
			ATRP	<i>t</i> BA		

during the polymerization. Furthermore, a combination of ATRP and NMP with the same initiator is possible as demonstrated by Tunca and Hizal *et al.*<sup>45,179–181</sup> Although both techniques are radical polymerizations and, hence, might interfere with each other, they can be applied subsequently: (i) NMP of styrene can be conducted without affecting the ATRP initiator in the absence of any metal catalyst<sup>45,180,181</sup> and (ii) ATRP of methacrylate can be conducted at lower temperature (60 °C) at which the nitroxide is still inactive and not able to mediate radical propagation.<sup>179</sup> Entry 38 shows such an alkyne-functionalized multifunctional initiator for ATRP and NMP.<sup>45,179–181</sup> The structure contains (i) 2-bromoisobutyrate as mediator for the ATRP polymerization of MMA, (ii) TEMPO as mediator for

NMP polymerization of styrene and an unprotected alkyne, whereas the fragments are linked *via* ester groups.

The unprotected alkyne is thermally stable up to 125 °C and the TEMPO-mediated polymerization of styrene seems not to interfere with the unprotected alkyne. Apparently, even after 17 h at 125 °C the polymerization was controlled and no significant loss of alkyne was observed for the resulting PS-macroinitiator ( $M_n = 10\,000\text{ g mol}^{-1}$ , PDI = 1.2) as judged by <sup>1</sup>H NMR spectroscopy and SEC measurements of the subsequent clicked structure.<sup>181</sup> By contrast, the ATRP of MMA was kept short in every case (30 min at 60 °C) to prevent significant amounts of side reaction with the catalytic system resulting in PMMA macroinitiator ( $M_n = 6\,000\text{ g mol}^{-1}$ , PDI = 1.2).<sup>179</sup>

However, the amount of side reactions is negligible in most cases due to the low concentration of alkyne-containing initiator.

Furthermore, alkyne-functionalized NMP initiators are combined with other controlled polymerization techniques by the incorporation of, e.g., alcohol groups for the ring-opening polymerization of  $\epsilon$ -caprolactone (Entry 39). These polymerization techniques do not interfere with each other and can be applied simultaneously<sup>182,183</sup> or subsequently.<sup>45,184</sup> For the consecutive procedure, first the ROP of  $\epsilon$ -CL with the initiator depicted in Entry 39 was conducted at 110 °C for 2 h using Sn(Oct)<sub>2</sub> as catalyst ( $M_n = 4\,000\text{ g mol}^{-1}$ , PDI = 1.1) followed by NMP of styrene at 125 °C for 15 h ( $M_n = 19\,000\text{ g mol}^{-1}$ , PDI = 1.3).<sup>45,184</sup> On the other hand, in a simultaneous one-pot approach St and  $\epsilon$ -CL were heated with Sn(Oct)<sub>2</sub> for 22 h at 120 °C ( $M_n = 12\,000\text{ g mol}^{-1}$ , PDI = 1.1).<sup>182</sup> For all examples, copolymers of PCL-*b*-PS with an alkyne as clickable function at the junction point were achieved, whereby the alkyne was not protected even in the polymerization at 120 °C for 22 h. Hence, the alkyne must be stable under the applied polymerization conditions of NMP and ROP.

In addition, since both polymerization techniques do not interfere with the azide-alkyne cycloaddition, 3-miktoarm star terpolymers can be constructed by conducting ROP of  $\epsilon$ -CL (with Sn(Oct)<sub>2</sub>), NMP of St (with initiator shown in Entry 39) and either simultaneously (one-pot/one-step) or subsequently (one-pot/two-step) clicking an azide-functionalized polymer with CuBr/PMDETA as catalyst.<sup>183</sup> Thereby, 3-arm stars of PEG-PCL-PS ( $M_n = 14\,000\text{ g mol}^{-1}$ , PDI = 1.3) and PMMA-PCL-PS ( $M_n = 14\,500\text{ g mol}^{-1}$ , PDI = 1.2) with the one-pot/one-step technique and stars of PtBA-PCL-PS ( $M_n = 16\,000\text{ g mol}^{-1}$ , PDI = 1.1) and PEG-PCL-PS ( $M_n = 15\,000\text{ g mol}^{-1}$ , PDI = 1.1) in the one pot/two step approach could be synthesized, respectively.<sup>183</sup>

Another type of an alkyne-functionalized macroinitiator ( $M_n = 7\,700\text{ g mol}^{-1}$ , PDI = 1.1–1.2) is depicted in Entry 40, whereas PtBoA is attached on both the initiating and the mediating fragment of the alkoxyamine.<sup>185</sup> The macroinitiator was obtained by a nitrene-mediated radical coupling reaction of activated ATRP-made PtBoA ( $M_n = 4\,300\text{ g mol}^{-1}$ , PDI = 1.2) in the presence of an alkyne-functionalized nitrene. To the best of our knowledge, this macroalkoxyamine had not yet been used as initiator in NMP. Nevertheless, it seems to be a potential candidate, since in a similar approach polystyrene midchain-functionalized with a parent alkoxyamine (not including the alkyne moiety) was used as initiator in NMP of St, *n*-BA and NIPAM for the chain extension towards ABA triblock copolymers.<sup>186,187</sup>

**Azide-functionalized initiators.** One of the first azide-functionalized structures that is capable for a controlled radical polymerization was published in 1998 by Hawker and coworkers.<sup>175</sup> In the common procedure (manganese-catalyzed radical coupling of nitroxides with styrenics for the synthesis of alkoxyamines) *p*-chloromethyl styrene was trapped with the commercial available TEMPO radical after radical activation and was subsequently reacted with sodium azide to yield an azide-functionalized initiator (Entry 41). However, this initiator was up to now to the best of our knowledge neither used in polymerizations nor used in combination with alkyne-azide cycloadditions. In this particular case, the azide was used to gain

an amino-functionalization by reduction with lithium aluminium hydride.

In a similar approach the *p*-(azidomethyl)phenylethyl-TIPNO was synthesized, whereby the *p*-chloromethyl styrene was functionalized with the azide prior to the radical coupling with TIPNO (Entry 42). The initiator was used in the polymerization of styrene ( $M_n = 9\,000\text{ g mol}^{-1}$ , PDI = 1.1 after 3 h, 120 °C) and *n*-butylacrylate ( $M_n = 6\,500\text{ g mol}^{-1}$ , PDI = 1.2–1.3 after 13 h at 120 °C), whereby the polymerization was controlled and no side reactions of the azide were discussed.<sup>174</sup>

In contrast, Voit *et al.* discussed that the polymerization of styrene with the azido-functionalized initiator depicted in Entry 42 failed due to the side reactions that were assigned to the cyclization of the azide with the vinylic double bond of the monomer.<sup>176</sup> Since the azide group is not thermally stable,<sup>49</sup> either postmodification or preclick approaches could be successfully utilized to prepare the  $\alpha$ -functionalized polymers. In the postmodification, *p*-(chloromethyl)phenylethyl-TIPNO was used in the polymerization of styrene and the chloro group was subsequently converted with sodium azide into azide (N<sub>3</sub>-PS:  $M_n = 8\,000\text{ g mol}^{-1}$ , PDI = 1.2). Following the preclick approach, an alkyne-functionalized moiety (Cbz-protected adenine derivative) was clicked onto the azide prior to the polymerization of styrene resulting in  $\alpha$ -functionalized PS ( $M_n = 52\,000\text{ g mol}^{-1}$ , PDI = 1.2).<sup>176</sup>

To study the steric and electronic influence of the triazole moiety for the initiation quality of the alkoxyamine shown in Entry 42, two different alkoxyamines were synthesized starting from 4-(chloromethyl)phenylethyl-TIPNO, whereby the chloro group was substituted either by azide or by 4-azidobenzoate to vary the distance of the azide to the alkoxyamine skeleton.<sup>188</sup> Polymerization of NIPAM using these azido-functionalized alkoxyamines as initiators failed in both cases. Therefore, the azido group was functionalized *via* 1,3 dipolar cycloaddition with either a 1,2-dihydroxyalkyl moiety, a barbituric acid moiety or a phenyl moiety. The initiators where the triazole was directly bound to the alkoxyamine group showed poor initiation. In contrast, the alkoxyamine with a rigid spacer revealed good control over the polymerization of NIPAM ( $M_n = 5\,000\text{ g mol}^{-1}$ , PDI = 1.2) and *n*-BA ( $M_n = 6\,000\text{ g mol}^{-1}$ , PDI = 1.2). The poor initiation efficiency in the first case was partly ascribed to an electronic influence but mostly to intramolecular hydrogen bonding between the propagating radical and the barbituric acid that hindered propagation. This was sterically prevented with the rigid spacer in the second case. In these preclick cases the azide moiety of the initiator described in Entry 42 opens the field towards versatile functionalized initiators *via* the facile incorporation of functional groups.

**Functional initiators for Diels–Alder reactions.** Besides an alkyne moiety also anthracene or furan-protected maleimide were attached to ATRP-NMP initiators as clickable groups for Diels–Alder reactions (Entry 43). The synthesis of these mikto-functional initiator starts from 2,2-bis(hydroxymethyl)propionic acid as the basic framework,<sup>189</sup> where the ATRP-initiating fragment (2-bromoisobutyrate), the NMP fragment (TEMPO) and the clickable moiety (protected maleimide or anthracene) were incorporated by esterification reactions.<sup>118,119,190</sup>

The anthracene-functionalized mikto-initiator depicted in Entry 43 was only used in the preclick approach, whereby the Diels–Alder reaction was conducted prior to the NMP of styrene followed by ATRP of *t*BA. With this strategy, different block copolymers were obtained: (i) H-shaped terpolymers<sup>119</sup> (PS)(*Pt*BA)-PEO-(*Pt*BA)(PS) ( $M_n = 18\,000\text{ g mol}^{-1}$ , PDI = 1.3) and (PS)(*Pt*BA)-PPO-(*Pt*BA)(PS) ( $M_n = 31\,000\text{ g mol}^{-1}$ , PDI = 1.3) and (ii) 3-miktoarm star polymer<sup>190</sup> PEG-PS-*Pt*BA ( $M_n = 18\,000\text{ g mol}^{-1}$ , PDI = 1.3). The protected maleimide-functionalized miktoinitiator described in Entry 43 was initially used in the ATRP of *t*BA ( $M_n = 4\,000\text{ g mol}^{-1}$ , PDI = 1.3) and subsequently “clicked” with anthracene-functionalized PCL prior to the NMP of styrene to obtain a 3-miktoarm terpolymer (PCL-*Pt*BA-PS) ( $M_n = 40\,000\text{ g mol}^{-1}$ , PDI = 1.7).<sup>118</sup> The high polydispersity index was ascribed to a loss of TEMPO during the Diels–Alder reaction at 100 °C, indicated by a shoulder in the SEC trace at lower molar masses.

The preclick approach for the anthracene or maleimide moiety in combination with NMP should be used, since the maleimide and anthracene moieties cause side reactions under the polymerization conditions of NMP. Hence, to the best of our knowledge no example for the postclick approach is yet reported.

## 5. Clickable monomers

Clickable monomers can be used to synthesize pendant functionalized polymers (Scheme 4) that can be easily modified in a grafting-onto approach *via* click chemistry. Thereby, the clickable monomer can be homopolymerized or copolymerized to obtain versatile random-, block- or comb polymers. Most widely used in controlled radical polymerization processes are MMA and St derivatives.

The polymerization of these click-functionalized monomers represents often a synthetic challenge, because the clickable unit as a reactive group is frequently in conflict with the radical polymerization conditions. In contrast to the initiator approach a higher amount of side reactions involving the clickable functionality is expected, which is caused by the higher concentration of the monomer used during the polymerization process compared to the initiator. This fact is in particularly pronounced for bulk polymerizations or for side reactions involving besides

the clickable unit other parts of the monomer, *e.g.* the vinyl group of azide-containing monomers, where cycloaddition between the double bond and the azide can occur. To circumvent such side reactions, either the clickable unit has to be protected, or polymerization time or temperature have to be reduced.

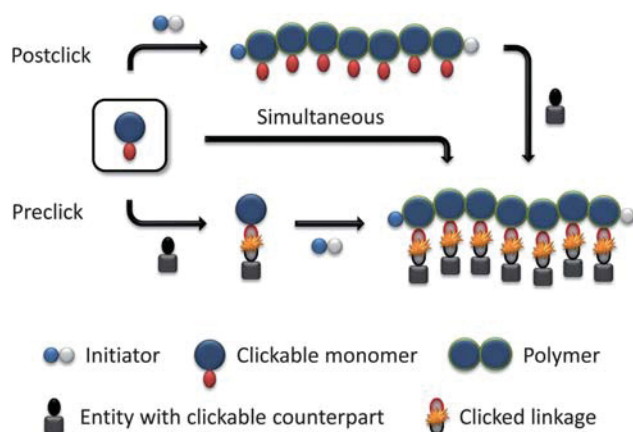
However, the degree of functionalization is much higher in this approach compared to the initiator one. Clickable initiators would provide polymers only with terminal functionalities, which would be one or two for linear polymers and equal the number of arms for star-shaped polymers. In contrast, homopolymerization of a clickable monomer would yield a polymer with functionalities as many as the number of repeating units. The degree of functionality can be decreased by copolymerization, which also decreases possible side reactions that are caused by the clickable monomers. In this section we discuss clickable monomers according to the functional groups, *i.e.* alkyne, azide, diene, thiol, para-fluoro and others. An overview over the clickable and clicked monomers is given in Tables 8–10.

### 5.1 Alkyne-containing monomers

The synthesis of alkyne-functionalized monomers is straightforward, whereby most synthetic routes involve the esterification of (meth)acryloyl chloride with propargyl alcohol or propargyl amine for (meth)acrylates<sup>3,66,153,191,192</sup> and acrylamides,<sup>95,193</sup> respectively. The propargyl derivatives can be protected by the reaction with trimethylsilyl chloride and 1,8-diazabicyclo[5.4.0]undec-7-ene catalyzed by silver chloride. The synthesis of alkyne-functionalized styrene is often accomplished *via* the Sonogashira reaction of 4-bromostyrene with (trimethylsilyl)acetylene.<sup>60,193–195</sup>

The protection of acetylene-functionalized monomers by the alkylsilyl group is of prime importance, because the terminal alkyne is known to be chemically<sup>196</sup> and thermally<sup>197</sup> not stable under the polymerization conditions required for the CRP techniques.<sup>194</sup> However, some researchers have used unprotected alkynes and indeed demonstrated that the terminal alkyne undergoes side reactions such as (i) radical addition to the triple bond,<sup>193</sup> (ii) chain transfer,<sup>198</sup> (iii) complexation of the terminal triple bond to copper-based ATRP catalysts and insertion reactions leading to insoluble crosslinked networks.<sup>77,193,199,200</sup> In one of these reports, Matyjaszewski and coworkers reported that the ATRP of unprotected propargyl methacrylate was hardly controllable (PDI values > 3), due to the involvement of the acetylene moiety during the catalyzed radical process.<sup>77</sup>

**Styrenes.** The first report on alkyne-functionalized styrene was reported in 2005 by Hawker and coworkers using protected 4-(trimethylsilylethynyl)styrene (St-C≡C-TMS) (Entry 44) in nitroxide-mediated polymerizations for the preparation of co- and terpolymers.<sup>193</sup> By utilizing the PhEt-TIPNO alkoxyamine as unimolecular initiator, poly(St-*co*-St-C≡CH) ( $M_n = 47\,000\text{ g mol}^{-1}$ , PDI = 1.2), poly(St-C≡CH-*co*-DMAM) ( $M_n = 40\,000\text{ g mol}^{-1}$ , PDI = 1.2) and poly(St-*r*-St-C≡CH-*r*-HEMA) ( $M_n = 32\,000\text{ g mol}^{-1}$ , PDI = 1.2) could be prepared in a controlled manner, whereby the alkyne monomer was incorporated into the polymers up to 10%. Without TMS-protection, significant amounts of crosslinked polymers at a higher content of alkyne-functionalized monomer or at high conversion were



**Scheme 4** Schematic representation of the strategies *via* clickable monomers.

**Table 8** Alkyne-containing monomers (poC = postclick, prC = preclick, simult = simultaneous)

Entry	Structure	Click	Strategy	CRP	Initiator/CTA (Abbr./Entry)	Comonomers	Ref
44		CuAAC	poC	RAFT NMP	MCPMDB PhEt-TIPNO	THPA, St St, DMAM, HEMA, GMA, tBOSi, tBA, THPA	194,203 60,193-195
45		CuAAC	poC	NMP RAFT	PhEt-TIPNO DDAT	St, tBOSi, AcOSi St	195,201 201
46		CuAAC	poC	NMP RAFT RAFT	PhEt-TIPNO BPIT 28	tBA AA NIPAM	193 205,206 156
47		CuAAC	poC	ATRP RAFT	15, TosCl, BMP CPDB, CPADB, CDB, CBDB, DDAT, MCPMDB	ε-CL, MMA, SMA, mPEG OEGMA, MMA, GMA	3,123,192,209 153,191,199,200,207,208
48		CuAAC	poC	ATRP NMP RAFT	BMPABE CPDB 17	- MMA -	69 214 66
49		ZnANC	poC	ATRP NMP	3 PhEt-TIPNO CPADB	NIPAM HEMA, DMAM NIPAM	95 193 215
50		CuAAC	poC prC	ATRP NMP ATRP RAFT	BPN, PEB BPO, TEMPO EBiB MPPCTTA	St St MMA St	48 210 213 67
51		CuAAC	poC	ATRP	PEB	St	216

observed. The efficiency and the orthogonality of the alkyne-azide click reaction were proven by one-pot functionalization either in a cascade or in a simultaneous approach. In related work, Voit *et al.* synthesized poly(*St-r-St-C≡CH-r-GMA*) ( $M_n = 30\,000\text{ g mol}^{-1}$ , PDI = 1.3) random terpolymers *via* NMP using the TMS-protected alkyne monomer. The deprotection with TBAF was performed without affecting the glycidyl moiety resulting in a pendant functionalized terpolymer bearing two orthogonal clickable moieties.<sup>60</sup>

Furthermore,  $\text{St-C}\equiv\text{CH}$  was used for the preparation of poly(*tBOS*-*b*-[*St-co-St-C}\equiv\text{CH}*]) ( $M_n = 60\,000\text{ g mol}^{-1}$ , PDI = 1.3–1.4) and poly(*pHSt-b*-[*St-co-St-C}\equiv\text{CH}*]) ( $M_n = 26\,000\text{ g mol}^{-1}$ , PDI = 1.2) diblock terpolymers which were applied in block copolymer lithography.<sup>195,201</sup>

In addition,  $\text{St-C}\equiv\text{C-TMS}$  was used in the synthesis of amphiphilic diblock terpolymers consisting of a hydrophilic poly(acrylic acid) block and a hydrophobic copolymer poly(*St-co-St-C}\equiv\text{CH}*).<sup>194</sup> Since acrylic acid can not be directly polymerized in a sufficiently controlled way with NMP<sup>202</sup> – due to decomposition of the nitroxide under acidic condition – one can use the protection/deprotection strategy. First, a *PtBA*-macroinitiator was applied in the nitroxide-mediated polymerization of *St* and  $\text{St-C}\equiv\text{C-TMS}$  leading to poly(*tBA-b*-[*St-co-St-C}\equiv\text{CTMS}*]) ( $M_n = 32\,000\text{ g mol}^{-1}$ , PDI = 1.2–1.3). However, deprotection of the *PtBA* block to PAA leads to a significant loss of alkyne functionality even of the protected one. Therefore, tetrahydropyran acrylate (THPA) was used which can be deprotected under milder conditions, but this compound was not stable under the temperature required for NMP. The *P*(THPA) macroinitiator could be polymerized *via* RAFT at 70 °C and was used in the copolymerization of styrene and 4-(trimethylsilylethynyl)styrene. Following the deprotection amphiphilic block copolymers *PAA-b*-[*PS-co-PSC}\equiv\text{CH}*] ( $M_n = 16\,000\text{ g mol}^{-1}$ , PDI = 1.2) were obtained that are capable to form micelles with a clickable hydrophobic core.<sup>194,203</sup>

In the discussed cases protected  $\text{St-C}\equiv\text{CH}$  was incorporated up to 20% in a statistical copolymerization with styrene. This might be sufficient for the specific attachment of functional groups by clicking, but for the tailoring of macroscopic properties homopolymers with pendant alkyne groups seem to be more promising. Voit and coworkers showed that by increasing the amount of protected 4-ethynylstyrene the control of nitroxide-mediated polymerization with PhEt-TIPNO as unimolecular initiator is lost indicated by polydispersity indices around 1.9 and large differences of the calculated molar masses to the observed ones for the homopolymer of poly( $\text{St-C}\equiv\text{C-TMS}$ ).<sup>195</sup> The authors assigned the loss of control to a shift of the active-dormant species equilibrium towards the active side caused by sterical hindrance and also to the recombination of the nitroxide and the TMS group of the propagating 4-(trimethylsilylethynyl) styrene radical. This assumption is supported by the fact that a controlled polymerization is obtained if an excess of free nitroxide is added to the polymerization medium. This shifts the equilibrium back to the dormant side and results in the synthesis of well-defined poly( $\text{St-C}\equiv\text{C-TMS}$ ) ( $M_n = 3\,500\text{ g mol}^{-1}$ , PDI = 1.2).<sup>195</sup>

To circumvent the sterical hindrance during the polymerization as well as to provide enhanced accessibility to the alkyne for the postmodification, 4-(3'-trimethylsilyl-ethynylmethoxy)styrene ( $\text{St-OMe-C}\equiv\text{CTMS}$ ) containing a methoxy group as a flexible spacer

was investigated (Entry 45). The synthesis of the monomer was performed by a substitution reaction of 4-hydroxystyrene with propargyl bromide and subsequent protection with TMS. The homopolymerization proceeded in a controlled manner without the necessity of any free nitroxide (poly( $\text{St-OMe-C}\equiv\text{CTMS}$ ):  $M_n = 6\,000\text{ g mol}^{-1}$ , PDI = 1.2–1.3). Besides, the TMS group is labile under basic and acidic conditions prohibiting the use of acetic acid as a polymerization enhancer. Moreover, the TMS group is thermally labile and a partial loss of the protecting group was observed for the reaction at 120 °C. Unfortunately, the more stable *t*-butyldimethyl-silyl (TBDMS) or triisopropylsilyl (TIPS) protected monomers could not be synthesized. With  $\text{St-OMe-C}\equiv\text{CTMS}$  as monomer in hand the following diblock copolymers were synthesized: poly(*tBOS*-*b*- $\text{St-OMe-C}\equiv\text{CH}$ ) ( $M_n = 52\,000\text{ g mol}^{-1}$ , PDI = 1.2), poly(*AcOS*-*b*- $\text{St-OMe-C}\equiv\text{CH}$ ) ( $M_n = 21\,000\text{ g mol}^{-1}$ , PDI = 1.4) as well as poly(*pHSt-b*- $\text{St-OMe-C}\equiv\text{CH}$ ) ( $M_n = 16\,000\text{ g mol}^{-1}$ , PDI = 1.2).<sup>195,201</sup>

Not only nitroxide-mediated polymerization but also the RAFT polymerization technique was used for the preparation of diblock copolymers poly(*St-b-St-OMe-C}\equiv\text{CH}*) with a trithiocarbonate RAFT agent.<sup>201</sup> Although alkyne-functionalized ATRP initiators are widely used for the polymerization of styrene, no alkyne-functionalized styrene derivative was polymerized *via* ATRP so far. A reason for that might be the higher polymerization temperature for the ATRP of styrene compared to other monomer classes promoting side reactions. It can be noted that the partial loss of the trimethylsilyl-protecting group at elevated temperatures leads to a higher amount of terminal acetylene compared to the initiator approach, which might cause a significant loss of control due to interference with the copper catalyst.

**Acrylates.** There are only a few examples using propargyl acrylates in CRP. A possible reason for that is the less controllable polymerization of acrylate monomers which can undergo some side reactions due to the formation of mid-chain radicals in poly(acrylates) (intermolecular transfer of radicals) resulting in branching and scission.<sup>204</sup> The triple bond at the monomer makes it even more difficult to gain control over the molecular structure.

The unprotected propargyl acrylate depicted in Entry 46 was copolymerized with acrylic acid at 60 °C by Caruso *et al.* using the RAFT method with a trithiocarbonate CTA resulting in a broad molar mass distribution ( $M_w = 86\,000\text{ g mol}^{-1}$  and a PDI value of 2.2).<sup>205</sup> In addition, a similar copolymer was prepared using a trithiocarbonate CTA yielding a copolymer with a molar mass of  $M_n = 53\,000\text{ g mol}^{-1}$  and a polydispersity index of 1.9. The broad mass distribution is attributed to branching of the unprotected alkyne-functionalized monomer.<sup>206</sup>

Furthermore, TMS-protected propargyl acrylate was randomly copolymerized with *tBA* using PhEt-TIPNO as initiator for NMP by Malkoch and coworkers, but no detailed discussion was provided regarding the obtained molar masses and polydispersity of the isolated polymers.<sup>193</sup>

**Methacrylates.** The TMS-protected propargyl methacrylate (Entry 47) can be polymerized under usual polymerization conditions for CRP (60–85 °C).<sup>3,153,191,192,207,208</sup> This type of monomer was mostly polymerized by ATRP or RAFT. In the case of RAFT polymerization a dithiobenzoate as chain transfer agent and AIBN as radical source was used. It is reported that for



the homopolymers molar masses up to 10 000 g mol<sup>-1</sup> are achievable.<sup>153</sup> The polymerizations were carried out for 3 to 16 h with protection of the terminal alkyne group resulting in well-defined polymers (PDI < 1.3). Also some block and random copolymers were prepared with different comonomers (MMA, OEGMA).<sup>208</sup> A kinetic study for propargyl methacrylate (Entry 47), including semilogarithmic kinetic plots of the RAFT polymerization of the propargyl methacrylate and the silyl-protected monomer was reported by Barner-Kowollik and coworkers. The authors demonstrated that the protected monomer polymerizes at a much lower rate than the nonprotected monomer.<sup>153,191</sup> Another RAFT copolymerization of the unprotected methacrylate (Entry 47) and MMA or GMA showed that the PDI values increase (PDI = 1.6–2.0,  $M_n$  = 15 000–25 000 g mol<sup>-1</sup>) and that under these polymerization conditions side reactions such as transfer and insertion reactions occur.<sup>199</sup>

TMS-protected propargyl methacrylate was also polymerized by ATRP. The first contribution was reported by Haddleton and coworkers using CuBr/*N*-ethyl-2-pyridylmethanimine as catalytic system. Kinetic studies indicated a living process and SEC measurements of the resulting polymers revealed a good control over the polymerization (PDI < 1.3).<sup>3</sup> This monomer is also used for the synthesis of block copolymers with poly( $\epsilon$ -caprolactone) as macroinitiator. A block copolymer ( $M_n$  = 14 100 g mol<sup>-1</sup>, PDI = 1.2) was obtained after the deprotection with TBAF and followed by the alkyne-azide cycloaddition leading to a functional graft copolymer.<sup>192</sup>

Drockenmuller *et al.* reported an *in situ* approach of ATRP polymerization and copper-catalyzed azide-alkyne click reaction using propargyl methacrylate as clickable monomer. The resulting functionalized copolymers revealed a broader molar mass distribution (PDI = 1.3–2.1) due to the use of unprotected alkyne.<sup>209</sup>

**Acrylamides.** The protected alkyne-functionalized acrylamide shown in Entry 48 is polymerized by ATRP using CuBr/Me<sub>6</sub>TREN as catalytic system and dansyl-bromide as initiator at 0 °C with NIPAM as comonomer ( $M_n$  = 13 900–19 600 g mol<sup>-1</sup>, PDI = 1.2–1.3).<sup>95</sup>

Additionally, the protected acrylamide was copolymerized with (*N,N*-dimethyl)acrylamide and TMS-protected 2-(hydroxyethyl)methacrylate *via* NMP using PhEt-TIPNO as initiator to prepare water-soluble random terpolymers.<sup>193</sup>

**Acrylonitrile.** The acrylonitrile monomer (AN) can be used without further functionalization for click reactions (Entry 49) since it contains nitrile groups which can be used for 1,3 dipolar cycloadditions with azides. Since this cycloaddition belongs to the list of reactions defined as click reaction by Sharpless and coworkers,<sup>13</sup> acrylonitrile can be in principle considered as a clickable monomer.

Acrylonitrile was polymerized *via* ATRP using 2-bromopropionitrile as initiator and CuBr/bpy as catalytic system by Du Prez and Matyjaszewski. The initiator contains the monomer group as initiating fragment that poses equal radical reactivity as the monomer itself providing fast initiation.<sup>48</sup> Thereby, poly(acrylonitrile) PAN ( $M_n$  = 40 000 g mol<sup>-1</sup>, PDI = 1.1) as well

as poly(AN-*b*-St) (PDI = 1.1) and poly(AN-*r*-St) ( $M_n$  = 8 500 g mol<sup>-1</sup>, PDI = 1.1) were prepared. For the block copolymer, first a PAN-macroinitiator was prepared followed by the polymerization of styrene as the second block to ensure high initiating rates and, hence, a narrow molar mass distribution.<sup>48</sup> In addition, acrylonitrile was polymerized *via* NMP using TEMPO/dibenzoylperoxide (BPO) as bimolecular initiator for the polymerization of the random copolymer poly(St-*r*-AN) ( $M_n$  = 10 000 g mol<sup>-1</sup>, PDI = 1.3–1.4) and the diblock polymer poly(St-*b*-[St-*r*-AN]) ( $M_n$  = 87 000 g mol<sup>-1</sup>, PDI = 1.2) that was initiated with a PS-macroinitiator.<sup>210</sup> Thereby the control increases with the content of acrylonitrile in the acrylonitrile/styrene feed.

Regarding possible postmodifications, it should be noted that the pendant nitrile group in polymeric materials is up to now efficiently modified only to the corresponding tetrazole ring using the reaction with sodium azide and zinc chloride as catalyst in DMF 120 °C for 40–50 h.<sup>48,210</sup> Herewith, the nitrile-azide cycloaddition is used to modify macroscopic properties rather than to place functional groups or to attach polymeric side chains.

The reason for this limitation lies within the nature of the ring formation of the tetrazoles: To allow an efficient ring formation under mild conditions, the azide should not be sterically hindered (which limits the use of polymeric azides), while the nitrile group has to be electron-poor (*e.g.* tosyl nitrile), which is not sufficiently fulfilled for the nitrile group along the backbone of (poly-)acrylonitrile.<sup>49,211,212</sup>

However, with the efficient modification to the corresponding tetrazole ring the macroscopic properties of the prepared diblock copolymers changes: (*i*) solubility and swellability in protic solvents increase, (*ii*) the morphology changes, since the tetrazole formation increases the incompatibility between the blocks<sup>210</sup> and (*iii*) the temperature stability for the tetrazole-modified material significantly decreases (by 60–120 °C) compared to the nitrile-based polymer.<sup>48</sup>

**Vinylacetylene.** The TMS-protected vinylacetylene (Entry 50) was polymerized using the ATRP process by Matyjaszewski.<sup>213</sup> This monomer was copolymerized with MMA using CuBr/2,2'-bipyridine catalyst and ethyl 2-bromoisobutyrate as initiator in anisole. Different environmental parameters such as temperature, time or ratio of copper to ligand to initiator were varied resulting in different polymers ( $M_n$  = 5 000–12 000 g mol<sup>-1</sup>, PDI = 1.1–1.5).<sup>213</sup>

Alkyne-functionalized maleimide (Entry 51) will be discussed in Section 6.1.2.7.

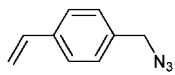
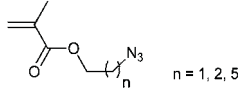
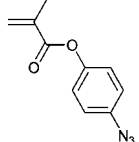
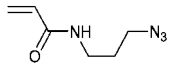
## 5.2 Azide-containing monomers

Azide-containing monomers based on (meth)acrylates or (meth)acrylamides are prepared by an esterification of 2-azidoethanol or 3-azidopropylamine with a (meth)acryloyl chloride or an activated acid of (meth)acrylic acid.<sup>77,90,108,217–220</sup> In addition, the route starting from the 2-hydroxyethyl methacrylate to the corresponding azide *via* the Mitsunobu reaction is described.<sup>221</sup> In the case of azide-functionalized styrene, the alkyne functionality is incorporated *via* substitution reaction of 4-vinylbenzyl chloride with sodium azide.<sup>83</sup>

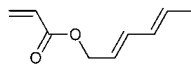
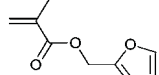
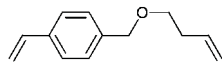
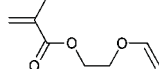
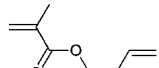
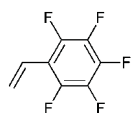
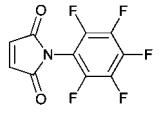
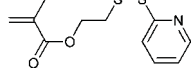
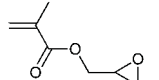
The used temperature represents an important criterion for the controlled polymerization of these monomers. The instability of the azide group at elevated temperatures is described, resulting in (i) the decomposition with evolution of nitrogen to form reactive

nitrenes that undergo insertion reactions<sup>49,217,222–225</sup> or (ii) cycloaddition with the monomer to form triazolines.<sup>49,105,108,226,227</sup> Both side reactions result in the formation of a crosslinked polymer. The higher concentration of azide groups in the

**Table 9** Azide-containing clickable monomers (poC = postclick, simult = simultaneous)

Entry	Structure	Click	Strategy	CRP	Initiator/CTA (Abbr./Entry)	Comonomers	Ref
52		CuAAC	simult	ATREP	5	St	83
53		CuAAC	poC	ATRP RAFT	EBiB, TosCl, CDB, CBDN, CPADB	MMA, DMAEMA, tBMA MMA	77,90,209,220,221 108,207,219,221
54		CuAAC	poC	RAFT	BICDT, CPDB	MMA, MA, St	217
55		CuAAC	poC	ATRP RAFT	3 CPADB	NIPAM NIPAM, DMA	95 218

**Table 10** Other click-functionalized monomers (poC = postclick)

Entry	Structure	Click	Strategy	CRP	Initiator/CTA	Comonomers	Ref
56		DA		poC	RAFT BDAT	St	228
57		DA		poC	ATRP EBiB, BBiBE	MMA, EHA	57,229–232
58		Thiol ene		poC	RAFT MCPMDB	St	127
59		Thiol ene		poC	RAFT CPADB	–	234
60		Thiol ene		poC	ATRP EBiB	MMA	127
61		Thiol para-fluoro, Amine para-fluoro		poC	NMP Blocbuilder®, PhEt-TIPNO	St	31,32
62		Thiol para-fluoro		poC	ATRP PEB	St	216
63		PySS		poC	RAFT CPADB TIPNO	HPMAM	235,236
64		RO RO		poC poC	NMP ATRP EBiB	St, MA tBMA, MMA	9,60 59,114,244

polymerization solution (1–2 M or bulk) compared to the initiator approach constrains the polymerization conditions of CRP to lower temperatures to gain sufficient control over the polymerization.<sup>77,90,95,108,217,219,220</sup> Nonetheless, there are also two reports published using normal ATRP conditions (65–70 °C) claiming that the polymerization proceeded in a controlled manner.<sup>207,218</sup> Regarding the orthogonality of ATRP and azide-containing monomers, it is known for azides to undergo the Staudinger reaction, *i.e.* reduction to amines, in the presence of phosphines that are typically used as ligand for iron complexes as the “new generation” catalytic systems in ATRP.<sup>6,15,49</sup>

**Styrenes.** One example for the simultaneous click chemistry and atom transfer radical emulsion polymerization (ATREP) is known for 4-vinylbenzyl azide (Entry 52).<sup>83</sup> This method allows the preparation of crosslinked PS nanoparticles by copolymerization of 4-vinylbenzyl azide and styrene and an alkyne-containing ATRP initiator with CuBr/PMDETA as the catalytic system.

**Methacrylates.** A kinetic study, including semi-logarithmic kinetic plots of the RAFT polymerization of an azide methacrylate derivative (Entry 53) is reported by Benicewicz at different temperatures and at different monomer conversions. The pseudo-first-order kinetic plots are reported for 40 °C as well as 30 °C showing a linear relationship between  $\ln([M]_0/[M]_t)$  and time, which indicates a constant level of radical concentration during the polymerization. At higher temperature (50 °C) a shoulder at higher molar masses could be observed which was caused by coupling or branching of the polymer chains. At 30 °C it was shown that the azide monomer can be polymerized by RAFT with a dithionaphthalate RAFT agent ( $M_n = 21\,500\text{ g mol}^{-1}$ , PDI = 1.1).<sup>108</sup> Benicewicz and coworkers also reported that the RAFT polymerization of 6-azidoethyl methacrylate showed a linear pseudo-first-order kinetic plot at 30 °C. It was noted that with higher monomer conversion (25%) a high molar mass shoulder was observed by SEC measurements.<sup>219</sup> 2-Azidoethyl methacrylate (Entry 53) was used for the copolymerization with MMA *via* ATRP or RAFT. The copolymer prepared by ATRP had a molar mass of  $M_n = 5\,400\text{ g mol}^{-1}$  and a PDI value of 1.2, whereas the copolymer prepared by RAFT had a molar mass of  $M_n = 7\,100\text{ g mol}^{-1}$  and a PDI value of 1.4. These copolymers were used for further functionalization with cyclooctyne derivatives (copper-free clicking).<sup>221</sup> The 4-azidophenyl methacrylate (Entry 54) can be copolymerized with different monomers in a controlled manner at room temperature by using a carbodithioate or a dithiobenzoate as initiator. Methyl acrylate, methyl methacrylate and styrene have been used as comonomers. The resulting copolymers were well-defined (PDI < 1.3) and in a molar mass ( $M_n$ ) range between 3 000 and 16 000  $\text{g mol}^{-1}$ .<sup>217</sup>

With the azide-functionalized monomer depicted in Entry 53 also a tandem click chemistry/ATRP procedure was applied by Drockenmuller *et al.* using CuBr/bpy as the catalytic system and TosCl as the initiator. Different copolymers with MMA were prepared ( $M_n < 22\,400\text{ g mol}^{-1}$ , PDI = 1.5).<sup>209</sup>

**Acrylamides.** There have been two reports published on the controlled radical polymerization of azido acrylamides (Entry 55). The first one is reported by Chang *et al.* for ATRP with a dansyl-

labeled initiator and CuBr/Me<sub>6</sub>TREN as catalyst. The polymerization was performed with NIPAM as comonomer at 0 °C to avoid side reactions ( $M_n = 9\,500\text{--}13\,300\text{ g mol}^{-1}$ , PDI = 1.2).<sup>95</sup> In another study, the authors polymerized 3-azidopropylacrylamide by RAFT with DMAM and NIPAM, where 4-cyanopentanoic acid dithiobenzoate was used as CTA and 4,4'-azobis(4-cyanopentanoic acid) as initiator to yield random copolymers ( $M_n = 14\,700\text{ g mol}^{-1}$ , PDI = 1.2).<sup>218</sup>

### 5.3 Monomers for Diels–Alder reactions

There are only a few examples for clickable monomers (dienophile or diene containing ones) that are suitable for Diels–Alder reactions. The furfuryl methacrylate is commercially available and therefore accessible for the controlled polymerization without further functionalization.

**Acrylates.** One report was published by Barner-Kowollik and Stenzel *et al.* using a hexa-2,4-dienyl acrylate (Entry 56), which was polymerized by RAFT using a trithiocarbonate chain transfer agent and styrene as comonomer ( $M_n = 5\,000\text{--}6\,000\text{ g mol}^{-1}$ , PDI = 1.2–1.4).<sup>228</sup>

**Methacrylates.** Singha *et al.* polymerized furfuryl methacrylate (FMA) (Entry 57) by ATRP (catalyst: CuCl/HMTETA, initiator: EBiB) at 90 °C. Moderate levels of monomer conversions (~60%) could be achieved during the homopolymerization of this type of monomer. Surprisingly, the polymers did not gel and preserved their low PDI values, which indicated no or negligible amounts of side reactions involving the addition of radicals to the furfuryl functionality. Semi-logarithmic kinetic plots revealed that the polydispersity decreased by increasing conversion.<sup>229</sup> Nonetheless, well-defined homopolymers ( $M_n = 6\,500\text{ g mol}^{-1}$ , PDI = 1.3) and copolymers with MMA ( $M_n = 10\,000\text{ g mol}^{-1}$ , PDI = 1.3) were obtained.<sup>57,229–231</sup> Furthermore, FMA was successfully used in the preparation of block copolymers with 2-ethylhexyl acrylate (EHA) and 1,2-bis(bromoisobutyryloxy)ethane (BBiBE) as initiator.<sup>232</sup> The ATRP reaction was conducted at 90 °C using CuCl/HMTETA as catalytic system. The obtained PFMA-*b*-PEHA-*b*-PFMA (up to  $M_n = 51\,000\text{ g mol}^{-1}$ , PDI = 1.3) was crosslinked with a bismaleimide to yield materials with self-healing properties.

### 5.4 Monomers for thiol-ene clicking

In the last years, the thiol-ene click reaction has attracted significant attention in the field of polymer science. These robust and efficient reactions have enormous advantages for the construction of polymeric structures. Recently, several reviews summarized the power of thiol-ene chemistry.<sup>19,28,53,233</sup>

Since thiol groups readily undergo side reactions under radical polymerization conditions, preferably ene-functionalized monomers were synthesized and used as clickable monomers. (Meth)acrylates containing a terminal double bond are prepared by an esterification of an alcohol (*e.g.* ethylene glycol vinyl ether or 3-butene-1-ol) with an acid chloride or an anhydride of (meth)acrylate acid.<sup>127,234</sup> Styrenes containing a terminal double bond are synthesized by substitution of a chloride group (*e.g.* from 4-vinylbenzyl chloride, using 3-butene-1-ol).<sup>127</sup> The controlled polymerization of this class of monomers is easily possible due to

the rather low reactivity of the unconjugated alkene group. Thus, no or less crosslinking occurs during the polymerization.<sup>127</sup>

**Styrenes.** There is only one report published for the polymerization of the ene-functionalized styrene derivative depicted in Entry 58. Hawker *et al.* reported a RAFT copolymerization to obtain alkene backbone-functionalized copolymers. The polymerization was performed with a dithiobenzoate as CTA at 75 °C resulting in a copolymer with St of a molar mass of  $M_n = 14\,000\text{ g mol}^{-1}$  and a PDI value of 1.1.<sup>127</sup>

**Methacrylates.** Vinyloxyethyl methacrylate (Entry 59) was polymerized by the RAFT process using a photoinitiator and a dithiobenzoate RAFT agent reported by Bulmus and coworkers.<sup>234</sup> Monomodal molar mass distributions were obtained at low monomer conversions (~25%) that broadened by increasing the polymerization time resulting in a hyperbranched polymer due to the incorporation of the vinyl ether group (PDI = 1.3–2.0).<sup>234</sup> Controlled polymerization of another alkene methacrylate (Entry 60) was described by Hawker and coworkers. The authors reported on the ATRP of but-3-enyl methacrylate. The copolymerization with MMA was initiated by ethyl 2-bromoisobutyrate and catalyzed by CuBr/PMDETA ( $M_n = 17\,000\text{ g mol}^{-1}$ , PDI = 1.2).<sup>127</sup>

### 5.5 Monomers for *para*-fluoro substitution

**Styrenes.** The commercially available pentafluorostyrene (Entry 61) can be used as a clickable monomer as recently shown by Schubert and coworkers. Thereby, the *para*-fluoro atom can be substituted in a postmodification by functionalized amines or thiols under mild conditions (see Section 2).<sup>31,32</sup> Pentafluorostyrene (PFS) was polymerized using the commercial available  $\beta$ -phosphonylated alkoxyamine (MMA-SG1: “BlocBuilder”) as unimolecular initiator for NMP polymerization at 110 °C. Thereby, homopolymer poly(PFS) ( $M_n = 3\,500\text{ g mol}^{-1}$ , PDI = 1.1), random copolymer poly(PFS-*r*-PS) ( $M_n = 9\,000\text{ g mol}^{-1}$ , PDI = 1.1) and diblock copolymers poly(PFS-*b*-PS) ( $M_n = 17\,000\text{ g mol}^{-1}$ , PDI = 1.2) could be prepared, where either a PFS- or a PS-macroinitiator was used.<sup>32</sup> Terpyridine-functionalized PhEt-TIPNO alkoxyamine as unimolecular initiator was also used for the NMP of PFS at 120 °C to yield poly(PFS) ( $M_n = 4\,500\text{ g mol}^{-1}$ , PDI = 1.1) and poly(PFS-*b*-PS) ( $M_n = 10\,000\text{ g mol}^{-1}$ , PDI = 1.2).<sup>31</sup>

The pentafluorophenyl-functionalized maleimide (Entry 62) will be discussed in Section 6.1.2.7.

### 5.6 Monomers for pyridyl disulfide exchange

In entry 63 a monomer is shown, where the pyridyl disulfide moiety is linked to methacrylate. The PySS group can be exchanged in a postmodification or premodification step by thiol functional compounds under mild reaction conditions, because of the facile leaving character of the 2-pyridinethione. The release of 2-pyridinethione allows the monitoring of the PySS exchange by UV/vis spectroscopy. This procedure is often used for the preparation of polymer bioconjugates (*e.g.* with oligopeptide) or for anticancer drugs, such as doxorubicin linked *via* the free thiol group.<sup>235,236</sup>

The monomer was used in RAFT polymerization with CPADB as CTA. These polymers were used as macro CTAs for the preparation of block copolymer of HPMAM resulting in different block segments with different molar mass ( $M_n = 13\,400\text{--}49\,000\text{ g mol}^{-1}$ , PDI = 1.2–1.3). These block copolymers were further crosslinked as micelles.<sup>235</sup>

Moreover, homopolymers of the PySS monomer were prepared by using the RAFT method by Bulmus *et al.* Different semilogarithmic plots are examined for this monomer indicating the controlled character of the polymerization. Numerous homopolymers were synthesized as basis for further bio-functionalization ( $M_n = 8\,000\text{--}12\,600\text{ g mol}^{-1}$ , PDI = 1.1–1.4).<sup>236</sup>

### 5.7 Monomers for ring-opening reactions

Ring-opening reaction of strained heterocycles are considered as a click reaction based on the spring-loaded character towards nucleophiles by Sharpless and coworkers.<sup>13</sup> For this purpose, glycidyl methacrylate (GMA) is a commercially available monomer, and thus can be used as a clickable monomer without further modification (Entry 64). CRP of GMA has been well studied by NMP,<sup>9</sup> RAFT<sup>237</sup> and ATRP.<sup>238–243</sup> For ATRP of GMA it is important to note that the epoxide might react with free ligand, which leads to unwanted branching. Thus, the catalyst has to be preformed before the addition of the monomer.<sup>59</sup> Moreover, any strong nucleophile should be avoided during polymerization. Apart from that, the epoxide is stable under the polymerization conditions even at elevated temperatures typically required for NMP.

With the “boom” of click chemistry in polymer science, the ring opening of epoxides with nucleophiles as a click-type reaction experienced also a revival in the last few years, but rather to introduce azides or alkynes than as a click reaction itself (Scheme 1, Entry 89). Why modifying towards another clickable functionality although the ring-opening reaction is an efficient click reaction itself? This is caused by the poor selectivity of epoxides. In contrast, the orthogonality is strongly increased for, *e.g.*, the azide-alkyne click reaction allowing the orthogonal functionalization in one-pot, simultaneous or cascade reactions.<sup>193</sup>

Various polymers containing glycidyl methacrylate were synthesized as basis for further click reactions: Poly(St-*r*-(C≡C-CH<sub>2</sub>-St)-*r*-GMA) was prepared *via* NMP with TIPNO as mediating nitroxide ( $M_n = 30\,000\text{ g mol}^{-1}$ , PDI = 1.3).<sup>60</sup> By ATRP the homopolymer as well as the random copolymers were synthesized (Entry 64): poly(GMA) with  $M_n = 27\,000\text{ g mol}^{-1}$  and PDI = 1.3,<sup>114</sup> poly(GMA-*r*-*t*BMA) with  $M_n = 8\,000\text{ g mol}^{-1}$  and PDI = 1.2<sup>244</sup> as well as poly(GMA-*r*-MMA) with  $M_n = 20\,000\text{ g mol}^{-1}$  and PDI = 1.2 to 1.5,<sup>59</sup> whereby the polydispersity index for the latter increases by increasing the fraction of GMA used in the feed.

### 5.8 Clicked monomers

Clicked monomers are formed by the azide-alkyne 1,3-dipolar cycloaddition and contain the triazole ring which is linked to the polymerizable vinyl group. There are only few examples of clicked monomers. Hawker *et al.* have described the RAFT polymerization of a series of 4-vinyl-1,2,3-triazoles (Entry 50). Different (co)polymers were prepared in a controlled manner using a dithioester.<sup>67</sup> Sumerlin *et al.* used propargyl acrylate

(Entry 46) that was clicked onto an azide-containing trithiocarbonate (Entry 29) for the RAFT polymerization of branched poly(*N*-isopropylacrylamide) (PDI = 1.5–2.1).<sup>156</sup> Also the chain extension of this macro-CTA with DMA was performed. 1-(3'-Aminopropyl)-4-acrylamido-1,2,3-triazole hydrochloride (Entry 48) was polymerized by the RAFT using a poly(NIPAM) macro-RAFT agent resulting in block copolymers ( $M_n = 19\,600\text{ g mol}^{-1}$ , PDI = 1.2).<sup>215</sup> Propargyl methacrylate (Entry 47) was clicked by a Cu-catalyzed 1,3-dipolar cycloaddition with 3-azido-7-diethylaminochromen-2-one and subsequently copolymerized with MMA by RAFT using 2-cyanoprop-2-yl dithiobenzoate (CPDB) as chain transfer agent ( $M_n = 10\,200\text{ g mol}^{-1}$ , PDI = 1.2).<sup>214</sup>

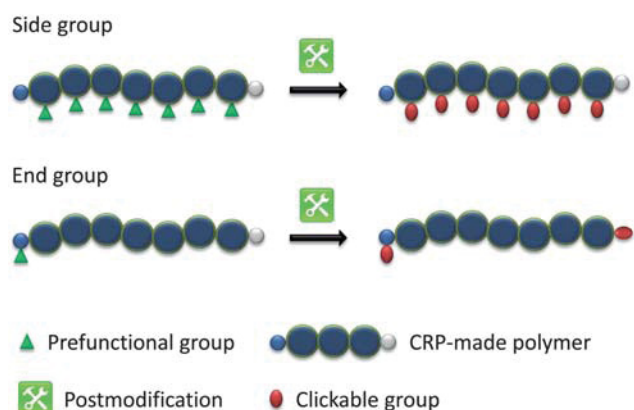
## 6. Postmodification

Postmodification reactions are used to transform latent functional groups into clickable units, whereby the polymer can be modified either at pendant or at terminal positions (Scheme 5). For the terminal modification the initiating side, the mediating side or both can be modified. An overview of the end-group modification approaches are depicted in Tables 11 and 12 and the side-group modifications are shown in Table 13, which will be discussed in the following.

### 6.1 End-group modification

Linear polymers prepared by controlled radical processes contain two functional end groups, one on the initiating end and the other one on the mediating end. Therefore, a polymer can be further functionalized on the  $\alpha$ - and/or the  $\omega$ -terminus. In particular for the  $\omega$ -terminus, unavoidable radical termination reactions during the polymerization such as recombination as well as disproportionation occur and, thus, parts of its functionality are lost to a certain amount. Assuming an efficient postmodification reaction, these side reactions for the prefunctional polymer can be considered as the bottleneck for the degree of functionalization that can be reached for  $\omega$ -functionalized polymers *via* the postmodification strategy.

**6.1.1 Modification on the  $\alpha$ -terminus.** The  $\alpha$ -terminus of the polymer is more preferred for modification in comparison to the  $\omega$ -terminus due to a higher end-group fidelity.



**Scheme 5** Schematic representation of the postmodification strategies.

**6.1.1.1 RAFT – Modification towards alkyne functionality.** An  $\alpha$ -endgroup modification of the initiating group was reported by Bertozzi *et al.*, where a pentafluorophenyl ester as a labile ester group (Entry 75) was attached to the initiating fragment. After polymerization the labile ester was cleaved with diisopropylethylamine in the presence of propargyl amine resulting in an  $\alpha$ -terminated alkyne polymer. Apparently, the trithiocarbonate was not attacked by the amine and, therefore, a defined polymer could be obtained.<sup>245</sup>


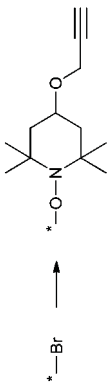
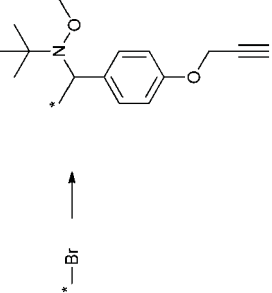

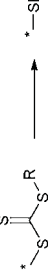


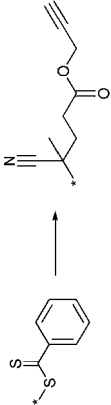
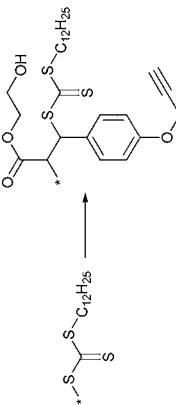
**6.1.1.2 NMP – Modification towards azide functionality.** Despite the versatility of functional groups that can be introduced as an initiating fragment on the  $\alpha$ -functionalized polymers prepared by NMP with functional alkoxyamines,<sup>175</sup> there is only one synthetic route reported for the transformation into a clickable moiety: The modification of the benzylic chloro group into an azide *via* a nucleophilic substitution with sodium azide (Entry 78, 79).

Initially, Hawker *et al.* described the postmodification from chloride into azide  $\alpha$ -functionalized polystyrene in 2004.<sup>246</sup> Thereby, the sodium azide was activated by the addition of catalytic amounts of 18-crown-6 ether while an excess of sodium azide was used. This postmodification was also utilized by Voit *et al.* using acetone as solvent and three equivalence of sodium azide at room temperature to achieve full conversion after several hours.<sup>176</sup> In 2008, Braslau *et al.* obtained azide-functionalized polystyrene by the reaction of the chloride counterpart in DMF with sodium azide (3 eq.) at 50 °C in the absence of crown ethers to almost full conversion.<sup>247</sup> Furthermore, the transformation was applied by O'Reilly *et al.* for the preparation of azido-functionalized poly(acrylic acid-*b*-styrene) ( $N_3CH_2$ -PhEt-PAA-*b*-PS) as clickable amphiphilic diblock copolymers. The postmodification of the benzylic chloro group attached to the PAA block was conducted in water at room temperature using a 5-fold excess of sodium azide to yield clickable micelles in water with azide groups on the outer shell.<sup>134</sup>


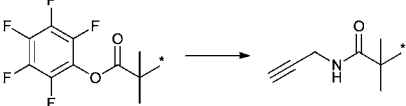
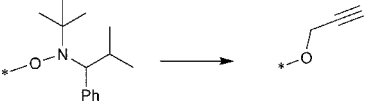
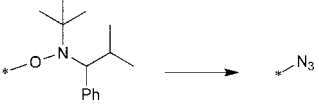
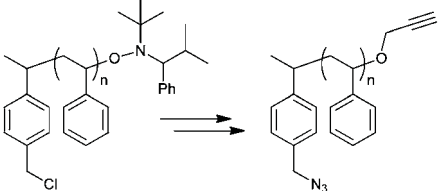
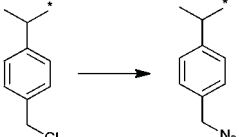
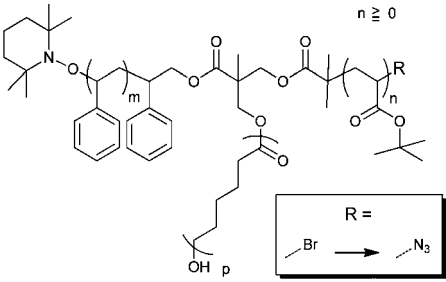
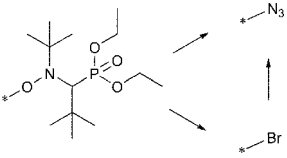
**6.1.2 Modification on the  $\omega$ -terminus.** The efficiency of the  $\omega$ -terminal modification depends on the stability of the mediating fragment of the polymer chain that is affected through side reactions inherent for controlled radical polymerization processes. In general, polymerizations intended for  $\omega$ -postmodification were kept at low conversions in order to avoid a significant loss of functionality.

**6.1.2.1 ATRP – Modification towards azide functionality.** The most prominent postmodification reaction towards a clickable functionality of ATRP-prepared polymers is the substitution of halides such as bromide against azide, since the halide is inherently present at the  $\omega$ -chain end after the ATRP process (Entry 65). The reaction is very efficient with sodium azide in DMF at room temperature, allowing for a specific transformation in the presence of distinct labile groups. In this context, it is important to note that Matyjaszewski and coworkers developed the method for this nucleophilic substitution in 1997/1998 for polystyrenes and polyacrylates to allow an easy access to amines over the azide *via* a reduction<sup>248</sup> or *via* the Staudinger process.<sup>249</sup> The authors also studied the rate constant for the substitution of selected model halogen compounds with sodium azide.<sup>250</sup>

Table 11 Postmodification – end group

Entry	Modification	Click	CRP	Type	Monomer	Ref
65		CuAAC	ATRP	Nucleophilic substitution	St, <i>t</i> BA, MA, OEGA, <i>t</i> BoA, MMA, GMA, OEGMA	59, 78–80, 90, 97, 98, 102, 114, 251–261
66		CuAAC	ATRP	Nitroxide radical coupling	St	263
67		CuAAC	ATRP	Nitroxide-mediated radical coupling	<i>t</i> BoA	185
68		DA	ATRP	Nucleophilic substitution	St, MMA, MA, <i>t</i> BoA	39, 266
69		Thiol-ene Thiol-yne MAdd	RAFT RAFT RAFT	Aminolysis Aminolysis Aminolysis	NIPAM, OPA, EA, HEA St NIPAM	116, 245, 267, 270, 275–278 141 116, 273
70		Thiol-ene Thiol-yne Thiol-isocyanate MAdd	RAFT RAFT RAFT RAFT	Aminolysis Aminolysis Aminolysis Aminolysis	DEAEMA, BA, NIPAM, MMA, HPMAM, OEGA NIPAM DEAEMA DEAEMA, NIPAM, MMA	50, 267–271 50 54 50, 233, 271, 272, 274
71		CuAAC	RAFT	Aminolysis, Substitution	MMA, DEGMA, LMA, St, NIPAM	280
72		CuAAC	RAFT	Radical exchange	St	143
73		CuAAC	RAFT	Radical insertion	St, MA	281

**Table 12** Postmodification – end group (continued)

Entry	Modification	Click	CRP	Type	Monomer	Ref
74		PySS	RAFT	Aminolysis, Substitution	NIPAM	267
75		CuAAC	RAFT	Ester cleavage	OPA	245
76		CuAAC	NMP	Oxidative cleavage	St	284
77		CuAAC	NMP	Radical exchange	St	247
78		CuAAC	NMP	i) Substitution ii) Oxidative cleavage	St	247
79		CuAAC	NMP	Substitution	St, <i>t</i> BA	134,176,247
80		CuAAC	NMP ROP ATRP	Substitution	St $\epsilon$ -CL <i>t</i> BA	71,72
81		CuAAC	NMP	Radical exchange, Substitution		285

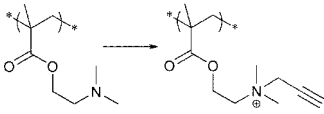
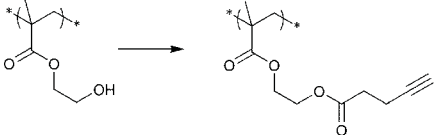
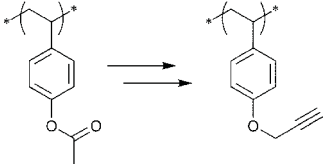
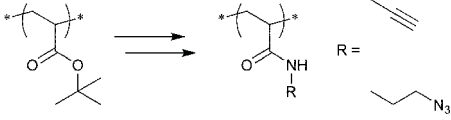
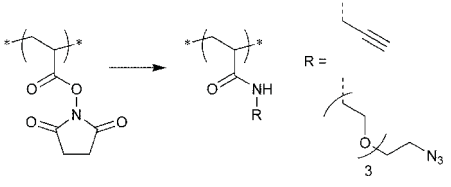
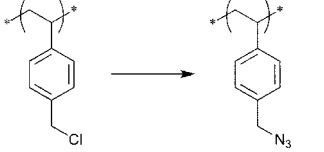
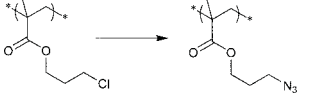
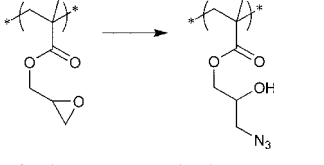
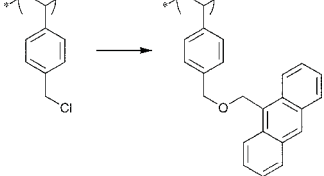
Up to now a lot of different polymers were postmodified *via* this azidation method. Poly(styrenes), poly(acrylates), poly(methacrylates) and their copolymers at different molar masses have been reported.<sup>59,78–80,90,97,98,102,114,251–261</sup> It should be noted that the azidation of poly(methacrylates) is significantly slower compared to poly(acrylates) and poly(styrenes) due to the tertiary bromine.<sup>262</sup> The modification can be used, *e.g.*, in combination with multifunctional initiators bearing functional termini for NMP or ROP (Entry **80**). The multifunctional initiator was used in NMP of styrene, ROP of  $\epsilon$ -caprolactone as well as ATRP of *t*BA followed by the quantitative substitution of the

bromine against azide, while the molar masses and the polydispersity indices retained.<sup>71,72</sup>

**6.1.2.2 ATRP – Modification towards alkyne functionality.** Only a few examples are described for polymers prepared by ATRP dealing with the exchange of the bromine end group against alkyne-functionalized groups.<sup>185,263</sup> Low molar masses and conversions are targeted by preparing the polymers to assure a high end-group fidelity of the  $\omega$ -terminating bromide.

Monteiro and coworkers used the high reactivity of PS towards cleavage of the bromine end group in the presence of

**Table 13** Postmodification – side group

Entry	Modification	Click	CRP	Type	Comonomers	Initiator	Ref
82		CuAAC	ATRP	Quaternization	DMAEMA, DEGMA, DEAEMA	EBiB	288
83		CuAAC	ATRP	Esterification	—	EBiB	289
84		CuAAC	NMP	i) Hydrolysis ii) Substitution	St	PhEt-TIPNO	291
85		CuAAC	NMP	i) Acidolysis ii) Amidation	St	PhEt-TIPNO	292,295
86		CuAAC	NMP	Amidation	St, <i>t</i> BA, AM	PhEt-TIPNO	193
87		CuAAC	NMP	Substitution	St, <i>t</i> BA	PhEt-TEMPO	117,292–294
88		CuAAC	RAFT	Substitution	AA	BPIT, PEDT	205,206
89		CuAAC	ATRP	Ring opening	MMA, <i>t</i> BMA	EBiB	59,104,114,244,290
90		DA	NMP	Etherification	St	PhEt-TEMPO	117,120

Cu(I)Br, Me<sub>6</sub>TREN and DMSO promoting a single electron transfer (SET) *via* the formation of nascent Cu(0).<sup>263</sup> The emerging carbon-centered radical was trapped by an alkyne-functionalized nitroxide (2,2,6,6-tetramethyl-4-(prop-2-ynoxy)piperidin-1-lyoxy)<sup>264</sup> to result in alkyne-terminated PS with near quantitative yields within 10 min at room temperature (Entry 66). A unique

feature of the nitroxide radical coupling (NRC) as a selective and highly efficient reaction is the reversible formation of the C–O bond of the alkoxyamine that undergoes homolytical cleavage upon heating. In this fashion, the coupled nitroxide can be substituted by an excess of other functional nitroxides (10-fold excess) at elevated temperatures.



Recently, Barner-Kowollik and coworkers established a new approach towards midchain-functionalized polymers by using nitrones in a dual radical capturing process.<sup>185,265</sup> Nitrones can rapidly react with carbon-centered radicals to form nitroxides that further trap radicals to form alkoxyamines. As such, nitrones can be used for efficient polymer conjugation by mediating the radical coupling reactions of macroradicals. The authors activated ATRP-made PiBoA with Cu(0)/PMDETA in toluene at 60 °C in the presence of an alkyne-functionalized nitron (2-fold excess), while the alkyne was protected with TMS.<sup>185</sup> In this vein, midchain alkyne-functionalized polymers as depicted in Entry 67 can be prepared in high yields as indicated by <sup>1</sup>H NMR spectroscopy (~90%). The midchain functional PiBoA was clicked after deprotection with either PS-N<sub>3</sub> or PiBoA-N<sub>3</sub> to form 3-arm star polymers.

As an additional feature, the prepared polymers bear an alkoxyamine functionality in the backbone that could in principle be used as a macroinitiator in a nitroxide-mediated polymerization for the insertion of another polymer block towards triblock copolymers. Hence, the present approach can also be considered as a preparation of clickable or clicked macroinitiators for NMP (Entry 40; Section 4.3).

**6.1.2.3 ATRP – Modification toward diene functionality for Diels–Alder reactions.** In Entry 68 a nucleophilic substitution of a bromo-terminated polymer with cyclopentadienyl as reported by Barner-Kowollik is described. This strategy allows the direct access to dienes which can be used for catalyst-free click reactions, *i.e.* Diels–Alder reaction. The reaction was performed with sodium cyclopentadienide (NaCp) or nickelocene (NiCp<sub>2</sub>) as the substituting agent at ambient temperature. It should be mentioned that side reactions can occur during the substitution with the more reactive NaCp, in particular for PMMA-Br, PiBoA-Br and PMA-Br, but not for PS-Br. It could be shown that the use of NiCp<sub>2</sub> using tributylphosphine and sodium iodide as promoters eliminates these side reactions. In this manner, cyclopentadienyl-functionalized polymers of PMMA, PiBoA, PMA and PS are reported (PDI < 1.3).<sup>39,266</sup>

**6.1.2.4 RAFT – Modification towards thiol functionality.** In recent years, an alternative click strategy has been established in polymer research for the design of complex macromolecular architectures. This strategy is based on the special chemical nature of thiol compounds that can be used for radical coupling processes in thiol-ene and thiol-yne reactions, as well as for nucleophilic addition reactions such as thiol-isocyanate addition or Michael addition. The radical-mediated addition of a thiol to an yne is a “sister” reaction to the radical thiol-ene reaction, whereby two thiols can be added (two-step process). All these reactions can be performed under mild conditions.

The ω-end of the polymer chains prepared by the RAFT polymerization can be easily modified to generate a reactive thiol group. In most of the reports a trithiocarbonate (Entry 69) or a dithiobenzoate (Entry 70) have been used as chain transfer agents for RAFT. These group can be easily modified into thiol groups. There are two synthetic pathways towards thiols: (i) Aminolysis with a primary amine<sup>50,54,141,245,267–275</sup> and (ii) reduction with NaBH<sub>4</sub>.<sup>276–278</sup> Care should be taken in this post-modification to prevent the coupling of two chains to form

a disulfide bridge, which are often visible by a shoulder at lower elution volumes in the SEC measurements. However, coupling of thiols can be easily reversed by addition of a reducing agent, *e.g.* phosphine derivatives.<sup>50,54,116,268,271,273,276</sup> Limitations of the thiol-ene reaction for polymer-polymer conjugation were recently described by Du Prez *et al.*<sup>53</sup>

In some cases, further purification of the ω-thiol functional polymers is necessary and dialysis or precipitation are the preferred techniques. A calorimetric method for the determination of the free thiol concentration was developed by Ellman.<sup>279</sup> Ellman’s reagent converts a thiol into a 5,5'-dithiobis(2-nitrobenzoic acid) derivative, which has a strong absorption and therefore the degree of functionalization can be determined.<sup>267,269,270,273,275</sup> Alternatively, this can be indirectly estimated by clicking a fluorescence dye (*e.g.* pyrene).<sup>274,276</sup> The degree of functionalization can be varied from 60% up to 99.5%. Often short polymer chains are used for the modification to provide high end-group fidelity on the mediating side ( $M_n < 10\,000\text{ g mol}^{-1}$ ). Different polymers were used for the modification towards thiols, *i.e.* acrylate-, methacrylate- and acrylamide derivatives.

An elegant example for the orthogonality of the Michael addition as nucleophilic thiol-ene reaction to the radical thiol-ene was recently described by Lowe *et al.*<sup>50</sup> By using the fact that the nucleophilic reaction of the thiols is selective for double bonds conjugated with electron-withdrawing groups (*e.g.* α,β-unsaturated carbonyl compounds), a consecutive reaction of a heterofunctional polymer with different thiols, first reacted *via* Michael addition and followed by the radical thiol-ene or thiol-yne reaction could be shown. The reverse case leads to the loss of orthogonality due to the unselective nature of the radical coupling.

**6.1.2.5 RAFT – Modification towards alkyne functionality.** An elegant approach to generate ω-end group functionalized triple bonds, which can be used for the Cu(I)-catalyzed cycloaddition, was reported by Theato and coworkers using butynyl methane thiosulfonate (Entry 71). Five different acetylene-terminated polymers (MMA, DEGMA, LMA, St, NIPAM) could be clicked to an azide.<sup>280</sup> Another approach towards alkyne-terminated polymer chains is the cleavage of the RAFT agent by a radical process (Entry 72).<sup>143</sup> Thereby, an excess of alkyne-modified initiator is used, which decomposes while generating radicals that react with the C = S of the thio-carbonylthio moiety in the polymer chain. Higher temperatures (80 °C) and a large excess of the initiator are necessary and it should be taken into account that side reactions during end-group modification can occur by means of recombination during insertion.<sup>143</sup> ABCD 4-miktoarm star polymers could be prepared by RAFT polymerization of styrene followed by an insertion reaction applying a large excess of 2-hydroxyethyl-3-(4-(prop-2-ynyloxy)phenyl) acrylate to stop the polymerization at 110 °C. Hence, a unprotected triple bond attached at the end of the polymer chain could be obtained (Entry 73). The reaction is not very efficient, because a large amount of unreacted macroinitiator is present after the diblock copolymerization.<sup>281</sup>

**6.1.2.6 RAFT – Modification towards pyridyl disulfide functionality.** Chemical modification of the ω-endgroup by aminolysis in the presence of 2,2'-dithiodipyridine was reported to generate a pyridyl-disulfide-terminated polymer chain (Entry

74). The pyridyl disulfide end groups allowed straightforward conjugation with oligonucleotides and peptides.<sup>267</sup>

**6.1.2.7 NMP – Conventional modification and possibilities.** Only a few examples are described dealing with the exchange of the nitroxide moiety on the polymer. The first study was conducted by Rizzardo, reducing the TEMPO to a hydroxy group with a mixture of zinc/acetic acid.<sup>282</sup> A radical-cleavage approach towards more versatile functional end groups was presented by Hawker and coworkers. Thereby, the propagating radical was trapped at the polymerization temperature by *N*-functionalized maleimides as non-self-polymerizing monomers, while the TIPNO nitroxide decomposed at elevated temperatures resulting in the maleimide-functionalized polymer.<sup>283</sup> The transformation yield for polystyrene, polyisoprene and poly(*n*-butylacrylate) was typically 90 to 95%, while no changes in molar masses and the polydispersity indices were observed.

This approach offers the possibility to introduce clickable units at the  $\omega$ -terminus by using functionalized maleimides. Following this strategy, Lutz and coworkers synthesized a library of functional maleimides and used them in the copolymerization with styrene *via* ATRP, while the maleimide was incorporated at a specific place in the polymer chain.<sup>216</sup> Among those, *N*-pentafluorophenyl maleimide or *N*-propargyl maleimide could be incorporated into the polymer, while the latter one had to be protected due to pronounced side reactions (Entry 51, 62). In principle, clickable  $\omega$ -functionalized polymers should be accessible using these monomers in the radical-cleavage procedure by Hawker as well.

**6.1.2.8 NMP – Modification towards alkyne functionality.** In contrast to the thermal cleavage of the alkoxyamine-terminated polymer, oxidative cleavage under much milder thermal conditions can be achieved by single electron oxidation with ceric ammonium nitrate (CAN).<sup>247,284</sup> After the oxidation the alkoxyamine cleaves heterolytically into a nitroxide and the cation-terminated polymer that can be trapped by nucleophiles. Braslau and coworkers treated TIPNO-terminated polystyrene with CAN and propargyl alcohol as nucleophile at room temperature under anhydrous conditions to obtain alkyne-functionalized PS (Entry 76) with an end-group fidelity of 65% as determined by UV-vis experiments.<sup>247</sup> Investigating PhEt-TEMPO as a model compound for TEMPO-terminated polymers, a heterolytic cleavage similar to the TIPNO counterpart was obtained. It could be shown that this method can also be used for TEMPO-terminated polymers. In contrast, polyacrylates terminated with TIPNO or TEMPO also undergo oxidative cleavage, but the cation-terminated polymer interferes with CAN by forming nitrate ester and prohibit further attachment of functional groups *via* the addition of nucleophiles.<sup>284</sup>

The modification of polystyrene that was prepared by NMP with commercially available  $\beta$ -phosphonylated alkoxyamine BlocBuilder® cannot be performed *via* the described oxidative cleavage with CAN due to the electronic and steric nature of SG1.<sup>285</sup>

**6.1.2.9 NMP – Modification towards azide functionality.** Terminal azide-functionalized polystyrene could be obtained starting from the nitroxide-terminated polymer through the

reaction with ethanesulfonyl azide (EtSO<sub>2</sub>N<sub>3</sub>) that was introduced by Renaud and Ollivier<sup>286</sup> as an azidation method for carbon radicals. Braslau and coworkers showed that polystyrene prepared by NMP reacts in the presence of an excess of EtSO<sub>2</sub>N<sub>3</sub> in *N*-methyl-2-pyrrolidinone at 120 °C to the azido-functionalized PS (Entry 77), although the azidation was incomplete as judged by labelling experiments with an alkyne-functionalized dye analyzed *via* UV-vis experiments.<sup>247</sup> Using PhEt-TIPNO as a model compound, the treatment with EtSO<sub>2</sub>N<sub>3</sub> led to less than 30% of the desired transformation.<sup>247</sup> This was explained by the weak electrophilic character of the styryl radical, since only electron-rich radicals can efficiently add onto EtSO<sub>2</sub>N<sub>3</sub>.<sup>287</sup> This also explains why polyacrylates could not be modified with this method.

The azidation reaction of nitroxide-terminated polystyrene was further studied by Bertin and coworkers for polystyrenes prepared with the commercial available BlocBuilder®.<sup>285</sup> Thereby, a one-step as well as a two-step approach towards the terminal azido-functionalized polymer were performed (Entry 81). In the one-step approach EtSO<sub>2</sub>N<sub>3</sub> was used under optimized reaction conditions using a large excess (50 eq.) at 90 °C. In the two-step approach the alkoxyamine was reacted at 75 °C in a radical exchange reaction with 2-bromoisobutyrate as solvent as well as the bromination agent to obtain the exchange of the nitroxide by bromine. Furthermore, this bromo-functionalized polymer was reacted with sodium azide following the well-known ATRP postmodification procedure at room temperature in DMF. For both approaches the azide-functionalization degree was around 70%.

### 6.1.3 Heteromodification on both termini

**6.1.3.1 NMP.** Since the azide group is stable against the mild conditions of the oxidative exchange of the nitroxide against propargyl alcohol by ceric ammonium nitrate (Section 4.1.1), alkyne-azide-functionalized heterotelechelic polystyrene could be efficiently synthesized in a two step synthesis as demonstrated by Braslau *et al.* (Entry 78).<sup>247</sup> At first the chloro group of the  $\alpha$ -functionalized polystyrene prepared by NMP was transformed into the azide followed by the oxidative cleavage reaction with CAN at room temperature and the *in situ* nucleophilic addition of propargyl alcohol.

## 6.2 Side-group modification

In contrast to the terminal functionalization, the modification of pendant groups is more influenced by steric or electronic effects, in particular for homopolymers, where every repeating unit has to be modified. Nonetheless, this method represents a convenient alternative route to multiple click-functionalized polymers, if the direct polymerization of these monomers is relatively more difficult and/or side reactions occur during the polymerization.

### 6.2.1 ATRP

**Modification towards alkyne functionality.** In Entry 82 the alkyne moiety could be selectively introduced by quaternization of the amine of 2-(dimethylamino)ethyl methacrylate (DMAEMA) with propargyl bromide at room temperature (Menschutkin reaction).<sup>288</sup> Due to sterical hindrance, the DMAEMA is more reactive towards quaternization than DEAEMA allowing for the selective modification of a terpolymer containing DEGMA,

DMAEMA and DEAEMA.<sup>288</sup> The purification of the quaternized copolymer was achieved simply by precipitation. The extent of quaternization of the DMAEMA units was evaluated by <sup>1</sup>H NMR spectroscopy to be 35%.

Alkynyl side groups were introduced into polymeric backbones of a linear poly(2-hydroxyethyl methacrylate) by an esterification reaction between the hydroxyl groups and 4-pentynoic acid that was activated by *N,N'*-dicyclohexylcarbodiimide (Entry **83**). The degree of functionalization was estimated by <sup>1</sup>H NMR spectroscopy to be close to 100%. No change of the apparent molar masses and PDI values occurred.<sup>289</sup>

**Modification towards azide functionality.** An efficient and convenient synthesis route to azides is the ring-opening reaction of epoxides as shown in Entry **89**. The oxirane ring is often opened with sodium azide in the presence of ammonium chloride to yield the corresponding 1-hydroxy-2-azido compounds. The reactions can be followed by IR spectroscopy of the characteristic vibration bands of the azide (2104 cm<sup>-1</sup>) and the epoxide ring (909 cm<sup>-1</sup>). This click reaction was applied for the preparation of copolymers with multiple azide groups, whereby different methacrylates are used, resulting in defined copolymers.<sup>59,104,114,244,290</sup>

### 6.2.2 RAFT

**Modification towards azide functionality.** In Entry **88**, a nucleophilic substitution of a pendant chloro group against azide was performed for a poly(3-chloropropyl acrylate-*co*-acrylic acid). The reaction was conducted with sodium azide at 80 °C and the final product was subsequently dialyzed. High molar mass copolymers were obtained:  $M_n = 86\,000$  and  $135\,000\text{ g mol}^{-1}$  with polydispersity indices of 2.2 and 1.4, respectively.<sup>205,206</sup>

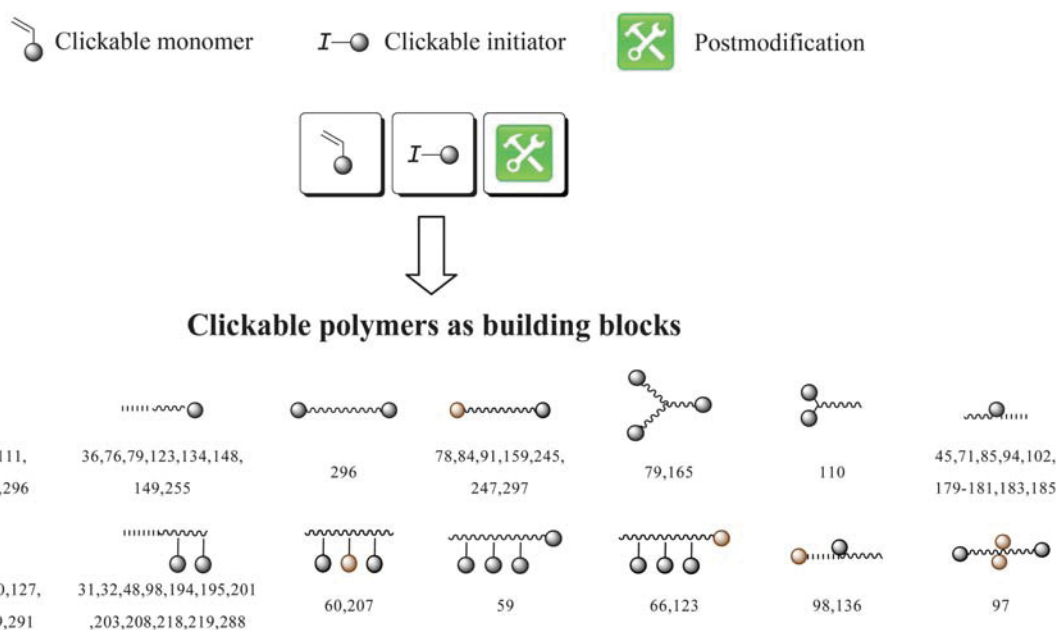
### 6.2.3 NMP

**Modification towards either alkyne or azide functionality.** A substitution reaction was carried out as pendant postmodification

for the random copolymer poly[styrene-*r*-(4-acetoxystyrene)] (Entry **84**).<sup>291</sup> The acetyl group was used as a protection for the phenolic hydroxy group that cannot be polymerized directly, since it acts as a radical scavenger. Deprotection was accomplished by using hydrazine monohydrate as a base for hydrolysis at room temperature to yield poly[styrene-*r*-(4-hydroxystyrene)]. The hydroxy group was further reacted with propargyl bromide under basic conditions in a Williamson ether synthesis to yield the clickable styrenic copolymer while retaining molar mass and polydispersity indices of the protected copolymer.<sup>291</sup>

Another postmodification strategy towards clickable side groups is the carbodiimide-mediated condensation which was demonstrated for the block copolymer poly(*t*BA-*b*-St) by Woolley and Hawker (Entry **85**).<sup>292</sup> First, the *t*-butyl group, acting as a protecting group, was cleaved using trifluoroacetic acid at room temperature. The resulting amphiphilic diblock polymer poly(acrylic acid-*b*-styrene) was assembled into micelles in water and partly functionalized with either 3-azidopropylamine or propargyl amine in a condensation reaction at room temperature using 1-[3'-(dimethylamino)propyl]-3-ethylcarbodiimide methiodide to activate the acid. The residual acid groups were crosslinked to obtain nanoparticles with azides or alkyne moieties on the outer shell.

Another postmodification strategy uses succinimide-functionalized acrylates as active ester for the condensation with amines under mild conditions.<sup>193</sup> The active ester is stable under the applied polymerization conditions and can be polymerized in a controlled way, while in contrast to alkyl acrylates no deprotection for further modification is required. Hereon, Malkoch *et al.* showed the preparation of random copolymers of *N*-(acryloyloxy)succinimide with either styrene, *t*-butylacrylate or acrylamide followed by a successful condensation reaction with propargyl amine or 1-amino-11-azido-3,6,9-trioxoundecane at 50 °C (Entry **86**). In addition, the amidation reaction does not interfere with the click reaction and can be used in a one-pot cascade reaction or simultaneously.<sup>193</sup>



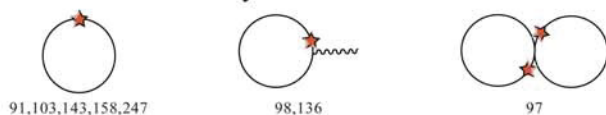
**Scheme 6** Schematic representation of clickable polymers: wavy = polymer chain; ●, ○ = orthogonal click functionalities, dashed = block segments.

## Clicked architectures

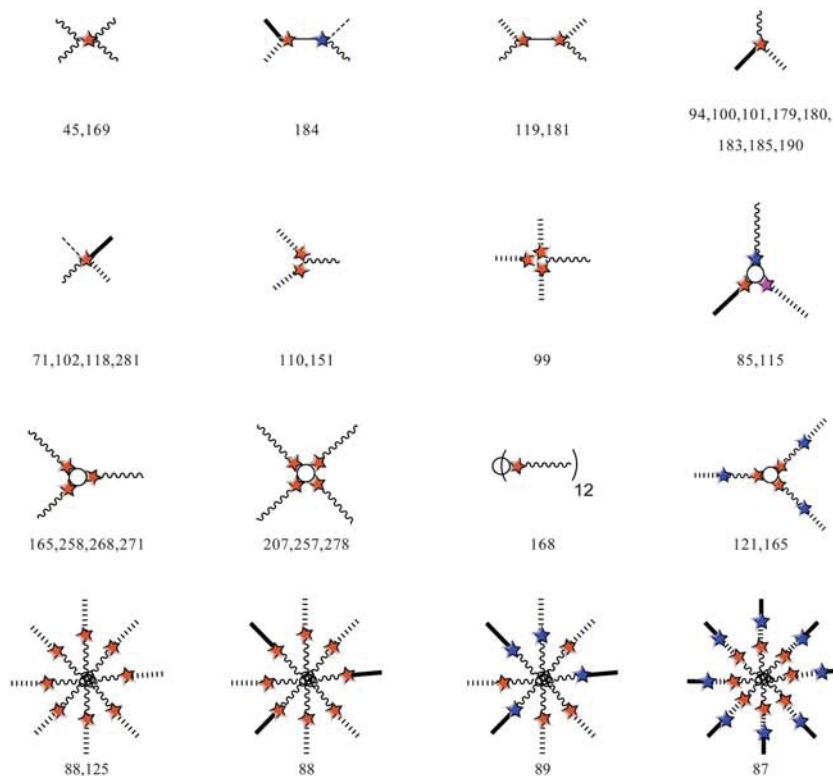
### Block copolymers



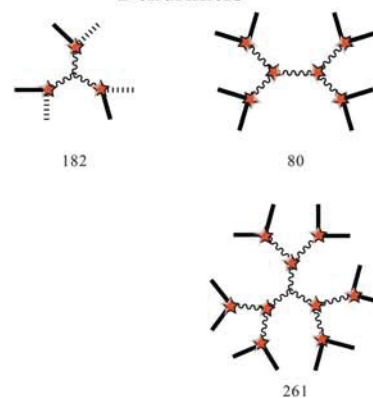
### Cyclic structures



### Star-like polymers



### Dendrimers



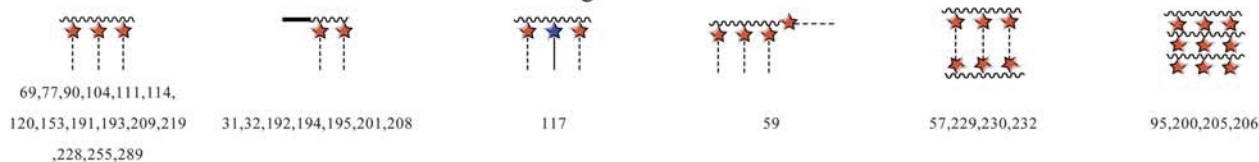
### Hyperbranched polymers

141,152,156,234

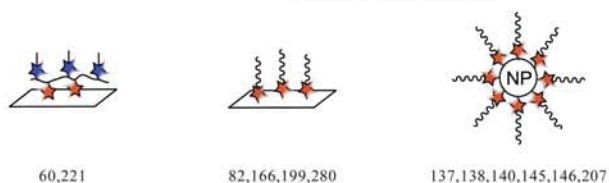
### Networks

83

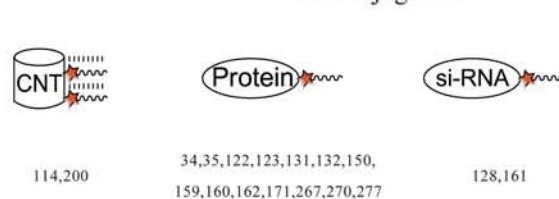
### Grafting and 2D architectures



### Surface attachment



### Bioconjugation



**Scheme 7** Schematic representation of selected clicked architectures: (wavy line = polymer chain; solid line = block segments; crosslinked polymer, star, blue star, pink star = different clicked functions, O = multifunctional core).

A facile approach towards pendant azide-functionalized polymers *via* postmodification is the reaction of benzylic chloride with sodium azide in a nucleophilic substitution reaction (Entry 87). The reaction is efficient at room temperature in DMF. Following this procedure, a random copolymer consisting of 4-(chloromethyl)styrene and styrene was transformed with sodium azide.<sup>293</sup> Furthermore, a random terpolymer consisting of 4-(chloromethyl)styrene, styrene as well as 4'-(anthracene-methyloxymethyl)styrene was efficiently modified to the pendant azido- and anthracene-containing derivative.<sup>117</sup> O'Reilly *et al.* modified the amphiphilic diblock copolymer poly[(acrylic acid)-*b*-styrene-*r*-4-chloromethylstyrene] *via* the described procedure to obtain, after crosslinking, nanoparticles with azide-functionalized cores.<sup>292</sup> In 2009, Ting *et al.* transformed homopolymers of 4-(chloromethyl)styrene as well as random and block copolymers with styrene at 60 °C in a mixture of DMSO/THF to the pendant azide-functionalized polymers.<sup>294</sup>

*Modification towards diene functionality for Diels–Alder reaction.* The pendant benzylic chloro group in 4-(chloromethyl)styrene containing polymers were also modified by the etherification reaction with 9-(oxymethyl)anthracene (Entry 90). Thereby, an excess of 9-(oxymethyl)anthracene was activated with sodium hydride to react with poly(styrene-*r*-4-chloromethylstyrene) to the anthracene-functionalized polymer at room temperature,<sup>117</sup> although the conversion only went to completion by using higher temperatures.<sup>120</sup>

## 7. Applications of clickable polymers

The concept of click chemistry combined with the concept of controlled radical polymerizations represent an ideal pair for the preparation of tailor-made macromolecular architectures.

The striking advantage of this combination can be clearly seen by the variety of clicked architectures that become possible by using clickable polymers as building blocks (Schemes 6 and 7). The schemes should provide an overview over the clickable and clicked architectures, while assigning assorted references. The origin for the large variety of architectures is the overcoming of limitations inherent for other techniques, which allows the design of new architectures prepared in high yields and with a wide range of accessible molar masses and constitutions. In this way, some block combinations become possible, which were not directly polymerizable due to disparate reactivities. An example for such an architecture is the block copolymer of styrene and ethylene glycol (EG) using the 1,3-dipolar cycloaddition of azides and acetylene of the respective end groups.

Utilizing the different approaches (clickable initiator, clickable monomer and postmodification) different types of highly functional polymers are accessible and can act as building blocks for the preparation of more complex structures. Several clickable polymers can be prepared: (i) End functional polymers on one or on both sites, (ii) mid-chain functional polymers, (iii) side-chain functional polymers and (iv) combinations of them (Scheme 6). These clickable polymers act as basic modules for further functionalization reactions to engineer more complex architectures (Scheme 7). Hereon, different linear block copolymers such as di-, ter- or quarterpolymers were prepared. The synthesis of different cyclic polymers such as eight-shaped or tadpole

polymers, which are limited for other non-click methods, has been realized using the click concept. These building blocks were also often used for the preparation of star-shaped polymers with 3 up to 12 arms as well as H-shaped or miktoarm star polymers. In this respect, two strategies arise for the synthesis of star-like polymers by clicking: (i) Using mid-chain functional polymers or (ii) end functional polymers onto a multifunctional core. Furthermore, several dendrimers and hyperbranched architectures were also realized by combining CRP and click chemistry. An elegant example represents the thiol-yne reaction for the preparation of hyperbranched polymers.

Another focus of polymer research is the grafting approach of side-chain functional polymers, which can be prepared by using the clickable monomer approach or the postmodification approach of pendant groups. The main advantage for this strategy is the facile tuning of polymer properties for a specific application. One clickable polymer backbone can act as building block for a variety of functionalization reactions (Scheme 6). Moreover, surface patterning is also of interest in material science. Polymers were clicked *via* CuAAC to different surfaces such as carbon nanotubes or nanoparticles (Si, Au). Also the construction of multilayer systems (layer-by-layer approach) are possible by using the 1,3-dipolar cycloaddition and CRP.

The interest in polymer-functionalized biomaterials strongly increased in the last years due to the facile access by using click chemistry for efficient conjugation and CRPs for tailoring the polymeric architectures. In this vein, different functional polymers were coupled with several proteins and siRNA.

## 8. Conclusion and outlook

In summary, it is clearly demonstrated in recent years that the combination of controlled/“living” radical polymerization (CRP) techniques and click reactions has become an inevitable route for preparing highly functional tailor-made macromolecules. This combination has been tremendously advanced since the introduction of the concept of click chemistry in 2001 by the cumulative efforts of a large number of research groups all over the globe. These developments on the preparation of new well-defined clickable polymers enabled straightforward access to demanding polymer structures such as cyclic and miktoarm star polymers.

Two combinations of CRP with click chemistry seem to be the perfect match: ATRP in combination with azide cycloaddition and RAFT with thio-click chemistry. Halogen-terminated polymers are directly obtained by ATRP and can be transformed to azide-terminated polymers using a simple azidation procedure. As a limitation, this combination may not be suitable for the preparation of clickable polymers of high molar masses, since a high end-group fidelity of the halogen-terminated polymers is only assured for low molar masses and low conversions. Even the most efficient postmodification reaction will not overcome this inherent problem. Nevertheless, ATRP and azide-alkyne click reactions are one of the most prominent combinations to prepare functional materials. Alternatively, thiol-terminated polymers are easily accessible from polymers prepared using the RAFT technique by reduction of the CTA end group. It has been demonstrated that these thiol-terminated polymers can be clicked not only to unsaturated double bonds but also to alkynes,

bromo, and *para*-fluoro groups making the combination of RAFT polymerizations with thio-click chemistry a powerful method. It should be noted that certain kinds of radical thiol-ene reactions do not fulfill the click criterion of a high reaction efficiency if they are applied for polymer-polymer conjugation.

We are confident that the combination of CRP and click chemistry methods will continue flourishing in the near future leading to new functional polymeric materials. Eventually, this will lead to a further establishment of CRP in combination with click chemistry as a scientific tool rather than being a separate research topic. Furthermore, it is evident that new trends in click chemistry, *e.g.* the development of advanced metal-free click reactions employing more reactive clickable units such as cyclooctynes as click counterparts to nitrones or nitrile oxides, will be combined with CRP methods in the near future, which will further expand the potential field of applications.

## Abbreviations

AcOSt	4-acetoxystyrene	DDAT	<i>S</i> -1-dodecyl- <i>S'</i> -( $\alpha,\alpha'$ -dimethyl- $\alpha''$ -acetic acid) trithiocarbonate
AA	acrylic acid	DDET	<i>S</i> -1-dodecyl- <i>S'</i> -( $\alpha,\alpha'$ -dimethyl- $\alpha''$ -ethyl acetate) trithiocarbonate
AIBN	azoisobutyronitrile	DEGMA	di(ethylene glycol) methylether methacrylate
AM	acrylamide	DIPEA	<i>S</i> -dodecyl- <i>S'</i> -( $\alpha,\alpha'$ -dimethylpentafluorophenyl acetate) trithiocarbonate
AN	acrylonitrile	DMAM	<i>N,N</i> -dimethylacrylamide
APBIB	3-azidopropyl 2-bromoisobutyrate	DEAM	<i>N,N</i> -diethylacrylamide
ATRP	atom transfer radical polymerization	DEAEMA	2-(diethylamino) ethyl methacrylate
ATREP	atom transfer radical emulsion polymerization	DMAEMA	2-(dimethylamino) ethyl methacrylate
BBiBE	1,2-bis(bromoisobutyryloxy)ethane	EBiB	ethyl 2-bromoisobutyrate
BDAT	<i>S,S'</i> -bis( $\alpha,\alpha'$ -dimethyl- $\alpha''$ -acetic acid) trithiocarbonate	EA	ethyl acrylate
BDB	benzyl dithiobenzoate	EEA	1-ethoxyethyl acrylate
BETP	benzyl 2-(ethylthiocarbonothioylthio) propanoate	EHA	2-ethylhexyl acrylate
BICDT	benzyl 1 <i>H</i> -imidazole-1-carbodithioate	EtSO <sub>2</sub> N <sub>3</sub>	ethanesulfonyl azide
bpy	2,2'-bipyridine	FMA	furfuryl methacrylate
BlocBuilder®	<i>N</i> -(2-methylpropyl)- <i>N</i> -(1-diethylphosphono-2,2-dimethylpropyl)- <i>O</i> -(2-carboxylprop-2-yl) hydroxylamine	GMA	glycidyl methacrylate
BMP	2-bromo-2-methyl-propionate	HEA	2-hydroxyethyl acrylate
BMPA	2-bromo-2-methyl-propionamide	HEMA	2-hydroxyethyl methacrylate
BMPABE	2-bromo-2-methyl-propionic acid benzyl ester	HMA	hostasol methacrylate
BPIT	butyl phthalimidomethyl trithiocarbonate	HMTETA	1,1,4,7,10,10-hexamethyl triethylenetetramine
BPN	2-bromopropionitrile	HPMA	2-hydroxypropyl methacrylate
BPO	dibenzoylperoxide	HPMAM	2-hydroxypropyl methacrylamide
BSPA	3-benzylsulfanyl-thiocarbonylsulfanyl propionic acid	<i>i</i> BoA	<i>i</i> -bornyl acrylate
CAN	ceric ammonium nitrate	<i>p</i> HSt	4-hydroxystyrene
CBDB	2-cyano-2-butyl dithiobenzoate	KSPMA	potassium 3-sulfopropyl methacrylate
CBDN	$\alpha$ -cyanobenzyl dithionaphthalate	LMA	lauryl methacrylate
CDB	2-phenylpropan-2-yl dithiobenzoate (cumyl dithiobenzoate)	MA	methyl acrylate
CNT	carbon nanotube	MAA	methacrylic acid
$\epsilon$ -CL	$\epsilon$ -caprolactone	MCPMDB	( <i>S</i> )-methoxycarbonylphenylmethyl dithiobenzoate
CPADB	(4-cyanopentanoic acid) dithiobenzoate	Me <sub>6</sub> TREN	tris(2-(dimethylamino)-ethyl) amine
CPDB	(2-(2-cyano-propyl)) dithiobenzoate	MMA	methyl methacrylate
CTA	chain transfer agent	mPEG	linear methoxy poly(ethylene glycol)
CRP	controlled radical polymerization	MPPCTTA	methyl 2-phenyl-2-(phenylcarbonothioylthio) acetate
		NaCp	cyclopentadienide
		<i>n</i> BA	<i>n</i> -butyl acrylate
		<i>n</i> BMA	<i>n</i> -butyl methacrylate
		NIPAM	<i>N</i> -isopropylacrylamide
		NiCp <sub>2</sub>	nickelocene
		NMP	nitroxide-mediated radical polymerization
		NP	nanoparticle
		NVP	<i>N</i> -vinylpyrrolidone
		OEGA	oligo(ethylene glycol) methylether acrylate
		OEGMA	oligo(ethylene glycol) methylether methacrylate
		OPA	(2-oxopropyl)acrylate
		PBP	propargyl 2-bromopropionate
		PDB	1-phenylethyl dithiobenzoate
		PEB	1-phenylethylbromide
		PEDT	<i>S</i> -1-phenylethyl- <i>S'</i> -dodecyl-trithiocarbonate
		PFPPCV	pentafluorophenyl-(4-phenylthiocarbonylthio-4-cyanovalerate)
		PFS	pentafluorostyrene
		PMDETA	<i>N,N,N',N',N''</i> -pentamethyldiethylene-triamine

poC	postclick
prC	preclick
RAFT	reversible addition-fragmentation chain transfer polymerization
ROP	ring-opening polymerization
SG1	<i>N</i> -(2-methylpropyl)- <i>N</i> -(1-diethylphosphono-2,2-dimethylpropyl)- <i>N</i> -oxyl
SMA	solketal methacrylate
St	styrene
<i>t</i> BA	<i>t</i> -butyl acrylate
<i>t</i> BMA	<i>t</i> -butyl methacrylate
TBAF	tetrabutylammonium fluoride
<i>t</i> BOST	4- <i>t</i> -butyloxystyrene
TBDMS	<i>t</i> -butyldimethyl-silyl
TEMPO	2,2,6,6-tetramethylpiperidinylnitroxide
THPA	tetrahydropyran acrylate
TIPNO	2,2,5-trimethyl-4-phenyl-3-azahexane-3-nitroxide
TIPS	triisopropylsilyl
TMS	trimethylsilyl
TosCl	<i>p</i> -toluenesulfonyl chloride
VAc	vinylacetate
VBA	vinylbenzyl azide
4VP	4-vinylpyridine.

Polymer abbreviations are formed by adding the suffix 'P' or 'poly' to the corresponding monomer abbreviation. The only exception is styrene, where the monomer is represented by St and the polymer by PS.

## Acknowledgements

Financial support of the Dutch Polymer Institute (DPI) and of the Thuringian Ministry for Education, Science and Culture (grant #B514-09051, NanoConSens) is gratefully acknowledged.

## Notes and references

- M. Szwarc, *Nature*, 1956, **178**, 1168–1169.
- M. Szwarc, M. Levy and R. Milkovich, *J. Am. Chem. Soc.*, 1956, **78**, 2656–2657.
- V. Ladmiral, G. Mantovani, G. J. Clarkson, S. Cauet, J. L. Irwin and D. M. Haddleton, *J. Am. Chem. Soc.*, 2006, **128**, 4823–4830.
- E. R. Gillies and J. M. J. Fréchet, *Drug Discovery Today*, 2005, **10**, 35–43.
- K. Matyjaszewski, *Prog. Polym. Sci.*, 2005, **30**, 858–875.
- M. Ouchi, T. Terashima and M. Sawamoto, *Chem. Rev.*, 2009, **109**, 4963–5050.
- K. Matyjaszewski and J. Xia, *Chem. Rev.*, 2001, **101**, 2921–2990.
- M. Kamigaito, T. Ando and M. Sawamoto, *Chem. Rev.*, 2001, **101**, 3689–3746.
- C. J. Hawker, A. W. Bosman and E. Harth, *Chem. Rev.*, 2001, **101**, 3661–3688.
- R. K. Iha, K. L. Wooley, A. M. Nyström, D. J. Burke, M. J. Kade and C. J. Hawker, *Chem. Rev.*, 2009, **109**, 5620–5686.
- G. Moad, E. Rizzardo and S. H. Thang, *Aust. J. Chem.*, 2006, **59**, 669–692.
- G. Moad, E. Rizzardo and S. H. Thang, *Aust. J. Chem.*, 2009, **62**, 1402–1472.
- H. C. Kolb, M. G. Finn and K. B. Sharpless, *Angew. Chem., Int. Ed.*, 2001, **40**, 2004–2021.
- D. Fournier, R. Hoogenboom and U. S. Schubert, *Chem. Soc. Rev.*, 2007, **36**, 1369–1380.
- W. H. Binder and R. Sachsenhofer, *Macromol. Rapid Commun.*, 2007, **28**, 15–54.
- Wolfgang H. Binder and Robert Sachsenhofer, *Macromol. Rapid Commun.*, 2008, **29**, 952–981.
- C. R. Becer, R. Hoogenboom and U. S. Schubert, *Angew. Chem., Int. Ed.*, 2009, **48**, 4900–4908.
- J.-F. Lutz, *Angew. Chem., Int. Ed.*, 2007, **46**, 1018–1025.
- A. B. Lowe, *Polym. Chem.*, 2010, **1**, 17–36.
- P. L. Golas and K. Matyjaszewski, *Chem. Soc. Rev.*, 2010, **39**, 1338–1354.
- C. Barner-Kowollik and A. J. Inglis, *Macromol. Chem. Phys.*, 2009, **210**, 987–992.
- D. D. Diaz, S. Punna, P. Holzer, A. K. McPherson, K. B. Sharpless, V. V. Fokin and M. G. Finn, *J. Polym. Sci., Part A: Polym. Chem.*, 2004, **42**, 4392–4403.
- P. Wu, A. K. Feldman, A. K. Nugent, C. J. Hawker, A. Scheel, B. Voit, J. Pyun, J. M. J. Fréchet, K. B. Sharpless and V. V. Fokin, *Angew. Chem., Int. Ed.*, 2004, **43**, 3928–3932.
- W. D. Sharpless, P. Wu, T. V. Hansen and J. G. Lindberg, *J. Chem. Educ.*, 2005, **82**, 1833–1836.
- J.-F. Lutz, *Angew. Chem., Int. Ed.*, 2008, **47**, 2182–2184.
- A. J. Inglis and C. Barner-Kowollik, *Macromol. Rapid Commun.*, 2010, **31**, 1247–1266.
- C. E. Hoyle, T. Y. Lee and T. Roper, *J. Polym. Sci., Part A: Polym. Chem.*, 2004, **42**, 5301–5338.
- C. E. Hoyle and C. N. Bowman, *Angew. Chem., Int. Ed.*, 2010, **49**, 1540–1573.
- A. B. Lowe, C. E. Hoyle and C. N. Bowman, *J. Mater. Chem.*, 2010, **20**, 4745–4750.
- R. Hoogenboom, *Angew. Chem., Int. Ed.*, 2010, **49**, 3415–3417.
- C. Ott, R. Hoogenboom and U. S. Schubert, *Chem. Commun.*, 2008, 3516–3518.
- C. R. Becer, K. Babiuch, D. Pilz, S. Hornig, T. Heinze, M. Gottschaldt and U. S. Schubert, *Macromolecules*, 2009, **42**, 2387–2394.
- I. Singh, Z. Zarafshani, J.-F. Lutz and F. Heaney, *Macromolecules*, 2009, **42**, 5411–5413.
- D. Bontempo, K. L. Heredia, B. A. Fish and H. D. Maynard, *J. Am. Chem. Soc.*, 2004, **126**, 15372–15373.
- K. L. Heredia, D. Bontempo, T. Ly, J. T. Byers, S. Halstenberg and H. D. Maynard, *J. Am. Chem. Soc.*, 2005, **127**, 16955–16960.
- J. Liu, V. Bulmus, C. Barner-Kowollik, M. H. Stenzel and T. P. Davis, *Macromol. Rapid Commun.*, 2007, **28**, 305–314.
- H. Durmaz, A. Dag, O. Altintas, T. Erdogan, G. Hizal and U. Tunca, *Macromolecules*, 2007, **40**, 191–198.
- S. Sinnwell, A. J. Inglis, T. P. Davis, M. H. Stenzel and C. Barner-Kowollik, *Chem. Commun.*, 2008, 2052–2054.
- A. J. Inglis, S. Sinnwell, M. H. Stenzel and C. Barner-Kowollik, *Angew. Chem. Int. Ed.*, 2009, **48**, 2411–2414.
- R. Huisgen, *Angew. Chem., Int. Ed. Engl.*, 1963, **2**, 565–598.
- P. Cintas, A. Barge, S. Tagliapietra, L. Boffa and G. Cravotto, *Nat. Protoc.*, 2010, **5**, 607–616.
- N. J. Agard, J. A. Prescher and C. R. Bertozzi, *J. Am. Chem. Soc.*, 2004, **126**, 15046–15047.
- S. S. v. Berkel, A. J. Dirks, S. A. Meeuwissen, D. L. L. Pingen, O. C. Boerman, P. Laverman, F. L. v. Delft, J. J. L. M. Cornelissen and F. P. J. T. Rutjes, *ChemBioChem*, 2008, **9**, 1805–1815.
- C. J. Duxbury, D. Cummins and A. Heise, *J. Polym. Sci., Part A: Polym. Chem.*, 2009, **47**, 3795–3802.
- E. Gungor, G. Hizal and U. Tunca, *J. Polym. Sci., Part A: Polym. Chem.*, 2008, **46**, 6703–6711.
- F. Himo, T. Lovell, R. Hilgraf, V. V. Rostovtsev, L. Noodleman, K. B. Sharpless and V. V. Fokin, *J. Am. Chem. Soc.*, 2005, **127**, 210–216.
- Z. P. Demko and K. B. Sharpless, *J. Org. Chem.*, 2001, **66**, 7945–7950.
- N. V. Tsarevsky, K. V. Bernaerts, B. Dufour, F. E. Du Prez and K. Matyjaszewski, *Macromolecules*, 2004, **37**, 9308–9313.
- S. Bräse, C. Gil, K. Knepper and V. Zimmermann, *Angew. Chem., Int. Ed.*, 2005, **44**, 5188–5240.
- B. Yu, J. W. Chan, C. E. Hoyle and A. B. Lowe, *J. Polym. Sci., Part A: Polym. Chem.*, 2009, **47**, 3544–3557.
- C. E. Hoyle, A. B. Lowe and C. N. Bowman, *Chem. Soc. Rev.*, 2010, **39**, 1355–1387.

- 52 K. L. Killops, L. M. Campos and C. J. Hawker, *J. Am. Chem. Soc.*, 2008, **130**, 5062–5064.
- 53 S. P. S. Koo, M. M. Stamenovic, R. A. Prasath, A. J. Inglis, F. E. Du Prez, C. Barner-Kowollik, W. V. Camp and T. Junkers, *J. Polym. Sci., Part A: Polym. Chem.*, 2010, **48**, 1699–1713.
- 54 H. Li, B. Yu, H. Matsushima, C. E. Hoyle and A. B. Lowe, *Macromolecules*, 2009, **42**, 6537–6542.
- 55 A. J. Inglis, M. H. Stenzel and C. Barner-Kowollik, *Macromol. Rapid Commun.*, 2009, **30**, 1792–1798.
- 56 A. Dag, H. Durmaz, V. Kirmizi, G. Hizal and U. Tunca, *Polym. Chem.*, 2010, **1**, 621–623.
- 57 A. A. Kavitha and N. K. Singha, *ACS Appl. Mater. Interfaces*, 2009, **1**, 1427–1436.
- 58 K. L. Heredia and H. D. Maynard, *Org. Biomol. Chem.*, 2007, **5**, 45–53.
- 59 N. V. Tsarevsky, S. A. Bencherif and K. Matyjaszewski, *Macromolecules*, 2007, **40**, 4439–4445.
- 60 S. Fleischmann, K. Hinrichs, U. Oertel, S. Reichelt, K.-J. Eichhorn and B. Voit, *Macromol. Rapid Commun.*, 2008, **29**, 1177–1185.
- 61 H. Kwart and K. King, *Chem. Rev.*, 1968, **68**, 415–447.
- 62 J. Sauer and R. Sustmann, *Angew. Chem., Int. Ed. Engl.*, 1980, **19**, 779–807.
- 63 T. Dispinar, R. Sanyal and A. Sanyal, *J. Polym. Sci., Part A: Polym. Chem.*, 2007, **45**, 4545–4551.
- 64 J. A. Syrett, G. Mantovani, W. R. S. Barton, D. Price and D. M. Haddleton, *Polym. Chem.*, 2010, **1**, 102–106.
- 65 A. J. Inglis, L. Nebhani, O. Altintas, F. G. Schmidt and C. Barner-Kowollik, *Macromolecules*, 2010, **43**, 5515–5520.
- 66 J. Geng, G. Mantovani, L. Tao, J. Nicolas, G. Chen, R. Wallis, D. A. Mitchell, B. R. G. Johnson, S. D. Evans and D. M. Haddleton, *J. Am. Chem. Soc.*, 2007, **129**, 15156–15163.
- 67 R. J. Thibault, K. Takizawa, P. Lowenheim, B. Helms, J. L. Mynar, J. M. J. Frechet and C. J. Hawker, *J. Am. Chem. Soc.*, 2006, **128**, 12084–12085.
- 68 V. L. G. Mantovani, L. Tao and D. M. Haddleton, *Chem. Commun.*, 2005, 2089–2091.
- 69 J. Geng, J. Lindqvist, G. Mantovani and D. M. Haddleton, *Angew. Chem., Int. Ed.*, 2008, **47**, 4180–4183.
- 70 L. Mespouille, M. Vachaudez, F. Suriano, P. Gerbaux, O. Coulembier, P. Degee, R. Flammang and P. Dubois, *Macromol. Rapid Commun.*, 2007, **28**, 2151–2158.
- 71 O. Altintas, G. Hizal and U. Tunca, *J. Polym. Sci., Part A: Polym. Chem.*, 2008, **46**, 1218–1228.
- 72 E. Gungor, H. Durmaz, G. Hizal and U. Tunca, *J. Polym. Sci., Part A: Polym. Chem.*, 2008, **46**, 4459–4468.
- 73 J. A. Opsteen and J. C. M. van Hest, *Chem. Commun.*, 2005, 57–59.
- 74 M. A. Bennett, *Chem. Rev.*, 1962, **62**, 611–652.
- 75 R. Nast, *Coord. Chem. Rev.*, 1982, **47**, 89–124.
- 76 A. Hasneen, H. S. Han and H.-J. Paik, *React. Funct. Polym.*, 2009, **69**, 681–687.
- 77 B. S. Sumerlin, N. V. Tsarevsky, G. Louche, R. Y. Lee and K. Matyjaszewski, *Macromolecules*, 2005, **38**, 7540–7545.
- 78 J. A. Opsteen and J. C. M. Van Hest, *J. Polym. Sci., Part A: Polym. Chem.*, 2007, **45**, 2913–2924.
- 79 Z. Zarafshani, O. Akdemir and J.-F. Lutz, *Macromol. Rapid Commun.*, 2008, **29**, 1161–1166.
- 80 C. N. Urbani, C. A. Bell, D. Lonsdale, M. R. Whittaker and M. J. Monteiro, *Macromolecules*, 2008, **41**, 76–86.
- 81 G. D. Fu, L. Q. Xu, F. Yao, K. Zhang, X. F. Wang, M. F. Zhu and S. Z. Nie, *ACS Appl. Mater. Interfaces*, 2009, **1**, 239–243.
- 82 G. J. Chen, L. Tao, G. Mantovani, V. Ladmiral, D. P. Burt, J. V. Macpherson and D. M. Haddleton, *Soft Matter*, 2007, **3**, 732–739.
- 83 L. Q. Xu, F. Yao, G. D. Fu and L. Shen, *Macromolecules*, 2009, **42**, 6385–6392.
- 84 N. V. Tsarevsky, B. S. Sumerlin and K. Matyjaszewski, *Macromolecules*, 2005, **38**, 3558–3561.
- 85 C. H. Li, Z. S. Ge, H. W. Liu and S. Y. Liu, *J. Polym. Sci., Part A: Polym. Chem.*, 2009, **47**, 4001–4013.
- 86 W. Lin, Q. Fu, Y. Zhang and J. Huang, *Macromolecules*, 2008, **41**, 4127–4135.
- 87 H. Durmaz, A. Dag, D. Gursoy, A. L. Demirel, G. Hizal and U. Tunca, *J. Polym. Sci., Part A: Polym. Chem.*, 2010, **48**, 1557–1564.
- 88 H. Durmaz, A. Dag, E. Erdogan, A. L. Demirel, G. Hizal and U. Tunca, *J. Polym. Sci., Part A: Polym. Chem.*, 2010, **48**, 99–108.
- 89 A. Dag, H. Durmaz, V. Kirmizi, G. Hizal and U. Tunca, *Polym. Chem.*, 2010, **1**, 621–623.
- 90 W. Van Camp, V. Germonpre, L. Mespouille, P. Dubois, E. J. Goethals and F. E. Du Prez, *React. Funct. Polym.*, 2007, **67**, 1168–1180.
- 91 J. Xu, J. Ye and S. Y. Liu, *Macromolecules*, 2007, **40**, 9103–9110.
- 92 L. Mespouille, M. Vachaudez, F. Suriano, P. Gerbaux, W. Van Camp, O. Coulembier, P. Degee, R. Flammang, F. Du Prez and P. Dubois, *React. Funct. Polym.*, 2008, **68**, 990–1003.
- 93 W. A. Braunecker and K. Matyjaszewski, *Prog. Polym. Sci.*, 2007, **32**, 93–146.
- 94 Y. F. Zhang, L. Hao, J. M. Hu, C. H. Li and S. Y. Liu, *Macromol. Rapid Commun.*, 2009, **30**, 941–947.
- 95 C. J. Huang and F. C. Chang, *Macromolecules*, 2009, **42**, 5155–5166.
- 96 J.-M. Schumers, J.-F. Gohy and C.-A. Fustin, *Polym. Chem.*, 2010, **1**, 161–163.
- 97 G. Y. Shi and C. Y. Pan, *Macromol. Rapid Commun.*, 2008, **29**, 1672–1678.
- 98 Y. Q. Dong, Y. Y. Tong, B. T. Dong, F. S. Du and Z. C. Li, *Macromolecules*, 2009, **42**, 2940–2948.
- 99 J. Zhu, X. L. Zhu, E. T. Kang and K. G. Neoh, *Polymer*, 2007, **48**, 6992–6999.
- 100 Y. F. Zhang, C. H. Li and S. Y. Liu, *J. Polym. Sci., Part A: Polym. Chem.*, 2009, **47**, 3066–3077.
- 101 G. H. Deng, D. Y. Ma and Z. Z. Xu, *Eur. Polym. J.*, 2007, **43**, 1179–1187.
- 102 G. W. Wang, X. L. Luo, C. Liu and J. L. Huang, *J. Polym. Sci., Part A: Polym. Chem.*, 2008, **46**, 2154–2166.
- 103 B. A. Laurent and S. M. Grayson, *J. Am. Chem. Soc.*, 2006, **128**, 4238–4239.
- 104 C. H. Li, Z. S. Ge, J. Fang and S. Y. Liu, *Macromolecules*, 2009, **42**, 2916–2924.
- 105 V. Ladmiral, T. M. Legge, Y. L. Zhao and S. Perrier, *Macromolecules*, 2008, **41**, 6728–6732.
- 106 W. Agut, D. Taton and S. Lecommandoux, *Macromolecules*, 2007, **40**, 5653–5661.
- 107 S. Pfeifer, Z. Zarafshani, N. Badi and J.-F. Lutz, *J. Am. Chem. Soc.*, 2009, **131**, 9195–9197.
- 108 Y. Li, J. W. Yang and B. C. Benicewicz, *J. Polym. Sci., Part A: Polym. Chem.*, 2007, **45**, 4300–4308.
- 109 M. Urien, H. Erothu, E. Cloutet, R. C. Hiorns, L. Vignau and H. Cramail, *Macromolecules*, 2008, **41**, 7033–7040.
- 110 C. H. Li, J. M. Hu, J. Yin and S. Y. Liu, *Macromolecules*, 2009, **42**, 5007–5016.
- 111 X. Jiang, M. C. Lok and W. E. Hennink, *Bioconjugate Chem.*, 2007, **18**, 2077–2084.
- 112 P. D. Topham, N. Sandon, E. S. Read, J. Madsen, A. J. Ryan and S. P. Armes, *Macromolecules*, 2008, **41**, 9542–9547.
- 113 A. Narumi, K. Fuchise, R. Kakuchi, A. Toda, T. Satoh, S. Kawaguchi, K. Sugiyama, A. Hirao and T. Kakuchi, *Macromol. Rapid Commun.*, 2008, **29**, 1126–1133.
- 114 Y. Zhang, H. K. He and C. Gao, *Macromolecules*, 2008, **41**, 9581–9594.
- 115 A. Dag, H. Durmaz, G. Hizal and U. Tunca, *J. Polym. Sci., Part A: Polym. Chem.*, 2008, **46**, 302–313.
- 116 M. Li, P. De, S. R. Gondi and B. S. Sumerlin, *J. Polym. Sci., Part A: Polym. Chem.*, 2008, **46**, 5093–5100.
- 117 A. Dag, H. Durmaz, E. Demir, G. Hizal and U. Tunca, *J. Polym. Sci., Part A: Polym. Chem.*, 2008, **46**, 6969–6977.
- 118 O. Altintas, G. Hizal and U. Tunca, *Des. Monomers Polym.*, 2009, **12**, 83–98.
- 119 H. Durmaz, F. Karatas, U. Tunca and G. Hizal, *J. Polym. Sci., Part A: Polym. Chem.*, 2006, **44**, 3947–3957.
- 120 B. Gacal, H. Durmaz, M. A. Tasdelen, G. Hizal, U. Tunca, Y. Yagci and A. L. Demirel, *Macromolecules*, 2006, **39**, 5330–5336.
- 121 H. Durmaz, A. Dag, A. Hizal, G. Hizal and U. Tunca, *J. Polym. Sci., Part A: Polym. Chem.*, 2008, **46**, 7091–7100.
- 122 G. Mantovani, F. Lecolley, L. Tao, D. M. Haddleton, J. Clerx, J. J. L. M. Cornelissen and K. Velonia, *J. Am. Chem. Soc.*, 2005, **127**, 2966–2973.
- 123 B. Le Droumaguet, G. Mantovani, D. M. Haddleton and K. Velonia, *J. Mater. Chem.*, 2007, **17**, 1916–1922.



- 124 M. Erdogan, G. Hizal, Ü. Tunca, D. Hayrabetyan and Ö. Pekcan, *Polymer*, 2002, **43**, 1925–1931.
- 125 A. Dag, H. Durmaz, U. Tunca and G. Hizal, *J. Polym. Sci., Part A: Polym. Chem.*, 2009, **47**, 178–187.
- 126 W. Zhang, W. Zhang, Z. Zhang, J. Zhu, Q. Pan and X. Zhu, *Polym. Bull.*, 2009, **63**, 467–483.
- 127 L. M. Campos, K. L. Killops, R. Sakai, J. M. J. Paulusse, D. Dameron, E. Drockenmüller, B. W. Messmore and C. J. Hawker, *Macromolecules*, 2008, **41**, 7063–7070.
- 128 V. Vázquez-Dorbatt, Z. P. Tolstyka, C.-W. Chang and H. D. Maynard, *Biomacromolecules*, 2009, **10**, 2207–2212.
- 129 A. Klaiherd, S. Ghosh and S. Thayumanavan, *Macromolecules*, 2007, **40**, 8518–8520.
- 130 N. V. Tsarevsky and K. Matyjaszewski, *Macromolecules*, 2002, **35**, 9009–9014.
- 131 H. D. Maynard, K. L. Heredia, R. C. Li, D. P. Parra and V. Vázquez-Dorbatt, *J. Mater. Chem.*, 2007, **17**, 4015–4017.
- 132 K. L. Heredia, Z. P. Tolstyka and H. D. Maynard, *Macromolecules*, 2007, **40**, 4772–4779.
- 133 D. Quemener, T. P. Davis, C. Barner-Kowollik and M. H. Stenzel, *Chem. Commun.*, 2006, 5051–5053.
- 134 R. K. O'Reilly, M. J. Joralemon, C. J. Hawker and K. L. Wooley, *J. Polym. Sci., Part A: Polym. Chem.*, 2006, **44**, 5203–5217.
- 135 S. R. S. Ting, A. M. Granville, D. Quemener, T. P. Davis, M. H. Stenzel and C. Barner-Kowollik, *Aust. J. Chem.*, 2007, **60**, 405–409.
- 136 G. Y. Shi, X. Z. Tang and C. Y. Pan, *J. Polym. Sci., Part A: Polym. Chem.*, 2008, **46**, 2390–2401.
- 137 R. Ranjan and W. J. Brittain, *Macromol. Rapid Commun.*, 2008, **29**, 1104–1110.
- 138 R. Ranjan and W. J. Brittain, *Macromol. Rapid Commun.*, 2007, **28**, 2084–2089.
- 139 A. J. D. Magenau, N. Martinez-Castro, D. A. Savin and R. F. Storey, *Macromolecules*, 2009, **42**, 8044–8051.
- 140 T. Zhang, Y. P. Wu, X. M. Pan, Z. H. Zheng, X. B. Ding and Y. X. Peng, *Eur. Polym. J.*, 2009, **45**, 1625–1633.
- 141 D. Konkolewicz, A. Gray-Weale and S. Perrier, *J. Am. Chem. Soc.*, 2009, **131**, 18075–18077.
- 142 N. Akeroyd, R. Pfuakwa and B. Klumperman, *Macromolecules*, 2009, **42**, 3014–3018.
- 143 A. S. Goldmann, D. Quemener, P. E. Millard, T. P. Davis, M. H. Stenzel, C. Barner-Kowollik and A. H. E. Mueller, *Polymer*, 2008, **49**, 2274–2281.
- 144 L. Barner, T. P. Davis, M. H. Stenzel and C. Barner-Kowollik, *Macromol. Rapid Commun.*, 2007, **28**, 539–559.
- 145 R. Ranjan and W. J. Brittain, *Macromolecules*, 2007, **40**, 6217–6223.
- 146 T. Zhang, Z. H. Zheng, X. B. Ding and Y. X. Peng, *Macromol. Rapid Commun.*, 2008, **29**, 1716–1720.
- 147 S. Püttick, D. J. Irvine, P. Licence and K. J. Thurecht, *J. Mater. Chem.*, 2009, **19**, 2679–2682.
- 148 S. R. Gondi, A. P. Vogt and B. S. Sumerlin, *Macromolecules*, 2007, **40**, 474–481.
- 149 P. De, S. R. Gondi and B. S. Sumerlin, *Biomacromolecules*, 2008, **9**, 1064–1070.
- 150 M. Li, P. De, S. R. Gondi and B. S. Sumerlin, *Macromol. Rapid Commun.*, 2008, **29**, 1172–1176.
- 151 A. Vora, K. Singh and D. C. Webster, *Polymer*, 2009, **50**, 2768–2774.
- 152 A. P. Vogt, S. R. Gondi and B. S. Sumerlin, *Aust. J. Chem.*, 2007, **60**, 396–399.
- 153 D. Quemener, M. Le Hellaye, C. Bissett, T. P. Davis, C. Barner-Kowollik and M. H. Stenzel, *J. Polym. Sci., Part A: Polym. Chem.*, 2008, **46**, 155–173.
- 154 J. Bernard, M. Save, B. Arathoon and B. Charleux, *J. Polym. Sci., Part A: Polym. Chem.*, 2008, **46**, 2845–2857.
- 155 F. Chen, Z. P. Cheng, J. Zhu, W. Zhang and X. L. Zhu, *Eur. Polym. J.*, 2008, **44**, 1789–1795.
- 156 A. P. Vogt and B. S. Sumerlin, *Macromolecules*, 2008, **41**, 7368–7373.
- 157 Z. S. An, W. Tang, M. H. Wu, Z. Jiao and G. D. Stucky, *Chem. Commun.*, 2008, 6501–6503.
- 158 X. P. Qiu, F. Tanaka and F. M. Winnik, *Macromolecules*, 2007, **40**, 7069–7071.
- 159 C. Boyer, J. Liu, V. Bulmus, T. P. Davis, C. Barner-Kowollik and M. H. Stenzel, *Macromolecules*, 2008, **41**, 5641–5650.
- 160 J. Liu, V. Bulmus, D. L. Herlambang, C. Barner-Kowollik, M. H. Stenzel and T. P. Davis, *Angew. Chem., Int. Ed.*, 2007, **46**, 3099–3103.
- 161 K. L. Heredia, T. H. Nguyen, C.-W. Chang, V. Bulmus, T. P. Davis and H. D. Maynard, *Chem. Commun.*, 2008, 3245–3247.
- 162 C. Boyer, V. Bulmus, J. Liu, T. P. Davis, M. H. Stenzel and C. Barner-Kowollik, *J. Am. Chem. Soc.*, 2007, **129**, 7145–7154.
- 163 C. Boyer, J. Liu, L. Wong, M. Tippett, V. Bulmus and T. P. Davis, *J. Polym. Sci., Part A: Polym. Chem.*, 2008, **46**, 7207–7224.
- 164 J. Liu, H. Liu, C. Boyer, V. Bulmus and T. P. Davis, *J. Polym. Sci., Part A: Polym. Chem.*, 2009, **47**, 899–912.
- 165 S. Sinnwell, A. J. Inglis, M. H. Stenzel and C. Barner-Kowollik, *Macromol. Rapid Commun.*, 2008, **29**, 1090–1096.
- 166 L. Nebhani, P. Gerstel, P. Atanasova, M. Bruns and C. Barner-Kowollik, *J. Polym. Sci., Part A: Polym. Chem.*, 2009, **47**, 7090–7095.
- 167 L. Nebhani, S. Sinnwell, C. Y. Lin, M. L. Coote, M. H. Stenzel and C. Barner-Kowollik, *J. Polym. Sci., Part A: Polym. Chem.*, 2009, **47**, 6053–6071.
- 168 S. Sinnwell, M. Lammens, M. H. Stenzel, F. E. Du Prez and C. Barner-Kowollik, *J. Polym. Sci., Part A: Polym. Chem.*, 2009, **47**, 2207–2213.
- 169 A. J. Inglis, S. Sinnwell, T. P. Davis, C. Barner-Kowollik and M. H. Stenzel, *Macromolecules*, 2008, **41**, 4120–4126.
- 170 S. Sinnwell, C. V. Synatschke, T. Junkers, M. H. Stenzel and C. Barner-Kowollik, *Macromolecules*, 2008, **41**, 7904–7912.
- 171 P. De, M. Li, S. R. Gondi and B. S. Sumerlin, *J. Am. Chem. Soc.*, 2008, **130**, 11288–11289.
- 172 S. Marque, H. Fischer, E. Baier and A. Studer, *J. Org. Chem.*, 2001, **66**, 1146–1156.
- 173 M. Rodlert, E. Harth, I. Rees and C. J. Hawker, *J. Polym. Sci., Part A: Polym. Chem.*, 2000, **38**, 4749–4763.
- 174 Nicole L. Hill and Rebecca Braslau, *J. Polym. Sci., Part A: Polym. Chem.*, 2007, **45**, 2341–2349.
- 175 J. Dao, D. Benoit and C. J. Hawker, *J. Polym. Sci., Part A: Polym. Chem.*, 1998, **36**, 2161–2167.
- 176 S. Fleischmann, H. Komber, D. Appelhans and B. I. Voit, *Macromol. Chem. Phys.*, 2007, **208**, 1050–1060.
- 177 G. F. D'Alelio and R. C. Evers, *J. Polym. Sci., Part A-1*, 1967, **5**, 999–1014.
- 178 L. B. Sessions, L. A. Miinea, K. D. Ericson, D. S. Glueck and R. B. Grubbs, *Macromolecules*, 2005, **38**, 2116–2121.
- 179 O. Altintas, G. Hizal and U. Tunca, *J. Polym. Sci., Part A: Polym. Chem.*, 2006, **44**, 5699–5707.
- 180 A. Gozgen, A. Dag, H. Durmaz, O. Sirkecioglu, G. Hizal and U. Tunca, *J. Polym. Sci., Part A: Polym. Chem.*, 2009, **47**, 497–504.
- 181 E. Gungor, G. Cote, T. Erdogan, H. Durmaz, A. L. Demirel, G. Hizal and U. Tunca, *J. Polym. Sci., Part A: Polym. Chem.*, 2007, **45**, 1055–1065.
- 182 O. Altintas, A. L. Demirel, G. Hizal and U. Tunca, *J. Polym. Sci., Part A: Polym. Chem.*, 2008, **46**, 5916–5928.
- 183 O. Altintas, B. Yankul, G. Hizal and U. Tunca, *J. Polym. Sci., Part A: Polym. Chem.*, 2007, **45**, 3588–3598.
- 184 E. Gungor, G. Hizal and U. Tunca, *J. Polym. Sci., Part A: Polym. Chem.*, 2009, **47**, 3409–3418.
- 185 E. H. H. Wong, M. H. Stenzel, T. Junkers and C. Barner-Kowollik, *Macromolecules*, 2010, **43**, 3785–3793.
- 186 T. Junkers, E. H. H. Wong, M. H. Stenzel and C. Barner-Kowollik, *Macromolecules*, 2009, **42**, 5027–5035.
- 187 E. H. H. Wong, T. Junkers and C. Barner-Kowollik, *J. Polym. Sci., Part A: Polym. Chem.*, 2008, **46**, 7273–7279.
- 188 W. H. Binder, D. Gloger, H. Weinstabl, G. Allmaier and E. Pittenauer, *Macromolecules*, 2007, **40**, 3097–3107.
- 189 U. Tunca, Z. Ozyurek, T. Erdogan and G. Hizal, *J. Polym. Sci., Part A: Polym. Chem.*, 2004, **42**, 4228–4236.
- 190 H. Durmaz, F. Karatas, U. Tunca and G. Hizal, *J. Polym. Sci., Part A: Polym. Chem.*, 2006, **44**, 499–509.
- 191 A. Krieg, C. R. Becer, R. Hoogenboom and U. S. Schubert, *Macromol. Symp.*, 2009, **275–276**, 73–81.
- 192 J. T. Wiltshire and G. G. Qiao, *J. Polym. Sci., Part A: Polym. Chem.*, 2009, **47**, 1485–1498.
- 193 M. Malkoch, R. J. Thibault, E. Drockenmüller, M. Messerschmidt, B. Voit, T. P. Russell and C. J. Hawker, *J. Am. Chem. Soc.*, 2005, **127**, 14942–14949.

- 194 R. K. O'Reilly, M. J. Joralemon, C. J. Hawker and K. L. Wooley, *Chem.-Eur. J.*, 2006, **12**, 6776–6786.
- 195 S. Fleischmann, H. Komber and B. Voit, *Macromolecules*, 2008, **41**, 5255–5264.
- 196 T. Ishizone, G. Uehara, A. Hirao, S. Nakahama and K. Tsuda, *Macromolecules*, 1998, **31**, 3764–3774.
- 197 F. Bertini, G. Audisio, J. Kiji and M. Fujita, *J. Anal. Appl. Pyrolysis*, 2003, **68–69**, 61–81.
- 198 M. M. Martin and E. B. Sanders, *J. Am. Chem. Soc.*, 1967, **89**, 3777–3782.
- 199 R.-V. Ostaci, D. Damiron, Y. Grohens, L. Léger and E. Drockenmüller, *Langmuir*, 2010, **26**, 1304–1310.
- 200 Y. Zhang, H. He, C. Gao and J. Y. Wu, *Langmuir*, 2009, **25**, 5814–5824.
- 201 J. Stadermann, S. Fleischmann, M. Messerschmidt, H. Komber and B. Voit, *Macromol. Symp.*, 2009, **275–276**, 35–42.
- 202 C. Ladaviere, N. Dorr and J. P. Claverie, *Macromolecules*, 2001, **34**, 5370–5372.
- 203 R. K. O'Reilly, M. J. Joralemon, C. J. Hawker and K. L. Wooley, *New J. Chem.*, 2007, **31**, 718–724.
- 204 T. Junkers and C. Barner-Kowollik, *J. Polym. Sci., Part A: Polym. Chem.*, 2008, **46**, 7585–7605.
- 205 G. K. Such, J. F. Quinn, A. Quinn, E. Tjijto and F. Caruso, *J. Am. Chem. Soc.*, 2006, **128**, 9318–9319.
- 206 G. K. Such, E. Tjijto, A. Postma, A. P. R. Johnston and F. Caruso, *Nano Lett.*, 2007, **7**, 1706–1710.
- 207 A. R. de Luzuriaga, N. Ormategui, H. J. Grande, I. Odriozola, J. A. Pornposo and I. Loinaz, *Macromol. Rapid Commun.*, 2008, **29**, 1156–1160.
- 208 X. W. Zhang, X. M. Lian, L. Liu, J. Zhang and H. Y. Zhao, *Macromolecules*, 2008, **41**, 7863–7869.
- 209 D. Damiron, M. Desorme, R. V. Ostaci, S. Al Akhrass, T. Hamaide and E. Drockenmüller, *J. Polym. Sci., Part A: Polym. Chem.*, 2009, **47**, 3803–3813.
- 210 D. Gromadzki, J. Lokaj, P. Cernoch, O. Diat, F. Nallet and P. Štěpánek, *Eur. Polym. J.*, 2008, **44**, 189–199.
- 211 M. Aldhoun, A. Massi and A. Dondoni, *J. Org. Chem.*, 2008, **73**, 9565–9575.
- 212 V. Aureggi and G. Sedelmeier, *Angew. Chem., Int. Ed.*, 2007, **46**, 8440–8444.
- 213 J. Aimi, L. A. McCullough and K. Matyjaszewski, *Macromolecules*, 2008, **41**, 9522–9524.
- 214 D. G. Li, J. Zhu, Z. P. Cheng, W. Zhang and X. L. Zhu, *React. Funct. Polym.*, 2009, **69**, 240–245.
- 215 Y. M. Zhou, K. Q. Jiang, Y. Q. Chen and S. Y. Liu, *J. Polym. Sci., Part A: Polym. Chem.*, 2008, **46**, 6518–6531.
- 216 S. Pfeifer and J.-F. Lutz, *Chem.-Eur. J.*, 2008, **14**, 10949–10957.
- 217 G. Li, H. T. Zheng and R. K. Bai, *Macromol. Rapid Commun.*, 2009, **30**, 442–447.
- 218 X. Z. Jiang, J. Y. Zhang, Y. M. Zhou, J. Xu and S. Y. Liu, *J. Polym. Sci., Part A: Polym. Chem.*, 2008, **46**, 860–871.
- 219 Y. Li and B. C. Benicewicz, *Macromolecules*, 2008, **41**, 7986–7992.
- 220 J. Y. Zhang, Y. M. Zhou, Z. Y. Zhu, Z. S. Ge and S. Y. Liu, *Macromolecules*, 2008, **41**, 1444–1454.
- 221 L. A. Canalle, S. S. v. Berkel, L. T. d. Haan and J. C. M. v. Hest, *Adv. Funct. Mater.*, 2009, **19**, 3464–3470.
- 222 L. González, A. Rodríguez, J. L. d. Benito and A. Marcos-Fernández, *J. Appl. Polym. Sci.*, 1997, **63**, 1353–1359.
- 223 J. E. Leffler and H. H. Gibson, *J. Am. Chem. Soc.*, 1968, **90**, 4117–4121.
- 224 C. J. Ruud, J. Jia and G. L. Baker, *Macromolecules*, 2000, **33**, 8184–8191.
- 225 C. K. Govindan, *Org. Process Res. Dev.*, 2002, **6**, 74–77.
- 226 G. T. Anderson, J. R. Henry and S. M. Weinreb, *J. Org. Chem.*, 1991, **56**, 6946–6948.
- 227 W. Broeckx, N. Overbergh, C. Samyn, G. Smets and G. L'abbé, *Tetrahedron*, 1971, **27**, 3527–3534.
- 228 A. Bousquet, C. Barner-Kowollik and M. H. Stenzel, *J. Polym. Sci., Part A: Polym. Chem.*, 2010, **48**, 1773–1781.
- 229 A. A. Kavitha and N. K. Singha, *Macromol. Chem. Phys.*, 2007, **208**, 2569–2577.
- 230 A. A. Kavitha and N. K. Singha, *J. Polym. Sci., Part A: Polym. Chem.*, 2007, **45**, 4441–4449.
- 231 A. A. Kavitha, A. Choudhury and N. K. Singha, *Macromol. Symp.*, 2006, **240**, 232–237.
- 232 A. A. Kavitha and N. K. Singha, *Macromolecules*, 2010, **43**, 3193–3205.
- 233 M. J. Kade, D. J. Burke and C. J. Hawker, *J. Polym. Sci., Part A: Polym. Chem.*, 2010, **48**, 743–750.
- 234 Z. Jia, J. Liu, T. P. Davis and V. Bulmus, *Polymer*, 2009, **50**, 5928–5932.
- 235 Z. Jia, L. Wong, T. P. Davis and V. Bulmus, *Biomacromolecules*, 2008, **9**, 3106–3113.
- 236 L. Wong, C. Boyer, Z. Jia, H. M. Zareie, T. P. Davis and V. Bulmus, *Biomacromolecules*, 2008, **9**, 1934–1944.
- 237 J. Zhu, Z. Di, X. Zhu and G. Chen, *J. Polym. Sci., Part A: Polym. Chem.*, 2004, **42**, 2558–2565.
- 238 K. Dayananda and R. Dhamodharan, *J. Polym. Sci., Part A: Polym. Chem.*, 2004, **42**, 902–915.
- 239 R. Krishnan and K. S. V. Srinivasan, *Macromolecules*, 2003, **36**, 1769–1771.
- 240 J. L. De La Fuente, P. F. Canamero and M. Fernandez-Garcia, *J. Polym. Sci., Part A: Polym. Chem.*, 2006, **44**, 1807–1816.
- 241 P. F. Cañamero, J. L. de la Fuente, E. L. Madruga and M. Fernández-García, *Macromol. Chem. Phys.*, 2004, **205**, 2221–2228.
- 242 R. Krishnan and K. S. V. Srinivasan, *Macromolecules*, 2004, **37**, 3614–3622.
- 243 G. Li, X. Zhu, J. Zhu, Z. Cheng and W. Zhang, *Polymer*, 2005, **46**, 12716–12721.
- 244 Y.-Y. Yuan, Q. Du, Y.-C. Wang and J. Wang, *Macromolecules*, 2010, **43**, 1739–1746.
- 245 K. Godula, D. Rabuka, K. T. Nam and C. R. Bertozzi, *Angew. Chem., Int. Ed.*, 2009, **48**, 4973–4976.
- 246 R. K. O'Reilly, C. J. Hawker and K. L. Wooley, *Polym. Prepr. (Am. Chem. Soc., Div. Polym. Chem.)*, 2004, **45**, 780.
- 247 G. O'Bryan, N. Ningnuek and R. Braslau, *Polymer*, 2008, **49**, 5241–5248.
- 248 K. Matyjaszewski, Y. Nakagawa and S. G. Gaynor, *Macromol. Rapid Commun.*, 1997, **18**, 1057–1066.
- 249 V. Coessens, Y. Nakagawa and K. Matyjaszewski, *Polym. Bull.*, 1998, **40**, 135–142.
- 250 V. Coessens and K. Matyjaszewski, *J. Macromol. Sci., Part A: Pure Appl. Chem.*, 1999, **36**, 667–679.
- 251 S. O. Kyeremateng, E. Amado, A. Blume and J. Kressler, *Macromol. Rapid Commun.*, 2008, **29**, 1140–1146.
- 252 A. Sinaga, P. Ravi, T. A. Hatton and K. C. Tam, *J. Polym. Sci., Part A: Polym. Chem.*, 2007, **45**, 2646–2656.
- 253 J.-F. Lutz, H. G. Börner and K. Weichenhan, *Macromol. Rapid Commun.*, 2005, **26**, 514–518.
- 254 J.-F. Lutz, H. G. Börner and K. Weichenhan, *Macromolecules*, 2006, **39**, 6376–6383.
- 255 Q. C. Liu and Y. M. Chen, *J. Polym. Sci., Part A: Polym. Chem.*, 2006, **44**, 6103–6113.
- 256 A. P. Vogt and B. S. Sumerlin, *Macromolecules*, 2006, **39**, 5286–5292.
- 257 H. F. Gao and K. Matyjaszewski, *Macromolecules*, 2006, **39**, 4960–4965.
- 258 O. Altintas, B. Yankul, G. Hizal and U. Tunca, *J. Polym. Sci., Part A: Polym. Chem.*, 2006, **44**, 6458–6465.
- 259 B. S. Lee, J. K. Lee, W. J. Kim, Y. H. Jung, S. J. Sim, J. Lee and I. S. Choi, *Biomacromolecules*, 2007, **8**, 744–749.
- 260 M. Degirmenci and N. Genli, *Macromol. Chem. Phys.*, 2009, **210**, 1617–1623.
- 261 Q. Liu, P. Zhao and Y. Chen, *J. Polym. Sci., Part A: Polym. Chem.*, 2007, **45**, 3330–3341.
- 262 P. L. Golas, N. V. Tsarevsky and K. Matyjaszewski, *Macromol. Rapid Commun.*, 2008, **29**, 1167–1171.
- 263 J. Kulis, C. A. Bell, A. S. Micallef, Z. Jia and M. J. Monteiro, *Macromolecules*, 2009, **42**, 8218–8227.
- 264 A. Gheorghie, A. Matsuno and O. Reiser, *Adv. Synth. Catal.*, 2006, **348**, 1016–1020.
- 265 E. H. H. Wong, C. Boyer, M. H. Stenzel, C. Barner-Kowollik and T. Junkers, *Chem. Commun.*, 2010, **46**, 1959–1961.
- 266 A. J. Inglis, T. Paulöhr and C. Barner-Kowollik, *Macromolecules*, 2010, **43**, 33–36.
- 267 C. Boyer, V. Bulmus and T. P. Davis, *Macromol. Rapid Commun.*, 2009, **30**, 493–497.
- 268 J. W. Chan, B. Yu, C. E. Hoyle and A. B. Lowe, *Polymer*, 2009, **50**, 3158–3168.

- 269 C. W. Chang, E. Bays, L. Tao, S. N. S. Alconcel and H. D. Maynard, *Chem. Commun.*, 2009, 3580–3582.
- 270 C. Boyer, A. Granville, T. P. Davis and V. Bulmus, *J. Polym. Sci., Part A: Polym. Chem.*, 2009, **47**, 3773–3794.
- 271 J. W. Chan, B. Yu, C. E. Hoyle and A. B. Lowe, *Chem. Commun.*, 2008, 4959–4961.
- 272 V. Lima, X. Jiang, J. Brokken-Zijp, P. J. Schoenmakers, B. Klumperman and R. V. D. Linde, *J. Polym. Sci., Part A: Polym. Chem.*, 2005, **43**, 959–973.
- 273 X.-P. Qiu and F. M. Winnik, *Macromol. Rapid Commun.*, 2006, **27**, 1648–1653.
- 274 M. Nakayama and T. Okano, *Biomacromolecules*, 2005, **6**, 2320–2327.
- 275 F. Segui, X.-P. Qiu and F. M. Winnik, *J. Polym. Sci., Part A: Polym. Chem.*, 2008, **46**, 314–326.
- 276 C. W. Scales, A. J. Convertine and C. L. McCormick, *Biomacromolecules*, 2006, **7**, 1389–1392.
- 277 H. Kakwere and S. Perrier, *J. Am. Chem. Soc.*, 2009, **131**, 1889–1895.
- 278 A. S. Goldmann, A. Walther, L. Nebhani, R. Joso, D. Ernst, K. Loos, C. Barner-Kowollik, L. Barner and A. H. E. Mueller, *Macromolecules*, 2009, **42**, 3707–3714.
- 279 G. L. Ellman, *Arch. Biochem. Biophys.*, 1958, **74**, 443–450.
- 280 P. J. Roth, D. Kessler, R. Zentel and P. Theato, *J. Polym. Sci., Part A: Polym. Chem.*, 2009, **47**, 3118–3130.
- 281 L. P. Yang, H. X. Zhou, G. Y. Shi, Y. Wang and C. Y. Pan, *J. Polym. Sci., Part A: Polym. Chem.*, 2008, **46**, 6641–6653.
- 282 D. H. Solomon, E. Rizzardo and P. Cacioli, US Patent, 4581 429, 1985.
- 283 E. Harth, C. J. Hawker, W. Fan and R. M. Waymouth, *Macromolecules*, 2001, **34**, 3856–3862.
- 284 G. O'Bryan and R. Braslau, *Macromolecules*, 2006, **39**, 9010–9017.
- 285 Y. Guillaeneuf, P.-E. Dufils, L. Autissier, M. Rollet, D. Gigmes and D. Bertin, *Macromolecules*, 2010, **43**, 91–100.
- 286 C. Ollivier and P. Renaud, *J. Am. Chem. Soc.*, 2001, **123**, 4717–4727.
- 287 P. Panchaud and P. Renaud, *J. Org. Chem.*, 2004, **69**, 3205–3207.
- 288 X. Z. Jiang, G. Y. Zhang, R. Narain and S. Y. Liu, *Langmuir*, 2009, **25**, 2046–2054.
- 289 H. Gao and K. Matyjaszewski, *J. Am. Chem. Soc.*, 2007, **129**, 6633–6639.
- 290 D. Cummins, C. J. Duxbury, P. Quaedflieg, P. Magusin, C. E. Koning and A. Heise, *Soft Matter*, 2009, **5**, 804–811.
- 291 B. Sieczkowska, M. Millaruelo, M. Messerschmidt and B. Voit, *Macromolecules*, 2007, **40**, 2361–2370.
- 292 R. K. O'Reilly, M. J. Joralemon, K. L. Wooley and C. J. Hawker, *Chem. Mater.*, 2005, **17**, 5976–5988.
- 293 G. Temel, B. Aydogan, N. Arsu and Y. Yagci, *Macromolecules*, 2009, **42**, 6098–6106.
- 294 W.-H. Ting, S. A. Dai, Y.-F. Shih, I.-K. Yang, W.-C. Su and R.-J. Jeng, *Polymer*, 2008, **49**, 1497–1505.
- 295 M. J. Joralemon, R. K. O'Reilly, C. J. Hawker and K. L. Wooley, *J. Am. Chem. Soc.*, 2005, **127**, 16892–16899.
- 296 P. L. Golas, N. V. Tsarevsky, B. S. Sumerlin and K. Matyjaszewski, *Macromolecules*, 2006, **39**, 6451–6457.
- 297 M.-A. Berthet, Z. Zarafshani, S. Pfeifer and J.-F. Lutz, *Macromolecules*, 2010, **43**, 44–50.



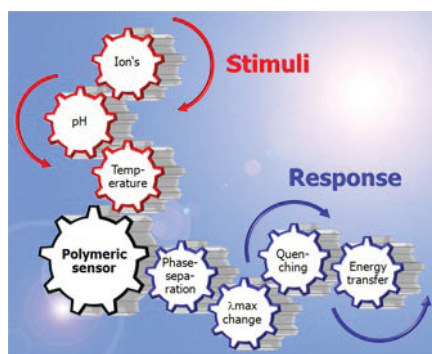
## Publication P2:

### *Aqueous polymeric sensors based on temperature-induced polymer phase transitions and solvatochromic dyes*

---

C. Pietsch, U. S. Schubert, R. Hoogenboom

*Chem. Commun.* **2011**, 47, 8750–8765



“Including cover page”

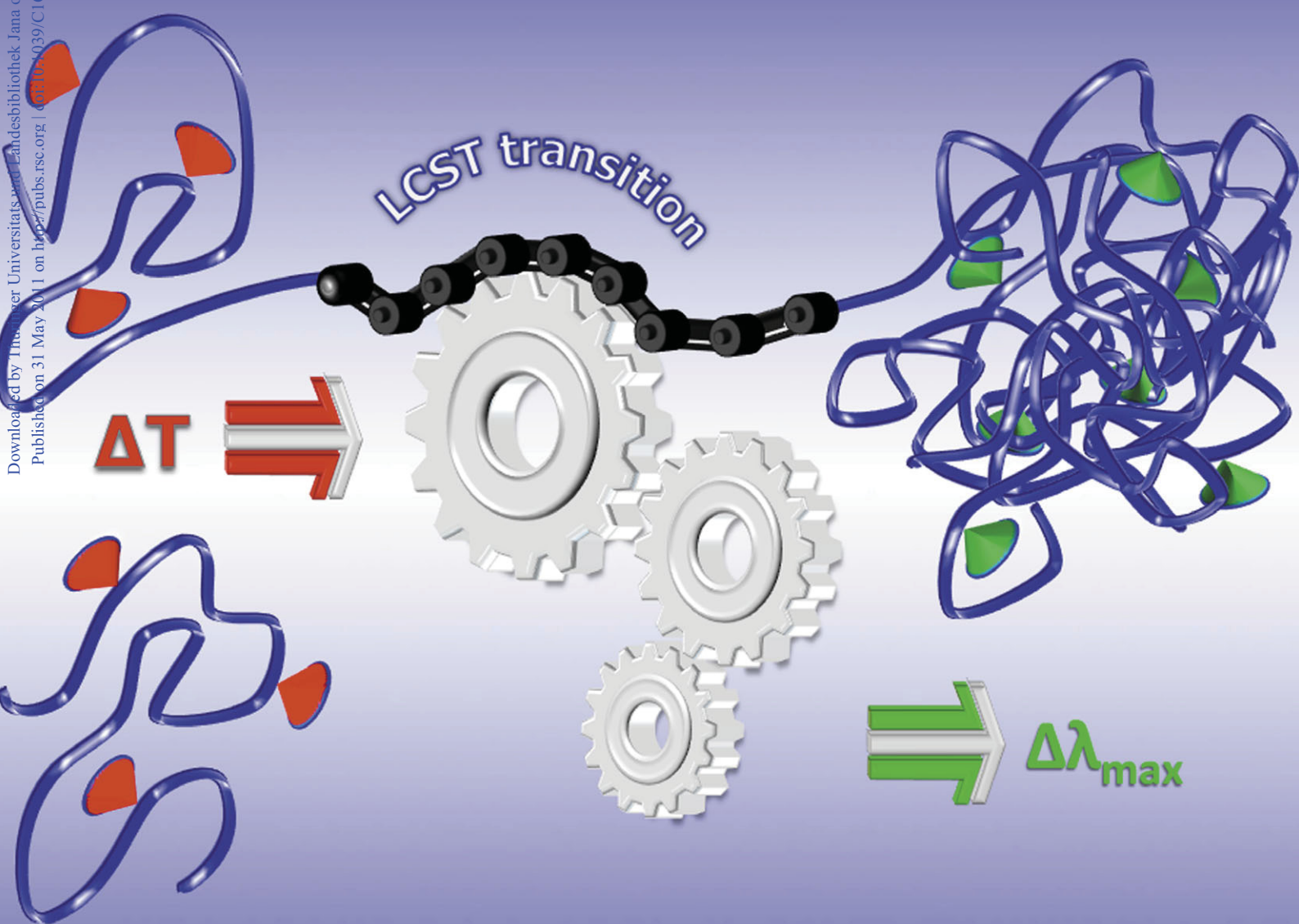


# ChemComm

Chemical Communications

[www.rsc.org/chemcomm](http://www.rsc.org/chemcomm)

Volume 47 | Number 31 | 21 August 2011 | Pages 8705–8980

Downloaded by Universitäts- und Landesbibliothek Jena on 26 July 2011  
Published on 31 May 2011 on [pubs.rsc.org](http://pubs.rsc.org) | DOI: 10.1039/C1CC11940K

ISSN 1359-7345

RSC Publishing

**FEATURE ARTICLE**Ulrich S. Schubert and Richard Hoogenboom *et al.*

Aqueous polymeric sensors based on temperature-induced polymer phase transitions and solvatochromic dyes





Cite this: *Chem. Commun.*, 2011, **47**, 8750–8765

www.rsc.org/chemcomm

## FEATURE ARTICLE

**Aqueous polymeric sensors based on temperature-induced polymer phase transitions and solvatochromic dyes**Christian Pietsch,<sup>ab</sup> Ulrich S. Schubert<sup>\*ab</sup> and Richard Hoogenboom<sup>\*c</sup>

Received 6th April 2011, Accepted 5th May 2011

DOI: 10.1039/c1cc11940k

This feature article provides, for the first time, an overview of the research that guided the way from fundamental studies of the thermo-responsive phase separation of aqueous polymer solutions to polymeric sensor systems. The incorporation of solvatochromic dyes into thermoresponsive polymers as well as the concepts of polymeric sensors are presented and discussed in detail.

**1. Introduction and motivation**

The determination of the temperature is one of the most important analytical methods in chemical laboratories. Among chemical,<sup>1–6</sup> pH,<sup>7,8</sup> chemomechanical<sup>9</sup> and calorimetric sensors, optical temperature<sup>10</sup> sensors play an important role in polymer science. A new class of optical temperature sensors has been developing since nearly 20 years and has received significant attention for the development of sensory materials in the

last years. These optical temperature sensors are supported by polymer chains or polymeric hydrogels that are responsible for sensing, which differentiate them from molecular optical sensors. Even though polymers already played an important role in sensor application as polymeric supporter or as polymeric matrix for the sensing dye units,<sup>1–13</sup> the here discussed relatively new class of sensors are based on stimuli-responsive polymers<sup>14–18</sup> that sharply respond with a solution phase transition to environmental parameter changes such as the temperature, pH value, UV/Vis light or chemical changes. Stimuli-responsive polymer systems can be polymers in solutions, hydro- or microgels, self-assembled aggregates and nanoparticles.<sup>7,10,14–21</sup> The access and the possibility to control the polymer properties<sup>22</sup> (e.g. molar mass or polymer architecture) and the flexibility of processing (e.g. coating or formation of nanoparticles) in combination with tunable solubility (e.g. ratio of hydrophobic/hydrophilic

<sup>a</sup>Laboratory of Organic and Macromolecular Chemistry (IOMC) and Jena Center for Soft Matter (JCSM), Friedrich-Schiller-University Jena, Humboldtstr. 10, 07743 Jena, Germany.

E-mail: ulrich.schubert@uni-jena.de, richard.hoogenboom@ugent.be

<sup>b</sup>Dutch Polymer Institute (DPI), P. O. Box 902, 5600 AX Eindhoven, The Netherlands

<sup>c</sup>Supramolecular Chemistry group, Department of Organic Chemistry, Ghent University, Krijgslaan 281 S4, 9000 Ghent, Belgium

**Christian Pietsch**

he spent two months at CSIRO (Melbourne, Australia), where he carried out research on RAFT polymerizations.

Christian Pietsch was born in 1984 in Naumburg/Saale (Germany) and studied chemistry at the Friedrich-Schiller-University Jena (Germany; 2003–2008) and accomplished the master thesis at the Eindhoven University of Technology (Netherlands) under the supervision of Prof. Ulrich S. Schubert. He continued as a PhD student in Jena working on stimuli-responsive copolymers as well as controlled radical polymerization techniques. Recently,

**Ulrich S. Schubert**

1999, followed by a temporal position as professor at the Center for Nanoscience, Universität München (Germany). From 2000 to 2007 he was Full-Professor at the Eindhoven University of Technology. Currently he holds a chair at the Friedrich-Schiller-University Jena.

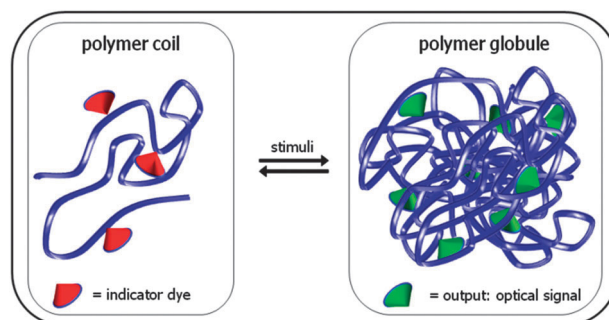
Prof. Ulrich S. Schubert studied chemistry at the Universities of Frankfurt and Bayreuth (both Germany) and the Virginia Commonwealth University, Richmond (USA). His PhD thesis was executed at the University of Bayreuth and the University of South Florida/Tampa. After postdoctoral training with Professor Lehn at the Université Strasbourg (France) he moved to the Technische Universität München (Germany) to obtain his Habilitation in

monomers) make them very promising and advantageous for sensor materials.

For sensing purposes, the polymer phase transition can be translated into a sensory signal by incorporation of solvatochromic dyes<sup>6,23</sup> that specifically change their optical or emissive properties upon changing environmental parameters or by reaction with analytes (Fig. 1). The high number of “indicator” dyes and the possibility of functionalization in combination with the tuneable polymer properties theoretically allow the specific detection of nearly every molecule or environmental parameter. Nevertheless, for an optimal performance the sensor system has to be very sensitive and selective for the response parameters. The optical signal transmission has some advantages over other methods; (i) the measurement can be performed without contact to the sample and therefore the analyte will be not destroyed during analysis and (ii) possibly even more important is that a continuous analyte/environmental parameter detection is possible if the polymeric sensor is reversible. Such continuous monitoring is quite difficult to realize, but necessary for on-line measurements.

The sensing approach based on combination of a responsive polymer phase transition and a solvatochromic dye allows simple and fast detection of, *e.g.*, the temperature by measuring the absorbance or fluorescence of the solution. The high sensitivities arise from the incorporated solvatochromic dye molecules, which respond to minor local environmental changes that occur upon the temperature induced polymer phase transition. For temperature-sensing in aqueous solution, the most important polymer phase transition is the so-called lower critical solution temperature (LCST), *i.e.* the polymer is dissolved at lower temperatures and precipitates upon increasing the temperature.

The driving force for the study of polymeric temperature sensors in the last 20 years is twofold: (i) the development of new functional (temperature) sensor systems utilizing stimuli-responsive polymers and (ii) to gain in depth understanding of



**Fig. 1** Schematic representation of the polymeric sensors based on polymer phase transitions (coil-to-globule) and solvatochromic dyes.

polymer chain conformations and/or phase transitions in solution. Widely used experimental techniques<sup>14</sup> for the determination of these coil-to-globule/LCST transitions are (i) calorimetry<sup>24–26</sup> (thermodynamics of phase separation), (ii) viscosity determination<sup>24</sup> (hydrodynamic consequences), (iii) light scattering measurements<sup>27–30</sup> (size of the coil or globule), (iv) UV/Vis or fluorescence spectroscopy<sup>31–34</sup> (molecular resolution of the thermo-reversible phase separation) and additionally, (v) IR<sup>35</sup> and NMR spectroscopy.

These techniques are used for fundamental research on stimuli-responsive polymers providing novel insights into the elementary mechanism like the equilibrium transition states or the kinetic/thermodynamic processes of the phase separation and the structure of individual polymer coils as well as the effects of various specific/non-specific interactions (hydrogen-bonding, electrostatic, hydrophobic/hydrophilic interactions) between the polymer chains, side/end-groups and/or the solvent.

At the end of the eighties, the first reports appeared on the combination of thermoresponsive polymers with (solvatochromic) chromophores as indicator dyes as a new method to study polymer phase transitions. Irie and Kungwachakun<sup>36</sup> studied azobenzene containing poly(*N*-isopropylacrylamide) (PNIPAM) copolymers as photoresponsive systems and Binkert *et al.*<sup>31</sup> reported a fluorescein labeled PNIPAM to investigate the local mobility of the polymer chains during the phase transition by fluorescence spectroscopy. Fundamental studies on fluorophores as indicators for stimuli-responsive polymers were reported by the Winnik group<sup>32,37</sup> in 1990 and shortly after by a research team led by Schild and Tirrell<sup>38</sup> based on PNIPAM in combination with the solvatochromic pyrene dye. Both groups used the non-radiative energy transfer between donor and acceptor chain labels to explore the inter-polymer interactions and the changes of the chain dimensions (hydrodynamic radius) during the coil-to-globule transition. Since 2003 a large number of polymeric fluorescent/solvatochromic temperature sensors have been developed based on these initially reported concepts to study coil to globule transitions. These polymeric thermometers represent important alternatives for conventional thermometers when, *e.g.*, the electromagnetic field or the ionic strengths are too strong for a conventional thermometer.

Additional information can be obtained with polymeric fluorescent sensors, because numerous parameters like fluorescence decay times, fluorescence intensity, quenching



**Richard Hoogenboom**

*Richard Hoogenboom was born in 1978 in Rotterdam (Netherlands) and studied chemical engineering at the Eindhoven University of Technology (TU/e; Netherlands). In 2005, he obtained his PhD under the supervision of Ulrich S. Schubert (TU/e) and continued working as project leader for the Dutch Polymer Institute. After postdoctoral training with Martin Möller at the RWTH Aachen (Humboldt fellowship) and Roeland*

*J. M. Nolte at the Radboud University Nijmegen (NWO veni-grant), he was appointed as associate professor at Ghent University in 2010. His research interests include stimuli-responsive polymers, supramolecular polymers, and poly-(2-oxazoline)s.*

efficiency, energy transfer and fluorescence polarization can be determined. The most challenging problems of optical sensors are the reversibility over a long time, the signal stability and photobleaching of the chromophore. Nonetheless, embedding the chromophore into a polymer backbone or in a nanoparticle/hydrogel protects the chromophore making the combination very promising. Additionally, potential fluctuations in signal intensity can be reduced by using ratiometric measurements.

The aim of this feature article is to provide a historical overview as well as detailed insights of aqueous polymeric sensors based on temperature-induced polymer phase transitions and solvatochromic dyes. The synthesis of the desired dye-functional macromolecules and the wide range of applications, such as temperature, pH value or ion sensors, biosensors, logical gates and drug delivery systems are discussed. The large variety of reported dye-functionalized polymeric materials and their optical behavior have been summarized in tables and will also be discussed briefly. For a more general application directed overview of responsive polymer sensors, the reader is referred to a recent perspective article.<sup>10</sup>

## 2. Incorporation of solvatochromic dyes in polymer backbones

The syntheses of responsive copolymers or hydrogels are mostly performed by radical polymerization techniques. The most commonly used technique is the free radical polymerization (FRP) in bulk or solution. Also radical emulsion polymerization is used to generate nanoparticles. In the last years controlled radical polymerization methods (CRP) are preferred due to the possibility to control the polymer architecture, composition and chain length. Atom transfer radical polymerization<sup>39</sup> (ATRP) or reversible addition–fragmentation chain transfer polymerization<sup>40</sup> (RAFT) have been mostly used for the construction of these polymeric sensors. Also living ionic or ring-opening polymerization are sometimes chosen as synthetic pathways to obtain dye-functionalized copolymers. Each of these techniques requires the use of a dedicated initiator or chain transfer agent/metal–ligand system to gain control over the polymerization. Several architectures like block, graft, statistical or star structures can be realized by these methods.

There are two major synthetic pathways to prepare dye-functionalized sensoric polymers: (i) the use of a dye-functionalized monomer or an initiator/chain transfer agent<sup>41</sup> or (ii) the functionalization of the polymer by post-polymerization modification<sup>42,43</sup> using *e.g.* an activated ester or an efficient “click” reaction,<sup>44–47</sup> which was successfully demonstrated for several functionalization strategies as well as for the preparation of different architectures. The advantage of the first strategy is that, it is relatively simple to control the ratio between the monomers (degree of functionalization). As a limitation, the dye-functional monomer must be compatible with the polymerization method. The main advantage of the post-polymerization modification approach is that the “activated copolymer” represents a universal scaffold for versatile dye functionalization (*e.g.* two different chromophores for FRET) allowing easy evaluation and comparison of the optical properties. In this post-polymerization modification

approach, reactive polymeric precursors are required, which can be activated esters,<sup>43</sup> like the pentafluorophenyl (meth)acrylate or *N*-[(meth)acryloxy] succinimide, or ‘clickable’ groups, such as acetylene or azide. A frequently applied synthetic pathway for the preparation of dye-functionalized monomers is the esterification of an alcohol or amine functionalized dye with a monomer comprising an activated acid, *e.g.* the acid chloride or anhydride of (meth)acrylic acid. Both the copolymerization and post-polymerization modification methods are very well suited for the preparation of dye-functionalized copolymers. Additionally, polymers bearing dyes at the chain termini can be prepared using functional initiators or terminating agents as well as by post-polymerization modification.

The degree of labelling, *i.e.* the amount of incorporated dye molecules, should be kept low independent of the preparation method to avoid a strong influence of the dye on the phase separation behavior, *e.g.* modification of the cloud point temperature, and to avoid self quenching effects caused by too high loading of fluorescence dyes.

## 3. Classification of LCST based polymeric temperature sensors

### 3.1 General concept of LCST based polymeric sensors

The concept of LCST based polymeric temperature sensors depends on the combination of polymer phase transitions and solvatochromic dyes. The temperature-induced polymer phase separation (demixing) in solution is called LCST and can be described by the Flory–Huggins theory.<sup>48</sup> During the coil-to-globule transitions the polymer chains change from a fully dissolved, hydrated state (hydrophilic) into a collapsed non-hydrated state (hydrophobic). This sharp entropy-driven collapse has a strong influence on the microenvironment of the repeating units of the polymer. The (majority of) water molecules are released into the bulk water during this transition and, therefore, a hydrophilic–hydrophobic (polarity) change occurs in the microenvironment of the polymer. By attaching a solvatochromic chromophore to the polymer chain, this microenvironmental polarity change during the temperature induced polymer phase transition can be translated into a colorimetric or fluorescent sensing signal.

The majority of such sensor designs are based on dye-functionalized stimuli-responsive PNIPAM<sup>14,24</sup> while more recently polymers based on poly(ethyleneglycol) (PEG) functionalized methacrylates,<sup>49–52</sup> *i.e.* POEGMA, became popular alternatives too. The popularity of PNIPAM is largely based on its LCST of 32 °C,<sup>14</sup> which is close to the human body temperature. In addition, the phase transition temperature is relatively insensitive to changes in concentration and pH making it rather robust. However, the phase transition does show slight hysteresis between heating and cooling due to vitrification of the precipitated polymer phase, which is related to the high glass transition temperature ( $T_g$ ) of PNIPAM. Since POEGMA has a very low  $T_g$  it shows excellent reversibility without hysteresis.<sup>51,52</sup> In addition, the phase transition temperature can easily be tuned by copolymerization of different OEGMA monomers and POEGMA shows superb

biocompatibility making it very well suited for biomedical applications, similar to PNIPAM.<sup>53,54</sup> As a limitation, the temperature sensing regime of LCST-based sensors is often limited to a narrow temperature range (around 10 to 20 °C) due to the sharp LCST phase transition. Nonetheless, the temperature range can be tuned over the full temperature range of ambient water (0 to 100 °C) by controlling the hydrophilic/hydrophobic balance of the polymer by copolymerization. Additionally, thermo-responsive polymers, *e.g.* PNIPAM or POEGMA, show a sharp phase transition and a good reversibility in water, which is crucial for accurate and reliable sensors.<sup>52</sup>

The chromophore, a fluorescence or visible solvatochromic dye, is of great importance for the performance of the temperature sensors. The chromophore should change its absorbance or emission behavior upon variation of the polymer microenvironment from exposure to water to exposure to the still relatively polar collapsed polymer globules. Dyes with negative solvatochromism reveal a hypsochromic shift with increasing solvent polarity and *vice versa* positive solvatochromic dyes exhibit a bathochromic shift. The effect is based on the different stabilization of the ground and/or excited state (by *e.g.* the polar water molecules) or interaction between the solvent/polymer and the chromophore.<sup>55</sup>

Even though the general LCST based sensor concept is based on an incorporated solvatochromic dye that directly translates the polarity change into a fluorescent or visible signal, different dye-based mechanisms can be exploited to translate the changes in polymer microenvironment during the LCST phase transition into a fluorescent or visible signal. These (complex) environmental parameters are, *e.g.*, viscosity changes, conformational changes or proton transfer.<sup>55</sup> The various dye sensing concepts can be categorized as follows: (i) fluorescence enhancement, (ii) fluorescence quenching, (iii) photoinduced electron transfer (PET), (iv) resonance energy transfer (RET), in particular the Förster resonance energy transfer (FRET), (v) excimer formation, (vi) batho/hypsochromic shift of emission or absorbance and (vii) photoisomerization.

Polymeric temperature sensors can be divided into two main classes: fluorescent and visible (absorbance) sensors. This classification not only divides the sensors according to the basic working principle, but also distinguishes the different detection methods by fluorescence and absorbance measurements and, accordingly, the resulting requirements for the sensors. From a synthetic point of view this classification provides a design criterion for choosing the right chromophore for a certain application, independent of the polymer properties. The different chromophores as well as their different sensing mechanisms in combination with various thermoresponsive polymers are discussed in the following subsections.

### 3.2 Fluorescence based temperature sensors

Fluorescent temperature sensors are discussed based on chromophores that show an emission, *i.e.* fluorophores, and are covalently attached to thermoresponsive polymers. In the following the fluorescent based temperature sensors are classified into chromophores that respond to temperature changes by (i) fluorescence enhancement, (ii) fluorescence quenching and

(iii) a batho/hypsochromic shift of emission. These different types of fluorescent temperature sensors are discussed in the following subsections together with other investigated simultaneous response factors. All the combinations of thermo-responsive polymers with chromophores, the temperature sensing regime and other investigated stimuli are summarized in Table 1.

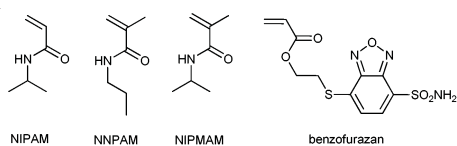
**3.2.1 Temperature induced fluorescence enhancement.** Since 2003 Uchiyama and Iwai *et al.*<sup>56–62</sup> reported on fluorescent thermometers, shown in entry 1, based on polarity sensitive benzofurazan derivatives (weakly fluorescent in hydrophilic and strongly fluorescent in hydrophobic microenvironment) in combination with thermoresponsive acrylamide copolymers (NIPAM, NNPAM and NIPMAM, Fig. 2).

A 13-fold increase of fluorescence intensity was demonstrated by increasing the temperature above the critical demixing point of the aqueous dye-functionalized polymer solution. The basic working principle of this sensor concept is based on the stronger fluorescence of the dye in a less polar environment, which is achieved upon temperature-induced demixing of the polymer solution. The authors studied the effect of different copolymer compositions on the response of the chromophore.<sup>58</sup> A similar increase of fluorescence intensity was observed for the different copolymers and it was shown that the standard deviation in fluorescence intensity for 10 repeating cycles is rather low (0.4–1.0%). Furthermore, microgels of these copolymers were reported by Iwai *et al.*<sup>59</sup> showing similar fluorescence behavior as the linear polymer chains, albeit the increase in fluorescence intensity is a bit lower (10 fold). By using a pH sensitive backbone, *N,N*-dimethylaminopropyl acrylamide, DMAPAM, in combination with *N-tert*-butylacrylamide NTBAM, the resulting copolymer exhibits both pH and temperature responsiveness.<sup>60</sup> This copolymer was studied with regard to logic gate applications with both pH value and temperature as input. Additionally, ionic components, 3-sulfopropyl acrylate (SPA) and (3-acrylamidopropyl) trimethylammonium salt (APTMA), were introduced to the polymer backbone by Uchiyama and coworkers<sup>61</sup> to expand the temperature range and to improve the temperature resolution. Several copolymers with different compositions were synthesized and studied. Incorporation of the benzofurazan moiety into PNIPAM nanogels resulted in enhanced fluorescence intensity above the cloud point temperature. These nanogels showed a sharper response in the presence of KCl ions and could be successfully used for intracellular thermometry.<sup>62</sup>

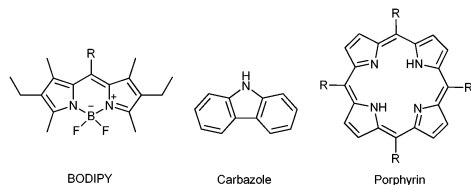
Porphyrim (entry 2, shown in Fig. 3) labeled NIPAM copolymers were studied by Avlasevich *et al.*<sup>66–69</sup> Different PNIPAM chain lengths and different porphyrim contents with and without metal complexation ( $Zn^{2+}$ ) were investigated. It could be shown that the fluorescence of porphyrim is quenched in cold water (*i.e.* by interchromophore interaction) and increasing the temperature above the cloud point temperature enhances the fluorescence intensity and quantum yield ( $\sim 6$  fold) caused by an increased rigidity and the formation of hydrophobic micro-domains in the globules. Porphyrim was also used by Yusa *et al.*<sup>70</sup> as the inner core of a 4-arm star-shaped poly(diethylacrylamide) (PDEAM) synthesized

**Table 1** Fluorescence based temperature sensors

Entry	Dye	Polymer	Stimuli [T-range °C]	Wavelength range (emission)	Repeat	Type	Ref.
1	Benzofurazan	NIPAM, NNPAM, NIPMAM, DMAPAM, NTBAM, SPA, APTMA, MPAM, DEAPAM, AA, NTAAM, NBCAM, NDMPAM	4–66 pH, K <sup>+</sup> , SO <sub>4</sub> <sup>2-</sup>	Em: 520–573 nm	10×	Microenvironmental polarity change	56–65
2	Porphyrin	NIPAM	28–38, Zn <sup>2+</sup>	Em: 660 nm, 723 nm	—	Microenvironmental polarity change	66–70
3	Rhodamine	NIPAM, NNPAM, NIPMAM PEO- <i>b</i> -NIPAM	10–50, pH, Hg <sup>2+</sup>	Em: 571 nm Em: 584 nm	2× 10×	Selective fluorescence enhancement, microenvironmental polarity change and micellar complexes and complexation of Hg <sup>2+</sup>	71, 72, 73
4	Tetraphenylethylene	NIPAM	25–50	Em: 468 nm	—	Aggregation-induced emission	74
5	Hemicyanine	NIPAM	20–40	Em: 572 nm	10×	Microenvironmental polarity change and tautomerism	75
6	BODIPY	NIPAM, DMAEMA, DEGMA, OEGMA	20–45	Em: 525 nm–575 nm	10×	Viscosity increase (rotation restricted), formation of H-dimers (H-aggregates) and quenching by AuNP	76–79
7	Naphthalimide	NIPAM	24–40, Hg <sup>2+</sup>	Em: 528 nm	—	Microenvironmental polarity change and Hg <sup>2+</sup> complexation	80
8	Fluorene	NIPAM Fluorene- <i>b</i> -NIPAM	22–40 15–40	Em: 388 nm Em: 430 nm	—	Microenvironmental polarity change and quenching	81, 82
9	4 <i>H</i> -Pyrene based dye (polymethine)	NIPAM, NIPMAM	30–60 35–40, Cu <sup>2+</sup>	Em: 570–600 nm Em: 620 nm	—	Microenvironmental polarity change and quenching by Cu <sup>2+</sup>	83, 84
10	Carbazole	NIPAM, St- <i>b</i> -NIPAM	25–45	Em: 360 nm	3×	Rotation restricted in the globule and excimer formation	38, 85, 86
11	Anthracene	NIPAM	15–40, pH	Em: 420 nm	—	PET with aggregation	87
12	Phenanthroline	NIPAM	20–40, Cu <sup>2+</sup> , pH	Em: 452 nm	—	Quenching by Cu <sup>2+</sup> , micellar formation	88, 89
13	Dansyl dye	NIPAM	20–45, Cu <sup>2+</sup>	Em: 490 nm	—	Quenching by Cu <sup>2+</sup>	90
14	Pyrene	NIPAM, <i>N</i> -alkylAM, MMA Hydroxypropyl cellulose <i>N</i> -VinylCLA- <i>co</i> -PEO, DEGMA, OEGMA- <i>b</i> -pyrene PEO- <i>b</i> -PPO- <i>b</i> -PEO	10–60	Em: 375, 396 nm → 480 nm	—	Change of excimer/monomer fluorescence and quenching by fullerene	32, 34, 37, 38, 91–105
15	Cy5.5	PEO- <i>b</i> -PPO- <i>b</i> -PEO	1–80	Em: 695 nm	—	Quenching in the micelle aggregation	106
16	2 <i>H</i> -Benzo[ <i>g</i> ]-chromen-2-one	NNPAM, NIPAM, NIPMAM, DMAPAM,	5–50	Em: 471 nm → 500 nm	—	Microenvironmental polarity change	107
17	Amino-phenyl-phenanthrene	NIPAM, MMA, NIPMAM MAA, DMAM, NNPAM,	20–60	Em: 481 nm → 434 nm	10×	Microenvironmental polarity change	63, 108–110
18	3-Hydroxyflavone	NIPAM	33–41	Em: 440 nm → 540 nm	10×	Tautomerism	111
19	6-Aminoquinoxaline	NIPAM, DMAM	30–40	Em: 515 nm → 497 nm	—	Microenvironmental polarity change	112
20	Alizarin red S	NIPAM- <i>co</i> -VPBA	20–40, diol	Em: 578 nm, 660 nm	—	Diol-boronic acid complex	113, 114
21	Benzoxazole	NIPAM	28–40, pH, Zn <sup>2+</sup>	Em: 425 nm → 500 nm	—	Keto-enol tautomerism and zinc complexation	115
22	Fluorescein	NIPAM, HEMA	28–33, pH	Em: 515 nm	—	pH change, micellar formation	89, 116, 117
23	Acridine	AM	2–50	Em: 491 nm	—	Tautomerism (pH change)	118
24	Aminoacetophenone thiosemicarbazone	NIPAM	15–35, pH	Em: 393 nm	—	Tautomerism (pH change)	119



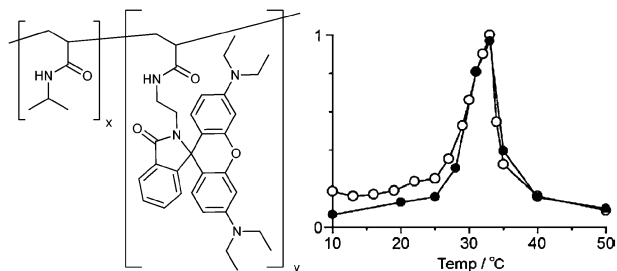
**Fig. 2** Schematic representation of the structures of acrylamides and the benzofurazan dye.<sup>58,61</sup>



**Fig. 3** Schematic representation of the structures of BODIPY, carbazole and porphyrin dyes.

by RAFT polymerization of a tetra functionalized porphyrin. The authors observed a reverse sensing behavior. Increasing the temperature above the cloud point led to a decrease in fluorescence intensity, which is caused by the different environment around the porphyrin core.

Rhodamine based PNIPAM copolymers, shown in entry 3, were synthesized by Hirai and coworkers.<sup>71,72</sup> These fluorescent thermometers showed a selective and reversible emission enhancement at a specific temperature range. This on/off emission response occurs only in acidic environment due to protonation of the nitrogen atoms in combination with a change from a spirocyclic to an open structure of 3. Below 25 °C the copolymer is non-fluorescent, between 25 and 35 °C the globule particle is fluorescent and above temperatures of 35 °C the emission is lost (Fig. 4). The authors discuss that the emission depends on the size of the globular particles, whereby the hydrophobicity in the globular particles is higher leading to emission enhancement. However, further increasing the temperature leads to further aggregation into very large particles (>200 μm) that scatter the incident light before it reaches the dye, resulting in a decrease in emission. A series of different acrylamide copolymers (NIPAM, NNPAM and NIPMAM) were functionalized with rhodamine to study the influence of the monomer composition and the polymer concentration on the sensing behavior in solution.<sup>72</sup> These copolymers show similar fluorescence enhancement behavior at a specific temperature interval in water.



**Fig. 4** Schematic representation of the structures of rhodamine based PNIPAM (left) and the emission enhancement at a specific temperature range (right). Reprinted with permission from ref. 71. Copyright © 2007 American Chemical Society.

A different type of fluorescent thermometer was designed by using the aggregation-induced emission effect of a tetraphenyl-ethylene dye, entry 4, covalently attached to PNIPAM.<sup>74</sup> The fluorescence of this chromophore was studied during the coil-to-globule (aggregation of polymer chains) transition and the authors could show a strong increase in emission at a specific temperature range. Entry 5 depicts a chromophore based on the cyanine family, a hemicyanine dye, which was attached to PNIPAM by Hirai *et al.*<sup>75</sup> The authors exploited the tautomerism of this chromophore, which has a benzenoid (nonfluorescent) and a quinoid (fluorescent) structure, for sensing since the equilibrium is shifted towards the quinoid form upon the temperature-induced polymer collapse. Based on this mechanism the fluorescence enhancement at 40 °C is 20-fold compared to the intensity at 25 °C. BODIPY (boron-dipyrromethene, entry 6, Fig. 3) labeled PNIPAM copolymers were prepared by Shiraishi *et al.*<sup>76</sup> via a pyridinium salt. These copolymers revealed a fluorescence enhancement based on the formation of viscous microdomains in the collapsed polymer globule. It is proposed that the higher viscosity restricts the rotation of the meso-pyridinium moiety, which suppresses the excited state of the BODIPY units. Additionally, a BODIPY monomer was copolymerized with *N,N*-dimethylaminoethyl methacrylate (DMAEMA) by the RAFT process revealing a fluorescence enhancement during the thermo-induced phase separation. The authors describe that the formation of dimers in the aggregates (H-dimer) is responsible for the strong increase in fluorescence intensity.<sup>77</sup> A BODIPY functionalized monomer (entry 6) was copolymerized with DEGMA and OEGMA to make random and block copolymers by Liras *et al.*<sup>78</sup> Increased fluorescence intensities and quantum yields were observed during the temperature-induced phase transition.

A responsive nanogel with naphthalimide units (entry 7) for the detection of temperature and Hg<sup>2+</sup> was created by Liu and coworkers.<sup>80</sup> Upon heating above the phase separation temperature, the fluorescence intensity underwent a 3.4-fold increase due to hydrophobic microenvironment changes. In the presence of Hg<sup>2+</sup> ions a 10 fold and 57 fold increase in fluorescence emission intensity was achieved at 25 and 40 °C, respectively. The strong increase in fluorescence emission is due to the Hg<sup>2+</sup> induced transformation of naphthalimide-thiourea to naphthalimide-imidazole derivatives of the chromophore. Chen *et al.*<sup>81</sup> labeled PNIPAM with fluorene (entry 8) derivatives. At pH values above 7 increasing temperature led to aggregation of the copolymer resulting in enhanced fluorescence intensity due to microenvironmental polarity change of PNIPAM, while at pH values below 7 the sidechain of the fluorene moieties is protonated and remains in solution. A push-pull chromophore based on 4*H*-pyrane and diphenyl amino structures (polymethine dye, entry 9) was attached to a hydrogel by Kim *et al.*<sup>83</sup> Again a fluorescence enhancement was observed by increasing the temperature above the LCST of PNIPAM ascribed to the polarity change. Another example of a fluorescence enhancement sensor was constructed from miktoarm star copolymers of PNIPAM<sub>3</sub>-(*N*-vinylcarbazole), entry 10.<sup>85</sup> The authors describe an increase of the fluorescence by a rotational restriction of carbazole (Fig. 3) in the precipitated globular state.

**3.2.2 Sensors based on fluorescence quenching.** Another strategy for the construction of fluorescent temperature sensors employs quenching processes.

Shiraishi *et al.*<sup>87</sup> reported a temperature-driven on/off fluorescent indicator based on 9-aminomethylanthracene (entry 11) and PNIPAM. The temperature induced demixing of the copolymer was studied in water at different pH values. The observed temperature-driven fluorescence quenching is based on the photoinduced electron transfer (PET) process, where interaction between the cationic amino group and the  $\pi$  electron-system of anthracene occurs.

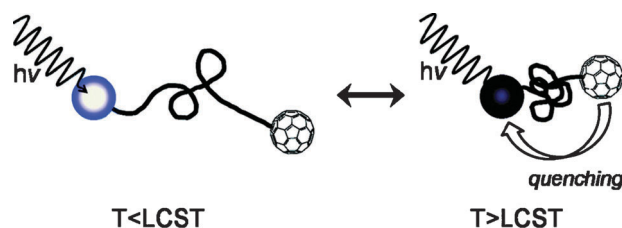
Another approach was reported based on a poly-(St-*b*-NIPAM) block copolymer micelles labeled with a carbazole dye (Fig. 3) in between the two block segments.<sup>86</sup> The authors showed a decrease of the fluorescence intensity (less excimer species) above the LCST by collapse of the PNIPAM block segments, while at low temperatures strong fluorescence is recorded due to the formation of more excimer species.

Tian *et al.*<sup>84</sup> reported a thermoresponsive polymer sensor labeled with dicyanomethylene-4*H*-pyrane moieties (entry 10) based on a fluorescence quenching mechanism (intramolecular charge transfer). The sensor shows multiple responsiveness to external stimuli, including pH value,  $\text{Cu}^{2+}$  ions and temperature in ethanol–water mixtures, and was also used for the construction of logic gates. It should be noted that the fluorescence quenching was observed only in neutral and acidic conditions. The authors suggest that the loss of the quenching is due to lower sensitivity of the copolymer to temperature (LCST behavior) in alkaline environments. Another example of selective  $\text{Cu}^{2+}$  ion recognition with a temperature sensor was reported by Liu *et al.*<sup>88</sup> using a microgel labeled with 1,10-phenanthroline (entry 12). Different metal-ions were investigated regarding the quenching process and only efficient quenching was observed for  $\text{Cu}^{2+}$  ions. Another example of a chemo- and temperature responsive hydrogel for detection of both temperature and  $\text{Cu}^{2+}$  ions was prepared by Liu *et al.*<sup>90</sup> A metal-chelating acceptor, picolineamine, and a fluorescent reporter, a dansyl-chromophore (5-(dimethyl-amino)naphthalene-1-sulfonyl dye, entry 13) were incorporated into PNIPAM. In the swollen state of the hydrogel,  $\text{Cu}^{2+}$  is selectively captured leading to emission quenching.

In a recent example, both pyrene (entry 14) and fullerene were covalently attached to the chain termini of PNIPAM (Fig. 5) and, alternatively, fullerene was attached on the side-chains of a pyrene end-functionalized PNIPAM.<sup>98</sup> In both cases, the pyrene fluorescence was quenched by increasing the temperature over the cloud point of PNIPAM due to the closer proximity of the pyrene and fullerene groups.

Water-soluble conjugated poly(fluorene)-*b*-poly(*N*-isopropylacrylamide) diblock copolymers were investigated by Liu and Wang *et al.*<sup>82</sup> showing self-assembly in aqueous solutions above the cloud point temperature of PNIPAM resulting in polyfluorene emission quenching.

Kim and Choi *et al.*<sup>106</sup> labeled the chain ends of a Pluronic<sup>®</sup> triblock copolymer consisting of ethylene oxide and propylene oxide with a Cy5.5 near-infrared fluorescent dye (entry 15). The copolymer exhibits temperature-induced aggregation behavior based on the LCST behavior of the



**Fig. 5** Temperature-induced quenching mechanism for both pyrene and fullerene end-group functionalized PNIPAM above the cloud point temperature (here denoted as LCST). Reprinted with permission from ref. 98. Copyright © 2009 American Chemical Society.

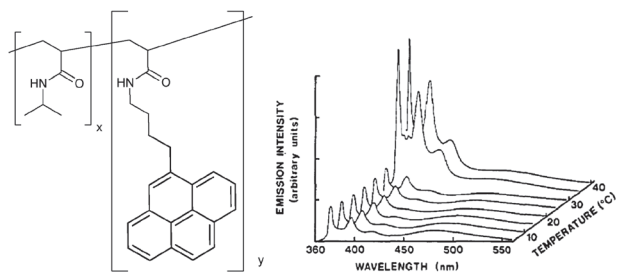
poly(propylene oxide) block covering a broad temperature interval from 0 to 80 °C. Accordingly, the near-infrared emission linearly decreases from 0 to 80 °C due to the transition from dissolved polymer chains to intermediate micelles (semi-quenched) to large aggregates (quenched).

A BODIPY (entry 6, Fig. 3) functionalized RAFT agent was used for the polymerization of NIPAM, followed by aminolysis to obtain a thiol end-group, which was used for the binding to gold nanoparticles.<sup>79</sup> By heating the copolymer over the cloud point temperature, the BODIPY fluorescence was quenched by the close proximity of these gold nanoparticles.

### 3.2.3 Sensors based on batho/hypsochromic emission shifts.

One of the most studied solvatochromic fluorescent dyes in chemistry is pyrene.<sup>120</sup> Pyrene is *e.g.* used in polymer science as a fluorescent probe for the determination of critical micelle concentrations (CMC) of block copolymers based on the sensitivity of the pyrene emission to the polarity of the solubilizing medium.<sup>121,122</sup> This special behavior of the fluorescent dye and the formation of excimers make the chromophore very useful for the investigation of the heat-induced phase transition to gain a molecular insight into the thermo-reversible phase separation. In the early nineties Winnik *et al.*<sup>32,34,37,91–93</sup> studied the phase transition of pyrene (entry 14) functionalized PNIPAM in water. The authors showed that the polymer phase transition has an influence on the pyrene excimer emission, *i.e.* a change in the ratio of excimer to monomer fluorescence from 375 and 396 nm (single pyrene emission) to ~480 nm of pyrene excimer emission (Fig. 6). Several parameters were investigated, like the effect of hydrophobically modified PNIPAM,<sup>91</sup> the excimer formation between naphthalene and pyrene moieties,<sup>34,95</sup> spin labeling<sup>93,94</sup> (stable radical of (2,2,6,6-tetramethylpiperidin-1-yl)oxyl, TEMPO derivative) and the influence of molar mass and pyrene content of the copolymer.

The non-radiative energy transfer between pyrene/naphthalene<sup>32</sup> or pyrene/carbazole<sup>38</sup> chain labels of PNIPAM was used to explore the interpolymer and polymer–solvent interactions by, *e.g.*, energy transfer efficiencies, which depend on the polymer chain dimensions (distance of chromophores). Several fundamental mechanisms of the polymer transition could be understood, including that for dilute solutions individual polymer chains are present below the LCST transition (no interpolymeric interactions) and that the macroscopic phase separation is caused by conformation changes triggered by temperature

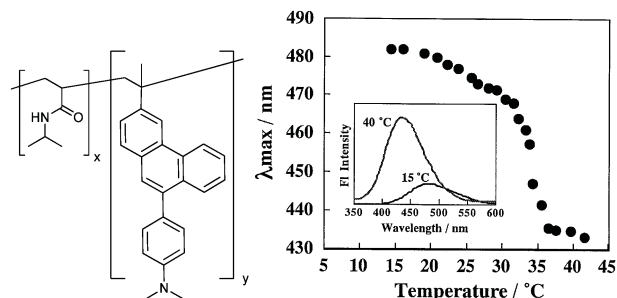


**Fig. 6** Pyrene labeled PNIPAM (left) and the effect of temperature on the monomer/excimer fluorescence by passing the cloud point temperature (right). Reprinted with permission from ref. 37. Copyright © 1990 American Chemical Society.

of polymer–water interactions (loss of hydrogen bonds) of PNIPAM. The phase separation is initiated by a gradual shrinking of the solvated polymer chain into a collapsed state followed by aggregation of individual chains into larger particles.

Hydroxy propyl cellulose, which exhibits a LCST transition at 42 °C, was also labeled with pyrene.<sup>96,97</sup> Under the phase separation temperature two types of excimer formation could be observed (one center vs. sandwich type) from ordered copolymer assemblies, but by increasing temperature the sandwich type predominates in the globule. In addition, pyrene-labeled poly(*N*-vinylcaprolactam) and PEO graft copolymers were investigated by Winnik *et al.*<sup>99,100</sup> to study the influence of the polymer phase transition on the pyrene excimer formation. PNIPAM with chain terminal pyrene groups was additionally investigated with regard to the LCST transition and excimer formation by several workgroups.<sup>103,104</sup> More recently, Hoogenboom *et al.*<sup>102</sup> reported a di(ethylene glycol) methyl ether methacrylate (DEGMA) copolymer labeled with pyrene as a fluorescent thermometer. Higher pyrene excimer emission was observed below the demixing temperature due to high polarity of the aqueous environment. In addition, the increased microviscosity in the collapsed polymer globules might hinder the excimer formation above the phase transition temperature. A block copolymer of poly(OEGMA-*b*-pyrene-methacrylate) was synthesized by Zhao *et al.*<sup>105</sup> revealing aqueous self-assembly into micelles and a temperature-induced change in the excimer/monomer fluorescence of pyrene.

The opposite polymer demixing transition in solution, namely the upper critical solution temperature (UCST), was investigated for the development of a fluorescent temperature sensor. Poly(methyl methacrylate), PMMA, with covalently attached pyrene groups was reported by Hoogenboom *et al.*<sup>101</sup> This UCST-type sensor revealed a broader temperature sensing range in aqueous ethanol (10 to 40 °C) compared to similar LCST based sensors. Uchiyama and Ohwada *et al.*<sup>107</sup> attached an environmentally sensitive 2*H*-benzo[*g*]chromen-2-one fluorophore (entry 16), which is nonfluorescent in aprotic solvents and strongly fluorescent in protic solvents, to PNIPAM. As expected a stronger fluorescence was observed for temperatures below the cloud point temperature and by increasing the temperature above the demixing point a blue shift of the maximum emission wavelength was observed together with a decrease in intensity due to the release of water molecules from the polymer chains.



**Fig. 7** Phenanthrene labeled PNIPAM (left) and (right) the effect of temperature on the maximum emission wavelength ( $\lambda_{\text{max}}$ ). Reprinted with permission from ref. 109. Copyright © 2000 Elsevier B.V.

Several copolymers and hydrogels of NIPAM with MMA, MAA, DMAM, NNIPAM, and NIPMAM were prepared with 9-(4-*N,N*-dimethylamino-phenyl)-phenanthrene derivative (entry 17) as covalently attached molecular fluorescent probe by Iwai *et al.* (Fig. 7).<sup>63,108–110</sup> The amount of comonomers incorporated in PNIPAM influences the LCST temperature (hydrophobic comonomers lower the LCST and hydrophilic comonomers increase it) and, therefore, a broader and tuneable temperature sensing range could be achieved. The amino-phenyl-phenanthrene dye exhibits intramolecular charge-transfer and shows a strong solvatochromism. When the PNIPAM precipitates upon heating, the maximum emission wavelength changes from 481 nm to 434 nm as shown in Fig. 7. This blue-shift was also observed for the various copolymers and is based on the change of the polarity of microenvironment.

A ratiometric thermometer was created by functionalizing a PNIPAM hydrogel with a 3-hydroxyflavone dye (entry 18).<sup>111</sup> The dye shows a dual-band emission associated with an excited state intramolecular charge transfer (green fluorescence) and a tautomer excited state intramolecular proton transfer (blue fluorescence), which depend on the polarity and the protic properties of the solvents. By heating the polymer solution over the cloud point a shift from blue emission to green emission was observed, which can be used for a ratiometric readout of the temperature. Matsumura and Katoh<sup>112</sup> used 6-aminoquinoxaline derivatives (entry 19) as chromophores for the copolymerization with NIPAM. The dye is used as a fluorescent probe for the phase separation by a change in the maximum emission wavelength ( $\lambda_{\text{max}}$ ) from 515 nm to 497 nm. In a final example, the alizarin red S dye (entry 20) was covalently linked to PNIPAM *via* diol–boronic acid complex formation and was investigated for logical operations<sup>114</sup> as well as for diol sensing<sup>113</sup> in combination with the aqueous temperature induced phase separation of PNIPAM.

**3.2.4 pH detection by fluorescence emission shift/enhancement during temperature induced phase separation.** Dye-labeled copolymer temperature sensors based on aqueous polymer phase transitions can also be used for the detection of the pH value since often a pH dependent emission shift is observed next to the temperature induced changes.

Recently Uchiyama and Ohwada *et al.*<sup>64,65</sup> synthesized several stimuli-responsive acrylamide copolymers with polarity sensitive benzofurazan dyes (entry 1). The sensor is based on the benzofurazan as indicator dye and several comonomers as



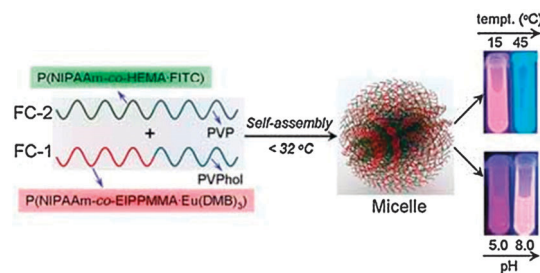
receptor units for ion recognition, e.g.  $K^+$  ions by crown ether complexation, sulfate ion detection by tris(3-aminopropyl)-amine units or  $H^+$  ion detection by DMAPAM. Multiple sensing of target ions ( $H^+$  or  $K^+$ ) in combination with temperature could be realized by suitable combinations of the different comonomers. A digital (on-off) fluorescent pH sensor was successfully created using this concept comprising an indicator dye and a receptor unit.<sup>64</sup>

A benzoxazole (entry 21) containing PNIPAM was used as a sensor for the pH value, zinc ion concentration and/or the temperature.<sup>115</sup> The dye shows a keto-enol tautomerism and can complex zinc ions under basic conditions resulting in an emission shift from 425 nm to 500 nm.

Fluorescein (entry 22) is a well-known fluorescent tracer in biology and is used for many applications. The fluorescence of fluorescein depends strongly on the pH value due to an equilibrium between the di-anion, mono-anion and neutral forms of the dye. Binkert *et al.*<sup>31</sup> investigated the local mobility of fluorescein labeled PNIPAM polymer chains with fluorescence spectroscopy (time resolved fluorescence depolarization). They observed a reduction of the label mobility and an enhancement of non-radiative transfer due to the coil (flexible) to globule transition.

A dual temperature and pH responsive PNIPAM copolymer was reported by Kanazawa *et al.*<sup>116</sup> based on fluorescein. The copolymer showed enhanced fluorescence intensity for low temperature, when the copolymer is in solution, which decreased by increasing the temperature. Similar to the parent fluorescein the copolymer revealed a pH depend fluorescence, where the highest values are achieved at alkaline conditions, while at acidic pH values the fluorescence is nearly lost. Additionally, cellular uptake of the copolymer was studied. A fluorescein based radical initiator was used for the ATRP of NIPAM and DMAM by Meng *et al.*<sup>117</sup> The LCST behaviors of the different copolymers were studied at different pH values by fluorescence spectroscopy showing an increase of fluorescence intensity for increasing pH values. Temperature and pH sensitive micellar complexes of poly(NIPAM-*co*-HEMA)-*b*-poly(4VP) labeled with fluorescein and poly(NIPAM-*co*-phenanthroline europium complex)-*b*-poly(4HSt) (Fig. 8) were synthesized by Zhang *et al.*<sup>89</sup> The size of the self-assembled structures changed during the LCST transition resulting in an aggregation of the micelles due to the collapse of PNIPAM. The self-assembly and fluorescent properties were found to be strongly dependent on the temperature and the pH value. The emission of fluorescein depends strongly on the pH value and, therefore, a shift in emission is observed. The temperature induced emission shift of the phenanthroline europium complex is due to a change from hydrophilic to hydrophobic of PNIPAM chains during the LCST transition.

Acridine-9-*N*-acrylamide (entry 23) was homo- and copolymerized with acrylamide (AM) by Su and coworkers<sup>118</sup> for the construction of temperature/pH sensors. The copolymer shows a linear relationship between the temperature and the fluorescence intensity and additionally a pH induced shift of the emission maximum due to the protonation of the nitrogen (tautomerism). A multifunctional fluorescent sensor was developed for the detection of the pH value and  $Hg^{2+}$  ions by Liu *et al.*<sup>73</sup> using a rhodamine B derivate (entry 3).



**Fig. 8** Poly(NIPAM-*co*-HEMA) labeled with fluorescein and a phenanthroline europium complex for pH and temperature detection. Reprinted with permission from ref. 89. Copyright © 2009 WILEY-VCH Verlag GmbH & Co. KGaA, Weinheim.

The detection sensitivity for both could be increased if the poly(ethylene glycol)-*b*-(NIPAM) copolymer is collapsed into micellar structures at elevated temperatures.

A pH and thermo sensitive polymeric material was realized by combining a *p*-aminoacetophenone thiosemicarbazone unit (entry 24) and a PNIPAM polymer chain. The fluorescence intensity could be significantly influenced by the addition of a base (tautomerism of thiosemicarbazone) resulting in emission decrease.<sup>119</sup>

### 3.3 FRET based sensors

The fluorescence resonance energy transfer (FRET) has also been exploited for the construction of polymeric sensors based on thermoresponsive polymers. The FRET energy transfer occurs between a donor molecule in the excited state and an acceptor (A) chromophore in the ground state, whereby the donor chromophores emit at wavelengths that overlap with the absorption spectrum of the acceptor, resulting in acceptor emission. The FRET process is a result of the long-range dipole-dipole interactions between the donor and acceptor.<sup>123</sup> FRET depends strongly on the distance between the donor and acceptor and allows the determination of this distance based on the efficiency of energy transfer. During the coil-to-globule transition of a thermoresponsive polymer, the interchain distances of the polymer coil are changing and therefore the FRET efficiency is influenced, which can be used to determine these interchain distances. The Winnik research group (entry 25)<sup>32</sup> as well as Schild and Tirrell (entry 26)<sup>38</sup> exploited the non-radiative energy transfer between donor and acceptor chain labels to study LCST polymer phase transitions for two cases: (i) the donor and acceptor are attached to the same polymer chain and (ii) a mixture of donor functionalized polymer chains with acceptor functionalized polymer chains. The FRET process was used to explore the interpolymer interactions and the mechanism of the coil-to-globule transition. The energy transfer efficiency was found to be higher above the LCST transition and the authors concluded that the mechanism of the phase separation is initiated by a gradual shrinking of the solvated polymer chain into a collapsed state followed by aggregation of individual chains into larger particles.<sup>32</sup> All the reported combinations of thermoresponsive polymers with, respectively, FRET pairs and the temperature sensing regime are summarized in Table 2.

**Table 2** FRET based temperature sensors

Entry	FRET pair (D/A)	Polymer	Stimuli [ <i>T</i> -range °C]	Wavelength range (D/A emission)	Type	Ref.
25	Naphthalene/pyrene	NIPAM	4–40	Em: 323 nm → 376, 480 nm	Chain length change (LCST)	32
26	Carbazole/pyrene	NIPAM	25–35	Em: 305 nm → 377 nm	Chain length change (LCST)	38
27	Cy5/Cy5.5 (Cyanine dyes)	NIPAM	23–43	Em: 674 nm → 697 nm	Chain length change (LCST)	124
28	Benzofurazan/rhodamine	St- <i>b</i> -NIPAM	25–36, pH, UV/Vis	Em: 518 nm → 580 nm	Photoisomerization and pH value change	125
29	Benzofurazan/spiropyran	NIPAM	25–50, UV, K <sup>+</sup>	Em: 527 nm → 588 nm	Chain length change (LCST) and swelling by UV light or K <sup>+</sup> ions	126, 127
30	Benzofurazan/spiropyran	NIPAM	20–35, UV/Vis	Em: 550 nm → 620 nm	Photoisomerization	128

Cyanine dyes (entry 27) were attached to PNIPAM core/shell microgels by Lyon *et al.*<sup>124</sup> in 2004 to study the structure–function relationship between the core and shell components. The swelling and thermoresponsive behavior of these microgels was investigated in detail *via* the FRET process. Investigations of the core swelling behavior in the presence of a shell allowed a geometric thickness determination.

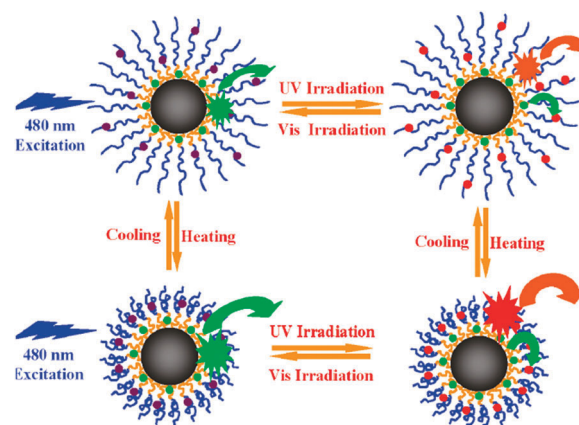
Liu and Cheng *et al.*<sup>125</sup> demonstrated three-state switching of fluorescence emission of a stimuli-responsive poly(St-*b*-NIPAM) block copolymer based on three chromophores (2 FRET pairs). These three chromophores give rise to two independent FRET processes based on benzofurazan/rhodamine and benzofurazan/spiropyran pairs (entry 28), which can be stimulated by the pH value, the temperature, and light irradiation. The reported diblock copolymer micelles act as a sensitive ratiometric fluorescent sensor for pH value and temperature.

Liu *et al.* recently developed thermo and light sensitive microgels based on the benzofurazan/rhodamine FRET pair (entry 29).<sup>126,127</sup> One type of microgel was designed to show temperature and light regulated FRET efficiencies, whereby the collapse of the microgels leads to an enhanced FRET efficiency due to the closer distance of the dyes. The authors incorporated a photocleavable 2-nitrobenzyl moiety, which could be used to change the optical properties of the microgel resulting in a less efficient FRET process.<sup>126</sup> In a second type of microgels (see also Section 4) Liu and coworkers introduced a crown-ether for the recognition of potassium ions as a ratiometric fluorescent probe. Also for this microgel the FRET process is enhanced by temperatures above the LCST, but in the presence of K<sup>+</sup> ions the re-swelling of the gel (larger volume) leads to less efficient FRET.<sup>127</sup>

Hybrid silica nanoparticles with PNIPAM brushes labeled with the benzofurazan/spiropyran FRET pair (entry 30) were reported by Liu *et al.* as temperature and UV/Vis light sensors (Fig. 9).<sup>128</sup> The spirobenzopyran shows two tautomeric structures, which can be switched by UV/Vis light (see Section 3.4.1) and, as a result, the FRET process could be turned off by irradiation with visible light. By passing the LCST transition the fluorescence ratio (FRET efficiency) of the dyes changed.

### 3.4 Absorbance based visible temperature sensors

In comparison to fluorescence based temperature sensors, only a small number of reports appeared on absorbance based



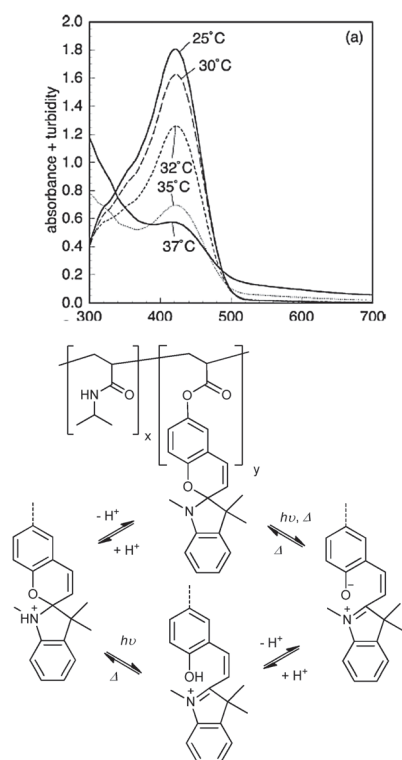
**Fig. 9** Hybrid silica nanoparticles with PNIPAM brushes showing an on/off FRET process. Reprinted with permission from ref. 128. Copyright © 2009 American Chemical Society.

temperature sensors; again PNIPAM based copolymers are primarily investigated. The majority of the absorbance based temperature sensors are based on chromophores that translate the polymer phase transition into a batho/hypso-chromic shift of absorbance. Nonetheless, this process can be a result of various mechanisms, like photoisomerization, tautomerism, photocrosslinking or complexation of the chromophore. The different types of reported absorbance temperature sensors are summarized in Table 3 and will be discussed in the following.

**3.4.1 Sensors based on batho/hypsochromic absorbance shifts.** Spiropyran (entry 31) is an often used photoresponsive dye since it can be switched by UV/Vis light between a colored open-ring structure (merocyanine) and a colorless spiro form with a closed-ring structure (Fig. 10). Both structures can be additionally protonated. Sumaru *et al.*<sup>129–134</sup> discussed the effects of irradiation with visible light on the absorption of PNIPAM functionalized with spiropyran during pH and/or temperature induced phase transitions. It was shown that the absorbance of spiropyran abruptly changed during the polymer phase transition, useful for logic gate operations. Based on this approach Sumaru and coworkers prepared a photo- and thermoresponsive gate membrane of a spiropyran functionalized PNIPAM hydrogel attached to a surface.<sup>132</sup> Garcia and Hu *et al.*<sup>135</sup> also used a PNIPAM hydrogel labeled with a spiropyran dye for photo-, thermo- and pH responsive sensing. In addition, complexation of Pb<sup>2+</sup> ions by the open

**Table 3** Absorbance based temperature sensors

Entry	Dye	Polymer	Stimuli [T-range °C]	Wavelength range (absorbance)	Repeat	Type	Ref.
31	Spiropyran	NIPAM, DEGMA, DMAM	10–50, pH UV/Vis, Pb <sup>2+</sup>	Abs: 519 → 546 nm Abs: 580 nm	—	Photoisomerization and microenvironmental polarity change, complexation	129–138, 140
32	Brooker's merocyanine	NIPAM	30–40, pH	Abs: 460 → 385 nm	—	Tautomerism, cyclodextrin complexation	139
33	Metalloporphyrin	NIPAM, HEMA, MAA	35–65, metal ions	Abs: 420 → 560 nm for different metal ions	8×	Different metal complexes and microenvironmental polarity change	141
34	Disperse red 1	DEGMA DEGMA-co-OEGMA	10–25, pH 86–96	Abs: 487 → 532 nm	—	Tautomerism of azo-dye	142
35	Azobenzene	NIPAM, DMAM, DMAEMA, NIPAM- <i>b</i> -PEO, DEGMA, OEGMA	20–60, UV/Vis	Abs: 320–365 nm and 425 nm	—	Photoisomerization ( <i>cis/trans</i> )	36, 140, 143–156
36	Copper chlorophyllin	NIPAM	25–40, UV/Vis	—	—	Heat-transfer by radiationless transition	157
37	Malachite green	NIPAM	25–35	Abs: 620 nm	—	Heat-transfer by radiationless transition	158
38	Naphthalene CBPQT <sup>4+</sup>	NIPAM	26–36	Abs: 450 nm	3×	Complexation	159
39	Leuco dye	NIPAM	25–35, UV/Vis	—	—	Halochromism	160
40	Fulgimide	NIPAM	26–36, UV/Vis	Abs: 325 → 525 nm	—	Photoisomerization	151



**Fig. 10** Absorbance spectra of spiropyrans chromophore in PNIPAM by heating over the LCST at pH 4 and the photoisomerization and protonation. Reprinted with permission from ref. 130. Copyright © 2007 Elsevier B.V.

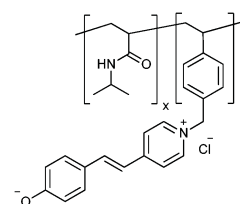
form of spiropyran was studied by Suzuki *et al.*<sup>136</sup> showing a colour shift by complexation.

A colorimetric thermometer with a linear and reversible batho/hypsochromic shift of the absorption spectrum of the attached spiropyran moieties in a temperature range of

10 to 34 °C was reported by Shiraishi *et al.*<sup>137</sup> In addition, a thermoresponsive poly(DEGMA-*b*-spiropyran) diblock copolymer was synthesized revealing double responsive micellization in aqueous solution.<sup>138</sup> The core of the micelles could be switched between both segments by temperature and UV/Vis light.

Brooker's merocyanine dye (4-[(1-methyl-4(*H*)-pyridinylidene)ethylidene]-2,5-cyclohexadien-1-one, entry 32, shows a strong negative solvatochromic effect in solution due to the presence of two tautomeric forms, a quinone and a zwitterion structure. This dye was covalently attached to PNIPAM *via* nitrogen quaternization (Fig. 11) by Ritter and Koopmans to act as an optical sensor in solution with a color shift for the temperature at different pH values.<sup>139</sup> Additionally, host-guest interactions with  $\beta$ -cyclodextrin were studied resulting in an absorbance shift of the dye.

In a recent example, a dual-sensing metalloporphyrin (entry 33) containing poly(NIPAM-*b*-HEMA-*b*-MAA) copolymer was demonstrated to act as a metal ion detector and sensitive thermometer.<sup>141</sup> The sensor exhibits a full-color tunable behavior and is based on different metal ion complexation by the porphyrin. These copolymers with different metal ions all revealed thermochromic properties by passing the LCST transition. Recently, a dual sensor that simultaneously senses the temperature and the pH value was developed by combination of a poly(DEGMA) copolymer with a pH



**Fig. 11** PNIPAM functionalized with Brooker's merocyanine.<sup>139</sup>

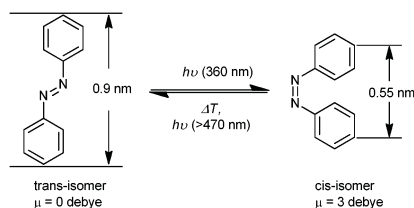


Fig. 12 Photoisomerization of azobenzene.<sup>144</sup>

responsive solvatochromic dye, namely disperse red 1 (entry 34).<sup>142</sup> At low pH values, the polymer undergoes a color change from 487 to 532 nm during the temperature-induced phase separation, while at neutral or basic conditions this shift is lost.

An interesting property of azobenzene derivatives (entry 35) is the photoisomerization of the *trans*- to the *cis*-isomer by irradiation with UV/Vis light (Fig. 12). During this photoisomerization the  $\pi^* \leftarrow \pi$  and  $\pi^* \leftarrow n$  transitions of the chromophore are affected resulting in a shift of the absorption band. This property of the azobenzene derivative can be used for photo sensor systems.

Azo-dyes were randomly incorporated in the polymer backbone by several working-groups by copolymerization of the dye-functionalized monomer with different monomers like NIPAM,<sup>36,140,143,145,147,149–152</sup> DMAM,<sup>140,144,146,153</sup> DMAEMA<sup>148,154</sup> and OEGMA.<sup>140,155,156</sup> The azobenzene copolymers were studied as light and thermo-sensitive materials. Additionally the effect of the pH value to the LCST<sup>154</sup> as well as the complexation of  $\alpha$ -cyclodextrin<sup>153</sup> were investigated. Suzuki and Tanaka<sup>157</sup> reported about a phase transition of copper chlorophyllin labeled (entry 36) PNIPAM gels induced by visible light and by temperature, which can be used as switches or as light sensors.

Another example for a photoresponsive microgel is based on PNIPAM and a malachite green dye (entry 37) for photomodulated material.<sup>158</sup> Irradiation of a malachite green containing hydrogel increases the temperature due to rapid nonradiative decay resulting in the collapse of the gel.

A naphthalene functionalized PNIPAM copolymer was used as a tool for the complexation of cyclophane cyclobis(paraquat-*p*-phenylene) (CBPQT<sup>4+</sup>), entry 38.<sup>159</sup> During the LCST-mediated transition of NIPAM a reversible decomplexation process occurs causing a large color shift due to the disassembly of the donor-acceptor complex, which shows great potential for the development of temperature sensors. A photo-induced phase transition of a PNIPAM hydrogel labeled with a bis(4-(dimethylamino)phenyl) (4-vinylphenyl)methyl leucocyanide (entry 39) dye, which shows a halochromism, was developed by Tanaka and Irie *et al.*<sup>160</sup> Equilibrium swelling curves of the gel were recorded as a function of temperature and UV light. The gel shows a very fast photoinduced transition and can be used in optical devices. Another photo-isomerizable chromophore represents the fulgimide dye (entry 40), which reveals an absorption band at 530 nm after UV irradiation. A series of thermo-responsive PNIPAM copolymers containing different amounts of fulgimide moieties has been synthesized and studied as molecular logic gates.<sup>151</sup>

#### 4. Applications of thermoresponsive polymeric sensors

In this section, the application potential of thermoresponsive polymeric sensors is highlighted based on selected examples. Not all design principles will be discussed in full detail, but the most important creative strategies and concepts will be explained. As is evident from the previous sections, a wide range of sensors for temperature, pH, UV/Vis light and ions have been developed by the combination of a polymer LCST transition with solvatochromic dyes. The large number of different chromophores and indicator dyes as well as the wide variety of available thermoresponsive (co)polymers provide almost unlimited potential for tailor-made sensors. In addition, recent studies demonstrate the extension of this concept towards biosensors, logic gates, microvalves or simultaneous dual sensors, which will be discussed in the following.

Logic gates that can (simultaneously) treat multiple inputs are extremely interesting for material science to develop molecular memory systems. In 2004, Uchiyama and Iwai *et al.*<sup>60</sup> developed a fluorescent polymeric logic gate with both temperature and pH as input values. The logic gate operation is based on the following concept (Fig. 13): the *N*-alkylacrylamide polymer backbone senses the changes in temperature by undergoing a LCST transition while the ionizable tertiary amine moieties in the polymer respond with a solubility change to the pH value. The incorporated polarity-sensitive benzofurazan dye records the accompanying changes in the microenvironmental polarity with a fluorescence signal as output.

Another very appealing application example is the development of a fluorescent nanogel as a thermometer for living cells.<sup>62</sup> A PNIPAM nanogel was prepared with incorporated water-sensitive benzofuran units that are quenched by contact with water. By increasing the temperature the nanogel, which was inside the cytoplasm of COS7 cells, showed a stronger fluorescence signal due to the collapse of the gel (Fig. 14). The temperature sensing accuracy was within 0.5 °C inside the living cells.

A dual sensor that simultaneously senses the temperature and the pH value was synthesized by Hoogenboom *et al.* as illustrated in Fig. 15.<sup>142</sup> The sensor is based on a thermo-responsive PDEGMA copolymer bearing disperse red 1 as a solvatochromic dye. The dual sensitive copolymer shows temperature responsiveness in the range from 10 to 20 °C

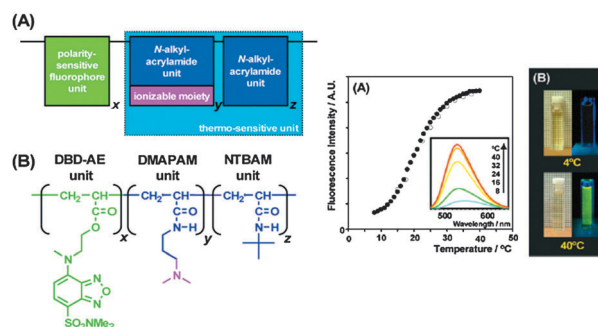
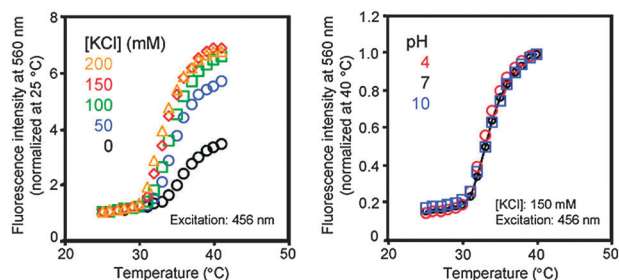
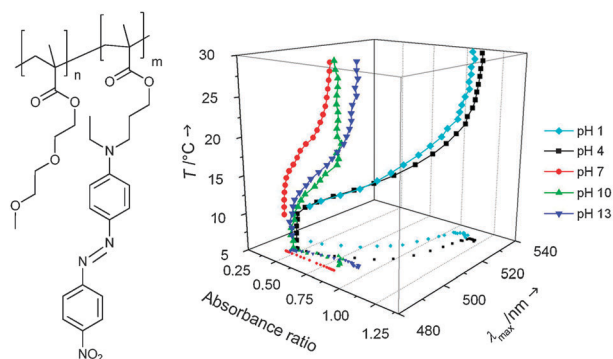


Fig. 13 Logic gates which can simultaneously treat multiple inputs. Reprinted with permission from ref. 60. Copyright © 2004 American Chemical Society.



**Fig. 14** Fluorescent nanogel as a thermometer for living cells. Reprinted with permission from ref. 62. Copyright © 2009 American Chemical Society.

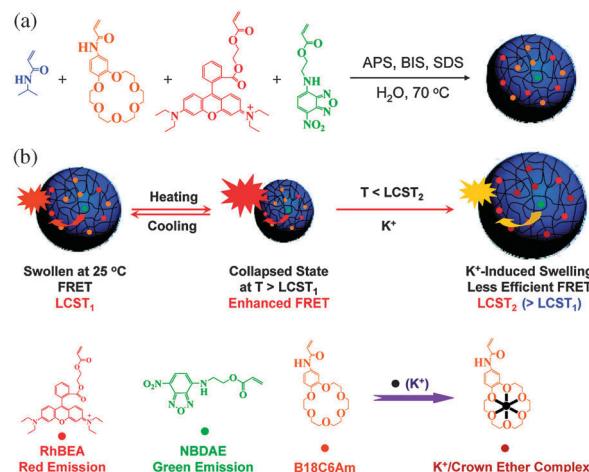


**Fig. 15** Dual sensor for temperature and pH value. Reprinted with permission from ref. 142. Copyright © 2009 WILEY-VCH Verlag GmbH & Co. KGaA, Weinheim.

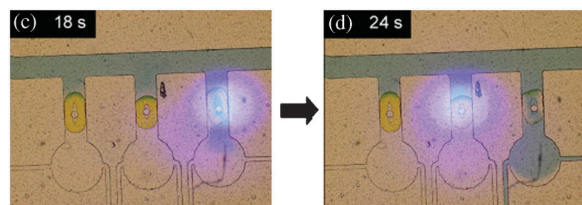
due to the phase separation of the PDEGMA and the chromophore exhibits a color change from 487 to 532 nm under acidic conditions due to protonation of the chromophore, while at basic conditions this shift is lost. By measuring a single absorption spectrum, the combination of absorption maximum as well as the absorbance ratio of the disperse red 1 dye provides information of both the temperature and pH value of the solution.

A ratiometric fluorescent  $K^+$  sensor based on a thermo-responsive PNIPAM microgel was designed by Liu *et al.*<sup>127</sup> 4-Acrylamidobenzo-18-crown-6 and two dyes for fluorescence resonance energy transfer, namely the donor benzoxadiazole and rhodamine-B as a FRET acceptor, were incorporated into the gel. The FRET process of the microgel is enhanced by temperatures above the LCST due to a shorter distance of the FRET pair. In addition, the presence of  $K^+$  ions induces a second volume phase transition (VPT) temperature leading to an increased distance between the dye pair resulting in less efficient FRET (Fig. 16).

Photoresponsive polymer gels based on PNIPAM functionalized with a spirobenzopyran chromophore were fabricated by Sumaru *et al.*<sup>133</sup> These polymer gels were exploited to develop a photoresponsive microvalve, which can be opened by local light irradiation. Blue light irradiation of the microgels causes a shrinkage of the PNIPAM gel (LCST) due to ring-closure of the spirobenzopyran causing a decrease in the cloud point temperature by its lower polarity compared to the ring-opened form. As a result of the microgel shrinkage the microvalves are opened (Fig. 17). Additionally,



**Fig. 16** Ratiometric fluorescent potassium sensor. Reprinted with permission from ref. 127. Copyright © 2010 American Chemical Society.



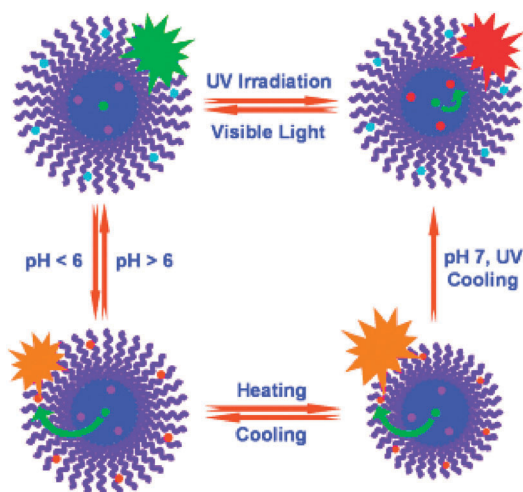
**Fig. 17** Photoresponsive polymer gel microvalves controlled by local light irradiation. Reprinted with permission from ref. 133. Copyright © 2007 Elsevier B.V.

the microvalves can be operated by temperature changes that also control the transition between the open and closed forms of spirobenzopyran. These microvalves facilitate non-contact, independent, and parallel fluid manipulation in microchips controlled by light irradiation or temperature.

A new type of multicolor fluorescent stimuli-responsive block copolymer was demonstrated to act as a sensitive ratiometric probe for both pH value and temperature. The concept is based on a thermo-responsive poly(*St-b*-NIPAM) diblock copolymer separately labeled with three different chromophores in the two block segments to comprise two FRET pairs (one type of donor dye and two types of acceptor dyes). The FRET process can be switched (on/off fluorescence) between the two acceptors stimulated by the pH value, or by UV/Vis light irradiation (Fig. 18). Fluorescence intensity changes of the micellar solution upon 5 cycles between pH 3 and pH 7 and upon UV irradiation (365 nm) and visible light irradiation (525 nm) were demonstrated.

## 5. Conclusions and outlook

This feature article illustrated the historical development of temperature-sensors based on thermo-responsive polymers in combination with solvatochromic dyes. In the early days, the incorporation of solvatochromic dyes was mostly exploited to provide a deeper fundamental understanding of the temperature-induced polymer phase transition. Only in the last decade, this concept has been widely adapted for the development of smart polymeric thermometers. The majority of these polymeric



**Fig. 18** Reversible three-state switching of FRET based thermo-responsive polymeric micelles. Reprinted with permission from ref. 125. Copyright © 2009 WILEY-VCH Verlag GmbH & Co. KGaA, Weinheim.

temperature sensors are based on the gold standard thermo-responsive polymer, PNIPAM, in combination with a wide variety of fluorescent dyes with a range of sensing mechanisms, including batho/hypsochromic shifts, fluorescence quenching/enhancing as well as FRET. In contrast, only a relatively small number of studies dealt with colorimetric sensors with solvatochromic visible dyes. More recently, there is a growing interest in using POEGMA based thermo-responsive polymers as alternatives to PNIPAM. Moreover, well-defined polymers with better defined phase transition temperatures became easily accessible through the development of controlled radical polymerization techniques. Finally, new application areas, besides simple temperature sensing, have been explored leading to polymers for logic gate operations, simultaneous dual sensors as well as smart valves.

This feature provides an up to date overview of this dynamic research field to already engaged scientists and will hopefully stimulate interested researchers to enter this exciting field of research that without doubt will lead to new innovative application concepts as well as more elegant and broadly applicable soluble polymeric thermometers in the coming years. Specific challenges for the near future are related to establishing the fundamental requirements for robust temperature sensors, such as the reversibility of the LCST transition over a long time (e.g. 1000 cycles), the signal stability and photobleaching effects of the chromophore in the polymer backbone and the biocompatibility or solubility. In principle the here discussed polymeric sensors are reversible and have potential for continuous sensing applications, but up to now most of the studies are limited to proof-of-principle concepts rather than continuous operation, which should also be addressed.

## Abbreviations

AA	acrylic acid,
APTMA	3-acrylamidopropyl trimethylammonium salt,
<i>N</i> -vinyl-CLA	<i>N</i> -vinyl-caprolactam,

DEAPAM	<i>N</i> -[3-(diethylamino)propyl] acrylamide,
DEAM	<i>N,N</i> -diethylacrylamide,
DEGMA	di(ethylene glycol) methylether methacrylate,
DMAEMA	2-(dimethylamino) ethyl methacrylate,
DMAM	<i>N,N</i> -dimethylacrylamide,
DMAPAM	<i>N</i> -[3-(dimethylamino)propyl] acrylamide,
HEMA	2-hydroxyethyl methacrylate,
4HSt	4-hydroxystyrene,
KSPMA	potassium 3-sulfopropyl methacrylate,
MAA	methacrylic acid,
MMA	methyl methacrylate,
PEG/PEO	linear poly(ethylene glycol),
PPO	poly(propylene oxide),
NBCAM	4-acrylamidobenzo-18-crown-6,
NDMPAM	<i>N</i> -(3,4-dimethoxyphenyl)acrylamide,
NIPAM	<i>N</i> -isopropylacrylamide,
NIPMAM	<i>N</i> -isopropylmethacrylamide,
NNPAM	<i>N-n</i> -propylacrylamide,
NTAAM	<i>N-tert</i> -amylacrylamide,
NTBAM	<i>N-tert</i> -butylacrylamide,
MPAM	<i>N</i> -(3-morpholin-4-ylpropyl)acrylamide,
OEGMA	oligo(ethylene glycol) methylether methacrylate,
SPA	3-sulfopropyl acrylate,
St	styrene,
4VP	4-vinylpyridine.

Polymer abbreviations are formed by adding the suffix 'P' or 'poly' to the corresponding monomer abbreviation.

## Acknowledgements

Financial support of the Dutch Polymer Institute (DPI) and the Netherlands Scientific Organisation (NWO; VENI-grant for RH and VICI-grant for USS) is gratefully acknowledged. We thank Dr Anja Schulz for helpful comments.

## Notes and references

- B. Adhikari and S. Majumdar, *Prog. Polym. Sci.*, 2004, **29**, 699–766.
- O. S. Wolfbeis, *J. Mater. Chem.*, 2005, **15**, 2657–2669.
- Optical Chemical Sensors*, ed. F. Baldini, *et al.*, Springer, Dordrecht, The Netherlands, 1 edn, 2006, vol. 224, pp. 297–322.
- C. McDonagh, C. S. Burke and B. D. MacCraith, *Chem. Rev.*, 2008, **108**, 400–422.
- O. S. Wolfbeis, *Adv. Mater.*, 2008, **20**, 3759–3763.
- M. I. J. Stich, L. H. Fischer and O. S. Wolfbeis, *Chem. Soc. Rev.*, 2010, **39**, 3102–3114.
- A. Richter, G. Paschew, S. Klatt, J. Lienig, K.-F. Arndt and H.-J. Adler, *Sensors*, 2008, **8**, 561–581.
- J. Han and K. Burgess, *Chem. Rev.*, 2009, **110**, 2709–2728.
- H.-J. Schneider, K. Kato and R. Strongin, *Sensors*, 2007, **7**, 1578–1611.
- J. Hu and S. Liu, *Macromolecules*, 2010, **43**, 8315–8330.
- H.-S. Peng, J. A. Stolwijk, L.-N. Sun, J. Wegener and O. S. Wolfbeis, *Angew. Chem., Int. Ed.*, 2010, **49**, 4246–4249.
- A. Grafe, K. Haupt and G. J. Mohr, *Anal. Chim. Acta*, 2006, **565**, 42–47.
- G. J. Mohr and O. S. Wolfbeis, *Anal. Chim. Acta*, 1994, **292**, 41–48.
- H. G. Schild, *Prog. Polym. Sci.*, 1992, **17**, 163–249.
- E. S. Gil and S. M. Hudson, *Prog. Polym. Sci.*, 2004, **29**, 1173–1222.

- 16 R. Liu, M. Fraylich and B. Saunders, *Colloid Polym. Sci.*, 2009, **287**, 627–643.
- 17 D. Roy, J. N. Cambre and B. S. Sumerlin, *Prog. Polym. Sci.*, 2010, **35**, 278–301.
- 18 S. Dai, P. Ravi and K. C. Tam, *Soft Matter*, 2009, **5**, 1987–2533.
- 19 D. Schmaljohann, *Adv. Drug Delivery Rev.*, 2006, **58**, 1655–1670.
- 20 M. Annaka and T. Tanaka, *Nature*, 1992, **355**, 430–432.
- 21 Y. Qiu and K. Park, *Adv. Drug Delivery Rev.*, 2001, **53**, 321–339.
- 22 K. Matyjaszewski, *Prog. Polym. Sci.*, 2005, **30**, 858–875.
- 23 C. Reichardt, *Chem. Rev.*, 1994, **94**, 2319–2358.
- 24 M. Heskins and J. E. Guillet, *J. Macromol. Sci., Part A: Pure Appl. Chem.*, 1968, **2**, 1441–1455.
- 25 H. G. Schild and D. A. Tirrell, *J. Phys. Chem.*, 1990, **94**, 4352–4356.
- 26 J. Zhao, R. Hoogenboom, G. Van Assche and B. Van Mele, *Macromolecules*, 2010, **43**, 6853–6860.
- 27 S. Fujishige, K. Kubota and I. Ando, *J. Phys. Chem.*, 1989, **93**, 3311–3313.
- 28 K. Kubota, S. Fujishige and I. Ando, *J. Phys. Chem.*, 1990, **94**, 5154–5158.
- 29 V. Aseyev, S. Hietala, A. Laukkanen, M. Nuopponen, O. Confortini, F. E. Du Prez and H. Tenhu, *Polymer*, 2005, **46**, 7118–7131.
- 30 P. Kujawa, F. Tanaka and F. M. Winnik, *Macromolecules*, 2006, **39**, 3048–3055.
- 31 P. Vyskocil, J. Ricka and T. Binkert, *Helv. Phys. Acta*, 1989, **62**, 243–245.
- 32 F. M. Winnik, *Polymer*, 1990, **31**, 2125–2134.
- 33 J. Duhamel, *Acc. Chem. Res.*, 2006, **39**, 953–960.
- 34 H. Ringsdorf, J. Simon and F. M. Winnik, *Macromolecules*, 1992, **25**, 7306–7312.
- 35 Y. Maeda, T. Higuchi and I. Ikeda, *Langmuir*, 2000, **16**, 7503–7509.
- 36 D. Kungwachakun and M. Irie, *Makromol. Chem. Rapid Commun.*, 1988, **9**, 243–246.
- 37 F. M. Winnik, *Macromolecules*, 1990, **23**, 233–242.
- 38 H. G. Schild and D. A. Tirrell, *Macromolecules*, 1992, **25**, 4553–4558.
- 39 K. Matyjaszewski and J. Xia, *Chem. Rev.*, 2001, **101**, 2921–2990.
- 40 G. Moad, E. Rizzardo and S. H. Thang, *Aust. J. Chem.*, 2009, **62**, 1402–1472.
- 41 M. Beija, M.-T. Charreyre and J. M. G. Martinho, *Prog. Polym. Sci.*, 2011, **36**, 568–602.
- 42 M. A. Gauthier, M. I. Gibson and H.-A. Klok, *Angew. Chem., Int. Ed.*, 2009, **48**, 48–58.
- 43 P. Theato, *J. Polym. Sci., Part A: Polym. Chem.*, 2008, **46**, 6677–6687.
- 44 H. C. Kolb, M. G. Finn and K. B. Sharpless, *Angew. Chem., Int. Ed.*, 2001, **40**, 2004–2021.
- 45 U. Mansfeld, C. Pietsch, R. Hoogenboom, C. R. Becer and U. S. Schubert, *Polym. Chem.*, 2010, **1**, 1560–1598.
- 46 D. Fournier, R. Hoogenboom and U. S. Schubert, *Chem. Soc. Rev.*, 2007, **36**, 1369–1380.
- 47 C. R. Becer, R. Hoogenboom and U. S. Schubert, *Angew. Chem., Int. Ed.*, 2009, **48**, 4900–4908.
- 48 U. W. Gedde, *Polymer Physics*, Kluwer Academic Publishers, Dordrecht, The Netherlands, 1st edn, 1995, pp. 55–69.
- 49 S. Han, M. Hagiwara and T. Ishizone, *Macromolecules*, 2003, **36**, 8312–8319.
- 50 S. Saeki, N. Kuwahara, M. Nakata and M. Kaneko, *Polymer*, 1976, **17**, 685–689.
- 51 Z. Hu, T. Cai and C. Chi, *Soft Matter*, 2010, **6**, 2115–2123.
- 52 J.-F. Lutz, Ö. Akdemir and A. Hoth, *J. Am. Chem. Soc.*, 2006, **128**, 13046–13047.
- 53 E. Wischerhoff, K. Uhlig, A. Lankenau, H. G. Börner, A. Laschewsky, C. Duschl and J.-F. Lutz, *Angew. Chem., Int. Ed.*, 2008, **47**, 5666–5668.
- 54 S. Tugulu, P. Silacci, N. Stergiopoulos and H.-A. Klok, *Biomaterials*, 2007, **28**, 2536–2546.
- 55 J. R. Lakowicz, *Principles of Fluorescence Spectroscopy*, Springer, New York, 3rd edn, 2006, pp. 205–235.
- 56 S. Uchiyama, Y. Matsumura, A. P. de Silva and K. Iwai, *Anal. Chem.*, 2003, **75**, 5926–5935.
- 57 C. Gota, S. Uchiyama, T. Yoshihara, S. Tobita and T. Ohwada, *J. Phys. Chem. B*, 2008, **112**, 2829–2836.
- 58 S. Uchiyama, Y. Matsumura, A. P. de Silva and K. Iwai, *Anal. Chem.*, 2004, **76**, 1793–1798.
- 59 K. Iwai, Y. Matsumura, S. Uchiyama and A. P. de Silva, *J. Mater. Chem.*, 2005, **15**, 2796–2800.
- 60 S. Uchiyama, N. Kawai, A. P. de Silva and K. Iwai, *J. Am. Chem. Soc.*, 2004, **126**, 3032–3033.
- 61 C. Gota, S. Uchiyama and T. Ohwada, *Analyst*, 2007, **132**, 121–126.
- 62 C. Gota, K. Okabe, T. Funatsu, Y. Harada and S. Uchiyama, *J. Am. Chem. Soc.*, 2009, **131**, 2766–2767.
- 63 Y. Matsumura and K. Iwai, *J. Colloid Interface Sci.*, 2006, **296**, 102–109.
- 64 S. Uchiyama and Y. Makino, *Chem. Commun.*, 2009, 2646–2648.
- 65 M. Onoda, S. Uchiyama and T. Ohwada, *Macromolecules*, 2007, **40**, 9651–9657.
- 66 V. N. Knyukshto, Y. S. Avlasevich, O. G. Kulinkovich and K. N. Solovyov, *J. Fluoresc.*, 1999, **9**, 371–378.
- 67 Y. S. Avlasevich, T. A. Chevtchouk, V. N. Knyukshto, O. G. Kulinkovich and K. N. Solovyov, *J. Porphyrins Phthalocyanines*, 2000, **4**, 579–587.
- 68 Y. S. Avlasevich, V. N. Knyukshto, O. G. Kulinkovich and K. N. Solovyov, *J. Appl. Spectrosc.*, 2000, **67**, 663–669.
- 69 Y. S. Avlasevich, O. G. Kulinkovich, V. N. Knyukshto, A. P. Losev and K. N. Solovyov, *J. Polym. Sci., Part A: Polym. Chem.*, 1997, **39**, 1155–1162, *Translated from Vysokomol. Soedin. A*, 1997, **1139**, 1740–1748.
- 70 S.-I. Yusa, T. Endo and M. Ito, *J. Polym. Sci., Part A: Polym. Chem.*, 2009, **47**, 6827–6838.
- 71 Y. Shiraishi, R. Miyamoto, X. Zhang and T. Hirai, *Org. Lett.*, 2007, **9**, 3921–3924.
- 72 Y. Shiraishi, R. Miyamoto and T. Hirai, *J. Photochem. Photobiol., A*, 2008, **200**, 432–437.
- 73 J. Hu, C. Li and S. Liu, *Langmuir*, 2010, **26**, 724–729.
- 74 L. Tang, J. K. Jin, A. J. Qin, W. Z. Yuan, Y. Mao, J. Mei, J. Z. Sun and B. Z. Tang, *Chem. Commun.*, 2009, 4974–4976.
- 75 Y. Shiraishi, R. Miyamoto and T. Hirai, *Langmuir*, 2008, **24**, 4273–4279.
- 76 D. Wang, R. Miyamoto, Y. Shiraishi and T. Hirai, *Langmuir*, 2009, **25**, 13176–13182.
- 77 A. Nagai, K. Kokado, J. Miyake and Y. Cyujo, *J. Polym. Sci., Part A: Polym. Chem.*, 2010, **48**, 627–634.
- 78 R. Paris, I. Quijada-Garrido, O. Garcia and M. Liras, *Macromolecules*, 2011, **44**, 80–86.
- 79 A. Nagai, R. Yoshii, T. Otsuka, K. Kokado and Y. Chujo, *Langmuir*, 2010, **26**, 15644–15649.
- 80 C. Li and S. Liu, *J. Mater. Chem.*, 2010, **20**, 10716–10723.
- 81 C. C. Yang, Y. Tian, A. K. Y. Jen and W. C. Chen, *J. Polym. Sci., Part A: Polym. Chem.*, 2006, **44**, 5495–5504.
- 82 W. Z. Wang, R. Wang, C. Zhang, S. Lu and T. X. Liu, *Polymer*, 2009, **50**, 1236–1245.
- 83 S.-H. Kim, I.-J. Hwang, S.-Y. Gwon and Y.-A. Son, *Dyes Pigm.*, 2010, **87**, 84–88.
- 84 Z. Q. Guo, W. H. Zhu, Y. Y. Xiong and H. Tian, *Macromolecules*, 2009, **42**, 1448–1453.
- 85 W. Zhang, Z. Zhang, Z. Cheng, Y. Tu, Y. Qiu and X. Zhu, *J. Polym. Sci., Part A: Polym. Chem.*, 2010, **48**, 4268–4278.
- 86 Q. Yan, J. Y. Yuan, W. Z. Yuan, M. Zhou, Y. W. Yin and C. Y. Pan, *Chem. Commun.*, 2008, 6188–6190.
- 87 Y. Shiraishi, R. Miyamoto and T. Hirai, *Tetrahedron Lett.*, 2007, **48**, 6660–6664.
- 88 T. Liu, J. Hu, J. Yin, Y. Zhang, C. Li and S. Liu, *Chem. Mater.*, 2009, **21**, 3439–3446.
- 89 Y. Y. Li, H. Cheng, J. L. Zhu, L. Yuan, Y. Dai, S. X. Cheng, X. Z. Zhang and R. X. Zhuo, *Adv. Mater.*, 2009, **21**, 2402–2406.
- 90 J. Yin, X. F. Guan, D. Wang and S. Y. Liu, *Langmuir*, 2009, **25**, 11367–11374.
- 91 H. Ringsdorf, J. Venzmer and F. M. Winnik, *Macromolecules*, 1991, **24**, 1678–1686.
- 92 F. M. Winnik, H. Ringsdorf and J. Venzmer, *Langmuir*, 1991, **7**, 912–917.
- 93 F. M. Winnik, M. F. Ottaviani, S. H. Bossman, W. S. Pan, M. Garcagaribay and N. J. Turro, *J. Phys. Chem.*, 1993, **97**, 12998–13005.
- 94 M. F. Ottaviani, F. M. Winnik, S. H. Bossmann and N. J. Turro, *Helv. Chim. Acta*, 2001, **84**, 2476–2492.

- 95 P. Kujawa, V. Aseyev, H. Tenhu and F. M. Winnik, *Macromolecules*, 2006, **39**, 7686–7693.
- 96 F. M. Winnik, N. Tamai, J. Yonezawa, Y. Nishimura and I. Yamazaki, *J. Phys. Chem.*, 1992, **96**, 1967–1972.
- 97 F. M. Winnik, *Macromolecules*, 1989, **22**, 734–742.
- 98 S. W. Hong, D. Y. Kim, J. U. Lee and W. H. Jo, *Macromolecules*, 2009, **42**, 2756–2761.
- 99 A. Laukkanen, F. M. Winnik and H. Tenhu, *Macromolecules*, 2005, **38**, 2439–2448.
- 100 A. Laukkanen, L. Valtola, F. M. Winnik and H. Tenhu, *Polymer*, 2005, **46**, 7055–7065.
- 101 C. Pietsch, R. Hoogenboom and U. S. Schubert, *Polym. Chem.*, 2010, **1**, 1005–1008.
- 102 C. Pietsch, A. Vollrath, R. Hoogenboom and U. S. Schubert, *Sensors*, 2010, **10**, 7979–7990.
- 103 Q. Duan, Y. Miura, A. Narumi, X. Shen, S.-I. Sato, T. Satoh and T. Kakuchi, *J. Polym. Sci., Part A: Polym. Chem.*, 2006, **44**, 1117–1124.
- 104 J. Rao, J. Xu, S. Luo and S. Liu, *Langmuir*, 2007, **23**, 11857–11865.
- 105 X. W. Zhang, X. M. Lian, L. Liu, J. Zhang and H. Y. Zhao, *Macromolecules*, 2008, **41**, 7863–7869.
- 106 S. Y. Lee, S. Lee, I. C. Youn, D. K. Yi, Y. T. Lim, B. H. Chung, J. F. Leary, I. C. Kwon, K. Kim and K. Choi, *Chem.–Eur. J.*, 2009, **15**, 6103–6106.
- 107 S. Uchiyama, K. Takehira, T. Yoshihara, S. Tobita and T. Ohwada, *Org. Lett.*, 2006, **8**, 5869–5872.
- 108 K. Iwai, N. Matsumoto, M. Niki and M. Yamamoto, *Mol. Cryst. Liq. Cryst.*, 1998, **315**, 53–58.
- 109 K. Iwai, K. Hanasaki and M. Yamamoto, *J. Lumin.*, 2000, **87–89**, 1289–1291.
- 110 Y. Matsumura and K. Iwai, *Polymer*, 2005, **46**, 10027–10034.
- 111 C.-Y. Chen and C.-T. Chen, *Chem. Commun.*, 2011, **47**, 994–996.
- 112 Y. Matsumura and A. Katoh, *J. Lumin.*, 2008, **128**, 625–630.
- 113 B. Elmas, S. Senel and A. Tuncel, *React. Funct. Polym.*, 2007, **67**, 87–96.
- 114 G. Pasparakis, M. Vamvakaki, N. Krasnogor and C. Alexander, *Soft Matter*, 2009, **5**, 3839–3841.
- 115 C. C. Yang, Y. Tian, C. Y. Chen, A. K. Y. Jen and W. C. Chen, *Macromol. Rapid Commun.*, 2007, **28**, 894–899.
- 116 H. Kobayashi, M. Nishikawa, C. Sakamoto, T. Nishio, H. Kanazawa and T. Okano, *Anal. Sci.*, 2009, **25**, 1043–1047.
- 117 X. J. Lu, L. F. Zhang, L. Z. Meng and Y. H. Liu, *Polym. Bull.*, 2007, **59**, 195–206.
- 118 X. Guan, X. Liu and Z. Su, *Eur. Polym. J.*, 2007, **43**, 3094–3105.
- 119 C. Li, L. Z. Meng, X. J. Lu, Z. Q. Wu, L. F. Zhang and Y. B. He, *Macromol. Chem. Phys.*, 2005, **206**, 1870–1877.
- 120 F. M. Winnik, *Chem. Rev.*, 1993, **93**, 587–614.
- 121 C. L. Zhao, M. A. Winnik, G. Riess and M. D. Croucher, *Langmuir*, 1990, **6**, 514–516.
- 122 G. Kwon, M. Naito, M. Yokoyama, T. Okano, Y. Sakurai and K. Kataoka, *Langmuir*, 1993, **9**, 945–949.
- 123 J. R. Lakowicz, *Principles of Fluorescence Spectroscopy*, Springer, New York, 3rd edn, 2006, pp. 443–475.
- 124 C. D. Jones, J. G. McGrath and L. A. Lyon, *J. Phys. Chem. B*, 2004, **108**, 12652–12657.
- 125 C. Li, Y. Zhang, J. Hu, J. Cheng and S. Liu, *Angew. Chem., Int. Ed.*, 2010, **49**, 5120–5124.
- 126 J. Yin, H. Hu, Y. Wu and S. Liu, *Polym. Chem.*, 2011, **2**, 363–371.
- 127 J. Yin, C. Li, D. Wang and S. Liu, *J. Phys. Chem. B*, 2010, **114**, 12213–12220.
- 128 T. Wu, G. Zou, J. M. Hu and S. Y. Liu, *Chem. Mater.*, 2009, **21**, 3788–3798.
- 129 M. Kameda, K. Sumaru, T. Kanamori and T. Shinbo, *Langmuir*, 2004, **20**, 9315–9319.
- 130 K. Sumaru, M. Kameda, T. Kanamori and T. Shinbo, *Macromolecules*, 2004, **37**, 4949–4955.
- 131 K. Sumaru, M. Kameda, T. Kanamori and T. Shinbo, *Macromolecules*, 2004, **37**, 7854–7856.
- 132 K. Sumaru, K. Ohi, T. Takagi, T. Kanamori and T. Shinbo, *Langmuir*, 2006, **22**, 4353–4356.
- 133 S. Sugiura, K. Sumaru, K. Ohi, K. Hiroki, T. Takagi and T. Kanamori, *Sens. Actuators, A*, 2007, **140**, 176–184.
- 134 J.-I. Edahiro, K. Sumaru, T. Takagi, T. Shinbo, T. Kanamori and M. Sudoh, *Eur. Polym. J.*, 2008, **44**, 300–307.
- 135 A. Garcia, M. Marquez, T. Cai, R. Rosario, Z. Hu, D. Gust, M. Hayes, S. A. Vail and C.-D. Park, *Langmuir*, 2007, **23**, 224–229.
- 136 T. Suzuki, T. Kato and H. Shinozaki, *Chem. Commun.*, 2004, 2036–2037.
- 137 Y. Shiraiishi, R. Miyamoto and T. Hirai, *Org. Lett.*, 2009, **11**, 1571–1574.
- 138 Q. Jin, G. Liu and J. Ji, *J. Polym. Sci., Part A: Polym. Chem.*, 2010, **48**, 2855–2861.
- 139 C. Koopmans and H. Ritter, *J. Am. Chem. Soc.*, 2007, **129**, 3502–3503, the authors termed the dye misleadingly Reichardt's dye.
- 140 Y. Zhao, L. Tremblay and Y. Zhao, *J. Polym. Sci., Part A: Polym. Chem.*, 2010, **48**, 4055–4066.
- 141 Q. Yan, J. Yuan, Y. Kang, Z. Cai, L. Zhou and Y. Yin, *Chem. Commun.*, 2010, **46**, 2781–2783.
- 142 C. Pietsch, R. Hoogenboom and U. S. Schubert, *Angew. Chem., Int. Ed.*, 2009, **48**, 5653–5656.
- 143 M. Irie and D. Kungwatchakun, *Proc. Jpn. Acad., Ser. B, Phys. Biol. Sci.*, 1992, **68**, 127–132.
- 144 R. Kröger, H. Menzel and M. L. Hallensleben, *Macromol. Chem. Phys.*, 1994, **195**, 2291–2298.
- 145 H. Akiyama and N. Tamaoki, *J. Polym. Sci., Part A: Polym. Chem.*, 2004, **42**, 5200–5214.
- 146 W. Yuan, G. Jiang, J. Wang, G. Wang, Y. Song and L. Jiang, *Macromolecules*, 2006, **39**, 1300–1303.
- 147 A. Desponds and R. Freitag, *Langmuir*, 2003, **19**, 6261–6270.
- 148 P. Ravi, S. L. Sin, L. H. Gan, Y. Y. Gan, K. C. Tam, X. L. Xia and X. Hu, *Polymer*, 2005, **46**, 137–146.
- 149 H. Akiyama and N. Tamaoki, *Macromolecules*, 2007, **40**, 5129–5132.
- 150 F. D. Jochum and P. Theato, *Polymer*, 2009, **50**, 3079–3085.
- 151 F. D. Jochum, F. R. Forst and P. Theato, *Macromol. Rapid Commun.*, 2010, **31**, 1456–1461.
- 152 F. D. Jochum and P. Theato, *Chem. Commun.*, 2010, **46**, 6717–6719.
- 153 C. Luo, F. Zuo, X. Ding, Z. Zheng, X. Cheng and Y. Peng, *J. Appl. Polym. Sci.*, 2008, **107**, 2118–2125.
- 154 X. Tang, X. Liang, L. Gao, X. Fan and Q. Zhou, *J. Polym. Sci., Part A: Polym. Chem.*, 2010, **48**, 2564–2570.
- 155 F. D. Jochum, L. zur Borg, P. J. Roth and P. Theato, *Macromolecules*, 2009, **42**, 7854–7862.
- 156 Y. Xiang, X. Xue, J. Zhu, Z. Zhang, W. Zhang, N. Zhou and X. Zhu, *Polym. Chem.*, 2010, **1**, 1453–1458.
- 157 A. Suzuki and T. Tanaka, *Nature*, 1990, **346**, 345–347.
- 158 S. Nayak and L. A. Lyon, *Chem. Mater.*, 2004, **16**, 2623–2627.
- 159 J. Bigot, M. Bria, S. T. Caldwell, F. Cazaux, A. Cooper, B. Charleux, G. Cooke, B. Fitzpatrick, D. Fournier, J. Lyskawa, M. Nutley, F. Stoffelbach and P. Woisel, *Chem. Commun.*, 2009, 5266–5268.
- 160 A. Mamada, T. Tanaka, D. Kungwatchakun and M. Irie, *Macromolecules*, 1990, **23**, 1517–1519.



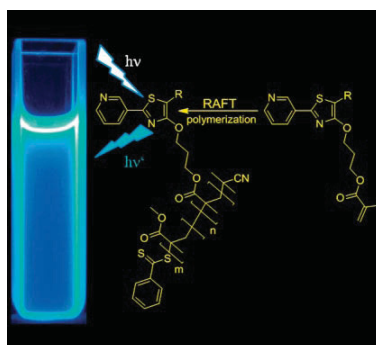
## Publication P3:

### *Blue-emitting polymers based on 4-hydroxythiazoles incorporated in a methacrylate backbone*

---

R. Menzel, A. Breul, C. Pietsch, J. Schäfer, C. Friebe, E. Tauscher,  
D. Weiß, B. Dietzek, J. Popp, R. Beckett, U. S. Schubert

*Macromol. Chem. Phys.* **2011**, *212*, 840–848



*“Including back cover page”*

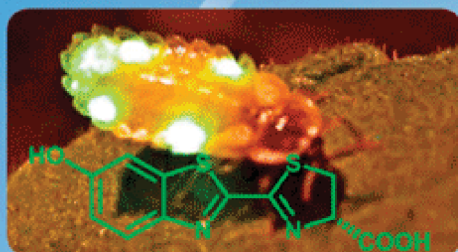
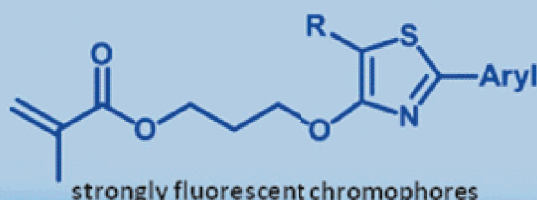




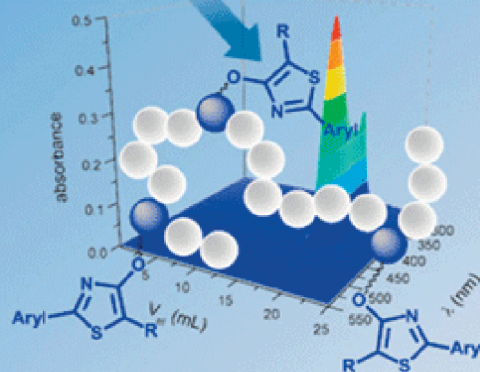
# Macromolecular Chemistry and Physics

Founded by  
Hermann Staudinger

## Thiazole-Dye Methacrylates Inspired by Nature



Firefly Luciferin



RAFT Polymerization

Special Series  
New Frontiers in  
Functional Polymers

8/2011

 WILEY-VCH



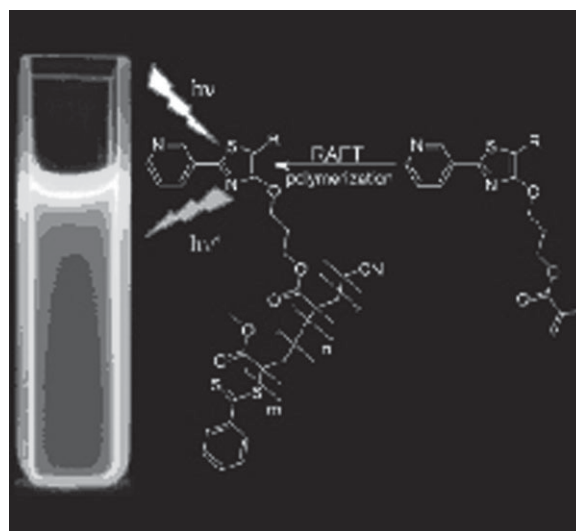
# Blue-Emitting Polymers Based on 4-Hydroxythiazoles Incorporated in a Methacrylate Backbone

Roberto Menzel, Alexander Breul, Christian Pietsch, Johann Schäfer, Christian Friebe, Eric Täuscher, Dieter Weiß, Benjamin Dietzek, Jürgen Popp,\* Rainer Beckert,\* Ulrich S. Schubert\*

The synthesis of two new monomers based on 4-hydroxythiazoles, with a non-classical chromophore structure similar to the luciferin dye of glowworms, is presented. These dyes are functionalized with methacrylates and copolymerized with methyl methacrylate using a RAFT polymerization process. The obtained polymers reveal PDI values below 1.2 and are characterized by NMR spectroscopy, SEC including a diode-array detector, UV-vis and fluorescence spectroscopy. In addition, thin films of the polymers are prepared by spin-coating and investigated regarding their optical properties.

## Introduction

Blue-light-emitting polymers, which have emerged from new fluorescent monomers, are the subject of intense research due to their potential applications in various fields, depending on the type of chromophore used. In



general, they have been successfully applied in organic light-emitting diodes (OLEDs),<sup>[1]</sup> as one emitting species for the construction of white polymer light-emitting diodes (WPLEDs),<sup>[2]</sup> as sensor molecules in biochemical and environmental applications,<sup>[3]</sup> or in dye-sensitized solar cells (DSSCs).<sup>[4]</sup> A further important research topic is the construction of antenna systems mimicking light-harvesting photosynthetic proteins in plants by incorporating donor and acceptor molecules in a polymer backbone to allow a fluorescence resonance energy transfer (FRET).<sup>[5]</sup> For this purpose, common  $\pi$ -conjugated polymers are not suitable due to the fact that their electronic properties strongly depend on the length of the polymer chain. Moreover, the synthesis of polymers with different conjugated chromophores is difficult.<sup>[6]</sup> Medintz

R. Menzel, A. Breul, C. Pietsch, C. Friebe, E. Täuscher, D. Weiß, R. Beckert, U. S. Schubert

Institute for Organic Chemistry and Macromolecular Chemistry (IOMC), Friedrich Schiller University Jena, Humboldtstr. 10, 07743, Jena, Germany

Fax: +49 3641 94 8202;

E-mail: ulrich.schubert@uni-jena.de, c6bera@uni-jena.de

J. Schäfer, B. Dietzek, J. Popp

Institute of Photonic Technology Jena, Albert-Einstein-Straße 9, 07745, Jena, Germany

B. Dietzek, J. Popp

Institute for Physical Chemistry (IPC), Friedrich Schiller University Jena, Helmholtzweg 4, 07743 Jena, Germany

Fax: +49 3641 94 8302; E-mail: juergen.popp@uni-jena.de

et al.<sup>[7]</sup> described that a directed energy transfer is not possible along a polymer chain because of the statistical distribution and the alternating distances between the dyes. However, recent publications provide examples for a non-directed, but reasonable, energy transfer along a polymer chain. For example, FRET was described for polymers containing a coumarin dye as well as a Ru(II) polypyridine complex,<sup>[8]</sup> for a linear Re(I) oligomer and a Ru(II) complex,<sup>[9]</sup> and for short, linear arrays of Ru(II) complexes and  $\pi$ -conjugated 1,4-diethynylenebenzene subunits.<sup>[10]</sup> In addition, tools are available to quantitatively describe FRET in different domains (e.g., polymers).<sup>[11]</sup>

Although a variety of blue-fluorescence (donor) molecules exist, the number of these incorporated into polymer backbones is relatively small. Usually, classic chromophores like coumarines, naphthalenes, pyrenes and quinolines are included, but often suffer from low quantum yields, strong solvent dependency of their electronic properties, excimer formation,<sup>[12]</sup> and a low photostability.<sup>[13]</sup> To overcome these restrictions, the generation of polymers containing a 4-hydroxy-1,3-thiazole unit as a non-classical fluorescence emitter has been desired. In contrary to other, small, heterocyclic compounds that are non- or only very-weakly fluorescent, alkylated derivatives of 4-hydroxy-1,3-thiazoles generally show a very-high room-temperature fluorescence, with quantum yields ranging from 0.7 up to unity, in combination with an unusually large Stokes shift.<sup>[14]</sup> In particular, the latter is essential for an efficient FRET in a donor/acceptor pair. In addition, the absorption and emission spectra of these dyes can be shifted over a wide range depending on the nature of the substituents of the thiazole chromophore.<sup>[15]</sup> From a synthetic point of view, the aromatic hydroxy group offers the advantage of an easy functionalization. Therefore, alkylation, as well as acylation reactions, can be performed under mild conditions.

Because of the highly fluorescent nature of the molecules, the chemical and, in comparison with other chromophores (e.g., rhodamines or fluoresceins), better photochemical stability, combined with an easy access and simple functionalization possibilities, 4-hydroxy-1,3-thiazoles are considered as promising candidates for the construction of functionalized luminescent materials.

Reversible addition-fragmentation chain transfer (RAFT) polymerization was chosen as an efficient method for the polymerization of dye-functionalized methacrylates.<sup>[16]</sup> RAFT allows good control over the characteristics of the accessible polymers, combined with a narrow molar-mass distribution and randomly distributed monomers. Furthermore, a large variety of different architectures can be produced, for example, blocks, combs and stars.<sup>[17]</sup>

## Experimental Part

### Materials and Instrumentation

All reagents were purchased from commercial sources (Biosolve, Fluka, Aldrich, Alfa Aesar and Acros Organics) and used directly without further purification. All solvents were of reagent grade, purified using common methods and distilled prior to use. Methyl methacrylate (MMA) was passed over a short neutral aluminum oxide column directly before use to remove the stabilizer. 2,2'-Azobisisobutyronitrile (AIBN) was recrystallized from methanol prior to use. All reactions were performed under an argon atmosphere in glassware equipped with a Teflon-coated magnetic stir bar. Size-exclusion chromatograms were recorded using a Shimadzu SCL-10A size-exclusion chromatography (SEC) system controller, an LC-10AD pump, an RID-10A refractive-index (RI) detector and a PLgel 5  $\mu$ m mixed-D column at 40 °C [eluent CHCl<sub>3</sub>:triethylamine (TEA):isopropyl alcohol (*i*-PrOH) = 94:4:2; flow rate 1 mL · min<sup>-1</sup>] applying linear poly(methyl methacrylate) (PMMA) standards. Further SEC experiments were carried out using a Shimadzu SCL-10A system controller, an LC-10AD pump, a CTO-10A VP oven, a PSS ETA-2010 viscosity detector and a PSS SDV pre/104/102 Å column at 40 °C [eluent: tetrahydrofuran (THF); flow rate 1 mL · min<sup>-1</sup>], applying universal calibration with polystyrene standards. 3D-SEC plots were recorded on a Waters SEC equipped with a DG-980-50 degasser, a HPLC 1515 pump, a column heater 1500 oven, and a 2996 photo diode-array (DAD) detector; dimethylacetamide (DMA) with 0.08% NH<sub>4</sub>PF<sub>6</sub> was used as solvent with a flow rate of 1 mL min<sup>-1</sup> at 50 °C on a Waters pre/Phenomenex Phenogel 103 Å/105 Å column. Gas-chromatography (GC) measurements were performed using an Interscience Trace GC with a Trace Column RTX-5 connected to a PAL autosampler. A spin coater from Laurell Technologies Corporation (North Wales, USA) was used for the preparation of the films. The surface topography and thickness of the polymer films were measured using a Wyko NT9100 optical interferometric profiler (Veeco, Mannheim, Germany). For this purpose, each film was scratched with a scalpel in a controlled manner. The depths of the scratches were measured using the optical profiler at five different positions on the film: the center and the four edges. <sup>1</sup>H and <sup>13</sup>C NMR spectra were recorded on a Bruker AC 250 (250 MHz), 300 (300 MHz) and 400 (400 MHz) spectrometer at 298 K. The chemical shifts are reported in parts per million relative to signals from the NMR solvents; coupling constants are given in Hz. The melting points were measured using a Galen III apparatus (Boëtius system). Reactions were monitored using thin-layer chromatography (TLC) on 0.2 mm Merck silica-gel plates (60 F254). The mass spectra were measured either using a Finnigan MAT S50 710 [electron impact (EI)] or MAZ 95 XL [fast atom bombardment (FAB)] system. Elemental analyses were carried out on a CHN-932 Automat Leco instrument. The UV-vis absorption and photoluminescence (PL) emission spectra were recorded using an Analytik Jena SPECORD 250 and a Jasco FP-6500 spectrometer, respectively, at 298 K. UV-vis and fluorescence spectra of the films were measured using a modified Hitachi F-4500 instrument. Absolute PL quantum yields were evaluated at 298 K using a Hamamatsu Photonic Multi-Channel Analyzer, C 10027. For this purpose, dilute solutions (10<sup>-6</sup> to 10<sup>-5</sup> M, 1 cm quartz cuvette) in CHCl<sub>3</sub> were used. As a reference, a quartz cuvette filled with the pristine solvent was utilized. The fluorescence lifetimes were obtained from streak-camera measurements. For this, a Ti:sapphire laser (Tsunami, Newport Spectra-Physics GmbH) was

used as the light source. The repetition rate was reduced to 4 kHz using a pulse selector (Model 3980, Newport Spectra-Physics GmbH) and afterwards the beam was frequency-doubled in a second-harmonic generator (Newport Spectra-Physics GmbH) to create the 435 nm pump beam.<sup>[18]</sup>

## Synthesis of the Monomers

### 5-Methyl-2-(pyridin-3-yl)thiazol-4-ol (**1a**)

2-Mercaptopropionic acid (10 mmol) and 3-pyridinecarbonitrile (8 mmol) were loaded into an argon-flushed Schlenk tube. Pyridine (10 mL) was added and the mixture was heated at 110 °C for 2 h. After the mixture was allowed to cool down to 60 °C, ethanol (EtOH, 50 mL) was added and the product precipitated as yellow crystals, which were collected by filtration, washed with EtOH and dried. The 4-hydroxythiazole is usually pure in terms of elemental analysis but can be recrystallized from *N,N*-dimethylformamide (DMF)/EtOH.

UV-vis (CH<sub>3</sub>CN):  $\lambda_{\max}$  (log  $\epsilon$ ) = 242 (3.52), 282 (3.38), 330 nm (3.65). MS (EI):  $m/z$  = 192 (M<sup>+</sup>), 105 (M<sup>+</sup> - C<sub>3</sub>H<sub>3</sub>OS). <sup>1</sup>H NMR (DMSO-*d*<sub>6</sub>):  $\delta$  = 2.25 (s, 3H), 7.39 (m, 1H), 8.09 (m, 1H), 8.58 (m, 1H), 8.98 (s, 1H), 10.18 (s, 1H). <sup>13</sup>C NMR (250 MHz, DMSO-*d*<sub>6</sub>):  $\delta$  = 159.7, 155.6, 150.5, 146.3, 132.6, 129.8, 124.6, 104.6, 9.5. (C<sub>9</sub>H<sub>8</sub>N<sub>2</sub>OS) (192.2): Calcd. C 56.23, H 4.19, N 14.57, S 16.68; Found C 56.20, H 4.23, N 14.72, S 16.66. Yield: 50%, yellow needles.

### 5-Phenyl-2-(pyridin-3-yl)thiazol-4-ol (**1b**)

A mixture of ethyl 2-bromophenylacetate (10 mmol) and pyridine-3-carbothioamide (10 mmol) was stirred in 100 mL of toluene under argon at between 100 and 110 °C for 3 h. The reaction was allowed to cool to room temperature. EtOH (50 mL) and pyridine (10 mL) were added to the brown suspension. The mixture was stirred for an additional 30 min, followed by filtration. The crude product was recrystallized from DMF/EtOH to yield the thiazole as yellow crystals.

UV-vis (DMSO):  $\lambda_{\max}$  (log  $\epsilon$ ) = 270 (3.85), 380 nm (4.22). MS (EI):  $m/z$  = 254 (M<sup>+</sup>), 150 (M<sup>+</sup> - C<sub>6</sub>H<sub>4</sub>N<sub>2</sub>), 138 (M<sup>+</sup> - C<sub>8</sub>H<sub>4</sub>O). <sup>1</sup>H NMR (DMSO-*d*<sub>6</sub>):  $\delta$  = 7.26 (m, 1H), 7.43 (t, <sup>3</sup>*J* = 7.4 Hz, 2H), 7.55 (m, 1H), 7.75 (d, <sup>3</sup>*J* = 7.3 Hz, 2H), 8.23 (m, 1H), 8.65 (d, <sup>4</sup>*J* = 1.4 Hz, 1H), 8.85 (d, <sup>4</sup>*J* = 1.6 Hz, 1H), 11.73 (s, 1H, OH). <sup>13</sup>C NMR (250 MHz, DMSO-*d*<sub>6</sub>):  $\delta$  = 159.2, 156.9, 151.2, 151.1, 146.4, 133.1, 131.9, 129.3, 126.8, 126.4, 124.7, 109.1. (C<sub>14</sub>H<sub>10</sub>N<sub>2</sub>OS) (254.3): Calcd. C 66.12, H 3.96, N 11.02, S 12.61; Found C 66.03, H 4.09, N 10.99, S 12.81. Yield: 77%, yellow crystals.

## General Procedure for the Etherification of the 4-Hydroxythiazoles

A solution of K<sub>2</sub>CO<sub>3</sub> (12 mmol in 5 mL H<sub>2</sub>O) was added to a mixture of the 4-hydroxythiazole (10 mmol) in 25 mL of dimethyl sulfoxide (DMSO). The red suspension was stirred for 30 min at room temperature (RT) and 3-chloropropan-1-ol (12 mmol) was added. Stirring was continued until no starting material was detected (indicated by TLC). The mixture was diluted with H<sub>2</sub>O (100 mL) and extracted with CHCl<sub>3</sub> (2 · 50 mL). The organic phase was additionally washed with H<sub>2</sub>O (3 · 50 mL), dried over MgSO<sub>4</sub> and concentrated in vacuo. The crude products were purified by column chromatography (silica, CHCl<sub>3</sub>/acetone 3:1) or Kugelrohr distillation.

### 3-[5-Methyl-2-(pyridin-3-yl)thiazol-4-yloxy]propan-1-ol (**2a**)

UV-vis (CH<sub>3</sub>CN):  $\lambda_{\max}$  (log  $\epsilon$ ) = 221 (3.85), 334 nm (3.98). MS (EI):  $m/z$  = 250 (M<sup>+</sup>), 192 (M<sup>+</sup> - C<sub>3</sub>H<sub>6</sub>O). <sup>1</sup>H NMR (250 MHz, CDCl<sub>3</sub>):  $\delta$  = 2.00 (p, <sup>3</sup>*J* = 5.9 Hz, 2H), 2.29 (s, 1H), 2.87 (s, 1H, OH), 3.83 (t, <sup>3</sup>*J* = 5.9 Hz, 2H), 4.50 (t, <sup>3</sup>*J* = 5.9 Hz, 1H), 7.31 (dd, <sup>3</sup>*J* = 8.0 Hz, <sup>3</sup>*J* = 4.9 Hz, 1H), 8.07 (m, 1H), 8.56 (dd, <sup>3</sup>*J* = 4.8 Hz, <sup>4</sup>*J* = 1.6 Hz, 1H), 9.00 (d, <sup>4</sup>*J* = 1.9 Hz, 1H). <sup>13</sup>C NMR (250 MHz, CDCl<sub>3</sub>):  $\delta$  = 160.28, 156.06, 150.00, 146.55, 132.38, 13.71, 123.65, 108.13, 68.05, 59.24, 32.72, 9.30. (C<sub>12</sub>H<sub>14</sub>N<sub>2</sub>O<sub>2</sub>S) (250.3): Calcd. C 57.58, H 5.64, N 11.19, S 12.81; Found C 57.32, H 5.34, N 11.35, S 12.88. Yield: 61%, orange solid.

### 3-[5-Phenyl-2-(pyridin-3-yl)thiazol-4-yloxy]propan-1-ol (**2b**)

UV-vis (CH<sub>3</sub>CN):  $\lambda_{\max}$  (log  $\epsilon$ ) = 233 (4.04), 267 (3.87), 363 nm (4.28). MS (EI):  $m/z$  = 312 (M<sup>+</sup>), 254 (M<sup>+</sup> - C<sub>3</sub>H<sub>6</sub>O). <sup>1</sup>H NMR (250 MHz, CDCl<sub>3</sub>):  $\delta$  = 2.12 (p, <sup>3</sup>*J* = 6.0 Hz, 2H), 2.65 (s, 1H), 3.89 (t, <sup>3</sup>*J* = 5.9 Hz, 2H), 4.69 (t, <sup>3</sup>*J* = 6.0 Hz, 2H), 7.27 (m, 1H), 7.37 (m, 3H), 7.73 (d, <sup>3</sup>*J* = 7.5 Hz, 2H), 8.16 (d, <sup>3</sup>*J* = 8.0 Hz, 1H), 8.62 (dd, <sup>3</sup>*J* = 4.8 Hz, <sup>4</sup>*J* = 1.3 Hz, 1H), 9.12 (d, <sup>4</sup>*J* = 1.9 Hz, 1H). <sup>13</sup>C NMR (250 MHz, CDCl<sub>3</sub>):  $\delta$  = 159.18, 156.82, 150.435, 146.78, 132.52, 131.07, 129.50, 128.75, 126.96, 126.87, 123.67, 112.86, 67.93, 59.36, 32.73. (C<sub>17</sub>H<sub>16</sub>N<sub>2</sub>O<sub>2</sub>S) (312.4): Calcd. C 65.36, H 5.16, N 8.97, S 10.26; Found C 65.01, H 4.83, N 8.69, S 10.19. Yield: 50%, orange solid.

## General Procedure for the Formation of the Methacrylates

The alkylated 4-hydroxythiazole (10 mmol) was added to a mixture of TEA (5.5 mL, 40 mmol) in 50 mL of dry CH<sub>2</sub>Cl<sub>2</sub>. After 5 min stirring, methacryloyl chloride (1.2 mL, 12 mmol, dissolved in 5 mL CH<sub>2</sub>Cl<sub>2</sub>) was added. The reaction was stirred at RT and monitored using TLC. After the reaction was finished (typically after 24 h), 50 mL of H<sub>2</sub>O were added and the organic phase was separated. The water phase was extracted with CH<sub>2</sub>Cl<sub>2</sub> (3 · 20 mL). The organic phases were combined, washed with additional water, dried over MgSO<sub>4</sub> and evaporated to dryness at *T* < 40 °C. The crude product was purified by column chromatography (silica, CHCl<sub>3</sub> to CHCl<sub>3</sub>:acetone 3:1).

### 3-[5-Methyl-2-(pyridin-3-yl)thiazol-4-yloxy]propyl methacrylate (**3a**)

UV-vis (CH<sub>3</sub>CN):  $\lambda_{\max}$  (log  $\epsilon$ ) = 222 (3.82), 335 nm (4.01). MS (EI):  $m/z$  = 319 (MH<sup>+</sup>), 127 (M<sup>+</sup> - C<sub>9</sub>H<sub>7</sub>N<sub>2</sub>OS). <sup>1</sup>H NMR (400 MHz, CDCl<sub>3</sub>):  $\delta$  = 1.94 (s, 3H), 2.16 (p, <sup>3</sup>*J* = 6.3 Hz, 2H), 2.30 (s, 3H), 4.35 (t, <sup>3</sup>*J* = 6.4 Hz, 2H), 4.47 (t, <sup>3</sup>*J* = 6.2 Hz, 2H), 5.55 (s, 1H), 6.11 (s, 1H), 7.31 (dd, <sup>3</sup>*J* = 7.9 Hz, *J* = 4.9 Hz, 1H), 8.09 (ddd, <sup>3</sup>*J* = 8.0 Hz, <sup>4</sup>*J* = 1.9 Hz, <sup>4</sup>*J* = 1.9 Hz, 1H), 8.57 (d, <sup>3</sup>*J* = 4.7 Hz, 1H), 9.05 (d, <sup>4</sup>*J* = 1.6 Hz, 1H). <sup>13</sup>C NMR (250 MHz, CDCl<sub>3</sub>):  $\delta$  = 167.35, 159.96, 155.86, 149.90, 146.64, 136.31, 132.34, 129.89, 125.42, 123.53, 107.94, 66.99, 61.53, 28.95, 18.28, 9.26. (C<sub>16</sub>H<sub>18</sub>N<sub>2</sub>O<sub>3</sub>S) (318.4): Calcd. C 60.36, H 5.70, N 8.80, S 10.07; Found C 60.01, H 5.79, N 8.67, S 9.97. Yield: 70%, orange oil.

### 3-[5-Phenyl-2-(pyridin-3-yl)thiazol-4-yloxy]propyl methacrylate (**3b**)

UV-vis (CH<sub>3</sub>CN):  $\lambda_{\max}$  (log  $\epsilon$ ) = 231 (4.08), 265 (3.90), 361 nm (4.30). MS (FAB):  $m/z$  = 381 (M<sup>+</sup>). <sup>1</sup>H NMR (250 MHz, CDCl<sub>3</sub>):  $\delta$  = 1.93 (s, 3H),

2.23 (p,  $^3J=6.3$  Hz, 2H), 4.37 (t,  $^3J=6.3$  Hz, 2H), 4.61 (t,  $^3J=6.3$  Hz, 2H), 5.54 (s, 1H), 6.11 (s, 1H), 7.30 (m, 4H), 7.69 (m, 2H), 8.11 (m, 1H), 8.59 (d,  $J=3.6$  Hz, 1H), 9.12 (s, 1H).  $^{13}\text{C}$  NMR (250 MHz,  $\text{CDCl}_3$ ):  $\delta=167.15, 158.74, 156.47, 150.24, 146.64, 136.13, 132.35, 130.98, 129.40, 128.61, 126.74, 126.68, 125.38, 123.45, 112.59, 67.12, 61.46, 28.850, 18.17$ . ( $\text{C}_{21}\text{H}_{20}\text{N}_2\text{O}_3\text{S}$ ) (380.5): Calcd. C 66.29, H 5.30, N 7.36, S 8.43; Found C 66.01, H 5.33, N 7.40, S 8.40. Yield: 65%, orange oil.

## Synthesis of the Polymers

### General Procedure for the RAFT Polymerization

The desired amounts of the monomers were transferred into reaction vials (5 mL closed microwave vials) and dissolved in toluene. Thereafter, calculated volumes of stock solutions of 2-cyanopropan-2-yl dithiobenzoate (CPDB) (0.07 M) and AIBN (0.03 M) in toluene were added. The ratio of [CPDB] to [AIBN] was adjusted to 4/1. The [monomer]/[initiator] ratio was always set to 100 with solution concentrations of  $2 \text{ mol} \cdot \text{L}^{-1}$ . Anisole (20%) was added as the internal standard for the GC measurements. The exact amounts of monomer, initiator, chain-transfer agent and solvent are listed in Table 1. Before closing the vials, the reaction solutions were purged with argon for 30 min. Subsequently, the reactions were heated in an oil bath to  $70^\circ\text{C}$  for the reaction times given in Table 1. The polymers were purified by precipitation into cold methanol followed by drying under reduced pressure at room temperature.

#### P(3a-*stat*-PMMA) (A)

UV-vis ( $\text{CHCl}_3$ ):  $\lambda_{\text{max}}$  (log  $\epsilon$  per dye unit) = 337 nm (3.51).  $^1\text{H}$  NMR ( $\text{CDCl}_3$ ):  $\delta=0.84$  (b,  $\text{CH}_3$  backbone), 1.00–2.00 (b,  $\text{CH}_2$  backbone and  $\text{CH}_2$  dye spacer,  $\text{CH}_3$  end group), 2.31 (b,  $\text{CH}_3$  dye), 3.60 (b,  $\text{OCH}_3$  methacrylate), 4.17 (b,  $\text{OCH}_2$  dye), 4.46 (b,  $\text{OCH}_2$  dye), 6.92, 7.37, 7.53 (b, Ar–H dithioester end group), 7.88, 8.13, 8.59, 9.07 (b, Ar–H pyridine substituent dye). GC: conversion = 60%. SEC ( $\text{CHCl}_3$ , PMMA standard):  $\overline{M}_n=7\ 400 \text{ g} \cdot \text{mol}^{-1}$ , PDI = 1.17, DP = 71,  $\overline{M}_{n,\text{theo}}=6\ 600 \text{ g} \cdot \text{mol}^{-1}$ .

#### P(3b-*stat*-PMMA) (B)

UV-vis ( $\text{CHCl}_3$ ):  $\lambda_{\text{max}}$  (log  $\epsilon$  per dye unit) = 366 nm (4.10).  $^1\text{H}$  NMR ( $\text{CDCl}_3$ ):  $\delta=0.84$  (b,  $\text{CH}_3$  backbone), 1.00–2.30 (b,  $\text{CH}_2$  backbone and dye spacer,  $\text{CH}_3$  end group), 3.60 (b,  $\text{OCH}_3$  methacrylate), 4.20 (b,  $\text{OCH}_2$  dye), 4.63 (b,  $\text{OCH}_2$  dye), 7.40, 7.53, 7.70, 7.88 (b, ArH

dithioester end group and phenyl substituent dye), 8.21, 8.66, 9.16 (b, Ar–H pyridine substituent dye). GC: conversion = 67%. SEC ( $\text{CHCl}_3$ , PMMA standard):  $\overline{M}_n=8\ 400 \text{ g} \cdot \text{mol}^{-1}$ , PDI = 1.19, DP = 77,  $\overline{M}_{n,\text{theo}}=7\ 500 \text{ g} \cdot \text{mol}^{-1}$ .

## Results and Discussion

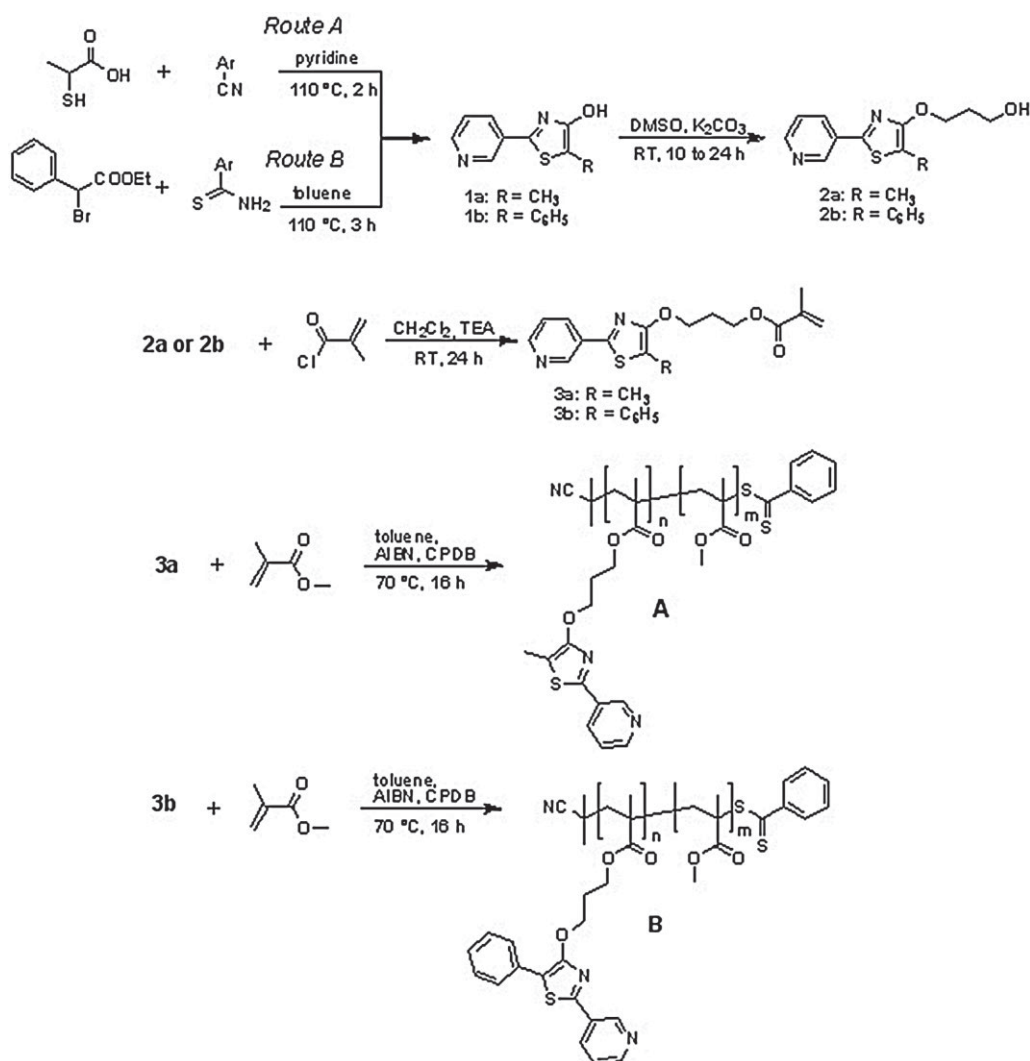
The current work describes the synthesis of blue emitters (as possible energy donors in a FRET process) that can be polymerized. For this purpose, the chromophore has to be connected via a spacer unit to the polymer backbone to gain a non-restricted arrangement of the chromophores, being one prerequisite for FRET to an acceptor molecule. To build up a possible acceptor, 2,2'-bipyridine or 2,2';6',2''-terpyridine ligands will be introduced in the polymer backbone to form the acceptor dye after complexation with ruthenium. Therefore, in order to avoid complex formation of the thiazoles with a Ru(II) precursor as demonstrated recently,<sup>[19]</sup> compounds with the thiazole linked in the *meta*-position to the pyridine moiety were synthesized.

Scheme 1 briefly shows the synthesis of the monomers and the polymers. The 4-hydroxy-1,3-thiazole derivatives can be prepared using two routes that are mainly determined by the availability of the starting materials. In route A, pyridine-2-carbonitrile reacts with thiolactic acid to form a 5-methyl-substituted thiazole. Route B is a modified Hantzsch thiazole synthesis. Here, pyridine-3-carbothioamide reacts with 2-bromo-2-phenylacetic acid to yield a 5-phenyl-substituted thiazole. For both routes, elevated temperatures (110 to  $120^\circ\text{C}$ ) and a base, typically pyridine, are required. Since the pyridine subunit of the thioamide can capture the hydrogen bromide formed in the reaction, the reaction in route B can also be carried out without an additional base, which results in higher yields. After the reaction, pyridine must be added to yield **1b** after deprotonation. It is worth mentioning that different thiolactic acids and  $\alpha$ -halogeno acids can be used to synthesize more complex structures and to efficiently tune the optical properties of the dyes.<sup>[20]</sup>

**Table 1.** Overview of selected reaction conditions used for the polymerizations at  $70^\circ\text{C}$  in toluene with CPDB:AIBN = 4,  $[\mathbf{3a}] = [\mathbf{3b}] = 0.06 \text{ M}$ .

Sample	$m$ (monomer)	$m$ (AIBN)	$m$ (CPDB)	Conc.	Reaction time
	mg	mg	mg	$\text{mol} \cdot \text{L}^{-1}$	h
A	55 ( <b>3a</b> ), 559.2 (MMA)	2.36	13.55	2.0	16
B	64 ( <b>3b</b> ), 544.6 (MMA)	2.30	12.41	2.0	16





■ Scheme 1. Schematic representations of the general synthetic routes to the monomers and polymers.

In the second step, compounds **1a** and **1b** were further functionalized by introducing the C3 spacer via a Williamson-type etherification of the hydroxy group with 3-chloropropan-1-ol or, alternatively, with 3-bromopropan-1-ol under mild conditions (K<sub>2</sub>CO<sub>3</sub>, room temperature). In the last step, an esterification of the formed aliphatic hydroxy group with methacryloyl chloride in dry CH<sub>2</sub>Cl<sub>2</sub> with TEA was carried out to yield the two monomers: 5-methyl-4-[3-(3-methylbuta-1,3-dien-2-yloxy)propoxy]-2-(pyridin-3-yl)thiazole (**3a**) and 4-[3-(3-methylbuta-1,3-dien-2-yloxy)propoxy]-5-phenyl-2-(pyridin-3-yl)thiazole (**3b**).

RAFT was selected as the polymerization method due to its good tolerance to functional groups. Other controlled-radical polymerization (CRP) techniques, such as nitroxide-mediated polymerization (NMP)<sup>[21]</sup> and atom-transfer radical polymerization (ATRP)<sup>[22]</sup> are less suitable. For ATRP polymerization, copper is required, which is difficult to

remove and, additionally, can be complexed by the thiazole dye leading to an inactivation of the copper. With the NMP technique, methacrylates cannot be polymerized in a controlled way.<sup>[21]</sup>

Hence, monomers **3a** and **3b** were copolymerized with methyl methacrylate (MMA) to yield polymers A and B, respectively. Standard conditions for the RAFT technique were applied (Scheme 1) utilizing CPDB as the chain-transfer agent, AIBN as the initiator and toluene as the solvent.

According to similar systems (copolymerization of pyrene or disperse red-1 methacrylates with MMA),<sup>[23]</sup> the reaction temperature was set to 70 °C with a reaction time of 16 h in order to ensure a complete polymerization of the monomers and to reach an optimal value of conversion combined with a low polydispersity index (PDI). The two obtained polymers revealed a narrow molar-mass distribu-

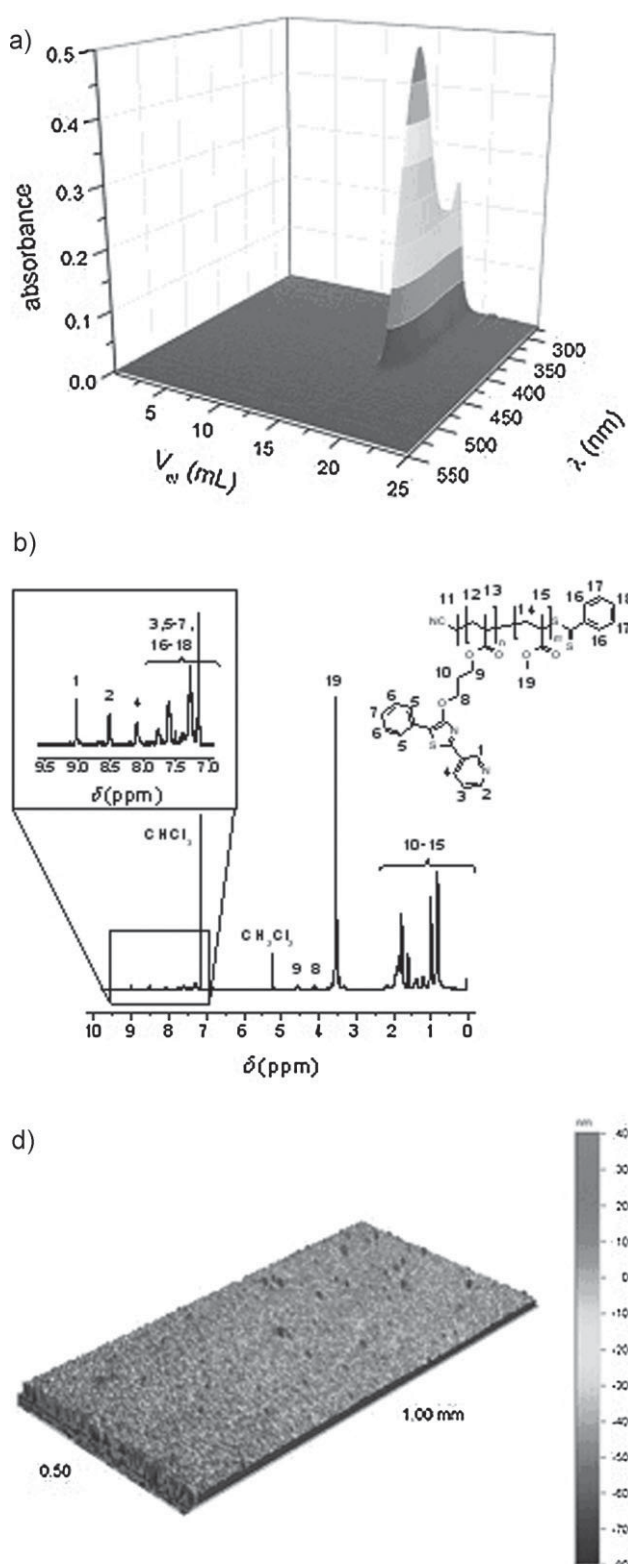


Figure 1. a) SEC (DMA,  $\text{NH}_4\text{PF}_6$ , DAD detector) of **B**; b)  $^1\text{H}$  NMR spectrum of **B** (300 MHz,  $\text{CHCl}_3$ ); c) Confocal-microscopy image of a spin-coated film of **B** ( $20 \text{ mg} \cdot \text{mL}^{-1}$ , chlorobenzene).

tion with PDI values below 1.2 (A: 1.17, B: 1.19) as well as a statistical distribution of the dye repeat units in the polymer, as supported by the SEC plots using a diode-array detector, depicted in Figure 1a. The ratio of dye to MMA is 2:98, as confirmed by the  $^1\text{H}$  NMR spectrum (Figure 1b). A kinetic study of the polymerizations was not carried out. The applied reaction conditions, investigated by a synthetic robot optimization, proved to be optimal for the RAFT polymerization of MMA.<sup>[24]</sup> The reactivity of the dye-functionalized monomers and MMA are similar, which is supported by the equal conversions of both monomers (approximately 65%, see Table 2). The proposed dye content of 3% was nearly reached for both polymers A and B (calculated from the integration of the  $^1\text{H}$  NMR spectra, see Table 2). Due to the low dye content of 2%, it is valid to assume that the hydrodynamic volume of PMMA was not significantly affected. Thus, polymers A and B are comparable to linear PMMA, which was used as the calibration standard (in SEC) to determine the  $\bar{M}_n$  values. The polymers show a good correlation between the theoretical  $\bar{M}_n$  values and those measured by SEC. Nevertheless, an absolute molar-mass detection was applied using an SEC equipped with a viscosity detector and a universal polystyrene (PS) calibration. The molar masses of the viscosity measurements are in good agreement with the obtained  $\bar{M}_n$  values using an RI detector as well as the theoretical ones. The results demonstrate that the monomers are well polymerizable and stable under RAFT conditions.

Furthermore, the polymers were tested regarding their film-forming behavior. For this purpose, films of the two polymers, shown for B in Figure 1c, were prepared by the spin-coating technique with a solution of A or B in chlorobenzene ( $20 \text{ mg} \cdot \text{mL}^{-1}$ ) at 2 000 rpm for 30 s. The obtained thin polymer films reached thicknesses of 95 nm (A) and 55 nm (B), respectively.

The absorption and emission spectra of the monomers, polymers and polymer films are shown in Figure 2 and the electronic properties are summarized in Table 3. Unless otherwise stated, the measurements were carried out at room temperature with chloroform as the solvent. Compounds of type 3 characteristically display an intense absorption in the UV region at about  $\lambda = 230 \text{ nm}$  (not shown) due to the pyridine moiety, which is mostly unaffected by the different thiazole cores. A second absorption for 3b occurs at about  $\lambda = 270 \text{ nm}$  due to the additional phenyl substituent in the 5-position (K-band). The most-important and strongest absorption originates from the thiazole subunit. The maximum is located at  $\lambda = 342 \text{ nm}$  for 3a and is bathochromically shifted to  $\lambda = 368 \text{ nm}$  for 3b due to the adjacent phenyl ring, which consequently lowers the gap between the  $S_0$  and  $S_1$  of the transition. The emission of the dyes is strongly related to the absorption and is located at  $\lambda = 410$  and  $446 \text{ nm}$  for 3a and 3b, respectively. A large Stokes shift of about  $5 000 \text{ cm}^{-1}$  can

Table 2. Selected characterization data for the obtained polymers.

Sample	[MMA]: [dye]	[M]:[CPDB]: [AIBN]	MMA	Dye	$\bar{M}_{n, \text{theo}}$	$\bar{M}_{n, \text{SEC}}$	PDI SEC	DP SEC	$\bar{M}_{n, \text{SEC}}$	PDI SEC	Dye
			conv. <sup>a)</sup>	conv. <sup>b)</sup>	(RI) <sup>c)</sup>	(RI) <sup>c)</sup>	(visco) <sup>d)</sup>	(visco) <sup>d)</sup>	content <sup>e)</sup>		
			%	%	$\text{g} \cdot \text{mol}^{-1}$	$\text{g} \cdot \text{mol}^{-1}$			$\text{g} \cdot \text{mol}^{-1}$		%
A	97:3	100:1:0.25	60	65	6 600	7 400	1.17	71	8 600	1.13	2
B	97:3	100:1:0.25	67	67	7 500	8 400	1.19	77	9 100	1.12	2

<sup>a)</sup>Calculated from the GC peak areas; <sup>b)</sup>Calculated from SEC (CHCl<sub>3</sub>) UV-detector peak areas:  $A_{\text{polymer}}/(A_{\text{polymer}} + A_{\text{monomer}})$ ; <sup>c)</sup>Calculated from SEC (CHCl<sub>3</sub>), PMMA calibration; <sup>d)</sup>Calculated from SEC (THF), visco detector and universal PS calibration; <sup>e)</sup>Calculated from integrated areas of aromatic dye signals and the -OCH<sub>3</sub> MMA signals.

Table 3. Absorption and fluorescence wavelengths, Stokes shifts, fluorescence lifetimes and quantum yields measured in CHCl<sub>3</sub> at room temperature.

Compound	$\lambda_{\text{abs}}$	$\lambda_{\text{fl}}$	Stokes shift	$\tau$	$\Phi$
	nm	nm	cm <sup>-1</sup>	ns	%
3a	342, 334 <sup>a)</sup>	410, 411 <sup>a)</sup>	4 850, 5 600 <sup>a)</sup>	2.2, 1.9 <sup>a)</sup>	29, 30 <sup>a)</sup>
3b	368, 361 <sup>a)</sup>	446, 447 <sup>a)</sup>	4 750, 5 300 <sup>a)</sup>	1.8, 1.5 <sup>a)</sup>	40, 34 <sup>a)</sup>
A (polymer)	338	409	5 150	2.1	31
B (polymer)	366	448	5 000	1.7	40
A (film)	325–335 <sup>b)</sup>	408	≈5 300 <sup>b)</sup>	–	–
B (film)	367	444	4 700	–	–

<sup>a)</sup>Measured in CH<sub>3</sub>CN; <sup>b)</sup>Superimposed with absorption from CPDB.

be observed. Measurements of the monomers carried out in a more-polar solvent, acetonitrile, led to similar results. The quantum yields, and, in agreement, the fluorescence lifetimes are slightly lower, whereas the Stokes shift becomes higher (typical for a  $\pi$ - $\pi^*$  transition). The obtained fluorescence lifetimes are in the normal range for such small molecules.<sup>[25]</sup>

By comparing the absorption and emission spectra of the monomers, polymers and films, they are found only to vary in the range of  $\lambda = \pm 6$  nm, which is basically within the range of the measurement errors. This implies that the optoelectronic properties of the monomers are unaffected by polymerization and thin-film formation. This is also consistent with the fluorescence decay curves of the monomers and polymers, shown in Figure 3. Moreover, no indication for an aggregation ( $\pi$ -stacking) of the dyes incorporated in the polymers, which would lead to a shorter lifetime or a shift of the absorption and/or emission maximum, can be observed. Additionally, the absorption of the chain-transfer agent (CPDB) can be seen for the polymer and film of A at approximately  $\lambda = 305$  nm due to the similar

extinction coefficients of **3a** to CPDB, which are also much lower as compared to **3b**.

## Conclusion

The synthesis and evaluation of polymers containing derivatives of 4-hydroxythiazoles as new light-harvesting and blue-fluorescing chromophores was performed. The electronic properties of these dyes can easily be tuned by varying the substituents at the thiazole core. In addition, they showed a good stability towards the applied RAFT conditions. Due to the C3 spacer, the electronic properties were almost unaffected by polymerization. Thin films of the polymers were prepared, which may be useful, for example, for the construction of dye-sensitized solar cells (DSSCs), in which the chromophores will act as light-harvesting antennas combined with primary electron donors, which allows charge injection into the wide-bandgap semiconductor material. Furthermore, the synthesized polymers could be useful for the construction of WPLEDs, in which the

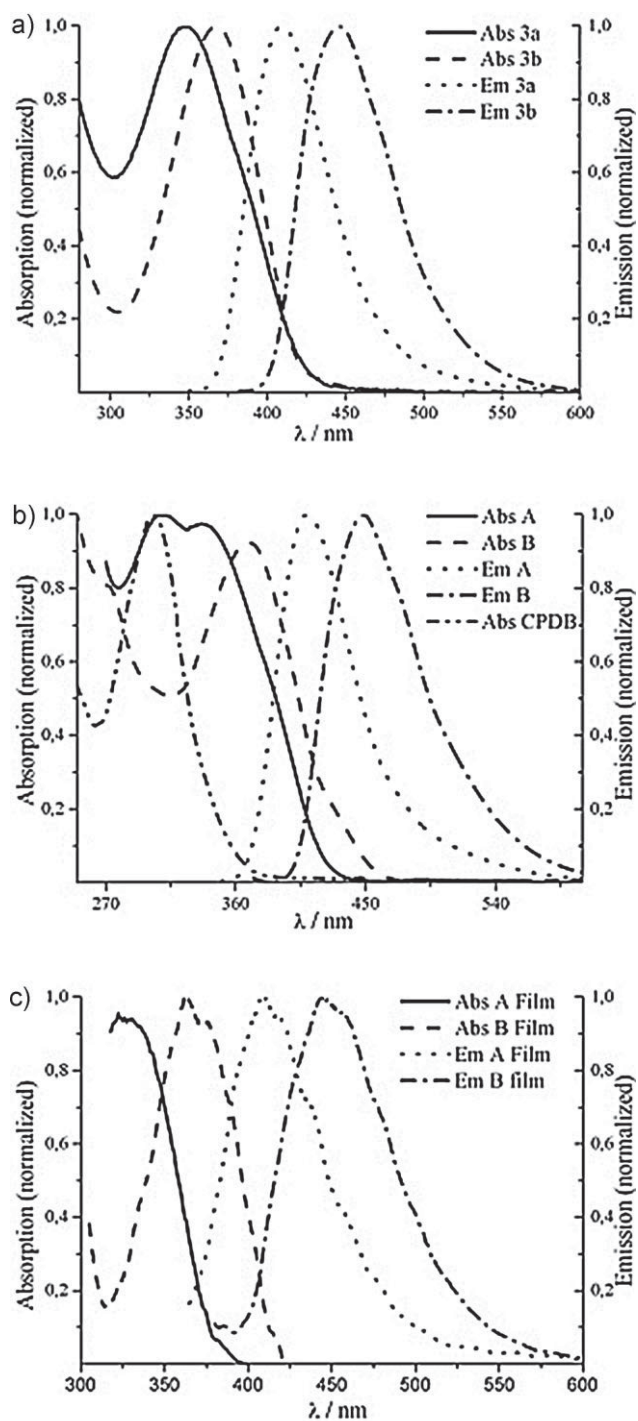


Figure 2. UV-vis absorption and emission spectra of (a) the monomers **3a**, **3b**, (b) polymers **A**, **B** and (c) films of **A** and **B** in  $\text{CHCl}_3$  at room temperature ( $c \approx 1 \times 10^{-6} \text{ mol} \cdot \text{L}^{-1}$ ).

presented thiazoles would account for the blue component. The capability of the thiazoles as FRET donors in polymers with either Ru(II) polypyridyl complexes or other long-wavelength-absorbing thiazoles as acceptors will be the basis for further applications.

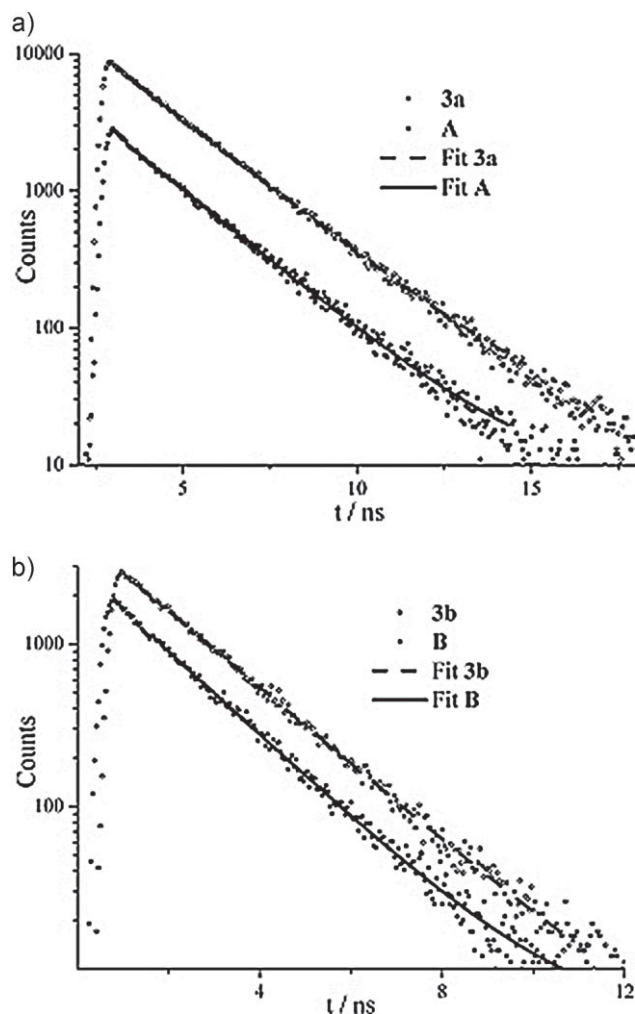


Figure 3. Monoexponential decay curves and fitting range of the monomers and polymers measured in  $\text{CHCl}_3$  at RT.

Acknowledgements: The authors thank the *Thuringian Ministry for Education, Science and Culture* [grant #B514-09049, Photonische Mizellen (PhotoMIC)] for financial support. B.D. acknowledges financial support by the *Fonds der Chemischen Industrie*.

Received: December 10, 2010; Published online: March 7, 2011;  
DOI: 10.1002/macp.201000752

Keywords: blue chromophores; donor dyes; fluorescence; reversible addition-fragmentation chain transfer (RAFT); thiazoles

- [1] [1a] A. C. Grimsdale, K. L. Chan, R. E. Martin, P. G. Jokisz, A. B. Holmes, *Chem. Rev.* **2009**, *109*, 897; [1b] O. Nuyken, S. Jungermann, V. Wiederhim, E. Bacher, K. Meerholz, *Monatsh. Chem.*, **2006**, *137*, 811.

- [2] [2a] P.-I. Shih, C.-F. Shu, Y.-L. Tung, Y. Chi, *Appl. Phys. Lett.* **2006**, *88*, 251110; [2b] J. Lu, H. Li, B. Yao, B. Zhao, C. Weng, G. Lei, P. Shen, Z. Xie, S. Tan, *J. Phys. Chem. B* **2009**, *113*, 4203; [2c] Z. Lin, Y.-D. Lin, C.-Y. Wu, P.-T. Chow, C.-H. Sun, T. J. Chow, *Macromolecules* **2010**, *43*, 5925.
- [3] [3a] K. Lee, L. K. Povlich, J. Kim, *Analyst* **2010**, *135*, 2179; [3b] D. T. McQuade, A. E. Pullen, T. M. Swager, *Chem. Rev.* **2000**, *100*, 2537; [3c] C.-C. Yang, Y. Tian, C.-Y. Chen, A. K.-Y. Jen, W.-C. Chen, *Macromol. Rapid Commun.* **2007**, *28*, 894.
- [4] [4a] X. Liu, R. Zhu, Y. Zhang, B. Liu, S. Ramakrishna, *Chem. Commun.* **2008**, 3789; [4b] W. Zhang, Z. Fang, M. Su, M. Saeys, B. Liu, *Macromol. Rapid Commun.* **2009**, *30*, 1533; [4c] G. D. Sharma, P. Suresh, J. A. Mikroyannidis, *Synth. Met.* **2010**, *160*, 1427, and references therein.
- [5] [5a] D. A. Friesen, T. Kajita, E. Danielson, T. J. Meyer, *Inorg. Chem.* **1998**, *37*, 2756; [5b] M. Sykora, K. A. Maxwell, J. M. DeSimone, T. J. Meyer, *Proc. Natl. Acad. Sci. USA* **2000**, *97*, 7687.
- [6] D. Y. Kim, H. N. Cho, C. Y. Kim, *Prog. Polym. Sci.* **2000**, *25*, 1089.
- [7] K. E. Sapsford, L. Berti, I. L. Medintz, *Angew. Chem. Int. Ed.* **2006**, *45*, 4562.
- [8] J. Serin, X. Schultze, A. Adronov, J. M. J. Fréchet, *Macromolecules*, **2002**, *35*, 5396.
- [9] Y. Yamamoto, Y. Tamaki, T. Yui, K. Koike, O. Ishitani, *J. Am. Chem. Soc.* **2010**, *132*, 11743, and references therein.
- [10] A. Harriman, A. Khatyr, R. Ziessel, *Res. Chem. Intermed.* **2007**, *33*, 49.
- [11] J. P. S. Farinha, J. M. G. Martinho, *J. Phys. Chem. C* **2008**, *112*, 10591.
- [12] M. Aguiar, F. E. Karasc, L. Akcelrud, *Macromolecules* **1995**, *28*, 4598.
- [13] A Guide to Fluorescent Probes and Labeling Technologies, in: *The Molecular Probes Handbook*, 11<sup>th</sup> edition, Molecular Probes Eugene **2010**, Chapter 1
- [14] U.-W. Grummt, D. Weiß, E. Birckner, R. Beckert, *J. Phys. Chem. A* **2007**, *111*, 1104.
- [15] K. Stippich, D. Weiß, A. Güther, H. Görls, R. Beckert, *J. Sulfur Chem.* **2009**, *30*, 109.
- [16] [16a] G. Moad, E. Rizzardo, S. H. Thang, *Polymer* **2008**, *49*, 1079; [16b] J. Chiefari, Y. Chong, F. Ercole, J. Krstina, J. Jeffery, T. Le, R. Mayadunne, G. Meijs, C. Moad, G. Moad, E. Rizzardo, S. Thang, *Macromolecules* **1998**, *31*, 5559.
- [17] [17a] A. J. Inglis, S. Sinnwell, T. P. Davis, C. Barner-Kowollik, M. H. Stenzel, *Macromolecules* **2008**, *41*, 4120; [17b] C. Weber, C. R. Becer, W. Guenther, R. Hoogenboom, U. S. Schubert, *Macromolecules* **2010**, *43*, 160; [17c] L. Barner, T. P. Davis, M. H. Stenzel, C. Barner-Kowollik, *Macromol. Rapid Commun.* **2007**, *28*, 539.
- [18] R. Siebert, D. Akimov, M. Schmitt, A. Winter, U. S. Schubert, B. Dietzek, J. Popp, *ChemPhysChem* **2009**, *10*, 910.
- [19] R. Menzel, E. Täuscher, D. Weiß, R. Beckert, H. Görls, *Z. Anorg. Allg. Chem.* **2010**, *636*, 1380.
- [20] E. Täuscher, D. Weiß, R. Beckert, H. Görls, *Synthesis* **2010**, *10*, 1603.
- [21] C. J. Hawker, A. W. Bosman, E. Harth, *Chem. Rev.* **2001**, *101*, 3661.
- [22] K. Matyjaszewski, J. Xia, *Chem. Rev.* **2001**, *101*, 2921.
- [23] [23a] C. Pietsch, R. Hoogenboom, U. S. Schubert, *Angew. Chem. Int. Ed.* **2009**, *48*, 5653; [23b] C. Pietsch, R. Hoogenboom, U. S. Schubert, *Polym. Chem.* **2010**, *1*, 1005.
- [24] [24a] M. W. M. Fijten, R. M. Paulus, U. S. Schubert, *J. Polym. Sci., Part A: Polym. Chem.* **2005**, *43*, 3831; [24b] M. W. M. Fijten, M. A. R. Meier, R. Hoogenboom, U. S. Schubert, *J. Polym. Sci., Part A: Polym. Chem.* **2004**, *42*, 5775.
- [25] M. Montalti, A. Credi, L. Prodi, M. T. Gandolfi, *Handbook of Photochemistry*, 3<sup>rd</sup> edition, Taylor & Francis, London 2006, Ch. 1.

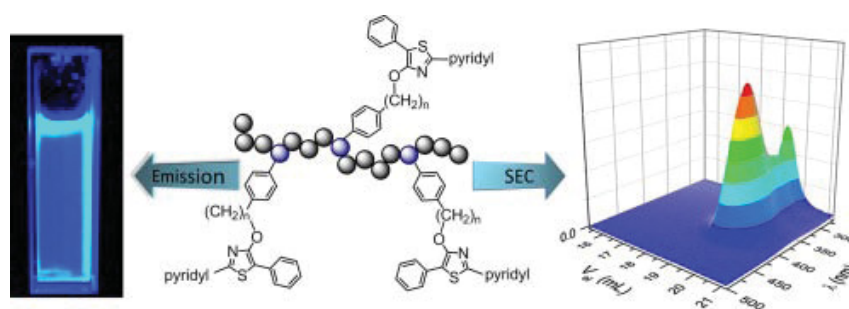


## Publication P4:

### *Blue emission of side-chain pendant 4-hydroxy-1,3-thiazoles in polystyrenes synthesized by RAFT polymerization*

A. M. Breul<sup>+</sup>, C. Pietsch<sup>+</sup>, R. Menzel, J. Schäfer, A. Teichler, M. D. Hager, J. Popp, B. Dietzek, R. Beckert, U. S. Schubert

*Eur. Polym. J.* **2012**, *48*, 1339–1347



<sup>+</sup> Both authors contributed equally to this paper







Contents lists available at SciVerse ScienceDirect

## European Polymer Journal

journal homepage: [www.elsevier.com/locate/europolj](http://www.elsevier.com/locate/europolj)

## Blue emitting side-chain pendant 4-hydroxy-1,3-thiazoles in polystyrenes synthesized by RAFT polymerization

Alexander M. Breul<sup>a,b,1</sup>, Christian Pietsch<sup>a,b,c,1</sup>, Roberto Menzel<sup>a,b</sup>, Johann Schäfer<sup>b,d</sup>, Anke Teichler<sup>a,b,c</sup>, Martin D. Hager<sup>a,b,c</sup>, Jürgen Popp<sup>b,d,e</sup>, Benjamin Dietzek<sup>b,d,e,\*</sup>, Rainer Beckert<sup>a,b,\*</sup>, Ulrich S. Schubert<sup>a,b,c,\*</sup>

<sup>a</sup>Laboratory of Organic and Macromolecular Chemistry (IOMC), Friedrich-Schiller-University Jena, Humboldtstr. 10, 07743 Jena, Germany

<sup>b</sup>Jena Center for Soft Matter (JCSM), Humboldtstr. 10, 07743 Jena, Germany

<sup>c</sup>Dutch Polymer Institute (DPI), P.O. Box 902, 5600 AX Eindhoven, The Netherlands

<sup>d</sup>Institute of Photonic Technologies (IPHT), Albert-Einstein-Straße 9, 07745 Jena, Germany

<sup>e</sup>Institute of Physical Chemistry (IPC), Friedrich-Schiller-University Jena, Helmholtzweg 4, 07743 Jena, Germany

## ARTICLE INFO

## Article history:

Received 24 November 2011

Received in revised form 23 March 2012

Accepted 26 March 2012

Available online 21 April 2012

## Keywords:

Blue chromophores

Donor dyes

Fluorescence

Reversible addition–fragmentation chain

transfer (RAFT)

Styrene

Thiazoles

## ABSTRACT

Blue emitting dyes bearing a luciferin analogous chromophore were attached to a polystyrene backbone. For this purpose, 4-hydroxy-1,3-thiazoles were functionalized with a styrene unit and polymerized using the reversible addition–fragmentation chain transfer (RAFT) polymerization technique. Two different chain transfer agents were investigated and one monomer was studied in terms of its kinetic behavior. The polymerization kinetics are presented and discussed in detail, showing a controlled polymerization behavior, resulting in well-defined copolymers with polydispersity indices below 1.2. The obtained polymers were characterized by size exclusion chromatography (SEC), <sup>1</sup>H NMR, MALDI-TOF MS and UV–vis absorption and fluorescence spectroscopy. In addition, the UV–vis absorption and emission behavior was investigated in thin films.

© 2012 Elsevier Ltd. All rights reserved.

### 1. Introduction

Fluorescent polymers derived from luminescent monomers are in the focus of intense research today [1–3]. A variety of different chromophores attracted high interest due to potential applications in various fields, for instance, their successful application in organic light emitting diodes (OLEDs) [2,4,5], as one emitting species in white polymer

light emitting diodes (WPLEDs) [2,6–8], as sensor molecules in biochemical and environmental applications [3,9–11], and dye sensitized solar cells [2,12–14]. Moreover, blue emitting monomers carry the potential of mimicking photosynthetic proteins in plants by incorporating the chromophores into polymers as donor molecules for Förster resonant energy transfer (FRET) process [15–21]. Main chain  $\pi$ -conjugated polymers are not attractive for this application due to the synthetic complexity and the dependence of the optical properties from the number of repeating units and, therefore, the distance between the chromophores [22]. In contrast, polymers which are functionalized with dye units in the side chain feature defined and predictable optical properties, independent from the degree of polymerization (DP) [23–26]. A homogeneous distribution of the dye in the polymer can be achieved by

\* Corresponding authors. Tel.: +49 (0)3641 948367; fax: +49 (0)3641 948302 (B. Dietzek), tel.: +49 (0)3641 948230; fax: +49 (0)3641 948212 (R. Beckert), tel.: +49 (0)3641 948200; fax: +49 (0)3641 948202 (U.S. Schubert).

E-mail addresses: [benjamin.dietzek@uni-jena.de](mailto:benjamin.dietzek@uni-jena.de) (B. Dietzek), [c6be-ra@uni-jena.de](mailto:c6be-ra@uni-jena.de) (R. Beckert), [ulrich.schubert@uni-jena.de](mailto:ulrich.schubert@uni-jena.de) (U.S. Schubert).

URL: <http://www.schubert-group.com> (U.S. Schubert).

<sup>1</sup> Both authors contributed equally to this work.

direct polymerization of functional monomers. Moreover, the degree of functionalization can be adjusted by the concentration of the labeled monomer in the overall monomer feed of the polymerization. Such polymers are of potential interest for a wide range of applications, e.g., in fluorescent nanoparticles for the investigation of biological substrates, in particular of living cells [27]. In contrast to common postpolymerization conjugations of dyes onto preformed particles, the direct polymerization leads to uniformly distributed dyes, resulting in an enhanced fluorescence of the particles, which are not vulnerable to dye-leakage [28].

Despite the large number of blue emitting molecules, e.g., coumarins [29], naphthalimides [30], pyrenes [31], and Nile blue [32], only a small part of them were incorporated into polymers so far. Moreover, many of these “conventional” dyes feature drawbacks, which have to be overcome; for instance, low quantum yields, strong solvent dependency of the electronic properties, excimer formation [33], and a low photostability [34]. A promising class of blue-emitting dyes are 1,3-thiazoles. These dyes generally feature very high room-temperature fluorescence, with quantum yields ranging from 0.7 up to unity, in combination with an unusually large Stokes shift [35,36]. Furthermore, the choice of different types of substituents strongly influences absorption and emission behavior in the UV and visible region of the electromagnetic spectrum [37]. In addition, the introduction of hydroxyl functionalities (i.e. 4-hydroxy-1,3-thiadiazoles) offers the possibility of an easy functionalization, in particular, alkylation as well as acylation, i.e. with styrene and methacrylate derivatives, respectively. The ease in synthetic access and functionalization combined with high fluorescence quantum yields, improved photostability compared to other chromophores (e.g., rhodamines, fluoresceins) as well as chemical stability made 4-hydroxy-1,3-thiazoles suitable for the fabrication of luminescent polymeric materials. Previously, it was demonstrated that 4-hydroxy-1,3-thiazoles can be successfully incorporated into poly (methyl methacrylate) (PMMA) backbones [23] by reversible addition–fragmentation chain transfer polymerization (RAFT) [38,39]. The advantage of RAFT is the good tolerance to functional groups (e.g., incorporation of dyes) [40,41] and the possibility to construct a wide range of different architectures, e.g., combs, blocks, and star copolymers [42–44]. A control over the molar mass and the polydispersity index (PDI) can be obtained by this type of controlled radical polymerization technique.

In comparison to methacrylates, styrene derivatives feature a better chemical stability, in particular, a better resistance towards hydrolysis.

In this contribution the synthesis and characterization of statistical thiazole-functionalized styrene copolymers are described. Two different chain transfer agents, 2-cyano-2-propyl dithiobenzoate (CPDB) and a trithiocarbonate (2-(butylthiocarbonothioylthio)propanoic acid, BTTCP) were investigated. Additionally, the copolymerization kinetics with styrene and one thiazole functionalized monomer were studied. Furthermore, absolute emission quantum yields and fluorescence lifetimes of the functionalized monomers and copolymers are determined using stationary UV–vis and time correlated single photon

counting measurements. Finally, the optical properties between a selected copolymer and its corresponding monomer unit in solution were compared to its behavior in thin films.

## 2. Experimental

### 2.1. Materials and instrumentation

All reagents were purchased from commercial sources (Biosolve, Fluka, Aldrich, Alfa Aesar and Acros Organics) and were used directly without further purification. All solvents were of reagent grade, purified using common methods and distilled prior to use. Styrene was passed over a short neutral aluminum oxide column directly before use to remove the stabilizer. 2,2'-Azobis(iso-butyronitrile) (AIBN) was recrystallized from methanol prior to use. **1a** [45] and **2a** [23] were synthesized according to literature methods. 2-Cyano-2-propyl dithiobenzoate (CPDB) was purchased from Sigma–Aldrich and 2-(butylthiocarbonothioylthio)propanoic acid (BTTCP) was kindly provided by BASF SE. All reactions were performed under an argon atmosphere in glassware equipped with a Teflon<sup>®</sup> coated magnetic stirring bar. Size exclusion chromatograms were recorded using a SEC Shimadzu SCL-10A system controller, a LC-10AD pump, a RID-10A refractive index detector and a PL gel 5  $\mu\text{m}$  mixed-D column at 40 °C (eluent  $\text{CHCl}_3$ :TEA:*i*-PrOH 94:4:2; flow rate 1 mL/min) applying linear polystyrene standards. GC measurements were performed on an Interscience Trace GC with a Trace Column RTX-5 connected to a PAL autosampler. A spin coater from Laurell Technologies Corporation (North Wales, USA) was used for the preparation of the films. The surface topography and thickness of the polymer films was measured by an optical interferometric profiler Wyko NT9100 (Veeco, Mannheim, Germany). For this purpose, each film was scratched with a scalpel in a controlled manner. At five different positions of the film, the center and the four edges, the depth of the scratch was measured with the optical profiler. <sup>1</sup>H and <sup>13</sup>C NMR spectra were recorded on Bruker AC 250 (250 MHz), 300 (300 MHz) and 400 (400 MHz) spectrometers at 298 K, respectively. The chemical shifts are reported in parts per million (ppm,  $\delta$  scale) relative to signals from the NMR solvents, coupling constants are given in Hz. The melting points were measured with a Galen III apparatus (Boëtius system). Reactions were monitored by TLC on 0.2 mm Merck silica gel plates (60 F254). The mass spectra were measured either with a Finnigan MAT SSQ 710 (EI) or a MAZ 95 XL (FAB) system. Elemental analyses were carried out on a CHN-932 Automat Leco instrument.

The UV–vis absorption and PL emission spectra were recorded on an Analytik Jena SPECORD 250 and a Jasco FP-6500 spectrometer, respectively, at 298 K. UV–vis and fluorescence spectra of the films were measured with a modified Hitachi F-4500. For this purpose, dilute solutions ( $10^{-6}$ – $10^{-5}$  M, 1 cm quartz cuvette) in  $\text{CHCl}_3$  were used. As reference, a quartz cuvette filled with the pristine solvent was utilized. Fluorescence lifetimes were obtained by streak camera measurements in the time-correlated

single-photon counting (TCSPC) mode. In the experiments a Ti:sapphire Laser (Tsunami, Newport Spectra-Physics GmbH) was used as light source. The pulse-to-pulse repetition rate was reduced to 800 kHz by a pulse selector (Model 3980, Newport Spectra-Physics GmbH). Afterwards the laser frequency was tripled using a setup described in recent publications [46]. Quantum yields measurements were performed with a Perkin Elmer Lambda 16 UV-vis spectrometer in perpendicular excitation-emission geometry, while the absorbance in the most red-shifted absorption maximum was <0.05. A detailed description of the respective setup is given in previous contributions [36].

## 2.2. Synthesis of the monomers

### 2.2.1. 5-Phenyl-2-(pyridin-2-yl)-4-(4-vinylbenzyloxy)thiazole (**1b**)

5-Phenyl-2-(pyridin-2-yl)thiazol-4-ol **1a** (2.54 g, 10 mmol) was dissolved in DMSO (20 mL) and  $K_2CO_3$  (1.74 g, 13 mmol, in 2 mL  $H_2O$ ) was added. The resulting orange solution was stirred for 20 min. Vinylbenzyl chloride (1.68 g, 11 mmol) was added and stirring was continued for 24 h at RT. After the reaction was finished (TLC),  $H_2O$  (300 mL) was added and the aqueous phase was extracted with  $CHCl_3$  ( $3 \times 50$  mL). The organic phase was washed with  $H_2O$  ( $3 \times 100$  mL), dried over  $MgSO_4$  and concentrated *in vacuo* at 40 °C. Flash chromatography (Silica,  $CH_2Cl_2$ ) yielded the pure compound as yellow solid. The product can also be recrystallized from EtOH/ $CHCl_3$  at -30 °C to obtain the ether as light yellow crystalline compound.

Yield: 3.11 g (8.4 mmol), 84%; yellow, fluffy needles: m.p. 85.5 °C;  $^1H$  NMR (250 MHz,  $CDCl_3$ ):  $\delta$  = 8.59 (d,  $J$  = 4.1 Hz, 1H), 8.15 (d,  $J$  = 7.9 Hz, 1H), 7.83–7.76 (m, 3H), 7.51–7.21 (m, 8H), 6.79 (dd,  $J$  = 10.8 Hz, 0.8 Hz, 1H), 5.80 (d,  $J$  = 17.6 Hz, 1H), 5.59 (s, 2H), 5.28 (d,  $J$  = 10.9 Hz, 1H).  $^{13}C$  NMR (63 MHz,  $CDCl_3$ ):  $\delta$  = 160.51, 159.83, 151.38, 149.51, 137.26, 137.02, 136.96, 136.54, 131.62, 128.79, 128.11, 127.02, 126.83, 126.39, 124.12, 118.91, 115.02, 114.08, 71.81. MS (micro ESI):  $m/z$  (%) = 393.1 ( $M^+ + Na$ , 100%), 371 ( $M^+ + H$ , 15%). MS (micro ESI-HRMS):  $m/z$  = 393.1029 [ $M + Na$ ] $^+$  requires for  $[C_{22}H_{17}N_2NaOS]^+$  = 393.1026.

### 2.2.2. 5-Phenyl-2-(pyridin-3-yl)-4-(3-(4-vinylbenzyloxy)propoxy)thiazole (**2b**)

NaH (77 mg, 1.92 mmol) of a NaH dispersion 60% in mineral oil) was added to a solution of 3-(5-phenyl-2-(pyridin-3-yl)thiazol-4-yloxy)propan-1-ol **2a** (500 mg, 1.60 mmol) in dry and degassed THF (10 mL) in a Schlenk tube under an argon atmosphere. The yellow slurry was stirred for 60 min followed by the addition of 4-vinylbenzyl chloride (292 mg, 1.92 mmol). Stirring was continued for 48 h. The reaction was aborted after this time because no significant progress was observed (TLC). The mixture was quenched with a saturated  $NH_4Cl$  solution (30 mL) and the organic phase was washed thoroughly with  $H_2O$  ( $3 \times 20$  mL) dried over  $MgSO_4$  and concentrated *in vacuo* at 40 °C. Column chromatography (silica,  $CH_2Cl_2$  to  $CH_2Cl_2/EtOAc$  10:1) yielded the product as a yellow oil.

Yield: 140 mg (0.33 mmol), 20%.  $^1H$  NMR (250 MHz,  $CDCl_3$ ):  $\delta$  = 9.15 (d,  $J$  = 1.7 Hz, 1H), 8.63 (dd,  $J$  = 4.8, 1.6 Hz, 1H), 8.25–8.11 (m, 1H), 7.74 (dd,  $J$  = 5.3, 3.4 Hz, 2H), 7.47–7.18 (m, 8H), 6.70 (dd,  $J$  = 17.6, 10.9 Hz, 1H), 5.72 (dd,  $J$  = 17.6, 0.8 Hz, 1H), 5.23 (dd,  $J$  = 10.9, 0.7 Hz, 1H), 4.66 (t,  $J$  = 6.2 Hz, 2H), 4.52 (s,  $J$  = 14.3 Hz, 2H), 3.82–3.61 (m, 2H), 2.37–2.04 (m, 2H).  $^{13}C$  NMR (63 MHz,  $CDCl_3$ ):  $\delta$  = 159.35, 156.68, 150.54, 147.02, 138.13, 137.05, 136.67, 132.68, 131.44, 129.79, 128.83, 127.92, 126.96, 126.89, 126.34, 123.74, 113.83, 112.68, 72.90, 67.91, 67.03, 30.14. MS (EI):  $m/z$  (%) = 428 ( $M^+$ , 6%), 117 (100%).

## 2.3. General polymerization procedure

The required amounts of the monomers (*i.e.*, styrene and dye-functionalized styrene) were transferred into the 5 mL reaction vial and dissolved in toluene. Thereafter, the calculated volumes of stock solutions of 2-cyano-2-propyl dithiobenzoate (CPDB) or 2-(butylthiocarbonothioylthio)propanoic acid (BTTCP) as well as 2,2'-azobis(*iso*-butyronitrile) (AIBN) in toluene were added. The ratio of [CTA] to [AIBN] was always 4/1. Before closing the vial, the reaction solution was purged with a flow of argon for 30 min. Subsequently, the reaction was performed in an oil bath at 70 °C for CPDB and 80 °C for BTTCP overnight (see Table 2 for exact reaction times and [M]/[CTA] ratios). The obtained polymers were purified by precipitation into cold methanol. The polymers were dried under reduced pressure at 40 °C. The conversion was measured by  $^1H$  NMR spectroscopy or by GC using anisole as internal standard.

### 2.3.1. P(**1b**-stat-styrene) (**A1**)

$^1H$  NMR ( $CDCl_3$ , 300 MHz):  $\delta$  = 8.61, 8.17 (Ar-H pyridine), 7.85, 7.55–6.3 (Ar-H), 5.62 ( $OCH_2$ ), 3.29, 2.5–0.7 (backbone). SEC ( $CHCl_3$ , PS standard):  $M_n$  = 3120 g/mol, PDI = 1.13. GC:  $conv_{styrene}$  = 26%;  $M_{n,theo}$  = 2900 g/mol. UV-vis ( $CHCl_3$ ):  $\lambda_{max}$  = 262, 370 nm.

### 2.3.2. P(**1b**-stat-styrene) (**A2**)

$^1H$  NMR ( $CDCl_3$ , 300 MHz):  $\delta$  = 8.62, 8.18 (Ar-H pyridine), 7.86, 7.55–6.3 (Ar-H), 5.63 ( $OCH_2$ ), 3.31, 2.45–0.7 (backbone). SEC ( $CHCl_3$ , PS standard):  $M_n$  = 8000 g/mol, PDI = 1.14.

### 2.3.3. P(**2b**-stat-styrene) (**B**)

$^1H$  NMR ( $CDCl_3$ , 300 MHz):  $\delta$  = 0.94, 1.11, 1.45, 1.87, 2.18 (b, backbone, initiator endgroup,  $CH_2$  spacer), 3.68, 4.45 (b,  $OCH_2$   $C_3$ -spacer), 4.67 (b,  $OCH_2$  benzyl), 6.59, 7.07, 7.35, 7.75 (b, Ar-H), 8.17, 8.61, 9.16 (b, Ar-H pyridine). SEC ( $CHCl_3$ , PS standard):  $M_n$  = 3000 g/mol;  $M_w$  = 3300 g/mol; PDI = 1.11. MALDI-TOF MS (DCTB matrix, AgI, linear mode):  $M_n$  = 2200 g/mol;  $M_w$  = 2700 g/mol; PDI = 1.14. GC:  $conv.$  = 23%;  $M_{n,theo}$  = 3100 g/mol. UV-vis ( $CHCl_3$ ):  $\lambda_{max}$  = 373 nm.

## 3. Results

This work demonstrates the synthesis and subsequent polymerization of blue emitting 1,3-thiazole

functionalized styrenes. For this purpose, two thiazoles (5-phenyl-2-(pyridin-2-yl)thiazol-4-ol **1a** and 3-(5-phenyl-2-(pyridin-3-yl)thiazol-4-yloxy)propan-1-ol **2a** have been etherified in dimethylformamide and THF, respectively, under basic conditions using  $K_2CO_3$  as base for **1a** and NaH for **2a**, respectively (Scheme 1). For the monomer synthesis of **1b**, the polymerizable styrene unit was directly attached to the chromophore. In addition, a C3 spacer was introduced in case of **2b** in order to enable a more flexible attachment of the chromophores. The structure of **1b** as chelating ligand could potentially allow complexation of metal ions, e.g., Ru(II) ions, whereas such reactions could be suppressed by the *meta*-substitution of the pyridine moiety in **2b**. Furthermore, the optical properties can be varied by additional substituents on the thiazoles [47].

As controlled radical polymerization (CRP) technique, the RAFT polymerization was carried out using AIBN as radical initiator, toluene as solvent and CPDB as chain transfer agent (CTA) for the polymerization of **2b**. In case of **1b**, 2-(butylthiocarbonothioylthio)propanoic acid (BTTCP) was utilized as CTA agent. As reaction conditions, in particular,  $[M]/[CTA]$  ratio, reaction time as well as temperature, analogous literature procedures known for the polymerization of styrene were applied (see Fig. 1 for SECs of **A1** and **A2** as well as Table 1 for the applied reaction conditions) [39,48]. All polymers revealed narrow molar mass distributions and an incorporation of the dyes in the polymer backbone which was proven by the 3D-SEC plot for polymer **B** in Fig. 2. Furthermore, the theoretical molar mass is in good agreement with the measured one

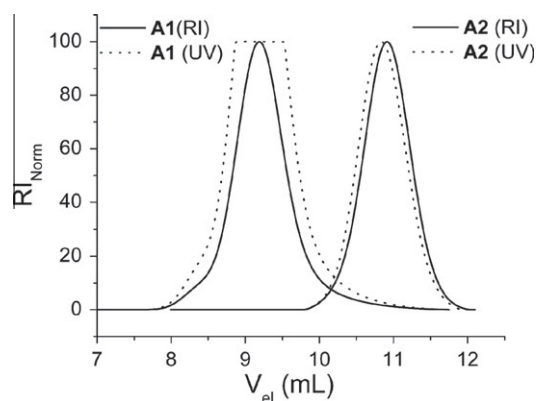
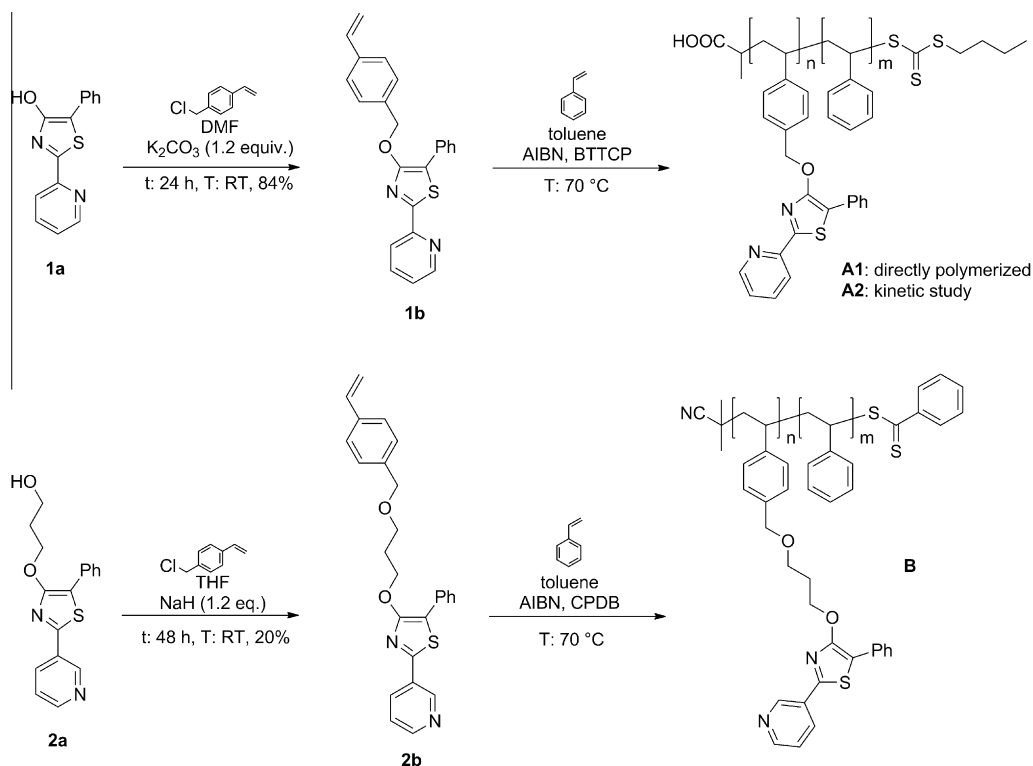


Fig. 1. Size exclusion chromatograms of copolymer **A1** and **A2** ( $CHCl_3$ ).

for both copolymers (for selected characterization data, see Table 2) and the targeted dye contents have been reached (see Fig. 3 for the  $^1H$  NMR spectra of **A** and **B**).

In addition, MALDI-TOF MS has been used as absolute characterization method in order to determine the exact molar mass. The spectrum (Fig. 4) depicts three distributions. The main distribution shows the incorporation of one thiazole functionalized unit in the backbone. Two minor distributions belong to a doubly dye-functionalized polymer chain as well as a non-functionalized one. In order to investigate if the non-functionalized polymer chain is just a result of the fragmentation in MALDI process or

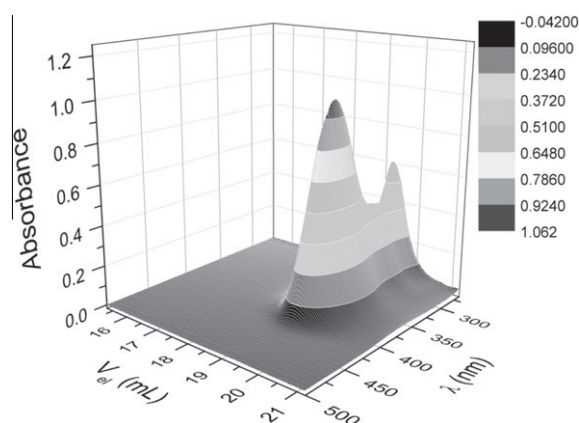


Scheme 1. Schematic representation of the synthesis of the discussed monomers and polymers.

**Table 1**

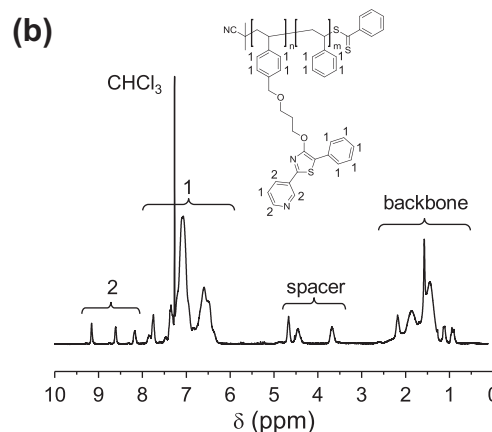
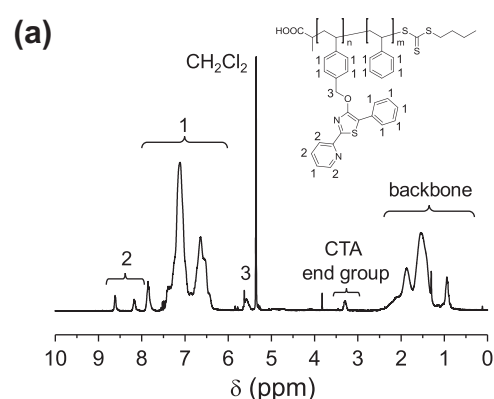
Overview over selected reaction conditions used for the polymerizations in toluene with CTA/AIBN = 4.

Sample	$m_{\text{monomer}}$ (g)	$m_{\text{AIBN}}$ (mg)	$m_{\text{CTA}}$ (mg)	Temp. (°C)	Conc. (mol/L)	Reaction time (h)
<b>A1</b>	0.396 (styrene) 0.074 (2b)	1.6	9.5 (BTTCP)	70	2.0	30
<b>A2</b>	1.65 (styrene) 0.071 (2b)	2.6	15.3 (BTTCP)	80	4.0	Kinetic study
<b>B</b>	0.245 (styrene) 0.112 (3b)	1.07	5.78 (CPDB)	70	2.0	16.5

**Fig. 2.** Characterization of **B** by SEC ( $\text{CHCl}_3$ ) using a DAD detector.

not, a kinetic study of a selected monomer (**1b**) was performed.

The polymerization kinetics were determined for the copolymerization of styrene and **1b** in toluene with BTTCP and a  $[M]/[BTTCP]$  ratio of 250 as depicted in Fig. 5 (for the according characterization data, see Table 3). The polymerization kinetics for the RAFT polymerizations have been investigated by determination of the styrene conversion using  $^1\text{H}$  NMR spectroscopy (styrene signals were overlapping with the thiazole styrene vinyl signals, therefore, estimation of the total conversion), and the molar masses as well as polydispersity indices by size exclusion chromatography (SEC). A linear slope of  $\ln([M]_0/[M]_t)$  could be observed for styrene for nearly 7 h, followed by a decrease in the slope. Such a decrease in  $\ln([M]_0/[M]_t)$  is commonly monitored due to either the occurrence of termination reactions (for styrene mostly recombination reactions) or a decrease in initiator concentration, which results from a steadily decreasing concentration of the radical source (AIBN) [49]. The decrease in radical concentration for the

**Fig. 3.**  $^1\text{H}$  NMR spectra of (a) **A1** (300 MHz,  $\text{CD}_2\text{Cl}_2$ ) and (b) **B** (300 MHz,  $\text{CDCl}_3$ ).

RAFT polymerization of styrene is described in literature by a recombination of the growing radical chains or by recombination of AIBN-derived cyanoisopropyl radicals

**Table 2**

Selected characterization data of the obtained polymers.

Sample	[styrene]:[dye]	CTA	$[M]:[CTA]:[AIBN]$	Conv. styrene <sup>a</sup> (%)	$M_{n,\text{theo}}$ (g/mol)	$M_{n,\text{SEC}}(\text{RI})^b$ (g/mol)	$\text{PDI}_{\text{SEC}}(\text{RI})^b$	$\text{DP}_{\text{SEC}}(\text{RI})^b$	Dye content (NMR) <sup>c</sup> (%)
<b>A1</b>	95:5	BTTCP	100:1:0.25	26	2900	3120	1.13	28	8.5
<b>A2</b>	247:3	BTTCP	250:1:0.25	34	9310	7910	1.15	74	4.3
<b>B</b>	90:10	CPDB	100:1:0.25	23	3100	3000	1.11	22	9

<sup>a</sup> Calculated from the vinyl integrals of the  $^1\text{H}$  NMR spectra using anisole as internal standard.

<sup>b</sup> Calculated from SEC ( $\text{CHCl}_3$ ), PS calibration.

<sup>c</sup> Calculated from the integrated areas of an aromatic dye signals (pyridine substituent) and the aromatic PS signals.

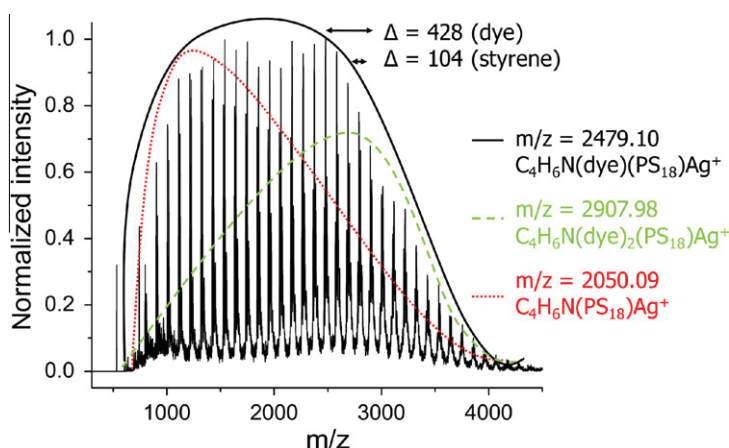


Fig. 4. Characterization of **B** by MALDI-TOF MS (DCTB matrix, AgI).

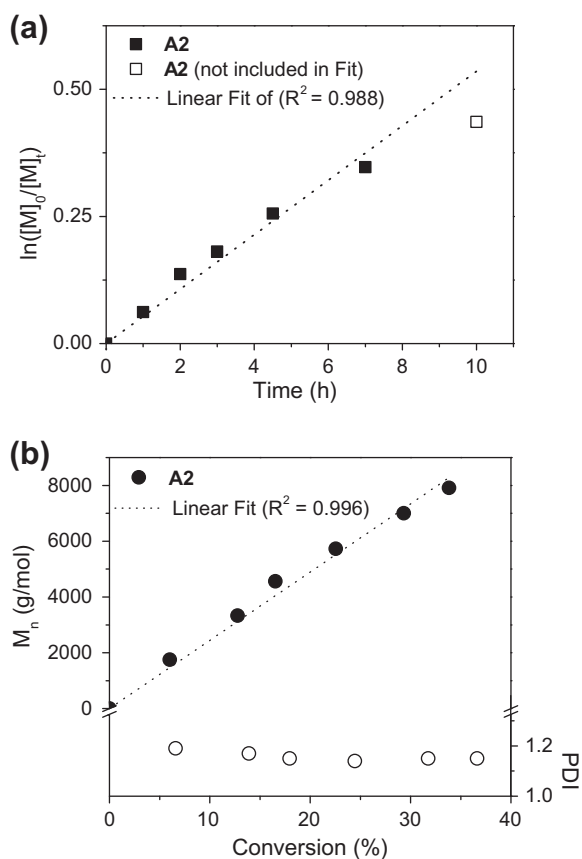


Fig. 5. (a) Kinetic analysis of the monomer conversion of styrene and 1,3-thiazole functionalized styrene during the RAFT polymerization at 80 °C in toluene with [BTTCP]:[AIBN] = 4 and [M] = 4 M. (b)  $M_n$  values and polydispersity indices versus monomer conversion for the copolymerization of styrene and 4-hydroxythiazole styrene.

[50]. A chain coupling reaction (e.g., by a shoulder at the high molar mass side) could not be observed in the SEC traces for the kinetic study as shown in Fig. 6. The decreasing radical concentration is also affected by the higher

temperatures of 80 °C resulting in a higher decomposition rate  $k_d$  of AIBN meaning that the  $t_{1/2}$  ( $t_{1/2} = \ln 2/k_d$ ) of AIBN at 80 °C in toluene is 1.2 h ( $k_d = 1.55 \times 10^{-4}$ ), whereas the  $t_{1/2}$  of AIBN is 4.8 h at 70 °C ( $k_d = 4.0 \times 10^{-5}$ ) [51]. The linear increase of the  $M_n$  values with the conversion in combination with low polydispersity indices (PDIs) below 1.2 evidences that the RAFT polymerization of styrene and the thiazole substituted styrene proceeded in a controlled way.

Copolymer **B** has been investigated, as example, in terms of the film forming behavior. For this purpose, spin-coating experiments have been carried out using *o*-dichlorobenzene as solvent (10 mg/mL) and a rotary speed of 2000 rpm for 30 s. A film thickness of 70 nm was reached using these parameters. The absorption and emission spectra have been investigated in diluted chloroform solutions at ambient temperature unless otherwise mentioned. The thiazoles feature an intense absorption in the UV region resulting from the pyridine moiety (not shown). The absorption of the *K*-band of the phenyl substituent at the 5-position can be observed at around  $\lambda = 270$  nm. The strongest absorption can be assigned to the thiazole core. In contrast to the pyridine moiety, the substituent on the 5-position strongly influences the absorption of the core. The position of the pyridine-nitrogen slightly shifts the location of the thiazole absorption maximum which is situated at  $\lambda = 371$  and 360 nm for **1b** (*ortho*-position) and **2b** (*meta*-position), respectively, whereas the location of the emission maximum is not significantly influenced in both cases at 445 (**1b**) and 447 (**2b**) nm (Fig. 7). As depicted in Fig. 8, the film of polymer **B** revealed the same absorbance and emission behavior as the monomers and polymers, respectively. The maxima are situated at the same wavelengths  $\pm 3$  nm, which is tolerable due to the measurements errors.

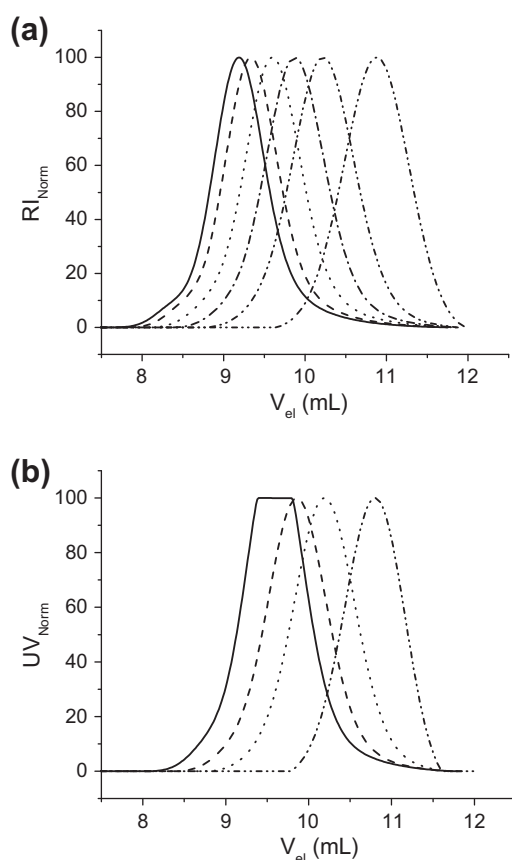
Stationary UV-vis and time correlated single photon counting measurements were performed in order to obtain absolute emission quantum yields and fluorescence lifetimes of the functionalized monomers **1b** and **2b** as well as the corresponding polymers **A** and **B** (Table 4). The quantum yields and fluorescence lifetimes (see Figs. 9

**Table 3**  
Kinetic investigations of copolymerization of styrene and thiazole-styrene (**1b**).

Sample	Time (h)	Combined conv. styrene and thiazole styrene <sup>a</sup> (%)	$M_{n,SEC}$ (RI) <sup>b</sup> (g/mol)	PDI <sub>SEC</sub> (RI) <sup>b</sup>
<b>A2-1</b>	1	6.0	1750	1.19
<b>A2-2</b>	2	12.8	3330	1.17
<b>A2-3</b>	3	16.5	4560	1.15
<b>A2-4</b>	4.5	22.6	5730	1.14
<b>A2-5</b>	7	29.3	7000	1.15
<b>A2-6</b>	10	33.8	7910	1.15

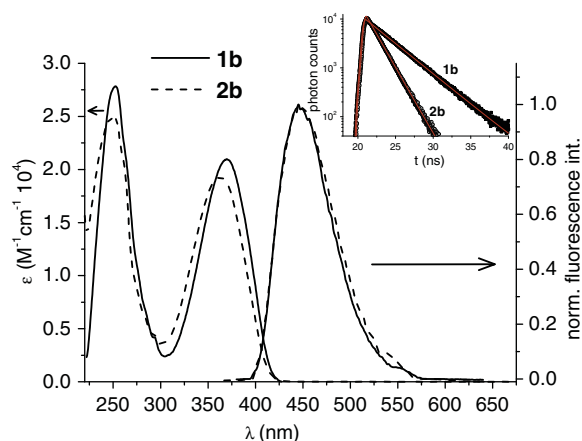
<sup>a</sup> Calculated from the vinyl signals of the <sup>1</sup>H NMR spectroscopy using anisole as internal standard.

<sup>b</sup> Calculated from SEC (CHCl<sub>3</sub>), PS calibration.

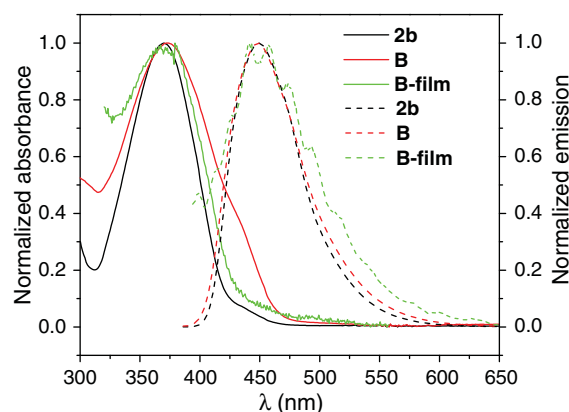


**Fig. 6.** SEC (CHCl<sub>3</sub>) traces of the kinetic analysis of poly(**1b**-stat-styrene) (**A2**) with (a) a RI and (b) a UV detector at 375 nm response (reaching the limit of the UV detector by sample **A2-4**).

and 10) are reduced in both polymers compared to the monomers. This behavior is typical for fluorescent polymers synthesized by the RAFT polymerization. This finding is related to the presence of the chain transfer agent used in the RAFT polymerization [52]. A decrease of the quantum yield and the fluorescence lifetime cannot be caused by the introduction of the alkyl-spacer unit separating the styrene and the thiazole, but by the formation of regio-



**Fig. 7.** UV-vis absorption spectra (CH<sub>3</sub>CN) as well as emission spectra of the monomers **1b** (solid line) and **2b** (dashed line); the inset shows the decay curves of the monomer **1b** (squares) and **2b** (open circles), solid lines illustrate the monoexponential fitted curves including the instrument response function.



**Fig. 8.** Comparison of absorption (solid) and emission spectra (dotted) of the monomer solution, polymer solution and polymer film of **2b** and **B**, respectively.

**Table 4**  
Fluorescence data measured in CH<sub>3</sub>CN at room temperature.

Compound	$\lambda_{abs}$ (nm) [log $\epsilon$ ]	$\lambda_{fl}$ (nm) <sup>a</sup>	Stoke-shift (cm <sup>-1</sup> ) <sup>b</sup>	$\tau$ (ns) <sup>c</sup>	$\Phi$ (%)
<b>1b</b>	253 [4.445],	445	4555	3.5	80
	370 [4.332]				
<b>2b</b>	250 [4.40],	447	5329	1.6	34
	361 [4.28]				
<b>A1</b>	253 (262 <sup>d</sup> ),	445	4555	3.2	51
	370 (380 <sup>d</sup> )				
<b>B</b>	250, 361	447	5329	1.4	18

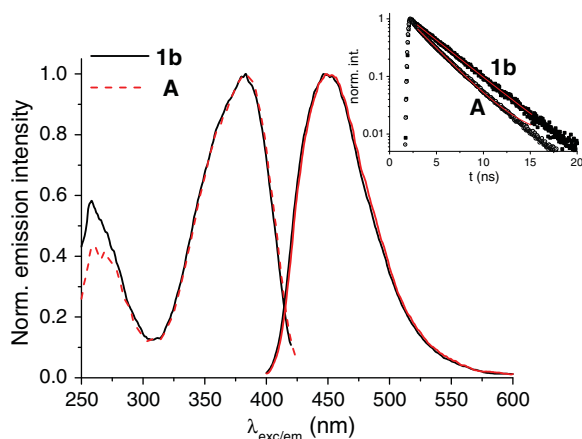
<sup>a</sup> Excitation in the absorption maximum.

<sup>b</sup> Related to the maximum of the longest wave-length absorption.

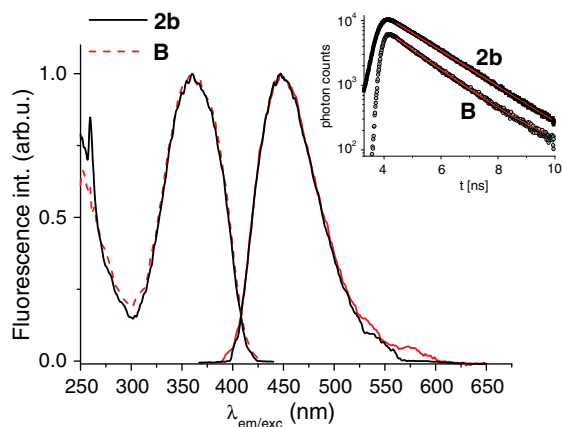
<sup>c</sup> Measured by time correlated single photon counting.

<sup>d</sup> Measured in chloroform.

somers of the pyridine substituent (*ortho*- and *meta*-position) as it is evident from a comparison of the data for the monomers **1b** and **2b** (Fig. 8). This is in agreement with previous work [36].



**Fig. 9.** Comparison of the monomer **1b** and polymer **A** emission ( $\lambda_{\text{exc}} = 380$  nm) as well as excitation spectra ( $\lambda_{\text{em}} = 447$  nm). The inset shows the fluorescence decay curve of **1b** and **A** in chloroform at 298 K.



**Fig. 10.** Comparison of the monomer **2b** and polymer **B** emission ( $\lambda_{\text{exc}} = 361$  nm) as well as excitation spectra ( $\lambda_{\text{em}} = 447$  nm). The inset shows the fluorescence decay curve of **2b** and **B** in acetonitrile at 298 K.

#### 4. Conclusion

The incorporation of thiazole functionalized styrenes into PS backbones as blue emissive chromophores was studied. For this purpose, two different polymerizable dyes were synthesized differing in the linker unit (with and without C3 spacer) which connects the chromophore to the backbone. The monomers were copolymerized with styrene in a controlled manner using the RAFT polymerization technique leading to well-defined polymers. A kinetic study supported a statistical incorporation of the thiazole units into the copolymer. The obtained polymers featured the same optical properties as the thiazoles monomers. As expected, the emission of the polymer was quenched by the dithioester or trithiocarbonate end-group, respectively, while this effect was unaffected by the introduction of a flexible C3 spacer moiety. Moreover, the polymers showed good thin film formation. Future investigations

will focus on donating the energy to other dye molecules and Ru(II) polypyridyl complexes in a FRET process.

#### Acknowledgments

The authors thank the Thuringian Ministry for Education, Science and Culture (Grant #B514-09049, Photonische Mizellen (PhotoMIC)) for financial support. B.D. acknowledges financial support by the Fonds der Chemischen Industrie. Additionally, the Dutch Polymer Institute (technology area HTE) is acknowledged for financial support.

#### References

- [1] Beija M, Charreyre MT, Martinho JMG. Dye-labelled polymer chains at specific sites: synthesis by living/controlled polymerization. *Prog Polym Sci* 2011;36(4):568–602.
- [2] Moad G, Chen M, Haeussler M, Postma A, Rizzardo E, Thang SH. Functional polymers for optoelectronic applications by RAFT polymerization. *Polym Chem* 2011;2(3):492–519.
- [3] Pietsch C, Schubert US, Hoogenboom R. Aqueous polymeric sensors based on temperature-induced polymer phase transitions and solvatochromic dyes. *Chem Commun* 2011;47(31):8750–65.
- [4] Grimsdale AC, Chan KL, Martin RE, Jokisz PG, Holmes AB. Synthesis of light-emitting conjugated polymers for applications in electroluminescent devices. *Chem Rev* 2009;109(3):897–1091.
- [5] Nuyken O, Jungermann S, Wiederhirm V, Bacher E, Meerholz K. Modern trends in organic light-emitting devices (OLEDs). *Monatsh Chem* 2006;137(7):811–24.
- [6] Shih PI, Shu CF, Tung YL, Chi Y. Efficient white-light-emitting diodes based on poly(*N*-vinylcarbazole) doped with blue fluorescent and orange phosphorescent materials. *Appl Phys Lett* 2006;88(25):251110.
- [7] Lu JJ, Li H, Yao B, Zhao B, Weng C, Lei GT, et al. Synergetic effect of efficient energy transfer and 3D  $\pi$ - $\pi$  stack for white emission based on the block copolymers containing nonconjugated spacer. *J Phys Chem B* 2009;113(13):4203–8.
- [8] Lin ZH, Lin YD, Wu CY, Chow PT, Sun CH, Chow TJ. White light-emitting devices based on star-shape polymers with a bisindolylmaleimide core. *Macromolecules* 2010;43(14):5925–31.
- [9] Lee K, Povlich LK, Kim J. Recent advances in fluorescent and colorimetric conjugated polymer-based biosensors. *Analyst* 2010;135(9):2179–89.
- [10] McQuade DT, Pullen AE, Swager TM. Conjugated polymer-based chemical sensors. *Chem Rev* 2000;100(7):2537–74.
- [11] Yang CC, Tian Y, Chen CY, Jen AKY, Chen WC. A novel benzoxazole-containing poly(*N*-isopropylacrylamide) copolymer as a multifunctional sensing material. *Macromol Rapid Commun* 2007;28(7):894–9.
- [12] Liu XZ, Zhu R, Zhang Y, Liu B, Ramakrishna S. Anionic benzothiadiazole containing polyfluorene and oligofluorene as organic sensitizers for dye-sensitized solar cells. *Chem Commun* 2008;32:3789–91.
- [13] Zhang W, Fang Z, Su MJ, Saeys M, Liu B. A triphenylamine-based conjugated polymer with donor- $\pi$ -acceptor architecture as organic sensitizer for dye-sensitized solar cells. *Macromol Rapid Commun* 2009;30(18):1533–7.
- [14] Sharma GD, Suresh P, Mikroyannidis JA. A phenylenevinylene copolymer with perylene bisimide units as organic sensitizer for dye-sensitized solar cells. *Synth Met* 2010;160(13–14):1427–32.
- [15] Friesen DA, Kajita T, Danielson E, Meyer TJ. Preparation and photophysical properties of amide-linked, polypyridylruthenium-derivatized polystyrene. *Inorg Chem* 1998;37(11):2756–62.
- [16] Sykora M, Maxwell KA, DeSimone JM, Meyer TJ. Mimicking the antenna-electron transfer properties of photosynthesis. *Proc Natl Acad Sci USA* 2000;97(14):7687–91.
- [17] Happ B, Schaefer J, Menzel R, Hager MD, Winter A, Popp J, et al. Synthesis and resonance energy transfer study on a random terpolymer containing a 2-(pyridine-2-yl)thiazole donor-type ligand and a luminescent [Ru(bpy)<sub>2</sub>(2-(triazol-4-yl)pyridine)]<sup>2+</sup> chromophore. *Macromolecules* 2011;44(16):6277–87.
- [18] Serin J, Schultze X, Adronov A, Fréchet JMJ. Synthesis and study of the absorption and luminescence properties of polymers containing



- Ru(BpyMe<sub>2</sub>)<sub>3</sub><sup>2+</sup> chromophores and coumarin laser dyes. *Macromolecules* 2002;35(14):5396–404.
- [19] Schultze X, Serin J, Adronov A, Frechet JM. Light harvesting and energy transfer in a ruthenium–coumarin-2 copolymer. *Chem Commun* 2001;13:1160–1.
- [20] Yamamoto Y, Tamaki Y, Yui T, Koike K, Ishitani O. New light-harvesting molecular systems constructed with a Ru(II) complex and a linear-shaped Re(I) oligomer. *J Am Chem Soc* 2010;132(33):11743–52.
- [21] Harriman A, Khatyr A, Ziessel R. The photophysical properties of short, linear arrays of ruthenium(II) tris(2,2'-bipyridine) complexes. *Res Chem Intermed* 2007;33(1–2):49–62.
- [22] Kim DY, Cho HN, Kim CY. Blue light emitting polymers. *Prog Polym Sci* 2000;25(8):1089–139.
- [23] Menzel R, Breul AM, Pietsch C, Schaefer J, Friebe C, Tauscher E, et al. Blue-emitting polymers based on 4-hydroxythiazoles incorporated in a methacrylate backbone. *Macromol Chem Phys* 2011;212(8):840–8.
- [24] Sommer M, Lang AS, Thelakkat M. Crystalline–crystalline donor–acceptor block copolymers. *Angew Chem Int Ed* 2008;47(41):7901–4.
- [25] Sommer M, Huttner S, Wunder S, Thelakkat M. Electron-conducting block copolymers: Morphological, optical, and electronic properties. *Adv Mater* 2008;20(13):2523–7.
- [26] Sommer M, Huttner S, Steiner U, Thelakkat M. Influence of molecular weight on the solar cell performance of double–crystalline donor–acceptor block copolymers. *Appl Phys Lett* 2009;95(18):183308.
- [27] Wang J, Tian SM, Petros RA, Napier ME, DeSimone JM. The complex role of multivalency in nanoparticles targeting the transferrin receptor for cancer therapies. *J Am Chem Soc* 2010;132(32):11306–13.
- [28] Thielbeer F, Chankeshwara SV, Bradley M. Polymerizable fluorescein derivatives: synthesis of fluorescent particles and their cellular uptake. *Biomacromolecules* 2011;12(12):4386–91.
- [29] Abd-El-Aziz AS, Shipman PO, Neeland EG, Corkery TC, Mohammed S, Harvey PD, et al. Benzo[f]- and benzo[h]coumarin-containing poly(methyl methacrylate)s and poly(methyl methacrylate)s with pendant coumarin-containing azo dyes. *Macromol Chem Phys* 2008;209(1):84–103.
- [30] Bojinov V, Grabchev I. Synthesis of new polymerizable 1,8-naphthalimide dyes containing a 2-hydroxyphenylbenzotriazole fragment. *Dyes Pigment* 2003;59(3):277–83.
- [31] Pietsch C, Vollrath A, Hoogenboom R, Schubert US. A fluorescent thermometer based on a pyrene-labeled thermoresponsive polymer. *Sensors* 2010;10(9):7979–90.
- [32] Chandrasekharan N, Ibrahim S, Kostov Y, Rao G. Ratiometric alcohol sensor based on a polymeric Nile blue. *Bioautomation* 2008;9:31–9.
- [33] Aguiar M, Karasz FE, Akcelrud L. Light-emitting polymers with pendant chromophoric groups. 1. Poly(stilbenyl-*p*-methoxystyrene). *Macromolecules* 1995;28(13):4598–602.
- [34] LifeTechnologies. The molecular probes handbook, a guide to fluorescent probes and labeling technologies. In: Johnson I, Spence MTZ, editors. 11th ed., Molecular Probes Eugene; 2010. p. 1–1076.
- [35] Grummt UW, Weiss D, Birckner E, Beckert R. Pyridylthiazoles: highly luminescent heterocyclic compounds. *J Phys Chem A* 2007;111(6):1104–10.
- [36] Dietzek B, Schaefer J, Menzel R, Weiss D, Beckert R, Popp J. Classification of novel thiazole compounds for sensitizing Ru-porphyrin complexes for artificial light harvesting. *J Lumin* 2011;131(6):1149–53.
- [37] Stippich K, Weiss D, Guether A, Goerls H, Beckert R. Novel luminescence dyes and ligands based on 4-hydroxythiazole. *J Sulfur Chem* 2009;30(2):109–18.
- [38] Chiefari J, Chong YK, Ercole F, Krstina J, Jeffery J, Le TPT, et al. Living free-radical polymerization by reversible addition–fragmentation chain transfer: the RAFT process. *Macromolecules* 1998;31(16):5559–62.
- [39] Moad G, Rizzardo E, Thang SH. Living radical polymerization by the RAFT process – a second update. *Aust J Chem* 2009;62(11):1402–72.
- [40] Pietsch C, Hoogenboom R, Schubert US. Soluble polymeric dual sensor for temperature and pH value. *Angew Chem Int Ed* 2009;48(31):5653–6.
- [41] Pietsch C, Hoogenboom R, Schubert US. PMMA based soluble polymeric temperature sensors based on UCST transition and solvatochromic dyes. *Polym Chem* 2010;1(7):1005–8.
- [42] Inglis AJ, Sinnwell S, Davis TP, Barner-Kowollik C, Stenzel MH. Reversible addition fragmentation chain transfer (RAFT) and hetero-Diels–Alder chemistry as a convenient conjugation tool for access to complex macromolecular designs. *Macromolecules* 2008;41(12):4120–6.
- [43] Weber C, Becer CR, Guenther W, Hoogenboom R, Schubert US. Dual responsive methacrylic acid and oligo(2-ethyl-2-oxazoline) containing graft copolymers. *Macromolecules* 2010;43(1):160–7.
- [44] Barner L, Davis TP, Stenzel MH, Barner-Kowollik C. Complex macromolecular architectures by reversible addition fragmentation chain transfer chemistry: theory and practice. *Macromol Rapid Commun* 2007;28(5):539–59.
- [45] Menzel R, Tauscher E, Weiss D, Beckert R, Goerls H. The combination of 4-hydroxythiazoles with azaheterocycles: efficient bidentate ligands for novel ruthenium complexes. *Z Anorg Allg Chem* 2010;636(7):1380–5.
- [46] Siebert R, Akimov D, Schmitt M, Winter A, Schubert US, Dietzek B, et al. Spectroscopic investigation of the ultrafast photoinduced dynamics in  $\pi$ -conjugated terpyridines. *ChemPhysChem* 2009;10(6):910–9.
- [47] Weiss D, Tauscher E, Beckert R, Fabian J, Assumpcao A, Goerls H. Classical heterocycles with surprising properties: the 4-hydroxy-1,3-thiazoles. *Tetrahedron Lett* 2011;52(18):2292–4.
- [48] Konkolewicz D, Siau M, Gray-Weale A, Hawke BS, Perrier S. Obtaining kinetic information from the chain-length distribution of polymers produced by RAFT. *J Phys Chem B* 2009;113(20):7086–94.
- [49] Chernikova EV, Tarasenko AV, Garina ES, Golubev VB. Controlled radical polymerization of styrene mediated by dithiobenzoates as reversible addition–fragmentation chain-transfer agents. *Polym Sci Ser A* 2006;48(10):1046–57.
- [50] Moad G, Chong YK, Mulder R, Rizzardo E, Thang San H. New features of the mechanism of RAFT polymerization. In: Matyjaszewski K, editor. *Controlled/living radical polymerization: progress in RAFT, DT, NMP & OMRP*. Washington DC: American Chemical Society; 2009. p. 3–18.
- [51] Brandrup J, Immergut EH, Grulke EA. *Polymer handbook*. 4th ed. New York: Wiley-Interscience; 1999.
- [52] Farinha JPS, Relogio P, Charreyre MT, Prazeres TJV, Martinho JMG. Understanding fluorescence quenching in polymers obtained by RAFT. *Macromolecules* 2007;40(13):4680–90.



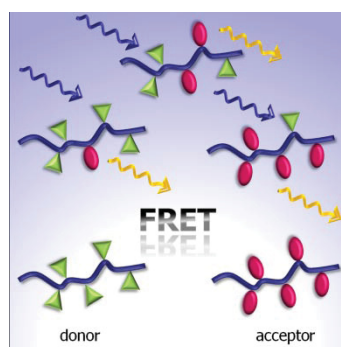
## Publication P5:

### *Förster resonance energy transfer in donor-acceptor 1,3-thiazole dyes in poly(methyl methacrylates)*

---

C. Pietsch<sup>+</sup>, J. Schäfer<sup>+</sup>, R. Menzel, R. Beckert, J. Popp, B. Dietzek,  
U. S. Schubert

*J. Polym. Sci., Part A: Polym. Chem.* **2013**, *51*, 4765–4773



<sup>+</sup> Both authors contributed equally to this paper



# Förster Resonance Energy Transfer in Poly(methyl methacrylates) Copolymers Bearing Donor–Acceptor 1,3-Thiazole Dyes

Christian Pietsch,<sup>1,2</sup> Johann Schäfer,<sup>3,4</sup> Roberto Menzel,<sup>1</sup> Rainer Beckert,<sup>1</sup>  
Jürgen Popp,<sup>2,3,4</sup> Benjamin Dietzek,<sup>2,3,4</sup> Ulrich S. Schubert<sup>1,2</sup>

<sup>1</sup>Laboratory of Organic and Macromolecular Chemistry (IOMC), Friedrich Schiller University  
Jena Humboldtstr. 10, 07743 Jena, Germany

<sup>2</sup>Jena Center for Soft Matter (JCSM), Friedrich Schiller University Jena, Philosophenweg 7, 07743 Jena, Germany

<sup>3</sup>Institute of Photonic Technology Jena e.V., Albert-Einstein-Str. 9, 07745 Jena, Germany

<sup>4</sup>Institute of Physical Chemistry (IPC) and Abbe Center of Photonics (ACP), Friedrich Schiller University Jena,  
Helmholtzweg 4, 07743 Jena, Germany

Correspondence to: B. Dietzek (E-mail: benjamin.dietzek@ipht-jena.de or ulrich.schubert@uni-jena.de)

Received 21 April 2013; accepted 24 July 2013; published online 9 September 2013

DOI: 10.1002/pola.26898

**ABSTRACT:** The Förster resonance energy transfer (FRET) properties in poly(methyl methacrylate) copolymers containing 2-(pyridine-2-yl) thiazole dyes were studied upon systematic variation of the donor-to-acceptor ratio. To this end, 2-(pyridine-2-yl) thiazole dyes specially designed for the usage as energy donor and acceptor molecules were incorporated within one polymer chain. Poly(methyl methacrylate) copolymers containing these donor and acceptor dyes were synthesized using the RAFT polymerization method. Copolymers with a molar mass ( $M_n$ ) of nearly 10,000 g/mol were achieved with dispersity index values ( $\mathcal{D}$ ) under 1.3. The presented copolymers act as a

model system for the FRET investigation. Förster resonance energy transfer properties of the copolymers are characterized by steady state as well as time resolved fluorescence spectroscopy. The results indicate that the energy transfer rates and the transfer efficiencies are tunable by variation of the donor-acceptor-ratio. © 2013 Wiley Periodicals, Inc. *J. Polym. Sci., Part A: Polym. Chem.* **2013**, *51*, 4765–4773

**KEYWORDS:** donor-acceptor systems; fluorescence; photophysics; FRET; reversible addition-fragmentation chain transfer (RAFT); thiazoles

**INTRODUCTION** The use of alternative energy sources has become an important research topic as conventional organic fuels are to decline and global warming due to the greenhouse effect becomes increasingly recognized. A key aspect to prevent both global warming and the long-term lack of fuels is the conversion of sunlight into electrical and chemical energy. The importance of this aspect is reflected in numerous recent technical developments from applications of solar cells to photocatalytic devices.<sup>1–7</sup> In particular photosynthetic systems that emerged in plants and algae over millions of years are of interest in this context. Light harvesting has been perfected by evolution to a point, which is not reached until now by artificial systems. Artificial photosynthetic systems are designed to mimic natural photosynthetic systems in that they are made of light-harvesting units, a photoactive center and a catalytic center.<sup>5,7–9</sup>

Hence, artificial light-harvesting systems based on polymeric and dendritic structures mimicking natural light-harvesting

systems have been designed and characterized.<sup>10–20</sup> Most design strategies aim to incorporating monomeric units into supramolecular assemblies with—ideally—only minor impact on the electronic properties of the monomers. Here, the dipole approximation of coulombic coupling between the monomeric units can be used to describe the donor-acceptor couplings, assuming temporally localized excitation within the supramolecular assembly. In order to allow for optimal energy transfer the spectral overlap of the donor emission with the acceptor absorption has to be optimized, the transition dipoles of donor and acceptor units should be aligned and the donor emission quantum yield must be high.<sup>21</sup> No interactions between donor and acceptor should exist, which induce changes in the emission and absorption line shape of the monomeric units, for example, inhomogeneous line broadening as well as coherent energy transfer dynamics.<sup>22</sup> These requirements can be met in nonconjugated polymers, which are accessible by multiple synthetic routes offering

Christian Pietsch and Johann Schäfer contributed equally to this work.  
Additional Supporting Information may be found in the online version of this article.

© 2013 Wiley Periodicals, Inc.

**TABLE 1** Overview of the Selected Reaction Conditions used for the Copolymerizations of MMA with **MD** and **MA**

Entry	Feed ratio [MMA]:[MD]:[MA]	$M_{n, SEC}$ g/mol <sup>a</sup>	$D^a$	DP (SEC)	$M_{n, SEC}$ g/mol <sup>b</sup>	$D^b$	Ratio <sup>1</sup> NMR % [MMA]:[MD]:[MA] <sup>c</sup>	Abs. units [MMA]:[MD]:[MA] <sup>d</sup>
<b>PD</b>	95:5:0	7,000	1.21	57	N/A	N/A	92.1:7.9:0	52:5:0
<b>PDA1</b>	94:5:1	10,600	1.20	76	8,900	1.18	87.7:10.8:1.5	67:8:1
<b>PDA2</b>	94:3:3	11,100	1.26	87	9,100	1.25	91.8:4.7:3.5	80:4:3
<b>PDA3</b>	94:1:5	12,400	1.26	102	9,800	1.30	83.6:1.6:4.8	95:2:5
<b>PA</b>	95:0:5	7,100	1.22	58	N/A	N/A	93.2:0:6.8	54:0:4

<sup>a</sup> Calculated from SEC (DMAc) using PMMA calibration.<sup>b</sup> Calculated from SEC (CHCl<sub>3</sub>) using PMMA calibration.<sup>c</sup> Calculated from integrated areas of (CH<sub>3</sub>)<sub>2</sub>N- signals the ester CH<sub>2</sub>-O-, and the CH<sub>3</sub>- side-group signals.<sup>d</sup> Rounded values.

the possibility of synthesizing a wide range of light-harvesting polymers.<sup>23–30</sup> A powerful polymerization technique in this context is the reversible addition-fragmentation chain-transfer polymerization (RAFT), which can be used for the construction of donor-acceptor copolymers with defined length and ratio of them.<sup>31–33</sup>

In this contribution FRET in novel 1,3-thiazole based donor-acceptor copolymers is discussed. In the copolymers at hand the excitation band of the acceptor molecules is expanded, making the polymers attractive to be used as light harvesting energy donors, for example, for ruthenium dyes.<sup>29</sup> Polymers with high photostability shall improve the overall performance of photocatalytic systems. Furthermore, applications of this system in dye sensitized solar cells as well as organic light-emitting diodes are conceivable or the use in biochemistry/medicine for FRET-microscopy for imaging of cell components.<sup>34,35</sup> The here presented copolymers act as a model system for FRET investigation. It is shown how the energy transfer efficiency is affected by the donor-acceptor-ratio.

## EXPERIMENTAL

### Materials

Methyl methacrylate (MMA) was purchased from Sigma-Aldrich and purified by stirring in the presence of an inhibitor-remover for hydroquinone or hydroquinone monomethyl ether (Aldrich) for 30 min before use. The initiator 2,2'-azobis(iso-butyronitrile) (AIBN) was recrystallized from methanol before use; 2-cyano-2-propyl dithiobenzoate (CPDB) chain transfer agent (CTA) was purchased from Sigma-Aldrich. The donor monomer 2-(pyridine-2-yl)-1,3-thiazole **MD**<sup>29</sup> and the acceptor monomer ((4-dimethylamino)phenyl)-2-(pyridine-2-yl)-1,3-thiazol **MA**<sup>36</sup> were synthesized according to literature. All analytical grade solvents were purchased from Sigma-Aldrich or Merck KGaA.

### General RAFT Polymerization Procedure

In a typical polymerization experiment, 282 mg of MMA ( $2.8 \times 10^{-3}$  mol), 57.1 mg of **MD** monomer ( $0.15 \times 10^{-3}$  mol) and 12.7 mg of **MA** monomer ( $0.03 \times 10^{-3}$  mol), 1.23 mg of AIBN initiator ( $8.0 \times 10^{-6}$  mol), 6.64 mg of CPDB (used as a CTA) RAFT agent ( $3.0 \times 10^{-5}$  mol), and toluene were

mixed together in a 10 mL glass vial as follows: MMA monomer, toluene followed by individual stock solutions of AIBN (initiator), and CPDB dissolved in toluene. The ratio between [CTA] and [AIBN] was 1:0.25 at a total monomer concentration of 2.0 mol/L. Before closing the vial, the reaction solutions were degassed by sparging argon for at least 30 min before use. Subsequently, the reaction was performed in an oil bath at 70 °C for 13 h. After the polymerization, acetone was added to the final mixtures, and the polymers were then precipitated into cold methanol. The utilized reaction conditions and [M]/[CTA] ratios are summarize in Table 1.

### Instrumentation

Size-exclusion chromatography (SEC) was performed on an Agilent1200 series system equipped with a G1310A pump, a G1362A refractive index and DAD G1315D detector and both a PSS Gram30 and a PSS Gram1000 column in series, whereby *N,N*-dimethyl-acetamide (DMAc) with 5 mmol lithium chloride was used as an eluent at 1 mL min<sup>-1</sup> flow rate and the column oven was set to 40 °C. The system was calibrated with poly(methyl methacrylate) standards. Further SEC experiments were performed on a Shimadzu system equipped with a SCL-10A system controller, a LC-10AD pump, a RID-10A refractive index detector, a UVD SPD-10AD UV/Vis detector and a PSS SDV linear S, 5 μm column (8 mm × 300 mm) with chloroform:triethylamine:2-propanol (94:4:2) as eluent and the column oven was set to 40 °C. A calibration with low polydispersity polymethylmethacrylate standards was used. Proton nuclear magnetic resonance (<sup>1</sup>H NMR) spectra were recorded on a Bruker AC 300 (300 MHz) spectrometer at 298 K. The chemical shifts are reported in parts per million (ppm, δ scale) relative to the signals of the NMR solvents.

The steady-state absorption spectra were recorded using a UV/Vis-NIR-spectrometer Varian Cary 5000. Molar extinction coefficients (ε) were obtained by measuring steady-state absorption of solutions in a 1 × 1 cm quartz glass sample cell. The concentration was kept below  $2.5 \times 10^{-5}$  mol L<sup>-1</sup>. Molar extinction coefficients were calculated from the arithmetic mean value of three measurements. Emission quantum yields (Φ<sub>F</sub>) in solution were measured on a LS50

**TABLE 2** Absorption and emission wavelengths ( $\lambda_{\text{abs}}$ ,  $\lambda_{\text{em}}$ ), Stokes shift ( $\nu$ ), fluorescence quantum yield ( $\Phi_F$ ), lifetime ( $\tau$ ), fluorescence rates ( $k_{\text{fl}}$ ), and nonradiative rates ( $k_{\text{nr}}$ ) obtained in chloroform at room temperature

Sample	[MMA]:[MD]:[MA]	$\lambda_{\text{abs}}/\text{nm}$ [log $\epsilon$ ]	$\lambda_{\text{em}}/\text{nm}$	$\nu$ ( $\text{cm}^{-1}$ )	$\Phi_F$	$\tau/\text{ns}^a$	$k_{\text{fl}}/\text{ns}^{-1b}$	$k_{\text{nr}}/\text{ns}^{-1c}$
	calc. rep. units							
<b>MD</b>	–	376 [4.346], 272 [3.955]	449	4,324	0.81	3.42	0.24	0.22
<b>MA</b>	–	416 [4.280], 281 [4.122]	526	4,969	0.61	3.52	0.17	0.24
<b>PD</b>	52.7: 4.5: –	376 [4.904], 274 [4.573]	448	4,274	0.60	2.78	0.22	0.28
<b>PDA1</b>	66.9: 8.2:1.1	377	449	4,253	0.46 <sup>d</sup>	2.42	–	–
<b>PDA2</b>	80.1: 4.1:3.1	386	525	6,859	–	1.86	–	–
<b>PDA3</b>	95.1: 1.6:4.9	408	526	5,498	–	1.64	–	–
<b>PA</b>	54.1: –:4.0	417 [4.819], 276 [5.535]	527	5,005	0.39	2.91	0.13	0.30

<sup>a</sup> For all of the polymers the mean lifetime  $\bar{\tau} = \sum f_i \tau_i$  is given instead of  $\tau$ , with  $f_i$  the fractional contribution of each decay component  $f_i = \alpha_i \tau_i / \sum_{j=1}^N \alpha_j \tau_j$ ,  $\alpha$  denotes the pre-exponential factor.

<sup>b</sup> Computed as  $\Phi_F/\tau$ .

<sup>c</sup>  $k_{\text{nr}} = (1 - \Phi)/\tau$ .

<sup>d</sup> Measured upon excitation at 376 nm.

PerkinElmer fluorescence spectrometer by comparing the corrected emission intensities of the compounds with the fluorescence intensity of the standard quinine sulphate in 0.1 M sulfuric acid ( $\Phi_F = 55\%$ ). The excitation wavelength was set to the most red-shifted absorption maximum of the donor molecule, and the extinction maximum was kept below 0.05. A spectro-fluorometer Jasco FP 6200 was used for measuring emission spectra. The chloroform used as solvent in spectroscopic measurements (ROTISOLV<sup>®</sup>  $\geq 99.8\%$ , UV/IR-Grade) was of spectroscopic grade.

From the spectra of donor and acceptor monomers of the classical Förster distance ( $R_0$ ) can be calculated to

$$R_0 = 0.211 \cdot (\kappa^2 n^{-4} Q_D J(\lambda))^{1/6} \quad (1)$$

Here, the orientation factor  $\kappa^2$  was set to 2/3, the refractive index  $n$  of chloroform was  $n = 1.445$  and  $Q_D$  is the emission quantum yield of the donor monomer.  $J(\lambda)$  is the overlap integral (see eq 2), while  $F_D(\lambda)$  refers to the donor emission and  $\epsilon_A(\lambda)$  for the molar acceptor absorption spectrum, the wavelength  $\lambda$  is measured in nanometer.<sup>21</sup>

$$J(\lambda) = \frac{\int_0^\infty F_D(\lambda) \epsilon_A(\lambda) \lambda^4 d\lambda}{\int_0^\infty F_D(\lambda) d\lambda} \quad (2)$$

### Time Correlated Single Photon Counting

Fluorescence lifetime measurements were performed with a streak camera in the time correlated single photon counting (TCSPC) mode. The emitted light was focused on the entrance slit of a Chromex 250IS imaging spectrograph and imaged to the streak scope C4334 (Hamamatsu) triggered by the C4792-01 unit. The sample was excited by a train of sub-picosecond pulses delivered by a Ti-sapphire laser (Tsunami, Newport Spectra-Physics GmbH). The fundamental of the Ti-sapphire output was frequency doubled in order to obtain pulses with a center wavelength of 375 nm. The repetition rate of the laser was adjusted to 0.4 MHz by a pulse selector (model 3980, Newport Spectra-Physics GmbH). All measurements were performed under magic angle configura-

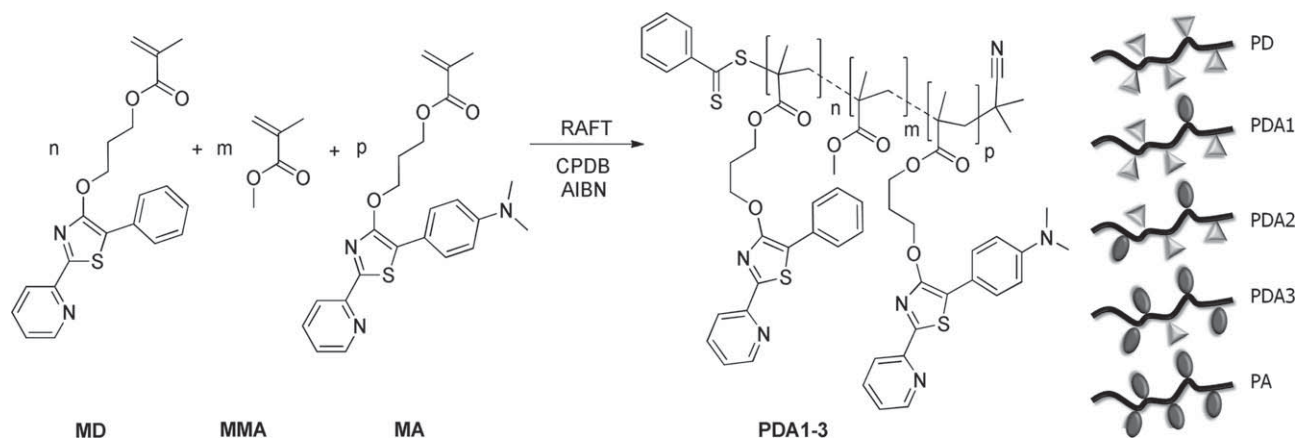
tion, that is, in perpendicular excitation emission geometry a Glan-Thompson polarizer was placed in the detection channel under 55° with respect to the polarization direction of the excitation pulses.

### RESULTS AND DISCUSSIONS

A series of five statistical donor-acceptor copolymers based on a PMMA was synthesized using RAFT polymerization. Within this series the donor-acceptor-ratio was varied (Scheme 1) starting from the donor copolymer (**PD**) followed by an increasing amount of acceptor (**PDA1-3**) ending by the acceptor copolymer (**PA**). The thiazole donor (**MD**) and acceptor monomers (**MA**) were explicitly synthesized to construct donor-acceptor systems (on flexible side-groups) along a polymer chain (Scheme 1). In doing so the thiazole structure of **MD** was expanded with an electron donating dimethylamino group at the phenyl ring in order to increase the charge transfer character (the pyridine acts as the electron acceptor) of the longest-wavelength  $\pi$ - $\pi^*$  transition. This induces a red shift of both the absorption and emission. The monomer **MA** exhibits a bathochromically shifted absorption (416 nm,  $\Delta = 40$  nm ( $2560$   $\text{cm}^{-1}$ )) and emission spectra (526 nm,  $\Delta = 77$  nm ( $3260$   $\text{cm}^{-1}$ )) together with a reduced quantum yield ( $\Phi_F = 61\%$ ) compared with **MD** in chloroform (compare Table 2).

The polymerizations were carried out using 2-cyano-2-propyl dithiobenzoate (CPDB) as CTA and AIBN as radical initiator (see Scheme 1) by applying similar conditions as previously described for the MMA thiazole copolymerization.<sup>25</sup>

The polymerizations of the monomers were performed in toluene with a monomer concentration of 2.0 mol L<sup>-1</sup>. The molar masses and dispersity indices ( $D$ ) measured by SEC are summarized in Table 1, demonstrating good control over the copolymer characteristics (Fig. 1). The monomer conversions of the MMA units were estimated by <sup>1</sup>H NMR spectroscopy via the signals of the protons of the corresponding double bonds. The conversion of all MMA units was around 65 to 80% after 13 h of polymerization time. After the



**FIGURE 1** Left: schematic representation of the RAFT polymerization of MMA with **MD** and **MA** using the CTA CPDB and the radical initiator AIBN. Right: illustration of the functionalized donor-acceptor copolymers **PD**, **PDA1-3** and **PA** (triangle = donor, cycle = acceptor).

polymerization the copolymers were precipitated three times into cold methanol to remove the unpolymerized monomers. For the finally derived copolymers, donor-acceptor-ratios were determined by  $^1\text{H}$  NMR spectroscopy using the integrated areas of the proton signals of the dimethylamino group ( $(\text{CH}_3)_2\text{N}$ - of **MA** at 3.0 ppm) and of the  $\text{CH}_2\text{-O}$ - signals of both dyes at 4.2 and 4.6 ppm (see Supporting Information). The observed ratios are in a good agreement with the monomer feed ratio.

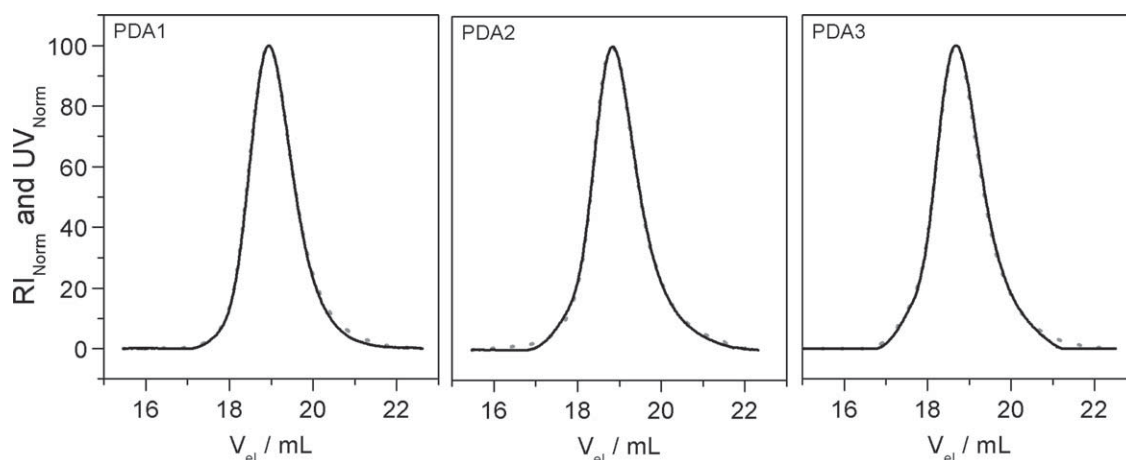
Concerning the absorption and emission spectra of the synthesized dyes it is possible to judge the quality of the donor-acceptor pair. From the steady state spectra the Förster distance was calculated: The emission spectrum of **MD** shows a distinct overlap with the absorption of **MA** (Fig. 2) and the overlap integral for FRET (eq 2) was calculated to  $J = 3.39 \times 10^{14} \text{ M}^{-1} \text{ cm}^{-1} \text{ nm}^4$ . For instance, this value exceeds overlap integrals, of poly(phenylene-vinylenes) regarding homo energy transfer within a polymer chain ( $J = 0.38$  to  $1.33 \times 10^{14} \text{ M}^{-1} \text{ cm}^{-1} \text{ nm}^4$ ).<sup>17</sup> Increasing the overlap

integral is important for an improved energy transfer rate  $k_{\text{FRET}}$  (eq 3), which is proportional to  $J(\lambda)$  (eq 2).

$$k_{\text{FRET}} = \frac{1}{\tau_D} \left( \frac{R_0}{R} \right)^6 \quad (3)$$

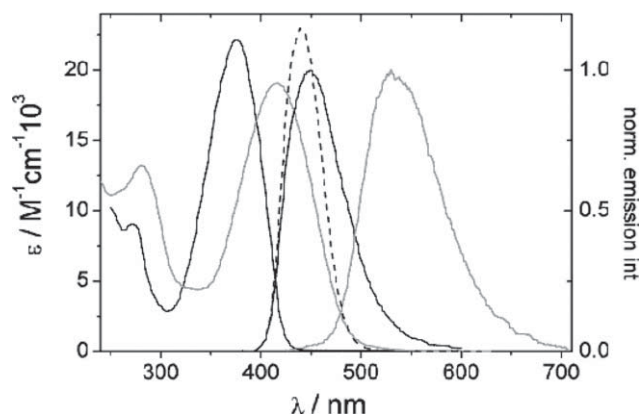
As a consequence of the large overlap the Förster distance  $R_0 = 39 \text{ \AA}$  also exceeds the Förster distances calculated for homo energy transfer in poly(phenylene-vinylenes) by more than  $10 \text{ \AA}$  (assuming a statistical orientation between donor and acceptor transition dipoles) and lies in the range of Förster distances calculated for blue emitting thiazoles.<sup>21</sup>

Upon energy transfer from **MD** (or **PD**) to **MA** (or **PA**) energy is lost due to nonradiative transfer of energy and relaxation processes (Table 2). This leads to a reduced overall emission quantum yield of **PDA1-3** compared with a system consisting of **MD** or **PD** alone. Hence, it is comprehensible that the overall emission quantum yield  $\Phi_F = 46\%$  of **PDA 1** (upon excitation at 376 nm) is reduced compared



**FIGURE 2** SEC traces of the synthesized donor-acceptor copolymers (**PDA1-3**) using a RI (solid black) and an UV detector ( $\lambda = 390 \text{ nm}$ , dotted grey).





**FIGURE 3** Absorption and emission spectra of **MD** (black lines) and **MA** (grey lines) in chloroform at room temperature. The dashed line represents the normalized integrand of the overlap integral for calculating the Förster distance.

with  $\Phi_F = 60\%$  for **PD** (see Table 2). Assuming no energy transfer in **PDA 1**, a quantum yield close to the value obtained for **PD** would be expected as—upon excitation at 376 nm—approximately 92% of the absorbance in **PDA 1** stem from donor units.<sup>37</sup> However, the measurements yield a value comparable to the quantum yield of **PA** ( $\Phi_F = 39\%$ ), indicating energy transfer in **PDA 1**.

Aside from the investigation of energy transfer it is important to know how polymerization affects the absorption and emission properties of the individual dyes. Upon polymerization of **MD** and **MA** to **PD** and **PA** no shift in the absorption and emission wavelengths is induced (Table 2, Figs. 3 and 4). However, the emission quantum yield and the mean lifetime of the chromophores is decreased, when connected to the polymer chain (Table 2). One possible deactivation pathways is opened by the RAFT-polymerization due to quenching by the dithiobenzoate (chain transfer agent) end-group or by self-quenching of the fluorophores.<sup>38</sup>

The influence of the polymerization on the chromophores is analyzed more in detail by monitoring the decay of their excited state. Here, a slight deviation from a mono-exponential fluorescence decay is observed and a further exponential is necessary to adequately fit the fluorescence traces from **PD** and **PA** (Table 4, see also Supporting Information). This indicates an additional rate constant, which accounts, for example, for exciplex formation of the thiazole with the dithiobenzoate end group. Similar effects have been reported for a coumarin dye embedded in a polymer.<sup>38</sup> Sometimes it is useful to characterize the fluorescence decay not only using exponential functions with discrete rate constants but with stretched exponential functions of the type of eq 4. For example, stretched exponential functions were used for measurements of Förster distance of dyes covalently bound to polymers.<sup>39</sup>

$$I(t) = I_0 \exp[-(t/\tau)^\beta] \quad (0 \leq \beta \leq 1) \quad (4)$$

Here, the parameter  $\beta$  reflects the extent of the deviation from a mono-exponential decay function. Data fitting using

eq 4 was applied to the fluorescence decay of **MD**, **MA**, and to the polymers **PD** and **PA** in order to account for discrete or non-discrete deactivation rates (Table 3). For the polymer fluorescence the parameter  $\beta$  is reduced compared with the monomers (Table 3). Thus, for the copolymers the fluorescence decay deviates stronger from a mono-exponential compared with the monomers. For **MD**  $\beta$  is 0.962, that is, the fluorescence decay nearly follows a mono-exponential decay. Copolymer **PA** exhibits the largest deviation from a mono-exponential decay ( $\beta = 0.814$ ) suggesting that in **PA** the acceptor fluorescence is more prone to be disturbed by environmental changes compared with the donor emission in **PD**. From the fit parameter  $\tau$  and  $\beta$  a mean lifetime  $\langle \tau \rangle$  can be calculated according to

$$\langle \tau \rangle = \frac{\tau}{\beta} \Gamma\left(\frac{1}{\beta}\right) \quad (5)$$

where  $\Gamma$  denotes the gamma function. The mean lifetimes  $\langle \tau \rangle$  are comparable to the mean experimental lifetimes  $\tau_{\text{exp}}$  obtained using exponential functions for curve fitting (Table 3). However  $\langle \tau \rangle$  is always shorter than  $\tau_{\text{exp}}$ . The original data together with the fitting curves and the weighted residuals are available in the Supporting Information.

After having detailed the fluorescence kinetics of monomers and the donor and acceptor polymers, **PD** and **PA**, respectively, now the investigation of the donor fluorescence in donor-acceptor polymers **PDA 1-3** is presented.

The distances between the chromophores within the copolymer chain is changed in the copolymer series **PDA 1-3** by variation of the amount of donor to acceptor chromophores. The series **PDA 1-3** have statistically distributed donor and acceptor molecules with calculated donor-acceptor-ratios of 8.2/1.1, 4.1/3.1 and 1.6/4.9, respectively (see Table 1). This leads to three cases of donor-acceptor copolymers: (i) donor-dominated copolymer, (ii) acceptor-dominated copolymer, (iii) a copolymer with a balanced donor-acceptor-ratio. This general classification is experimentally derivable from steady-state absorption and emission spectra (Fig. 5). The spectra resemble the spectra of either the donor or the acceptor depending on the donor-acceptor-ratio, that is, the absorption spectra of **PDA 1-3** can be considered as linear combinations of the spectra from **PD** and **PA** (Fig. 4). When the contribution of each compound to the spectra is known, it is possible to determine energy transfer efficiencies in **PDA 1-3**, as detailed in the Supporting Information. Briefly, it is assumed that the absorbance of the donor-acceptor copolymers is a linear combination of the absorbance of **PD**

**TABLE 3** Comparison of Stretched Exponential Fitting Results with Exponential Fit

Entry	$\tau/\text{ns}$	$\beta$	$\tau > / \text{ns}$	$\tau_{\text{exp}}/\text{ns}$
<b>MD</b>	3.22	0.962	3.28	3.42
<b>MA</b>	3.14	0.919	3.27	3.52
<b>PD</b>	2.40	0.899	2.53	2.78
<b>PA</b>	2.13	0.814	2.38	2.91

**TABLE 4** Data of Energy Transfer Analysis: Donor-Acceptor-MMA-Ratio [MMA]:[MD]:[MA], Lifetime  $\tau$ , Energy Transfer Efficiency  $E$ , Average Transfer Rate per Donor Chromophore  $k_{\text{FRET}}$ 

Sample	[MMA]:[MD]:[MA]	$\tau/\text{ns}$ ( $f_i$ ) <sup>a</sup>	$E$ (%) <sup>b</sup>	$k_{\text{FRET}}/\text{ns}^{-1\text{c}}$	$k_{\text{FRET}}\cdot[\text{MD}]/\text{ns}^{-1}$	$k_{\text{FRET}}\cdot[\text{MD}]:[\text{MA}]/\text{ns}^{-1}$
<b>PD</b>	52.7: 4.5: –	3.055 (0.87), 1.574 (0.13)	–	–	–	–
<b>PA</b>	54.1: –:4.0	3.101 (0.92), 0.854 (0.08)	–	–	–	–
<b>PDA1</b>	66.9: 8.2:1.1	2.561 (0.94), 0.315 (0.06)	35 (50)	0.19 (0.36)	1.56 (2.95)	1.42 (2.68)
<b>PDA2</b>	80.1: 4.1:3.1	2.359 (0.74), 0.506 (0.21), 0.065 (0.04)	74 (76)	1.02 (1.14)	4.18 (4.67)	1.35 (1.51)
<b>PDA3</b>	95.1: 1.6:4.9	2.301 (0.64), 0.615 (0.23), 0.188 (0.09),0.026 (0.04)	87 (85)	2.40 (2.04)	3.84 (3.26)	0.78 (0.67)

$k_{\text{FRET}}\cdot[\text{MD}]$  ( $[\text{MD}]/[\text{MA}]$  is the number of donor/acceptor molecules in a polymer) is a measure for the overall energy transfer rate to acceptors in a polymer chain.  $k_{\text{FRET}}\cdot[\text{MD}]:[\text{MA}]$  is a measure for the energy transfer rate to an individual acceptor molecule in the polymer.

<sup>a</sup> In brackets the fractional contribution of each decay component  $f_i = \alpha_i \tau_i / \sum_{j=1}^N \alpha_j \tau_j$  is given, the  $\alpha$ 's denote the pre-exponential factors.

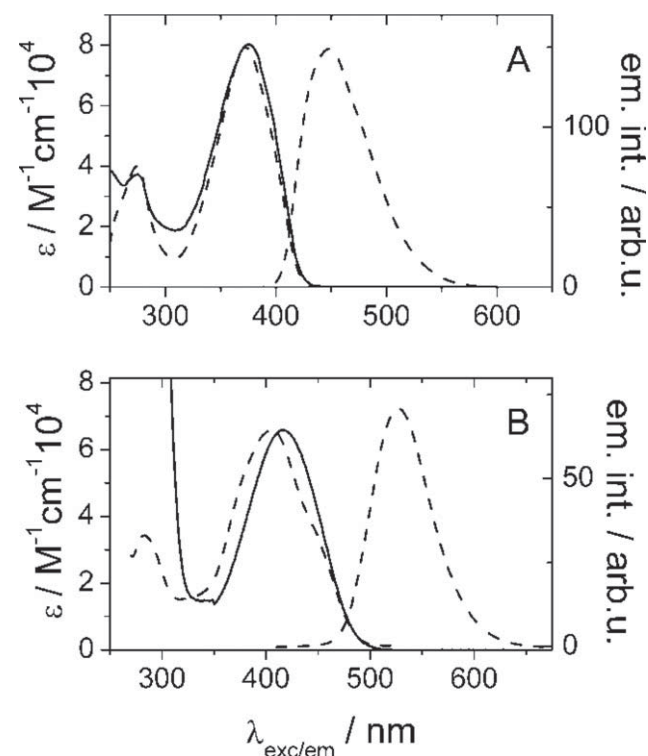
<sup>b</sup> Transfer efficiency  $E$  was calculated by  $E = 1 - \frac{\int I_{\text{DA}}(t) dt}{\int I_{\text{D}}(t) dt}$ , with  $I(t) = \sum \alpha_i \tau_i$  the  $\alpha$ 's are normalized to unity. Transfer efficiencies calculated from

the analysis of steady state spectra (see Supporting Information) are put in brackets.

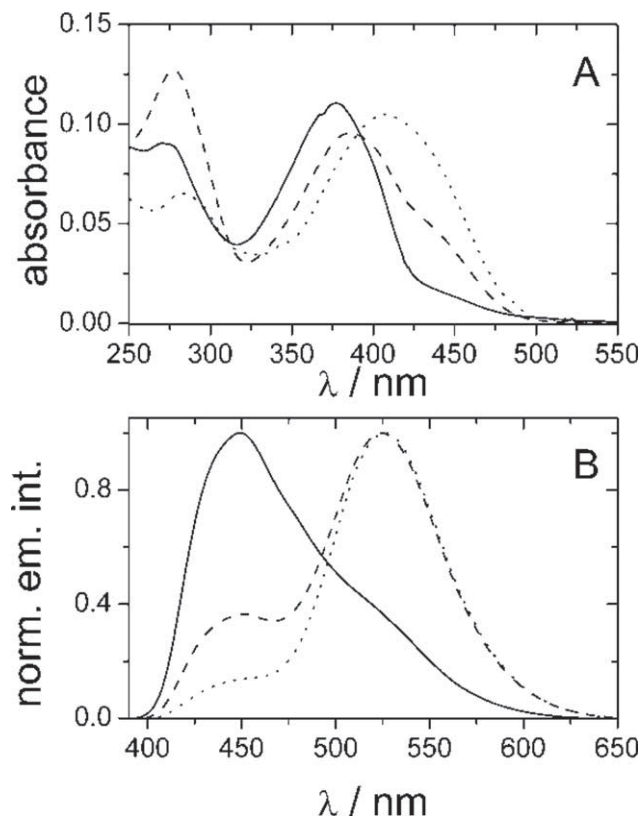
<sup>c</sup> The transfer rate  $k_{\text{FRET}}$  is determined by using the calculated transfer efficiency  $E$  and the mean lifetime  $\tau_{\text{D}}$  of the donor reference **PD**:  $k_{\text{FRET}} = \frac{E}{E-1} \cdot \frac{1}{\tau_{\text{D}}}$ . In brackets the calculated transfer rate is given using results from steady state measurements.

and **PA**. To determine the contributions of donor and acceptor units to the absorption spectra of **PDA 1-3** a non-negative constraint least square fit was used. From the

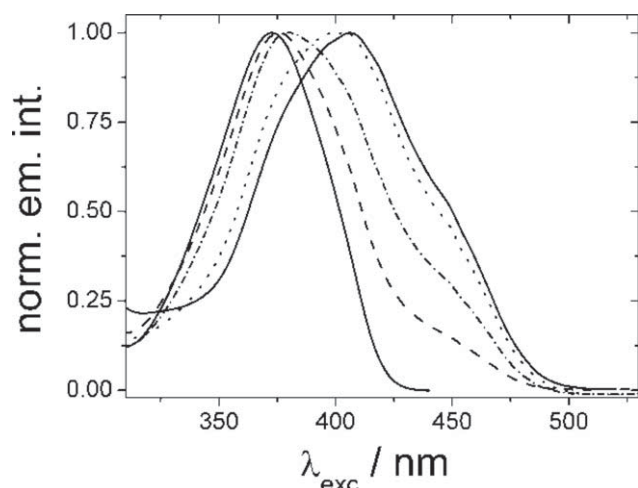
results the percentage of the donor molecules to the overall absorbance of the donor-acceptor copolymer and the transfer efficiencies (shown in Table 4) are calculated.<sup>29</sup>



**FIGURE 4** Absorption spectra (solid line), excitation and emission spectra (dashed line) measured in chloroform at room temperature. (A) For **PD**, the emission (excitation) wavelength was set to  $\lambda_{\text{Ex}} = 376$  nm ( $\lambda_{\text{Em}} = 455$  nm). (B) For **PA** the excitation wavelength was  $\lambda_{\text{Ex}} = 400$  nm, emission wavelength  $\lambda_{\text{Em}} = 530$  nm.



**FIGURE 5** Absorption spectra (A) and normalized emission spectra (B) of **PDA1** (solid line), **PDA2** (dashed line) and **PDA3** (dotted lines) measured in chloroform at room temperature. The excitation wavelength was  $\lambda_{\text{Ex}} = 376$  nm.



**FIGURE 6** Excitation spectra of donor and acceptor copolymers **PD** and **PA** (solid) and of the donor-acceptor polymers **PDA1** (dashed), **PDA2** (dashed-dotted) and **PDA3** (dotted) recorded by monitoring the emission at 450 nm for **PD**, 525 nm for **PA**, and 592 nm for **PDA1**, **PDA2**, and **PDA3** in chloroform at room temperature.

The focus of the discussion is now shifted to consider FRET in these polymers. In this context, we shall start with a qualitative discussion, which is based on an inspection of the fluorescence excitation spectra of the acceptor emission (Fig. 5).

The excitation spectrum of **PDA 1** (see Fig. 6) resembles that of **PD** reflecting the majority of donor molecules in the polymer, that is, the acceptor is excited mainly by the donor molecules. The spectra of **PDA 2** differs from the fluorescence excitation spectrum of **PDA 1** in that the shoulder at about 440 nm is more pronounced in the latter case. For **PDA 3** only a marginal contribution from the excitation through donor molecules is apparent, as visible by a slight blue shift and a broadening of the excitation spectrum compared with **PA**. This does not imply that no donor-acceptor energy migration takes place, but rather that direct excitation of acceptor molecules dominates over energy transfer. For **PDA2** both donor and acceptor contribute to the fluorescence excitation spectrum.

Transfer efficiencies are determined by eq 6 using the experimental donor fluorescence intensities of **PDA 1-3** and of the donor reference system **PD**. The parameter  $I_{DA}$  and  $I_D$  (see Supporting Information and Fig. 4) represent the intensities of the donor fluorescence in the donor-acceptor copolymers (**PDA 1-3**) and the donor reference system (**PD**), respectively.

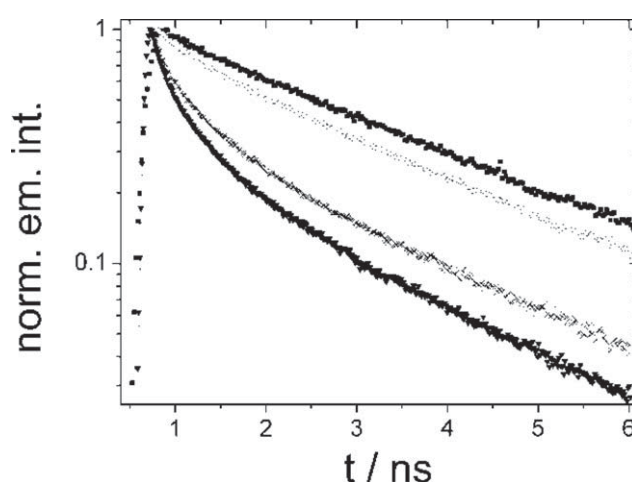
$$E = 1 - \frac{I_{DA}}{I_D} = 1 - \frac{\int I_{DA}(t) dt}{\int I_D(t) dt} \quad (6)$$

Time-resolved measurements as well as steady state measurements were performed in order to determine transfer efficiencies and transfer rates. In doing so, only the donor fluorescence was analyzed. The acceptor fluorescence is not

taken into account for determining the transfer efficiency from excitation spectra.<sup>40</sup> This is done as the donor fluorescence spectrally overlaps with the acceptor fluorescence thereby obscuring the transfer efficiency value. Accordingly, the normalized fluorescence decay traces of the excited donor in **PD** and **PDA 1-3** were analyzed (Figs. 6 and 7).

The emissions traces of the donor-acceptor polymers show a faster decay than that of the donor polymer **PD**. Furthermore, the emission decay in the series **PDA 1-3** is accelerated upon reducing the donor-acceptor-ratio. This indicates a more efficient quenching of the donor molecules if more acceptors are present. This argument is based on the assumption that the polymers **PDA 1-3** occupy the same spatial volume although the degrees of polymerization are not exactly identical (see Table 2). The donor mean lifetime of **PDA 1** (2.42 ns) almost equals that of **PD** (2.78 ns) (see also Table 2). This approach to the lifetime of the reference system **PD** for large donor-acceptor-ratios justifies the usage of **PD** as reference, because it verifies eq 6: that is, the transfer efficiency approaches zero for large donor-acceptor-ratios. Therefore energy transfer efficiencies for **PDA 1-3** were calculated in reference to the fluorescence intensity of **PD** (Table 4). The transfer efficiency increases from 0.35 to 0.74 and 0.87 for **PDA1**, **PDA2** and **PDA3**, respectively.

Noteworthy, the complexity of the donor-emission decay in **PDA 1-3** depends on the donor-acceptor-ratio. When the donor molecules are surrounded by more acceptors more exponentials are necessary in order to fit/to account for the experimental data (Table 4). The donor decay of **PDA 3** is described adequately by a fit using four exponentials. This indicates that a lifetime-distribution should be favored in describing the data as compared with a sum of discrete rates.<sup>41</sup> The distribution of lifetimes is physically based on different distances between donor and acceptor molecules



**FIGURE 7** Normalized photon counting decay traces of the donor fluorescence of **PD** (filled squares—topmost curve), **PDA 1** (open circles—second curve from top), **PDA 2** (crosses), and **PDA 3** (filled triangles—fastest decay, i.e. bottom curve), measured in chloroform at room temperature.

within the polymers, differently oriented donor and acceptor dipoles and potentially alterations in the chain-mobility, which cause different transfer rates for individual donor fluorophores in the copolymer. As none of the before mentioned effects causes discrete modes of emission but rather affects the distribution of emission lifetimes, an average transfer rate per donor molecule is calculated using the experimentally accessible transfer efficiencies. The absolute transfer rates in the copolymer depend on the number of donor molecules bound to the polymer chain and on the calculated average transfer rate per donor molecule. Thus, a weighting of the average transfer rates was performed by multiplying the respective values with the number of donor molecules of the polymer backbone – as determined by NMR spectroscopy (Table 4). Thus, the estimates for the absolute transfer rates show a strong dependence on the donor-acceptor-ratio. For **PDA 1** the absolute transfer rate suffers from a small number of acceptor molecules within the polymer chain, which could receive the electronic energy from donor molecules. The situation is differently for **PDA 3** in which the donor molecules transfer most of the absorbed energy to acceptors. However, due to the low content of donors in the copolymer the absorption cross section of the polymer chain is reduced. As a consequence, the absolute energy transfer rate in **PDA 2** exceeds the rate estimates for **PDA 1** and **PDA 3**, indicating that a balanced donor-acceptor-ratio in copolymers of the type **PDA** yields a maximum energy flow to acceptor dyes. This is of interest for the preparation of dye sensitized solar cells (DSSC) with incorporated energy relay dyes.<sup>3</sup> In particular in solid-state DSSC with restricted thickness of a few micrometers, where not all the incoming light is absorbed, polymers like **PDA2** enhance the light-harvesting efficiency.

In addition, energy focusing is very important, that is, concentrating energy transfer to a single acceptor, for example, a reaction center. In order to provide a measure of the energy focusing in the polymers the absolute energy transfer rate—discussed before—was divided by the number of acceptors in a polymer chain (Table 4).

The resulting values point to the dependence of energy focusing on the donor-acceptor-ratio: **PDA 1** exhibits the largest value (1.42) indicating that high donor-acceptor-ratio leads to a better energy focusing. Thus, in systems demanding efficient energy focusing, that is, artificial photosynthetic systems, the copolymer **PDA 1** is more favorable compared with copolymers **PDA 2-3**.<sup>7</sup>

## CONCLUSIONS

PMMA-based copolymers containing thiazole donor and thiazole acceptor dyes were synthesized using the RAFT polymerization method. A series of statistical donor-acceptor copolymers have been prepared, with compositions changes from donor copolymer to acceptor copolymer. These donor-acceptor macromolecules were used as a model system for the investigation regarding an antenna structure for light-harvesting systems. The polymerization of these thiazole

dyes into the polymer backbone leads only to minor changes in their photophysical properties of the individual dyes in solution. Fluorescence excitation spectrum decay curves as well as life time measurements showed that energy was transferred from the donor to the acceptor moiety along the copolymer chain, that is, due to small spacing of the donor/acceptor dyes or due to the formation of a random coil, which brings the fluorophores in close proximity.

The fluorescence of the incorporated donor dyes is highly quenched by acceptor molecules due to the energy transfer with an efficiency up to 87%. This study shows the strong influence of the ratio between the donor and acceptor chromophore for the energy transfer. The copolymers presented in this study can act as antenna structures for light harvesting systems. For the first time, it was shown that a balanced donor-acceptor-ratio leads to the most effective energy transfer while a high acceptor content leads to an efficient energy focusing.

## ACKNOWLEDGMENTS

We thank L. Steuer for their support. Financial support of the Dutch Polymer Institute (DPI, technology area HTE), the Carl-Zeiss-Foundation (Strukturantrag JCSM), the Thuringian Ministry for Education, Science and Culture (Grant no. #514-09049, Photonische Mizellen (PhotoMIC)), and the Fonds der Chemischen Industrie is gratefully acknowledged.

## REFERENCES AND NOTES

- 1 M. Grätzel, *Nature* **2001**, *414*, 338–344.
- 2 C. Siegers, B. Oláh, U. Würfel, J. Hohl-Ebinger, A. Hinsch, R. Haag, *Sol. Energy Mater. Sol. Cells* **2009**, *93*, 552–563.
- 3 B. E. Hardin, E. T. Hoke, P. B. Armstrong, J. H. Yum, P. Comte, T. Torres, J. M. J. Fréchet, M. K. Nazeeruddin, M. Grätzel, M. D. McGehee, *Nat. Photonics* **2009**, *3*, 406–411.
- 4 B. Loges, A. Boddien, F. Gärtner, H. Junge, M. Beller, *Top. Catal.* **2010**, *53*, 902–914.
- 5 C. Wang, Z. Xie, K. E. deKrafft, W. Lin, *ACS Appl. Mater. Interfaces* **2012**, *4*, 2288–2294.
- 6 A. Fihri, V. Artero, M. Razavet, C. Baffert, W. Leibl, M. Fontecave, *Angew. Chem. Int. Engl. Ed.* **2008**, *47*, 564–567.
- 7 L. Duan, F. Bozoglian, S. Mandal, B. Stewart, T. Privalov, A. Llobet, L. Sun, *Nat. Chem.* **2012**, *4*, 418–423.
- 8 Z. Xie, C. Wang, K. E. deKrafft, W. Lin, *J. Am. Chem. Soc.* **2011**, *133*, 2056–2059.
- 9 S. Tschierlei, M. Presselt, C. Kuhnt, A. Yartsev, T. Pascher, V. Sundström, M. Karnahl, M. Schwalbe, B. Schäfer, S. Rau, M. Schmitt, B. Dietzek, J. Popp, *Chem. Eur. J.* **2009**, *15*, 7678–7688.
- 10 J. Serin, X. Schultze, A. Adronov, J. M. J. Fréchet, *Macromolecules* **2002**, *35*, 5396–5404.
- 11 A. Adronov, D. R. Robello, J. M. J. Fréchet, *J. Polym. Sci. Part A: Polym. Chem.* **2001**, *39*, 1366–1373.
- 12 C. N. Fleming, K. A. Maxwell, J. M. DeSimone, T. J. Meyer, J. M. Papanikolas, *J. Am. Chem. Soc.* **2001**, *123*, 10336–10347.
- 13 F. V. R. Neuwahl, R. Righini, A. Adronov, P. R. L. Malenfant, J. M. J. Fréchet, *J. Phys. Chem. B* **2001**, *105*, 1307–1312.

- 14 X. Schultze, J. Serin, A. Adronov, J. M. J. Fréchet, *Chem. Commun.* **2001**, 1160–1161.
- 15 C. Devadoss, P. Bharathi, J. S. Moore, *Nature* **1996**, *383*, 9635–9644.
- 16 S. L. Gilat, A. Adronov, J. M. J. Fréchet, *Angew. Chem. Int. Engl. Ed.* **1999**, *38*, 1422–1427.
- 17 A. J. Tilley, M. Chen, S. M. Danczak, K. P. Ghiggino, J. M. White, *Polym. Chem.* **2012**, *3*, 892–899.
- 18 T. A. Smith, K. P. Ghiggino, *Polym. Int.* **2006**, *55*, 772–779.
- 19 K. P. Ghiggino, T. D. M. Bell, E. N. Hooley, *Faraday Discuss.* **2012**, *155*, 79–88.
- 20 V. Gulbinas, I. Mineviciute, D. Hertel, R. Wellander, A. Yartsev, V. Sundstrom, *J. Chem. Phys.* **2007**, *127*, 144907.
- 21 J. Schäfer, R. Menzel, D. Weiß, B. Dietzek, R. Beckert, J. Popp, *J. Lumin.* **2011**, *131*, 1149–1153.
- 22 G. D. Scholes, *Annu. Rev. Phys. Chem.* **2003**, *54*, 57–87.
- 23 J. N. Younathan, W. E. Jones, T. J. Meyer, *J. Phys. Chem.* **1991**, *95*, 488–492.
- 24 C. N. Fleming, L. M. Dupray, J. M. Papanikolas, T. J. Meyer, *J. Phys. Chem. A* **2002**, *106*, 2328–2334.
- 25 R. Menzel, A. Breul, C. Pietsch, J. Schäfer, C. Friebe, E. Täuscher, D. Weiß, B. Dietzek, J. Popp, R. Beckert, U. S. Schubert, *Macromol. Chem. Phys.* **2011**, *212*, 840–848.
- 26 A. M. Breul, C. Pietsch, R. Menzel, J. Schäfer, A. Teichler, M. D. Hager, J. Popp, B. Dietzek, R. Beckert, U. S. Schubert, *Eur. Polym. J.* **2012**, *48*, 1339–1347.
- 27 A. M. Breul, J. Schäfer, C. Friebe, F. Schlütter, R. M. Paulus, G. Festag, M. D. Hager, A. Winter, B. Dietzek, J. Popp, U. S. Schubert, *Macromol. Chem. Phys.* **2012**, *213*, 808–819.
- 28 A. M. Breul, J. Schäfer, G. M. Pavlov, A. Teichler, S. Höppener, C. Weber, J. Nowotny, L. Blankenburg, J. Popp, M. D. Hager, B. Dietzek, U. S. Schubert, *J. Polym. Sci. Part A: Polym. Chem.* **2012**, *50*, 3192–3205.
- 29 B. Happ, J. Schaefer, R. Menzel, M. D. Hager, A. Winter, J. Popp, R. Beckert, B. Dietzek, U. S. Schubert, *Macromolecules* **2011**, *2*, 6277–6287.
- 30 P. J. Roth, M. Haase, T. Basché, P. Theato, R. Zentel, *Macromolecules* **2009**, *43*, 895–902.
- 31 J. Chiefari, Y. K. Chong, F. Ercole, J. Krstina, J. Jeffery, T. P. T. Le, R. T. A. Mayadunne, G. F. Meijs, C. L. Moad, G. Moad, E. Rizzardo, S. H. Thang, *Macromolecules* **1998**, *31*, 5559–5562.
- 32 G. Moad, E. Rizzardo, S. H. Thang, *Aust. J. Chem.* **2009**, *62*, 1402–1472.
- 33 G. Moad, M. Chen, M. Haussler, A. Postma, E. Rizzardo, S. H. Thang, *Polym. Chem.* **2011**, *2*, 492–519.
- 34 E. A. Jares-Erijman, T. M. Jovin, *Nat. Biotechnol.* **2003**, *21*, 1387–1395.
- 35 B. N. G. Giepmans, S. R. Adams, M. H. Ellisman, R. Y. Tsien, *Science* **2006**, *312*, 217–224.
- 36 A. Vollrath, D. Pretzel, C. Pietsch, I. Perevyazko, R. Menzel, S. Schubert, G. M. Pavlov, D. Weiß, R. Beckert, U. S. Schubert, *Macromol. Rapid Commun.* **2012**, *33*, 1791–1797.
- 37 The contribution of the donor molecules to the absolute absorption of PDA 1 was calculated by a quantitative analysis of the absorbance spectra (see Supporting Information).
- 38 J. Farinha, R. Paula, M. Charreyre, T. J. V. Prazeres, J. M. G. Martinho, *Macromolecules* **2007**, *40*, 4680–4691.
- 39 N. Felorzabih, P. Froimowicz, J. C. Haley, G. R. Bardajee, B. Li, E. Bovero, F. C. J. M. van Veggel, M. A. Winnik, *J. Phys. Chem. B* **2009**, *113*, 2262–2272.
- 40 F. Bai, S. E. Webber, *Macromolecules* **1986**, *19*, 2484–2494.
- 41 J. P. S. Farinha, J. M. G. Martinho, *J. Phys. Chem. C* **2008**, *112*, 10591–10601.

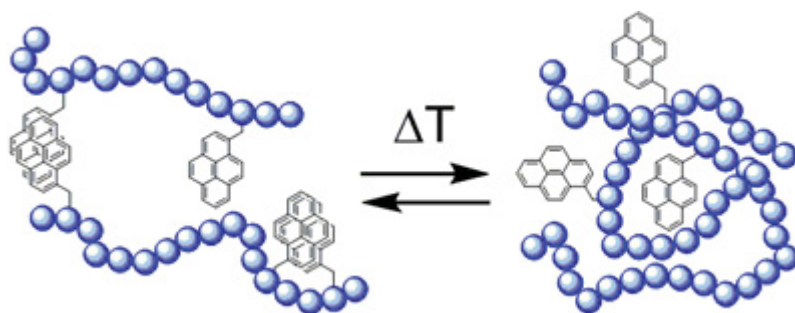


Publication P6:  
*A fluorescent thermometer based on a pyrene-labeled  
thermoresponsive polymer*

---

C. Pietsch, A. Vollrath, R. Hoogenboom, U. S. Schubert

*Sensors* **2010**, *10*, 7979–7990







Article

## A Fluorescent Thermometer Based on a Pyrene-Labeled Thermoresponsive Polymer

Christian Pietsch <sup>1,2</sup>, Antje Vollrath <sup>1</sup>, Richard Hoogenboom <sup>3,4,\*</sup> and Ulrich S. Schubert <sup>1,2,3</sup>

<sup>1</sup> Laboratory of Organic and Macromolecular Chemistry, Friedrich-Schiller-University Jena, Humboldtstrasse 10, 07743 Jena, Germany; E-Mails: christian.pietsch@uni-jena.de (C.P.); antje.vollrath@uni-jena.de (A.V.); ulrich.schubert@uni-jena.de (U.S.S.)

<sup>2</sup> Dutch Polymer Institute (DPI), John F. Kennedylaan 2, 5612 AB Eindhoven, Netherlands

<sup>3</sup> Laboratory of Macromolecular Chemistry and Nanoscience, Eindhoven University of Technology, P.O. Box 513, 5600 MB Eindhoven, Netherlands

<sup>4</sup> Supramolecular Chemistry group, Department of Organic Chemistry, Ghent University, Krijgslaan 281 S4, 9000 Ghent, Belgium

\* Author to whom correspondence should be addressed; E-Mail: richard.hoogenboom@ugent.be.

Received: 21 June 2010; in revised form: 23 July 2010 / Accepted: 20 August 2010 /

Published: 27 August 2010

---

**Abstract:** Thermoresponsive polymers that undergo a solubility transition by variation of the temperature are important materials for the development of ‘smart’ materials. In this contribution we exploit the solubility phase transition of poly(methoxy diethylene glycol methacrylate), which is accompanied by a transition from hydrophilic to hydrophobic, for the development of a fluorescent thermometer. To translate the polymer phase transition into a fluorescent response, the polymer was functionalized with pyrene resulting in a change of the emission based on the microenvironment. This approach led to a soluble polymeric fluorescent thermometer with a temperature range from 11 °C to 21 °C. The polymer phase transition that occurs during sensing is studied in detail by dynamic light scattering.

**Keywords:** pyrene; DEGMA; stimuli-responsive polymer; lower critical solution temperature (LCST); RAFT polymerization; solvatochromism; fluorescent thermometer

---

## 1. Introduction

In recent years, dye-functionalization of thermoresponsive polymers has received significant attention for the development of sensory materials [1-12]. This approach allows simple and fast detection of the temperature by measuring the absorbance or fluorescence of a polymer solution. The high sensitivities arise from the incorporated solvatochromic dye molecules [13,14], which respond to minor local environmental changes that occur upon the temperature induced polymer phase transition. Such optical thermometers are desirable for remote sensing of the temperature based on the reversible temperature induced polymer phase transition. These thermometers can be used if the electromagnetic field or the ionic strengths are too strong for a conventional thermometer. A variety of optical polymeric thermometers have been reported as sensing materials. Hirai and co-workers classified these types of responsive polymers in three classes [5,9]: (i) heat-induced fluorescence enhancement, (ii) heat-induced fluorescence quenching, and (iii) selective emission enhancement at a specific temperature range. A further class is based on (iv) a temperature-dependent batho-chromic/hypso-chromic shift of the absorption or emission wavelengths [3,6,11,15,16]. Such solvatochromic dyes change color in response to changes of the solvent polarity. Recently, it was reported that combining a solvatochromic dye with a temperature-responsive polymer leads to a color change upon changing the temperature, as in the dissolved state the dye is in contact with water while in the collapsed state the dye is dissolved in the less polar precipitated polymer globule. Such optical polymeric sensors can be used for a wide range of applications, such as biosensors [2], drug delivery [17,18], logic gates [4,10,19,20], and optical sensing [1,5-9,11,12].

The majority of these sensor materials are based on stimuli-responsive polymers, exhibiting a lower critical solution temperature (LCST) in solution, sometimes also called coil-to-globule transition. Such LCST polymers are water-soluble at low temperatures and undergo a sharp entropy-driven collapse with increasing temperature. As a result the temperature sensing regime of LCST-based sensors is often limited to the detection of a narrow temperature range (around 10 °C). The LCST behavior of polymers in solution can be described by the Flory-Huggins theory [21].

Besides the most commonly studied poly(*N*-isopropylacrylamide) (PNIPAM) [17,22], a number of poly(ethyleneglycol) (PEG) based polymers have been reported to exhibit LCST behavior. In particular, ethyleneglycol methyl ether methacrylate-based polymers have attracted attention as thermoresponsive materials and as alternatives to PNIPAM [23-27]. It has been demonstrated that oligoethylene glycol methyl ether methacrylate-based polymers exhibit similar desirable thermoresponsive properties in water as PNIPAM while showing less hysteresis between heating and cooling.

The strong interest in PEG base methacrylates is based on the easy preparation of well-defined structures by controlled radical polymerization (CRP) techniques. In this work we used the reversible addition fragmentation chain transfer (RAFT) technique as polymerization method [28,29]. In particular, we used di(ethylene glycol) methyl ether methacrylate (DEGMA) copolymers, which have a low LCST of around 25 °C and this class of polymers has superb biocompatibility [30,31].

The fluorescent dye pyrene is a very hydrophobic molecule and has limited solubility in polar solvents like water. Pyrene is one of the most studied fluorescent dyes in chemistry. In the early nineties Winnik and co-workers studied the heat-induced phase transition in water of a pyrene

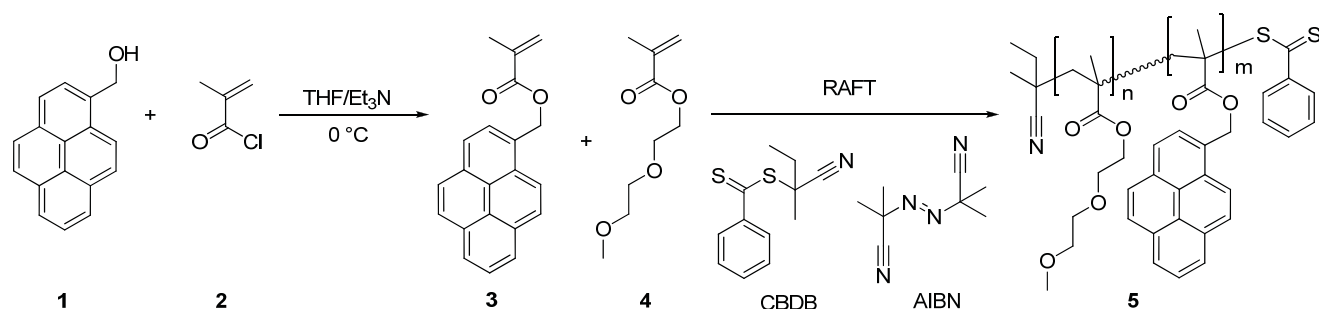
functionalized poly(NIPAM) [32,33]. It could be shown that the phase transition has an influence on the pyrene eximer emission. Pyrene is also used in polymer chemistry as fluorescent probe to determine the critical micelle concentration of block copolymers based on the sensitivity of the pyrene emission to the polarity of the solubilizing medium [34,35]. It could be shown that the ratio of the intensity of the pyrene monomer emission (in total five vibronic bands) of the first ( $I_1$  at 373 nm) and third peak ( $I_3$  at 384 nm) represents a sensitive parameter, which is characteristic for the polarity of the environment [36]. Also the relative intensity of the first and the fifth peak can be used as sensitive parameter for the polarity of the medium ( $I_5$  at 393 nm). In addition, pyrene shows a second emission band at higher concentration corresponding to an excited dimer (excimer fluorescence > 450 nm). This excimer fluorescence band appears at higher wavelengths in comparison to the emission band of the monomer fluorescence (red shift) [37].

In the current work, we developed an optical fluorescent temperature sensors with a temperature sensing regime based on the LCST transition of pyrene functionalized poly(DEGMA) in water. The synthesis and characterization of this copolymer are reported. In addition, the temperature sensing ability of the copolymer is discussed based on fluorescence spectroscopy and dynamic light scattering (DLS).

## 2. Results and Discussion

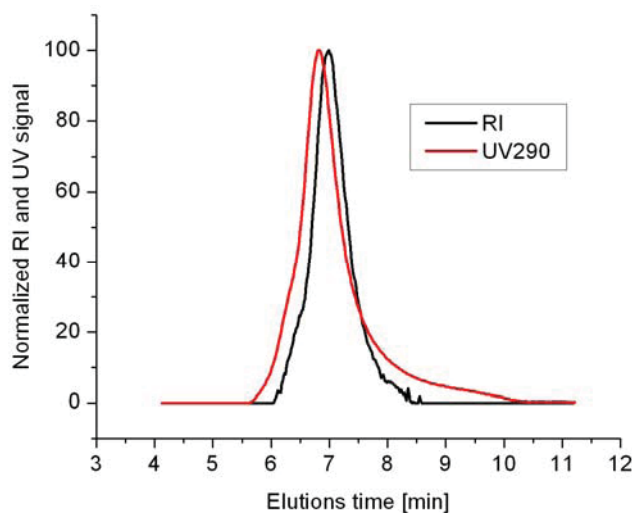
The synthesis route of the pyrene-labeled copolymer poly(DEGMA-*stat*-PyMMA) (**5**), is depicted in Scheme 1. The polymerization was performed using the RAFT process [28,29] to ensure the preparation of well-defined copolymers allowing a straightforward interpretation of the sensing results. As a first step the polymerizable pyrene dye methacrylate monomer (PyMMA, **3**) was synthesized by an esterification reaction of the hydroxyl group of pyrene-1-methanol (**1**) with methacryloyl chloride (**2**) [12]. In a further step, PyMMA (**3**) was statistically copolymerized with di(ethylene glycol) methylether methacrylate (DEGMA, **4**) by RAFT polymerization. 2-Cyano-2-butyl dithiobenzoate (CBDB) was used as chain transfer agent and azoisobutyronitrile (AIBN) as radical initiator (Scheme 1). The synthesis was performed at 70 °C for 12 hours with toluene as solvent. The monomer to RAFT agent ratio was 100 using 5% of dye-functionalized monomer, aiming for a degree of polymerization of 100.

**Scheme 1.** Schematic representation of the synthesis of the pyrene-functionalized monomer and the subsequent RAFT copolymerization with DEGMA.



The size exclusion chromatograms display a narrow molar mass distribution with low PDI values ( $PDI < 1.20$ ). The chromatograms were recorded with both a RI (black line) and a UV detector (red line) revealing nearly the same distribution clearly demonstrating that the pyrene dye is incorporated in the copolymer since PDEGMA does not absorb at 290 nm (Figure 1).

**Figure 1.** Size exclusion chromatograms of copolymer **5**.



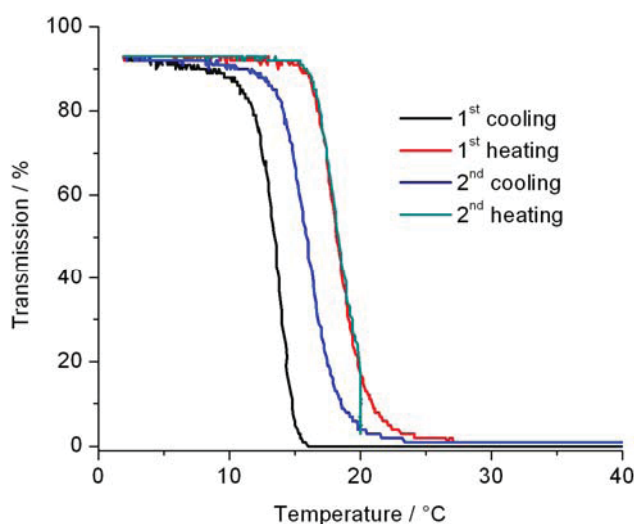
The shift in the retention time between the RI and UV detector is due to the placement of the detectors in series, *i.e.*, the eluent first passes the UV-detector and then the RI detector. The molar mass of copolymer **5** was determined to be 29,000 g/mol, with a polydispersity index of 1.20 calculated for the RI-trace with poly(styrene) standards. A broader molar mass distribution is obtained with the UV detector, which is due to the different sensitivities of both detectors, *i.e.*, higher sensitivity of the UV detector, especially in the oligomer region. In addition, the RI detector detects all repeat units while the UV detector only detects the incorporate pyrene molecules. As such, low molar mass oligomers will not be substantially detected by the RI detector, but when a few of these are dye-labeled they will appear in the UV-detector.

The ratio between the DEGMA units and the pyrene side groups in the copolymer chain was determined to be 4.5 mol% using  $^1\text{H-NMR}$  spectroscopy based on the respective aromatic pyrene signals and the backbone or side-chain signals of the polymer. In addition, the pyrene content was found to be 5.0 mol% based on the UV-vis extinction coefficient of the copolymer. These two values are in good agreement and are within the experimental error of the two applied techniques.

The temperature induced phase transition of the poly(DEGMA-*stat*-PyMMA) copolymer **5** was explored by turbidimetry. Figure 2 shows the change in turbidity (determined at 500 nm) of copolymer **5** in water at a concentration of 2.5 mg/mL. This concentration was chosen since at lower concentration the cloud point is more difficult to detect, because less polymer chains will aggregate during the phase transition at lower concentrations resulting in the formation of smaller precipitated particles that scatter less light. Figure 2 clearly demonstrates that at low temperatures the polymer solution has close to 100% transmittance indicative of a clear polymer solution. Upon increasing the temperature, the polymer chains precipitate resulting in the formation of large aggregates that scatter away the light as indicated by 0% transmittance. The difference in the turbidity curves during first and

second cooling are due to the influence of the history of the solid polymer particles that is still present in the first cooling run while this history is erased during complete dissolution in the first heating run. The temperature at 50% transmission represents the cloud point (CP) of the polymer solution, which is 18.3 °C for both heating runs. During these heating runs, the solubility of the polymer at temperatures below the CP is based on the formation of a large number of hydrogen bonds between the repeating units of the polymer chain (ethylene glycol units) and water molecules that form a hydration shell. Upon increasing the temperature the hydrogen bonds are weakened and finally broken resulting in the loss of the hydration shell leaving the non-hydrated hydrophobic polymer chains behind. At the CP, the polymer chain collapses and the water is released into the bulk water. This polymer phase transition is driven by the increase of entropy of releasing the water molecules into the bulk water. Below the CP, the polymers are well solvated and, thus, are exposed to the polar aqueous environment while in the precipitated state above the CP the polymer globule is less polar. This polarity transition around the polymer chains is the basis for the sensing ability of the poly(DEGMA-*stat*-PyMMA) copolymer **5** that will be discussed in the following.

**Figure 2.** Turbidity *versus* temperature plot for an aqueous solution of copolymer **5** (2.5 mg mL<sup>-1</sup>).



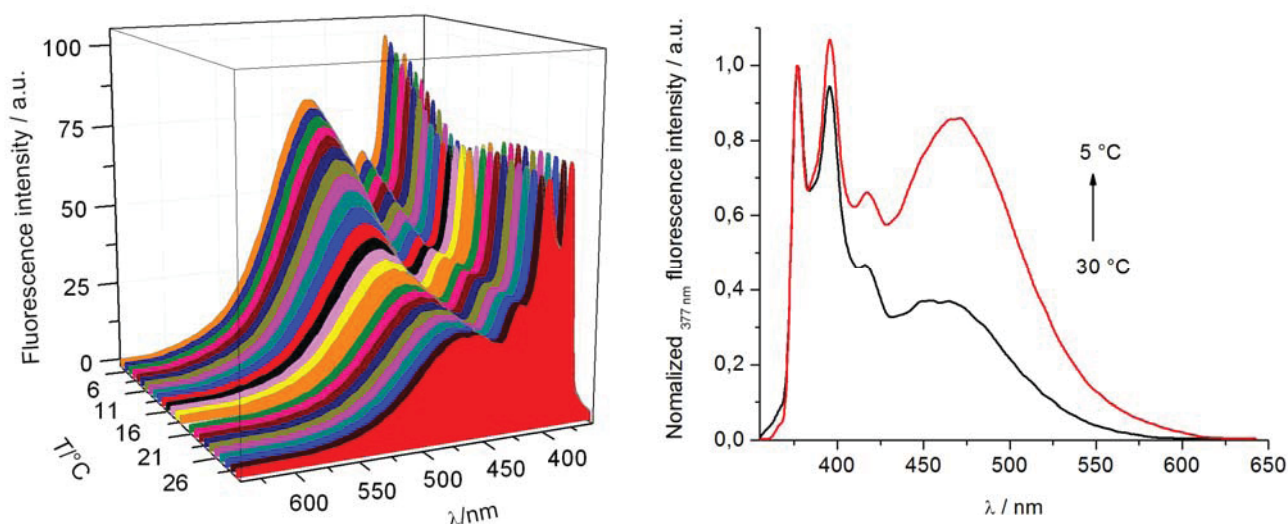
The temperature sensing ability of the pyrene-labeled copolymer **5** in aqueous solution was investigated by temperature controlled fluorescence spectroscopy at a polymer concentration of 1 mg/mL. Figure 3a shows the resulting waterfall plot of the fluorescence spectra recorded in between 5 °C to 30 °C ( $\lambda_{exc} = 342$  nm; one spectra per degree). Three characteristic pyrene emission bands are observed at 467 nm (broad), 377 nm and 395 nm, which are assigned to the excimer emission ( $I_E > 450$  nm) and the individual pyrene molecule emission ( $I_1$  at 377 nm and  $I_5$  at 395 nm) of the pyrene units in the copolymer. This 3D representation clearly demonstrates that the intensity of  $I_E$  at 467 nm increases with decreasing temperature, along with a small red shift of the excimer emission from 462 to 471 nm (Figure 3b).

The stronger excimer emission at lower temperatures can be related to the high polarity of the aqueous environment, which enhances the hydrophobic association of individual pyrene molecules. This association is further facilitated by the high mobility of the hydrated polymer chains in solution. At higher temperatures, in the precipitated state, the polarity around the pyrene molecules is lower

compared to the hydrated state lowering the formation of excimers. In addition, the increased microviscosity in the collapsed polymer globules might also hinder the excimer formation.

The ratio of  $I_5/I_1$  ( $I_5$  at 395 nm and  $I_1$  at 377 nm) is 1.07 at 5 °C, which is quite similar to the value in ethanol of 1.06 indicating that the pyrene molecules are not fully exposed to the solvent, *i.e.*, they apparently form hydrophobic clusters as is also indicated by the excimer emission. This  $I_5/I_1$  ratio is linearly decreasing during the polymer phase transition upon heating and finally reaches a value of 0.94 at 30 °C, which is similar to the value of acidic acid of 0.95 [36], surprisingly indicating a more polar environment in the precipitated state. This increased polarity is most likely due to breaking of the hydrophobic pyrene clusters and, therefore, the pyrene groups can interact (e.g., dipole-dipole) with the polar ethylene oxide side chains of the polymer chain.

**Figure 3.** (a) Waterfall plot of the fluorescence spectra as a function of temperature (excitation wavelength 342 nm) and (b) normalized fluorescence intensity (377 nm) at 5 °C (red) and 30 °C (black) of a solution of pyrene-labeled copolymer **5** in water at 1.0 mg mL<sup>-1</sup>.



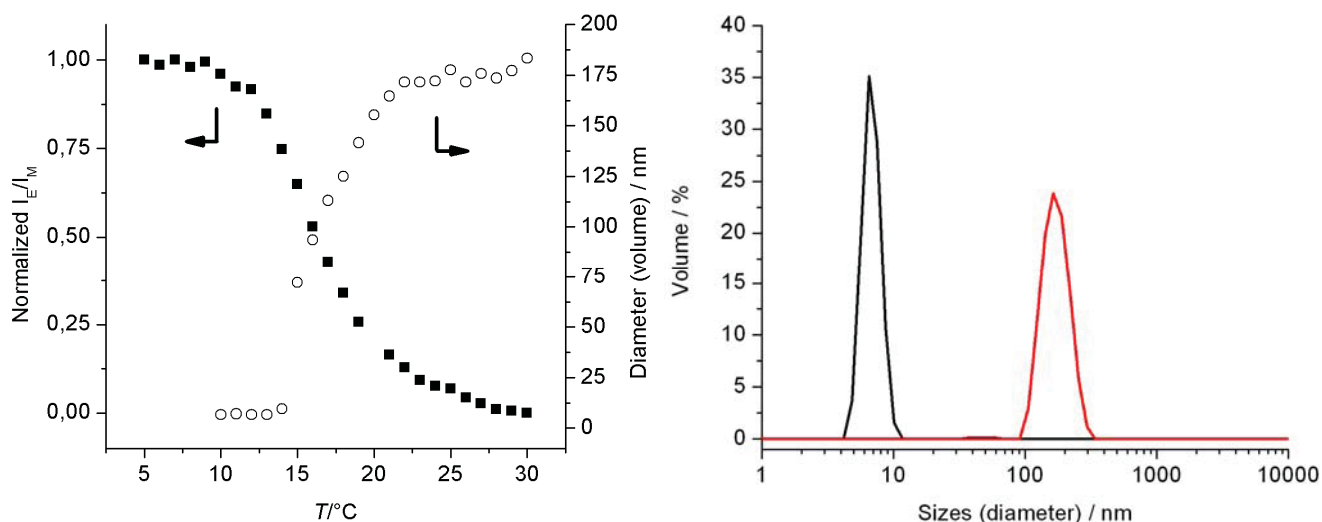
To quantify the sensing ability of the pyrene-labeled copolymer **5**, the normalized ratio of excimer emission to monomer emission intensities ( $I_E/I_M$ ) *versus* temperature was investigated since this ratio is expected to be independent from fluctuations in polymer concentration making the read-out of the sensor more robust (Figure 4a). Three distinct regimes are present in  $I_E/I_M$  *versus* temperature plot. Below 10 °C when the polymer is fully soluble in aqueous solution, the  $I_E/I_M$  ratio is constant. A strong decrease in  $I_E/I_M$  is observed upon increasing the temperature from 11 °C and 21 °C, which can be regarded as the temperature sensing regime of copolymer **5**. Finally, above 21 °C the  $I_E/I_M$  ratio only shows a minor decrease, which might be attributed to increased chain mobility within the precipitated polymer globules rather than a polymer phase transition. The close similarity of the  $I_E/I_M$  ratio and the turbidimetry results clearly demonstrates that indeed the polymer phase transition can be employed for the development of a fluorescent thermometer.

The temperature induced phase transition of copolymer **5** was investigated in further detail by dynamic light scattering as a function of temperature (DLS; Figure 4). Representative size distributions of the polymer globules at temperatures below and above the phase transition are illustrated in Figure 4b (CONTIN analysis). Below the CP at 10 °C the polymer globule has a hydrodynamic radius of 7 nm

corresponding to individual hydrated polymer chains. Above the CP at 30 °C where polymer chains are precipitated, larger aggregates with a hydrodynamic radius of 183 nm are observed. Apparently, the polymer concentration is low enough to prevent further aggregation into micrometer sized particles. It is rather surprising that the precipitated polymer aggregates have a narrow size distribution with a  $PDI_{\text{particle}}$  value of 0.060 (obtained from the Cumulants analysis).

The hydrodynamic radius of the polymer globules is plotted as a function of temperature in Figure 4a, revealing a very similar temperature transition as previously observed by turbidimetry investigations as well as the  $I_E/I_M$  ratio. From 10 to 14 °C the particle size is constant around 7 nm, indicating the presence of individual hydrated polymer chains in solution. A further increase in temperature results in a strong increase in the diameter of the polymer globules indicative of a temperature induced aggregation. The demixing point of the polymer solution might be regarded to be 15 °C where the Z average diameter of the aggregates is already 78 nm with a  $PDI_{\text{particle}}$  of 0.222 (Cumulant analysis). In between 16 and 20 °C the polymer chains are further dehydrated making them more hydrophobic resulting in further aggregation of the initial aggregates as evidenced by the increase of the hydrodynamic radius. Heating beyond the polymer phase transition, *i.e.*, above 21 °C, does not further affect the size of the aggregates. These DLS results are in very good agreement with the sensing behavior of the copolymer confirming that the change in pyrene emission is based on the temperature induced polymer phase transition.

**Figure 4.** (a) The ratio of excimer (467 nm) to monomer (395 nm) emission intensities ( $I_E/I_M$ , black squares) and the hydrodynamic radius of the polymer globules (DLS, open circles) of copolymer **5** at 1.0 mg mL<sup>-1</sup> as function of temperature. (b) The hydrodynamic radius of the polymer globules at 5 °C (black) and 30 °C (red) as determined by DLS at 1.0 mg mL<sup>-1</sup> (CONTIN routine).



### 3. Experimental Section

#### 3.1. Materials

Di(ethylene glycol) methylether methacrylate (DEGMA) was purchased from Sigma-Aldrich and was purified with an inhibitor-remover before use. Pyrene-1-methanol was purchased from

Sigma-Aldrich and was used without purification. Azobis(isobutyronitrile) (AIBN, Aldrich) was recrystallized from methanol prior to use. 2-Cyano-2-butyl dithiobenzoate (CBDB) [38] was prepared according to a literature procedure for a related compound. All analytical grade solvents were purchased from Biosolve Ltd. or Fluka. The deuterated solvents ( $\text{CDCl}_3$  or  $\text{CD}_2\text{Cl}_2$ ) for NMR spectroscopy were obtained from Cambridge Isotope Laboratories.

### 3.2. Instrumentation

Size-exclusion chromatography (SEC) was performed on a Shimadzu system equipped with a SCL-10A system controller, a LC-10AD pump, a RID-10A refractive index detector, a SPD-10A UV detector at 290 nm and a PSS SDV column with chloroform-triethylamine-2-propanol (94:4:2) as eluent and the column oven was set to 50 °C (polystyrene calibration). Poly(styrene) (PS) samples were used as calibration standards.

Nuclear magnetic resonance spectra were recorded on a Varian Mercury 400 MHz spectrometer at 298 K. Chemical shifts are reported in parts per million (ppm) calibrated to an internal standard, tetramethylsilane (TMS) in deuterated solvents ( $\text{CDCl}_3$  or  $\text{CD}_2\text{Cl}_2$ ).

UV/vis spectra were recorded on a Perkin-Elmer Lambda-45 UV/vis spectrophotometer. For fluorescence measurements a Perkin-Elmer Luminescence Spectrometer LS 50B with a PTP-1 Peltier Temperature Programmer were used. For the temperature measurements on these spectrophotometers a temperature profile with a temperature rate of 0.5 °C/min was used.

Elemental analyses were carried out on a EuroVector EuroEA300 elemental analyzer for CHNSO. The cloud point measurements for the identification of the LCST behavior were performed by heating the polymer (2.5 mg/mL) in water from 0 to 105 °C with a heating rate of 1.0 °C per minute followed by cooling to 0 °C at a cooling rate of 1.0 °C per minute after keeping it 10 minutes at 105 °C. This cycle was repeated two times. During these controlled cycles the transmission through the solutions was monitored in a Crystall16™ from Avantium Technologies. The cloud points are reported as the 50% transmittance temperature in the second heating run.

Dynamic light scattering (DLS) measurements were carried out on a Zetasizer Nano ZS (Malvern Instruments, Malvern, U.K.) operating with a laser beam at 633 nm and a scattering angle of 173°. The polymer was dissolved in water (1.0 mg/mL) and transferred into a quartz cuvette. The DLS measurements were performed between 10 and 30 °C using steps of 1 °C and an equilibrium time of 120 seconds. The solution was measured three times for 60 seconds at every temperature. The mean particle size was approximated as the effective (Z average) diameter and the width of the distribution as the polydispersity index ( $\text{PDI}_{\text{particle}}$ ) that was obtained by the Cumulants method assuming a spherical shape. Furthermore, the particle size distribution was calculated applying the NNLS mode (CONTIN routine).

### 3.3. Synthesis of pyrene-1-ylmethyl-methacrylate (PyMMA) monomer (3)

To a solution of triethylamine (1.80 mL, 12.8 mmol) in anhydrous THF (50 mL), pyrene-1-ylmethanol (1.0 g, 4.3 mmol) was added. Methacryloyl chloride (1.24 mL, 12.8 mmol) was added dropwise to this clear solution at 0 °C. The reaction was then stirred at room temperature overnight (24 hours total reaction time). Subsequently, the reaction medium was filtered and the



solvent was evaporated under reduced pressure. Afterwards the solid residue was dissolved in diethyl ether and washed with water. After evaporation of the diethyl ether, the crude monomer was purified by recrystallization from ethanol at 40 °C. Yield: 40%. GC-MS:  $m/z$  (%) = 300 (38) [ $M^+$ ], 215 (100) [ $M^+ - C_4H_5O_2$ ], 203 (9) [ $C_6H_{10}^+ H^+$ ], 189 (8), 107 (5), 94 (9), 41 (10) [all aromatic fragmentation].  $^1H$ -NMR (400 MHz,  $CDCl_3$ ):  $\delta$  = 8.32–8.00 (m, 9H, aromatic  $H^{2-10}$ ), 6.16 (s, 1H,  $H^{12}$ ), 5.91 (s, 2H,  $H^{11}$ ), 5.57 (s, 1H,  $H^{12}$ ), 1.98 (s, 3H,  $H^{13}$ ) ppm.  $^{13}C$ -NMR (100 MHz,  $CDCl_3$ ):  $\delta$  = 167.4 (C=O), 136.2, 131.7, 131.2, 130.7, 129.5, 129.0, 128.1, 127.8, 127.6, 127.3, 126.1, 126.0, 125.5, 125.4, 124.9, 124.6, 124.5, 122.9 (16 aromatic C and  $-C=CH_2$ ), 65.0 ( $-CH_2-O$ ), 18.4 ( $-CH_3$ ) ppm. Elemental analysis:  $C_{21}H_{16}O_2$  (300.35): cal.: C 83.98% H 5.37%; found: C 84.08% H 5.64%. UV/vis (*n*-heptane):  $\lambda_{max}/nm$  ( $\epsilon/(M^{-1}\cdot cm^{-1})$ ): 201 (16,120), 233 (26,060), 242 (46,680), 265 (16,350), 276 (31,270), 312 (7,760), 326 (20,210), 342 (32,520). Fluorescence (THF):  $\lambda_{max}/nm$ : 377, 394, 416 (shoulder), 435 (shoulder).

### 3.4. Synthesis of poly(DEGMA-*stat*-PyMMA) copolymer 5

Poly(MMA-*stat*-PyMMA) was prepared in a closed reaction vessel with a [DEGMA]:[PyMMA]:[CBDB]:[AIBN] ratio of 95:5:1:0.25. AIBN (1.64 mg, 0.01 mmol), PyMMA (60.1 mg, 0.2 mmol) and CBDB (9.41 mg, 0.04 mmol) were dissolved in a solution of DEGMA (0.70 mL, 3.8 mmol) and toluene (1.30 mL). Before the polymerization, the solution was degassed with argon for 30 min. The reaction mixture was heated to 70 °C for 12 hours. Afterwards the polymer mixture was diluted with dichloromethane and precipitated twice in *n*-hexane resulting in a pink viscous oil.  $^1H$ -NMR (400 MHz,  $CD_2Cl_2$ ):  $\delta$  = 8.51–8.02 (m, 46H, H pyrene), 7.89 (m, 1H, H RAFT-agent), 7.56 (m, 1H, H RAFT-agent), 7.39 (m, 2H, H RAFT-agent), 5.76 (s, 8H,  $-CH_2-O-$ ), 4.10 (s, 175H,  $-CH_2-O-$ ), 3.67, 3.61 and 3.53 (s, 568H,  $-CH_2-CH_2-$ ), 3.36 (s, 297H,  $-O-CH_3$ ), 1.98–0.88 (m, 500H,  $-CH_2-$  and  $-CH_3$ ) ppm. UV/vis (1,4-dioxane):  $\lambda_{max}/nm$  [ $\epsilon/(M^{-1}\cdot cm^{-1})$ ]: 244 (369,580), 266 (183,240), 277 (337,030), 314 (90,630), 328 (214,340), 342 (316,000). Fluorescence ( $H_2O$ ):  $\lambda_{max}/nm$ : 377, 395, 467. Select characterization and composition data are given in Tables 1 and 2.

**Table 1.** Selected characterization data of the precipitated poly(DEGMA-*stat*-PyMMA).

Sample	Ratio n/m	Yield [mg]	$M_n$ [g/mol] <sup>a</sup>	PDI <sup>a</sup>
5	95/5	551	29,000	1.20

<sup>a</sup> Obtained from SEC (RI) using  $CHCl_3$  eluent and PS standards.

**Table 2.** Composition of poly(DEGMA-*stat*-PyMMA).

Sample	Theo. ratio DEGMA/PyMMA n/m	Composition <sup>a</sup> $^1H$ -NMR signal [%]	Composition <sup>b</sup> UV/vis pyrene [%]
5	95/5	4.5	5.0

<sup>a</sup> Obtained from the proton integrals of the pyrene and backbone using  $^1H$ -NMR spectroscopy;

<sup>b</sup> Obtained from the  $\epsilon$  of the UV/vis spectrum using the Lambert-Beer-Law and  $M_n$  of SEC.

#### 4. Conclusions

A well-defined fluorescent thermoresponsive copolymer based on poly(DEGMA) side-chain functionalized with pyrene has been synthesized by RAFT polymerization. It could be demonstrated by temperature controlled fluorescence investigations that this polymer acts as a soluble fluorescent temperature sensor in water. At temperatures below the polymer phase transition, the polymer chains are hydrated as demonstrated by DLS and, thus, the pyrene molecules are exposed to the polar aqueous environment driving excimer formation. Above the LCST phase transition of the polymer, the polymer chains are dehydrated and demix from the aqueous solution providing a less polar environment for the pyrene inside the polymer aggregates. During the phase transition, a gradual decrease in  $I_E/I_M$  ratio is observed, which can be used to detect the temperature of the solution in between 11 °C and 21 °C, *i.e.*, the temperature sensing regime. Interpretation of the  $I_E/I_M$  ratio as sensing signal is believed to make the sensor more robust compared to looking at individual emission intensities since it will be less dependent on polymer concentration. Turbidimetry and DLS demonstrated that the polymer phase transition also occurred in the observed temperature sensing regime confirming that indeed the polymer phase transition induces the change in  $I_E/I_M$  ratio of the attached pyrene molecules.

#### Acknowledgements

The Dutch Polymer Institute (DPI) and the Netherlands Scientific Organisation (NWO; Veni-grant for RH and VICI award for USS) are acknowledged for financial support.

#### References

1. Tang, L.; Jin, J.K.; Qin, A.J.; Yuan, W.Z.; Mao, Y.; Mei, J.; Sun, J.Z.; Tang, B.Z. A fluorescent thermometer operating in aggregation-induced emission mechanism: Probing thermal transitions of PNIPAM in water. *Chem. Commun.* **2009**, *7*, 4974-4976.
2. Gota, C.; Okabe, K.; Funatsu, T.; Harada, Y.; Uchiyama, S. Hydrophilic fluorescent nanogel thermometer for intracellular thermometry. *J. Am. Chem. Soc.* **2009**, *131*, 2766-2767.
3. Koopmans, C.; Ritter, H. Color change of N-isopropylacrylamide copolymer bearing Reichardt's dye as optical sensor for lower critical solution temperature and for host-guest interaction with beta-cyclodextrin. *J. Am. Chem. Soc.* **2007**, *129*, 3502-3503.
4. Uchiyama, S.; Kawai, N.; de Silva, A.P.; Iwai, K. Fluorescent polymeric AND logic gate with temperature and pH as inputs. *J. Am. Chem. Soc.* **2004**, *126*, 3032-3033.
5. Shiraishi, Y.; Miyamoto, R.; Hirai, T. A hemicyanine-conjugated copolymer as a highly sensitive fluorescent thermometer. *Langmuir* **2008**, *24*, 4273-4279.
6. Pietsch, C.; Hoogenboom, R.; Schubert, U.S. Soluble polymeric dual sensor for temperature and pH value. *Angew. Chem. Int. Ed.* **2009**, *48*, 5653-5656.
7. Wang, D.; Miyamoto, R.; Shiraishi, Y.; Hirai, T. BODIPY-conjugated thermoresponsive copolymer as a fluorescent thermometer based on polymer microviscosity. *Langmuir* **2009**, *25*, 13176-13182.
8. Shiraishi, Y.; Miyamoto, R.; Hirai, T. Spiropyran-conjugated thermoresponsive copolymer as a colorimetric thermometer with linear and reversible color change. *Org. Lett.* **2009**, *11*, 1571-1574.

9. Shiraishi, Y.; Miyamoto, R.; Zhang, X.; Hirai, T. Rhodamine-based fluorescent thermometer exhibiting selective emission enhancement at a specific temperature range. *Org. Lett.* **2007**, *9*, 3921-3924.
10. Guo, Z.Q.; Zhu, W.H.; Xiong, Y.Y.; Tian, H. Multiple logic fluorescent thermometer system based on N-isopropylmethacrylamide copolymer bearing dicyanomethylene-4H-pyran moiety. *Macromolecules* **2009**, *42*, 1448-1453.
11. Yan, Q.; Yuan, J.; Kang, Y.; Cai, Z.; Zhou, L.; Yin, Y. Dual-sensing porphyrin-containing copolymer nanosensor as full-spectrum colorimeter and ultra-sensitive thermometer. *Chem. Commun.* **2010**, *46*, 2781-2783.
12. Pietsch, C.; Hoogenboom, R.; Schubert, U.S. PMMA based soluble polymeric temperature sensors based on UCST transition and solvatochromic dyes. *Polym. Chem.* **2010**, *1*, 1005-1008.
13. Reichardt, C. Solvatochromic dyes as solvent polarity indicators. *Chem. Rev.* **1994**, *94*, 2319-2358.
14. Suppan, P. Invited review solvatochromic shifts: The influence of the medium on the energy of electronic states. *J. Photochem. Photobiol. A Chem.* **1990**, *50*, 293-330.
15. Matsumura, Y.; Iwai, K. Thermo-responsive behavior and microenvironments of poly(N-isopropylacrylamide) microgel particles as studied by fluorescent label method. *J. Colloid Interface Sci.* **2006**, *296*, 102-109.
16. Roth, I.; Jbarah, A.A.; Holze, R.; Friedrich, M.; Spange, S. 2-nitro-1,4-diaminobenzene-functionalized poly(vinyl amine)s as water-soluble UV-Vis-sensitive pH sensors. *Macromol. Rapid Commun.* **2006**, *27*, 193-199.
17. Aoshima, S.; Kanaoka, S. Synthesis of stimuli-responsive polymers by living polymerization: Poly(N-isopropylacrylamide) and poly(vinyl ether)s. *Adv. Polym. Sci.* **2008**, *210*, 169-208.
18. Schmaljohann, D. Thermo- and pH-responsive polymers in drug delivery. *Adv. Drug Deliv. Rev.* **2006**, *58*, 1655-1670.
19. Uchiyama, S.; Makino, Y. Digital fluorescent pH sensors. *Chem. Commun.* **2009**, 2646-2648.
20. Yan, Q.; Yuan, J.Y.; Yuan, W.Z.; Zhou, M.; Yin, Y.W.; Pan, C.Y. Copolymer logical switches adjusted through core-shell micelles: from temperature response to fluorescence response. *Chem. Commun.* **2008**, 6188-6190.
21. Gedde, U.W. *Polymer Physics*, 1st ed.; Kluwer Academic Publishers: Dordrecht, The Netherlands, 1995; pp. 55-69.
22. Schild, H.G. Poly(N-isopropylacrylamide): Experiment, theory and application. *Progr. Polym. Sci.* **1992**, *17*, 163-249.
23. Fournier, D.; Hoogenboom, R.; Thijs, H.M.L.; Paulus, R.M.; Schubert, U.S. Tunable pH- and temperature-sensitive copolymer libraries by reversible addition-fragmentation chain transfer copolymerizations of methacrylates. *Macromolecules* **2007**, *40*, 915-920.
24. Becer, C.R.; Hahn, S.; Fijten, M.W.M.; Thijs, H.M.L.; Hoogenboom, R.; Schubert, U.S. Libraries of methacrylic acid and oligo(ethylene glycol) methacrylate copolymers with LCST behavior. *J. Polym. Sci. A Polym. Chem.* **2008**, *46*, 7138-7147.
25. Lutz, J.-F. Polymerization of oligo(ethylene glycol) (meth)acrylates: Toward new generations of smart biocompatible materials. *J. Polym. Sci. A Polym. Chem.* **2008**, *46*, 3459-3470.

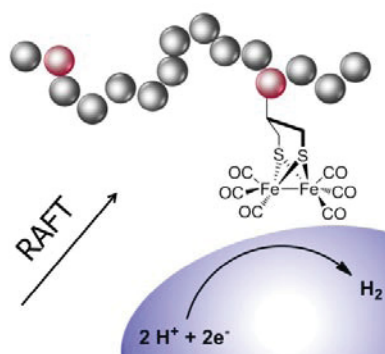
26. Lutz, J.-F.; Hoth, A. Preparation of Ideal PEG analogues with a tunable thermosensitivity by controlled radical copolymerization of 2-(2-methoxyethoxy)ethyl methacrylate and oligo(ethylene glycol) methacrylate. *Macromolecules* **2005**, *39*, 893-896.
27. Pietsch, C.; Fijten, M.W.M.; Lambermont-Thijs, H.M.L.; Hoogenboom, R.; Schubert, U.S. Unexpected reactivity for the RAFT copolymerization of oligo(ethylene glycol) methacrylates. *J. Polym. Sci. A Polym. Chem.* **2009**, *47*, 2811-2820.
28. Moad, G.; Rizzardo, E.; Thang, S.H. Living radical polymerization by the RAFT process. *Aust. J. Chem.* **2005**, *58*, 379-410.
29. Moad, G.; Rizzardo, E.; Thang, S.H. Living radical polymerization by the RAFT process—A second update. *Aust. J. Chem.* **2009**, *62*, 1402-1472.
30. Tugulu, S.; Silacci, P.; Stergiopoulos, N.; Klok, H.-A. RGD-Functionalized polymer brushes as substrates for the integrin specific adhesion of human umbilical vein endothelial cells. *Biomaterials* **2007**, *28*, 2536-2546.
31. Wischerhoff, E.; Uhlig, K.; Lankenau, A.; Börner, H.G.; Laschewsky, A.; Duschl, C.; Lutz, J.-F. Controlled cell adhesion on PEG-based switchable surfaces. *Angew. Chem. Int. Ed.* **2008**, *47*, 5666-5668.
32. Winnik, F.M. Fluorescence studies of aqueous solutions of poly(N-isopropylacrylamide) below and above their LCST. *Macromolecules* **1990**, *23*, 233-242.
33. Ringsdorf, H.; Venzmer, J.; Winnik, F.M. Fluorescence studies of hydrophobically modified poly(N-isopropylacrylamides). *Macromolecules* **1991**, *24*, 1678-1686.
34. Kwon, G.; Naito, M.; Yokoyama, M.; Okano, T.; Sakurai, Y.; Kataoka, K. Micelles based on AB block copolymers of poly(ethylene oxide) and poly(.beta.-benzyl L-aspartate). *Langmuir* **1993**, *9*, 945-949.
35. Zhao, C.L.; Winnik, M.A.; Riess, G.; Croucher, M.D. Fluorescence probe techniques used to study micelle formation in water-soluble block copolymers. *Langmuir* **1990**, *6*, 514-516.
36. Kalyanasundaram, K.; Thomas, J.K. Environmental effects on vibronic band intensities in pyrene monomer fluorescence and their application in studies of micellar systems. *J. Am. Chem. Soc.* **1977**, *99*, 2039-2044.
37. Förster, T. Excimers. *Angew. Chem. Int. Ed.* **1969**, *8*, 333-343.
38. Bouhadir, G.; Legrand, N.; Quiclet-Sire, B.; Zard, S.Z.; A new practical synthesis of tertiary S-alkyl dithiocarbonates and related derivatives. *Tetrahedron Lett.* **1999**, *40*, 277-280.

Publication P7:  
*Controlled radical polymerization of styrene-based models of the  
active site of the [FeFe]-hydrogenase*

---

D. Heine, C. Pietsch, U. S. Schubert, W. Weigand

*J. Polym. Sci., Part A: Polym. Chem.* **2013**, *51*, 2171–2180.

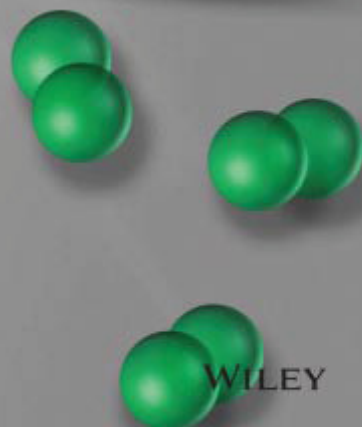
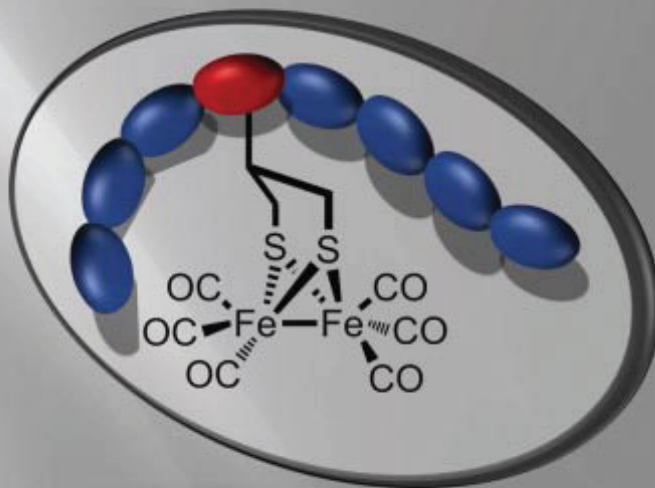
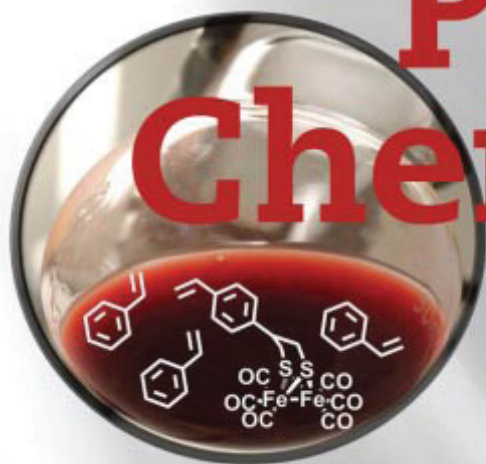


"Including cover page"



JOURNAL OF POLYMER SCIENCE | PART A

# Polymer Chemistry



VOL 51 NO 19 15 MAY 2013  
WWW.POLYMER-CHEMISTRY.ORG



WILEY





# Controlled Radical Polymerization of Styrene-Based Models of the Active Site of the [FeFe]-Hydrogenase

Daniel Heine,<sup>1\*</sup> Christian Pietsch,<sup>2,3,4</sup> Ulrich S. Schubert,<sup>2,3,4</sup> Wolfgang Weigand<sup>1,3</sup>

<sup>1</sup>Institute of Inorganic and Analytical Chemistry, Friedrich-Schiller-University Jena, Humboldtstrasse 8, 07743 Jena, Germany

<sup>2</sup>Laboratory of Organic and Macromolecular Chemistry (IOMC) Friedrich-Schiller-University Jena, Humboldtstraße 10, 07743 Jena, Germany

<sup>3</sup>Jena Center for Soft Matter (JCSM), Philosophenweg 7, 07743 Jena, Germany

<sup>4</sup>Dutch Polymer Institute (DPI), John F. Kennedylaan 2, 5612 AB Eindhoven, The Netherlands

Correspondence to: U. S. Schubert (E-mail: ulrich.schubert@uni-jena.de) or W. Weigand (E-mail: wolfgang.weigand@uni-jena.de)

Received 5 November 2012; revised 23 December 2012; accepted 8 January 2013; published online 14 February 2013

DOI: 10.1002/pola.26584

**ABSTRACT:** Within this study, we report on the first controlled radical polymerization of styrene-based models of the active site of the [FeFe]-hydrogenase. Three different model complexes based on styrene were prepared including propanedithiolato-bridged, 2-azapropanedithiolato-bridged, and bifunctional styrene iron complex. These model complexes were copolymerized with styrene using free radical and the reversible addition-fragmentation chain transfer polymerization method. The polymerization behavior of the hydrogenase models is discussed and analyzed in detail. It could be shown that the model complex can be incorporated into copolymers. The obtained copolymers exhibit narrow molar mass distribu-

tions. The presence of the [FeFe]-hydrogenase models were proven by atomic absorption spectrometry, NMR and IR spectroscopy as well as cyclovoltammetric measurements. It could be shown that the [FeFe]-hydrogenase mimic copolymers, as well as the monomeric originating complexes exhibit electrocatalytic proton reduction at a low potential of  $-2.2$  V. © 2013 Wiley Periodicals, Inc. *J. Polym. Sci., Part A: Polym. Chem.* **2013**, *51*, 2171–2180

**KEYWORDS:** biomimetic; electrochemistry; hydrogenase models; metal-polymer complexes; organometallic catalysts; reversible addition fragmentation chain transfer

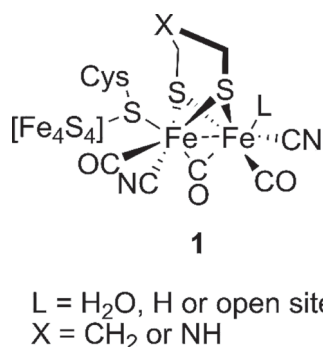
**INTRODUCTION** Hydrogen plays a crucial role in metabolism as well as in the energy balance of different microorganisms, like bacteria or algae. Nature provides a highly efficient tool for hydrogen evolution and uptake, the enzyme hydrogenase.<sup>1,2</sup> Hydrogenases—proteins that are able to convert protons catalytically into hydrogen in a reversible two electron redox process—are key elements of this hydrogen-based metabolism.<sup>3</sup> Thereby the [FeFe]-hydrogenases are seen as the main enzymes for proton reduction. As the structural discovery of the active center,<sup>4,5</sup> numerous attempts have been commenced to synthesize biomimetic models of this so-called “H-Cluster”, showing comparable catalytic efficiency to the enzyme<sup>6–10</sup> (Fig. 1). However, it is obvious, that the efficient performance of the natural enzyme is based on the supporting effect of the surrounding protein environment.

The embedding of active “core structures” into an appropriate polymer might be a suitable substitution of these protein environments. An artificial polymeric structure could provide some of the cavities and proton access channels that are

highly important for the stability and efficiency of the enzyme, like it is in its native environments.<sup>11</sup> For this purpose, block copolymers with defined superstructures could be the ultimate goal. Preferable tools for this synthetic challenge are controlled radical polymerization techniques. Up to now, only few attempts were established to incorporate the subsite of the so-called “H-Cluster” into oligomeric or polymeric materials. It has been reported that models of the active site of the [FeFe]-hydrogenase could successfully be incorporated into electropolymer films<sup>12,13</sup> and tentagel resin beads.<sup>11</sup> Direct polymerization of an alkynyl containing [FeFe]-hydrogenase model could be achieved using Rh, WCl<sub>6</sub>, and SnPh<sub>4</sub> as catalysts.<sup>14,15</sup> Another strategy uses “click” chemistry namely aromatic diazides to incorporate the model complexes in polymers.<sup>16,17</sup> In contrast to these approaches the radical polymerization method is without question one of the most common techniques for the preparation of polymers. However, no radical polymerization of a model complex of the active site of the [FeFe]-hydrogenase has been reported previously. In this contribution, we describe the

\*Present address: Daniel Heine, Leibniz Institute for Natural Product Research and Infection Biology e.V. Hans-Knöll-Institute (HKI), Beutenbergstraße 11a, 07745 Jena, Germany.

© 2013 Wiley Periodicals, Inc.



**FIGURE 1** Schematic representation of the active site of [FeFe]-hydrogenase, the H-Cluster.

syntheses of styrene based hydrogenase models and their incorporation into different copolymers by controlled living radical polymerization techniques. The advantage of controlled radical polymerization methods is the simple control over the molar mass, the molar mass distribution, the ratio between the monomers and the possibility to synthesize block copolymers with different functionality. A series of poly(styrene)-based copolymers containing a [FeFe] cluster were synthesized by reversible addition-fragmentation chain transfer (RAFT) polymerization.<sup>18,19</sup> The focus of this contribution is the development and polymerization of [FeFe]-hydrogenase models, its characterization and the proof of incorporation of the clusters into the copolymers.

## EXPERIMENTAL

### Materials

Styrene (St) was purchased from Sigma-Aldrich and purified by stirring in the presence of inhibitor-remover for hydroquinone or hydroquinone monomethyl ether (Aldrich) for 30 min prior to use. 2,2'-Azobis(*iso*-butyronitrile) (AIBN) was recrystallized from methanol prior to use. 2-Cyano-2-propyl dithiobenzoate (CPDB) was purchased from Sigma-Aldrich and 2-(butylthiocarbothioylthio)propanoic acid (CTA2) was a kind gift from BASF SE and used as received. All other solvents and reagents were purchased from commercial sources. Chemical syntheses were performed under argon atmosphere, using general schlenk techniques.

### Instrumentation

Mass spectra were recorded on a MAT SSQ 710 (Finnigan) and a MAT 95 XL (Finnigan), NMR spectra were recorded on Avance 200, AC 300, Avance 400, and Avance 600 NMR spectrometers (Bruker). Elemental analysis were performed on a Vario EL III CHNS (Elementar Analysensysteme) and IR Spectra on a 2000 FT-IR spectrometer (Perkin-Elmer). Size-exclusion chromatography (SEC) was performed on a Shimadzu system equipped with a SCL-10A system controller, a LC-10AD pump, a RID-10A refractive index detector, a SPD-10AD VP UV/VIS detector and a PSS SDV linear S, 5- $\mu$ m column (8  $\times$  300 mm<sup>2</sup>) with chloroform:triethylamine:2-propanol (94:4:2) as eluent and the column oven was set to 40 °C. A calibration with low polydispersity polystyrene ( $M_n$  from 376 to 128,000 g mol<sup>-1</sup>) standards was used. In addition,

further SEC experiments were carried out using an Agilent1200 series system, a G1310A pump, a G1362A refractive index detector and both a PSS Gram30 and a PSS Gram1000 column in series, whereby *N,N*-dimethylacetamide with 5 mmol lithium chloride was used as an eluent at 1 mL min<sup>-1</sup> flow rate and the column oven was set to 40 °C. The system was calibrated with polystyrene ( $M_n$  from 374 to 1,040,000 g mol<sup>-1</sup>) standards. A triple detection including viscosity, light scattering and RI measurements were performed on a Shimadzu SEC system, equipped with a system controller SCL-10A, a LC-10AD pump, a RID-10A refractive index detector, a UV/VIS detector SPD-10A, a PSS ETA-2010 differential viscometer, a PSS SLD 7000 (BIC) MALS detector (at  $\lambda = 635$  nm), a degasser DGU-14A and a CTO-10A column oven and two PSS SDV linear M columns utilizing THF as eluent with a flow rate of 1 mL min<sup>-1</sup>. A universal calibration with low polydispersity polystyrene ( $M_n$  from 374 to 1,040,000 g mol<sup>-1</sup>) standards was used.

Measurements of cyclic voltammograms were accomplished using a PGSTAT 30 (Metrohm) and a 663 VA STAND (Metrohm) with a glassy carbon working electrode, a Ag/Ag<sup>+</sup> reference electrode and a platinum counter electrode. [*n*Bu<sub>4</sub>N][PF<sub>6</sub>] was used as supporting electrolyte. All solutions were purged with nitrogen for 10 min prior to use. Potentials are given against Fc/Fc<sup>+</sup>. Differential scanning calorimetry (DSC) was performed on a Netzsch DSC 204 F1 Phoenix under nitrogen atmosphere with a heating rate of 10 K min<sup>-1</sup> from -20 to 180 °C. A nova400 (Analytik Jena, Germany) flame atomic absorption spectrometer equipped with an iron hollow cathode lamp (operating at 248.3 nm, Analytik Jena, Germany) was used for the analyses of the amount of iron. The instrumental parameters were adjusted according the manufacturer's recommendation. Fe was determined in aqueous medium between 0.1 and 2.0 mg L<sup>-1</sup>. The complexes and polymers were decomposed to release iron with conc. nitric acid and hydrogen peroxide at 180 °C and 10 bar for 15 min.

### Monomer Synthesis

#### Diethyl 2-(4-vinylbenzyl) Malonate 2

To a solution of diethyl malonate (9 mL, 59.4 mmol) in dry THF (50 mL) sodium hydride (60% in mineral oil, 2.38 g, 59.4 mmol) was slowly added. The reaction mixture was treated with a solution of 4-vinylbenzyl chloride **1** (9.05 g, 59.4 mmol) in dry THF (10 mL) and stirred at room temperature for 17 h. The slightly yellow solution was concentrated under reduced pressure and water (15 mL) was added. The mixture was extracted with dichloromethane (3  $\times$  15 mL) and the combined organic layers were dried (Na<sub>2</sub>SO<sub>4</sub>) and concentrated *in vacuo*. The crude product was purified by column chromatography (gradient elution *n*-hexane—dichloromethane) over silica gel to give 9.64 g of compound **2** as a colorless, viscous oil. Yield: 91% (based on recovered starting material). Bp 48 °C (7.6 10<sup>-1</sup> mbar).

<sup>1</sup>H NMR (200 MHz; CDCl<sub>3</sub>,  $\delta$ , ppm): 7.21 [m, 4H]; 6.64 [dd, 1H;  $J_{trans} = 17.6$ ;  $J_{cis} = 10.9$  Hz]; 5.67 [d, 1H,  $J_{trans} = 17.6$  Hz]; 5.17 [d, 1H,  $J_{cis} = 10.9$  Hz]; 4.13 [q, 4H,  $J = 7.1$  Hz];

3.61 [t, 1H,  $J = 7.8$  Hz]; 3.17 [d, 2H;  $J = 7.8$  Hz]; 1.18 [t, 6H,  $J = 7.1$  Hz].  $^{13}\text{C}$  NMR (50 MHz;  $\text{CDCl}_3$ ,  $\delta$ , ppm): 168.6 (C=O); 137.4 (ArC); 136.3 (CH=CH<sub>2</sub>); 136.0 (ArC); 128.9 (2 ArC); 126.2 (2 ArC); 113.3 (CH=CH<sub>2</sub>); 61.3 (CH<sub>2</sub>CH<sub>3</sub>); 53.6 (CH<sub>2</sub>CH(CO)<sub>2</sub>); 34.2 (CH<sub>2</sub>CH(CO)<sub>2</sub>); 13.8 (CH<sub>2</sub>CH<sub>3</sub>). IR:  $\nu = 1750$  (C=O); 1629 (C=C)  $\text{cm}^{-1}$ . EIMS [ $m/z$  (%): 276 ([M]<sup>+</sup>); 202 ([M-74]<sup>+</sup>). Anal. calcd for C<sub>16</sub>H<sub>20</sub>O<sub>4</sub>: C 69.54, H 7.30; found: C 70.82, H 7.89.

### 2-(4-Vinylbenzyl)propane-1,3-diol **3**

Lithium aluminum hydride (3.26 g, 85.8 mmol) was dissolved in dry diethyl ether (20 mL). To the stirred suspension was slowly added diethyl 2-(4-vinylbenzyl) malonate **2** (4.23 g, 15.3 mmol) in dry diethyl ether and the reaction mixture was stirred at room temperature for 40 h. Afterwards the reaction was quenched by addition of ice. Hydrochloric acid (2 M) was added until the precipitation disappeared. The layers were separated and the aqueous layer was extracted with diethyl ether (2 × 20 mL). Purification by column chromatography (*n*-hexane/ethyl acetate = 1/3) gave product **3** (1.05 g) as white solid. Yield: 36%. mp 39.4 °C.

$^1\text{H}$  NMR (400 MHz;  $\text{CDCl}_3$ ,  $\delta$ , ppm): 7.20 [m, 4H]; 6.67 [dd, 1H,  $J_{trans} = 17.8$  Hz,  $J_{cis} = 10.9$  Hz]; 5.70 [d, 1H,  $J_{trans} = 17.8$  Hz]; 5.20 [d, 1H,  $J_{cis} = 10.9$ ]; 3.72 [s, 2H]; 3.62 [m, 4H]; 2.55 [d, 2H,  $J = 7.4$  Hz]; 1.96 [m, 1H].  $^{13}\text{C}$  NMR (100 MHz;  $\text{CDCl}_3$ ,  $\delta$ , ppm): 139.5 (ArC); 136.4 (CH=CH<sub>2</sub>); 135.3 (ArC); 129.0 (2 ArC); 126.1 (2 ArC); 113.0 (CH=CH<sub>2</sub>); 64.1 (CH<sub>2</sub>OH); 43.8 (CH(CH<sub>2</sub>OH)<sub>2</sub>); 33.8 (CH<sub>2</sub>CH(CH<sub>2</sub>)). IR  $\nu = 3307$  (OH); 1629 (C=C)  $\text{cm}^{-1}$ . EIMS [ $m/z$  (%): 192 ([M]<sup>+</sup>); 174 ([M-18]<sup>+</sup>); 156 ([M-36]<sup>+</sup>), 143 ([M-18-31]<sup>+</sup>). Anal. calcd for C<sub>12</sub>H<sub>16</sub>O<sub>2</sub>: C 74.97, H 8.39; found: C 74.31, H 8.42.

### 2-(4-Vinylbenzyl)propane-1,3-diyl bis(4-methylbenzenesulfonate) **3a**

To a cooled solution (0 °C) of 2-(4-vinylbenzyl)propane-1,3-diol **3** (130 mg, 0.68 mmol) in pyridine (2 mL) was added 4-toluene-sulfonyl chloride (260 mg, 1.36 mmol) and the suspension was stirred at room temperature for 18 h. Afterwards the mixture was given into ice water and the aqueous solution was extracted with dichloromethane (3 × 5 mL). The combined organic layers were washed with water, dried (Na<sub>2</sub>SO<sub>4</sub>) and concentrated *in vacuo*. Purification by column chromatography over silica gel (dichloromethane) gave 222 mg of a white solid. Yield: 66%. Mp 119.5 °C.

$^1\text{H}$  NMR (400 MHz;  $\text{CDCl}_3$ ,  $\delta$ , ppm): 7.51 [m, 8H]; 7.05 [m, 4H]; 6.64 [dd, 1H,  $J_{trans} = 17.6$  Hz,  $J_{cis} = 10.9$  Hz]; 5.68 [d, 1H,  $J_{trans} = 17.6$ ]; 5.21 [d, 1H,  $J_{cis} = 10.9$ ]; 3.91 [m, 4H]; 2.55 [d, 2H,  $J = 7.5$  Hz]; 2.44 [s, 6H]; 2.22 [m, 1H].  $^{13}\text{C}$  NMR (100 MHz;  $\text{CDCl}_3$ ,  $\delta$ , ppm): 145.1 (2 ArC); 136.9 (ArC); 136.3 (CH=CH<sub>2</sub>); 136.1 (ArC); 132.4 (2 ArC); 129.9 (4 ArC); 129.0 (2 ArC); 127.9 (4 ArC); 126.4 (2 ArC); 113.7 (CH=CH<sub>2</sub>); 68.2 (CH<sub>2</sub>O); 40.0 (CH(CH<sub>2</sub>O)<sub>2</sub>); 32.9 (CH<sub>2</sub>CH(CH<sub>2</sub>)); 21.6 (2 CH<sub>3</sub>). IR:  $\nu = 1665$  (C=C); 1178 (S=O)  $\text{cm}^{-1}$ . FAB-MS [ $m/z$  (nba)]: 501 ([M+H]<sup>+</sup>). EIMS [ $m/z$  (%): 328 ([M-172]<sup>+</sup>); 156 ([M-2 × 172]<sup>+</sup>). Anal. calcd for C<sub>26</sub>H<sub>28</sub>O<sub>6</sub>S<sub>2</sub>: C 62.38, H 5.64, S 12.81; found: C 62.27, H 5.36, S 12.57.

### [Fe<sub>2</sub>((SCH<sub>2</sub>)<sub>2</sub>CH(CH<sub>2</sub>C<sub>6</sub>H<sub>4</sub>CHCH<sub>2</sub>))(CO)<sub>6</sub>] **4**

To a cooled solution (-78 °C) of [Fe<sub>2</sub>S<sub>2</sub>(CO)<sub>6</sub>] (57 mg, 0.17 mmol) in dry THF (3 mL) a 1 M solution of LiEt<sub>3</sub>BH (0.34 mL, 34 mmol) was added. After stirring for 15 min **3a** (70 mg, 0.14 mmol) in dry THF was added and the solution was allowed to warm to room temperature. After 16 h stirring the mixture was concentrated under reduced pressure and the crude product was purified by column chromatography (*n*-hexane) over silica gel to give 29.5 mg of a red solid. Yield: 40%.

$^1\text{H}$  NMR (200 MHz;  $\text{CDCl}_3$ ,  $\delta$ , ppm): 7.14 [m, 4H]; 6.67 [dd, 1H,  $J_{trans} = 17.6$  Hz,  $J_{cis} = 10.7$  Hz]; 5.70 [d, 1H,  $J_{trans} = 17.6$  Hz]; 5.21 [d, 1H,  $J_{cis} = 10.7$  Hz]; 2.55 [d, 2H,  $J = 11.4$  Hz]; 2.43 [d, 2H,  $J = 5.4$  Hz]; 1.53 [m, 1H]; 1.37 [m, 2H].  $^{13}\text{C}$  NMR (100 MHz;  $\text{CDCl}_3$ ,  $\delta$ , ppm): 207.5 (CO); 207.1 (CO); 136.6 (ArC); 135.9 (CH=CH<sub>2</sub>); 135.8 (ArC); 128.5 (2 ArC); 126.2 (2 ArC); 113.4 (CH=CH<sub>2</sub>); 45.0 (CH(CH<sub>2</sub>S)<sub>2</sub>); 42.5 (CH<sub>2</sub>CH(CH<sub>2</sub>)<sub>2</sub>); 28.4 (CH<sub>2</sub>S). IR:  $\nu = 2073$ , 2033, 2003 and 1989 (CO)  $\text{cm}^{-1}$ . EIMS [ $m/z$  (%): 502 ([M]<sup>+</sup>); 334 ([M-6 × 28]<sup>+</sup>). Anal. calcd for C<sub>18</sub>H<sub>14</sub>Fe<sub>2</sub>O<sub>6</sub>S<sub>2</sub> × 0.3 C<sub>6</sub>H<sub>14</sub>: C 45.04, H 3.47, S 12.15; found: C 45.69, H 3.42, S 12.71.

### 2-(4-Vinylbenzyl)isoindoline-1,3-dione **5**

The compound was prepared according to a literature procedure,<sup>20</sup> using 5 g (32.8 mmol) of 4-vinylbenzyl chloride **1**. In total 8.49 g (32 mmol) of 2-(4-vinylbenzyl)isoindoline-1,3-dione **5** was obtained. Yield: 98% mp 119.5 °C.

$^1\text{H}$  NMR (200 MHz;  $\text{CDCl}_3$ ,  $\delta$ , ppm): 7.76 [m, 4H]; 7.35 [m, 4H]; 6.65 [dd, 1H;  $J_{trans} = 17.6$  Hz,  $J_{cis} = 10.9$  Hz]; 5.69 [d, 1H,  $J_{trans} = 17.6$  Hz]; 5.2 [d, 1H,  $J_{cis} = 10.9$  Hz]; 4.81 [s, 2H].

### 4-(Methylamino) Styrene **6**

The synthesis of **6** was performed *via* hydrazinolysis of **5**.<sup>20</sup> By using 2 g (7.6 mmol) of **5**, 0.98 g (7.4 mmol) of **6** could be obtained. Yield: 97%.

$^1\text{H}$  NMR (200 MHz;  $\text{CDCl}_3$ ,  $\delta$ , ppm): 7.30 [m, 4H]; 6.69 [dd, 1H;  $J_{trans} = 17.6$  Hz,  $J_{cis} = 10.9$  Hz]; 5.71 [d, 1H,  $J_{trans} = 17.6$  Hz]; 5.20 [d, 1H,  $J_{cis} = 10.9$  Hz]; 3.83 [s, 2H]; 1.58 [s, 2H].

### [Fe<sub>2</sub>((SCH<sub>2</sub>)<sub>2</sub>N(CH<sub>2</sub>C<sub>6</sub>H<sub>4</sub>CHCH<sub>2</sub>))(CO)<sub>6</sub>] **7**

4-Methylamino styrene (280 mg, 2.1 mmol) was added to paraformaldehyde (130 mg, 4.3 mmol) in dry THF and stirred at room temperature for 5 h to give the aminomethylation mixture. To a cooled solution (-78 °C) of [Fe<sub>2</sub>S<sub>2</sub>(CO)<sub>6</sub>] (72 mg, 0.21 mmol) in dry THF (5 mL) was slowly given a 1 M solution of LiEt<sub>3</sub>BH (0.42 mL, 42 mmol). After stirring for 15 min trifluoroacetic acid was added (50  $\mu\text{L}$ ) and after another 15 min the deep red solution was given to the pre-cooled (-78 °C) aminomethylation mixture. The solution was slowly allowed to warm to room temperature followed stirring for additional 17 h. The solvent was removed at reduced pressure and the crude product was isolated by column chromatography (*n*-hexane/dichloromethane = 10:1), resulting in 49 mg of a red solid. Yield: 46%.

$^1\text{H}$  NMR (200 MHz;  $\text{CDCl}_3$ ,  $\delta$ , ppm): 7.20 [m, 4H]; 6.67 [m, 1H]; 5.71 [d, 1H,  $J_{trans} = 17.8$  Hz]; 5.23 [d, 1H,  $J_{cis} = 11.1$  Hz]; 3.64 [s, 2H]; 3.28 [s, 4H].  $^{13}\text{C}$  NMR (100 MHz;  $\text{CDCl}_3$ ,  $\delta$ ,

ppm): 207.8 (CO); 137.3 (ArC); 136.3 (CH=CH<sub>2</sub>); 135.4 (ArC); 128.9 (2 ArC); 126.5 (2 ArC); 114.2 (CH=CH<sub>2</sub>); 61.7 (CH<sub>2</sub>N(CH<sub>2</sub>)<sub>2</sub>); 52.4 (CH<sub>2</sub>S). IR:  $\nu$  = 2073, 2032, and 1994 (CO) cm<sup>-1</sup>. EIMS [*m/z* (%): 503 ([M]<sup>+</sup>); 335 ([M-6 × 28]<sup>+</sup>). Anal. calcd for C<sub>17</sub>H<sub>13</sub>Fe<sub>2</sub>NO<sub>6</sub>S<sub>2</sub> × 0.3 C<sub>6</sub>H<sub>14</sub>: C 42.70, H 3.28, N 2.65, S 12.10; found: C 41.14, H 3.32, N 2.24, S 12.43.

### [Fe<sub>2</sub>(μ-SCH<sub>2</sub>)<sub>2</sub>(C<sub>6</sub>H<sub>4</sub>CHCH<sub>2</sub>)<sub>2</sub>(CO)<sub>6</sub>] **8**

To a cooled solution (-78 °C) of Fe<sub>2</sub>S<sub>2</sub>(CO)<sub>6</sub> (100 mg; 0.29 mmol) in dry THF (5 mL) was slowly given 1 M LiEt<sub>3</sub>BH (0.6 mL; 0.6 mmol). After 15 minutes **1** (150 mg; 1 mmol) was added. The solution was slowly allowed to warm to temperature, resulting in a red colored solution. Afterwards, the solvent was removed under reduced pressure and the crude product was purified by column chromatography (*n*-hexane) to give 69 mg of a red solid. Yield: 41%.

<sup>1</sup>H NMR (200 MHz; CDCl<sub>3</sub>,  $\delta$ , ppm): 7.22 [m, 8H]; 6.69 [m, 2H]; 5.74 [m, 2H]; 5.25 [m, 2H]; 3.60 [s, 2H]; 3.19 [s, 2H]. <sup>13</sup>C NMR (100 MHz; CDCl<sub>3</sub>,  $\delta$ , ppm): 208.5 (CO); 138.4, 138.0, 137.2, 136.9 (4 ArC); 136.3 (2 CH=CH<sub>2</sub>); 129.5, 128.7, 126.7, 126.5 (8 ArCH), 114.3 (CH=C<sup>1</sup>H<sub>2</sub>), 114.1 (CH=C<sup>2</sup>H<sub>2</sub>), 42.8 (C<sup>1</sup>H<sub>2</sub>), 28.4 (C<sup>2</sup>H<sub>2</sub>). IR:  $\nu$  = 2070; 2034 and 1989 (CO) cm<sup>-1</sup>. EIMS [*m/z* (%): 578 ([M]<sup>+</sup>); 410 ([M-6 × 28]<sup>+</sup>). Anal. calcd for C<sub>24</sub>H<sub>18</sub>O<sub>6</sub>Fe<sub>2</sub>S<sub>2</sub> × 0.5C<sub>6</sub>H<sub>14</sub>: C 52.19, H 4.06, S 10.32; found: C 52.20; H 3.73, S 10.06.

### Benzyl (diethoxyphosphoryl)dithioformate (CTA1)

The compound was prepared according to a literature procedure.<sup>21</sup> Yield: 72%.

<sup>1</sup>H NMR (300 MHz, CDCl<sub>3</sub>,  $\delta$ , ppm): 7.36 [s, 5H]; 4.42 [s, 2H, SCH<sub>2</sub>Ph]; 4.25 [m, 4H, POCH<sub>2</sub>]; 1.36 [d, 6H, *J* = 7.1 Hz]. <sup>13</sup>C NMR (75.5 MHz; CDCl<sub>3</sub>,  $\delta$ , ppm): 228.2 (PCSS); 133.9, 129.3, 128.8, 127.9 (4 ArC); 64.7 (d, *J*<sub>CP</sub> = 6.9 Hz, POCH<sub>2</sub>); 40.6 (d, *J*<sub>CP</sub> = 2.7 Hz, SCH<sub>2</sub>Ph); 16.2 (d, *J*<sub>CP</sub> = 6.2 Hz, CH<sub>3</sub>).

### General Procedure for RAFT Copolymerization

In a typical RAFT copolymerization experiment, 1.24 g of styrene (11.9 mmol), 55.5 mg of **8** (0.096 mmol), 1.97 mg of AIBN initiator (0.012 mmol), 11.44 mg of 2-(butylthio-carbonothioylthio)propanoic acid (CTA2) RAFT agent (0.048 mmol) and toluene (1.34 mL) were mixed together in a reaction vial as follows. Both styrene and **8**, toluene as solvent, anisole (0.3 mL) as internal standard and individual stock solutions of AIBN (initiator) and CTA2 dissolved in toluene were added. The monomer concentration was kept at 4.0 mol L<sup>-1</sup> for the polymerization experiment. The vials were closed and degassed by sparging argon for at least 30 min prior to use. Subsequently, the reaction solution was placed in a preheated oil bath at 80 °C for 12 h. The copolymers were purified by precipitation into a large volume of cold methanol and dried under reduced pressure. Conversion was measured by <sup>1</sup>H NMR spectroscopy using anisole as internal standard. For more experimental details see Table 1.

### Free Radical Polymerization

The same protocol as for the RAFT polymerization, with the exception of the addition of the CTA agent, was used. For more experimental details see Table 1.

## RESULTS AND DISCUSSION

### Syntheses of [FeFe]-Hydrogenase Monomers

The first objective of our work was to synthesize polymerizable [FeFe]-hydrogenase models. For this purpose, we choose styrene based models due to the synthesis access and the high monomer stability against hydrolysis. The [FeFe] cluster is connected to the styrene unit via a bridged configuration. Because of the uncertainty of the bridgehead atom, which is represented in nature by nitrogen or carbon atoms, synthetic models of the [FeFe]-hydrogenase mostly include either a propanedithiolato or an 2-aza-1,3-propanedithiolato subunit. This led us to the intention to design polymerizable systems

**TABLE 1** Overview of Reaction Conditions and Characterization Data of the Obtained Copolymers Via RAFT Copolymerization

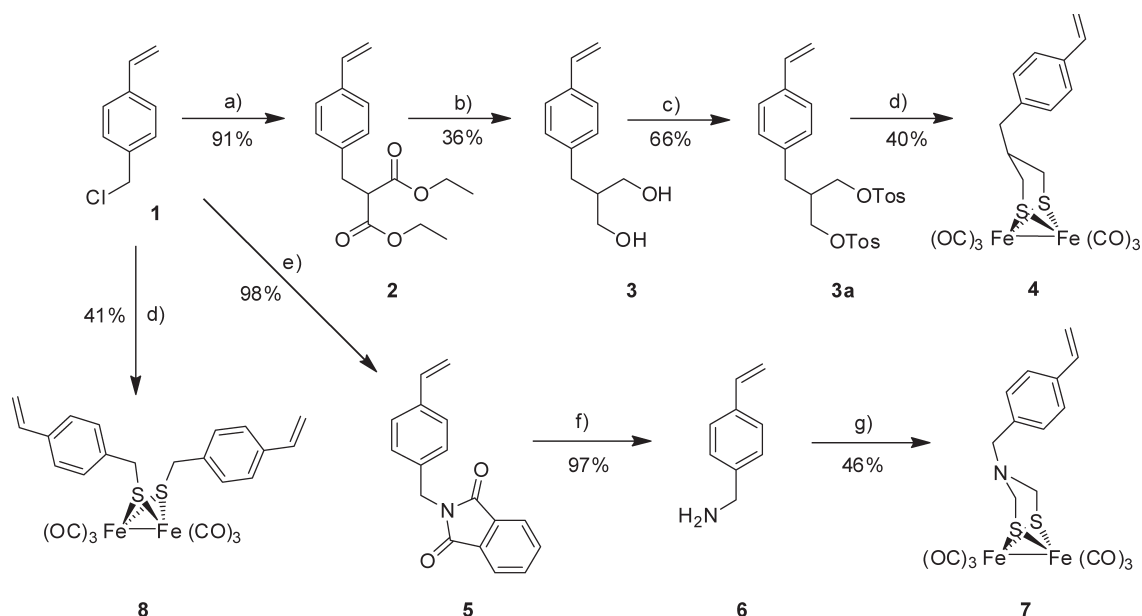
Sample	[M]/[FeFe]/ CTA <sup>a</sup>	Initiator	[M]/[FeFe]: [CTA]:[Initiator] <sup>a</sup>	<i>T</i> (°C)	<i>C</i> <sub>monomer</sub> (mol L <sup>-1</sup> )	<i>T</i> (h)	<i>M</i> <sub>n</sub> [g mol <sup>-1</sup> ] <sup>b</sup>	PDI <sup>b</sup>	Conv.
<b>09</b>	St/ <b>8</b> /-	AIBN	245/5:-:1	70	2.0	13	28,400 <sup>c</sup>	5.4 <sup>c</sup>	n/a
<b>10</b>	St/ <b>4</b> /CTA1	AIBN	199/1:1:0.25	70	4.0	18	7,400	1.23	n/a
<b>11</b>	St/ <b>8</b> /CTA2	AIBN	248/2:1:0.25	80	4.0	14	9,700	1.24	32
<b>12</b>	St/ <b>7</b> /CTA2	AIBN	95/5: 1:0.25	80	2.0	10	- <sup>d</sup>	- <sup>d</sup>	0
<b>13</b>	St-/CTA2	VAZO88	100/0: :0.25	80	4.37	15	5,000	1.08	33
<b>14</b>	St/ <b>8</b> /CTA2	VAZO88	96/4:1:0.25	80	4.37	28	3,100	1.31	n/a
<b>15</b>	AA/ <b>8</b> /CTA2	AIBN	98/2:1:0.25	70	2.0	6 (7; 6)	- <sup>d</sup>	- <sup>d</sup>	0
<b>16</b>	St-/CPDB	AIBN	100/0: :0.25	70	2.0	16	4,500	1.11	35
<b>17</b>	St/ <b>8</b> /CPDB	AIBN	98/2:1:0.25	70	2.0	24	2,800	1.18	n/a
<b>17re</b>	St/ <b>8</b> /CPDB	AIBN	98/2:1:0.25	70	2.0	26	6,000	1.6	n/a

<sup>a</sup> M = monomer, [FeFe] = [FeFe]-hydrogenase mimic, CTA = chain transfer agent; molar feed ratios.

<sup>b</sup> Calculated from SEC (CHCl<sub>3</sub>) using PS calibration.

<sup>c</sup> Calculated from SEC (DMAc) using PS calibration.

<sup>d</sup> No polymer obtained.



**FIGURE 2** Schematic representation of the syntheses of styrene-based [FeFe]-hydrogenase models. (a) diethyl malonate, NaH; (b) LiAlH<sub>4</sub>; (c) 4-toluenesulfonyl chloride, pyridine; (d) Fe<sub>2</sub>S<sub>2</sub>(CO)<sub>6</sub>, LiEt<sub>3</sub>BH; (e) potassium phthalimide, DMF; (f) hydrazine hydrate; (g) I: HCHO II: Fe<sub>2</sub>(SH)<sub>2</sub>(CO)<sub>6</sub>.

related to the active site of the [FeFe]-hydrogenase, that matches both prospects, namely an *N* or a *C* bridgehead atom (7 vs. 4).

The synthesis of the propanedithiolato-bridged model 4 was established by reacting 4-vinylbenzyl chloride 1 with diethyl malonate under the presence of sodium hydride (Fig. 2).

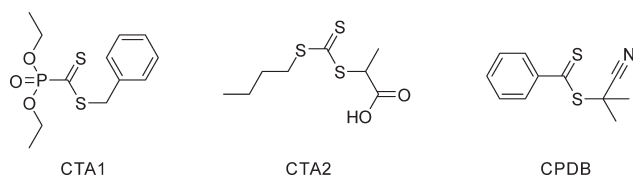
The resulting diethyl 2-(4-vinylbenzyl) malonate 2 was reduced with lithium aluminum hydride to diol 3. The introduction of a tosylate as leaving group was accomplished by the reaction with 4-toluenesulfonyl chloride. Reaction with the reduced cluster Fe<sub>2</sub>S<sub>2</sub>(CO)<sub>6</sub><sup>2-</sup> at -78 °C resulted in the formation of the styrene-based [FeFe]-hydrogenase model 4. Contrary, the synthesis of the 2-aza-1,3-propanedithiolato-bridged model 7 was established by condensation reaction of 4-methylamino styrene 6 with 2 equivalents of formaldehyde and diiron carbonyl sulfide. Amine 6 was synthesized, following a literature procedure reported by Bertini.<sup>20</sup> Beside both the bridged model complexes 4 and 7 we also focused on a monomer that has an easier synthesis access (1 step procedure, Fig. 2). For this purpose we synthesized complex 8 from the reaction of 4-vinylbenzylchloride and the Fe<sub>2</sub>S<sub>2</sub>(CO)<sub>6</sub><sup>2-</sup> cluster after reduction with LiEt<sub>3</sub>BH. In addition complex 8 is able to form cross-linked copolymer systems.

### Polymerization of Styrene [FeFe]-Hydrogenase Models

Literature reports based on polymerization of metal containing monomers indicate a considerable difference concerning certain polymerization parameters. The behavior of metalloence derivatives in radical polymerizations were extensively studied, in particular in the case of vinyl ferrocene.<sup>22-27</sup> On the one hand iron containing monomers like vinyl ferrocene or ferrocenyl (meth)acrylates are already known for interactions with the propagating radical. The reported difficulties

in the polymerization behavior are based on a termination reaction via an electron transfer from the ferrocene nucleus to the radical.<sup>25,27,28</sup> This termination reaction would cause the polymerization to slow down or even completely inhibit the polymerization. Also, H-abstraction of the methylene group in  $\alpha$ -position by a radical may occur, which leads to chain transfer side reactions.<sup>28</sup> On the other hand the temperatures, which are required in radical polymerization, play an important role due to possible decomposition of the metal complex. Literature reports about styrene monomers containing metal clusters and their polymerization are quite rare. Pitman and Withers report about a tricobalt nonacarbonyl styrene complex and both groups observed a partially decomposition during the polymerization.<sup>26,29</sup> Contrary, Pomogailo et al.<sup>30-34</sup> reported about the preparation and copolymerization (styrene or acrylonitrile) of osmium, iron and rhodium-based trinuclear cluster monomers. The authors described that all attempts to homopolymerize these cluster type monomers have not been successful.<sup>34</sup>

The styrene derivative 8 provides a good starting point for free radical polymerization experiments. In a first experiment, [FeFe]-hydrogenase model 8 could be successfully polymerized using AIBN as radical initiator with a ratio 8/styrene of 5/245 at 70 °C in toluene. The copolymer exhibits very strong signals for the CO vibration in the IR-region at 2067, 2033, and 1987 cm<sup>-1</sup>. The signals are not differing strongly to these of the monomeric model 8. Because of the possibility of cross-linking, copolymer 9 features a molar mass of  $M_n = 28.400$  g/mol and a PDI value of 5.4. This experiment proves the stability and the possibility to copolymerize the [2Fe2S]-core under classical conditions of a free radical polymerization. In the next step we tried to use the RAFT polymerization<sup>18,19,35,36</sup> technique for the controlled



**FIGURE 3** Schematic representation of the CTA agents used in the controlled radical polymerization of the [FeFe]-hydrogenase models.

radical polymerization of these [FeFe]-hydrogenase models. We have chosen the RAFT process to obtain well-defined copolymers due to several reasons. The RAFT process tolerates a wide range of monomers and functional groups and was already used for the polymerization of ferrocenyl (meth)acrylates.<sup>28</sup> The RAFT polymerization method was performed using AIBN as radical starter and different chain transfer agents (CTA) for styrene derivatives were investigated to obtain good control over the polymerization (Fig. 3). Within this series, the ratios of [FeFe]-hydrogenase models to styrene were varied.

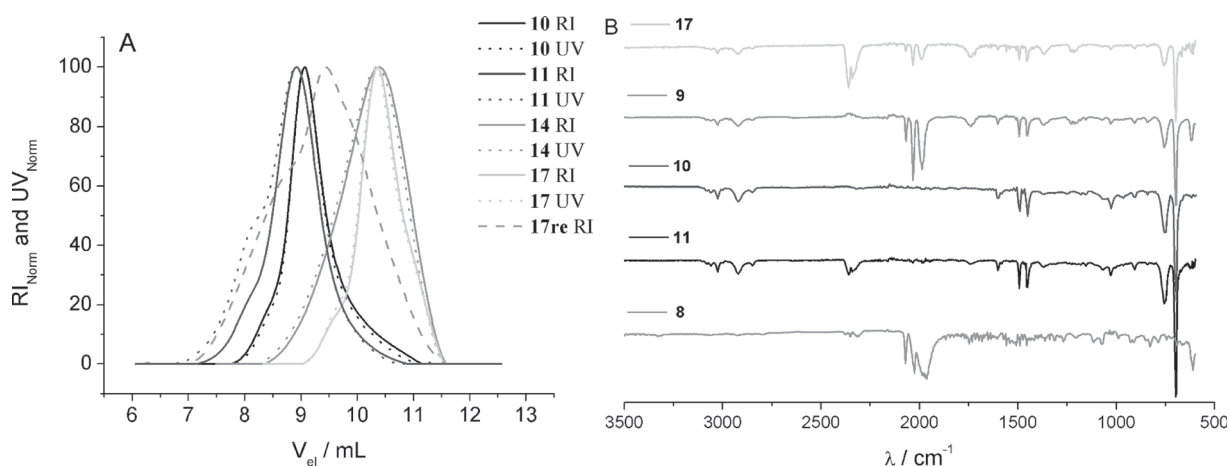
The addition of RAFT agent benzyl (diethoxyphosphoryl) dithioformate (CTA1) led to a controlled copolymerization of **4** and styrene as shown by the data in Table 1 and the SEC trace in Figure 4(a). The obtained copolymer **10** has a molar mass of  $7400 \text{ g mol}^{-1}$  with a PDI value of 1.23. Still, the ratio between the [FeFe] cluster and styrene is low (1/199), but for this reason ensures isolated catalytic centers. Three weak signals in the IR-region at 2079, 2044, and  $1987 \text{ cm}^{-1}$  [Fig. 4(b)] as well as the absorption of the copolymer on the SEC profile [Fig. 4(a)] indicates the presence of the [FeFe]-core in the obtained copolymer **10**. Model complexes of the [FeFe]-hydrogenase bearing a propandithiolato-bridge have been described to show a strong absorbance in the near-UV region and in the region around 460 nm (charge transfer transitions).<sup>37</sup> The measurement of the UV absorbance of the polymer should, therefore, be a suitable tool to monitor qualitatively the incorporation of the intact [FeFe]-core unit.

Using a mixture of complex **8**/styrene with a ratio of 2:248 in the presence of 2-(((butylsulfanyl) carbonothioyl) sulfanyl) propanoic acid (CTA2) at  $80 \text{ }^\circ\text{C}$  leads to the formation of a copolymer (**11**) with a molar mass ( $M_n$ ) of  $9700 \text{ g/mol}$ . The signals of the CO-vibration of **11** in the IR-spectrum are present at 2033 and  $1986 \text{ cm}^{-1}$  [Fig. 4(b)]. The low PDI value of 1.24, the nearly monomodal distribution in the SEC profile [Fig. 4(a)] and the remaining signal of one proton of the alkenyl-group in the  $^1\text{H}$  NMR-spectrum of copolymer **11** indicates that most of the [2Fe2S]-centers are linked to the polymer backbone by only one out of two possible connecting groups. Therefore, we assume that the amount of cross-linking is decreased to a minimum due to the higher CTA content and the low monomer conversion.

However, the polymerization of hydrogenase model **7** under RAFT-conditions failed (**12**, Table 1), leading to a black-colored solution that did not show any polymer. Although severe problems are reported for the RAFT polymerization of primary amines, the RAFT polymerization of tertiary amines should not be challenging.<sup>19</sup> The reason may be the aminolysis of the CTA agent and this is mainly based on primary or secondary amines.<sup>38–40</sup>

Another reason might be the decomposition of the [FeFe] model **7** under the RAFT conditions due to the different bridgehead atom in the cluster ( $N$  atom, Fig. 2). An evidence for decomposition of the iron cluster is the color change of the solution after the polymerization into black.

In addition to the critical polymerization of hydrogenase model **7**, two RAFT polymerizations with and without hydrogenase model **8** were performed to investigate a possible interference of the iron cluster with the propagating radical. The RAFT polymerization of styrene at  $80 \text{ }^\circ\text{C}$  with 1,1'-azobis(cyclohexanecarbonitrile) (VAZO88) initiator results in a polystyrene (**13**) with a molar mass ( $M_n$ ) of  $5000 \text{ g mol}^{-1}$  and a PDI value of 1.08. A conversion of styrene of 33% was reached after 15 h. The same procedure was used for the polymerization of the hydrogenase model **8** with a ratio St/**8** of 96/4. After 28 h polymerization time a copolymer



**FIGURE 4** (a) SEC trace of the synthesized copolymers (UV/VIS detector at 490 nm) and (b): IR spectra of different [FeFe] cluster copolymers and styrene monomer **8**.

TABLE 2 Molar Mass Comparison of Selected Copolymers

Sample	$M_n$ (RI) [g mol <sup>-1</sup> ] <sup>a</sup>	PDI <sup>a</sup>	$M_n$ (RI) [g mol <sup>-1</sup> ] <sup>b</sup>	PDI <sup>b</sup>	$M_v$ (visco) [g mol <sup>-1</sup> ] <sup>b</sup>	PDI <sup>b</sup>	$M_w$ (MALS) [g mol <sup>-1</sup> ] <sup>b</sup>	PDI <sup>b</sup>
<b>11</b>	9,700	1.24	8,400	1.38	10,100	1.32	13,300	1.56
<b>17re</b>	6,000	1.6	4,500	1.80	9,200	1.86	10,700	2.01

<sup>a</sup> Calculated from SEC (CHCl<sub>3</sub>) using PS calibration.

<sup>b</sup> Average value of three individual measurements, calculated from SEC (THF) using universal PS calibration.

(**14**, Table 1) with  $M_n = 3100$  g mol<sup>-1</sup> and a PDI value of 1.31 was obtained. The copolymerization of the iron-cluster complex is slower than the homopolymerization of styrene, which could be an indication for inhibition and/or possible interference with the radicals that would slow down the polymerization rate. The iron center could catch the radical (termination step), as it was already observed for different iron containing monomers.<sup>25,27,28</sup> As a consequence the radical concentration inside the solution is reduced, leading to a decreased polymerization rate. Conversely, this observation might simply be deduced to a slower polymerization rate of the *para*-alkylstyrene moiety which shows a reduced reactivity in radical polymerizations in comparison to styrenes. This effect was already reported, for example, for 4-methylstyrene<sup>41</sup> and for 4-ethylstyrene.<sup>42</sup>

We further sought for a possible RAFT copolymerization of acrylic acid and complex **8** (Table 1, **15**) in ethanol. Unfortunately, no polymers were visible in the SEC trace after 7 h polymerization time. Even after some re-initiation with AIBN (same and double amount of AIBN), no polymer could be observed. We assumed therefore a strong interaction of the acrylic acid monomers and the iron clusters inhibiting completely the polymerization.

Another CTA (2-cyanopropyl-dithiobenzoate, CPDB) was used for the copolymerization of monomer **8** to investigate if this CTA is another suitable initiator for the copolymerization. After 24 h polymerization time copolymer **17** with a molar

mass ( $M_n$ ) of 2800 g/mol and a narrow mass distribution [Fig. 4(a)] was observed. For this approach the *bis*(styrene)iron complex **8** was used together with styrene in a ratio of 98/2.

As a result, a considerably slower polymerization rate was observed. After 16 h the RAFT polymerization of styrene results in a polymer (**16**) with a molar mass ( $M_n$ ) of 4500 g mol<sup>-1</sup> (PDI 1.11). However, when using hydrogenase model **8** nearly half the molar mass ( $M_n = 2800$  g mol<sup>-1</sup>, PDI 1.18) was only obtained (Table 1). It should also be noted that due to the low conversion and the large St/FeFe feed ratio it might be possible that not all copolymer chains are functionalized with the iron cluster. A reinitiation for further polymerization of copolymer **17** with AIBN was performed to investigate the "living" character of the copolymer. Indeed, a chain extension could be observed, but on the other hand it results in a broader molar mass distribution of polymer **17re** with a PDI value of 1.6 and a molar mass of 6000 g mol<sup>-1</sup>, due to the possibility of cross-linking and low amounts of incomplete chain extension.

A molar mass calculation was performed for selected samples using a triple detection including a RI, a viscosity and a MALS detector (Table 2). For this estimation three individual measurements were performed showing a monomodal distribution for copolymer **11** and **17re**. The results confirmed the molar masses as obtained by the conventional calculation, besides the  $M_w$  by MALS detection, where the signal to

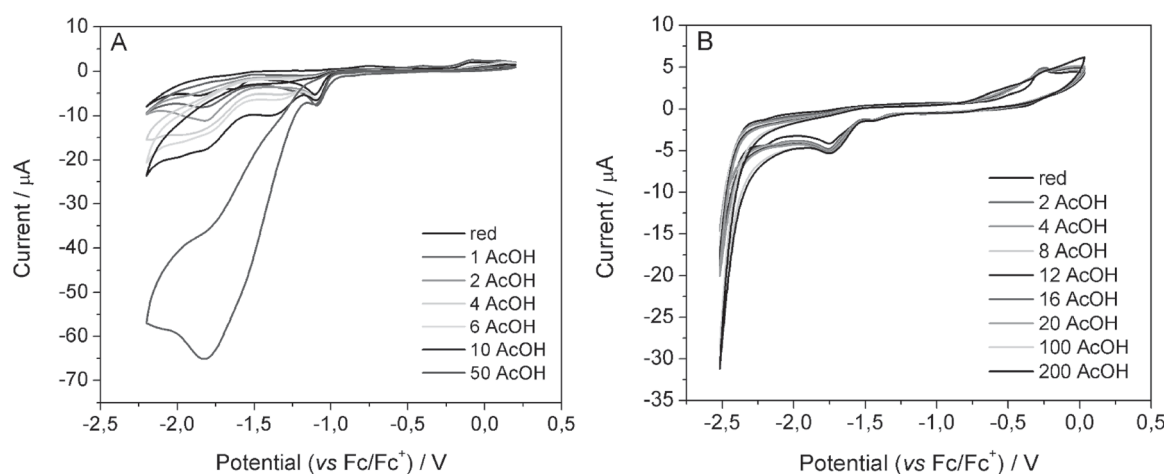


FIGURE 5 (a): Cyclic voltammogram under addition of acetic acid (AcOH) of monomer **8** and (b): Cyclic voltammogram under addition of acetic acid (AcOH) of copolymer **17re**.

**TABLE 3** Characterization of Monomeric and Polymeric Styrene-Based [FeFe]-Hydrogenase Models

Sample	IR-Signal (cm <sup>-1</sup> )	$E_{pc}/V^a$ (Fe <sup>1</sup> Fe <sup>1</sup> /Fe <sup>0</sup> Fe <sup>1</sup> )	$E_{pc}/V^a$ (Fe <sup>0</sup> Fe <sup>1</sup> /Fe <sup>0</sup> Fe <sup>0</sup> )	$E_{pa}/V^a$ (Fe <sup>1</sup> Fe <sup>1</sup> /Fe <sup>1</sup> Fe <sup>2</sup> )	St/[FeFe] Ratio <sup>b</sup> <sup>1</sup> H NMR (mol %)	Fe <sub>Theo</sub> (mass %) <sup>c</sup>	Fe <sub>Exp</sub> (mass %) <sup>d</sup>
<b>4</b>	2,073, 2,033, 1,989	-1.64	-2.28	0.85	—	n/a	n/a
<b>7</b>	2,073, 2,032, 1,994	-1.72	-2.25	0.44	—	n/a	n/a
<b>8</b>	2,070, 2,034, 1,989,	-1.73	-2.26	0.62	—	19.3	17.5
<b>9</b>	2,067, 2,033, 1,987	-1.72	-2.20	n/a	89/11	1.97	1.59
<b>10</b>	2,079, 2,044, 1,987,	-1.58	-1.85	0.81	98.8/1.2	0.53	n/a
<b>11</b>	2,033, 1,986	-1.75	-2.22	0.47	98.2/1.8	0.83	0.39
<b>17re</b>	2,069, 2,033, 1,986	-1.75	-2.21	0.26	95.6/4.4	1.97	3.5

<sup>a</sup> Performed in dichloromethane or DMF, supporting electrolyte: [nBu<sub>4</sub>N][PF<sub>6</sub>], scan rate: 0.1 V s<sup>-1</sup> against Fc/Fc<sup>+</sup> (Fc = ferrocene).

<sup>b</sup> Calculated from the integral of the -CH<sub>2</sub>-Ar signal of the [FeFe]-bridge and that of the backbone polystyrene signals in the <sup>1</sup>H NMR spectra, whereby St means styrene and [FeFe] the [FeFe]-hydrogenase mimic.

<sup>c</sup> Calculated according to formula: Fe<sub>Theo</sub> (mass %) = 2 m × M<sub>Fe</sub> / (n × M<sub>St</sub> + m × M<sub>[FeFe]</sub>) using the feed ratio to estimate the n and m values.

<sup>d</sup> Determined by AAS spectrometry.

noise ratio is too poor due to the low molar mass of the analyzed samples.

### Cyclovoltammetric, AAS, and NMR Measurements

The electrochemical properties of the model compounds were examined by cyclic voltammetry. Monomer clusters **4** and **7** show a quasi-reversible signal of the first reduction event at -1.64 and -1.72 V [Fig. 5(a)], which turns into a reversible signals under elevation of the scan rate to 1 V s<sup>-1</sup>. By contrast, compound **8** exhibits an irreversible signal in this region, which appears at -1.73 V. This might be explained by a decreased stability of the complex after reduction. Oxidation occurs in a less similar range, starting with compound **7** at 0.44 V. All synthesized styrene based complexes showing an electrocatalytic proton reduction after addition of acetic acid due to a rising signal at the second reduction event.

The electrochemical investigation of polymers is often quite challenging due to low solubility or in general broader signals. Nevertheless, we were able to observe all expected signals without major difficulties. In general larger amounts of the copolymers are necessary. The cyclovoltammetric investigation of the copolymers **9-11** and **17re** revealed a redox behavior comparable to these of the related monomeric compounds [Fig. 5(b)].

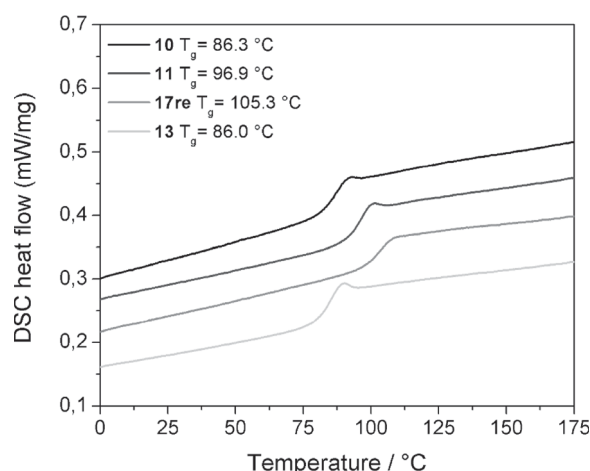
All copolymers of monomer **8** show an increased first and second reduction event at around -1.7 and -2.2 V, respectively. However, copolymer **10** differs from these values being reduced rather early starting with a first reduction event emerging at -1.58 V and a second reduction event at -1.85 V. The reduction is obviously performed at a milder potential compared to that of the polymers **9** and **11**, which are derived from styrene-based monomer **8**.

Addition of acetic acid led to a rising second reduction signal which, therefore, indicates an electrocatalytic proton reduction in acidic solution. Taken together, the cyclovoltammetric examinations implicate that the incorporation of the [FeFe]-hydrogenase model into a large polymer does not inhibit the catalytic ability of the model complexes **4** and **8**. The per-

formance of the [2Fe2S]-clusters is therefore still active in the polymer chain.

The amount of [2Fe2S]-clusters incorporated into the polymer correlates most likely with the ratio of iron present in the polymeric material. Therefore, we considered atomic absorption spectrometry (AAS) as possible tool to gain insights into the degree of [FeFe] clusters incorporated. As all polymers are insoluble in water, a chemical extraction under strong acidic condition prior to the measurements was performed. The theoretical amount of iron in the polymeric samples is in good agreement with the experimental ones (Table 3). Measurement errors of the AAS investigation are probably related to the pre-treatment and the chemical extraction of the polymeric material. In addition the assigned amounts of incorporated iron clusters were supported by calculations using <sup>1</sup>H NMR spectroscopy. All calculated amounts are in a good agreement with the theoretical values and are shown in Table 3.

Representative DSC traces are shown in Figure 6. A glass transition temperature (*T*<sub>g</sub>) of homo polystyrene **13** was



**FIGURE 6** DSC response (third heating cycle) of the investigated [FeFe] cluster polystyrene copolymers.



observed at 86 °C. The  $T_g$  of the iron-cluster copolymers vary in a temperature range from 86.3 to 105.3 °C (with a heat capacity ( $\Delta C_p$ ) of about 0.35 Jg<sup>-1</sup> K<sup>-1</sup>) probably due to a different content of [2Fe2S] clusters. On the one hand this behavior can be explained by the decreased chain mobility in cases of higher contents of the bulky cluster. On the other hand differences may be deduced to a higher “crosslinking” of the *bis*(styrene) complex containing copolymers. Finally one cannot exclude that the observed variations in the DSC traces may also arise from differences in the molar mass of the copolymers.

## CONCLUSIONS

Three different styrene-based monomers connected to a model of the active site of the [FeFe]-hydrogenase were synthesized. The modified styrene derivatives with a carbon bridgehead atom could be successfully copolymerized by a controlled radical polymerization technique. In contrast to that, the nitrogen bridged complex could not be copolymerized despite several attempts. All functional copolymers show a moderate to even strong absorbance in the area of the carbonyl-vibration in the IR-region, indicating the incorporation of the [2Fe2S]-hexacarbonyl-cluster. It could be shown that the biomimetic metal centers keep their activity and redox behavior after polymerization and inclusion into the copolymer chain. Furthermore, electrocatalytic proton reduction could be proven. The content of catalytic [2Fe2S]-clusters could be determined using ASS-measurements and <sup>1</sup>H NMR spectroscopy. With this work, we contribute to efforts in immobilizing [FeFe]-hydrogenase mimics to readily processable copolymers. We are convinced that our work will support future developments in the field of polymer-bound metallorganic catalysts, able to produce hydrogen in a highly efficient manner.

## ACKNOWLEDGMENTS

The authors like to thank U.P. Apfel for important discussions, S. Köhn for AAS measurements, C. Friebe for CV investigations, R. Paulus for DSC analysis and G. Festag for SEC measurements. Financial support of the Dutch Polymer Institute (DPI, technology area HTE) and the Carl-Zeiss-Foundation (Strukturantrag JCSM) are gratefully acknowledged.

## REFERENCES AND NOTES

- 1 A. I. Krasna, D. Rittenberg, *J. Am. Chem. Soc.* **1954**, *76*, 3015–3020.
- 2 Frey, M. *ChemBioChem* **2002**, *3*, 153–160.
- 3 M. W. W. Adams, *FEMS Microbiol. Lett.* **1990**, *75*, 219–237.
- 4 J. W. Peters, W. N. Lanzilotta, B. J. Lemon, L. C. Seefeldt, *Science* **1998**, *282*, 1853–1858.
- 5 Y. Nicolet, C. Piras, P. Legrand, C. E. Hatchikian, J. C. Fontecilla-Camps, *Structure* **1999**, *7*, 13–23.
- 6 B. E. Barton, T. B. Rauchfuss, *J. Am. Chem. Soc.* **2010**, *132*, 14877–14885.
- 7 D. J. Evans, C. J. Pickett, *Chem. Soc. Rev.* **2003**, *32*, 268–275.
- 8 C. D. Tard, C. J. Pickett, *Chem. Rev.* **2009**, *109*, 2245–2274.
- 9 U.-P. Apfel, Y. Halpin, M. Gottschaldt, H. Görls, J. G. Vos, W. Weigand, *Eur. J. Inorg. Chem.* **2008**, 5112–5118.
- 10 M. Y. Darensbourg, W. Weigand, *Eur. J. Inorg. Chem.* **2011**, 917–918.
- 11 K. N. Green, J. L. Hess, C. M. Thomas, M. Y. Darensbourg, *Dalton Trans.* **2009**, 4344–4350.
- 12 S. K. Ibrahim, X. Liu, C. Tard, C. J. Pickett, *Chem. Commun.* **2007**, 1535–1537.
- 13 S. Ibrahim, P. M. Woi, Y. Alias, C. J. Pickett, *Chem. Commun.* **2010**, *46*, 8189–8191.
- 14 X. Liu, X. Ru, Y. Li, K. Zhang, D. Chen, *Int. J. Hydrogen Energy* **2011**, *36*, 9612–9619.
- 15 X. Ru, X. Zeng, Z. Li, J. D. Evans, C. Zhan, Y. Tang, L. Wang, X. Liu, *J. Polym. Sci. Part A: Polym. Chem.* **2010**, *48*, 2410–2417.
- 16 C. Zhan, X. Wang, Z. Wei, D. J. Evans, X. Ru, X. Zeng, X. Liu, *Dalton Trans.* **2010**, *39*, 11255–11262.
- 17 L. Wang, Z. Xiao, X. Ru, X. Liu, *RSC Adv.* **2011**, *1*, 1211–1219.
- 18 J. Chiefari, Y. K. Chong, F. Ercole, J. Krstina, J. Jeffery, T. P. T. Le, R. T. A. Mayadunne, G. F. Meijs, C. L. Moad, G. Moad, E. Rizzardo, S. H. Thang, *Macromolecules* **1998**, *31*, 5559–5562.
- 19 G. Moad, E. Rizzardo, S. H. Thang, *Aust. J. Chem.* **2009**, *62*, 1402–1472.
- 20 V. Bertini, S. Alfei, M. Poggi, F. Lucchesini, N. Picci, F. lemma, *Tetrahedron* **2004**, *60*, 11407–11414.
- 21 M. Laus, R. Papa, K. Sparnacci, A. Alberti, M. Benaglia, D. Macciantelli, *Macromolecules* **2001**, *34*, 7269–7275.
- 22 M. G. Baldwin, K. E. Johnson, *J. Polym. Sci. Part A-1 Polym. Chem.* **1967**, *5*, 2091–2098.
- 23 J. C. Lai, T. Rounsfell, C. U. Pittman, *J. Polym. Sci. Part A-1 Polym. Chem.* **1971**, *9*, 651–662.
- 24 M. H. George, G. F. Hayes, *J. Polym. Sci. Polym. Chem.* **1973**, *11*, 471–477.
- 25 M. H. George, G. F. Hayes, *J. Polym. Sci. Polym. Chem.* **1975**, *13*, 1049–1070.
- 26 C. U. Pittman, M. D. Rausch, *Pure Appl. Chem.* **1986**, *58*, 617–622.
- 27 C. Pittman, *J. Inorg. Organomet. Polym. Mater.* **2005**, *15*, 33–55.
- 28 C. Herfurth, D. Voll, J. Buller, J. Weiss, C. Barner-Kowollik, A. Laschewsky, *J. Polym. Sci. Part A: Polym. Chem.* **2012**, *50*, 108–118.
- 29 D. Seyferth, H. P. Withers, *Inorg. Chem.* **1983**, *22*, 2931–2936.
- 30 V. A. Maksakov, V. P. Kirin, S. N. Konchenko, N. M. Bravaya, A. D. Pomogailo, A. V. Virovets, N. V. Podberezskaya, I. G. Barakovskaya, S. V. Tkachev, *Russ. Chem. Bull.* **1993**, *42*, 1236–1241.
- 31 Y. Shul’ga, O. Roshchupkina, G. Dzhardimalieva, I. Cherushevich, A. Dodonov, Y. Baldokhin, P. Kolotykin, A. Rozenberg, A. Pomogailo, *Russ. Chem. Bull.* **1993**, *42*, 1661–1665.
- 32 N. M. Bravaya, A. D. Pomogailo, V. A. Maksakov, V. P. Kirin, V. P. Grachev, A. I. Kuzaez, *Russ. Chem. Bull.* **1995**, *44*, 1062–1067.
- 33 S. I. Pomogailo, G. V. Shilov, V. A. Ershova, A. V. Virovets, V. M. Pogrebnyak, N. V. Podberezskaya, A. V. Golovin, G. I. Dzhardimalieva, A. D. Pomogailo, *J. Organomet. Chem.* **2005**, *690*, 4258–4264.
- 34 S. I. Pomogailo, G. I. Dzhardimalieva, V. A. Ershova, S. M. Aldoshin, A. D. Pomogailo, *Macromol. Symp.* **2002**, *186*, 155–160.

- 35** C. Pietsch, M. W. M. Fijten, H. M. L. Lambermont-Thijs, R. Hoogenboom, U. S. Schubert, *J. Polym. Sci. Part A: Polym. Chem.* **2009**, *47*, 2811–2820.
- 36** A. M. Breul, C. Pietsch, R. Menzel, J. Schäfer, A. Teichler, M. D. Hager, J. Popp, B. Dietzek, R. Beckert, U. S. Schubert, *Eur. Polym. J.* **2012**, *48*, 1339–1347.
- 37** A. T. Fiedler, T. C. Brunold, *Inorg. Chem.* **2005**, *44*, 1794–1809.
- 38** H. Willcock, R. K. O'Reilly, *Polym. Chem.* **2010**, *1*, 149–157.
- 39** G. Moad, E. Rizzardo, S. H. Thang, *Polym. Int.* **2011**, *60*, 9–25.
- 40** U. Mansfeld, C. Pietsch, R. Hoogenboom, C. R. Becer, U. S. Schubert, *Polym. Chem.* **2010**, *1*, 1560–1598.
- 41** R. W. H. Berry, A. J. Ludlow, R. J. Mazza, *Macromol. Chem. Phys.* **1997**, *198*, 1579–1595.
- 42** I. A. Barker, J. El Harfi, K. Adlington, S. M. Howdle, D. J. Irvine, *Macromolecules*, **2012**, *45*, 9258–9266.

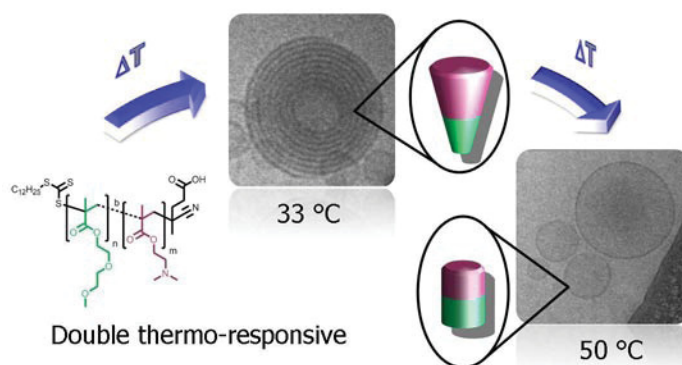
## Publication P8:

### *Thermo-induced self-assembly of responsive poly(DMAEMA-*b*-DEGMA) block copolymers into multi- and uni-lamellar vesicles*

---

C. Pietsch, U. Mansfeld, C. Guerrero-Sanchez, S. Hoepfner, A. Vollrath, M. Wagner, R. Hoogenboom, S. Saubern, S. H. Thang, C. R. Becer, J. Chiefari, U. S. Schubert

*Macromolecules*, **2012**, *45*, 9292–9302



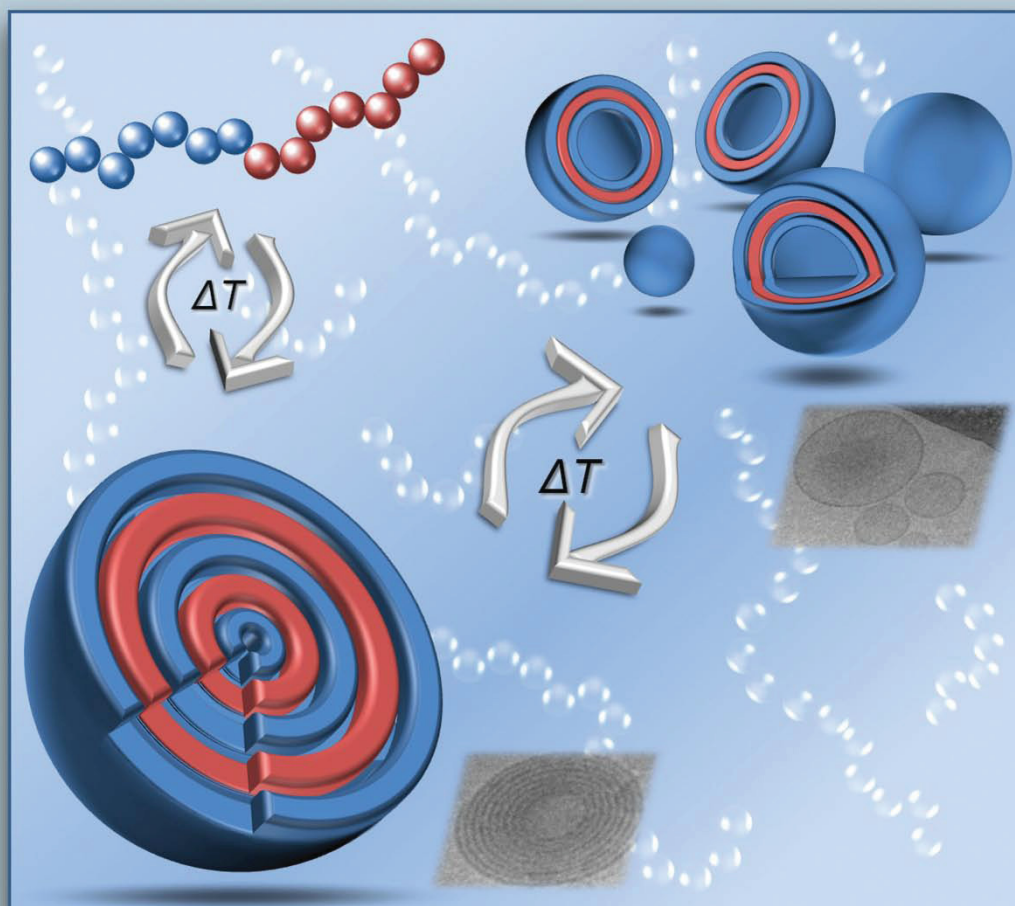
*"Including cover page"*



# Macromolecules

December 11, 2012  
Volume 45  
Number 23

[pubs.acs.org/Macromolecules](http://pubs.acs.org/Macromolecules)



ACS Publications  
MOST TRUSTED. MOST CITED. MOST READ.

[www.acs.org](http://www.acs.org)



# Thermo-Induced Self-Assembly of Responsive Poly(DMAEMA-*b*-DEGMA) Block Copolymers into Multi- and Unilamellar Vesicles

Christian Pietsch,<sup>†,‡,§</sup> Ulrich Mansfeld,<sup>†,‡,§</sup> Carlos Guerrero-Sanchez,<sup>||</sup> Stephanie Hoepfener,<sup>†,‡,§</sup> Antje Vollrath,<sup>†,‡</sup> Michael Wagner,<sup>†,‡</sup> Richard Hoogenboom,<sup>⊥</sup> Simon Saubern,<sup>||</sup> San H. Thang,<sup>||</sup> C. Remzi Becer,<sup>#</sup> John Chiefari,<sup>||</sup> and Ulrich S. Schubert<sup>\*,†,‡,§</sup>

<sup>†</sup> Laboratory of Organic and Macromolecular Chemistry (IOMC) Friedrich-Schiller-University Jena, Humboldtstrasse 10, 07743 Jena, Germany

<sup>‡</sup> Jena Center for Soft Matter (JCSM), Humboldtstrasse 10, 07743 Jena, Germany

<sup>§</sup> Dutch Polymer Institute (DPI), John F. Kennedylaan 2, 5612 AB Eindhoven, The Netherlands

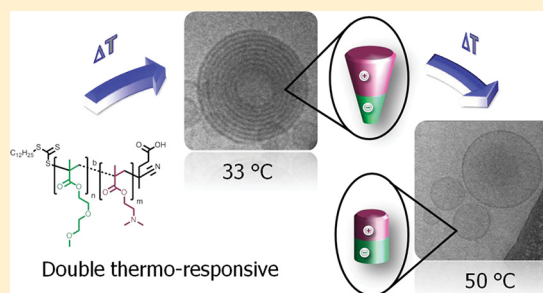
<sup>||</sup> CSIRO, Materials Science and Engineering, Bag 10, Clayton South, 3169 Victoria, Australia

<sup>⊥</sup> Supramolecular Chemistry Group, Department of Organic Chemistry, Ghent University, Krijgslaan 281 S4, 9000 Ghent, Belgium

<sup>#</sup> Department of Chemistry, University of Warwick, CV4 7AL Coventry, United Kingdom

## Supporting Information

**ABSTRACT:** A series of thermoresponsive diblock copolymers of poly[2-(dimethylamino)ethyl methacrylate-*block*-di(ethyleneglycol) methyl ether methacrylate], poly(DMAEMA-*b*-DEGMA), were synthesized by reversible addition–fragmentation chain transfer (RAFT) polymerizations. The series consist of diblock and quasi diblock copolymers. Sequential monomer addition was used for the quasi diblock copolymer synthesis and the macro-chain transfer approach was utilized for the block copolymer synthesis. The focus of this contribution is the controlled variation of the ratios of DMAEMA to DEGMA in the copolymer composition, resulting in a systematic polymer library. One of the investigated block copolymer systems showed double lower critical solution temperature (LCST) behavior in water and was further investigated. The phase transitions of this block copolymer were studied in aqueous solutions by turbidimetry, dynamic light scattering (DLS), variable temperature proton nuclear magnetic resonance (<sup>1</sup>H NMR) spectroscopy, zeta potential, and cryo transmission electron microscopy (cryo-TEM). The block copolymer undergoes a two-step thermo-induced self-assembly, which results in the formation of multilamellar vesicles after the first LCST temperature and to unilamellar vesicles above the second LCST transition. An interplay of ionic interactions as well as the change of the corresponding volume fraction during the LCST transitions were identified as the driving force for the double responsive behavior.



## INTRODUCTION

Stimuli-responsive polymers, which undergo phase transitions in response to an external stimulus, have gained the interest of many researchers in the past decade.<sup>1–5</sup> Such “smart” materials can act with a property change in response to changes in temperature, pH value, electric potential, light, or magnetic field.<sup>6–10</sup> The area of stimuli-responsive polymers represents nowadays a strongly growing field in polymer research, in particular the investigation regarding lower critical solution temperature behavior has attracted significant interest. Particular attention in this context has been paid to the thermosensitive self-organization of amphiphilic block copolymers, especially on the formation of micelles or vesicular structures in aqueous solution. Numerous reports on the micellization of diblock copolymers containing thermosensitive block segments are described.<sup>4,6,7,11–13</sup> The formed vesicles or

polymersomes are usually spherical shell structures with a hydrophobic core-layer and a hydrophilic internal and external corona made from amphiphilic block copolymers.<sup>14–16</sup> Polymer vesicles, which respond to external stimuli such as a change in temperature or the pH value, represent attractive candidates for applications in encapsulation or drug delivery systems.<sup>3,17,18</sup>

LCST polymers are soluble below a certain temperature because of the formation of hydrogen bonds between water molecules of the hydration shell and the polymer chains. By passing the cloud point temperature ( $T_{CP}$ ), the polymer starts to precipitate due to the breaking of hydrogen bonds and due to hydrophobic polymer–polymer interactions because the

Received: September 7, 2012

Revised: November 2, 2012

Published: November 19, 2012

**Table 1. Overview of the Selected Reaction Conditions Used for the Polymerizations of DMAEMA and DEGMA Using an Automated Parallel Synthesizer**

sample	structure	ratio 1st polym DMAEMA/CTA <sup>a</sup>	ratio 2nd polym DEGMA/macroCTA <sup>a</sup>	concn [mol/L]	polym time [h]
H1	homo	90:1		3.0	10.0
B1	quasi		10:1	2.0	6.0
H2	homo	80:1		3.0	10.0
B2	quasi		20:1	2.0	6.0
H5	homo	45:1		3.0	10.0
B5	quasi		55:1	2.0	6.0

<sup>a</sup>Molar ratios of the reaction solution.

entropy term becomes dominant in the Gibbs equation. Besides the gold standard poly(*N*-isopropylacrylamide) (poly(NIPAM)) with a LCST of 32 °C,<sup>1</sup> a number of poly(ethyleneglycol) functionalized (meth)acrylates have been reported to exhibit LCST behavior.<sup>19–21</sup> In particular, different oligo(ethylene glycol) methyl ether methacrylate (OEGMA)-based polymers received significant attention as temperature sensitive materials. The large interest is fueled by the easy preparation of well-defined OEGMA-based copolymers by reversible deactivation radical polymerization (RDRP) techniques such as reversible addition–fragmentation chain transfer (RAFT) polymerizations.<sup>22–24</sup> By variation of the side chain length, the  $T_{CP}$  of these copolymers can be tuned, which makes them very attractive systems.<sup>19,25,26</sup> The homopolymer of di(ethylene glycol) methyl ether methacrylate (DEGMA) (two repeating units of ethylene glycol) has a  $T_{CP}$  around 27 °C, which can be increased by copolymerizing with a more hydrophilic monomer.<sup>19,20,26,27</sup> 2-(Dimethylamino)ethyl methacrylate (DMAEMA) has been used as such a comonomer, resulting in a pH- and temperature-responsive copolymer.<sup>28</sup> Poly(DMAEMA) is used in various applications, e.g., in gene delivery systems of transfection agents.<sup>29–31</sup> Various  $T_{CP}$ 's of poly(DMAEMA) have been reported in literature ranging from 20 to 80 °C, which is an indication that the LCST strongly depends on the used molar masses.<sup>28,32–38</sup> Furthermore, the  $T_{CP}$  strongly depends on variations in the pH value due to partial (de)protonation of the basic nitrogen atoms of DMAEMA.<sup>28,35–39</sup>

Block copolymers can be responsive to two different stimuli at the same time, such as temperature and the pH value, as demonstrated for block copolymers of (poly(NIPAM-*b*-AA))<sup>40</sup> and poly(DMAEMA-*b*-MMA).<sup>41</sup> Furthermore, different copolymer brushes of DMAEMA with DEGMA and *tert*-butyl methacrylate (*t*BMA), investigated by Matyjaszewski et al., showed dual responsive properties.<sup>38</sup> The pH and temperature responsive properties were also investigated for different poly(DMAEMA-*co*-DEGMA) hydrogels.<sup>37</sup> Poly(DMAEMA-*b*-DEGMA) block copolymers were recently used to control the self-assembly of virus particles.<sup>42</sup>

The thermoresponsive self-organization of amphiphilic block copolymers in aqueous solution has been described in the literature for several systems.<sup>6,7,11–13,43–47</sup> For example, the self-assembly of double thermoresponsive block copolymers of poly(*N*-*n*-propylacrylamide-*b*-*N*-ethylacrylamide) was reported.<sup>48</sup> Furthermore, the thermo-induced micellization transition of the block copolymer solution of poly(tri(ethylene glycol) methyl ether acrylate)-*b*-poly(4-vinylbenzyl methoxytris(oxyethylene) ether) was described.<sup>49</sup> The formation of double hydrophilic diblock copolymers to vesicle and micelle structures have been studied in detail by Lecomman-

doux and co-workers using poly((dimethylamino)ethyl methacrylate-*b*-glutamic acid).<sup>50</sup> However, the thermo-induced self-assembly of poly(DMAEMA-*b*-DEGMA) is, to the best of our knowledge, not yet reported.

In this contribution, a series of thermoresponsive diblock copolymers of poly(DMAEMA-*b*-DEGMA) was synthesized by RAFT polymerization ranging from pure block to gradient block copolymer (quasi diblock) structures. The macro-chain transfer approach was used for the preparation of these block copolymers. The ratios of DMAEMA to DEGMA were systematically varied, while the degree of polymerization was kept constant. The self-assembly behavior as well as the LCST of the responsive polymers were measured by turbidimetry. Within this series of block copolymers, a double-responsive behavior was observed for one particular composition and the self-assembly characteristic was further investigated by dynamic light scattering, temperature-dependent <sup>1</sup>H NMR spectroscopy, zeta potential analysis, and cryogenic transmission electron microscopy. The formation of spherical structures, like multilamellar and unilamellar vesicles at elevated temperatures, was observed and a model for the formation of these structures was developed.

## EXPERIMENTAL SECTION

**Materials.** Di(ethylene glycol) methyl ether methacrylate (DEGMA) and 2-(dimethylamino)ethyl methacrylate (DMAEMA) were purchased from Sigma-Aldrich and purified by stirring in the presence of inhibitor-remover for hydroquinone or hydroquinone monomethyl ether (Aldrich) for 30 min prior to use. The initiator, 1,1'-azobis(cyclohexane carbonitrile) (VAZO-88), was obtained from DuPont. 4-Cyano-4-[(dodecylsulfanylthiocarbonyl)sulfanyl]pentanoic acid (DTTCP) chain transfer agent (CTA) was prepared according to a literature procedure.<sup>23,51</sup> All analytical grade solvents were purchased from Sigma-Aldrich or Merck KGaA.

**Polymerization in an Automated Parallel Synthesizer.** The quasi block copolymerizations were performed in a Chemspeed Accelerator SLT automated synthesizer using the sequential monomer addition and following similar experimental procedures as reported elsewhere.<sup>52–54</sup> In a typical polymerization experiment, 864 mg of DMAEMA monomer ( $5.5 \times 10^{-3}$  mol), 0.73 mg of VAZO-88 initiator ( $3.0 \times 10^{-6}$  mol), 24.1 mg of DTTCP (used as a CTA) RAFT agent ( $6.00 \times 10^{-5}$  mol), and *N,N*-dimethylformamide (DMF) were mixed together in a 13 mL glass reactor of an automated parallel synthesizer as follows: DMAEMA monomer, DMF solvent reservoir, and individual stock solutions of VAZO-88 (initiator) and DTTCP (CTA) dissolved in DMF were degassed by sparging nitrogen for at least 15 min prior to use. All these reagents were added and combined into one of the reactors of the parallel synthesizer using its automated liquid handling system in order to reach the aforementioned amounts and a monomer concentration of 3.0 M; the ratio of RAFT agent to initiator was 1:0.05. Trioxane dissolved in the DMAEMA monomer was utilized, at a concentration of 5 mg mL<sup>-1</sup> of total reaction mixture, as internal standard to determine the monomer conversion by <sup>1</sup>H



NMR measurements in deuterated chloroform ( $\text{CDCl}_3$ ). Once in the reactor, the reaction mixture was subjected to three freeze–pump–thaw cycles between  $-70$  and  $-10$  °C (5 mbar vacuum for 2 min each cycle) in the parallel synthesizer.<sup>53</sup> Thereafter, the reaction mixtures were heated up to 90 °C and vortexed at 600 rpm for 10 h; the coldfinger reflux condensers were set to 7 °C during the reaction. After the polymerization, samples of 75  $\mu\text{L}$  were withdrawn with the liquid handling system of the apparatus and transferred into NMR tubes and size exclusion chromatography (SEC) vials, which were filled with their corresponding solvent for analysis. The first polymerization step proceeded up to a certain conversion, which resulted in a poly(DMAEMA) macro-chain transfer agents (macro-CTAs). Thereafter, the polymers were chain extended with DEGMA using similar conditions as described above. The DEGMA concentration was kept at 2.0 mol  $\text{L}^{-1}$  for each polymerization experiment. Table 1 summarizes the utilized reaction conditions and  $[\text{M}]/[\text{CTA}]$  ratios. After completion of the polymerization, dichloromethane ( $\text{CH}_2\text{Cl}_2$ ) was added to the final mixtures and the polymers were then manually precipitated into *n*-hexane (with adding  $\text{CH}_2\text{Cl}_2$ , DMF is soluble in *n*-hexane). Afterward, the copolymers were dried in a vacuum oven at 40 °C.

**Polymerization via Classical Conditions.** Block copolymers were also synthesized using the macro-CTA approach with a precipitation step in between to obtain pure block segments. The desired amounts of the monomer (e.g., 2.36 g, 15.0 mmol of DMAEMA) were transferred into Schlenk type reactors and were diluted with DMF. Thereafter, the calculated volumes of stock solutions of CTA (DTTCP, 0.15 mmol, 60.55 mg) as well as the initiator (VAZO-88, 0.008 mmol, 1.83 mg) were added. The ratio between  $[\text{CTA}]$  and  $[\text{VAZO-88}]$  was 1:0.05. The prepared solutions were degassed using four freeze–pump–thaw cycles. Subsequently, the reaction was performed in an oil bath at 90 °C for 10 h. After the polymerization,  $\text{CH}_2\text{Cl}_2$  was added to the final mixtures and the polymers were then manually precipitated into *n*-hexane (with adding  $\text{CH}_2\text{Cl}_2$ , DMF is soluble in *n*-hexane). Afterward, the polymers were dried in a vacuum oven at 40 °C. The final poly(DMAEMA)s were used as a macro-CTA and chain extended with DEGMA using similar conditions as described above. The utilized reaction conditions and  $[\text{M}]/[\text{CTA}]$  ratios are summarized in Table 2. All monomer conversions were measured by  $^1\text{H}$  NMR spectroscopy using trioxane as internal standard. The molar masses of the obtained polymers were measured by SEC.

**Instrumentation.** Size-exclusion chromatography (SEC) was performed on a system comprising a Waters 590 HPLC pump and a Waters 410 refractive index detector equipped with three Waters Styragel columns (HT2, HT3, HT4, each 300 mm  $\times$  7.8 mm, providing an effective molar mass range of 100–600000  $\text{g mol}^{-1}$ ). The

**Table 2. Overview of the Selected Reaction Conditions Used for the Polymerizations of DMAEMA and DEGMA via the Schlenk Technique**

sample	structure	ratio feed 1st polym monomer/CTA <sup>a</sup>	ratio feed 2nd polym monomer/macroCTA <sup>a</sup>	concn [mol/L]	polym time [h]
H3	homo	(DMAEMA) 100:1		2.0	10.0
B3	block		(DEGMA) 100:1	1.0	7.5
H4	homo	(DMAEMA) 100:1		3.0	8.0
B4	block		(DEGMA) 100:1	1.0	6.0
H6	homo	(DEGMA) 100:1		2.0	8.0
B6	block		(DMAEMA) 50:1	1.0	6.0

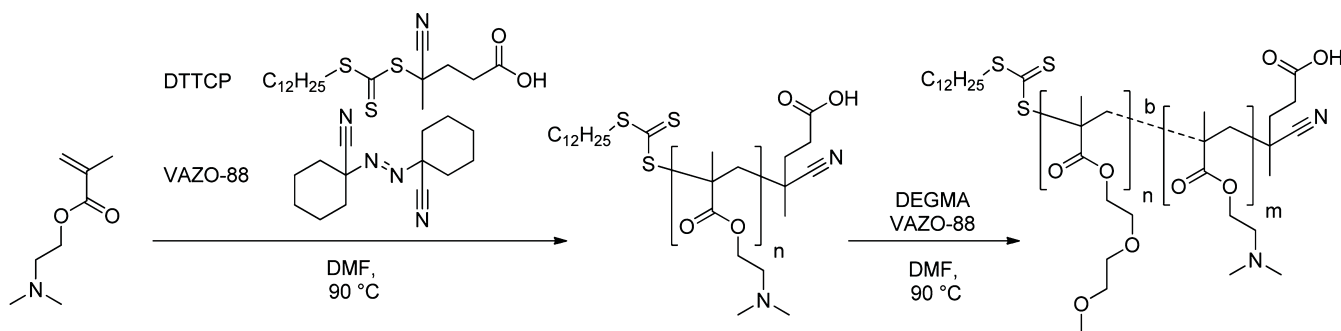
<sup>a</sup>Molar ratios of the reaction solution.

eluent was DMF (containing 0.45% w/v LiBr) at 80 °C with a flow rate of 1 mL  $\text{min}^{-1}$ . Number ( $M_n$ ) and weight-average ( $M_w$ ) molar masses were evaluated using Waters Millennium software. A polynomial was used to fit the log  $M$  vs time calibration curve, which was linear across the molar mass ranges. The SEC columns were calibrated with low polydispersity polystyrene standards (Polymer Laboratories) ranging from  $M_n$  3100 to 650000  $\text{g mol}^{-1}$ . Further SEC experiments were performed on a Shimadzu system equipped with a SCL-10A system controller, a LC-10AD pump, a RID-10A refractive index detector, and a PSS SDV linear S, 5  $\mu\text{m}$  column (8 mm  $\times$  300 mm) with chloroform/triethylamine/2-propanol (94:4:2) as eluent, and the column oven was set to 40 °C. A calibration with low polydispersity polystyrene standards (ranging  $M_n$  from 376 to 128000  $\text{g mol}^{-1}$ ) was used. In addition, further SEC experiments were carried out using an Agilent1200 series system, a G1310A pump, a G1362A refractive index detector, and both a PSS Gram30 and a PSS Gram1000 column in series, whereby *N,N*-dimethylacetamide (DMAc) with 5 mmol lithium chloride was used as an eluent at 1 mL  $\text{min}^{-1}$  flow rate, and the column oven was set to 40 °C. The system was calibrated with polystyrene ( $M_n$  from 374  $\text{g mol}^{-1}$  to 1040000  $\text{g mol}^{-1}$ ) standards. Proton nuclear magnetic resonance ( $^1\text{H}$  NMR) spectra were recorded on a Bruker AC 300 (300 MHz) and 400 (400 MHz) spectrometer at 298 K. The chemical shifts are reported in parts per million (ppm,  $\delta$  scale) relative to the signals from the NMR solvents. The temperature variable  $^1\text{H}$  NMR spectroscopy was recorded on a Bruker AC 400 (400 MHz) spectrometer in deuterium oxide ( $\text{D}_2\text{O}$ ) at a polymer concentration of 5.0 mg  $\text{mL}^{-1}$ . At each temperature step (5 °C) from 25 to 65 °C, the polymer solution was equilibrated for 3 min. Conversions were calculated from  $^1\text{H}$  NMR spectra using 1,3,5-trioxane as an internal standard. The cloud point measurements for the identification of the LCST behavior were performed by heating the polymer (1.0, 2.5, 5.0, and 10.0 mg  $\text{mL}^{-1}$ , respectively) in deionized water from 0 to 105 °C with a heating rate of 1.0 °C  $\text{min}^{-1}$  followed by cooling to 0 °C at a cooling rate of 1.0 °C  $\text{min}^{-1}$  after keeping it 10 min at 105 °C. This cycle was repeated three times. During these controlled cycles, the transmission through the solutions was monitored in a Crystal16 from Avantium Technologies. The cloud points are reported as the 50% transmittance temperature in the second heating run.

High-throughput dynamic light scattering (HT-DLS) measurements were performed on the DynaPro Plate Reader Plus (Wyatt Technology Corporation, Santa Barbara, CA) equipped with a 60 mV linearly polarized gallium arsenide (GaAs) laser of  $\lambda = 832.5$  nm and operating at an angle of 156°. The samples were heated from 25 to 65 °C in a 96-well plate using 10 °C heating steps, and after 5 min equilibration time, each well was measured collecting five acquisitions. The data were analyzed with the Dynamics software version 6.20 by the method of cumulants.<sup>55</sup> The percent of polydispersity is given by  $\%Pd = 100(\mu_2)/\mu_1^2$ , where  $\mu_1$  and  $\mu_2$  are the first- and the second-order cumulant, respectively. The level of homogeneity is considered high when the percent polydispersity is less than 15%. If the level of homogeneity is low (percent polydispersity larger than 30%), the particle population can be considered as being polydisperse. DLS measurements were also carried out on a Zetasizer Nano ZS (Malvern Instruments, Malvern, UK) operating with a laser beam at 633 nm and a scattering angle of 173°. The sample was heated in a quartz cuvette from 25 up to 65 °C in 1 °C steps. At each temperature step, the sample was equilibrated for 120 s and then measured three times including three runs for 30 s. The intensity and the volume distribution of the particle size were calculated applying the NNLS mode.

Electrophoretic light scattering was used to measure the electrokinetic potential, also known as zeta potential. The measurements were performed using a Zetasizer Nano ZS (Malvern Instruments) by applying laser Doppler velocimetry. For each measurement, 20 runs were carried out using the slow-field reversal and fast-field reversal mode at 150 V. Each experiment was performed in triplicate from 25 to 65 °C in 5 °C steps. The zeta potential ( $\zeta$ ) was calculated from the electrophoretic mobility ( $\mu$ ) according to the Henry equation. The Henry coefficient  $f(\text{ka})$  was calculated according to Oshima.<sup>56</sup>

**Scheme 1. Schematic Representation of the Poly(DMAEMA-*b*-DEGMA) Formation Using RAFT Polymerization with the CTA DTTCP and the Radical Initiator VAZO-88**



**Table 3. Composition of the Block Copolymers of Poly(DMAEMA-*b*-DEGMA) from SEC and <sup>1</sup>H NMR Spectroscopy with Increasing Ratio of DEGMA Starting from DMAEMA Homopolymer**

sample <sup>a</sup>	SEC (DMF) <sup>b</sup>		SEC (DMAc) <sup>c</sup>		SEC (CHCl <sub>3</sub> ) <sup>d</sup>		conv. <sup>e</sup> [%]	M <sub>n,theo</sub> <sup>f</sup> [g/mol]	ratio [%]	<sup>1</sup> H NMR <sup>g</sup> DMAEMA/DEGMA
	M <sub>n</sub> [g/mol]	PDI	M <sub>n</sub> [g/mol]	PDI	M <sub>n</sub> [g/mol]	PDI				
H1 (h)	18600	1.16					81 <sup>(M1)</sup>	10200		100:0
H2 (h)	15200	1.17					62 <sup>(M1)</sup>	6200		100:0
H3 (h)	17600	1.22					80 <sup>(M1)</sup>	13000		100:0
H4 (h)	15200	1.21	13500	1.43	28700	1.22	83 <sup>(M1)</sup>	13300		100:0
H5 (h)	8800	1.16					75 <sup>(M1)</sup>	5400		100:0
B1 (q)	20800	1.29	24700	1.44	29700	1.36	39 <sup>(M2)</sup>	12600		94:6
B2 (q)	21800	1.25	24100	1.41	30200	1.34	70 <sup>(M2)</sup>	10900		87:13
B3 (b)	26900	1.27	27400	1.52	<i>h</i>	<i>h</i>	65 <sup>(M2)</sup>	25400		66:34
B4 (b)	35100	1.54	36600	1.48	<i>h</i>	<i>h</i>	53 <sup>(M2)</sup>	23300		64:36
B5 (q)	39700	1.35	24000	1.70	<i>h</i>	<i>h</i>	85 <sup>(M2)</sup>	15300		51:49
B6 (b)	26600	1.32	27100	1.33	33500	1.24	40 <sup>(M1)</sup>	20800		20:80
H6 (h)	23600	1.23	23700	1.29	27800	1.20	76 <sup>(M2)</sup>	14500		0:100

<sup>a</sup>Copolymer structure: h = homopolymer, q = quasi diblock copolymer, b = diblock copolymer. <sup>b</sup>Calculated from SEC (DMF) using PS calibration. <sup>c</sup>Calculated from SEC (DMAc) using PS calibration. <sup>d</sup>Calculated from SEC (CHCl<sub>3</sub>/triethylamine/2-propanol = 94/4/2) using PS calibration. <sup>e</sup>Calculated from vinyl integrals of <sup>1</sup>H NMR spectra using trioxane as internal standard, M1 = DMAEMA and M2 = DEGMA. <sup>f</sup>Calculated according to formula (M<sub>n,theo</sub> = ([M]/[CTA] × conv × M<sub>monomer</sub>) + M<sub>CTA</sub>), besides for block copolymers where M<sub>CTA</sub> is M<sub>macroCTA</sub>. <sup>g</sup>Calculated from integrated areas of DMAEMA signals ((CH<sub>3</sub>)<sub>2</sub>N-) and the DEGMA (CH<sub>2</sub>-O-) side-group signals. <sup>h</sup>Block copolymer reached the exclusion limit of the SEC.

Cryogenic transmission electron microscopy (cryo-TEM) measurements were performed on a Philips CM120 operating at an acceleration voltage of 120 kV. Images were recorded with a bottom mounted 1 k × 1 k CCD camera. The samples for TEM investigations were prepared and stored at room temperature prior to the investigation (5 mg mL<sup>-1</sup>). For the temperature-dependent investigation, the samples were preheated under frequent agitation for at least 30 min in a water bath at 35 and 50 °C, respectively. A drop of the polymer solution (5 μL) was rapidly placed with a preheated microliter pipet on a perforated carbon grid (Quantifoil R2/2) within an in-house-built controlled environment vitrification system (CEVS) with a saturated water atmosphere. The temperature within the CEVS was adjusted to 38 and 55 °C to ensure that the sample is investigated above the corresponding cloud point temperatures. Prior to the blotting, the liquid was allowed to equilibrate on the grids for at least 2 min to avoid preparation artifacts. The controlled saturated humidity and defined temperature minimizes temperature alterations of the sample due to evaporation effects. The samples were rapidly blotted and plunged into a cryogen reservoir containing liquid ethane. After preparation, the samples were stored and measured at a temperature below -176 °C to avoid the formation of crystalline ice layers. To avoid further preparation artifacts, similar blotting times were used at different temperatures.

## RESULTS AND DISCUSSION

**Synthesis of the Poly(DMAEMA-*b*-DEGMA) Library.** A library of double thermoresponsive poly(DMAEMA-*b*-

DEGMA) diblock copolymers was synthesized using the RAFT polymerization technique in a sequential monomer addition approach. Within this series, the ratios of DMAEMA and DEGMA were varied ranging from 100% DMAEMA to 100% DEGMA with composition changes in 20% steps. Two possibilities of the macro-chain transfer approach were explored, namely with and without a precipitation step after the first polymerization. Using a parallel robot platform, the second DEGMA monomer was added before the full conversion of DMAEMA was reached, resulting in quasi diblock structures. The polymerizations were carried out using 4-cyano-4-[(dodecylsulfanylthiocarbonyl)sulfanyl]pentanoic acid (DTTCP) as CTA and VAZO-88 as radical initiator (see Scheme 1), applying similar conditions as previously described for the MMA polymerization,<sup>57</sup> namely 90 °C with a ratio of DTTCP to VAZO-88 of 20:1.

The quasi diblock copolymers were synthesized in a Chemspeed Accelerator SLT106 automated platform and the diblock copolymers under classical conditions (Schlenk technique) using the same polymerization conditions. The first block segment was polymerized in DMF at a concentration of 3.0 mol L<sup>-1</sup>, followed by the polymerization of DEGMA with a monomer concentration of 2.0 mol L<sup>-1</sup>. For B6, this order was reversed, meaning that first DEGMA was polymerized and

Table 4. Cloud Point Temperatures from Turbidimetry Measurement of the Homo and Block Copolymers

sample DMAEMA/DEGMA [%]	cloud points by turbidimetry (2nd heating run) in °C <sup>a</sup>							
	H4 100:0	B1 94:6	B2 87:13	B3 66:34	B4 64:36	B5 <sup>c</sup> 51:49	B6 20:80	H6 0:100
10 mg mL <sup>-1</sup>	45.4	43.6	40.7	m <sup>b</sup>	m <sup>b</sup>	32.5:48.0	29.4	25.1
5.0 mg mL <sup>-1</sup>	46.7	44.5	41.7	m <sup>b</sup>	m <sup>b</sup>	33:~49 32:~48 <sup>d</sup>	30.0	25.9
2.5 mg mL <sup>-1</sup>	49.0	46.0	43.2	m <sup>b</sup>	m <sup>b</sup>	34:~46	30.5	28.0
1.0 mg mL <sup>-1</sup>	57.4	48.2	45.3	m <sup>b</sup>	m <sup>b</sup>	~41	31.5	36.4

<sup>a</sup>Estimated in deionized water at 50% transmission for the second heating run. <sup>b</sup>No clear phase separation transition. <sup>c</sup>Estimated at the local maximum at the half %value of transmission. <sup>d</sup>Estimated in D<sub>2</sub>O.

then the corresponding DMAEMA block. In Table 3, the molar masses and polydispersity indices (PDI) measured by SEC are summarized, demonstrating good control over the first blocks (PDI < 1.23) and relatively good control for most block copolymers (PDI < 1.35, except B4). The obtained diblock copolymers were characterized by SEC in DMF, DMAc, and chloroform as eluent, using a refractive index detector (see Supporting Information (SI)). The hydrodynamic volume of poly(DMAEMA) depends strongly on the solvent and, additionally, it is known that interactions with the column material<sup>58</sup> occur due to the basic nitrogen atoms, therefore, different SEC systems were used to characterize the block copolymers. Nevertheless, the obtained values should be handled with care because of both the calibration with polystyrene and the possibility of column interactions.<sup>59</sup>

The monomer conversions of DMAEMA and DEGMA were estimated by <sup>1</sup>H NMR spectroscopy. The conversion of DMAEMA was around 70–80% after 10 h of polymerization. Then the polymerization was stopped to retain high RAFT end-group functionality. A clear molar mass shift could be observed for the block copolymers in the SEC analysis. For the final copolymers, the ratio between both block segments were determined by <sup>1</sup>H NMR spectroscopy using the integrated areas of DMAEMA signals ((CH<sub>3</sub>)<sub>2</sub>N– at 2.26 ppm) and the DEGMA (CH<sub>2</sub>–O– at 3.54–3.66 ppm) ethylene glycol side-group signals (Figure S6, SI). The observed ratios are in a good agreement with the monomer feed ratio.

**Thermoresponsive Properties of Poly(DMAEMA-*b*-DEGMA).** Heating solutions of the polymers in deionized water induces a LCST transition, i.e., the solutions become turbid above the characteristic  $T_{CP}$ , indicating the collapse of the polymer chains (two-phase system). The  $T_{CP}$ 's of the homo- and block copolymers were determined by turbidimetry measurements in deionized water at four different concentrations (1.0, 2.5, 5.0, and 10.0 mg mL<sup>-1</sup>) and are listed in Table 4. All thermo-induced transitions of the copolymers were found to be fully reversible (SI, Figure S7).

The  $T_{CP}$  of the homopolymer poly(DEGMA), H6, is 25.9 °C at 5.0 mg mL<sup>-1</sup>, which correspond well with the literature value of 27 °C.<sup>19,20,27</sup> With increasing amount of DMAEMA, the observed demixing points increase and the highest  $T_{CP}$  is observed for the homopolymer of poly(DMAEMA), H4, namely 46.7 °C at 5.0 mg mL<sup>-1</sup> (see also Figure 1). This observed effect is due to the increased hydrophilicity of the “end-group” by the incorporation of the PDMAEMA block. In some cases, namely for B3 and B4, the solutions showed only weak transitions, presumably due to the formation of mainly smaller aggregates. All  $T_{CP}$  transitions from the turbidimetry measurement of the block copolymers are plotted in Figure 1 against the molar ratio of PDMAEMA to provide a better

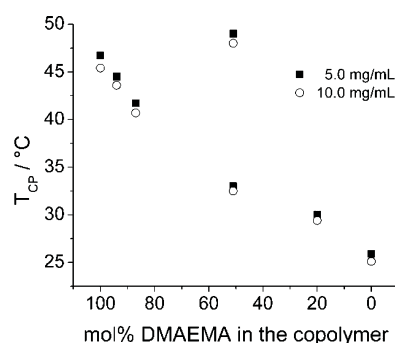
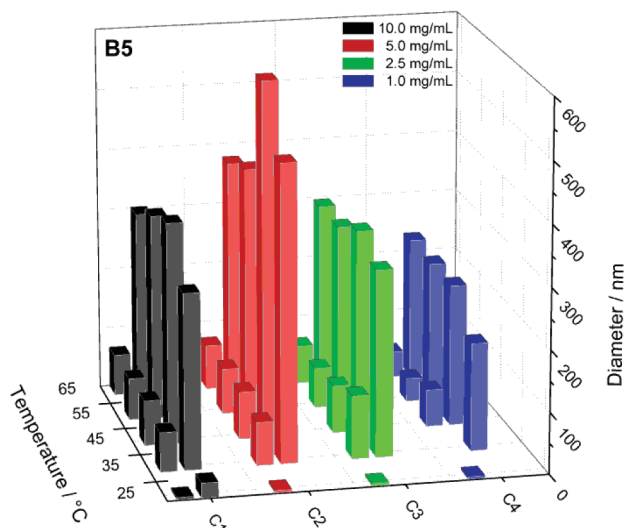


Figure 1. Cloud points ( $T_{CP}$ ) of the studied block copolymers of poly(DMAEMA-*b*-DEGMA) at 5.0 and 10.0 mg mL<sup>-1</sup>.

overview. A roughly linear behavior of the  $T_{CP}$  transitions with increasing amount of mol% DMAEMA in the block copolymers could be observed. Differences between the pure and the quasi diblock copolymer were not observed in the turbidimetry measurements; apparently the gradient is too small to have an influence. For all samples, a lower  $T_{CP}$  is observed with higher concentration due to the statistical influence during the aggregation behavior. Two  $T_{CP}$  values were observed for B5 (see Table 4 and Figure 1), indicating the double thermo-responsive behavior in aqueous solution. The turbidimetry curve of this copolymer shows a weak transition at 33 °C followed by a rearrangement and, therefore, a second transition at 49 °C (see also Figure S8 SI).

Due to its double-responsive behavior, the B5 block copolymer was selected for detailed structural analysis, as it shows the most interesting thermoresponsive behavior of the tested copolymers.

The LCST transition was further investigated in detail by DLS measurements as function of temperature for B5. To efficiently characterize different concentrations of this block copolymer, a high-throughput DLS plate reader setup was used. The demixing values were estimated by this DLS setup in deionized water at four different concentrations (1.0, 2.5, 5.0, and 10.0 mg mL<sup>-1</sup>) starting from 25 °C and heating up to 65 °C in 10 °C steps. The temperature induced collapse of the quasi diblock copolymer B5 (~50% of each block segment) resulted in the appearance of two size distributions (Figure 2), one with a diameter of 40 nm and a second of around 300 nm. The size of the agglomerates of B5 is nearly constant also by further increasing the temperature. In addition, the polymer concentration has no significant influence on the size of the self-assembled structures of the block copolymer. The self-assembled structures might be micelles (ca. 40 nm) and larger vesicular structures (300–400 nm), although no conclusive assignment can be made based on the DLS results alone. To



**Figure 2.** Hydrodynamic diameters of the copolymer coils and globules of **B5** (showing two distribution) at different concentration as function of temperature.

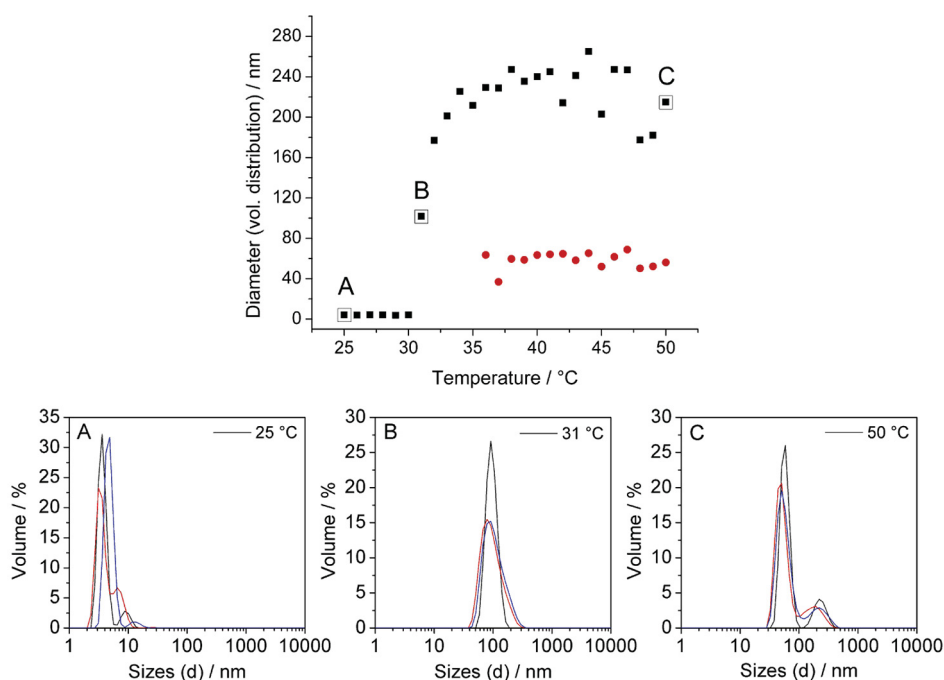
evaluate the aggregation behavior of the chosen copolymer, **B5** was investigated in further detail using a DLS Zetasizer (Malvern).

The experiment was performed in deionized water at a concentration of  $1.0 \text{ mg mL}^{-1}$ , and the temperature run was set up between 25 and  $50 \text{ }^{\circ}\text{C}$ , with heating in  $1 \text{ }^{\circ}\text{C}$  steps to have a closer look at the phase transitions. A repeated temperature run ranging from 25 to  $65 \text{ }^{\circ}\text{C}$  is plotted in the SI (Figure S10), showing a similar size distribution of the observed self-assembled aggregates. No changes in the size above  $50 \text{ }^{\circ}\text{C}$  are observed. The distribution of the block copolymer assemblies at temperatures below and above the phase

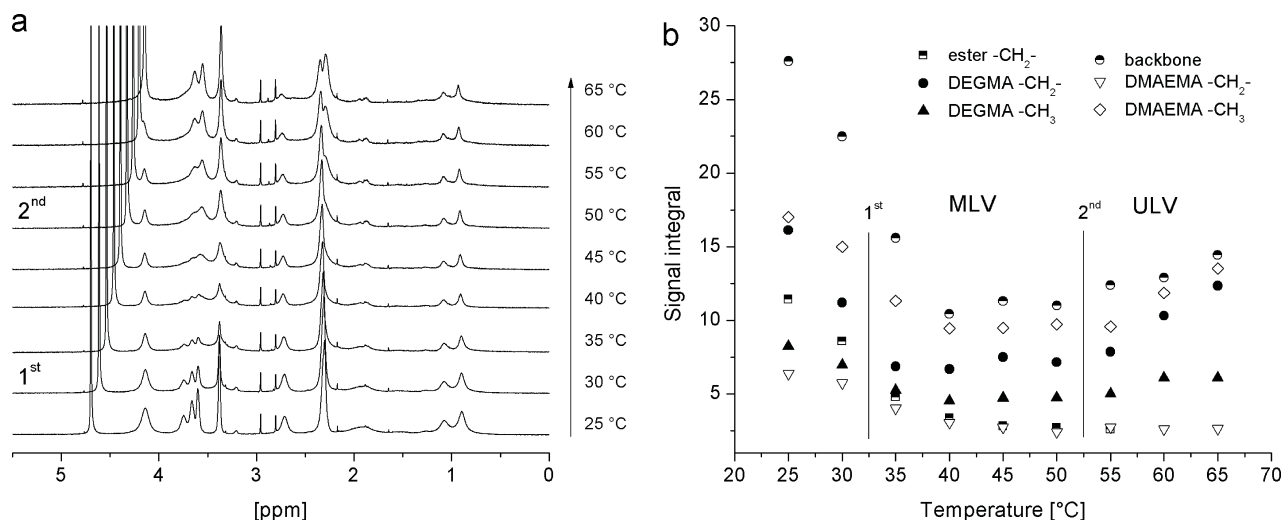
transition is illustrated in Figure 3 (volume distribution; intensity distribution is plotted in the SI, Figure S10). Below the cloud point at  $25 \text{ }^{\circ}\text{C}$ , the polymer chains are fully soluble and, therefore, a hydrodynamic diameter smaller than  $10 \text{ nm}$  was obtained, corresponding most probably to individual hydrated polymer chains, taking into account also the molecular dimensions of the block copolymers. An increase in temperature results in an increase in the diameter of the polymer aggregates to  $\sim 100 \text{ nm}$ , indicating the temperature-induced aggregation of the polymer chains. The first transition of the polymer solution is observed at a temperature of  $31 \text{ }^{\circ}\text{C}$ , i.e., when the collapse of the PDEGMA takes place.

The hydrodynamic diameter of these aggregates is around  $100 \text{ nm}$  as displayed in Figure 3. By further increasing the temperature, a rearrangement is observed, which is reflected in the appearance of a second distribution. Above  $36 \text{ }^{\circ}\text{C}$ , two distributions are formed with a hydrodynamic diameter of  $65$  and  $240 \text{ nm}$ , respectively. The formed structures appear to be thermodynamically stable in solution, as the aggregate size remains constant even at further increased temperatures.

The temperature induced phase transition of the selected block copolymer **B5** was further investigated by temperature dependent  $^1\text{H}$  NMR spectroscopy to obtain a deeper insight into the aggregation behavior. The phase transition was investigated in  $\text{D}_2\text{O}$  at a concentration of  $5.0 \text{ mg mL}^{-1}$ . At each temperature step ( $5 \text{ }^{\circ}\text{C}$ ), the polymer solution was equilibrated for  $3 \text{ min}$  (it should be noted here that the time scale of the temperature induced formation of micellar structures and larger aggregates is faster than the typical acquisition times required by the NMR spectrometer). The  $^1\text{H}$  NMR spectrum of the block copolymer at  $25 \text{ }^{\circ}\text{C}$  shows the characteristic signals of poly(DMAEMA-*b*-DEGMA); the corresponding temperature series is plotted in Figure 4. In the  $^1\text{H}$  NMR spectra, the signals at  $3.3\text{--}3.9 \text{ ppm}$  represent the ethylene glycol and  $-\text{OCH}_3$  groups (EG) of poly(DEGMA)



**Figure 3.** The hydrodynamic diameter (volume distribution, average value of three estimations) of the block copolymer chains and globules of **B5** at  $1.0 \text{ mg mL}^{-1}$  is plotted as a function of temperature. (A–C) Hydrodynamic size distribution (three measurements) at the respective temperature.



**Figure 4.** Temperature dependent <sup>1</sup>H NMR spectra (a) in D<sub>2</sub>O of B5 (5 mg mL<sup>-1</sup>) showing the evolution of the -CH<sub>2</sub>- and CH<sub>3</sub>- signals of poly(DEGMA) block at 3.3 ppm and 3.5–3.9 ppm, and the -CH<sub>2</sub>- and CH<sub>3</sub>-resonance of the poly(DMAEMA) block segment at 2.7 and 2.3 ppm as well as the polymer backbone in a temperature range from 25 to 65 °C. On the right side (b), the integrals of the block copolymer signals are plotted against the temperature (MLV = multilamellar vesicles and ULV = unilamellar vesicles, see also Figures 5 and 6).

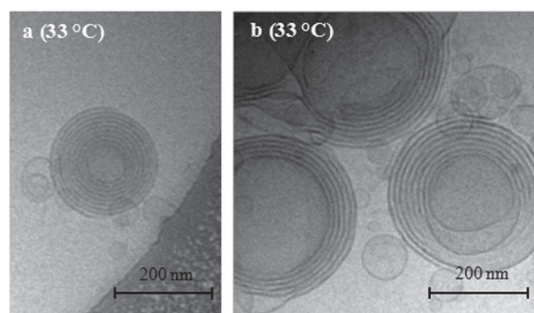
and the signals at 2.3 ppm (CH<sub>3</sub>-N-) represent the poly(DMAEMA) block. The position of the small DMF signals, which are left after the precipitation and drying processes, were used as reference signal (adjustment of changes due to the temperature increase, whereby the DMF is unaffected) and all spectra were normalized in intensity to the D<sub>2</sub>O signal. It is observable (Figure 4) that the DEGMA signals at 3.5–3.9 ppm decrease significantly, denoting the collapse of the DEGMA block which is induced by the temperature increase from 25 to 40 °C. Also, all other signals (backbone at 0.8–1.5 ppm and DMAEMA at 2.3 and 2.8 ppm) decrease by increasing temperature, leading to broad signals due to the reduced flexibility of the polymer chains (see Figure 4). The PDMAEMA block is still visible at 45 °C (CH<sub>3</sub>-N- at 2.2 ppm) as it is supposed that it forms a kind of corona around the hydrophobic PDEGMA aggregates.

Unexpectedly, further increasing the temperature from 50 to 65 °C is accompanied by an increase for some signals corresponding to DMAEMA and to DEGMA (Figure 4b), respectively. These signals are visible for the DMAEMA group (CH<sub>3</sub>-N-) at 2.2 ppm, for the EG groups of DEGMA at 3.6 and 3.7 ppm as well as for the -OCH<sub>3</sub> group at 3.3 ppm. The shifted signals indicate a different microenvironment of (at least parts of) the DMAEMA and DEGMA groups and are supposed to correlate to the corresponding rearrangement of the block copolymer. This second assembly might be induced by the collapse of the DMAEMA block (at 49 °C vs the homopolymer of poly(DMAEMA) at 47 °C as listed in Table 4 for a concentration of 5.0 mg mL<sup>-1</sup>), which appears to be at these temperatures more hydrophobic than in the previous configuration (hydrophilic corona), thus resulting in a structural change. The transformation of the PDMAEMA block is indicated by the high-field shift of the DMAEMA signal, which provides a higher electron density at the methyl groups (CH<sub>3</sub>-N-) caused by the breaking of the H-bonds.

There might also be a migration of the more polar DEGMA groups (higher amount of oxygen atoms in the structure) to the surface of the collapsed structures to stabilize them in aqueous solution. This migration could lead then to a partial hydration of the DEGMA chains, which causes the reappearance of the

corresponding signals in the NMR spectra (Figure 4a at 3.6–3.7 ppm).

**Self-Assembly of Poly(DMAEMA-*b*-DEGMA).** The double responsive behavior of poly(DMAEMA-*b*-DEGMA) motivated the utilization of cryo-TEM to visualize the associated structures. The sample preparation was performed at different temperatures, and the samples were instantaneously vitrified after an equilibration time of ~2 min to preserve the aggregate structure at the blotting temperature. The cryo-TEM images of solutions which were vitrified at a blotting temperature of approximately 33 °C are depicted in Figure 5.



**Figure 5.** Cryo-TEM images (a,b) of B5 block copolymer solution at ~33 °C in H<sub>2</sub>O (preheated, 5.0 mg mL<sup>-1</sup>) showing the formation of multilamellar vesicles and additionally unilamellar vesicles.

At this temperature, which is above the *T*<sub>CP</sub> of PDEGMA and below the *T*<sub>CP</sub> of PDMAEMA, the presence of large multilamellar vesicles (MLV) with a diameter of approximately 200 nm and unilamellar vesicles (ULV), which are observed to be significantly smaller (40 to 90 nm), is observed. The cryo-TEM micrograph shows that the MLVs have a layered structure with comparable distance between the individual lamellae and represent an onion-like form. In this case, a molecular arrangement of the copolymer can be assumed that resembles the structure depicted in Figure 5 (PDEGMA dark; PDMAEMA light).

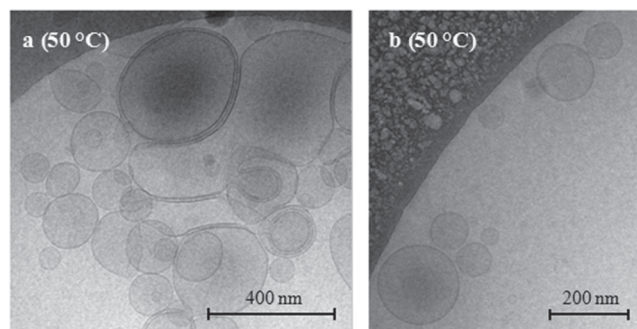
The formation of MLV is based on one hand on the hydrophilic–hydrophobic character of the block copolymers

and on the other hand on the volume fractions of the individual blocks, respectively. The self-assembly of amphiphiles into well-defined structures, such as vesicles, derives from the hydrophobic attraction at the hydrocarbon–water interface, which induces the molecules to associate, and the hydrophilic part that remain in contact with water.<sup>60</sup> For thermosensitive block copolymers, the individual blocks shows a selective, thermally driven solubility and, therefore, the overall hydrophilic–hydrophobic character can be changed by temperature. At 33 °C, the PDEGMA block is collapsed and therefore hydrophobic, while the PDMAEMA block is hydrophilic and is still in solution due to the fact that the blotting temperature remains below the  $T_{CP}$  of PDMAEMA.

The formation of micelles or vesicle structures depends for block copolymers on their ratio between both hydrophobic and hydrophilic segments.<sup>6,7,45,60</sup> Classically, the “critical packing parameter” is used to define the morphology of the resultant self-assembled structure. The ratio of DMAEMA to DEGMA in the block copolymer **B5** is 51% to 49%. With this composition, the formation of micelles or vesicles can be expected.<sup>6,45</sup> In the present case, the block copolymers revealed a tendency for the formation of multilamellar vesicles. The number of shells in these MLVs is up to nine layers for the block copolymer with a significant size distribution of the formed MLVs. The measured size of the different vesicles is between 225 nm (Figure 5a) and 325 nm (Figure 5b), which is in the same size range as obtained by the DLS measurements (approximately 220 nm). The shell thickness of the MLV of PDMAEMA block (Figure 5a) is approximately 5–8 nm. This value is significantly smaller and can be correlated to the polymer chain length (DMAEMA block has DP of ~45, which equals the length of 11.5 nm when completely stretched) to an interdigitated, very compact arrangement of the PDMAEMA chains.<sup>60</sup> This observation is also supported by the NMR investigations, which show reduced signals of the PDMAEMA block at this temperature. The precipitated PDEGMA core is approximately 6 nm in thickness, which suggests very densely packed chains, which is also supported by the strong dark contrast which is found in the cryo-TEM images.

The polymer was subsequently heated to a temperature above the  $T_{CP}$  of DMEAEMA, and the resulting structures were investigated by means of cryo-TEM in the same fashion as described above. In contrast to the sample which was investigated at 33 °C, the formation of preferentially unilamellar, large vesicles is observed. MLVs with a large number of shells are not observed anymore. In Figure 6, the cryo-TEM images of **B5** block copolymer solution acquired at ~50 °C (a,b) showed the formation of large unilamellar vesicles in aqueous solution.

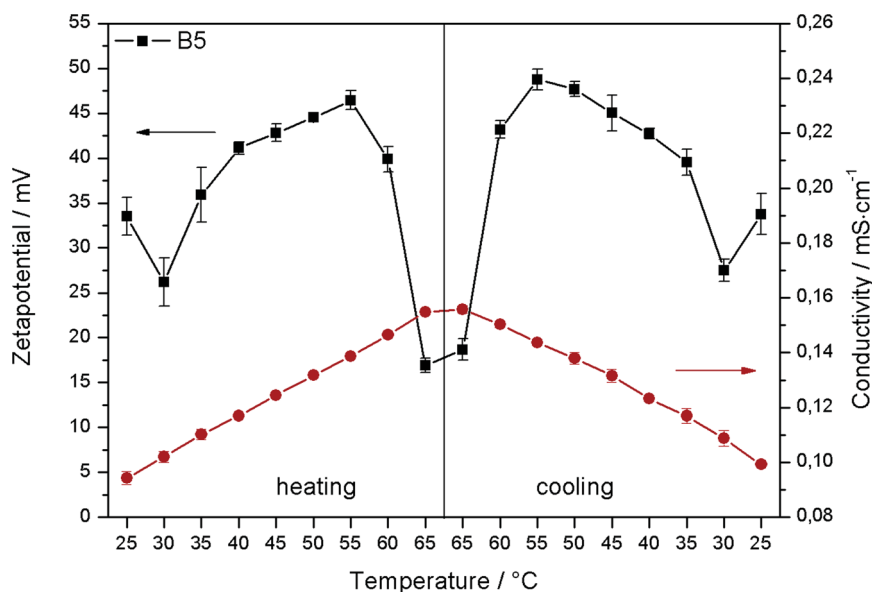
The thermoresponsive behavior of the selected block copolymer **B5** was further investigated by temperature variable zeta potential (also known as electrokinetic potential) measurements to gain a deeper insight in the polyelectrolyte nature of the block copolymer during the polymer phase transitions (Figure 7). The phase transition was investigated in water at a concentration of 2.5 mg mL<sup>-1</sup> in the temperature range from 25 to 65 °C during both heating and cooling with temperature steps of 5 °C. The conductivity (red cycles, Figure 7) of the copolymer solution was also measured, indicating a small increase of charge carrier mobility or concentration with increasing temperature, i.e., caused by the increased autodissociation of water. After the cooling cycle, the conductivity of the solution reaches nearly the starting value at 25 °C. The zeta



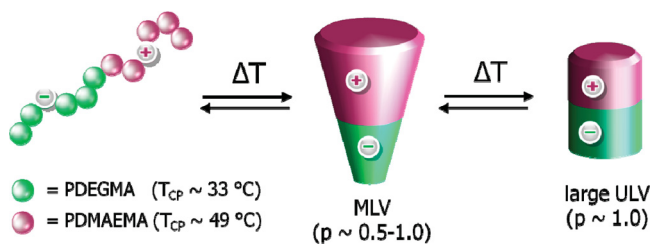
**Figure 6.** Cryo-TEM image (a,b) of **B5** block copolymer solution at ~50 °C in H<sub>2</sub>O (preheated, 5.0 mg mL<sup>-1</sup>) showing the formation of large unilamellar vesicles.

potential measurements show that two reversible thermo-induced transitions are present without showing any hysteresis behavior in the graph (Figure 7, black squares). The first transition takes place at around 30 °C and the second transition around 55–60 °C, whereby a strong decrease in the zeta potential is observed. Over the measured temperature range from 25 to 65 °C, a positive potential was measured due to the cationically charged protonated DMAEMA groups. The high value of the zeta potential indicates stable aggregates (usually a potential >25 mV indicates a stable system), which cannot further assemble together due to repulsion forces. In contrast, the pure PDEGMA homopolymer **H6** revealed a negative potential (partially negative charges due to oxygen atoms and carboxylic acid end groups) over the complete temperature range (see SI, Figure S11). On the basis of these results, it can be assumed that the collapse of the PDEGMA block at 30 °C is associated with an enhancement of the negative charges on the surface of the collapsed aggregates (SI, Figure S11), which support the formation of MLVs. The assembly is promoted by electrostatic interactions between the positive charged PDMAEMA block (corona) and the negatively charged collapsed PDEGMA block. This layer-by-layer assembly above the first transition temperature lowers the overall zeta potential of the aggregates. The charge compensation by the layer-by-layer assembly in MLV structures represents an important thermodynamic contribution to the stability of the self-assembled structures. If the temperature is raised above 50 °C, the DMAEMA block starts to collapse. During this collapse, a migration of the DMAEMA chains to the hydrophobic surface of the PDEGMA layer might occur as observed by <sup>1</sup>H NMR. This effect changes the electrostatic balance of the MLV structures, i.e., the charge compensation, and ultimately leads to the preferential formation of ULV structures. This change of the charge balance is reflected in the corresponding zeta potential values (Figure 7).

On the basis of these experimental observations, a model for the aggregation of the double responsive transition of the block copolymer structures at different temperatures was developed, which is schematically illustrated in Figure 8. In this configuration, the PDEGMA block (negatively charged) becomes insoluble at the first LCST transition temperature and is collapsed in the lamellar structure. The still-soluble PDMAEMA block (positively charged) stabilizes the individual shells by a layer-by-layer assembly and promotes the preferential formation of multilamellar onion-like vesicles. With further increasing temperature also the solubility of the PDMAEMA decreases. As a result, the volume of the



**Figure 7.** Temperature variable zeta potential measurements (black squares, average value of five estimations) of block copolymer **B5** solution at 2.5 mg mL<sup>-1</sup> showing two reversible temperature-induced transitions. Also the conductivity (red cycles) of the copolymer solution was measured.



**Figure 8.** Proposed model for the aggregation of the double responsive transition of the block copolymer. In the figure, represent red cycles DEGMA and green cycles DMAEMA units.

hydrophobic part of the copolymer increases and the interbilayer energy changes. Simultaneously, the decreasing size of the hydrophilic corona block is seen as an additional driving force for the modified aggregation behavior due to altered volume fraction and space requirements.

This effect was, e.g., observed for PS-*b*-PAA aggregates,<sup>61</sup> where shorter corona fractions generally resulted in the formation of larger structures.<sup>62</sup> Additionally, the altered charge balance within the structures favors the formation of larger and unilamellar vesicles.

This structural transitions explain also the <sup>1</sup>H NMR observations showing that after the first transition the respective poly(DEGMA) signals disappeared. This could be a direct consequence of the narrow environment, which is formed in the multilamellar vesicle system. As observed from the cryo-TEM images, it can be assumed that above 50 °C a structural transition toward unilamellar vesicles takes place. In this configuration, the packing density of the macromolecules becomes less pronounced, which could be a possible explanation of the reappearance of the poly(DMAEMA) signal in the <sup>1</sup>H NMR spectrum.

## CONCLUSION

The RAFT polymerization method was used for the preparation of a library of double thermoresponsive diblock copolymers, namely poly(DMAEMA-*b*-DEGMA). A series of poly(DMAEMA-*b*-DEGMA) copolymers have been prepared,

with compositions ranging from PDMAEMA to PDEGMA in steps of 20 mol%. The phase transitions of these block copolymers in aqueous solutions were studied in detail by turbidimetry. Higher cloud points of the poly(DMAEMA-*b*-DEGMA) with increasing amount of mol% DMAEMA in the block copolymer were observed. Within this series of block copolymers, a block ratio of 50:50 resulted in a double-responsive LCST behavior. This block copolymer was further investigated to elucidate the self-assembly behavior in detail. Variable temperature <sup>1</sup>H NMR spectroscopy, zeta potential, and cryo-TEM investigations revealed the temperature induced formation of multilamellar vesicular structures at elevated temperature which convert into unilamellar vesicles at higher temperatures. On the basis of the measurements, an illustrative model for the reversible temperature-induced self-assembly is given based on the initial formation of multilamellar vesicular (MLV) aggregates that further assemble into unilamellar vesicle (ULV) structures. This transition could be assigned to the changes of the volume ratios as well as to the ionic interplay between the block copolymers at different temperatures. In particular, the ionic contributions of the negatively charged PDEGMA block and the positively charged PDMAEMA block are supposed to support the layer-by-layer assembly at 33 °C, which favors the formation of multilamellar vesicles (MLV). Further increase of the temperature changes again the volume ratio between the blocks as the solubility of the second block occurs, furthermore the second LCST transition is associated with a changed electrostatic balance between the blocks. This results in the preferential transition of MLVs to ULVs. The present study assumes a facile interplay of the volume ratio and the changes of the ionic interactions. However, both contributions cannot be separated by the investigation of only one polymer. In further studies, the formation of self-assembled structures of different block copolymers and at different pH values will be investigated to gain a deeper understanding of the aggregation process.

The design and self-assembly of such thermoresponsive migrating block copolymers will provide new possibilities for delivery vehicles (for therapies), e.g., temperature-controlled

release of drugs, and will provide important deeper insights into the LCST transition and the formation of MLVs.

## ■ ASSOCIATED CONTENT

### ● Supporting Information

SEC curves of poly(DMAEMA-*b*-DEGMA), turbidity curves and zeta potential measurements. This material is available free of charge via the Internet at <http://pubs.acs.org>.

## ■ AUTHOR INFORMATION

### Corresponding Author

\*E-mail: [ulrich.schubert@uni-jena.de](mailto:ulrich.schubert@uni-jena.de).

### Notes

The authors declare no competing financial interest.

## ■ ACKNOWLEDGMENTS

We thank W. Günther and G. Sentis for the temperature dependent NMR measurements. Financial support of the Dutch Polymer Institute (DPI, technology area HTE) and the Carl-Zeiss-Foundation (Strukturantrag JCSM) is gratefully acknowledged. C.P. acknowledges also financial support by CSIRO.

## ■ REFERENCES

- (1) Schild, H. G. *Prog. Polym. Sci.* **1992**, *17* (2), 163–249.
- (2) Gil, E. S.; Hudson, S. M. *Prog. Polym. Sci.* **2004**, *29* (12), 1173–1222.
- (3) Schmaljohann, D. *Adv. Drug Delivery Rev.* **2006**, *58* (15), 1655–1670.
- (4) Dimitrov, I.; Trzebicka, B.; Müller, A. H. E.; Dworak, A.; Tsvetanov, C. B. *Prog. Polym. Sci.* **2007**, *32* (11), 1275–1343.
- (5) Weber, C.; Hoogenboom, R.; Schubert, U. S. *Prog. Polym. Sci.* **2012**, *37* (5), 686–714.
- (6) Du, J.; O'Reilly, R. K. *Soft Matter* **2009**, *5* (19), 3544–3561.
- (7) Li, M.-H.; Keller, P. *Soft Matter* **2009**, *5* (5), 927–937.
- (8) Hu, J.; Liu, S. *Macromolecules* **2010**, *43* (20), 8315–8330.
- (9) Pietsch, C.; Schubert, U. S.; Hoogenboom, R. *Chem. Commun.* **2011**, *47* (31), 8750–8765.
- (10) Pietsch, C.; Hoogenboom, R.; Schubert, U. S. *Angew. Chem., Int. Ed.* **2009**, *48* (31), 5653–5656.
- (11) Qin, S.; Geng, Y.; Discher, D. E.; Yang, S. *Adv. Mater.* **2006**, *18* (21), 2905–2909.
- (12) Li, Y.; Lokitz, B. S.; McCormick, C. L. *Angew. Chem., Int. Ed.* **2006**, *45* (35), 5792–5795.
- (13) Hoogenboom, R.; Rogers, S.; Can, A.; Becer, C. R.; Guerrero-Sanchez, C.; Wouters, D.; Hoepfener, S.; Schubert, U. S. *Chem. Commun.* **2009**, *37*, 5582–5584.
- (14) Discher, B. M.; Won, Y.-Y.; Ege, D. S.; Lee, J. C.-M.; Bates, F. S.; Discher, D. E.; Hammer, D. A. *Science* **1999**, *284* (5417), 1143–1146.
- (15) Discher, D. E.; Eisenberg, A. *Science* **2002**, *297* (5583), 967–973.
- (16) Antonietti, M.; Förster, S. *Adv. Mater.* **2003**, *15* (16), 1323–1333.
- (17) Coelho, J.; Ferreira, P.; Alves, P.; Cordeiro, R.; Fonseca, A.; Góis, J.; Gil, M. *EPMA J.* **2010**, *1* (1), 164–209.
- (18) Onaca, O.; Enea, R.; Hughes, D. W.; Meier, W. *Macromol. Biosci.* **2009**, *9* (2), 129–139.
- (19) Han, S.; Hagiwara, M.; Ishizone, T. *Macromolecules* **2003**, *36* (22), 8312–8319.
- (20) Lutz, J.-F.; Hoth, A. *Macromolecules* **2005**, *39* (2), 893–896.
- (21) Lutz, J.-F. *J. Polym. Sci., Part A: Polym. Chem.* **2008**, *46* (11), 3459–3470.
- (22) Moad, G.; Rizzardo, E.; Thang, S. H. *Aust. J. Chem.* **2009**, *62* (11), 1402–1472.
- (23) Keddie, D. J.; Moad, G.; Rizzardo, E.; Thang, S. H. *Macromolecules* **2012**, *45* (13), 5321–5342.
- (24) Pietsch, C.; Fijten, M. W. M.; Lambermont-Thijs, H. M. L.; Hoogenboom, R.; Schubert, U. S. *J. Polym. Sci., Part A: Polym. Chem.* **2009**, *47* (11), 2811–2820.
- (25) Lutz, J.-F.; Akdemir, Ö.; Hoth, A. *J. Am. Chem. Soc.* **2006**, *128* (40), 13046–13047.
- (26) Becer, C. R.; Hahn, S.; Fijten, M. W. M.; Thijs, H. M. L.; Hoogenboom, R.; Schubert, U. S. *J. Polym. Sci., Part A: Polym. Chem.* **2008**, *46* (21), 7138–7147.
- (27) Ishizone, T.; Seki, A.; Hagiwara, M.; Han, S.; Yokoyama, H.; Oyane, A.; Deffieux, A.; Carlotti, S. *Macromolecules* **2008**, *41* (8), 2963–2967.
- (28) Fournier, D.; Hoogenboom, R.; Thijs, H. M. L.; Paulus, R. M.; Schubert, U. S. *Macromolecules* **2007**, *40* (4), 915–920.
- (29) Üzgün, S.; Akdemir, Ö.; Hasenpusch, G.; Maucksch, C.; Golas, M. M.; Sander, B.; Stark, H.; Imker, R.; Lutz, J.-F.; Rudolph, C. *Biomacromolecules* **2009**, *11* (1), 39–50.
- (30) Cai, J.; Yue, Y.; Rui, D.; Zhang, Y.; Liu, S.; Wu, C. *Macromolecules* **2011**, *44* (7), 2050–2057.
- (31) Hinton, T. M.; Guerrero-Sanchez, C.; Graham, J. E.; Le, T.; Muir, B. W.; Shi, S.; Tizard, M. L. V.; Gunatillake, P. A.; McLean, K. M.; Thang, S. H. *Biomaterials* **2012**, *33* (30), 7631–7642.
- (32) Cho, S. H.; Jhon, M. S.; Yuk, S. H.; Lee, H. B. *J. Polym. Sci., Part B: Polym. Phys.* **1997**, *35* (4), 595–598.
- (33) Bütün, V.; Armes, S. P.; Billingham, N. C. *Polymer* **2001**, *42* (14), 5993–6008.
- (34) Liu, Q.; Yu, Z.; Ni, P. *Colloid Polym. Sci.* **2004**, *282* (4), 387–393.
- (35) Plamper, F. A.; Ruppel, M.; Schmalz, A.; Borisov, O.; Ballauff, M.; Müller, A. H. E. *Macromolecules* **2007**, *40* (23), 8361–8366.
- (36) Plamper, F. A.; Schmalz, A.; Müller, A. H. E. *J. Am. Chem. Soc.* **2007**, *129* (47), 14538–14539.
- (37) Paris, R.; Quijada-Garrido, I. *Eur. Polym. J.* **2010**, *46* (11), 2156–2163.
- (38) Yamamoto, S.-i.; Pietrasik, J.; Matyjaszewski, K. *Macromolecules* **2008**, *41* (19), 7013–7020.
- (39) van de Wetering, P.; Zuidam, N. J.; van Steenbergen, M. J.; van der Houwen, O. A. G. J.; Underberg, W. J. M.; Hennink, W. E. *Macromolecules* **1998**, *31* (23), 8063–8068.
- (40) Schilli, C. M.; Zhang, M.; Rizzardo, E.; Thang, S. H.; Chong, Y. K.; Edwards, K.; Karlsson, G.; Müller, A. H. E. *Macromolecules* **2004**, *37* (21), 7861–7866.
- (41) Baines, F. L.; Billingham, N. C.; Armes, S. P. *Macromolecules* **1996**, *29* (10), 3416–3420.
- (42) Kostiainen, M. A.; Pietsch, C.; Hoogenboom, R.; Nolte, R. J. M.; Cornelissen, J. J. L. M. *Adv. Funct. Mater.* **2011**, *21* (11), 2012–2019.
- (43) Arotgaréna, M.; Heise, B.; Ishaya, S.; Laschewsky, A. *J. Am. Chem. Soc.* **2002**, *124* (14), 3787–3793.
- (44) Kotsuchibashi, Y.; Ebara, M.; Yamamoto, K.; Aoyagi, T. *Polym. Chem.* **2011**, *2* (6), 1362–1367.
- (45) Blanz, A.; Armes, S. P.; Ryan, A. J. *Macromol. Rapid Commun.* **2009**, *30* (4–5), 267–277.
- (46) Liu, S.; Armes, S. P. *J. Am. Chem. Soc.* **2001**, *123* (40), 9910–9911.
- (47) Xu, J.; Luo, S.; Shi, W.; Liu, S. *Langmuir* **2005**, *22* (3), 989–997.
- (48) Weiss, J.; Bottcher, C.; Laschewsky, A. *Soft Matter* **2011**, *7* (2), 483–492.
- (49) Hua, F.; Jiang, X.; Zhao, B. *Macromolecules* **2006**, *39* (10), 3476–3479.
- (50) Agut, W.; Brulet, A.; Schatz, C.; Taton, D.; Lecommandoux, S. *Langmuir* **2010**, *26* (13), 10546–10554.
- (51) Farnham, W. B., PCT Int. Appl. WO 2005113493, A1 20051201, 2005.
- (52) Keddie, D. J.; Guerrero-Sanchez, C.; Moad, G.; Rizzardo, E.; Thang, S. H. *Macromolecules* **2011**, *44* (17), 6738–6745.
- (53) Guerrero-Sanchez, C.; Keddie, D. J.; Saubern, S.; Chiefari, J. *ACS Comb. Sci.* **2012**, *14* (7), 389–394.
- (54) Keddie, D. J.; Guerrero-Sanchez, C.; Moad, G.; Mulder, R. J.; Rizzardo, E.; Thang, S. H. *Macromolecules* **2012**, *45* (10), 4205–4215.
- (55) Koppel, D. E. *J. Chem. Phys.* **1972**, *57* (11), 4814–4820.



- (56) Ohshima, H. *J. Colloid Interface Sci.* **1994**, *168* (1), 269–271.
- (57) Moad, G.; Chong, Y. K.; Postma, A.; Rizzardo, E.; Thang, S. H. *Polymer* **2005**, *46* (19), 8458–8468.
- (58) Sahnoun, M.; Charreyre, M.-T.; Veron, L.; Delair, T.; D'Agosto, F. *J. Polym. Sci., Part A: Polym. Chem.* **2005**, *43* (16), 3551–3565.
- (59) Guillaneuf, Y.; Castignolles, P. *J. Polym. Sci., Part A: Polym. Chem.* **2008**, *46* (3), 897–911.
- (60) Israelachvili, J. N., *Intermolecular and Surface Forces*. 3rd ed.; Elsevier, Academic Press: Amsterdam, 2011.
- (61) Zhang, L.; Eisenberg, A. *J. Am. Chem. Soc.* **1996**, *118* (13), 3168–3181.
- (62) Holder, S. J.; Sommerdijk, N. A. J. M.; Williams, S. J.; Nolte, R. J. M.; Hiorns, R. C.; Jones, R. G. *Chem. Commun.* **1998**, *14*, 1445–1446.



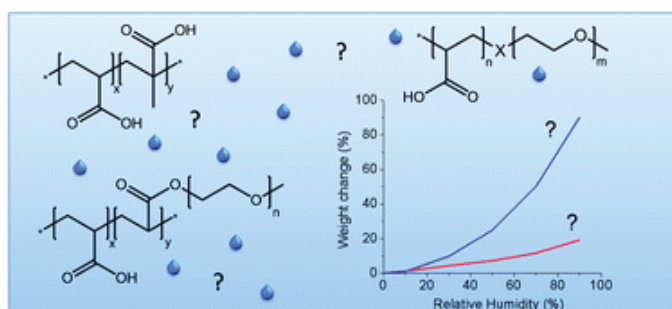
## Publication P9:

### *Dual hydrophilic polymers based on (meth)acrylic acid and poly(ethylene glycol) – synthesis and water uptake behavior*

---

A. Krieg, C. Pietsch, A. Baumgaertel, M. D. Hager, C. R. Becer,  
U. S. Schubert

*Polym. Chem.* **2010**, *1*, 1669–1676





# Dual hydrophilic polymers based on (meth)acrylic acid and poly(ethylene glycol) – synthesis and water uptake behavior†

Andreas Krieg,<sup>ac</sup> Christian Pietsch,<sup>ac</sup> Anja Baumgaertel,<sup>ac</sup> Martin D. Hager,<sup>ac</sup> C. Remzi Becer<sup>\*abc</sup> and Ulrich S. Schubert<sup>\*abc</sup>

Received 16th May 2010, Accepted 8th July 2010

DOI: 10.1039/c0py00156b

Synthesis and characterization of dual hydrophilic random and block copolymers of acrylic acid (AA) or methacrylic acid (MAA) with poly(ethylene glycol) (PEG) *via* different controlled radical polymerization techniques are discussed. Initially, reversible addition fragmentation chain transfer (RAFT) polymerization was employed to synthesize homo, random and block copolymers of AA and MAA in ethanol. The polymers were characterized in detail by means of size exclusion chromatography (SEC), <sup>1</sup>H NMR spectroscopy, matrix assisted laser desorption ionization time of flight (MALDI-TOF) mass spectrometry as well as MALDI-TOF MS coupled with collision induced dissociation (CID) to identify the end groups and the repeating units. Following that, atom transfer radical polymerization (ATRP) and RAFT polymerization were employed for the preparation of block copolymers using a PEG macroinitiator and a PEG macro chain transfer agent. Moreover, graft copolymers that contain oligo(ethyleneglycol) pendant groups and AA or MAA have been prepared using the RAFT polymerization process. Additionally, selected homo or block copolymers were tested for their water-uptake properties using a thermal gravimetric analyzer with a controlled humidity chamber. An advantageous behavior of the copolymers compared to the related homopolymers was reached with the obtained ability to absorb moisture over the complete humidity range as well as to a very high absolute water uptake.

## Introduction

Water-soluble polymers with various architectures are of great interest in the field of polymer science due to their wide range of possible applications, *i.e.* in drug-delivery systems, dispersing agents and absorbent materials.<sup>1–4</sup> The most widely used structures to construct dual hydrophilic polymers are based on acrylic acid (AA), methacrylic acid (MAA) and poly(ethylene glycol) (PEG). AA and MAA can be polymerized by controlled radical polymerization techniques whereas PEG can be obtained by ionic polymerization.<sup>5–7</sup> Various polymeric architectures can be constructed using these monomers or polymers. However, the synthesis and characterization of well-defined water soluble polymers requires not only dedicated reaction conditions and catalysts but also suitable analytical instruments to precisely assign their structures.

There are two main approaches which are possible for obtaining polymers of desired architectures. The first possibility is the reaction of end group or side group functionalized polymers with the second block or functional side group to form

block or graft copolymers, respectively. The reactions which are nowadays employed in this route are mainly found among the so called “click” reactions.<sup>8–10</sup> The other possibility is the construction of the desired compositions and architectures directly by the polymerization process itself. Therefore, macroinitiators, macromonomers or macro chain transfer agents (macro-CTA) have to be prepared according to the targeted polymeric structures.<sup>11</sup> In the present study, the latter approach was applied to obtain linear as well as graft block and random copolymers.

Controlled radical polymerization (CRP) techniques provide enormous possibilities for synthesizing well-defined polymers with controlled architectures and molar masses. For instance, reversible addition fragmentation chain transfer (RAFT) polymerization allows the use of acidic monomers and also the use of polar solvents like ethanol. Therefore, this technique is the most widely employed method to prepare water soluble polymers.<sup>12</sup> However, the CTA has to be carefully selected depending on the nature of the monomer.<sup>13–15</sup>

Alternatively, transition metal-catalyzed controlled radical polymerization techniques provide good control over the polymerization of several monomers.<sup>16</sup> Unfortunately, these techniques, namely atom transfer radical polymerization (ATRP) and single electron transfer controlled radical polymerization (SET-LRP), are based on the oxidation reduction equilibrium of the transition metal and ligand complex which can be disturbed in the presence of acidic monomers.<sup>17–19</sup> As a consequence, protected monomers have to be used during the polymerization.

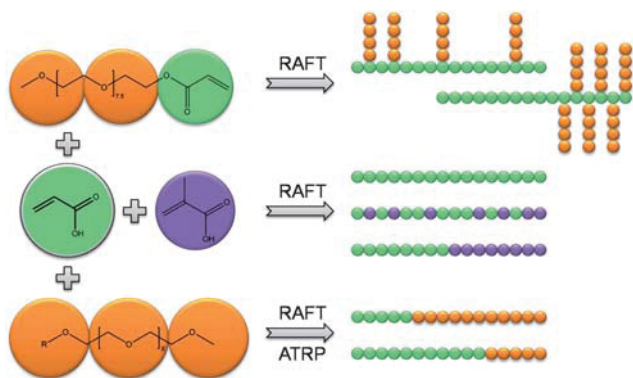
While actual studies are, for example, investigating the morphology of dual hydrophilic copolymers, *e.g.* P(AA-*co*-EG)

<sup>a</sup>Laboratory of Organic and Macromolecular Chemistry, Friedrich-Schiller-University Jena, Humboldtstrasse 10, 07743 Jena, Germany. E-mail: ulrich.schubert@uni-jena.de

<sup>b</sup>Laboratory of Macromolecular Chemistry and Nanoscience, Eindhoven University of Technology, PO Box 513, 5600, MB, Eindhoven, The Netherlands. E-mail: c.r.becer@warwick.ac.uk

<sup>c</sup>Dutch Polymer Institute (DPI), John F. Kennedylaan 2, 5612, AB, Eindhoven, The Netherlands

† Electronic supplementary information (ESI) available: Comparison of measured and calculated isotopic patterns for MS-MS spectra. See DOI: 10.1039/c0py00156b



**Scheme 1** A schematic representation of the monomers used and the block and random copolymer architectures obtained by different synthetic approaches.

nanofibers, like recently reported by Charleux *et al.*,<sup>20</sup> the present contribution focuses on structural investigation and the study of the water uptake behavior.

Water uptake properties of polymers are relatively rarely investigated, but represent a very important polymer characteristic and play a crucial role in several applications of polymers such as personal care products,<sup>21–23</sup> coatings, composite materials, cement,<sup>24</sup> membranes and sensors,<sup>25</sup> agriculture products,<sup>26–30</sup> biomedical materials,<sup>31–33</sup> insulation of underwater cables<sup>34</sup> or recreational activities (*e.g.* artificial snow). Researchers have focused on the modification and optimization of polymers in terms of water absorbency, absorption–desorption rates and gel strength (in cross-linked systems).<sup>35</sup> Moisture uptake can be measured directly from water or from a humid atmosphere. However, most of the reported research has focused on the investigation of cross-linked polymer systems (super absorbent polymers) in direct contact with water. Other measurements require the use of conditioned desiccators and several days to weeks of measurement time until the samples are saturated with water molecules. Alternatively, water uptake properties of polymeric materials can be measured by a thermal gravimetric analyzer with a controlled humidity chamber. This technique requires a very small amount of sample (a few milligrams) and the measurement can be performed in any form, such as in powder, liquid or crosslinked gel.

Different strategies to synthesize dual hydrophilic polymers in various architectures were studied, as illustrated in Scheme 1. Homopolymers, block and random copolymers of AA and MAA have been prepared using RAFT polymerization. Moreover, graft copolymers were prepared using oligo(ethylene glycol) acrylate (OEGA) and AA or MAA. Furthermore, macroinitiator and macro chain transfer agents were synthesized in order to use those in the block copolymerization. ATRP and RAFT polymerization were employed to synthesize PEG-*b*-AA and PEG-*b*-MAA block copolymers. Finally, these polymers are tested for their water uptake properties.

## Experimental section

### Materials

Poly(ethylene glycol) monomethyl ether (mPEG<sub>1k</sub>: CH<sub>3</sub>-PEG<sub>22</sub>-OH,  $M_n = 1000 \text{ g mol}^{-1}$ , PDI = 1.07 and mPEG<sub>2k</sub>: CH<sub>3</sub>-PEG<sub>44</sub>-

OH,  $M_n = 2000 \text{ g mol}^{-1}$ , PDI = 1.08) were purchased from Sigma-Aldrich. The monomers acrylic acid (AA), methacrylic acid (MAA), *tert*-butyl acrylate (*t*BuA) and oligo(ethylene glycol) acrylate ( $M_n = 480 \text{ g mol}^{-1}$ ) (OEGA<sub>480</sub>) were purchased from Sigma-Aldrich and passed through a column with inhibitor remover by Sigma-Aldrich before using. CuBr, *N,N',N'',N'''*-pentamethyl diethylene triamine (PMDETA) and ethyl 2-bromo-isobutyrate (EtBriB) were purchased from Sigma-Aldrich and used as received without further purification. 2-(Butylthio-carbonothioylthio) propanoic acid (BPTC) and 2-cyano-2-butylthiobenzoate (CBDB) were synthesized according to the literature and used without further purification.<sup>36,37</sup> Azobis(isobutyronitrile) (AIBN) was received from Sigma-Aldrich and recrystallized from methanol before using. Other solvents and reagents were used as received without further purification.

### Instrumentation

<sup>1</sup>H NMR spectra were recorded in CDCl<sub>3</sub> or DMSO-*d*<sub>6</sub> on a Bruker AC 300 MHz using the residual solvent resonance as an internal standard. Size exclusion chromatography (SEC) was performed on a Shimadzu system equipped with a SCL-10A system controller, a LC-10AD pump, a RID-10A refractive index detector and both a PSS Gram30 and a PSS Gram1000 column in series, whereby *N,N*-dimethylacetamide (DMAc) with 5 mmol lithium chloride (LiCl) was used as an eluent at 1 mL min<sup>-1</sup> flow rate and the column oven was set to 60 °C. The system was calibrated with polystyrene (370 g mol<sup>-1</sup>–67 500 g mol<sup>-1</sup>) and poly(methyl methacrylate) (2000 g mol<sup>-1</sup>–88 000 g mol<sup>-1</sup>) standards, respectively. For the measurement of the matrix assisted laser desorption/ionization (MALDI) spectra an Ultraflex III TOF/TOF (Bruker Daltonics, Bremen, Germany) instrument was used. The instrument was equipped with a Nd:YAG laser and a collision cell. All spectra were measured in the positive reflector or linear mode. The instrument was calibrated prior to each measurement with an external PMMA standard from PSS Polymer Standards Services GmbH (Mainz, Germany). Monomer conversions were determined by gas chromatography (GC) using anisole as internal standard. The number-average molar mass ( $M_n$ ) and the polydispersity index (PDI) were determined by size-exclusion chromatography (SEC) using chloroform or *N,N*-dimethyl acetamide (DMAc) as solvents depending on the solubility behavior of the samples. The water-uptake measurements of the polymers were investigated on a Q5000 SA thermogravimetric analyzer from TA Instruments containing a microbalance in which the sample and reference pans were enclosed in a humidity and temperature controlled chamber. The temperature in the Q5000 SA was controlled by Peltier elements. Dried N<sub>2</sub> gas flow (200 mL min<sup>-1</sup>) was split into two parts, of which one part was wetted by passing it through a water-saturated chamber. The desired relative humidity (RH) for the measurements could subsequently be obtained by mixing proper proportions (regulated by mass-flow controllers) of dry and wet stream.

### Synthesis

**Homopolymerization of AA and MAA via RAFT.** AA and MAA were homopolymerized separately by RAFT

polymerization. The general procedure was introduced as follows. A mixture 288 mg AA or 344 mg MAA (4 mmol) with 6.6 mg AIBN (0.04 mmol) and 38 mg CTA (0.16 mmol BPTC for PAA or 0.16 mmol CBDB for PMAA) was dissolved in 1.5 mL absolute ethanol and 0.2 mL anisole in a capped vial leading to a final monomer concentration of 2 mol L<sup>-1</sup>. The reaction mixture was bubbled with argon for half an hour and the  $t_0$ -sample was withdrawn for the subsequent GC measurements. The reaction solution was placed in a preheated oil bath at 70 °C. After the desired period of time the mixture was cooled to ambient temperature and a  $t_{\text{end}}$ -sample for GC was taken. The solution was diluted by adding 2 mL ethanol and precipitated into 75 mL ethyl acetate. The solid polymer obtained was dried, washed with diethyl ether and dried again until the mass of the polymer was constant.

**Block copolymerization of MAA and AA via RAFT.** The PMAA homopolymer was synthesized by RAFT polymerization as described above. To 0.288 mg AA (4 mmol) the prepared PMAA macro-CTA was added to such an extent that the desired monomer/CTA ratio was reached. Furthermore, 0.25 eq. AIBN relative to the PMAA macro-CTA (1 eq.) were added, and the whole mixture was diluted in 3.3 mL ethanol and 0.4 mL anisole leading to a final AA concentration of 1 mol L<sup>-1</sup>. The reaction mixture was bubbled with argon for half an hour, and the  $t_0$ -sample was withdrawn for the subsequent GC measurements. The reaction solution was placed in a preheated oil bath at 70 °C. After the desired period of time, the mixture was cooled to ambient temperature and a  $t_{\text{end}}$ -sample for GC was taken. The solution was precipitated into 75 mL ethyl acetate. The solid polymer obtained was dried, washed with diethyl ether and dried again until the mass of the polymer was constant.

**Random copolymerization of MAA and AA via RAFT.** The P(MAA-*r*-AA) random copolymers were prepared by RAFT polymerization according to the general procedure as follows. AA and MAA were mixed in a desired ratio leading to a final total amount of monomer of 4 mmol. With 3.3 mg AIBN (0.02 mmol) and 16 mg CBDB (0.08 mmol), the monomers were dissolved in 1.5 mL absolute ethanol and 0.2 mL anisole in a capped vial leading to a final total monomer concentration of 2 mol L<sup>-1</sup>. The reaction mixture was bubbled with argon for half an hour and the  $t_0$ -sample was withdrawn for the subsequent GC measurements. The reaction solution was placed in a preheated oil bath at 70 °C. After the desired period of time, the mixture was cooled to ambient temperature, and a  $t_{\text{end}}$ -sample for GC was taken. The solution was diluted by adding 2 mL ethanol and precipitated into 75 mL ethyl acetate. The solid polymer obtained was dried, washed with diethyl ether and dried again until the mass of the polymer was constant.

**Homopolymerization of OEGA<sub>480</sub> via RAFT.** OEGA was polymerized by RAFT polymerization. A mixture of 480 mg OEGA<sub>480</sub> (1 mmol), 29.8 mg BPTC (0.125 mmol) and 2 mg AIBN (0.013 mmol) were dissolved in 2 mL absolute ethanol in a capped vial leading to a final monomer concentration of 0.5 mol L<sup>-1</sup>. The reaction mixture was bubbled with argon for half an hour and the  $t_0$ -sample was withdrawn for the subsequent SEC measurements. The reaction solution was placed in

a preheated oil bath at 70 °C. After 5 h, the mixture was cooled to ambient temperature and a  $t_{\text{end}}$ -sample for GPC was taken. The solution was precipitated into cold diethyl ether.

**Random copolymerization of AA and OEGA<sub>480</sub> via RAFT.** A mixture of AA (35 or 70 eq.), OEGA<sub>480</sub> (5 eq.), BPTC (1 eq.) and AIBN (0.25 eq.) was dissolved in absolute ethanol with a total monomer concentration of 4 mol L<sup>-1</sup>. The reaction solution was purged with argon for 60 min and placed in a preheated oil bath (70 °C). After 6 h the reaction was stopped and the solution was precipitated into cold ethyl acetate. The final polymer was obtained after washing with cold diethyl ether to remove ethyl acetate residues. It was dried until the mass of the polymer was constant. The determination of the conversion were done by GC using anisole as internal standard.

**Block copolymerization of AA and OEGA<sub>480</sub> via RAFT.** These block copolymers were prepared in a sequential monomer addition process using the RAFT method, whereby AA was polymerized at first resulting in a macro chain transfer agent. To a mixture of BPTC (1 eq.) and AIBN (0.25 eq.) AA (35 or 70 eq.) was added and the mixture was dissolved in absolute ethanol in a capped vial with a total monomer concentration of 3.5 mol L<sup>-1</sup>. The reaction solution was purged with argon for 60 min and placed in a preheated oil bath (70 °C). After 5 h OEGA<sub>480</sub> ([OEGA<sub>480</sub>]<sub>0</sub> = 0.5 mol L<sup>-1</sup>) was added *via* a syringe to this capped vial (OEGA<sub>480</sub> : PAA : AIBN = 5 : 1 : 0.25) and the solution was further heated for 6 h. The polymer was isolated by precipitation into cold ethyl acetate and washed with diethyl ether to remove the residual monomer and solvent. The polymer was dried until the mass of the sample was constant.

**Synthesis of PEG macroinitiator for ATRP (PEG-EBriB).** 2-Bromo-2-methyl-propionate end-functionalized mPEG<sub>1k</sub> was synthesized by reacting 2-bromo-2-methyl-propionyl bromide and mPEG<sub>1k</sub> in the presence of triethylamine at room temperature in dry THF.

<sup>1</sup>H NMR (300 MHz, CDCl<sub>3</sub>) δ = 4.31 (*m*, CH<sub>2</sub>-OCO), 3.63 (*m*, O-CH<sub>2</sub>), 3.36 (*m*, CH<sub>3</sub>-O), 1.92 (*s*, (CH<sub>3</sub>)<sub>2</sub>CBr) ppm.

**Synthesis of PEG macro chain transfer agent for RAFT (PEG-BPTC).** mPEG<sub>2k</sub> end-functionalized with BPTC was synthesized by reacting 2-(butylthiocarbonothioylthio) propanoyl benzo-triazolid and mPEG<sub>2k</sub> in the presence of triethylamine in dry THF.

<sup>1</sup>H NMR (300 MHz, CDCl<sub>3</sub>) δ = 4.73 (CH-SCS<sub>2</sub>), 4.20 (CH<sub>2</sub>-OCO), 3.55 (CH<sub>2</sub>-O), 3.28 (CH<sub>3</sub>-O), 3.26 (CH<sub>2</sub>-SCS<sub>2</sub>), 1.59 (CH<sub>2</sub>(CH<sub>2</sub>)<sub>2</sub>), 1.50 (CH<sub>3</sub>-CH), 1.33 (CH<sub>2</sub>-CH<sub>3</sub>), 0.84 (CH<sub>2</sub>-CH<sub>3</sub>) ppm.

**Synthesis of PEG-*b*-AA via ATRP.** Poly(ethylene glycol-*block-tert*-butyl acrylate) (PEG-*b*-*t*BA) was synthesized by ATRP. 0.058 mL PMDETA (48 mg, 0.28 mmol) and 40 mg CuBr (0.28 mmol) were dissolved in 2.5 mL anisole and flushed with argon. After the formation of the complex 200 mg (0.2 mmol) PEG<sub>1k</sub>-EBriB ( $M_n = 1040$  g mol<sup>-1</sup> according to MALDI-TOF MS) and 1.45 mL *t*BuA (1.28 g, 10 mmol) were added. The reaction mixture was further degassed with argon, and a  $t_0$ -sample for GC was taken *via* syringe. The closed vial was placed in

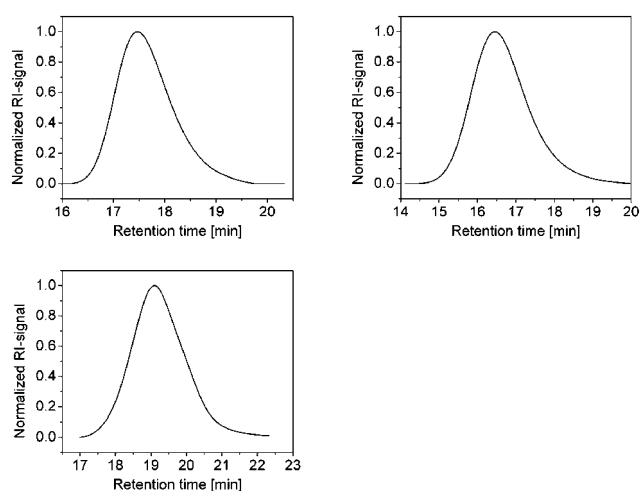
a preheated oil bath at 90 °C and reacted for 4 h. Afterwards, a  $t_{\text{end}}$ -sample for GC was withdrawn and the mixture was passed over a short  $\text{Al}_2\text{O}_3$  column to remove the copper catalyst and precipitated into a methanol–water mixture. The dried polymer was stirred with 5 equivalence of trifluoroacetic acid relative to the *tert*-butyl functionalities for 24 h to cleave the *tert*-butyl groups that will finally yield P(EG-*b*-AA).

**Synthesis of P(EG-*b*-AA) via RAFT.** Poly(ethylene glycol-*block*-acrylic acid) (P(EG-*b*-AA)) was synthesized by RAFT polymerization. In a capped vial, a mixture of 200 mg PEG<sub>2k</sub>-CTA (0.1 mmol) ( $M_n = 2000 \text{ g mol}^{-1}$  according to MALDI-TOF MS), 343  $\mu\text{L}$  AA (360 mg, 5 mmol) and 3.3 mg AIBN (0.02 mmol) was dissolved in 0.250 mL anisole and 1.9 mL ethanol. After flushing the solution with argon for 30 min, a  $t_0$ -sample for GC was taken and the mixture was placed in a preheated oil bath at 70 °C and reacted for 5 h. The reaction solution was cooled to ambient temperature, and a  $t_{\text{end}}$ -sample for GC was withdrawn. Subsequently, 2.5 mL ethanol were added and the solution was precipitated into cold diethyl ether.

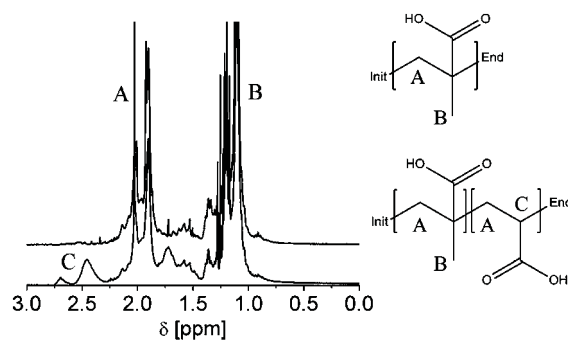
## Results and discussion

The synthesis of polymers based on AA or MAA *via* CRP techniques can be challenging due to the acidic nature, as described previously. Therefore, the RAFT polymerization was preferred over ATRP to obtain the desired polymers. However, a dedicated CTA is necessary to successfully polymerize both acrylic and also methacrylic monomers. CBDB is an adequate CTA to reach control in the present case and allowed the preparation of the desired random and block copolymers of AA and MAA. The obtained SEC results of homopolymers, random- and block copolymers of AA and MAA are shown in Fig. 1.

The relatively similar structures of AA and MAA raise the question about the possibilities to determine the compositions of the obtained polymers. An indirect approach is the calculation of molar mass and polymer composition in correlation to the monomer conversion during the polymerization which can be determined by GC. On the other hand,  $^1\text{H}$  NMR spectroscopy



**Fig. 1** SEC traces of PAA (top left), P(MAA-*r*-AA) (top right) and P(MAA-*b*-AA) (bottom left).



**Fig. 2**  $^1\text{H}$  NMR spectra (300 MHz,  $\text{CDCl}_3$ ) of P(MAA) (top) and P(MAA-*co*-AA) (bottom) with the corresponding schematic representation of the polymer structures.

allows to distinguish between both compounds in the final polymer; thereby a selective and quantitative analysis of the real polymer composition can be performed (Fig. 2).

The conversion of the monomers were calculated using both GC and  $^1\text{H}$  NMR spectroscopy. This allows the direct calculation of the polymer composition. The comparison of the obtained values using both approaches shows a rather good agreement in most cases. It has to be considered that possible solvent residues, in particular those with alkyl functionalities, can lead to an overestimation of the MAA content using the  $^1\text{H}$  NMR technique.

The versatility of the RAFT technique allowed the synthesis of various polymers with different compositions. A comparison of the prepared polymers including their characteristic data obtained by several analytical techniques, *i.e.* GC, SEC, and  $^1\text{H}$  NMR spectroscopy, is provided in Table 1.

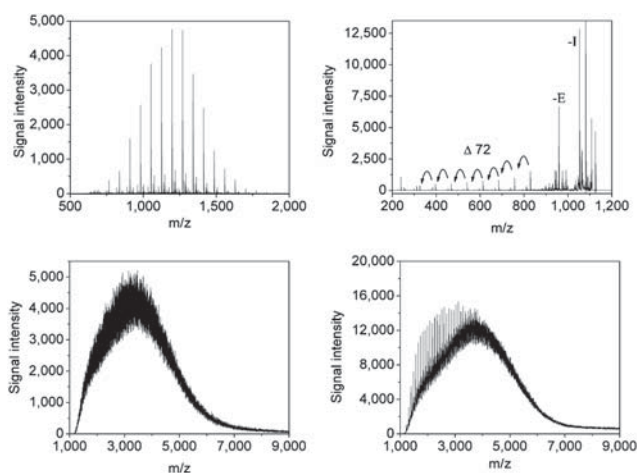
SEC is a widely used technique in polymer analysis. The obvious discrepancy between the theoretical molar masses and the experimental values in the current case is caused by the significantly larger hydrodynamic volume of the polymers prepared in comparison to the polymer standards used for the calibration of the SEC (PS calibration). A route to circumvent this problem is the use of a direct molar mass determination technique, *i.e.* MALDI-TOF mass spectrometry. Since the exact determination of polymeric structures is one of the most important goals in polymer research, this technique represents a very powerful tool. The combination of a mass spectrometric analysis of a polymer, providing a molar mass distribution, with the subsequent fragmentation of single and distinct macromolecules offers a great possibility to analyze polymers down to their precise structure and composition. The prerequisite for such a tandem mass spectrometric analysis is the selective admittance of already desorbed and ionized molecules into a gas filled collision cell. Further fragmentation occurs inside, which is kinetically induced by the collision gas (argon or nitrogen). Fig. 3 shows the analysis of the selected polymers by MALDI-TOF MS and tandem-MS technique. However, besides the stated advantages, one should be aware of potential disadvantages of the MALDI-TOF MS technique. Due to its rather harsh ionization method, fragmentations can occur during the measurement process itself leading to fragments not representing the real polymer structure. Furthermore, possible ionization biases can make an accurate molar mass determination difficult. MS



**Table 1** Representative data of homopolymers (H), random (R) and block (B) copolymers of AA and MAA synthesized *via* RAFT polymerization

Run	MAA (feed)	AA (feed)	MAA <sup>a</sup> (conv.)	AA <sup>a</sup> (conv.)	$M_{n,theo}^b$ /g mol <sup>-1</sup>	$M_{n,SEC}^c$ /g mol <sup>-1</sup>	PDI <sup>c</sup>	MAA : AA (GC)	MAA : AA <sup>d</sup> ( <sup>1</sup> H NMR)
H1	—	30	—	0.84	2053	4300	1.19	0 : 1	0 : 1
H2	25	—	0.54	—	1396	3600	1.31	1 : 0	1 : 0
R <sub>1</sub>	20	48	0.96	0.60	3960	7900	1.26	0.39 : 0.61	0.40 : 0.60
R <sub>2</sub>	25	25	0.87	0.55	3099	6400	1.25	0.61 : 0.39	0.60 : 0.40
R3	11	67	0.88	0.43	3146	6900	1.21	0.26 : 0.74	0.33 : 0.67
B1	18	35	0.99	0.50	3027	6000	1.34	0.50 : 0.50	0.71 : 0.29
B2	20	25	0.95	0.45	2679	4300	1.39	0.63 : 0.37	0.67 : 0.33
B3	20	60	0.96	0.3	3182	7300	1.28	0.53 : 0.47	0.55 : 0.44

<sup>a</sup> Conversion values were determined by GC. <sup>b</sup> Calculated according to formula ( $M_{n,theo} = ([M]/[CTA]) \times conv. \times M_{Monomer} + M_{CTA}$ ). <sup>c</sup> Calculated according to PS standards. <sup>d</sup> The ratios were calculated from the corresponding peaks shown in Fig. 2.



**Fig. 3** Representative MALDI-TOF mass spectra of PAA (H1) (top left), P(MAA-*r*-AA) (R3) (bottom left) and P(MAA-*b*-AA) (B3) (bottom right). Tandem MS spectrum of PAA (top right).

techniques applying softer ionization methods, *e.g.* electron spray ionization (ESI), can add further insights.<sup>38</sup>

The MALDI-TOF mass spectrum of the homopolymer allows the assignment of molecular structures corresponding to the obtained distributions. The distance between the signals of each distribution corresponds to the molar mass of the monomer unit. The main distribution represents the expected structure plus the charge carrying sodium ion. The three minor signal distributions are probably caused by fragmentations during the MALDI measurement itself. One of these fractions can for example be assigned to the expected structure after the loss of the *n*-butyl substituent from the end-group.

Furthermore, tandem mass spectrometry is possible providing an even deeper insight into the polymeric structure. The major signals in the high molar mass region can be assigned to the desired structure after losing H<sub>2</sub>O (−18) and CO<sub>2</sub> (−44) due to anhydrite formation, decarboxylation reactions and combinations of both.<sup>39</sup> The two important signals marked as −I and −E represent the polymer after loss of the initiator group (−I) or the chain transfer agent end group (−E). The Δ72 distribution in the middle mass region represents the different chain lengths, which can be formed by fragmentation of different amounts of repeating units of AA.

The clear structure of the homopolymer mass spectra is lost in the case of the random and block copolymers. The large amount of possible monomer combinations and, thereby, the wide range of resulting molar masses leads to complex spectra. Single signal assignments are no longer possible.

The resulting  $M_n$  values correspond to the expected molar masses calculated from the monomer. In case of the block copolymer, residual homopolymer of the unconverted first block is visible on the low molar mass shoulder of the distribution. However, it is not possible to draw any quantitative conclusions concerning the amount of remaining homopolymer from the MALDI-TOF mass spectra.

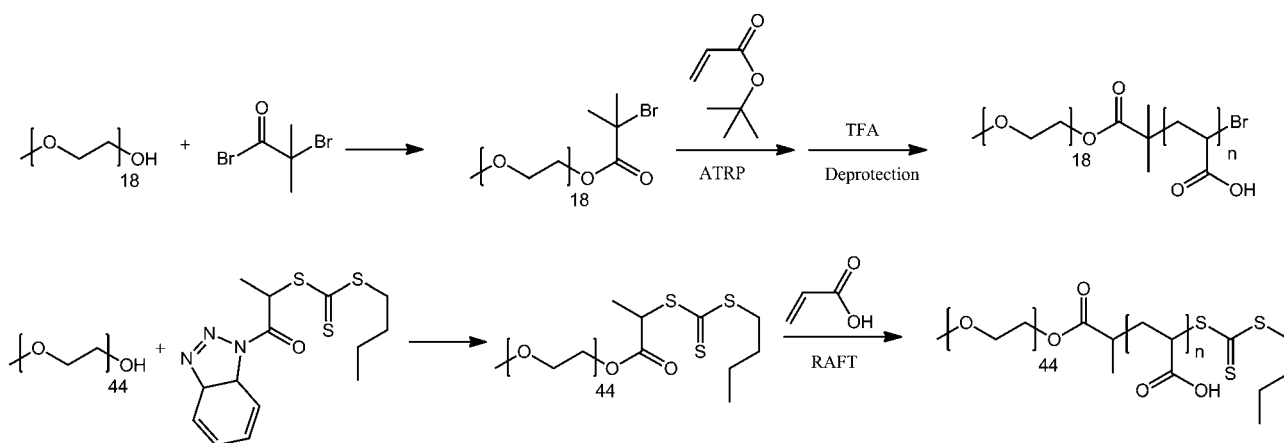
Dual hydrophilic block copolymers composed of EG and AA are a versatile polymer class suitable for many applications, *e.g.* to control structure and size of mineral particles.<sup>40</sup> The synthetic approach mainly utilized towards these polymers up to now is the synthesis of a macro-initiator suitable for ATRP by an esterification reaction. Subsequently a protected acrylic monomer, *e.g.* *t*-butyl acrylate (*t*-BuA), is polymerized onto this macroinitiator, providing the desired poly(EG-*b*-AA) after a deprotection step.

A second possibility, with the advantage of avoiding the deprotection step, is the synthesis of a macro chain transfer agent applicable for a RAFT polymerization of acrylic acid. A visualization of both synthetic approaches is provided in Scheme 2. In the present study, both methods were applied to obtain P(EO-*b*-AA) block copolymers. In Table 2, the characteristic data for all polymers prepared using both approaches are summarized.

The macroinitiator synthesis as well as the polymerization and deprotection steps could be followed *via* MALDI-TOF mass spectrometry. The resulting spectra including the assigned structures are provided exemplarily for the ATRP approach in Fig. 4.

The main distribution could be assigned to the desired product plus a sodium ion. Also the second largest distribution represents an acceptable product with the only difference being a hydroxyl end-group at the second chain-end of the macroinitiator. Only a very small educt specific distribution is observed. An overlay of the MALDI-TOF mass spectra of the macroinitiator and its block copolymer with *t*BuA before and AA after deprotection illustrates the controlled synthesis of the block copolymer as well as its subsequent deprotection.

The approach *via* the RAFT-polymerization enabled the synthesis of comparably well-defined polymers. The

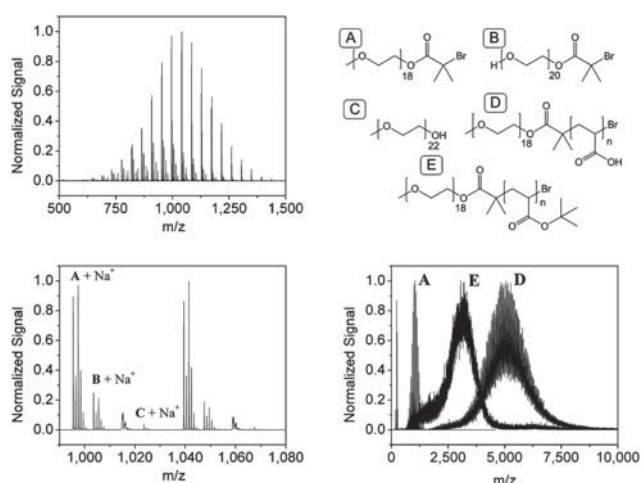


**Scheme 2** A schematic representation of the ATRP macroinitiator approach (top) and the RAFT macro chain transfer agent approach (bottom) towards P(EG-*b*-AA) block copolymers.

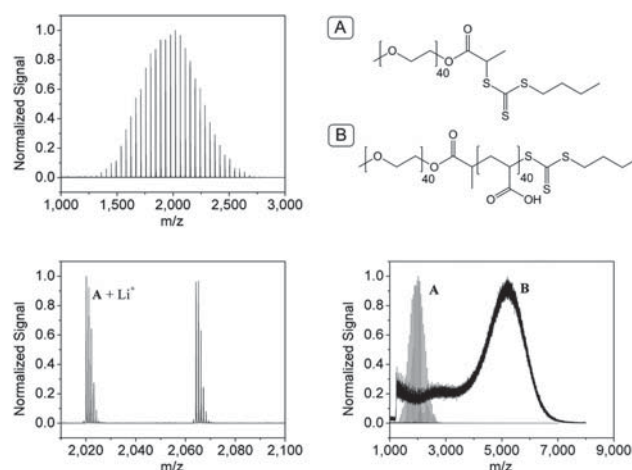
**Table 2** Characteristic data of the polymers which were included in the synthesis of P(EG-*b*-AA) via the ATRP or the RAFT route, respectively

Type	$M_n^a$ /g mol <sup>-1</sup>	PDI <sup>a</sup>	$M_p^b$ /g mol <sup>-1</sup>	$M_n^c$ /g mol <sup>-1</sup>	Comp. <sup>d</sup> EG : A.
mPEG <sub>1k</sub>	1700	1.06	1000	—	—
mPEG-Br	2100	1.07	1040	—	1 : 0
P(EG- <i>b</i> - <i>t</i> BuA)	4100	1.09	5050	5250	0.32 : 0.68
P(EG- <i>b</i> -AA)	8500	1.22	3100	3390	0.33 : 0.67
mPEG <sub>2k</sub>	—	—	—	1950	1 : 0
mPEG-CTA	2900	1.08	2000	2130	1 : 0
P(EG- <i>b</i> -AA)	12 000	1.27	5300	5480	0.49 : 0.51

<sup>a</sup> Determined by SEC analysis according to PS standards. <sup>b</sup> Determined by MALDI-TOF/MS analysis. <sup>c</sup> Determined by <sup>1</sup>H NMR measurements. <sup>d</sup> The ratios were calculated from the corresponding peaks.



**Fig. 4** MALDI-TOF mass spectrum of the PEG macroinitiator (top left), its magnification (bottom left) and an overlay of the MALDI-TOF mass spectra of macro-initiator, P(EG-*b*-*t*BuA) and P(EG-*b*-AA) (bottom right) with a schematic representation of the assigned structures (top right).

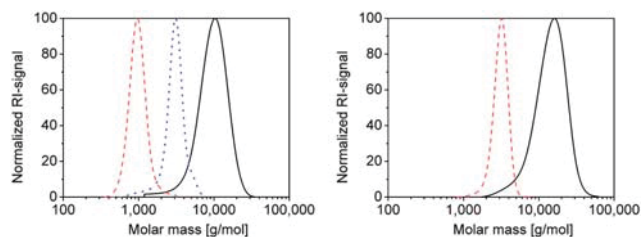


**Fig. 5** MALDI-TOF mass spectrum of the mPEG macro-CTA (top left), magnification of the main distribution (bottom left) and an overlay of the MALDI-TOF mass spectra of the macro chain transfer agent and the prepared P(EG-*b*-AA) (bottom right) with a schematic representation of the assigned structures (top right).

MALDI-TOF mass spectra are provided in Fig. 5. The starting material and product resulted in the same molar mass and are thereby not distinguishable by MALDI-TOF/MS. Nevertheless, the desired structure could be proven by tandem MS analysis leading to a MS spectrum of the product which is different to mPEG-OH.

The SEC analysis revealed once more the difference in hydrodynamic volume between polymers containing acrylic acid and the usual standard polymers used to calibrate the SEC. Fig. 6 visualizes the SEC results obtained for the P(EG-*b*-AA) polymers in comparison to their precursors prepared by the ATRP and the RAFT approach. To obtain comparable results PS-calibrations were used to calculate molar masses and PDI values. Nevertheless nearly quantitative conversions between different states of the block copolymer synthesis could be observed using SEC analysis.

The routes described led to linear block copolymers P(EG-*b*-AA). The copolymerization of AA and oligo(ethylene glycol)



**Fig. 6** Overlay of SEC traces of polymers obtained from the ATRP approach (P(EG-*b*-AA) (—), P(EG-*b*-tBuA) (····), mPEG macroinitiator (---) (left) and the ones obtained during the RAFT approach (P(EG-*b*-AA) (—) and mPEG macro-CTA (---) (right).

acrylate ( $M_n = 480 \text{ g mol}^{-1}$ ) (OEGA<sub>480</sub>) will lead to graft block and random copolymers. The chosen technique to obtain these polymers was the RAFT polymerization using BPTC as CTA and AIBN as radical source.

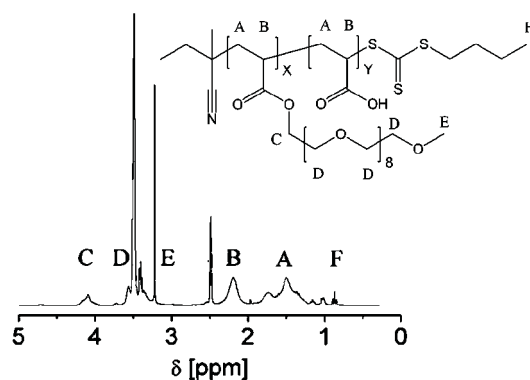
The resulting polymers including characterizing data obtained by SEC and <sup>1</sup>H NMR measurements are summarized in Table 3.

The specific separated signals obtained by <sup>1</sup>H NMR spectroscopy enabled the determination of the relative and even the absolute polymer composition as seen in Fig. 7. The accuracy of the determination of the absolute composition is of course dependent on a quantitative end-group functionalization. Analysis *via* SEC revealed narrow molar mass distributions

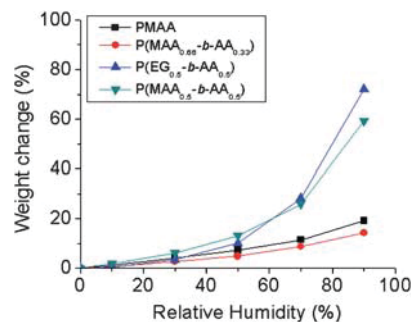
**Table 3** Characteristic data of the block (B) and random (R) copolymers of AA and OEGA<sub>480</sub>

Sample	Feed	$M_n$ (theor.) <sup>a</sup> /g mol <sup>-1</sup>	$M_n$ <sup>b</sup> (SEC) /g mol <sup>-1</sup>	PDI <sup>b</sup> (SEC)	Comp. <sup>c</sup> ( <sup>1</sup> H NMR)
POEGA <sub>480</sub>	0/8	3800	3000	1.15	—
R4	35/5	4800	6400	1.28	0.81 : 0.19
R5	45/5	5700	7100	1.21	—
R6	70/5	7700	8100	1.38	0.91 : 0.09
B4	35/5	4800	6000	1.20	0.87 : 0.13
B5	45/5	5700	6600	1.25	—
B6	70/5	7700	11 000	1.20	0.93 : 0.07

<sup>a</sup> Calculated according to formula ( $M_n(\text{theor.}) = ([M]/[CTA]) \times \text{conv.} \times M_{\text{Monomer}} + M_{\text{CTA}}$ ). <sup>b</sup> Calculated according to PS standards. <sup>c</sup> The ratios were calculated from the corresponding peaks shown in Fig. 7.



**Fig. 7** <sup>1</sup>H NMR spectrum for P(AA-*co*-OEGA<sub>480</sub>) with the corresponding schematic representation of the structure and the signal assignments (300 MHz, DMSO-*d*<sub>6</sub>).



**Fig. 8** Water uptake measurements of P(MAA-*b*-AA) with varying composition and P(EG-*b*-AA).

which led to different molar mass values due to the discrepancy in the hydrodynamic volume relative to the polystyrene standards used for calibration.

To investigate the water uptake behavior of the prepared polymers, thermogravimetric analysis of dried polymer samples were performed under changing humidity. In previous studies the water uptake of several linear polymers including PEG, PAA and poly(sodium acrylate) was investigated and reported.<sup>4</sup> These measurements showed the remarkable difference of the absorption behavior of pure PAA and the sodium salt of PAA as well as PEG. The highest water uptake at 90% relative humidity was observed for the PAA sodium salt (88%) and PEG (73%) whereas pure PAA could take up only 33%. In difference to the other two polymers, PAA absorbs water during the whole range of air humidity (10 to 90%) while PEG and PAA sodium salt do not absorb relevant amounts of water before a humidity level of at least 40% (PAA sodium salt) or even 70% (PEG) is reached.

In the present work the water uptake of P(MAA-*b*-AA) copolymers and P(EG-*b*-AA) was investigated. The results are shown in Fig. 8. While the ratio of MAA and AA in the corresponding block copolymers seems to have only a small influence, the total water uptake is surprisingly high in particular for **B3** (59% at 90% humidity).

An interesting result was observed in case of the P(EG<sub>40</sub>-*b*-AA<sub>42</sub>) block copolymer. The high water uptake of PEG at high humidity levels could be combined with the early starting uptake of water of PAA at lower humidity levels. Therefore, the resulting combined water uptake behavior could overcome the disadvantages of each homopolymer leading to the ability to absorb moisture over the complete humidity range as well as to a very high absolute water uptake level.

## Conclusions

Dual hydrophilic copolymers consisting of acrylic acid and methacrylic acid could be synthesized successfully. Random as well as block copolymers were prepared by controlled radical polymerization, *i.e.* the RAFT technique. The materials obtained were characterized by multiple analytical techniques like SEC, MALDI-TOF mass spectrometry, <sup>1</sup>H NMR spectroscopy, and water uptake measurements.

Well-defined dual hydrophilic linear and graft block copolymers based on acrylic acid and poly(ethylene glycol) could be prepared by RAFT and ATRP. The synthesized precursors, *i.e.*

macroinitiator and macro chain transfer agent, and the final block copolymers were characterized by SEC analysis, <sup>1</sup>H NMR spectroscopy, and MALDI-TOF mass spectrometry. Additionally, the successful synthesis of well-defined block and random copolymers consisting of acrylic acid and oligo(ethylene glycol) acrylate led to dual hydrophilic copolymers of branched architecture. The synthesized polymers were characterized by <sup>1</sup>H NMR spectroscopy and size exclusion chromatography (SEC).

During further investigations of the water uptake behavior of several selected polymers, an interesting water absorbing hybrid behavior could be observed for the P(EG-*b*-AA) block copolymer. The disadvantage of PEG, which is not able to absorb moisture below 70% humidity in a larger amount, could be overcome while keeping the final absolute water uptake at a high level of above 70%.

## Acknowledgements

The authors thank the Dutch Polymer Institute (DPI) and the Thuringer Kultusministerium for financial support. The help from Juergen Vitz performing the water uptake measurements is greatly acknowledged.

## References

- D. E. Discher and A. Eisenberg, *Science*, 2002, **297**, 967.
- M. P. Patel, M. B. Johnstone, F. J. Hughes and M. Braden, *Biomaterials*, 2001, **22**, 81.
- Y. Oda, S. Kanaoka and S. Aoshima, *J. Polym. Sci., Part A: Polym. Chem.*, 2010, **48**, 1207.
- H. M. L. Thijs, C. R. Becer, C. Guerrero-Sanchez, D. Fournier, R. Hoogenboom and U. S. Schubert, *J. Mater. Chem.*, 2007, **17**, 4864.
- J. J. Kiefer, P. Somasundaran and K. P. Ananthapadmanabhan, *Langmuir*, 1993, **9**, 1187.
- S. J. Hou, E. L. Chaikof, D. Taton and Y. Gnanou, *Macromolecules*, 2003, **36**, 3874.
- C. R. Becer, S. Hahn, M. W. M. Fijten, H. M. L. Thijs, R. Hoogenboom and U. S. Schubert, *J. Polym. Sci., Part A: Polym. Chem.*, 2008, **46**, 7138.
- H. C. Kolb, M. G. Finn and K. B. Sharpless, *Angew. Chem., Int. Ed.*, 2001, **40**, 2004.
- C. R. Becer, R. Hoogenboom and U. S. Schubert, *Angew. Chem., Int. Ed.*, 2009, **48**, 4900.
- J. F. Lutz, *Angew. Chem., Int. Ed.*, 2007, **46**, 1018.
- G. Moad, E. Rizzardo and S. H. Thang, *Aust. J. Chem.*, 2009, **62**, 1402.
- A. B. Lowe and C. L. McCormick, *Prog. Polym. Sci.*, 2007, **32**, 283.
- G. Moad, E. Rizzardo and S. H. Thang, *Aust. J. Chem.*, 2006, **59**, 669.
- J. Chiefari, Y. K. Chong, F. Ercole, J. Krstina, J. Jeffery, T. P. T. Le, R. T. A. Mayadunne, G. F. Meijs, C. L. Moad, G. Moad, E. Rizzardo and S. H. Thang, *Macromolecules*, 1998, **31**, 5559.
- M. Benaglia, M. Chen, Y. K. Chong, G. Moad, E. Rizzardo and S. H. Thang, *Macromolecules*, 2009, **42**, 9384.
- M. Ouchi, T. Terashima and M. Sawamoto, *Chem. Rev.*, 2009, **109**, 4963.
- B. M. Rosen and V. Percec, *Chem. Rev.*, 2009, **109**, 5069.
- M. Kamigaito, T. Ando and M. Sawamoto, *Chem. Rev.*, 2001, **101**, 3689.
- K. Matyjaszewski and J. Xia, *Chem. Rev.*, 2001, **101**, 2921.
- S. Boissé, J. Rieger, K. Belal, A. Di-Cicco, P. Beauvier, M.-H. Li and B. Charleux, *Chem. Commun.*, 2010, **46**, 1950.
- U. I. Sires and S. B. Mallory, *Postgrad. Med.*, 1995, **98**, 79.
- M. Gourmand and J. M. Corpart, *Actual. Chim.*, 1999, **11**, 46.
- F. L. Buchholz, S. R. Pesce and C. L. Powell, *J. Appl. Polym. Sci.*, 2005, **98**, 2493.
- O. M. Jensen and P. F. Hansen, *Cem. Concr. Res.*, 2001, **31**, 647.
- D. Gao, R. B. Heimann, J. Lerchner, J. Seidel and G. Wolf, *J. Mater. Sci.*, 2001, **36**, 4567.
- M. P. Raju and K. M. Raju, *J. Polym. Mater.*, 2001, **18**, 149.
- S. J. Kohls, D. D. Baker, D. A. Kremer and J. O. Dawson, *Plant Soil*, 1999, **214**, 105.
- K. M. Raju and M. P. Raju, *Polym. Int.*, 2001, **50**, 946.
- P. Chen, W. Zhang, W. Luo and Y. J. Fang, *J. Appl. Polym. Sci.*, 2004, **93**, 1748.
- K. S. Kazanskii and S. A. Dubrovskii, *Adv. Polym. Sci.*, 1992, **104**, 97.
- L. C. Doug and A. S. Hoffman, *J. Controlled Release*, 1991, **15**, 141.
- P. Colombo, *Adv. Drug Delivery Rev.*, 1993, **11**, 37.
- P. Kuzma, A. J. Moo-Young, D. Moro, H. Quandt, C. W. Bardin and P. H. Schlegel, *Macromol. Symp.*, 1996, **109**, 15.
- F. L. Buchholz and N. A. Peppas, *ACS Symp. Ser.*, 1994, **573**, 128.
- M. Bakass, A. Mokhlisse and M. Lallemand, *J. Appl. Polym. Sci.*, 2001, **82**, 1541.
- J.-S. Song and M. A. Winnik, *Macromolecules*, 2006, **39**, 8318.
- C. J. Ferguson, R. J. Hughes, D. Nguyen, B. T. T. Pham, R. G. Gilbert, A. K. Serelis, C. H. Such and B. S. Hawkett, *Macromolecules*, 2005, **38**, 2191.
- T. Gruending, S. Weidner, J. Falkenhagen and C. Barner-Kowollik, *Polym. Chem.*, 2010, **1**, 599.
- R. Giordanengo, S. Viel, B. A. Breton, A. Thévand and L. Charlesa, *J. Am. Soc. Mass Spectrom.*, 2009, **20**, 25.
- M. Sedláč, M. Antonietti and H. Coelfen, *Macromol. Chem. Phys.*, 1998, **199**, 247.

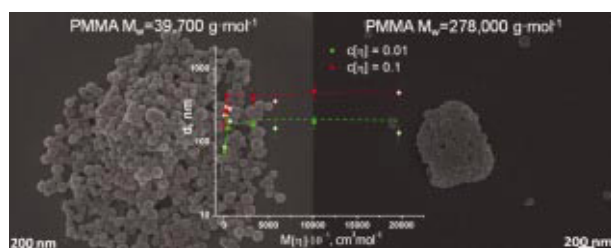
## Publication P10:

### *Nanoprecipitation of poly(methyl methacrylate)-based nanoparticles: effect of the molar mass and polymer behavior*

---

I. Y. Perevyazko, A. Vollrath, C. Pietsch, S. Schubert, G. M. Pavlov,  
U. S. Schubert

*J. Polym. Sci., Part A: Polym. Chem.* **2012**, *50*, 2906–2913





# Nanoprecipitation of Poly(methyl methacrylate)-Based Nanoparticles: Effect of the Molar Mass and Polymer Behavior

Igor Y. Perevyazko,<sup>1,2</sup> Antje Vollrath,<sup>1,2</sup> Christian Pietsch,<sup>1,2,3</sup> Stephanie Schubert,<sup>1,2,4</sup> Georgy M. Pavlov,<sup>1,2</sup> Ulrich S. Schubert<sup>1,2,3</sup>

<sup>1</sup>Laboratory of Organic and Macromolecular Chemistry (IOMC) Friedrich-Schiller-University, D-07743 Jena, Germany

<sup>2</sup>Jena Center for Soft Matter (JCSM), Friedrich-Schiller-University, D-07743 Jena, Germany

<sup>3</sup>Dutch Polymer Institute (DPI), Eindhoven 5600 AX, The Netherlands

<sup>4</sup>Institute of Pharmacy, Department of Pharmaceutical Technology, Friedrich-Schiller-University, D-07743 Jena, Germany

Correspondence to: U. S. Schubert (E-mail: ulrich.schubert@uni-jena.de)

Received 8 March 2012; accepted 14 March 2012; published online 28 April 2012

DOI: 10.1002/pola.26071

**ABSTRACT:** The current investigation describes in detail the influence of the polymer molar mass as well as polymer-solvent interactions on the formation of nanoparticles using the nanoprecipitation methodology. For this purpose, a homologous series of poly(methyl methacrylate)s with molar masses ranging from 7,700 to 274,000 g mol<sup>-1</sup> was prepared. Subsequently nanoprecipitation was performed in an automated and systematic manner using liquid handling robots and a variation of different initial concentrations of the polymers and solvent/nonsolvent ratios. To elucidate information about the polymer behavior in the solvents used for the nanoprecipitation proce-

dures (acetone, tetrahydrofuran), intrinsic viscosity measurements were performed. The nanoparticle formulations were examined in terms of particle size and size distribution, particle shape as well as zeta-potential. The conditions for the preparation of stable and uniform nanoparticles, regardless of molar mass and hydrodynamic volume of the initial polymer, were determined. © 2012 Wiley Periodicals, Inc. *J Polym Sci Part A: Polym Chem* 50: 2906–2913, 2012

**KEYWORDS:** nanoparticles; nanoprecipitation; molar mass; PMMA; synthetic polymers; ultracentrifugation; viscosity

**INTRODUCTION** Polymeric nanoparticles have been extensively studied in the last decades as potential drug delivery devices. Nanoparticle formation using the nanoprecipitation method<sup>1</sup> is nowadays a commonly used technique. Among the numerous other manufacturing methods, it is known to be a very simple and convenient way for the production of polymeric nanoparticles with desired sizes.<sup>2,3</sup> A variety of different polymers can be used, such as poly(lactide-co-glycolide),<sup>4</sup> poly( $\epsilon$ -caprolactone),<sup>5</sup> poly(acrylics), poly(styrene), poly(methyl methacrylate) (PMMA), and its different copolymers as well as various amphiphilic block copolymers.<sup>6–9</sup> Nanoprecipitation represents a process based on the diffusion of the organic solution (i.e., polymer solvent) into an aqueous phase leading to the precipitation of the polymer into small colloidal particles. The formation of nanoparticles by the process complies with the nucleation theory and consists of several steps like particle nucleation, molecular growing, and aggregation.<sup>10,11</sup> Stable nanoparticle suspensions are only formed applying specific conditions, which promote a supersaturation of polymer molecules in a ternary polymer/solvent/nonsolvent system and shifts it into a metastable region (Ouzo region).<sup>9,11–13</sup> This region is located

between the binodal (miscibility limit curve) and spinodal (stability limit curve) on a three component phase diagram based on the hydrophobic solute, the solvent, and the nonsolvent. The resulting properties of the particles primarily depend on the polymer behavior in the organic phase but also on the nature and ratio of the external phase as well as on concentration and nature of the used surfactants.<sup>14–18</sup> It could be shown repeatedly that the particle size is strongly affected by the initial polymer concentration: higher concentrations lead to an increasing number of molecules per volume of the solvent, which, in turn, leads to the formation of larger particles. At the same time, the ratio between solvent and nonsolvent was found to have a more complex, nonlinear influence on the size of the particles.<sup>9,18,19</sup> Thorough investigation of the molar mass influence on the production of biodegradable nanoparticles based on poly(lactic acid) was first presented by Legrand et al.<sup>16</sup> This study was designed to determine in detail and to extend the understanding of the effect of the polymer characteristics, in particular the molar mass, on the nanoprecipitation results of synthetic polymers. For this purpose, PMMA samples were investigated in a wide range of molar masses (between  $M_w$

= 7,700 and 274,000 g mol<sup>-1</sup>) to obtain information about the polymer-solvent interactions and the size of the particles formed. The investigations were carried out in two solvents, namely acetone and tetrahydrofuran (THF). Nanoparticles were prepared in a reproducible and systematic manner by using a liquid handling robot.<sup>19</sup> All formulations were subsequently characterized using dynamic light scattering (DLS) for a fast size determination. In addition, selected samples were studied by analytical ultracentrifugation (AUC) and scanning electron microscopy (SEM).

## EXPERIMENTAL

### Synthesis of the PMMA Polymers

Methyl methacrylate (MMA) and 2-cyano-2-propyl dithiobenzoate (CPDB) were purchased from Sigma-Aldrich. MMA was purified by treating the monomer with inhibitor-remover (Aldrich). The initiator 2,2'-azobisisobutyronitrile (AIBN) was recrystallized from methanol prior to use. All analytical grade solvents were purchased from commercial sources (Fluka, Aldrich, Alfa Caesar and Acros Organics).

The following procedure illustrates the standard conditions for the reversible addition-fragmentation chain transfer (RAFT) polymerization of MMA.<sup>20,21</sup> The desired amount of MMA (3.0 mL, 28.12 mmol) was transferred into a reaction vial and dissolved in ethanol (1 mL). Thereafter, the calculated volumes of stock solutions of CPDB (5.19 mg, 0.023 mmol) as well as AIBN (1.92 mg, 0.012 mmol) in ethanol were added. Before closing the vial, the reaction solution was purged with a flow of argon for at least 30 min. Subsequently, the reaction was performed in an oil bath at 70 °C (see Table 1 for exact reaction times, MMA concentration and [M]/[chain transfer agent, CTA] ratios). After the polymerization, acetone was added to the final mixtures, and the polymers were then manually precipitated in cold methanol. The polymers were dried under reduced pressure at 40 °C.

### Size-Exclusion Chromatography

Size-exclusion chromatography (SEC) was performed using an Agilent1200 series system, a G1310A pump, a G1362A refractive index detector and both a PSS Gram30 and a PSS Gram1000 column in series, whereby *N,N*-dimethylacetamide with 5 mmol lithium chloride was used as an eluent at 1 mL min<sup>-1</sup> flow rate. The column oven was set to 40 °C. The system was calibrated with PMMA standards of narrow dispersity.

### Sedimentation Velocity Experiments

Sedimentation velocity experiments were performed with a ProteomeLab XLI Protein Characterization System analytical ultracentrifuge (Beckman Coulter, Brea, CA), using conventional double-sector Epon centerpieces of 12-mm optical path length and a four hole rotor. Rotor speed was 3,000 to 20,000 rpm, depending on the sample. Cells were filled with 420 μL of nanoparticle suspension at the initial concentration and 440 μL of solvent (H<sub>2</sub>O). The nanoparticle suspensions were used without further purification. Before the run, the rotor was equilibrated for ~2 h at 20 °C in the centrifuge. Sedimentation profiles were obtained every 15 s by in-

**TABLE 1** Selected Characterization Data of the Obtained PMMA Polymers

Sample	[M]:[CTA]: [AIBN]	Conc. mol L <sup>-1</sup>	Time, h	<i>M</i> <sub>w, SEC</sub> g mol <sup>-1</sup>	PDI <sub>SEC</sub>	DP <sub>SEC</sub>
1	40:1:0.25	2.0	13	7,700	1.13	66
2	200:1:0.25	2.0	13	20,200	1.17	170
3	400:1:0.25	2.0	20.5	39,700	1.26	312
4	1,200:1:0.5	7.03	16	106,000	1.25	846
5	4,000:1:0.5	7.03	16	274,000	1.34	2,035

terference optics. For the analysis of the particle size distribution, the sedimentation velocity data were treated by ls-g\*(s) analysis with a Tikhonov-Phillips regularization procedure (confidence level of 0.9 was used) implemented into the Sedfit program. This method is based on a boundary modeling of a superposition of sedimentation profiles of ideal nondiffusing particles.<sup>22</sup> For the appropriate size determination by sedimentation velocity, the knowledge of the partial specific volume is essential. A value of  $v = 0.78 \pm 0.01 \text{ cm}^3 \text{ g}^{-1}$  was used, which was determined previously for PMMA and its copolymers.<sup>8</sup>

### DLS and Zeta Potential

DLS was performed on the DynaPro Plate Reader Plus (Wyatt Technology Corporation, Santa Barbara, CA) equipped with a 60 mV linearly polarized gallium arsenide (GaAs) laser at 832.5 nm and operating at an angle of 156°. The data were analyzed with the Dynamics software ver. 6.10 by the method of cumulants. The percent of polydispersity is given by,

$$\% Pd = 100 \frac{\mu_2}{\mu_1^2} \quad (1)$$

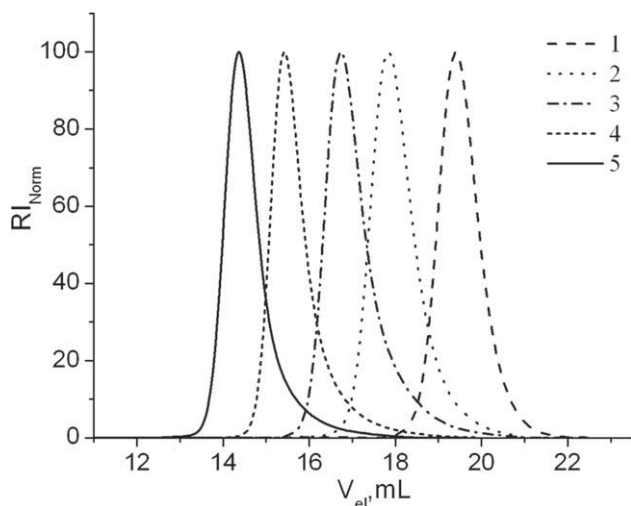
where  $\mu_1$  and  $\mu_2$  are the first and the second order cumulant, respectively.

For selected samples, the determination of the particles size and zeta potential measurements was performed using a Zetasizer Nano ZS (Malvern instruments, Malvern, UK). In these measurements, a laser beam at 633 nm was used and a scattering angle of 173°. Each sample was measured in triplicate at 25 °C for 30 s in a low volume polycarbonate cell. For this purpose, 20 μL nanoparticle suspensions were diluted with 1 mL demineralized, filtered water. The mean particle size was approximated as the effective (Z average) diameter obtained by the cumulant method.

### SEM

The nanoparticle suspensions were diluted with filtered, deionized water to a final concentration of 1 mg mL<sup>-1</sup>. They were characterized using a LEO-1450 VP SEM (Leo, Oberkochen, Germany), operating at 10 kV. One droplet (15–20 μL) of the suspension was placed on a mica surface and lyophilized for 3 h. Finally, the sample was coated with platinum,





**FIGURE 1** SEC chromatograms of the obtained PMMA polymers used. 1 – ( $M_w = 7,700 \text{ g mol}^{-1}$ ), 2 – ( $M_w = 20,200 \text{ g mol}^{-1}$ ), 3 – ( $M_w = 39,700 \text{ g mol}^{-1}$ ), 4 – ( $M_w = 106,000 \text{ g mol}^{-1}$ ), and 5 – ( $M_w = 274,000 \text{ g mol}^{-1}$ ).

using a BAL-TEC SCD005 sputtering device (Balzers, Lichtenstein) and applying a current of 60 mA for 80 s.

### Viscosity Measurements

Viscosity measurements were conducted using a AMVn (Anton Paar, Graz, Austria) rolling ball viscometer with a manually filled capillary with an internal diameter of 0.9 mm. The viscosities of the solution,  $\eta$ , and of the solvent,  $\eta_0$ , were obtained from the rolling times of the steel ball, measured at three inclination angles ( $30^\circ$ ,  $50^\circ$ , and  $70^\circ$ ) of the capillary. The viscosity of each solution was calculated from the average of six measurements; the measurements were conducted at  $20^\circ \text{C}$ .

### Preparation of the Nanoparticle Suspensions

Nanoparticles were prepared by the nanoprecipitation method from a stock polymer solution in acetone or THF at different concentrations of the polymers. The initial polymer solutions were filtered via a  $0.45 \mu\text{m}$  filter. To formulate the particles in a 96-well microtiter plate, a pipetting robot (FasTrans, Analytik Jena GmbH, Jena, Germany) was used. Nanoprecipitation was performed in an automated way by the fast injection of the polymer solution into a well containing different amounts of water depending on the solvent/nonsolvent ratio. The effective final volume of the well was  $300 \mu\text{L}$ . The nanosuspension formed was then mixed three times by aspiration and release of a volume of  $200 \mu\text{L}$ . Subsequently, the plate was placed in a fume hood, where the organic solvent was completely removed from the suspension by evaporation.

## RESULTS AND DISCUSSION

### Synthesis and Characterization of the Polymers

A range of PMMA samples were synthesized using the RAFT polymerization technique. The RAFT polymerization was carried out using AIBN as radical initiator, ethanol as solvent,

and CPDB as CTA. Different molar masses of PMMA were obtained by changing the polymerization time, the MMA concentration and the  $[M]:[CTA]$  ratio (see Table 1 for detailed reaction conditions). High molar masses up to  $M_w = 274,000 \text{ g mol}^{-1}$  could be realized via the RAFT process. All PMMA samples are well-defined with polydispersity indices ranging from 1.13 to 1.34. The SEC chromatographs of the different PMMAs are depicted in Figure 1.

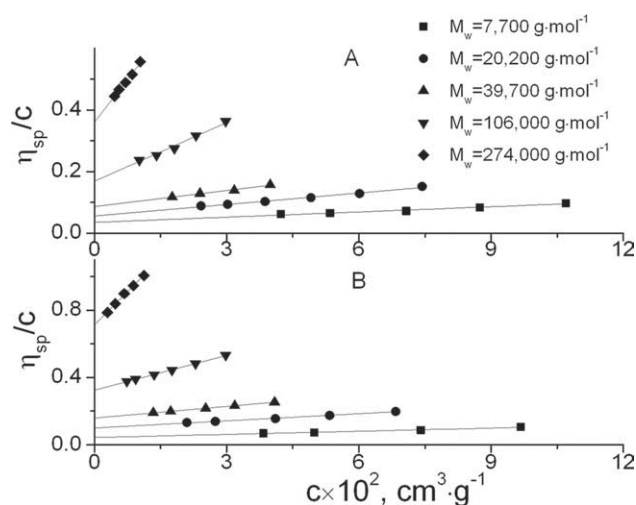
### Intrinsic Viscosity Measurements

Prior to compare the influence of various PMMA samples on the nanoparticle formation, intrinsic viscosity measurements of polymer solutions were performed. The knowledge of the intrinsic viscosity is essential to evaluate the interaction between the polymer and solvent molecules at various polymer molar masses. The intrinsic viscosities were obtained by applying Huggins' extrapolation to zero concentration procedure:

$$\frac{\eta_{sp}}{c} = [\eta] + k'[\eta]^2c + \dots \quad (2)$$

where  $[\eta]$  and  $\eta_{sp}$  are the intrinsic and specific viscosity respectively,  $k'$  is the Huggins dimensionless parameter (interaction parameter), and  $c$  is the polymer concentration. The resulting plot of the reduced viscosity and the concentration for the samples investigated in acetone and THF is presented in Figure 2. As expected, solutions of PMMA in acetone have a lower viscosity in comparison to THF. According to Flory's equation,<sup>23</sup> this can indicate that the volume of the polymer coil in acetone is lower than in THF solutions. The corresponding values of the intrinsic viscosity are listed in Table 2. It is also well known that for a homologous series of macromolecules the intrinsic viscosity can be related to the molar mass through scaling relations of the Kuhn-Mark-Houwink-Sakurada type (KMHS relations):<sup>23</sup>

$$[\eta] = K_\eta \cdot M^a \quad (3)$$



**FIGURE 2** Dependence of the reduced viscosity on the polymer concentration for PMMA samples in acetone (A) and THF (B), respectively. Lines represent linear fitting procedures.

**TABLE 2** Intrinsic Viscosity Data for the PMMA Polymers

Sample	$[\eta]_{\text{acetone}}, \text{cm}^3 \text{g}^{-1}$	$[\eta]_{\text{THF}}, \text{cm}^3 \text{g}^{-1}$
1	$4.1 \pm 0.5$	$6 \pm 1$
2	$6.2 \pm 0.6$	$10.6 \pm 0.5$
3	$9.2 \pm 0.6$	$16.3 \pm 0.6$
4	$19 \pm 1$	$33.2 \pm 0.5$
5	$37 \pm 1$	$71.8 \pm 0.5$

The parameters of this equation are characteristic for the polymer-solvent system. They can be evaluated from the log-log dependence of the  $[\eta]$  versus  $M_w$ . The exponent in the KMHS equation varies in the range of  $0.5 < a < 0.85$  for random coils. A value of 0.5 is indicating theta solvent conditions, which means that the polymer coil behaves as an undisturbed Gaussian coil. In this study, the following values:  $K_\eta = 1.33 \cdot 10^{-2}$ ,  $a = 0.63$  and  $K_\eta = 0.70 \cdot 10^{-2}$ ,  $a = 0.74$  were found for the polymer solution in acetone and THF, respectively. This, in turn, testifies a good affinity of the polymer to the solvents. However, according to the collected data THF seems to be a thermodynamically better solvent for the PMMA than acetone.

### Nanoparticle Formation

To study the influence of the polymer molar mass on the nanoparticle formation via nanoprecipitation, it is crucial to maintain the same initial conditions for each nanoprecipitation process. The characteristic "degree of dilution" assesses the contribution of the different intrinsic viscosities of polymer solutions, which were introduced and represented by the Debye parameter:  $c \cdot [\eta]$ , where  $c$  is the polymer concentration and  $[\eta]$  is the intrinsic viscosity of the polymer. The degree of dilution evaluates the volume fraction of the macromolecular coils in the solution. If the value of  $c \cdot [\eta] \ll 1$ , the solution can be considered as diluted, and no overlapping of the macromolecular coils occurs.

In detail, the nanoparticles were precipitated from 12 different initial polymer solutions with concentrations (logarithmically scattered) corresponding to the following range of  $c \cdot [\eta]$  values: 0.004–0.120. Each solution was then combined with eight different proportions of water in a way that the solvent/nonsolvent ratio was ranged from 0.1 to 0.5 (again scattered logarithmically) representing in total 96 different populations of nanoparticles. The same procedure was applied for each PMMA sample. After preparation, one can notice a visually observable trend in appearance following the changes made in the nanoprecipitation process. At the lowest concentrations, a faintly opalescent suspension was obtained; with increasing concentration, the opalescence became more apparent. The particles suspensions were analyzed after complete evaporation of acetone or THF, respectively. Initially, the DLS plate reader was used for the particle characterization. Figure 3 shows a size distribution as a function of initial polymer concentration and solvent/nonsolvent ratio of nanoparticles based on **PMMA 1**. The size of the particles is increasing from around 70 to 180 nm

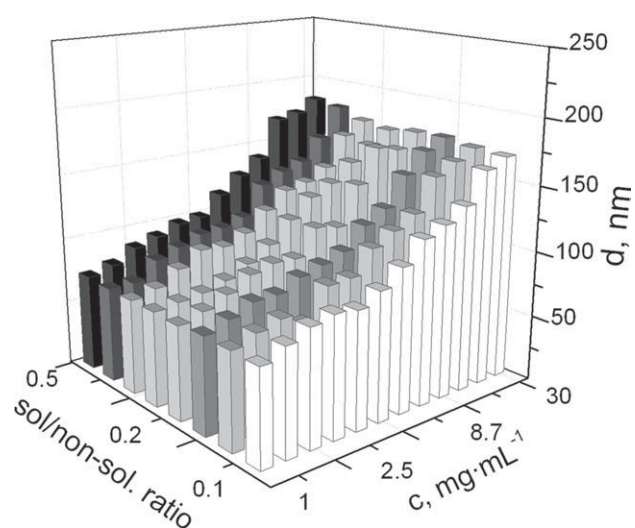
depending on the concentration (degree of dilution) and solvent/nonsolvent ratio. The polydispersity of the nanoparticles based on **PMMA 1** to **PMMA 3** increases from  $5 \pm 2\%$  to  $20 \pm 5\%$  for the lowest and highest concentration, respectively. In the case of particles based on **PMMA 4** and **PMMA 5**, the nanoparticle suspensions were found to be more polydisperse; the polydispersity constitutes  $12 \pm 3\%$  and  $30 \pm 16\%$  for the lowest and highest concentration, respectively.

### Morphology Study

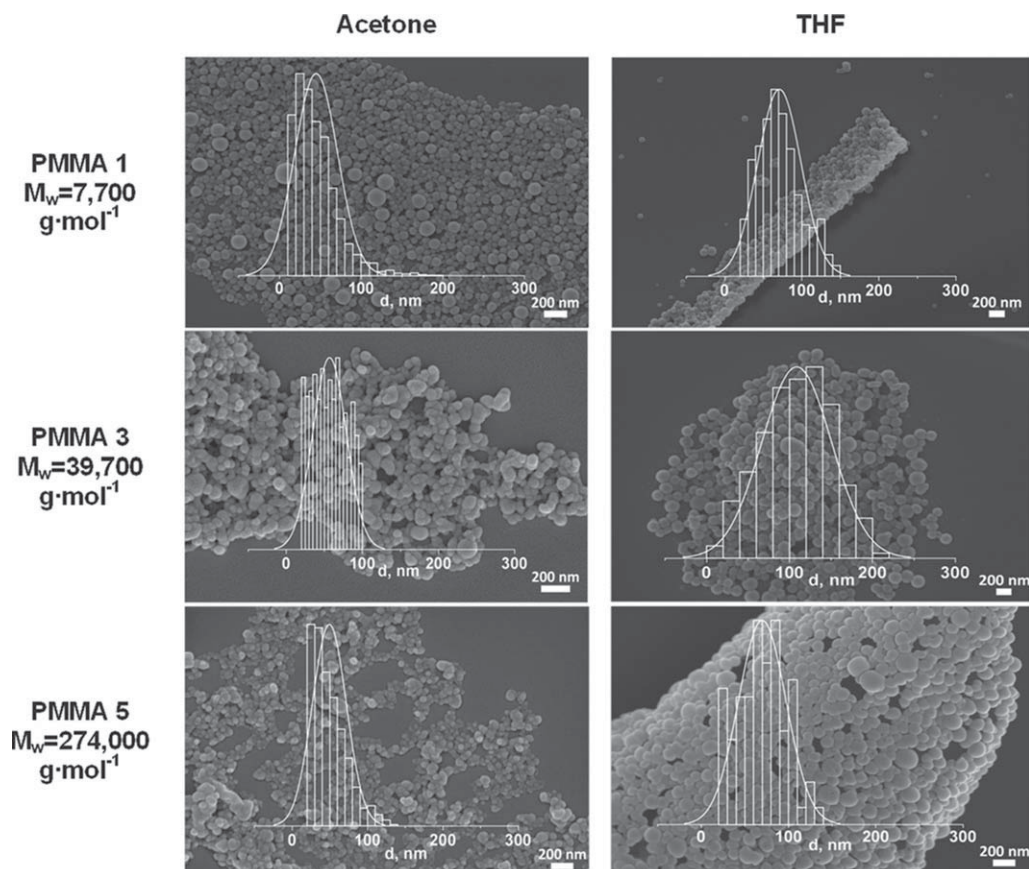
In Figure 4, the SEM micrographs and the corresponding size-distributions, determined by ImageJ analysis, are shown for nanoparticles based on **PMMA 1**, **3**, and **5** prepared in acetone and THF, respectively, at a degree of dilution  $c \cdot [\eta] = 0.01$  and a solvent/nonsolvent ratio of 0.1. The sizes of the particles of **PMMA 1**, **3**, and **5** were virtually the same. The calculated weight average particle size constitutes  $74 \pm 4$  nm for the preparation procedure in acetone and  $100 \pm 20$  nm for the THF preparations. However, particles prepared from acetone solution are only uniform and spherically shaped for the low molar mass **PMMA 1** ( $M_w = 7,700 \text{ g mol}^{-1}$ ), whereas with increasing molar mass less spherical particles with rough surfaces appeared. In contrast, particles prepared from THF solution are spherical and uniform within the whole molar mass range.

### Sedimentation Velocity Experiments

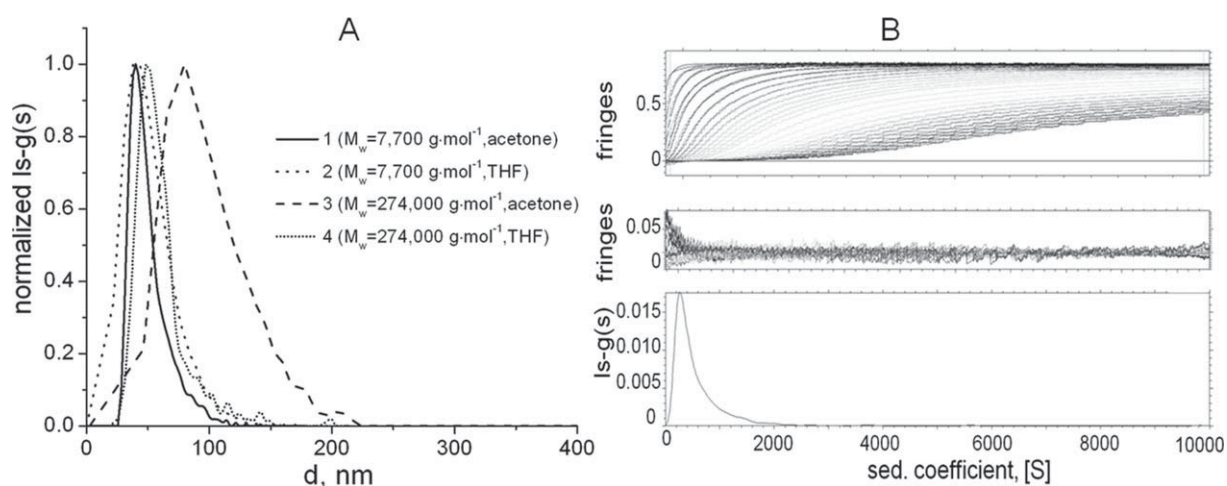
Sedimentation velocity analyses were performed for various nanoparticle suspensions in water to gain detailed information about the size distribution of the particles. In Figure 5(A) typical size-distributions obtained by AUC are shown for **PMMA 1** and **PMMA 5** particles. The differential distribution of sedimentation coefficients were subsequently



**FIGURE 3** 3D representation of the nanoprecipitation experiment using a PMMA with  $M_w = 7,700 \text{ g mol}^{-1}$ : an average particle size (Z-axis) as function of initial polymer concentration (X-axis) and solvent/nonsolvent ratio (Y-axis). Sizes were obtained by DLS measurements. The nanoparticles were prepared by dropping a polymer acetone solution into water.



**FIGURE 4** SEM images and corresponding size-distributions of nanoparticles prepared from polymer solutions of PMMA with different molar masses in acetone and THF. The particles were prepared by dropping a polymer solution into water. The initial polymer concentration was adjusted to obtain the same degree of dilution ( $c[\eta] = 0.01$ ) of all polymer solutions. Solvent/nonsolvent ratio was kept constant at 0.1.



**FIGURE 5** A: Comparison of normalized size-distributions obtained by sedimentation velocity experiment for the nanoparticles based on **PMMA 1** ( $M_w = 7,700 \text{ g mol}^{-1}$ ) and **PMMA 5** ( $M_w = 274,000 \text{ g mol}^{-1}$ ) in acetone and THF. The initial polymer concentration corresponds to the degree of dilution  $c[\eta] = 0.01$  at a solvent/nonsolvent ratio of 0.1. B: Example of sedimentation velocity experiments for nanoparticles based on **PMMA 1** in acetone. The experiment was carried out at 3,000 rpm, scans were collected every 15 s. Top panel: superposition of sedimentation profiles obtained with interference optics at 20 °C. Middle: corresponding residual plots. Bottom: differential distribution  $Is-g(s)$  of the sedimentation coefficients. The distributions were obtained with a regularization procedure at a confidence level of 0.9.

transformed into the size distribution, and an average diameter was calculated according to the Stokes-Einstein equation assuming a spherical shape of the particles. Particles prepared from acetone solution are slightly smaller comparing to the THF preparation. The majority of the particles prepared from the different molar mass samples at similar degree of dilution  $c[\eta] = 0.01$  have virtually the same sizes:  $74 \pm 5$  nm and  $100 \pm 20$  nm for the particles prepared from acetone and THF polymer solution, respectively. However, it should be noted that the distributions of high molar mass samples are slightly shifted to larger diameters.

### Zeta-Potential Measurements

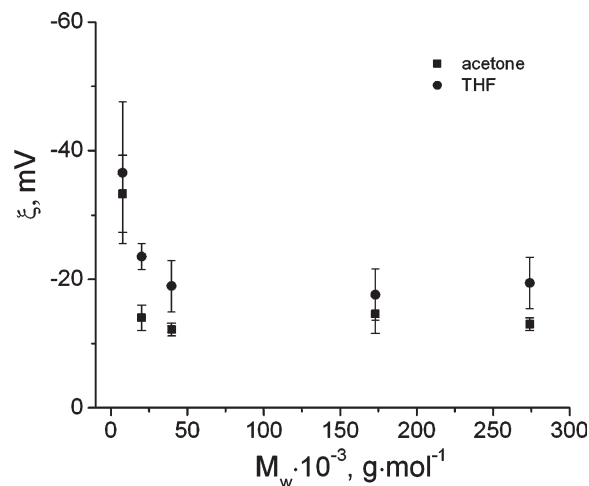
The surface charge of particles represents an additional important parameter for the characteristics of nanoparticles besides size and shape. In particular, the stability of nanoparticle suspensions as well as the cellular uptake are strongly affected by the zeta-potential. The correlation between zeta-potential and initial polymer molar mass is presented in Figure 6. The magnitude of the zeta-potential decreases with increasing molar mass of the initial polymer. The maximum value was observed for the nanoparticles based on **PMMA 1** and constitutes  $-33$  and  $-37$  mV for the acetone and THF preparations, respectively. The minimum values were observed for the particles based on **PMMA 3**, which do not change significantly at larger molar mass:  $-(13 \pm 1)$  mV and  $-(20 \pm 3)$  mV for the acetone and THF preparations, respectively.

### DISCUSSION

Many factors have to be taken into account to obtain stable nanoparticle suspension with desired size and properties during the nanoprecipitation process. It was shown before that one of the key-factors, which define the particle size, is the initial polymer concentration: the higher the concentration of the polymer in the organic phase, the lower the velocity of diffusion owing to the increasing viscosity of the polymer solution; consequently, more polymer molecules per unit volume of solvent are present, and the resulting particles will have a larger size.<sup>13,15,16</sup> However, equality of the initial polymer concentration will not reflect the same conditions for the nanoprecipitation process in case of polymers with various molar mass or different chemical structure, since macromolecular coils will occupy different volumes owing to the different length of a polymer chain. Furthermore, the volume of the macromolecular coil of a polymer depends on the equilibrium rigidity of the chain and on the nature of the polymer-solvent interaction. A physical quantity, which reflects the volume occupied by the polymer molecule, is the intrinsic viscosity.

$$[\eta] = \phi \frac{\langle h^2 \rangle^{3/2}}{M} \quad (4)$$

where  $\langle h^2 \rangle$  is the mean square end-to-end distance of the coil,  $\Phi$  is the Flory hydrodynamic parameter, and  $M$  is the molar mass of the polymer. The product of the intrinsic viscosity  $[\eta]$  and the concentration of the solution (Debye pa-



**FIGURE 6** Zeta-potential of the nanoparticles as a function of initial polymer molar mass. The nanoparticles were obtained by nanoprecipitation of polymers dissolved in acetone and THF. The initial polymer concentration corresponds to the degree of dilution  $c[\eta] = 0.01$  at a solvent/nonsolvent ratio of 0.1.

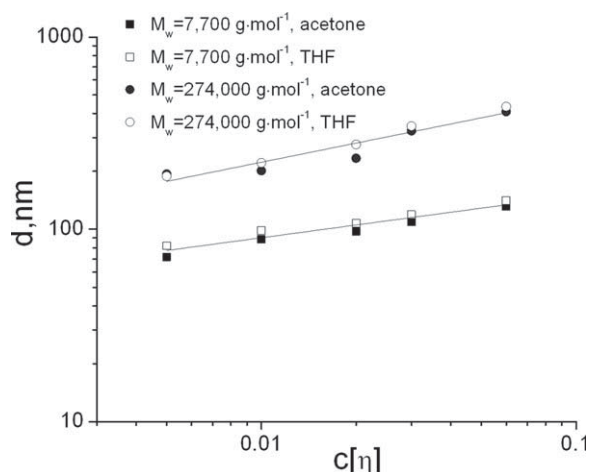
rameter) represents a good approximation of the volume fraction of the macromolecular coils in the solution  $\phi$  and can be specified as follows:

$$\phi \equiv \frac{nv}{V} = \frac{mvN_A}{VM} = \frac{c \times 0.36 \langle h^2 \rangle^{3/2} N_A}{M} = \left( \frac{0.36N_A}{\phi} \right) c[\eta] \approx c[\eta] \quad (5)$$

$$v = 0.36 \langle h^2 \rangle^{3/2} \quad (6)$$

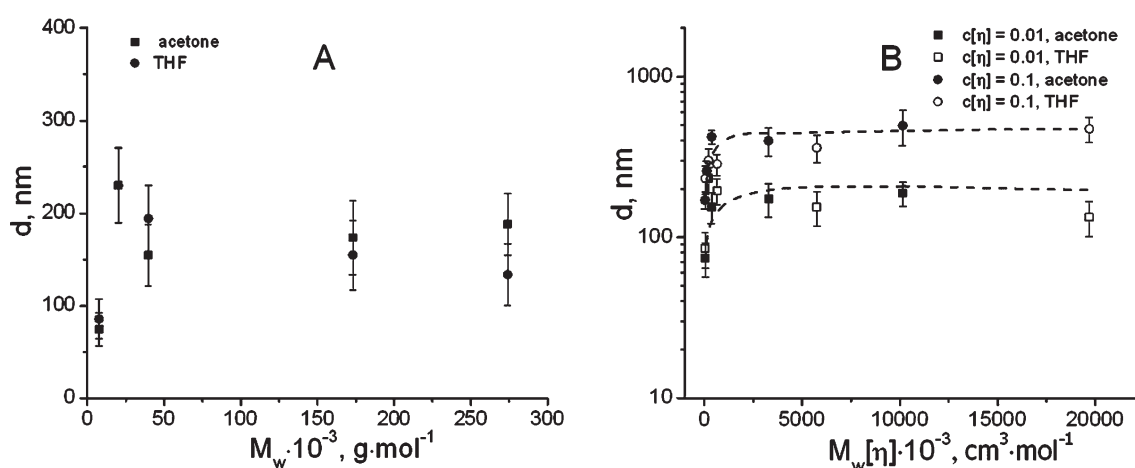
Therein,  $v$  is the volume occupied by the macromolecular coil in solution,  $m$  is the mass of the polymer in volume  $V$ ,  $N_A$  is the Avogadro number. If  $c[\eta] \ll 1$ , the polymer solution can be considered as diluted-then, no overlapping of macromolecular coils occurs.

Based on these data, nanoparticle suspensions were prepared with a degree of dilution from  $0.004 < c[\eta] < 0.12$ . In Figure 7, the size of the nanoparticles as a function of the Debye parameter is presented in a double logarithmic scale. A comparison is made for particles prepared from the polymer solutions of **PMMA 1** and **PMMA 5** in acetone and THF, respectively. As expected, the particles size increases as the solution becomes more concentrated-corresponding to the higher values of the Debye parameter. However, the slopes of the regression lines (0.20 and 0.32 for **PMMA 1** and **PMMA 5**, respectively) show that the size increases more rapidly for the nanoparticles on the basis of high molar mass polymer. It is further obvious that higher molar mass polymers lead to the formation of the particles with larger diameters, which actually contradicts data obtained from SEM and AUC. Such a difference in sizes can be related to the fact that, in accordance with the measured values of zeta-potential, nanoparticles on the basis of high molar mass polymers (**PMMA**



**FIGURE 7** Double logarithmic dependence of the particle diameters on the degree of dilution (Debye parameter) obtained by DLS measurements. Nanoparticles based on **PMMA 1** ( $M_w = 7,700 \text{ g mol}^{-1}$ ) and **PMMA 5** ( $M_w = 274,000 \text{ g mol}^{-1}$ ) in acetone and THF.

**4, PMMA 5**) were found to have low values of surface charge. This, in turn, can provoke formation of agglomerates, which will influence the final particle distribution. The resulting comparison of the particles sizes (an average from the AUC, DLS, and SEM data) as a function of the polymer molar mass is presented in Figure 8(A). Indeed, a slight increase of the particle sizes with the molar mass is noticeable. This effect is more evident when the particles were nanoprecipitated from the polymer solution in acetone. It can also be concluded that, regardless to the solvent used, the increase in particle size is followed by a plateau. A maximum size could be observed for the particles based on **PMMA 2** with  $M_w = 20,200 \text{ g mol}^{-1}$ . Figure 8(B) represents the semi logarithmic dependence of the particle size on the



**FIGURE 8** A: Dependence of the resulting weight average sizes on the initial polymer molar mass for the nanoparticles obtained by nanoprecipitation of polymers dissolved in acetone and THF. Initial polymer concentrations correspond to the degree of dilution  $c[\eta] = 0.01$ . B: Semi logarithmic dependence of the particle size on the product of polymer molar mass and intrinsic viscosity. Initial polymer concentrations correspond to the degree of dilution  $c[\eta] = 0.01$  and  $c[\eta] = 0.1$  in acetone and THF. Deviations are related to the difference in the nanoparticle sizes obtained from various characterization techniques (AUC, DLS, and SEM).

product of molar mass  $M$  on the intrinsic viscosity  $[\eta]$  for two values of  $c[\eta]$ : 1, 2 – 0.01 and 3, 4 – 0.1. Since this work was generally performed using dilute polymer solutions, the parameter  $M[\eta]$  will reflect the volume of the macromolecular coils in the initial solution. It is clear that in both cases an increase of the volume of the macromolecular coil leads to the formation of nanoparticles with larger sizes. The magnitude of the particle size increases  $\sim 2.5$ –3 times compared to the first data point. With further increase of the macromolecular volume, the size of the nanoparticles remains constant within the experimental error. It is also clear that in case of more concentrated solutions ( $c[\eta] = 0.1$ ) the final nanoparticle size is larger. It was generally observed that stable nanoparticle suspensions were only produced when  $c[\eta] \leq 0.1$ . Applying concentrations corresponding to the values of  $c[\eta] > 0.1$ , nanoparticle suspensions were found to be highly polydisperse, with diameters larger than 500 nm. Such a behavior may testify to the shift beyond the Ouzo region. Regardless to concentration and molar mass, the particles obtained from the polymer solution in acetone are relatively smaller than those prepared from THF solution. This size difference can simply be related to the lower viscosity of the acetone polymer solution in comparison to THF. SEM micrographs showed the formation of more uniform nanoparticles if THF was used as solvent. This is in agreement with the viscosity data, which show higher values of the exponent in the KMHS equation for the polymer in THF solution resulting in the higher affinity of the polymer to the solvent. When acetone was used as solvent, uniform nanoparticles with smooth surfaces were only observed in case of **PMMA 1** based nanoparticles.

## CONCLUSION

To obtain well-defined particles on the basis of a certain polymer, it is crucial to work with highly diluted polymer solutions. Regardless to the polymer molar mass,

hydrodynamic volume and solvent quality, the formation of stable nanoparticle suspensions could only be observed at a Debye parameter  $c[\eta] \ll 0.1$ . According to this, it could be shown that the key factor during the particle preparation is the volume fraction occupied by the polymer macromolecular coil in the initial solution instead of the polymer concentration. The morphology of the nanoparticles depends on the affinity of the polymer molecules to the solvent. It appeared that "good" solvents are preferable to formulate uniform nanoparticles with smooth surfaces. Taking together these findings, it can be concluded that knowledge of the hydrodynamic properties of the initial polymer solution is essential for tuning and optimizing conditions for the nanoprecipitation process.

#### ACKNOWLEDGMENTS

The authors are grateful to the Thuringian Ministry for Education, Science, and Culture (grant #B514-09051, NanoConSens), to the Carl-Zeiss Stiftung (Strukturantrag JCSM) and to the Dutch Polymer Institute (DPI, Technology Area HTE) for financial support.

#### REFERENCES AND NOTES

- 1 Fessi, H.; Puisieux, F.; Devissaguet, J. P.; Ammoury, N.; Benita, S. *Int. J. Pharm.* **1989**, *55*, R1–R4.
- 2 Mora-Huertas, C. E.; Fessi, H.; Elaissari, A. *Int. J. Pharm.* **2010**, *385*, 113–142.
- 3 Vauthier, C.; Bouchemal, K. *Pharm. Res.* **2009**, *26*, 1025–1058.
- 4 Govender, T.; Stolnik, S.; Garnett, M. C.; Illum, L.; Davis, S. S. *J. Controlled Release* **1999**, *57*, 171–185.
- 5 Zhang, H.; Cui, W.; Bei, J.; Wang, S. *Polym. Degrad. Stab.* **2006**, *91*, 1929–1936.
- 6 Dutta, P.; Shrivastava, S.; Dey, J. *Macromol. Biosci.* **2009**, *9*, 1116–1126.
- 7 Hornig, S.; Heinze, T.; Becer, C. R.; Schubert, U. S. *J. Mater. Chem.* **2009**, *19*, 3838–3840.
- 8 Perevyazko, I.; Vollrath, A.; Hornig, S.; Pavlov, G. M.; Schubert, U. S. *J. Polym. Sci., Part A: Polym. Chem.* **2010**, *48*, 3924–3931.
- 9 Aubry, J.; Ganachaud, F.; Cohen Addad, J. P.; Cabane, B. *Langmuir* **2009**, *25*, 1970–1979.
- 10 Horn, D.; Rieger, J. *Angew. Chem. Int. Ed.* **2001**, *40*, 4330–4361.
- 11 Brick, M. C.; Palmer, H. J.; Whitesides, T. H. *Langmuir* **2003**, *19*, 6367–6380.
- 12 Vitale, S. A.; Katz, J. L. *Langmuir* **2003**, *19*, 4105–4110.
- 13 Beck-Broichsitter, M.; Rytting, E.; Lehardt, T.; Wang, X.; Kissel, T. *Eur. J. Pharm. Sci.* **2010**, *41*, 244–253.
- 14 Chorny, M.; Fishbein, I.; Danenberg, H. D.; Golomb, G. *J. Controlled Release* **2002**, *83*, 389–400.
- 15 Plasari, E.; Grisoni, P. H.; Villermaux, J. *Chem. Eng. Res. Des.* **1997**, *75*, 237–244.
- 16 Legrand, P.; Lesieur, S.; Bochot, A.; Gref, R.; Raatjes, W.; Barratt, G.; Vauthier, C. *Int. J. Pharm.* **2007**, *344*, 33–43.
- 17 Galindo-Rodriguez, S.; Allémann, E.; Fessi, H.; Doelker, E. *Pharm. Res.* **2004**, *21*, 1428–1439.
- 18 Stainmesse, S.; Orecchioni, A. M.; Nakache, E.; Puisieux, F.; Fessi, H. *Colloid. Polym. Sci.* **1995**, *273*, 505–511.
- 19 Perevyazko, I. Y.; Delaney, J. T.; Vollrath, A.; Pavlov, G. M.; Schubert, S.; Schubert, U. S. *Soft Matter* **2011**, *7*, 5030–5035.
- 20 Moad, G.; Rizzardo, E.; Thang, S. H. *Aust. J. Chem.* **2009**, *62*, 1402–1472.
- 21 Chiefari, J.; Chong, Y. K.; Ercole, F.; Krstina, J.; Jeffery, J.; Le, T. P. T.; Mayadunne, R. T. A.; Meijs, G. F.; Moad, C. L.; Moad, G.; Rizzardo, E.; Thang, S. H. *Macromolecules* **1998**, *31*, 5559–5562.
- 22 Schuck, P.; Rossmannith, P. *Biopolymers* **2000**, *54*, 328–341.
- 23 Fujita, H. *Polymer Solutions*; Elsevier: Amsterdam, **1990**.

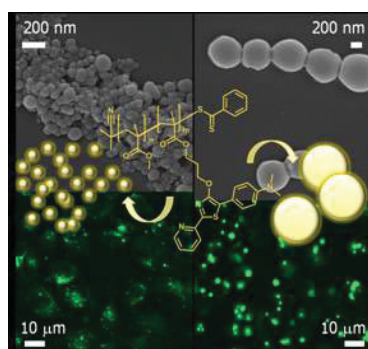
## Publication P11:

### *Preparation, cellular internalization and biocompatibility of highly fluorescent PMMA nanoparticles*

---

A. Vollrath, D. Pretzel, C. Pietsch, I. Y. Perevyazko, R. Menzel, S. Schubert, G. M. Pavlov, D. Weiß, R. Beckert, U. S. Schubert

*Macromol. Rapid Commun.* **2012**, 33, 1791–1797



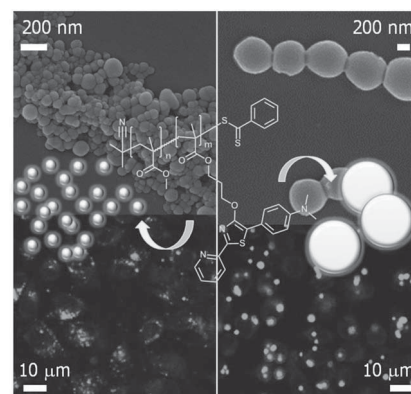




# Preparation, Cellular Internalization, and Biocompatibility of Highly Fluorescent PMMA Nanoparticles

Antje Vollrath, David Pretzel, Christian Pietsch, Igor Perevyazko, Stephanie Schubert, George M. Pavlov, Ulrich S. Schubert\*

Methacrylate monomers were functionalized with a 4-hydroxythiazole chromophore and copolymerized with methyl methacrylate via RAFT. Nanoparticles of 120 and 500 nm in size were prepared without using stabilizers/surfactants. For comparative studies, preparative ultracentrifugation was applied for the separation into small and large particle fractions. All suspensions were characterized by DLS, AUC, and SEM and tested regarding their stability during centrifugation and re-suspension, autoclavation, and incubation in cell culture media. In vitro studies with mouse fibroblast cell line and differently sized NP showed a particle uptake into cells. Biocompatibility, non-toxicity, and hemocompatibility were demonstrated using a XTT assay, a live/dead staining, and an erythrocyte aggregation and hemolysis assay.



## 1. Introduction

Recent progress in the area of nanosciences enabled the development of various nanoparticle (NP) devices as powerful tools in the pharmaceutical area for drug delivery

systems, but also in other scientific fields, for example, chemistry, biology, and electronics.<sup>[1–3]</sup> In particular for diagnostic applications, like live cell imaging, the investigation of labeled nanosystems (1 to 1000 nm) is rapidly expanding.<sup>[4–8]</sup> Such nanodevices can consist of various materials, such as silica, carbon, metal oxides, pure metals, and polymers.<sup>[6,9,10]</sup> In particular, quantum dots have revolutionized the biological research with their fascinating light-emitting properties, though still having safety issues due to the liberation of heavy metals.<sup>[2,11]</sup> The use of fluorescent polymeric NP represents a suitable alternative to avoid the obstacle of the potential toxicity of metal-based NP. A diversity of biocompatible polymers, such as poly(lactide-*co*-glycolide) and poly( $\epsilon$ -caprolactone), are used for formulation.<sup>[12–14]</sup> The incorporation of dyes into the polymer shell during NP preparation or the use of labeled polymer systems provides a protection against external influences while keeping their spectral properties, which are essential for the subsequent analysis of particle–cell interactions via confocal laser scanning microscopy.<sup>[7,13,15]</sup> A further benefit of polymeric NP is the variety of formulation techniques such as emulsification–solvent diffusion,

A. Vollrath, D. Pretzel, C. Pietsch, I. Perevyazko, G. M. Pavlov, U. S. Schubert

Laboratory of Organic and Macromolecular Chemistry, Friedrich-Schiller-University Jena, Humboldtstr. 10, 07743 Jena, Germany  
E-mail: ulrich.schubert@uni-jena.de

C. Pietsch, U. S. Schubert

Dutch Polymer Institute (DPI), Post Office Box 902, Eindhoven 5600 AX, the Netherlands  
S. Schubert, U. S. Schubert

Jena Center for Soft Matter (JCMS), Friedrich-Schiller-University Jena, Humboldtstr. 10, 07743 Jena, Germany  
S. Schubert

Institute of Pharmacy, Department of Pharmaceutical Technology Friedrich-Schiller-University Jena, Otto-Schott-Str. 41, 07745 Jena, Germany

nanoprecipitation, spray drying, salting out, and milling processes.<sup>[16–18]</sup> By using the appropriate conditions for formulation, specific drugs can be encapsulated resulting in labeled drug carriers of desired sizes and with suitable charges.<sup>[16,18,19]</sup>

In the herein presented study, polymethylmethacrylate (PMMA) copolymers were chosen as a model system to demonstrate that functional PMMA-based nanoparticles are well suitable for diagnostic applications such as the imaging of cells. The biocompatibility of PMMA microspheres enables their use in many biomedical applications, for example, as injectable dermal fillers, as PMMA-based NPs for in vitro gene delivery approaches, and also for orthopedic bone reconstruction.<sup>[20–28]</sup> For the design of labeled nanosystems, a luciferin-based 4-hydroxythiazole derivative was incorporated into the PMMA polymer backbone, showing benefits as high fluorescence at room temperature with high quantum yields, easy adjustment of the fluorescent properties, and excellent stability.<sup>[29,30]</sup> For this purpose, methacrylates were functionalized with the thiazole chromophore (MA<sup>y</sup>) and then copolymerized with methyl methacrylate (MMA) using the reversible addition–fragmentation chain transfer (RAFT) polymerization technique.<sup>[29,31–33]</sup> For the NP preparation, nanoprecipitation (solvent-evaporation) was chosen as a simple, fast, reliable, and cost-effective method.<sup>[34–36]</sup> Different particle sizes were obtained by varying the initial conditions of the formulation. Additionally, preparative ultracentrifugation (pUC) was utilized for the fractionation of particles into discretely sized NP suspensions. It provides another dimension of physical control of the size distribution of particles on the nanoscale.<sup>[14,37–39]</sup>

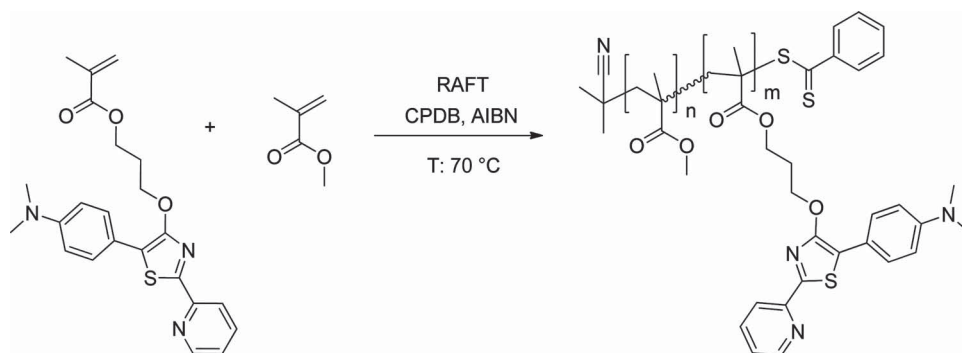
Since the size strongly influences the biodistribution of NPs and the way of internalization into target cells, it is imperative to have well-defined particles with narrow size distributions. Unfortunately, it is a matter of fact that in literature the accuracy of particle size determination is disputable.<sup>[40–42]</sup> Consequently, in this distribution,

all suspensions were characterized comprehensively by dynamic light scattering (DLS), scanning electron microscopy (SEM), and analytical ultracentrifugation (AUC) to allow a detailed characterization of the NPs.<sup>[43]</sup> The stability of the resulting nanosuspensions after long-time storage, autoclavation, and incubation in cell culture media was studied by measurements of size and zeta potential. The internalization of the differently sized nanoparticles into adherent cells was monitored by confocal laser scanning microscopy (CLSM). The biocompatibility of the particle suspensions in terms of their non-toxicity was proven by XTT cytotoxicity assay and microscopic evaluation of viability after a live/dead staining. Compatibility with blood was analyzed by checking the induction of hemolysis and aggregation of erythrocytes.

## 2. Results and Discussion

### 2.1. Synthesis of P(MMA-*stat*-MA<sup>y</sup>)

The yellow light-emitting thiazole-dye 3-((5-(4-(dimethylamino)phenyl)-2-(pyridin-3-yl)thiazol-4-yl)oxy)propan-1-ol was attached to the methacrylate monomer by an esterification reaction. The non-classical 4-hydroxy-1,3-thiazole chromophore structure is similar to the luciferin dye of fireflies and shows excellent fluorescent properties.<sup>[44]</sup> The resulting dye-functionalized methacrylate MA<sup>y</sup> was copolymerized statistically with MMAs using the RAFT polymerization methodology (Scheme 1).<sup>[31–33]</sup> The reaction was carried out using AIBN as a radical initiator, toluene as a solvent, and 2-cyano-2-propyl dithiobenzoate (CPDB) as a chain transfer agent. The ratio of MMA to the dye-functionalized monomers was 69:1, leading to a final conversion rate of 70% of the copolymers with a DP of 100. The dye-functionalized methacrylates were statistically distributed in the polymer backbone due to the same reactivity of both monomers.<sup>[29]</sup> The low degree of labeling (1 to 3%) ensured the preservation of the properties of the PMMA



■ Scheme 1. Schematic representation of the synthesis of p(MMA-*stat*-MA<sup>y</sup>).

**Table 1.** Summary of the size distributions of the nanoparticles based on p(MMA-*stat*-MA<sup>y</sup>).

Sample	$d_{\text{DLS}}$ [nm]	$\text{PDI}_{\text{particle}}$	$d_{\text{SEM}}$ [nm]	$d_{\text{AUC}}$ [nm]	$\zeta$ [mV]
<b>S1</b>	118	0.10	111	120	-36
<b>L1</b>	488	0.03	696	503	-35
<b>S2</b>	120	0.26	131	97	-32
<b>L2</b>	597	0.19	502	381	-33

homopolymer. As determined by SEC, the final p(MMA-*stat*-MA<sup>y</sup>) revealed a molar mass ( $\bar{M}_n$ ) of 8500 g mol<sup>-1</sup> with a polydispersity index value of 1.19 (Table S1, Supporting Information). Similar molar mass distributions recorded by both RI and UV detector clearly demonstrate that the thiazole dye was incorporated into the copolymer. The ratio of the MMA units and the thiazole dye in the copolymer was determined to be 2.9 mol% by <sup>1</sup>H NMR spectroscopy. The final copolymer showed the same absorbance and emission behavior like the monomeric thiazole chromophore (solvent acetonitrile;  $\lambda_{\text{Abs}} = 413$  nm,  $\lambda_{\text{Em}} = 557$  nm, Stokes-shift 6259 cm<sup>-1</sup>, Figure S1, Supporting Information) with a quantum yield of  $\Phi_{\text{PL}} = 0.29$ .

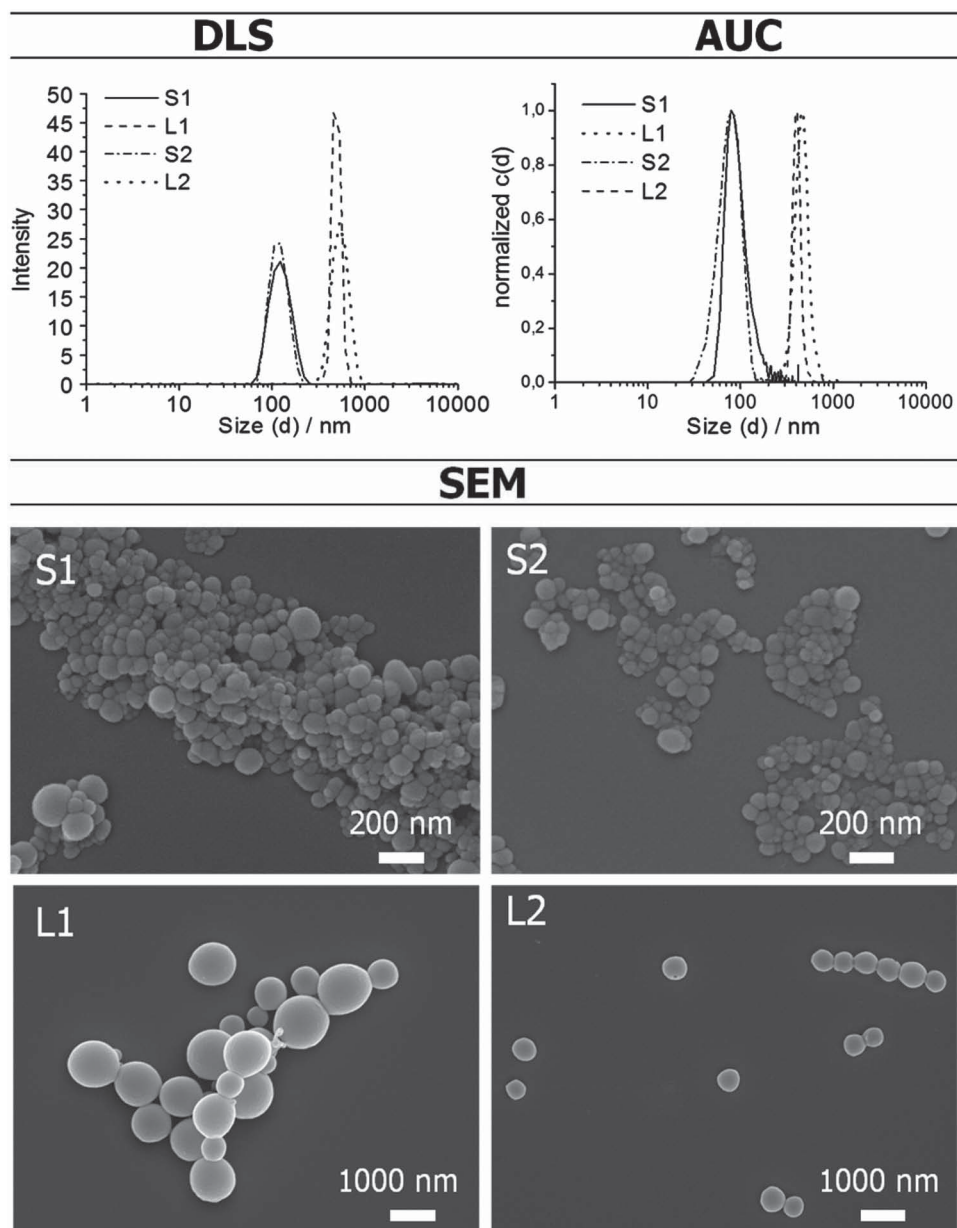
## 2.2. Nanoparticle Preparation and Characterization

The so-called nanoprecipitation or solvent evaporation process was found to be a suitable method for the preparation of differently sized NPs. Therefore, this simple, fast, and cost effective technique was applied for the preparation of p(MMA-*stat*-MA<sup>y</sup>) NPs.<sup>[34,45]</sup> The final particle size was tuned by variation of the initial polymer concentration in the organic phase and/or by changing the dropping method (polymer solution into water or water into polymer solution).<sup>[46]</sup> In order to obtain small particles (**S1**), a polymer solution with a concentration of 4 mg mL<sup>-1</sup> was dropped into water. For larger particles (**L1**), water was dropped into the polymer solution with a concentration of 3 mg mL<sup>-1</sup>. In general, a solvent/non-solvent ratio of 0.25 was used and continuous stirring was applied. After evaporation of the acetone, the particle sizes were examined by DLS. The Z-average diameter for the nanoparticles suspensions **S1** and **L1** was determined to be  $d_{\text{S1}} = 118$  nm ( $\text{PDI}_{\text{P}} = 0.10$ ) and  $d_{\text{L1}} = 488$  nm ( $\text{PDI}_{\text{P}} = 0.03$ ), respectively (Table 1). The resulting size distributions were monomodal (Figure 1). In addition to nanoprecipitation, preparative ultracentrifugation (pUC)<sup>[47]</sup> in a density gradient was used for the separation of defined NP. For pUC, a thin layer of a particle suspension to be fractionated is layered on the top of a solution containing the density gradient. When a centrifugal field is applied, the various components move through the gradient at different rates depending on their sizes, densities, and shapes.<sup>[37–39,48]</sup> In this respect, a particle

suspension with a broad size distribution was separated by pUC into fractions **S2** and **L2**. DLS and AUC measurements indicated particle sizes of  $d_{\text{S2}} = 120$  nm ( $\text{PDI}_{\text{P}} = 0.29$ ) and  $d_{\text{L2}} = 600$  nm ( $\text{PDI}_{\text{P}} = 0.19$ , Table 1). The small increase of the  $\text{PDI}_{\text{P}}$  values of **S2** and **L2** compared with **S1** and **L1** might be caused by a slight agglomeration of the NP during the pUC treatment. The zeta potential of all suspensions were in the same range ( $\zeta = -32$  to  $-36$  mV) and thereby testified a good stability of the NP in suspension. SEM investigations were performed to obtain further information about the size and shape of the particles (Figure 1). The small particles **S1** and **S2** revealed more irregular shapes than the larger ones (**L1** and **L2**), which might be caused by the preparation technique, that is, dropping acetone in water, which is characterized by the fast exchange of the solvent against the non-solvent environment.<sup>[34,35]</sup> For the small particles, the calculated diameters were in good agreement with the DLS results ( $d_{\text{S1}} = 111$  nm,  $d_{\text{S2}} = 131$  nm), whereas the large particle samples were characterized by slightly increased sizes in the particle fractions ( $d_{\text{L1}} = 696$  nm,  $d_{\text{L2}} = 502$  nm, Table 1). Complementary, the analysis of the samples by AUC revealed diameters of  $d_{\text{S1}} = 120$  nm and  $d_{\text{L1}} = 503$  nm as well as  $d_{\text{S2}} = 97$  nm and  $d_{\text{L2}} = 381$  nm, respectively. In order to exclude the occurrence of bulk precipitation and Ostwald ripening even over a long period of time, the nanosuspensions were stored at 5 °C for 6 months and examined again regarding their zeta potential and size distribution. No signs of instability of the initial nanosuspensions were found in terms of agglomeration or creaming up. It should be mentioned that no surfactants were added to inhibit particle aggregation. In addition, samples of the initial NP suspension were analyzed by DLS and SEM after centrifugation at 24.650 g for 20 min, autoclavation, lyophilization, and subsequent resuspension. Neither the size distributions nor the zeta potential values changed, which ensured the high stability of the p(MMA-*stat*-MA<sup>y</sup>) nanoparticles. The absorption and emission spectra of the nanosuspensions in comparison to the monomer were equal within the range of the measurement errors ( $\pm 5$  nm). This implies that the fluorescence properties of the monomers were unaffected by polymerization and NP formation.

## 2.3. Biological Experiments

In order to prove the efficient internalization of the particles into cells, mouse fibroblasts L929 were incubated with 120 and 500 nm sized nanosuspensions prepared by nanoprecipitation and pUC separation, respectively. The internalization of the NP into the cells was monitored by CLSM (representative micrographs are shown in Figure 2). On the basis of the relative size distribution of their corresponding fluorescence signal, a clear discrimination of small and large particles was possible. Furthermore, a concentration-dependent internalization of all



**Figure 1.** Size distributions of the particles in water ( $c = 0.5 \text{ mg mL}^{-1}$ ) obtained by DLS and AUC as well as SEM images of the particle suspensions.

fluorescent NP into the cytoplasm in the range of  $c = 0.1$  to  $10 \text{ } \mu\text{g mL}^{-1}$  was observed. The more particles added for incubation with adherent cells, the more particles were consequently found in the cytoplasm. It was further obvious that the pUC prepared samples **S2** and **L2** were internalized to a higher degree than the particles **S1** and **L1**. This might be due to traces of sucrose attached to the particle surface. As described in literature, carbohydrate moieties can act as ligands for diverse receptors. Hence, their appearance on the particle surface could lead to an enhanced cellular recognition and internalization of the particle **S2** and **L2**.<sup>[49–51]</sup>

It is known that PMMA particles are phagocytosable and it can be assumed that the cellular uptake of PMMA particles in the size range studied is presumable mediated in a similar fashion via an endocytotic pathway.<sup>[27]</sup> The negative surface charge of the PMMA NP does not alter the cellular uptake and most probably yields to a reduction of the non specific binding of anionic proteins present in the cell culture medium and also in the body fluid, for example, in the blood, thus rendering opportunities for in vivo administration of NP.<sup>[26]</sup>

For diagnostic applications, the biocompatibility and non-toxicity of the nanosuspensions are important

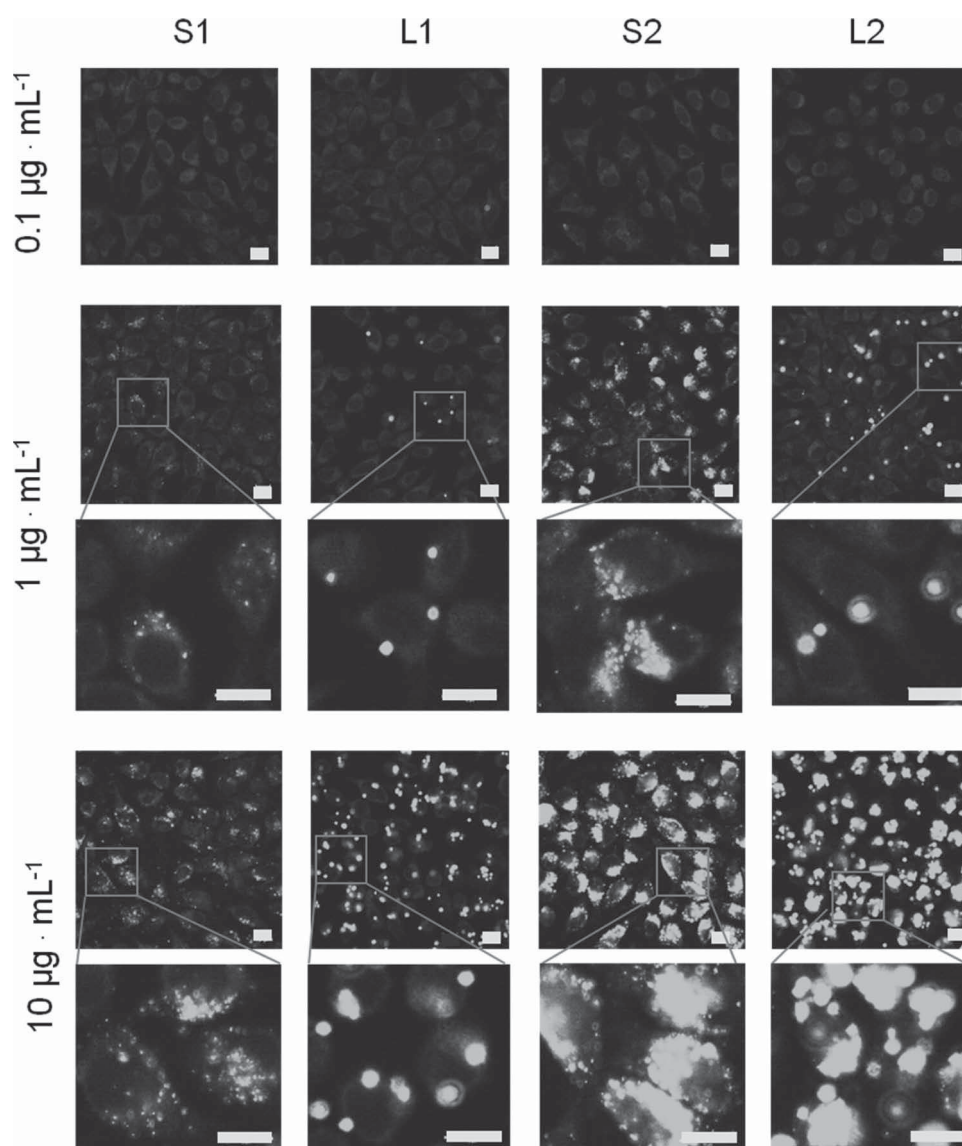


Figure 2. Confocal fluorescence images of L929 cells after 24 h incubation with polymeric p(MMA-*stat*-MA)<sup>y</sup> nanoparticles. Cells incubated with polymer free culture medium served as control (not shown). All images were obtained with identical instrument settings (scale bars 10 μm).

prerequisites. The *in vitro* cytotoxicity experiment was performed on the basis of the XTT assay using L929 mouse fibroblasts, according to the German standard institution guideline DIN ISO 10993-5 as a reference for biomaterial testing. After 24 h of incubation with different NP concentrations ( $c = 0.1\text{--}10\ \mu\text{g mL}^{-1}$ ), the metabolic activity of cells treated with test-samples was found to be on the level of untreated controls, which proves the absence of a toxic effect mediated by the NPs (Figure S2, Supporting Information). A detailed live/dead microscopy study of cells that were treated with NP confirmed the cell-membrane integrity (exclusion of red fluorescent PI from cell nuclei) and their excellent viability (strong green fluorescence

of FDA in cytoplasm) (Figure S3, Supporting Information). In addition, the interaction of NP suspensions with blood cells was investigated in terms of their potential to induce hemolysis (membrane damage and cell disruption) and/or aggregation of erythrocytes, one of the major cellular blood components. Whereas the treatment of erythrocytes with 1% Triton X-100 as positive control led to a complete disruption of the erythrocytes and subsequent release of the incorporated hemoglobin, none of the NP suspensions nor the PBS-treated negative control showed any hemolytic activity, indicating the absence of any harmful effect on the erythrocyte membrane integrity (Figure S4, Supporting Information). Furthermore,

the capability of NP suspensions to induce a formation of erythrocyte aggregates as an unwanted sign of blood incompatibility was studied microscopically and photometrically. None of the NP suspensions induced any red blood cell aggregation, even at the highest concentration of  $10 \mu\text{g mL}^{-1}$  (Figure S5 and S6, Supporting Information). In contrast, the treatment with 25 kDa bPEI as positive control caused the clear formation of aggregates, whereas PBS-treated samples used as negative control did not yield in any aggregate formation. This observed absence of any nanoparticle-mediated blood incompatibility is in line with clinical evaluations of PMMA membranes dedicated for the use in blood dialysis.<sup>[26]</sup> It is reported that due to their relatively hydrophobic and anionic surface PMMA particles show less nonspecific protein and peptide binding, and, thereby reduce the initial steps of opsonization leading to cell recognition/binding and possible immunological reactions.<sup>[52]</sup> It is known that PMMA NP may be ingested and most probably can pass through the epithelial barrier and will likely end up in the bloodstream. Large particles are usually trapped by the liver,<sup>[53]</sup> while smaller pass on and are captured by the kidneys.<sup>[54]</sup> However, because of the very low toxicity documented for PMMA NPs, even in view of a chronic/continuous disease treatment *in vivo*, the possibility of obtaining sustainable effects by using PMMA NPs is presumably realistic. In addition, the good stability of the nanoparticles during autoclavation, centrifugation, and lyophilization/resuspension is basic requirements for the possible administration of lyophilized, resuspended/reconstituted, and autoclaved particles.

### 3. Conclusion

Consequently, the 4-hydroxythiazole-functionalized PMMA NPs are suitable for fluorescence-based long-term studies of biological processes at the molecular level. On the contrary to traditional fluorophores, the PMMA NPs combine small size and high photostability, and, in contrast to widely used quantum dots, they do not contain hazardous components, which need to be shielded by protective layers. The bio-analytical applications based on functionalized polymeric PMMA NPs are of emerging interest and provide opportunities like minimal-invasive intracellular monitoring of key components like pH value and oxygen content as well as ions like calcium, potassium or sodium. They can be combined with state-of-the-art imaging techniques like flow cytometry, fluorescence microscopy, and sophisticated imaging approaches, such as confocal imaging providing the opportunity for 3D analysis. In combination with dyes emitting in the near-infrared wavelength range, it offers an optical window for *in vivo* tissue imaging into several mm depth. By the immobilization of ligands to the

PMMA particles surface, also a specific binding to biomolecules can be mediated, thereby enabling approaches like specific cell targeting.<sup>[55]</sup>

### Supporting Information

Supporting Information is available from the Wiley Online Library or from the author.

Acknowledgements: The Thüringer Ministerium für Bildung, Wissenschaft und Kultur (TMBWK, ProExzellenz-Programm NanoConSens) is acknowledged for financial support. We gratefully thank Roberto Menzel and Prof. Dr. Rainer Beckert, Friedrich-Schiller-University of Jena, for providing the 4-hydroxyl thiazole dye and Steffi Stumpf and Dr. Frank Steininger, EMZ Jena, for assistance in the SEM investigations.

Received: May 13, 2012; Revised: June 28, 2012; Published online: August 7, 2012; DOI: 10.1002/marc.201200329

Keywords: fluorescent nanoparticles; 4-hydroxythiazoles; nanoprecipitation; particle size distribution; preparative ultracentrifugation; analytical ultracentrifugation; poly(methyl methacrylate); size-dependent cell uptake; solvent-evaporation technique

- [1] D. F. Emerich, C. G. Thanos, *J. Drug Targeting* **2007**, *15*, 163.
- [2] W. J. Stark, *Angew. Chem. Int. Ed.* **2011**, *50*, 1242.
- [3] N. Sanvicens, M. P. Marco, *Trends Biotechnol.* **2008**, *26*, 425.
- [4] A. Merkoci, *Biosens. Bioelectron.* **2010**, *26*, 1164.
- [5] C. J. Xu, L. Y. Mu, I. Roes, D. Miranda-Nieves, M. Nahrendorf, J. A. Ankrum, W. A. Zhao, J. M. Karp, *Nanotechnology* **2011**, *22*, 1.
- [6] K. H. Chung, M. Y. Cho, M. H. Sung, H. Poo, Y. T. Lim, *Chem. Commun.* **2011**, *47*, 8889.
- [7] G. Tosi, L. Bondioli, B. Ruozi, L. Badiali, G. M. Severini, S. Biffi, A. De Vita, B. Bortot, D. Dolcetta, F. Forni, M. A. Vandelli, *J. Neural Transm.* **2011**, *118*, 145.
- [8] M. Mahmoudi, V. Serpooshan, S. Laurent, *Nanoscale* **2011**, *3*, 3007.
- [9] A. H. Faraji, P. Wipf, *Biorg. Med. Chem.* **2009**, *17*, 2950.
- [10] H. S. Cho, Z. Dong, G. M. Pauletti, J. Zhang, H. Xu, H. Gu, L. Wang, R. C. Ewing, C. Huth, F. Wang, D. Shi, *ACS Nano* **2010**, *4*, 5398.
- [11] K. H. Lee, *J. Nucl. Med.* **2007**, *48*, 1408.
- [12] Z. Zili, S. Sfar, H. Fessi, *Int. J. Pharm.* **2005**, *294*, 261.
- [13] G. Tosi, F. Rivasi, F. Gandolfi, L. Costantino, M. A. Vandelli, F. Forni, *Biomaterials* **2005**, *26*, 4189.
- [14] M. Gaumet, R. Gurny, F. Delie, *Int. J. Pharm.* **2007**, *342*, 222.
- [15] A. E. Nel, L. Maedler, D. Velegol, T. Xia, E. M. V. Hoek, P. Somasundaran, F. Klaessig, V. Castranova, M. Thompson, *Nat. Mater.* **2009**, *8*, 543.
- [16] C. Vauthier, K. Bouchemal, *Pharm. Res.* **2009**, *26*, 1025.
- [17] R. A. Jain, *Biomaterials* **2000**, *21*, 2475.
- [18] J. P. Rao, K. E. Geckeler, *Prog. Polym. Sci.* **2011**, *36*, 887.
- [19] C. Pinto Reis, R. J. Neufeld, A. J. Ribeiro, F. Veiga, *Nanomed. Nanotechnol. Biol. Med.* **2006**, *1*, 8.

- [20] C. H. Lohmann, D. D. Dean, G. Koster, D. Casasola, G. H. Buchhorn, U. Fink, Z. Schwartz, B. D. Boyan, *Biomaterials* **2002**, *23*, 1855.
- [21] L. Araujo, M. Sheppard, R. Lobenberg, J. Kreuter, *Int. J. Pharm.* **1999**, *176*, 209.
- [22] I. Perevyazko, A. Vollrath, S. Hornig, G. M. Pavlov, U. S. Schubert, *J. Polym. Sci., Part A: Polym. Chem.* **2010**, *48*, 3924.
- [23] A. Vollrath, S. Schubert, N. Windhab, C. Biskup, U. S. Schubert, *Macromol. Rapid Commun.* **2010**, *31*, 2053.
- [24] J. W. Yoo, N. Giri, C. H. Lee, *Int. J. Pharm.* **2011**, *403*, 262.
- [25] R. Q. Frazer, R. T. Byron, P. B. Osborne, K. P. West, *J. Long. Term Eff. Med. Implants* **2005**, *15*, 629.
- [26] H. Horikawa, H. Naitoh, M. Agatsuma, S. Hashimoto, T. Miyazaki, H. Nagasaka, A. Fujimori, *Kidney Dial.* **1994**, *94*.
- [27] A. Bettencourt, A. J. Almeida, *J. Microencapsul.* **2012**, *29*, 353.
- [28] M. L. W. Knetsch, N. Olthof, L. H. Koole, *J. Biomed. Mater. Res., Part A* **2007**, *82A*, 947.
- [29] R. Menzel, A. Breul, C. Pietsch, J. Schaefer, C. Friebe, E. Tauscher, D. Weiss, B. Dietzek, J. Popp, R. Beckert, U. S. Schubert, *Macromol. Chem. Phys.* **2011**, *212*, 840.
- [30] D. Weiss, R. Menzel, E. Tauscher, R. Beckert, H. Goerls, *Z. Anorg. Allg. Chem.* **2010**, *636*, 1380.
- [31] G. Moad, S. H. Thang, *Aust. J. Chem.* **2009**, *62*, 1379.
- [32] R. Hoogenboom, C. Pietsch, U. S. Schubert, *Polym. Chem.* **2010**, *1*, 1005.
- [33] J. Chiefari, Y. K. Chong, F. Ercole, J. Krstina, J. Jeffery, T. P. T. Le, R. T. A. Mayadunne, G. F. Meijs, C. L. Moad, G. Moad, E. Rizzardo, S. H. Thang, *Macromolecules* **1998**, *31*, 5559.
- [34] H. Fessi, F. Puisieux, J. P. Devissaguet, N. Ammoury, S. Benita, *Int. J. Pharm.* **1989**, *55*, R1.
- [35] S. Schubert, J. T. Delaney, U. S. Schubert, *Soft Matter* **2011**, *7*, 1581.
- [36] U. Bilati, E. Allemann, E. Doelker, *Eur. J. Pharm. Sci.* **2005**, *24*, 67.
- [37] F. Bonaccorso, T. Hasan, P. H. Tan, C. Sciascia, G. Privitera, G. Di Marco, P. G. Gucciardi, A. C. Ferrari, *J. Phys. Chem. C* **2010**, *114*, 17267.
- [38] V. Vogel, K. Langer, S. Balthasar, P. Schuck, W. Maechtle, W. Haase, J. van den Broek, C. Tziatzios, D. Schubert, *Prog. Colloid Polym. Sci.* **2002**, *119*, 31.
- [39] H. Pertoft, *J. Biochem. Bioph. Methods* **2000**, *44*, 1.
- [40] M. Gaumet, A. Vargas, R. Gurny, F. Delie, *Eur. J. Pharm. Biopharm.* **2008**, *69*, 1.
- [41] M. Gaumet, R. Gurny, F. Delie, *Eur. J. Pharm. Sci.* **2009**, *36*, 465.
- [42] C. He, Y. Hu, L. Yin, C. Tang, C. Yin, *Biomaterials* **2010**, *31*, 3657.
- [43] J. C. Giddings, *Science* **1993**, *260*, 1456.
- [44] E. Tauscher, D. Weiss, R. Beckert, J. Fabian, A. Assumpcao, H. Goerls, *Tetrahedron Lett.* **2011**, *52*, 2292.
- [45] S. Hornig, T. Heinze, C. R. Becer, U. S. Schubert, *J. Mater. Chem.* **2009**, *19*, 3838.
- [46] I. Y. Perevyazko, J. T. Delaney, Jr., A. Vollrath, G. M. Pavlov, S. Schubert, U. S. Schubert, *Soft Matter* **2011**, *7*, 5030.
- [47] M. K. Brakke, *J. Am. Chem. Soc.* **1951**, *73*, 1847.
- [48] X. Sun, S. M. Tabakman, W. S. Seo, L. Zhang, G. Zhang, S. Sherlock, L. Bai, H. Dai, *Angew. Chem. Int. Ed.* **2009**, *48*, 939.
- [49] S. R. S. Ting, G. Chen, M. H. Stenzel, *Polym. Chem.* **2010**, *1*, 1392.
- [50] J. J. Lundquist, E. J. Toone, *Chem. Rev.* **2002**, *102*, 555.
- [51] C. R. Becer, M. I. Gibson, J. Geng, R. Ilyas, R. Wallis, D. A. Mitchell, D. M. Haddleton, *J. Am. Chem. Soc.* **2010**, *132*, 15130.
- [52] D. H. Sun, M. C. D. Trindade, Y. Nakashima, W. J. Maloney, S. B. Goodman, D. J. Schurman, R. L. Smith, *J. Biomed. Mater. Res., Part A* **2003**, *65A*, 290.
- [53] G. Borchard, J. Kreuter, *Pharm. Res.* **1996**, *13*, 1055.
- [54] A. M. Gatti, F. Rivasi, *Biomaterials* **2002**, *23*, 2381.
- [55] Y. K. Gong, F. M. Winnik, *Nanoscale* **2012**, *4*, 360.

# Preparation, Cellular Internalization, and Biocompatibility of Highly Fluorescent PMMA Nanoparticles

Antje Vollrath, David Pretzel, Christian Pietsch, Igor Perevyazko, Stephanie Schubert, George M. Pavlov, Ulrich S. Schubert\*

DOI: 10.1002/marc.201200329

The authors regret that there were important omissions in the above article. The synthesis of the yellow light-emitting thiazole-dye 3-((5-(4-(dimethylamino)phenyl)-2-(pyridin-3-yl)thiazol-4-yl)oxy)propan-1-ol as well as the corresponding methacrylate monomer was not described in reference 29 of the manuscript or in reference 1 of the Supporting Information (in this publication only the related blue emitting monomer is described). The resulting yellow and blue polymers were both investigated – however, due to the non-visibility of the blue polymer only the yellow one was continued in the published study. In order to allow an exact reproduction of the monomer synthesis, a detailed description has been added as Supporting Information of this Correction.

In the original version of the above article, three co-authors' names (Roberto Menzel, Dieter Weiß, and Rainer Beckert) were missing from the byline and affiliation. The correct author byline is as follows:

Antje Vollrath, David Pretzel, Christian Pietsch, Igor Perevyazko, Roberto Menzel, Stephanie Schubert, George M. Pavlov, Dieter Weiß, Rainer Beckert, Ulrich S. Schubert\*

Finally, the Acknowledgments section in the above article should be replaced with the following paragraph.

The Thüringer Ministerium für Bildung, Wissenschaft und Kultur (TMBWK, ProExzellenz-Programm NanoConSens) is acknowledged for financial support. We gratefully thank Steffi Stumpf and Dr. Frank Steininger, EMZ Jena, for assistance in the SEM investigations.

A. Vollrath, D. Pretzel, C. Pietsch, I. Perevyazko, R. Menzel,  
G. M. Pavlov, D. Weiß, R. Beckert, U. S. Schubert  
Laboratory of Organic and Macromolecular Chemistry (IOMC),  
Friedrich-Schiller-University Jena, Humboldtstr. 10,  
07743 Jena, Germany  
E-mail: ulrich.schubert@uni-jena.de  
C. Pietsch, I. Perevyazko, G. M. Pavlov, U. S. Schubert  
Dutch Polymer Institute (DPI), Post Office Box 902,  
Eindhoven 5600 AX, The Netherlands  
S. Schubert, R. Beckert, U. S. Schubert  
Jena Center for Soft Matter (JCMS), Friedrich-Schiller-  
University Jena, Humboldtstr. 10, 07743 Jena, Germany  
Stephanie Schubert  
Institute of Pharmacy, Department of Pharmaceutical  
Technology Friedrich-Schiller-University Jena,  
Otto-Schott-Str. 41, 07745 Jena, Germany



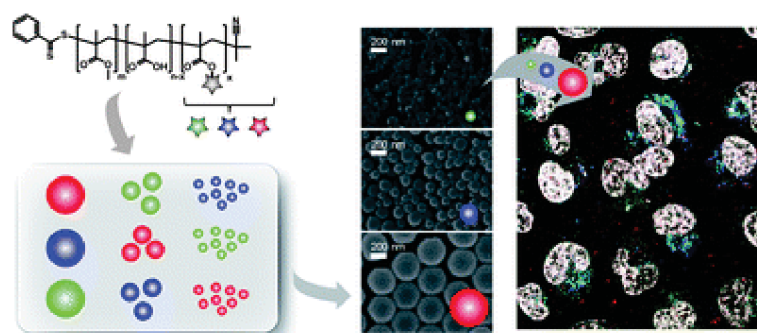
## Publication P12:

### *A toolbox of different sized and labeled PMMA nanoparticles for cellular uptake investigations*

---

A. Vollrath, A. Schallon, C. Pietsch, S. Schubert, T. Nomoto, Y. Matsumoto,  
K. Kataoka, U. S. Schubert

*Soft Matter*, **2013**, *9*, 99–108





## A toolbox of differently sized and labeled PMMA nanoparticles for cellular uptake investigation†

Cite this: *Soft Matter*, 2013, 9, 99

Antje Vollrath,<sup>ab</sup> Anja Schallon,<sup>ab</sup> Christian Pietsch,<sup>ab</sup> Stephanie Schubert,<sup>bc</sup> Takahiro Nomoto,<sup>d</sup> Yu Matsumoto,<sup>e</sup> Kazunori Kataoka<sup>\*defg</sup> and Ulrich S. Schubert<sup>\*ab</sup>

The cellular internalization of defined PMMA nanoparticles was investigated. For this purpose, the biocompatible copolymer p(MMA-*stat*-MAA)<sub>0.91:0.09</sub> was synthesized by RAFT polymerization and labeled with three different fluorescent dyes ( $\lambda_{\text{Ex}} = 493, 557, \text{ and } 653 \text{ nm}$ ). Nanoparticles were formulated from the differently labeled copolymers into samples with relatively narrow size distribution (diameter  $d < 100 \text{ nm}$ ,  $100 \text{ to } 200 \text{ nm}$ ,  $>300 \text{ nm}$ ) under appropriate conditions of nanoprecipitation and were subsequently characterized by DLS and SEM. Mixtures of the differently sized nanoparticle samples were applied for internalization studies using monolayer cultured HeLa cells. The localization of the nanoparticles was detected after certain time points up to 24 h by CLSM, using LysoTracker as a marker for late endosomes and lysosomes. In investigations by flow cytometry, a fast uptake of medium sized nanoparticles was found, whereas the large and small nanoparticles exhibited a slower internalization. However, small and medium sized nanoparticles were detected in the late endosomes/lysosomes, whereas the large nanoparticles exhibit little co-localization with LysoTracker. Moreover, it could be shown by using different inhibitors for clathrin-dependent (chlorpromazine), caveolin-dependent (filipin III) endocytosis and macropinocytosis (EIPA) that nanoparticles with  $d < 200 \text{ nm}$  were internalized *via* clathrin-dependent endocytosis, whereas those with  $d > 300 \text{ nm}$  were internalized *via* macropinocytosis.

Received 20th August 2012

Accepted 25th September 2012

DOI: 10.1039/c2sm26928g

[www.rsc.org/softmatter](http://www.rsc.org/softmatter)

### Introduction

Polymeric nanoparticles (NPs) can provide manifold opportunities for drug and gene delivery,<sup>1,2</sup> because molecules and particles at the nanometer scale offer important benefits like an enhanced permeability and retention effect (EPR), resulting in an improved bioavailability and fewer side effects. In addition, NPs offer the possibility of delivering nucleic acids (siRNA, DNA), proteins or other active substances into targeted organs or cells.<sup>1–6</sup> However, many points in the field of nanotechnology

still need to be considered very carefully with regard to unknown long-time consequences such as the accumulation of the particles in the vessels/liver, the uptake through skin and lungs, and the removal by the reticuloendothelial system.<sup>7</sup> Hence, a detailed understanding of the interaction of NPs with their environment is essential for the development of defined drug delivery systems as well as for specific diagnostic applications.

Since the last decade, a number of studies have been published investigating the cellular uptake mechanisms of NPs with respect to various physical, chemical, and biological parameters.<sup>8–13</sup> The size of the NPs was found to play the key role in the final particle–cell interaction.<sup>14–16</sup> In detail, depending on their size, particles can enter cells either by phagocytosis or pinocytosis; the latter mechanism can be further subdivided into clathrin- and caveolin-dependent endocytosis as well as clathrin/caveolin-independent endocytosis such as macropinocytosis.<sup>17–20</sup> Phagocytosis and macropinocytosis are processes to engulf large particles up to the range of  $10 \mu\text{m}$ , whereas the clathrin- and caveolin-dependent endocytosis are the main processes for the internalization of smaller particles below  $500 \text{ nm}$ .<sup>18</sup> In addition, the shape of the NPs significantly influences uptake of NPs by phagocytosis. Rod-like and oblate ellipsoidal NPs with a high aspect ratio were taken up more efficiently in comparison to their spherical counterparts, due to their higher surface area and, therefore, a better attachment to

<sup>a</sup>Laboratory of Organic and Macromolecular Chemistry (IOMC), Friedrich Schiller University Jena, Humboldtstrasse 10, 07743 Jena, Germany. E-mail: [ulrich.schubert@uni-jena.de](mailto:ulrich.schubert@uni-jena.de)

<sup>b</sup>Jena Center for Soft Matter (JCSM), Friedrich Schiller University Jena, Philosophenweg 7, 07743 Jena, Germany

<sup>c</sup>Institute of Pharmacy, Department of Pharmaceutical Technology, Friedrich Schiller University Jena, Otto-Schott-Str. 41, 07745 Jena, Germany

<sup>d</sup>Department of Bioengineering, Graduate School of Engineering, The University of Tokyo, 7-3-1 Hongo, Bunkyo-ku, Tokyo 113-8656, Japan

<sup>e</sup>Center for Disease Biology and Integrative Medicine, Graduate School of Medicine, The University of Tokyo, 7-3-1 Hongo, Bunkyo-ku, Tokyo 113-0033, Japan

<sup>f</sup>Department of Materials Engineering, Graduate School of Engineering, The University of Tokyo, 7-3-1 Hongo, Bunkyo-ku, Tokyo 113-8656, Japan

<sup>g</sup>Center for NanoBio Integration (CNBI), The University of Tokyo, 7-3-1 Hongo, Bunkyo-ku, Tokyo 113-8656, Japan. E-mail: [kataoka@bmw.t.u-tokyo.ac.jp](mailto:kataoka@bmw.t.u-tokyo.ac.jp)

† Electronic supplementary information (ESI) available: See DOI: 10.1039/c2sm26928g

the cell membrane.<sup>13,16,21,22</sup> In addition, the internalization of particles into the cells is influenced by their surface charge: an increased positive charge leads to a higher cellular uptake due to electrostatic interactions with the negatively charged cell membrane.<sup>23</sup> As the surface of NPs can be further functionalized with different reactive groups (COOH and NH<sub>2</sub>), amino acids, sugar units, antibodies, or peptides, cellular uptake of NPs can be inhibited or advanced.<sup>24–26</sup> Nevertheless, no final conclusion can be drawn about the size, shape and charge dependency of cellular uptake of NPs, as the studies published so far are all based on different materials. Inorganic (gold,<sup>27,28</sup> silica particles,<sup>29,30</sup> and quantum dots<sup>31</sup>) and organic (poly(lactic-co-glycolic acid) (PLGA),<sup>15</sup> polystyrene (PS),<sup>32,33</sup> and chitosan<sup>34,35</sup>) materials were studied and many contradictory results were reported by different investigators.<sup>36</sup> Furthermore, cell internalization studies frequently used NP beads with non-defined surfaces because conventional preparation techniques (e.g. the emulsion technique) require the use of surfactants, which also influence cellular uptake.<sup>37</sup> Hence, further studies on NP–cell-interactions with well-defined NPs, in the absence of any surfactants, would be helpful to gain a better insight into the involved parameters and structure–property relationships.

The present study aims at investigating the cell interaction of polymeric NPs with well-defined characteristics based on poly(methyl methacrylate) (PMMA) derivatives, poly(methyl methacrylate)-*stat*-poly(methacrylic acid) (p(MMA-*stat*-MAA)) copolymer. The p(MMA-*stat*-MAA) copolymer is based on the same monomers as the pharmaceutically important coating material EUDRAGIT® S100, which is applied for pH-dependent drug release.<sup>31</sup> Recently, it has been demonstrated that PMMA systems are suitable for diagnostic applications in cell imaging and as a gene carrier due to their non-toxicity and good biocompatibility.<sup>38–41</sup> Here, the poly(methacrylic acid) segment of p(MMA-*stat*-MAA) was labeled with various dyes (DY-495 (green), DY-547 (orange), and DY-647 (red)) for tracking of the NPs.<sup>42</sup> NPs of the labeled p(MMA-*stat*-MAA) copolymers (p(MMA-*stat*-MAA<sup>dye</sup> (green, orange, or red))) were prepared by the solvent-evaporation (nanoprecipitation) method<sup>43</sup> and characterized comprehensively by dynamic light scattering (DLS) and scanning electron microscopy (SEM).<sup>44</sup> The stability of the NPs was demonstrated by DLS measurements after autoclave treatment, after incubation in cell culture media, and during pH titration studies, respectively. Cytotoxicity assays were performed to prove the biocompatibility and non-toxicity of the NPs. The cellular uptake studies used HeLa cells and three differently sized and individually labeled NPs. Flow cytometry was applied for studies on time- and concentration-dependent cellular uptake and confocal laser scanning microscopy (CLSM) for cellular distribution and co-localization studies. In addition, cellular internalization was investigated by inhibitors of clathrin- and caveolin-dependent endocytosis as well as of macropinocytosis.

## Experimental

### Materials

All reagents were purchased from commercial sources (Fluka and Sigma Aldrich). MMA and MAA were purchased from Sigma Aldrich and purified with an inhibitor-remover before use. 2,2'-

Azobis(iso-butyronitrile) (AIBN) was recrystallized from methanol prior to use. 2-Cyano-2-propyl dithiobenzoate (CPDB) was purchased from Sigma Aldrich. Purified *N,N*-dimethylacetamide (DMA) and dimethylformamide (DMF) were obtained from VWR. The fluorescent dyes  $\lambda = 495$  nm (DY-495),  $\lambda = 557$  nm (DY-547), and  $\lambda = 653$  nm (DY-647) were purchased from DYOMICS GmbH. AlamarBlue, LysoTracker Green, and Opti-MEM were obtained from Life Technologies. Hoechst 33342, 5-(*N*-ethyl-*N*-isopropyl)amiloride (EIPA), filipin III, and chlorpromazine were purchased from Sigma Aldrich. Cell culture materials were received from Greiner Bio One, cell culture media and solutions from Biochrome, Greiner, and PAA. Unless otherwise stated, the chemicals were used without further purification.

### Synthesis of p(MMA-*stat*-MAA)

P(MMA-*stat*-MAA) was prepared by copolymerization of MMA with MAA using the reversible addition–fragmentation chain transfer (RAFT) polymerization method.<sup>37,38</sup> In a typical RAFT copolymerization experiment, 4.325 g of MMA monomer ( $43.2 \times 10^{-3}$  mol), 0.413 g of MAA monomer ( $4.8 \times 10^{-3}$  mol), 19.7 mg of AIBN initiator ( $0.12 \times 10^{-3}$  mol), 106.3 mg of CPDB RAFT agent ( $0.48 \times 10^{-3}$  mol) and 5.8 mL of ethanol were mixed together with anisole as the internal standard (1.2 mL) in a 25 mL reaction vial. The monomer concentration was kept at 4 mol L<sup>-1</sup>. Subsequently, the reaction solution was placed in a preheated oil bath at 70 °C for 10 hours. The copolymer was purified by precipitation into a large volume of cold diethyl ether and dried under reduced pressure. Conversion was measured by <sup>1</sup>H NMR spectroscopy using anisole as the internal standard. <sup>1</sup>H NMR (DMSO-d<sub>6</sub>, 300 MHz):  $\delta = 12.5$  (–OH), 7.83, 7.64, and 6.46 (Ar–H, CPDB), 3.55 (OCH<sub>3</sub>), 2.25–0.3 (backbone) ppm. SEC (DMA, LiCl, and PMMA standard):  $M_n = 16\,000$  g mol<sup>-1</sup> and PDI = 1.19. Elemental analysis: p(MMA-*stat*-MAA) C: 58.18 and H: 7.91%.

### Labeling of p(MMA-*stat*-MAA)

500 mg of the p(MMA-*stat*-MAA) polymer ( $3.1 \times 10^{-4}$  mol) were dissolved in 2 mL of dried DMF, and 50  $\mu$ L ( $3.0 \times 10^{-4}$  mol) of 1-ethyl-3-(3-dimethylaminopropyl)carbodiimide (EDC) was added as well as 500  $\mu$ L of a stock solution ( $c = 0.1$  mg mL<sup>-1</sup> in DMF) of the desired dye DY-495 (green,  $8.5 \times 10^{-8}$  mol), DY-547 (orange,  $7.5 \times 10^{-8}$  mol), or DY-647 (red,  $7.1 \times 10^{-8}$  mol). The labeled polymers were purified by repeated precipitation in water and extensive dialysis afterwards. The products were obtained by freeze drying in 70% overall yield. SEC (DMA, LiCl, and PMMA standard): p(MMA-*stat*-MAA<sup>green</sup>):  $M_n = 23\,500$  g mol<sup>-1</sup> and PDI = 1.21; p(MMA-*stat*-MAA<sup>orange</sup>):  $M_n = 21\,800$  g mol<sup>-1</sup> and PDI = 1.22; p(MMA-*stat*-MAA<sup>red</sup>):  $M_n = 23\,800$  g mol<sup>-1</sup> and PDI = 1.22; elemental analysis: p(MMA-*stat*-MAA<sup>green</sup>) C: 56.85, H: 8.18, and N: 2.43; p(MMA-*stat*-MAA<sup>orange</sup>) C: 58.51, H: 8.12, and N: 2.40; p(MMA-*stat*-MAA<sup>red</sup>) C: 58.17, H: 8.08, and N: 2.46.

### Preparation of the NP suspension

NPs were prepared by nanoprecipitation with subsequent solvent evaporation. For this purpose, the polymers were dissolved in acetone and filtered through a 2  $\mu$ m filter prior to use.

NP suspensions with different sizes were prepared by variation of the initial conditions of the formulation. For the small (diameter  $d < 100$  nm) and medium (100 to 200 nm) sized NPs, the acetone solution was dropped into deionized water (AW) with a concentration of  $1 \text{ mg mL}^{-1}$  and  $10 \text{ mg mL}^{-1}$ , respectively. By dropping water to the polymer solution (WA) with a concentration of  $4 \text{ mg mL}^{-1}$ , large NPs ( $d > 300$  nm) were prepared. For all suspensions, the acetone–water ratio was chosen to be 0.25. Furthermore, the dropping speed was approximately  $50 \mu\text{L}$  per second, and the stirring speed was set to 1000 rpm (Magnetic Stirrer MR Hei-Standard). Afterwards, the acetone was evaporated from the solution by stirring overnight at room temperature, the suspensions were filtered using a filter paper and diluted to a final concentration of  $0.5 \text{ mg mL}^{-1}$ . The suspensions were stored in a fridge at  $4^\circ\text{C}$  and before further usage they were vortexed to ensure a homogenous particle suspension.

### Dynamic light scattering (DLS) and zeta potential measurements

For DLS investigations, a Zetasizer Nano ZS (Malvern Instruments, Malvern, UK) operating with a laser beam at 633 nm and a scattering angle of  $173^\circ$  was used. Each sample was analyzed in triplicate at  $25^\circ\text{C}$  in a polycarbonate zeta cell. For size measurements, three runs were applied for 30 s; for the zeta potential measurements, three runs were applied for 10 s. The intensity, volume and number distribution of the NPs were calculated applying the NNLS mode.

### Scanning electron microscopy (SEM)

SEM images were obtained using a LEO-1450 VP, Leo Elektronenmikroskopie GmbH, Oberkochen, Germany. The sputter coating device BAL-TEC SCD005 (Balzers, Liechtenstein; 60 mA, 80 s) was used. The system was operated from 8 to 10 kV.

### Cell lines and culture conditions

The HeLa (CCL-2, ATCC) and L929 (CCL-1, ATCC) cell lines used in the uptake and cytotoxicity experiments were maintained in suitable cell culture media supplemented with 10% fetal calf serum (FCS),  $100 \mu\text{g mL}^{-1}$  streptomycin,  $100 \text{ IU mL}^{-1}$  penicillin, and 2 mM L-glutamine (4 mM for L929). The cells were cultured at  $37^\circ\text{C}$  in a humidified 5%  $\text{CO}_2$  atmosphere.

### Flow cytometry analysis

For the determination of cellular uptake of NPs *via* flow cytometry,  $10^5$  cells per well were seeded in 12-well plates and incubated for 24 h. Thirty minutes prior to the incubation with the NPs, the cells were rinsed with PBS and supplemented with OptiMEM. The NPs were added to the cells and the plates were incubated for the indicated time. Afterwards, the cells were harvested by trypsinization and resuspended in PBS supplemented with 10% FCS. To determine the relative uptake of NPs, 10 000 cells were quantified by flow cytometry using a Cytomics FC 500 (Beckman Coulter).

### Microscopy studies

HeLa cells were cultured on 35 mm glass dishes (Iwaki, Japan) at  $2 \times 10^5$  cells per dish. After 24 h, the medium was exchanged with OptiMEM, and the cells were incubated for 30 min before the addition of the NP suspensions. The nuclei and the late endosomes/lysosomes were stained with Hoechst 33342 and LysoTracker Green, respectively, before CLSM imaging. CLSM images were acquired 24 h after the administration of NPs, using a Zeiss LSM 780 (Carl Zeiss). Excitation wavelengths were 405 nm, 488 nm, 561 nm and 633 nm for Hoechst 33342, LysoTracker Green or DY-495 stained NPs, DY-547 stained NPs, and DY-647 stained NPs, respectively. Co-localization was quantified, using Imaris software (Bitplane AG, Zurich, Switzerland).

### Inhibition of endosomal pathways

The cells were seeded as described before. The growth media were changed to OptiMEM and incubated for 30 min before  $10 \mu\text{g mL}^{-1}$  chlorpromazine,  $1 \mu\text{g mL}^{-1}$  filipin III, or  $100 \mu\text{M}$  EIPA were added and incubated for a further 30 min. Afterwards, the NPs were added, and the cells were incubated for the indicated time.

### Cell viability

For L929 cells, the cytotoxicity assay was performed according to ISO10993-5. In detail, the cells were seeded at 10 000 cells per well in a 96-well plate and incubated for 24 h. No cells were seeded in the outer wells. The growth media were replaced by OptiMEM. Afterwards, NP dilutions in the concentration range from 78 to  $254 \mu\text{g mL}^{-1}$  were added, and the cells were incubated at  $37^\circ\text{C}$  for further 24 h. Subsequently, the medium was replaced by DPBS and AlamarBlue, as recommended by the supplier. After incubation for 4 h, the fluorescence was measured at Ex 570/Em 610 nm in a microplate reader (Genios Pro, Tecan GmbH), with untreated cells serving as controls.

## Results and discussions

### Polymer preparation and characterization

To provide the possibility of functionalization after the polymerization, carboxylic acid groups were introduced into the PMMA chain. Therefore, MMA was copolymerized with MAA using the RAFT polymerization method.<sup>37,38</sup> This technique allows the synthesis of tailored polymers with control over molar mass and the composition of the copolymer, *i.e.*, the ratio between MAA and MMA.

In the copolymerization reaction, a final conversion of 87% (both monomers) was reached. MMA and MAA are statistically distributed in the polymer backbone due to the same reactivity ratio of the MMA and MAA units.<sup>45</sup> The ratio between both MMA and MAA in p(MMA-*stat*-MAA) was determined by  $^1\text{H}$  NMR spectroscopy. The observed ratio of 91 to 9% agrees well with the theoretical value of 90 to 10%. The low content of MAA ensures the stability at  $\text{pH} > 7$  of the NPs and seems to be beneficial for a well-defined NP formation in aqueous systems. A molar mass of  $M_n = 16\,000 \text{ g mol}^{-1}$  with a polydispersity

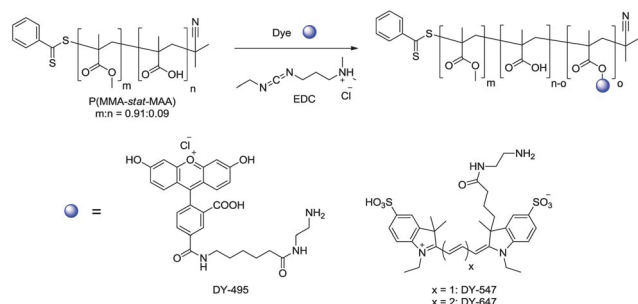
**Table 1** Selected characterization data of the p(MMA-*stat*-MAA)<sub>0.91:0.09</sub> polymer and the fluorescent labeled p(MMA-*stat*-MA<sup>dye</sup>) copolymers

Sample	$M_n^a$ [g mol <sup>-1</sup> ]	PDI <sub>SEC</sub> (RI) <sup>a</sup>	C [%]	H [%]	N [%]
P(MMA- <i>stat</i> -MAA) <sub>0.91:0.09</sub>	16 000	1.15	58.18	7.91	—
P(MMA- <i>stat</i> -MA <sup>green</sup> )	23 500	1.21	56.85	8.18	2.43
P(MMA- <i>stat</i> -MA <sup>orange</sup> )	21 800	1.22	58.51	8.12	2.40
P(MMA- <i>stat</i> -MA <sup>red</sup> )	23 800	1.22	58.17	8.08	2.46

<sup>a</sup> Calculated from SEC (DMA and LiCl) and PMMA calibration.

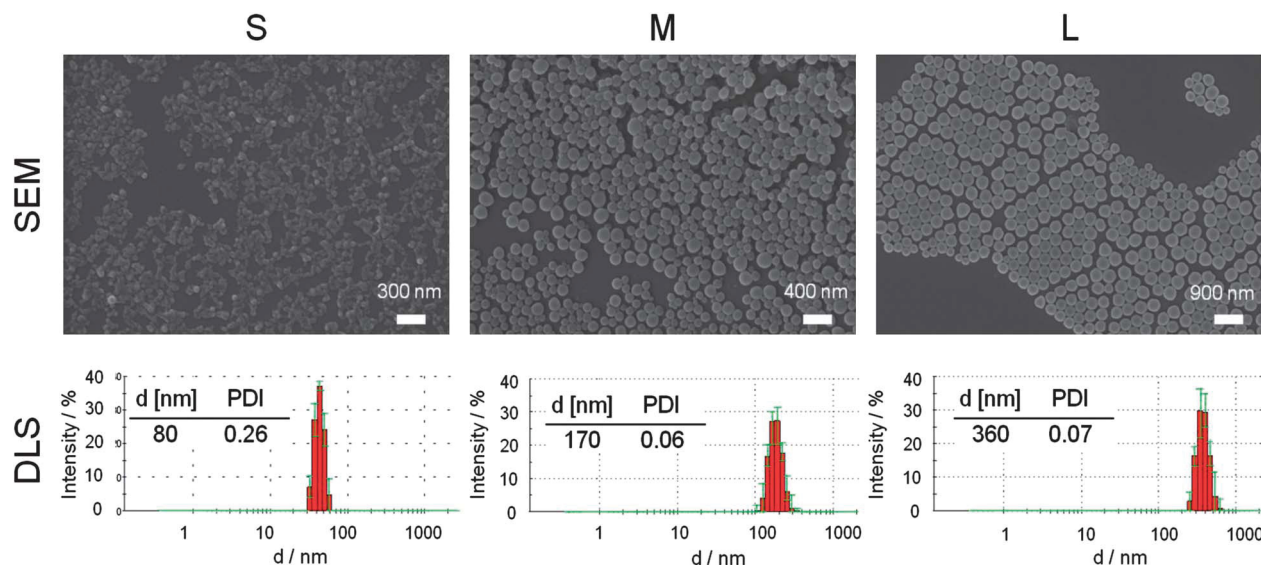
index of 1.15 (DMA, LiCl) was determined by size exclusion chromatography (SEC) for the final copolymer p(MMA-*stat*-MAA)<sub>0.91:0.09</sub> (Table 1).

In order to obtain differently labeled polymers, three different dyes (DY-495, DY-547 and DY-647) were chosen, because the dyes provide high quantum yields, good photostability, and are available with different functional groups (Scheme 1).<sup>42</sup> The labeling procedure was performed by the reaction of the COOH groups with the NH<sub>2</sub>-functionalized dyes using EDC as the coupling reagent. The absence of free dye was proven by fluorescence measurements of the washing water after purification. The fluorescence emission spectra of the labeled copolymers p(MMA-*stat*-MA<sup>green</sup>), p(MMA-*stat*-MA<sup>orange</sup>), and p(MMA-*stat*-MA<sup>red</sup>) are displayed in the ESI, Fig. S1.† All the copolymers show distinct peaks at 525 nm, 568 nm, and 668 nm, respectively. In comparison to the initial emission of the pure dyes, no significant change in the fluorescence behavior was obtained even after conjugation into the copolymer segments. A comparison of the SEC graphs of the unmodified p(MMA-*stat*-MAA) and the labeled copolymers revealed a slight change in the elution volume, indicating that the molar mass slightly increased due to dye conjugation and that the polymer was not degraded or cross-linked during the labeling procedure. The overlay of the diode array detector (DAD) and refractive index (RI) traces of the labeled samples confirm the covalent attachment of the dyes (ESI, Fig. S2†). Furthermore, the elemental analysis revealed an increase in the nitrogen content, which also indicates the attachment of the dyes in the polymer backbone.

**Scheme 1** Schematic representation of the reaction of p(MMA-*stat*-MAA)<sub>0.91:0.09</sub> with the DY-495, DY-547, and DY-647 using EDC as a coupling reagent.

## Preparation and characterization of NPs

Differently sized NPs were prepared by nanoprecipitation with subsequent solvent evaporation, a technique, which is not only simple and cost-effective but also fast and easy.<sup>43</sup> By variation of the initial conditions of the formulation, such as the solvent/non-solvent ratio and the concentration of the polymer solution, well-defined NPs with different sizes can be prepared. In comparison to other procedures commonly used, *e.g.*, the emulsification technique, no surfactants are necessary for the NP preparation. This represents an important benefit of the nanoprecipitation technique. It was proven that surfactants significantly affect the interaction of NPs with cells as well as their cellular uptake.<sup>37</sup> Using nanoprecipitation, it is known that the final NP sizes can be tuned from 50 nm up to 1 μm by varying the initial polymer concentration in the organic phase and/or by changing the dropping method (polymer solution into water or water into polymer solution). In order to yield small (S;  $d < 100$  nm), medium (M;  $d$  between 100 and 200 nm), and large (L,  $d > 300$  nm) NPs, different nanoprecipitation conditions were applied. By dropping the acetone-polymer solution into water, smaller NPs were obtained in comparison to the reverse technique. For the preparation of the small NPs, polymer acetone solutions with a concentration of 1 mg mL<sup>-1</sup> were dropped into water. For the medium sized NPs the same procedure with an increased concentration of 10 mg mL<sup>-1</sup> was used. The large NPs were generated by dropping water into polymer solutions with a concentration of 4 mg mL<sup>-1</sup>. For all suspensions, a solvent/non-solvent ratio of 0.25 and no surfactants were used. After subsequent removal of the acetone by overnight evaporation, the NPs were filtered, diluted to a concentration of 0.5 mg mL<sup>-1</sup>, and characterized by DLS and SEM. These complementary techniques give sufficient information about the size, shape, and surface characteristics of the particle systems.<sup>44</sup> For the small NPs, a size of 80 (±10) nm was measured by DLS in water. The medium NPs revealed a size of 150 (±10) nm, whereas for the large NPs a size of 400 (±50) nm was obtained. Low PDI<sup>P</sup> values confirm a narrow size distribution of the NPs, which was further verified by the SEM investigations. A detailed analysis of a representative small, medium and large NP batch is displayed in Fig. 1. As the major focus of this research was set on the influence of the size on the cell internalization, a charge effect needs to be excluded. Thus, only a low degree of labeling was performed in order to keep the charge density similar. The zeta potential of the NP was measured in water (pH = 6), resulting in comparable values with 30 ± 10 mV for all nanoparticle suspensions. The zeta potential values larger than 20 mV further indicate high repulsion forces and colloidal stability of the NPs in suspension. However, the stability of the NPs should also be confirmed under different conditions, and, therefore, a NP suspension with medium sized NPs was investigated in more detail. For this purpose, all NPs were centrifuged at 15 000 rpm for 20 min, autoclaved, or incubated in PBS or cell culture media as well as titrated in the pH range of 4 to 10. The resulting suspensions were analyzed again by DLS and SEM. Neither the size distribution nor the zeta potential value changed, which proves the



**Fig. 1** Representative SEM images and DLS intensity size distribution with corresponding Z average value and polydispersity PDI<sup>P</sup> of the small, medium and large particles of the p(MMA-*stat*-MA<sup>dye</sup>) copolymer.

high stability of the p(MMA-*stat*-MA<sup>dye</sup>) NPs (ESI, Fig. S3<sup>†</sup>). In combination with the easily tunable NP size, the absence of surfactants, and the variety on possible modifications/labels of the original polymers, the NPs represent excellent and well-defined materials for further cell internalization experiments.

#### Cytotoxicity of the polymers in L929 cells

To evaluate the cytotoxicity of the NPs, we used L929 cells, because they were commonly used for the investigation of cytotoxicity, as they are sensitive and recommended by ISO10993-5. For the cell experiments, the NPs (which originally were in distilled water) were buffered with DPBS before being added to the cells. In preliminary experiments, cytotoxicity tests with AlamarBlue were performed for 24 h, to evaluate the metabolic activity of L929 cells exposed to the NPs. Small (<100 nm) and large (>300 nm) labeled NPs were investigated. As shown in Fig. S4 (ESI<sup>†</sup>), all types of NPs did not cause a significant cytotoxicity after 24 h of incubation at the investigated concentrations up to 260  $\mu\text{g}$  NPs per mL ( $p > 0.01$ ; ANOVA). Moreover, neither size nor labeling of the NPs showed an influence on the cytotoxicity. This is in agreement with studies of other groups using EUDRAGIT S100.<sup>38–40</sup> Thus, the NPs used here are not toxic even at the maximum concentration of 150  $\mu\text{g}$  mL<sup>-1</sup>.

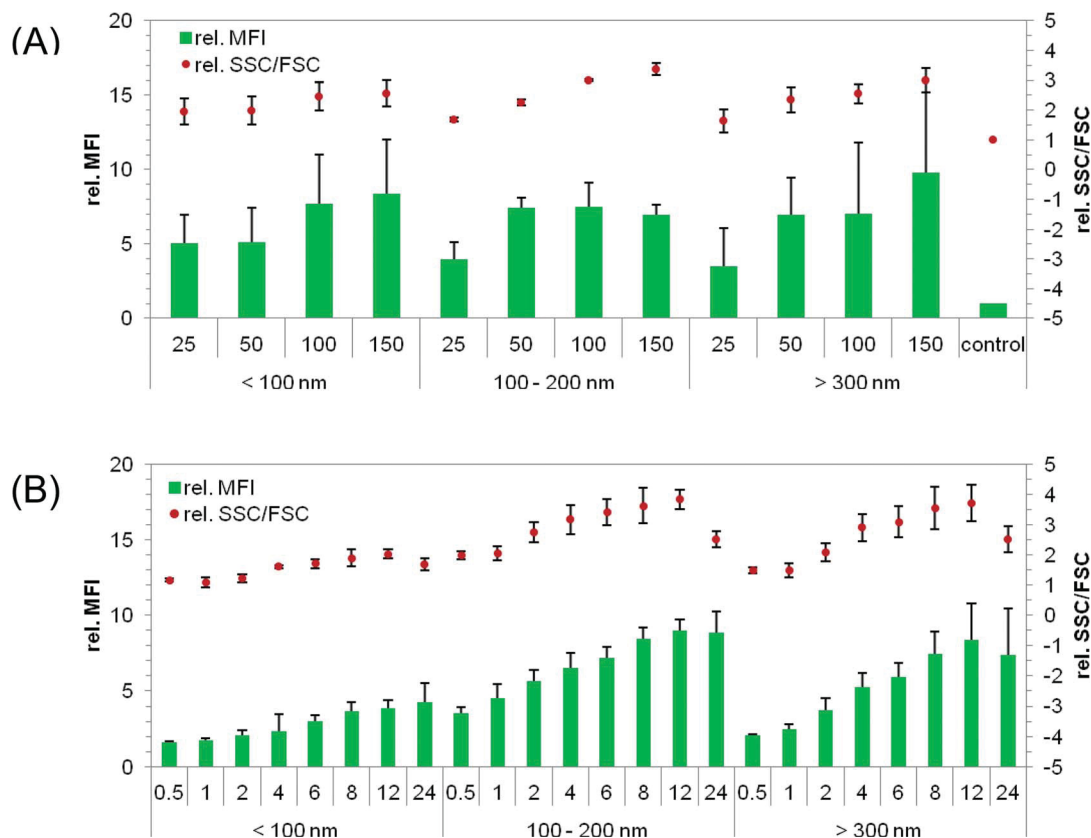
#### Validation of cellular uptake measurement by flow cytometry *via* fluorescence and side scatter

To investigate cellular uptake of the NPs into HeLa cells by flow cytometry, we first confirmed the validation of cellular uptake measurement by flow cytometry. The fluorescence channel as well as the side scatter (SSC) and forward scatter (FSC) channels were used. The SSC is directly related to the cell granularity and was used as an indicator of cellular uptake.<sup>46</sup> On the other hand, the FSC is correlated with the cell size and was used as an additional factor. After overnight incubation with the NPs, the cells showed a high cellular uptake that was detected by the

fluorescence intensity measurements. This result was also confirmed by an increase in the SSC channel (ESI, Fig. S5<sup>†</sup>): the SSC signal increased with the increase of the incubation time, whereas the FSC signal did not change. Moreover, a strong correlation between fluorescence and SSC was detected when HeLa cells were incubated with increasing sizes of DY-547 labeled NPs. To exclude a high influence of NPs on the cell surface, the outer fluorescence was quenched with trypan. No differences in the non-quenched ones could be observed. Therefore, the uptake of NPs can be detected by fluorescence and SSC measurements.

#### Dependency of cellular uptake on the NP concentration

A concentration-dependent cellular uptake was investigated after 24 h using four different NP concentrations (25, 50, 100, and 150  $\mu\text{g}$  mL<sup>-1</sup>, respectively). The cellular uptake was quantified using flow cytometry. It should be noted that larger NPs contain a higher content of labeled polymers leading to an increased fluorescence signal compared to smaller NPs. To suppress the influence of the cell size on granularity, the SSC was measured relative to the FSC as the cofactor. For analysis, the fluorescence (mean fluorescence intensity = MFI) and SSC/FSC of the treated cells were plotted relative to untreated cells (Fig. 2). It was observed that higher NP concentrations lead to an increase in MFI and SSC/FSC (Fig. 2A). In particular, for the medium and large sized NPs, a clear concentration-dependent cellular uptake was observed. In detail, for incubation with 150  $\mu\text{g}$  mL<sup>-1</sup>, a three times higher relative SSC/FSC value was obtained for the medium and large sized NPs ( $3.4 \pm 0.2$  and  $3 \pm 0.4$ , respectively) in comparison to the control cells. For the small NPs only a relative SSC/FSC value of  $2.6 \pm 0.4$  was detected. The fluorescence measurement also confirmed these results, but is influenced by the amount of fluorescent polymer per particle. The number of “positive cells” (cells that



**Fig. 2** Cellular uptake of NPs into HeLa cells measured by flow cytometry: the cells were seeded at a concentration of  $10^5$  cells per mL 24 h before particle incubation with NPs. The uptake of NPs was investigated in serum-reduced media and measured by two methods: the relative change of fluorescence (MFI) and granularity (SSC/FSC) compared to non-treated cells. (A) Different concentrations of differently sized particles were analyzed after 24 h of incubation. (B) Time-dependent uptake of 50  $\mu\text{g}$  NPs per mL. Data represent mean  $\pm$  SD,  $n \geq 3$ .

internalize NPs) was increased with higher NP concentration: 95% positive cells were found for  $c = 150 \mu\text{g mL}^{-1}$  and 75% for  $50 \mu\text{g mL}^{-1}$ , respectively (data not shown). Furthermore, the relative SSC/FSC as well as the relative MFI showed no significant differences between small, medium and large NPs at  $50 \mu\text{g mL}^{-1}$  ( $p > 0.05$ ). It could be shown that all NPs were taken up by HeLa cells at the used concentrations.

#### Cultivation conditions – influence on the NP uptake by HeLa cells

The majority of experiments were performed with serum-reduced media (OptiMEM), but additionally the cellular uptake of NPs was further investigated in growth media to exclude an influence of serum proteins on the uptake. No significant differences could be obtained between serum-reduced and serum-containing (growth media) conditions for  $50 \mu\text{g mL}^{-1}$  small and large NPs. In all cases, 60% to 70% of positive cells and an increased SSC/FSC signal could be detected after 24 h. The results indicate that the used media have no influence on the cellular uptake.

#### Dependency of cellular uptake on the incubation time

The size of the NPs showed no influence on the cytotoxicity and cellular uptake after 24 h incubation at a NP concentration of  $50 \mu\text{g mL}^{-1}$  as described above. To gain a deeper understanding

of the cellular uptake, a time-dependent cellular uptake was evaluated. In these experiments, HeLa cells were incubated with p(MMA-*stat*-MA<sup>orange</sup>) NPs for 30 min up to 24 h, and MFI as well as SSC/FSC were analyzed by flow cytometry. In Fig. 2B, the cellular uptake is presented as relative MFI and SSC/FSC of treated cells to non-treated cells. It could be observed that all the NPs were taken up by the cells in a time-dependent manner. In detail, small NPs < 100 nm reached a relative MFI of around 4 and an increase of SSC/FSC of around 2 after 24 h at  $50 \mu\text{g mL}^{-1}$ . This is in agreement with the results observed by the concentration-dependent uptake in Fig. 2A. A significant increase ( $p < 0.01$ ) in granularity (relative SSC/FSC) was detectable after 4 h incubation. The highest relative SSC/FSC was found after 12 h incubation. This was also the case for medium and large sized NPs (medium NP: MFI 8.5, SSC/FSC 3.5; large NP: MFI 7.5–8, SSC/FSC 3.5). Furthermore, no significant differences were detected between medium and large NPs after 4 to 24 h incubation ( $p > 0.05$ ). The internalization of all NPs reached a plateau after 8 h, as indicated by the lack of further significant increase in fluorescence and granularity ( $p > 0.05$ ). A difference in the cellular uptake of the differently sized NPs was, however, observed at early time points. In detail, small NPs < 100 nm and large NPs > 300 nm showed no increase in granularity for 2 h and 1 h, respectively ( $p > 0.05$ ). In contrast to this, an increase in granularity was detectable with medium sized NPs ( $p < 0.01$ ),

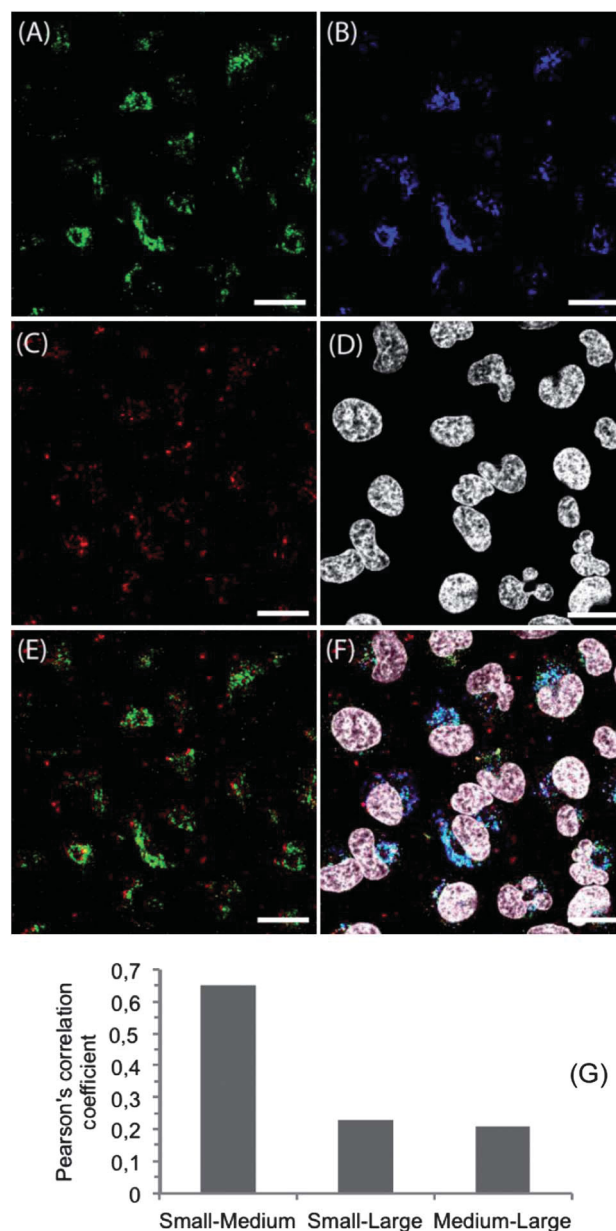


which can be due to different reasons. First of all, the effect may be caused by different endosomal pathways. The delayed cellular uptake of small NPs can also be explained by a slower sedimentation of the NPs compared to the larger ones. This could lead to a later contact between the membrane of cells and NPs, and an eventual delayed cellular uptake. Besides, a decrease in relative SSC/FSC was observed at 24 h compared to that at 12 h in particular with medium and large sized NPs. This could not be observed by fluorescence. The reason for this decrease in granularity is not understood by now and requires further investigations.

In conclusion, medium NPs of 100 to 200 nm were found to have the fastest cellular uptake in HeLa cells compared to smaller and larger ones. A fast cellular uptake of medium sized NPs could be due to fast sedimentation and fast internalization into cells, indicating an endosomal pathway. Large NPs were taken up very slowly despite fast sedimentation, indicating a macropinocytotic uptake, because endosomal pathways like clathrin- or caveolin-dependent endocytosis are faster compared to macropinocytosis.<sup>47</sup>

### Intracellular localization study of differently sized NPs

The cellular uptake mechanisms of HeLa cells were investigated by CLSM. For this purpose, the intracellular distribution of NPs after 24 h incubation was studied in living cells. Small NP<sup>green</sup>, medium NP<sup>orange</sup> and large NP<sup>red</sup> suspensions were used at 50  $\mu\text{g mL}^{-1}$  each. The nuclei of the cells were stained with Hoechst 33342. A representative NP distribution in HeLa cells is presented in Fig. 3. Cells containing NPs of different sizes are plotted separately (Fig. 3A–C) as well as the corresponding cell nuclei (Fig. 3D). In addition, two overlays are presented. The overlay of all channels is presented in Fig. 3F. No NPs could be observed in the cell nuclei. The intracellular distribution of small and medium sized NPs is comparable. In detail, a peri-nuclear localization was observed (compare Fig. 3A and B) in the cytoplasm. Hence, a strong co-localization was found with NPs below 200 nm. In contrast, the intracellular localization of small and large NPs is different, as presented in Fig. 3A and C, and merged in Fig. 3E. Co-localizations between small and large sized NPs would be indicated by yellow signals. Here, only a few yellow signals were detectable indicating only some co-localization. This could also be observed in Fig. 3F, where the observed cyan staining indicates a co-localization of small and medium sized NPs, whereas only a few purple (co-localization of medium and large NPs) and yellow signals could be found. Furthermore the co-localization was quantified by Pearson's correlation coefficient (PCC) (Fig. 3G). The PCC between the small and medium sized NPs showed the highest value, suggesting that the small and medium sized NPs might have a similar cellular uptake pathway. To exclude the possibility that this cellular distribution is caused by the dye, other NPs with comparable sizes but different dyes were investigated (*e.g.* small NP<sup>orange</sup> and large NP<sup>green</sup>). This combination of NPs was also incubated with HeLa cells and treated as described before. Thereby, the intracellular distribution shows no dependency on the dye and, thus, indicates no influence of the chemical nature



**Fig. 3** Confocal microscope images of HeLa cells incubated with NPs. Cells were seeded at a density of  $10^5$  cells per mL for 24 h in medium before particle incubation. NPs with different sizes and labels (A: small NP<sup>green</sup>, B: medium NP<sup>orange</sup>, C: large NP<sup>red</sup>) were added at 50  $\mu\text{g mL}^{-1}$  simultaneously and incubated for 24 h. (D) Cell nuclei were stained with Hoechst 33342. (E) Overlay of small NP<sup>green</sup> and large NP<sup>red</sup>. (F) Overlay image of labeled NPs and cell nuclei. (G) Pearson's correlation coefficient of labeled NPs. The scale bars indicate 20  $\mu\text{m}$ .

of dyes used on the uptake behavior of HeLa cells. Additionally, HeLa cells incubated with small, medium, and large NPs at 4  $^{\circ}\text{C}$  revealed no fluorescence inside the cells (ESI, Fig. S6<sup>†</sup>). This indicates an active cellular uptake mechanism of all sized NPs *via* endocytosis. Hence, a different intracellular distribution of large NPs (>300 nm) compared to small (<100 nm) and medium (100 to 200 nm) sized NPs was clearly proven. This indicates a different internalization of NPs below 200 nm compared to larger ones. Furthermore, the microscopy data support the results observed by flow cytometry, where differences in time-dependent uptake

could be found with regard to the NP size. Although, medium and large sized NPs sediment faster onto the cells, the large NPs were not internalized within the first hour, whereas medium sized NPs were detected in cells after 30 min.

### Investigation of cellular pathways

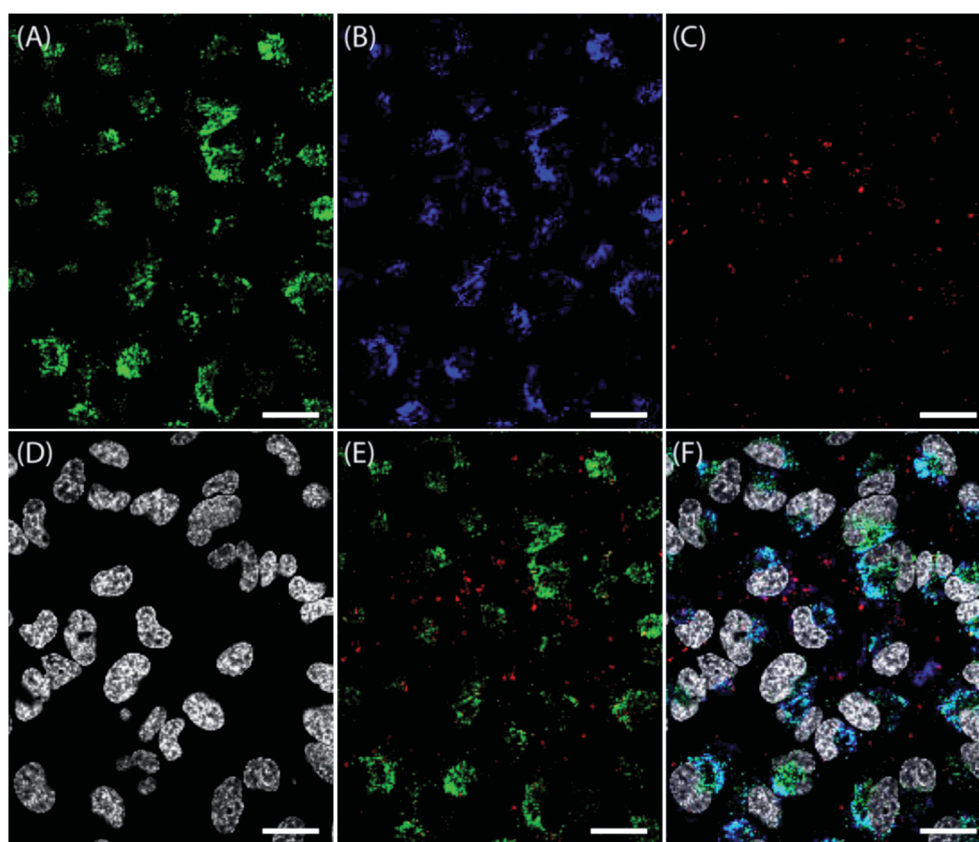
The intracellular localization and the cellular uptake kinetics of NPs showed strong dependency on size (Fig. 2B and 3). To further elucidate this observation, the intracellular localization was investigated by using LysoTracker, a well known substance for staining acidic late endosomes and lysosomes. As NPs <200 nm showed the same cellular localization in all experiments, only medium (100 to 200 nm) NPs are presented here. They show a stronger fluorescence signal and could be detected more easily compared to small NPs, due to more labeled polymers inside the NPs. In Fig. 4, the stained lysosomes (A), medium NPs (B), large NPs (C), and cell nuclei (D) are presented. Moreover, the overlay of lysosomes and large NPs (E) and the overlay of all dyes used (F) are shown. Again, no NPs were found in the nuclei. It should be noted that almost all medium sized NPs were detected in the late endosomes or lysosomes indicated by a high PCC of 0.61 and a cyan staining in Fig. 4F due to the merging of medium sized NP<sup>orange</sup> (plotted in blue) with LysoTracker (A). An adverse intracellular localization was found by using large NPs

showing little co-localization with medium sized NPs and a PCC of 0.19, as described before. Furthermore, little co-localization was observed with late endosomes or lysosomes, indicated by slight yellow signals in Fig. 4E and a PCC of only 0.15.

The large NPs were taken up by the cells, but the internalization or the cellular pathway seems to be different to the medium ones. Whereas smaller NPs revealed a fate in late endosomes or lysosomes, the cellular uptake mechanism of larger NPs is not fully understood. It can be postulated that NPs smaller than 200 nm were internalized *via* endocytosis and ended up in the late endosomes or lysosomes. The missing co-localization of larger NPs > 300 nm with late endosomes or lysosomes indicates an uptake mechanism that does not end in the lysosomes at the investigated time points, as a release of NPs into the cytoplasm is not supported.

### Inhibition of endocytic pathways

To investigate the cellular uptake mechanism of differently sized NPs, internalization routes were inhibited. Chlorpromazine was used for inhibition of clathrin-dependent and filipin III for inhibition of caveolin-dependent endocytosis. It was described in the literature that NPs < 200 nm are predominantly taken up by these pathways.<sup>18,48</sup> In contrast to smaller NPs, larger NPs can be taken up by macropinocytosis or phagocytosis and were inhibited by



**Fig. 4** Confocal microscope images of HeLa cells incubated with particles. Cells were seeded at a density of  $10^5$  cells per mL for 24 h. The medium was changed and incubated for 30 min. NPs at different sizes and labels (B: medium NP<sup>orange</sup>; C: large NP<sup>red</sup>) were added at  $50 \mu\text{g mL}^{-1}$  simultaneously and incubated for 24 h. (A) LysoTracker Green was added 10 min before microscopic analysis and incubated at  $37^\circ\text{C}$  to stain acidic late endosomes and lysosomes. (D) Cell nuclei were stained with Hoechst 33342. (E) Overlay of stained lysosomes and large NP<sup>red</sup>. (F) Overlay image of labeled NPs, lysosomes and cell nuclei. The scale bars indicate 20  $\mu\text{m}$ .

EIPA.<sup>18,48</sup> The NP internalization was analyzed by flow cytometry (ESI, Fig. S7†). Inhibition of cellular uptake was investigated with small and large sized NPs, as it was shown that the intracellular localization of small and medium sized NPs is comparable. As mentioned above, the MFI and the SSC/FSC showed no strong increase after 2 h (Fig. 2), because the NP concentration in cells has an influence on the signal intensity of SSC/FSC and MFI. As the cells internalize only a few NPs after 2 hours, the SSC/FSC and MFI could not be used in this case. Therefore, the percentage of cells taking up NPs was used (ESI, Fig. S7†). In the case of using small NPs and the three different inhibitors, it was found that NPs < 200 nm were excluded not by filipin III and EIPA but by chlorpromazine, indicating an uptake *via* clathrin-dependent endocytosis. To prove this result, CLSM studies were also performed. In Fig. S8 (ESI†), medium sized NPs (green) were not detectable in cells incubated with chlorpromazine (A) but detectable in cells incubated with filipin III. As controls, polystyrene (PS) beads of 150 nm were used (blue emission). These PS beads could be excluded by filipin III, indicating an uptake *via* caveolin-dependent endocytosis, as also confirmed in the literature.<sup>18</sup> This suggests that surfactants, which are usually necessary to prepare commercial NPs, have an influence on the uptake in cells. By using inhibitors, it can be assumed that NPs < 200 nm internalize *via* clathrin-dependent endocytosis, in particular the 100 nm NPs used in this study. In the case of internalization of large NPs, an exclusion could be observed by using EIPA, but not when chlorpromazine and filipin III are used (ESI, Fig. S7†), indicating an uptake of larger NPs *via* macropinocytosis. As already reported in the literature,<sup>49</sup> EIPA caused also a weak inhibition of small sized NPs. These blocking study of differently sized NPs showed that defined small p(MMA-*stat*-MAA) NPs were predominantly taken up by clathrin-dependent endocytosis, whereas larger ones were predominantly taken up by macropinocytosis.

## Conclusion

The preparation of a differently labeled p(MMA-*stat*-MAA) copolymer and its nanoprecipitation into defined NPs with various sizes (<100 nm, 100 to 200 nm, and >300 nm) without the usage of surfactants were demonstrated. These tailor-made NPs are promising for studying the influence of the surface, charge or size of the NPs on their internalization into cells, as no stabilizers were used, which have an influence on cellular uptake. We showed that the size itself of the NPs has a strong influence on the uptake in HeLa cells. This is further influenced by the concentration used and incubation time. The medium sized NPs were taken up faster compared to small and large ones. All NPs were found inside the cells, whereas small and medium sized NPs showed the same cellular distribution and were detectable in lysosomes. In contrast, large NPs showed less co-localization with smaller NPs and were not detectable in the lysosomes. By using inhibitors, we have shown that clathrin-dependent endocytosis is the predominant pathway for smaller NPs < 200 nm, whereas macropinocytosis is responsible for larger NPs. In further studies, the influence of the zeta potential and of the additional functional groups on the particle surface will be studied, again in the absence of surfactants.

## Acknowledgements

The financial support from the Thuringian Ministry for Education, Science and Culture (grant #B514-09051, Nano-ConSens), the Deutsche Forschungsgemeinschaft (Japan-Germany exchange program, DFG and JSPS), the Carl-Zeiss Foundation (JCSM Strukturantrag), the Funding Program for World-Leading Innovative R&D on Science and Technology (FIRST Program, JSPS), and the Core Research Program for Evolutional Science and Technology (CREST) from the Japan Science and Technology Corporation (JST) is gratefully acknowledged. We express our gratitude to Steffi Stumpf, EMZ Jena, for assistance in the SEM investigations, Melanie Nikolajski, University of Jena, for help with the pH dependent zeta measurements, Tomoya Suma, the University of Tokyo, for help with FC studies, and Dr Xueying Liu, the University of Tokyo, for the CLSM measurements.

## References

- 1 K. Riehemann, S. W. Schneider, T. A. Luger, B. Godin, M. Ferrari and H. Fuchs, *Angew. Chem., Int. Ed.*, 2009, **48**, 872.
- 2 N. Sanvicens and M. P. Marco, *Trends Biotechnol.*, 2008, **26**, 425.
- 3 J. Fang, H. Nakamura and H. Maeda, *Adv. Drug Delivery Rev.*, 2011, **63**, 136.
- 4 K. Miyata, T. Nomoto, H. Takemoto, H. J. Kim, Y. Matsumoto, M. Oba, N. Nishiyama and K. Kataoka, *Abstr. Pap. Am. Chem. Soc.*, 2010, **110**, 178.
- 5 Y. Liu, H. Miyoshi and M. Nakamura, *Int. J. Cancer*, 2007, **120**, 2527.
- 6 X. A. Wu and H. M. Mansour, *Int. J. Nanotechnol.*, 2011, **8**, 115.
- 7 G. Oberdorster, V. Stone and K. Donaldson, *Nanotoxicology*, 2007, **1**, 2.
- 8 J. A. Kim, C. Aberg, A. Salvati and K. A. Dawson, *Nat. Nanotechnol.*, 2012, **7**, 62.
- 9 V. Mailander and K. Landfester, *Biomacromolecules*, 2009, **10**, 2379.
- 10 L. E. Euliss, J. A. DuPont, S. Gratton and J. M. DeSimone, *Chem. Soc. Rev.*, 2006, **35**, 1095.
- 11 F. Alexis, E. Pridgen, L. K. Molnar and O. C. Farokhzad, *Mol. Pharmacol.*, 2008, **5**, 505.
- 12 M. Mahmoudi, I. Lynch, M. R. Ejtehadi, M. P. Monopoli, F. B. Bombelli and S. Laurent, *Chem. Rev.*, 2011, **111**, 5610.
- 13 J. Wang, J. D. Byrne, M. E. Napier and J. M. DeSimone, *Small*, 2011, **7**, 1919.
- 14 G. M. Whitesides, *Nat. Biotechnol.*, 2003, **21**, 1161.
- 15 M. Gaumet, R. Gurny and F. Delie, *Eur. J. Pharm. Sci.*, 2009, **36**, 465.
- 16 J. P. Best, Y. Yan and F. Caruso, *Adv. Healthcare Mater.*, 2012, **1**, 35.
- 17 G. Sahay, D. Y. Alakhova and A. V. Kabanov, *J. Controlled Release*, 2010, **145**, 182.
- 18 J. Rejman, V. Oberle, I. S. Zuhorn and D. Hoekstra, *Biochem. J.*, 2004, **377**, 159.

- 19 H. J. Gao, W. D. Shi and L. B. Freund, *Proc. Natl. Acad. Sci. U. S. A.*, 2005, **102**, 9469.
- 20 S. Zhang, J. Li, G. Lykotrafitis, G. Bao and S. Suresh, *Adv. Mater.*, 2009, **21**, 419.
- 21 S. E. A. Gratton, P. A. Ropp, P. D. Pohlhaus, J. C. Luft, V. J. Madden, M. E. Napier and J. M. DeSimone, *Proc. Natl. Acad. Sci. U. S. A.*, 2008, **105**, 11613.
- 22 N. Doshi and S. Mitragotri, *PLoS One*, 2010, **5**, 1.
- 23 J. Dausend, A. Musyanovych, M. Dass, P. Walther, H. Schrezenmeier, K. Landfester and V. Mailander, *Macromol. Biosci.*, 2008, **8**, 1135.
- 24 A. Musyanovych, J. Dausend, M. Dass, P. Walther, V. Mailaender and K. Landfester, *Acta Biomater.*, 2011, **7**, 4160.
- 25 S. Lorenz, C. P. Hauser, B. Autenrieth, C. K. Weiss, K. Landfester and V. Mailander, *Macromol. Biosci.*, 2010, **10**, 1034.
- 26 M. Gaumet, R. Gurny and F. Delie, *Int. J. Pharm.*, 2010, **390**, 45.
- 27 W. Jiang, B. Y. S. Kim, J. T. Rutka and W. C. W. Chan, *Nat. Nanotechnol.*, 2008, **3**, 145.
- 28 Arnida, M. M. Janat-Amsbury, A. Ray, C. M. Peterson and H. Ghandehari, *Eur. J. Pharm. Biopharm.*, 2011, **77**, 417.
- 29 W.-K. Oh, S. Kim, M. Choi, C. Kim, Y. S. Jeong, B.-R. Cho, J.-S. Hahn and J. Jang, *ACS Nano*, 2010, **4**, 5301.
- 30 P. Decuzzi, B. Godin, T. Tanaka, S. Y. Lee, C. Chiappini, X. Liu and M. Ferrari, *J. Controlled Release*, 2010, **141**, 320.
- 31 Z. Popovic, W. Liu, V. P. Chauhan, J. Lee, C. Wong, A. B. Greytak, N. Insin, D. G. Nocera, D. Fukumura, R. K. Jain and M. G. Bawendi, *Angew. Chem., Int. Ed.*, 2010, **49**, 8649.
- 32 W. Zauner, N. A. Farrow and A. M. R. Haines, *J. Controlled Release*, 2001, **71**, 39.
- 33 O. Lunov, T. Syrovets, C. Loos, J. Beil, M. Delecher, K. Tron, G. U. Nienhaus, A. Musyanovych, V. Mailander, K. Landfester and T. Simmet, *ACS Nano*, 2011, **5**, 1657.
- 34 C. He, Y. Hu, L. Yin, C. Tang and C. Yin, *Biomaterials*, 2010, **31**, 3657.
- 35 Y.-L. Chiu, Y.-C. Ho, Y.-M. Chen, S.-F. Peng, C.-J. Ke, K.-J. Chen, F.-L. Mi and H.-W. Sung, *J. Controlled Release*, 2010, **146**, 152.
- 36 T.-G. Iversen, T. Skotland and K. Sandvig, *Nano Today*, 2011, **6**, 176.
- 37 S. K. Sahoo, J. Panyam, S. Prabha and V. Labhassetwar, *J. Controlled Release*, 2002, **82**, 105.
- 38 M. Feng and P. Li, *Acta Pharm. Sinica*, 2005, **40**, 893.
- 39 K. M. Ho, W. Y. Li, C. H. Wong and P. Li, *Colloid Polym. Sci.*, 2010, **288**, 1503.
- 40 P.-J. Lou, W.-F. Cheng, Y.-C. Chung, C.-Y. Cheng, L.-H. Chiu and T.-H. Young, *J. Biomed. Mater. Res., Part A*, 2009, **88**, 849.
- 41 A. Vollrath, D. Pretzel, C. Pietsch, I. Perevyazko, S. Schubert, G. M. Pavlov and U. S. Schubert, *Macromol. Rapid Commun.*, 2012, DOI: 10.1002/marc.201200329.
- 42 J. Pauli, T. Vag, R. Haag, M. Spieles, M. Wenzel, W. A. Kaiser, U. Resch-Genger and I. Hilger, *Eur. J. Med. Chem.*, 2009, **44**, 3496.
- 43 S. Schubert, J. T. Delaney and U. S. Schubert, *Soft Matter*, 2011, **7**, 1581.
- 44 I. Y. Perevyazko, A. Vollrath, S. Hornig, G. M. Pavlov and U. S. Schubert, *J. Polym. Sci., Part A: Polym. Chem.*, 2010, **48**, 3924.
- 45 J. Brandrup, E. H. Immergut and E. A. Grulke, in *Polymer Handbook*, Wiley-Interscience, 4th edn, 1999.
- 46 A. Palecanda and L. Kobzik, *Methods*, 2000, **21**, 241.
- 47 C. S. S. R. Kumar, "Nanocomposites, Nanomaterials for Life Sciences", in *Nanocomposites*, Wiley-VCH, 1st edn, 2010, p. 466.
- 48 S. Grosse, Y. Aron, G. Thevenot, M. Monsigny and I. Fajac, *J. Controlled Release*, 2007, **122**, 111.
- 49 M. Fretz, J. Jin, R. Conibere, N. A. Penning, S. Al-Taei, G. Storm, S. Futaki, T. Takeuchi, I. Nakase and A. T. Jones, *J. Controlled Release*, 2006, **116**, 247.